CONTEMPORARY PROBLEMS OF

POWER ENGINEERING AND ENVIRONMENTAL PROTECTION

Editors:
Krzysztof Pikoń
Magdalena Bogacka

eit InnoEnergy Knowledge Innovation Community
Silesian University of Technology

Edited by Krzysztof Pikoń and Magdalena Bogacka

CONTEMPORARY PROBLEMS OF POWER ENGINEERING AND ENVIRONMENTAL PROTECTION 2019

Gliwice, 2020

Scientific Editors: Krzysztof Pikoń, Magdalena Bogacka

Technical Editors: Novi Dwi Saksiwi, Mateo Toro Cárdenas, Michał Rabiej, Dawid Brzózka

Cover design: Novi Dwi Saksiwi, Ichwaldo Haries Sendyartha

List of Reviewers:

dr Sunil Kumar Sahu
prof. dr hab. Teresa Grzybek
dr hab. inż. Małgorzata Wilk, prof. AGH
dr inż. Karol Sztekler
dr Xiayan Ye
dr inż. Magdalena Bogacka
dr Anna Grobelak
prof. dr hab. Leszek Czepirski
dr Shareq Mohd Nazir
dr hab. inż. Roman Korab, prof. PŚ
dr hab inż. Jacek Kalina
dr inż. Karolina Petela
dr inż. Karol Sztekler
dr hab. inż. Witold Nocoń, prof. PŚ
dr inż. Ziemowit Ostrowski
dr inż. Tomasz Bury
dr inż. Marcin Landrat
dr inż. Aleksandra Lipczyńska
dr inż. Sylwia Zelek-Pogudz

ISBN 978-83-950087-6-4

Published by Department of Technologies and Installations for Waste Management,

Silesian University of Technology

Available online: waste.polsl.pl

Contemporary Problems of Power Engineering and Environmental Protection – Energy Transition

In the modern era, industrial development and growth in the population and in the economy have led to significant increases in energy demand. To attend this demand all sources have been used and improved technically in the course of years, from conventional generation to renewables. However, the impact to the environment has only been a topic of interest during recent years. In that context, efforts around the globe to reduce global greenhouse gases emissions and massive consumption of natural resources resulted in the creation of new and cleaner technologies and processes. This book represents a mean to help in the diffusion of research and development made by young scientists in a variety of fields related with Environmental Protection and Energy.

The monograph "Contemporary Problems of Power Engineering and Environmental Protection" is the seventh volume of the scientific edition. This monograph consists of the manuscripts prepared by young scientists, mainly students as well as scholars from different research fields who presented them during the 7th Conference on Environmental Protection and Energy. This event is focused on soil protection, air and water resources, waste utilization, renewable sources of energy, hydro energy, wind energy, biomass, geothermal energy, energy systems, energy efficiency, LCA, influence on the natural environment and dispersed power engineering. The conference took place on 6th of December 2019 in Centre of New Technologies in Silesian University of Technology, Gliwice, Poland. This was an excellent opportunity to share the knowledge and ideas of young scientists who wanted to make a difference and contribute to a better future, in harmony with the natural environment while securing energy needs of the society.

The event, as from the beginning, was organised entirely by the students of Silesian University of Technology as part of Project Management course and as one of the essential elements of "learning by doing" approach.

MSc Energy Transition program's goal is to establish a future generation of engineers with innovative thinking who are ready to lead the implementation of contemporary energy systems and circular economy strategies. Moreover, the international atmosphere with close industrial connections shed more light to the application of theory knowledge in the real engineering environment. This conference is an excellent example for acquiring business and soft skills, active part of the program's curriculum, as a significate added value in student's professional profile.

We are proud of students' commitment, dedication and skills demonstrated toward the conference which made this a big success and, we are happy to see them getting themselves improved through each step of this event.

We would like to express our appreciation to InnoEnergy for supporting MSc Energy Transition program and the 7th Conference on Environmental Protection and Energy.

Mateo Toro Cárdenas

Table of contents

Developing a more sustainable food source for rising population of India

Kapilkumar Ingle[1, 2], Alexander Golberg[3]

[1]Department of Ecology, University of Szeged, Közép fasor 52, H-6726 Szeged, Hungary
[2]Doctoral School of Environmental Sciences, University of Szeged, Rerrich Béla tér 1, H-6720 Szeged, Hungary
[3]Porter School of Environment and Earth Science, Tel Aviv University, Israel

Abstract

Seaweeds have strong potential to play role in regular diet and to provide various nutrients for sound health. However, to develop seaweed as a food is challenging task due to public acceptance, availability of material and cultivation potential of seaweed. India has strong potential of seaweed cultivation but Indian seaweed industry is still in primary stage and seaweed is not part of Indian cuisine. In this short overview, we are addressing possible challenges and hurdles in implementation of commercial cultivation of seaweeds in Indian seawater. There are very limited research papers available on this issue addressing the challenges. Large scale coastal or offshore seaweed cultivation needs long and uniform seashore not only geographically but by rules and regulations too. This paper is addressing few important requirements which can open the door of Indian seaweed sector as a new and sustainable food source.

Keywords: Indian seawater, *Ulva*, seaweed cultivation, food security

1. Introduction

India and China are most populous, agrarian, labor intensive, fastest growing economies in the world [1] but with several social and environmental problems [2] with improvement in the 'Quality of Life' (QoL) of urban people which results in the migration of people towards cities for better life [3] from rural and tribal areas. These things make Indian government more conscious about the environmental and social concern of developmental projects. Indian economy is recovering again to grow speedily in recent time with increasing demand of food and fuel. Marine macroalgae or seaweed can be sustainable food resource for growing Indian population. But Indian seaweed sector is still in primary stages while China is number one producer of seaweed in the world.

Marine environment contains about eighty per cent of world plant diversity, includes thousands of marine seaweed species which play important role in many East and Southeast countries ecologically and economically [4]. Seaweed generally known as seaweed are multicellular photosynthetic plants, consists of leaf like structure called thallus. The color derived from chlorophyll and natural pigments of thallus classified seaweed in green (Chlorophyta), brown (Phaeophyta) and red algae (Rhodophyta). In many Asian countries, raw seaweed or seaweed products are used as source of food which contains source of almost vitamins, essential minerals and dietary fibers etc [5].

The cultivation of seaweed in marine environment is not responsible for competition with terrestrial crops for land and water, have recently gained much attention as a potential candidate for future feedstock for biorefinery. Compared to other terrestrial biomass crops seaweed have high rate of fixation of CO_2, which is one more benefit of carbon dioxide remediation[6]. However, the large scale of seaweed cultivation can be responsible for positive and negative impact on coastal and marine ecosystems [7]. The scale up low cost production of seaweed is still great challenge to fulfill the need of developing India.

In this short review we are focusing on possible barriers to establish such large scale cultivation project of seaweeds in India.

2. Basic challenges for macroalgal cultivation

Biorefinery is the term in use from last nearly four decades which refers to the production of bio-based products including food, cattle feed, chemical, medicinal products and fuel from biomass [8]. Now days this term is emerging research field [9] and getting attraction to be used for algal biomass. The major requirements for establishing biorefinery from seaweed are shown in fig. 1. However, there are many challenges in cultivating seaweed in Indian seawater and utilize that as a food in regular Indian diet.

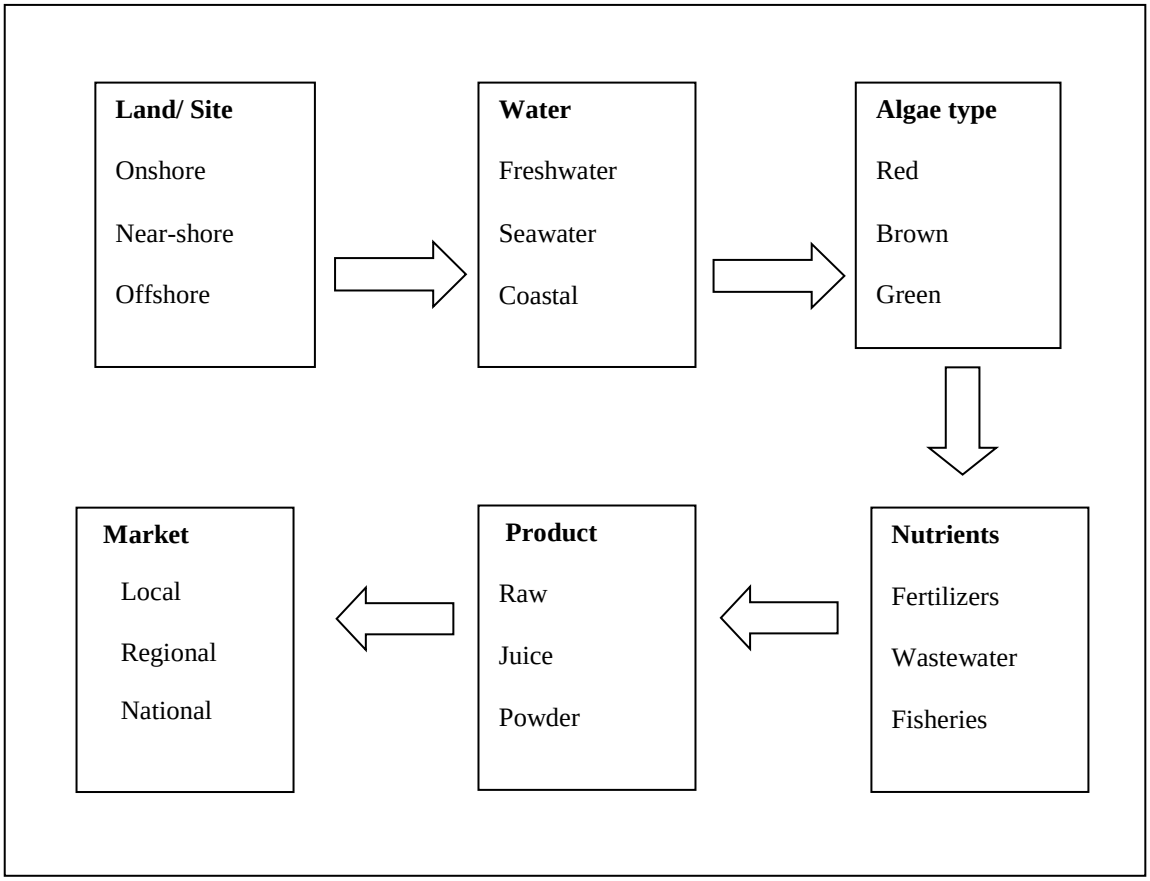

Fig. 2.1. Options available and suitable for the basic requirements for seaweed food product

Many seaweed have potential to accumulate and store the nutrients to use them in the period of unavailability of sufficient nutrients [10] and can grow in favorable conditions. Seaweeds can be either directly harvested or cultivated. However, its availability and chemical composition vary with area of ocean or sea, available nutrients in that area, seasonal changes and climate variations. It is possible to cultivate seaweeds in a pond on few hectors land but land acquisition is one of the most difficult tasks in India now a days. The governmental price of any land is very much less than market price which can create various social issues. With this the Indian agriculture sector facing various challenges as illiteracy, weak socio-economic conditions, lack of technical knowledge and environmental awareness, small landholdings, weather dependent farming systems, poor infrastructures and lack of sufficient bureaucratic procedures which all make farmers and rural people more sensitive economically. The suicide of farmer is the darker side of Indian agriculture. This thing makes government to think before establishing any new development project which need agricultural or rural side land. To overcome this limitation the coastal bay development for biomass cultivation is good option for project proponents.

The washing of seaweed after collection will need freshwater which can make fermentation of seaweed. The offshore or near-shore cultivation of seaweed can provide the sufficient water source for biomass production and it can be reused for various purposes. The green algae are nearly similar to terrestrial plants on the basis of chemical composition and many species show the seawater habitat. Few among those species have good economic value as food, medicine and source for obtaining various chemicals easily available worldwide as shown in fig.2. Seaweed are available naturally in various coastal region of India among those the coastal belt of south India and coast of Gujarat state are most important as their abundant availability. But still seaweed as a source of food is unknown for many Indians and not popular India. Fast growing rate and high carbohydrate contains can make *Ulva* species more popular for cultivation. There are various species of genus *Ulva* found in Indian coast and ocean but *Ulva fasciata* shows higher polysaccharides content and has potential to grow worldwide.

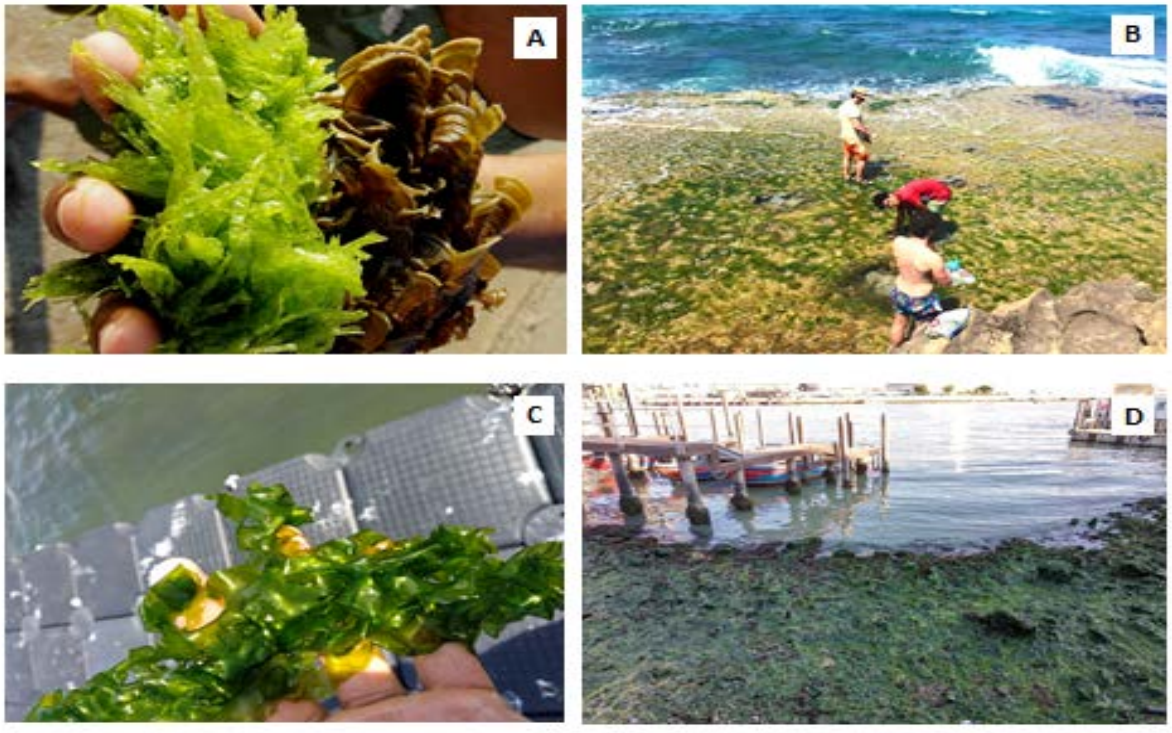

Fig. 2.2. Seaweeds from Mediterranean Sea. A. From Tel Aviv coast. B. Northern Israel coastal area shows various seaweeds. C. Seaweed *Ulva* from Chioggia, Italy. D. Venice lagoon is full of seaweed species particularly *Ulva*.

Summer in India is generally very hot with nearly more than 45 ^{0}C areal temperature in coastal areas. Such temperature is lethal for many seaweed but nutrient storage helps them to increase tolerance level to high temperature by production of heat shock proteins [11]. Though the temperature helps in photosynthesis, the unavailability of nutrients [12] become responsible for the reduction of growth rate due to slowing the process of photosynthesis. But in case of nutrient availability by nutrient loading or by boundary layer refreshing due to high flow rate[11], seaweed show maximum growth rate. The nutrient level is high in coastal water in the season of raining particularly due to addition of agricultural water runoff in rivers and then to coast. Eastern coast of India shows mouths of many rivers which take part actively in incensement of nutrient level of coastal water. Such things are become responsible for eutrophication at many places and with this special addition of nutrients in coastal water for seaweed cultivation of also responsible for eutrophication [13]. But well managed cultivation of seaweed where the nutrients are available with fish and mussel culture can be effective in terms of high and low nutrient condition [14].

Local market will be available as per requirement. The facilities should be available for the transportation of product to market. With this, it is necessary to find possible uses of other products of biomass. The collection

system and distributors need the storage and transportation. Perfect technology, the equipment and necessary experimental set up and well skilled technician is the most important need for this part of project. To make all these requirements cost effective it is necessary to find alternatives with possible benefits. The skilled and unskilled manpower is necessary in the project which has positive social impacts.

3. *Ulva* cultivation requirements

As other plants, *Ulva* also required sufficient temperature and nutrients with favorable environment. Other environmental factors most important for *Ulva* are salinity, water exchange to deliver nutrients and carbon dioxide. *Ulva* has tolerance capacity to salinity level and sunlight, temperature. However, these capacities vary in species to species and depend on the location. The sunlight and temperature are dependent on the seasonal variations which can impact on growth and contents of *Ulva*. In *Ulva* most important sugar is rhamnose which can shows variations in different seasons [15]. Winter season make seaweeds more flexible to resist waves than the summer [15]. With this, rainy season can increase the risks of accumulation of pollutants, chemicals, and heavy metals due to run off from land to ocean.

3.1. Temperature

The temperature plays important role on the metabolic rate and reproduction of *Ulva* similar as all photosynthetic plants. India is located in the high temperature zone and many seaweeds are sensitive to higher temperature. Temperature more than optimum [16] level can destabilize protein in seaweed and became responsible for cellular damage, and further leads in death of seaweed [17]. The species which are highly tolerable to temperature and have potential to recover back after damage are useful for cultivation in large scale. In offshore environment the temperature of seawater is generally cooler than the seawater from coastal sites [18]. This thing can be beneficial for the cultivation of seaweed if there are sufficient nutrients available at offshore sites.

3.2. Salinity

The salinity of major part of seawater throughout the world is in between 34 to 35 ppt [19]. Indian seawater salinity is also in that range just shows little less value in coastal water compare the offshore seawater. In case of India, the eastern costal area is less saline than western coast[19]. The higher salinity than optimal seaweed can show cellular dehydration [20]. Alteration of inorganic and organic components present in the cell makes seaweed little tough to balance the osmotic pressure but for commercial cultivation the seaweed should capable to tolerate wide range of the salinity [11].

3.3. Water movement

In general the movements of water below 0.1 m/s is known as low water motion [21] and above 0.25 m/s is known as high water motion [22]. The movement of seawater or water motion is important need of seaweed cultivation as it is related to their growth rate[23]. Water motion is responsible for the exchange of carbon dioxide and nutrients present in seaweed and water. In case of slow water movement, the thallus of seaweed shows the large boundary layer which obstacles to get sufficient carbon dioxide [11] and results in reduction of growth rate [24]. In high water motion seaweed need to develop strong holdfast [25] which adversely impacts on growth of other part. In case of low water motion can show increase in grazing, abundance of epiphytes. In case of eastern coast of India, the Bay of Bengal is adversely famous for the deadliest cyclones and storms in the world [26]. In this background it is challenging to make cultivation particularly at offshore environment at eastern coast of India.

3.4. Turbidity

The transparency of seawater is the challenging factor for large scale cultivation as it is directly related with other factors such as temperature, pH and link to climate change too[27]. Offshore environment shows transparent water compare to coastal water and particularly at the time of rainy season. The rainy season, many rivers are responsible for influx of large quantity of muddy water in the coastal areas[27]. The turbidity

is responsible to absorption and scattering of sunlight and can be leads to increase in the seawater temperature [28]. This can impact on the photosynthesis rate of seaweed. But clear seawater can also be responsible for the negative impact on seaweed [29].

4. Main challenges in the large-scale cultivation

4.1. Diseases

Large scale seaweed can be affected by diseases and become responsible for heavy economic loss [30]. There are many viral, bacterial and fungal diseases due to pathogens making the commercially cultivated seaweed as hosts. Sometimes few endophytes are hosted by many seaweed [31] which are not responsible for diseases but make some changes in host plants [32]. Adverse environmental conditions can provide opportunities to biological factors such as bacteria, fungus to grow [33]. The bacteria like E. coli get nutrient source from seaweed, grow fast and can create risk to human health. The decay of infected seaweed is also one more problem if it comes to beach in large quantity.

4.2. Epiphytes

Epiphytes on seaweed are generally the seawater plants such as diatoms, polysiphonia which are dependent on the seaweed for food. Epiphytes cover the major surface of seaweed and create pores on seaweed. However, few seaweed developed diverse protective systems, both chemical and mechanical, to eliminate the parasitic microbes [34]. Many epiphytes do not show any harm to seaweed directly but can compete with host seaweed for sunlight and nutrients [35]. Few times the epiphytes are responsible for the attraction of grazers towards them and seaweed.

4.3. Grazers

Seaweed are the important source of food for various kinds of water herbivores [36]. There are various kinds of primary consumers are available there in that ecosystem which can multiply and become more in numbers due to large scale seaweed cultivation. These organisms called as grazers and they can be bivalves, ascidians, amphipods, polychaetes, gastropods or sponges or fishes and so on. Seaweed cultivation in southern coast of India is facing problem of grazers particularly the rabbit fish which is herbivorous fish [35].These small sized herbivorous fish is responsible for big economic loss for seaweed cultivation.

5. Conclusion

The challenges in front of developing the seaweed as a food source for indian regular diet are related with the successful cultivation of large-scale cultivation of macroalgae in Indian seawater. There is strong need of finding possibilities of such cultivation by changing not only overcoming the environmental challenges but also finding strong policy support. The clear policy with well define need of marine food resources, support to tackle the problem of challenges and hurdle in this area section is the primary need in this sector. The success in this will be the important steps to develop this resource.

Acknowledgement

Author is Stipendium Hungaricum student working in the University of Szeged, Hungary for his PhD.

References

[1] H.K. Sandhu, Agricultural Development in India and China : a Comparative Study, 1 (2012) 45–55.

[2] K.N. Ingle, K. Harada, C.N. Wei, K. Minamoto, A. Ueda, Policy framework for formulating environmental management strategy for sustainable development of tanneries in India., Environ. Health Prev. Med. 16 (2011) 123–128. https://doi.org/10.1007/s12199-010-0168-8.

[3] J.-W. Wang, Z.-T. Cui, H.-W. Cui, C.-N. Wei, K. Harada, K. Minamoto, K. Ueda, K.N. Ingle, C.-G. Zhang, A. Ueda, Quality of life associated with perceived stigma and discrimination among the floating population in Shanghai, China: a qualitative study, Health Promot. Int. 25 (2010) 394–402. https://doi.org/10.1093/heapro/daq039.

[4] A.J. Smit, Medicinal and pharmaceutical uses of seaweed natural products: a review., J. Appl. Phycol. 16 (2004) 245–262. https://doi.org/10.1023/B.

[5] K. Ito, K. Hori, Seaweed: chemical composmon and potential food uses, Food Rev. Int. 5 (1989) 101–144. https://doi.org/10.1080/87559128909540845.

[6] K. Gao, K.R. McKinley, Use of macroalgae for marine biomass production and CO2 remediation: a review, J. Appl. Phycol. 6 (1994) 45–60. https://doi.org/10.1007/BF02185904.

[7] A.D. Hughes, M.S. Kelly, K.D. Black, M.S. Stanley, Biogas from Macroalgae: is it time to revisit the idea?, Biotechnol. Biofuels. 5 (2012) 86. https://doi.org/10.1186/1754-6834-5-86.

[8] A.-D. González-Delgado, V. Kafarov, Microalgae based biorefinery: Issues to consider, CTyF - Ciencia, Tecnol. y Futur. 4 (2011) 5–22.

[9] K.A. Jung, S.-R. Lim, Y. Kim, J.M. Park, Potentials of macroalgae as feedstocks for biorefinery, Bioresour. Technol. 135 (2013) 182–190. https://doi.org/10.1016/j.biortech.2012.10.025.

[10] D.M. Young EB, Berges JA, Physiological responses of intertidal marine brown algae to nitrogen deprivation and resupply of nitrate and ammonium, Physiol. Plant. 135 (2009) 400–411. https://doi.org/10.1111/j.1399-3054.2008.01199.x.

[11] P.D. Kerrison, M.S. Stanley, M.D. Edwards, K.D. Black, A.D. Hughes, The cultivation of European kelp for bioenergy: Site and species selection, Biomass and Bioenergy. 80 (2015) 229–242. https://doi.org/10.1016/j.biombioe.2015.04.035.

[12] K. Sajotun, Seasonal Lamina Growth in two Age Groups of Laminaria saccharina (L.) Lamour. in Western Norway, Bot. Mar. 36 (1993) 433–442. https://doi.org/10.1515/botm.1993.36.5.433.

[13] D.L. Sun S, Wang F, Li CL, Qin S, Zhou MJ, Emerging challenges : Massive green algae blooms in the Yellow Sea, Nat Preced. (2008).

[14] J.C. Sanderson, M.J. Dring, K. Davidson, M.S. Kelly, Culture, yield and bioremediation potential of Palmaria palmata (Linnaeus) Weber & Mohr and Saccharina latissima (Linnaeus) C.E. Lane, C. Mayes, Druehl & G.W. Saunders adjacent to fish farm cages in northwest Scotland, Aquaculture. 354–355 (2012) 128–135. https://doi.org/10.1016/j.aquaculture.2012.03.019.

[15] X. Briand, P. Morand, Anaerobic digestion of *Ulva* sp. 1. Relationship between *Ulva* composition and methanisation, J. Appl. Phycol. 9 (1997) 511–524. https://doi.org/10.1023/A:1007972026328.

[16] M.P. Lesser, OXIDATIVE STRESS IN MARINE ENVIRONMENTS: Biochemistry and Physiological Ecology, Annu. Rev. Physiol. 68 (2006) 253–278. https://doi.org/10.1146/annurev.physiol.68.040104.110001.

[17] J. Bruhn, V. a. Gerard, Photoinhibition and recovery of the kelp Laminaria saccharina at optimal and superoptimal temperatures, Mar. Biol. 125 (1996) 639–648. https://doi.org/10.1007/BF00349245.

[18] E. Reith, E. Deurwaarder, K. Hemmes, Bio-offshore: grootschalige teelt van zeewieren in combinatie met offshore windparken in de Noordzee, (2005).

[19] CSIR-NIO, SAGAR - A pocketbook on the ocean with special reference to the waters around India,

(n.d.). http://www.nio.org/index/option/com_nomenu/task/show/tid/2/id/140.

[20] M. Kumar, P. Kumari, C.R.K. Reddy, B. Jha, Salinity and desiccation induced oxidative stress acclimation in seaweeds, 2014. https://doi.org/10.1016/B978-0-12-408062-1.00004-4.

[21] W.N. Wheeler, Effect of boundary layer transport on the fixation of carbon by the giant kelp Macrocystis pyrifera, Mar. Biol. 56 (1980) 103–110. https://doi.org/10.1007/BF00397128.

[22] C.L. Stevens, C.L. Hurd, Boundary-layers around bladed aquatic macrophytes, Hydrobiologia. 346 (1997) 119–128. https://doi.org/10.1023/A:1002914015683.

[23] B.H. Buck, C.M. Buchholz, Response of offshore cultivated Laminaria saccharina to hydrodynamic forcing in the North Sea, Aquaculture. 250 (2005) 674–691. https://doi.org/10.1016/j.aquaculture.2005.04.062.

[24] C.L. Hurd, Water motion, marine macroalgal physiology, and production, J. Phycol. 36 (2000) 453–472. https://doi.org/10.1046/j.1529-8817.2000.99139.x.

[25] S. Kawamata, Adaptive mechanical tolerance and dislodgement velocity of the kelp Laminaria japonica in wave-induced water motion, Mar. Ecol. Prog. Ser. 211 (2001) 89–104. https://doi.org/10.3354/meps211089.

[26] C. Antony, A.S. Unnikrishnan, Observed characteristics of tide-surge interaction along the east coast of india and the head of bay of bengal, Estuar. Coast. Shelf Sci. 131 (2013) 6–11. https://doi.org/10.1016/j.ecss.2013.08.004.

[27] V. Meleder, J. Populus, B. Guillaumont, T. Perrot, P. Mouquet, Predictive modelling of seabed habitats: Case study of subtidal kelp forests on the coast of Brittany, France, Mar. Biol. 157 (2010) 1525–1541. https://doi.org/10.1007/s00227-010-1426-4.

[28] H. Arakawa, Ocean turbidity and its effects on marine organisms., (n.d.).

[29] M.J. Dring, A. Wagner, K. Luning, Contribution of the UV component of natural sunlight to photoinhibition of photosynthesis in six species of subtidal brown and red seaweeds, Plant, Cell Environ. 24 (2001) 1153–1164. https://doi.org/10.1046/j.1365-3040.2001.00765.x.

[30] C.M.M. Gachon, T. Sime-Ngando, M. Strittmatter, A. Chambouvet, G.H. Kim, Algal diseases: Spotlight on a black box, Trends Plant Sci. 15 (2010) 633–640. https://doi.org/10.1016/j.tplants.2010.08.005.

[31] F. Weinberger, G. Pohnert, M.L. Berndt, K. Bouarab, B. Kloareg, P. Potin, Apoplastic oxidation of L-asparagine is involved in the control of the green algal endophyte Acrochaete operculata Correa & Nielsen by the red seaweed Chondrus crispus Stackhouse, J. Exp. Bot. 56 (2005) 1317–1326. https://doi.org/10.1093/jxb/eri132.

[32] G.C. Zuccarello, D. Moon, L.J. Goff, A phylogenetic study of parasitic genera placed in the family choreocolacaceae (Rhodophyta), J. Phycol. 40 (2004) 937–945. https://doi.org/10.1111/j.1529-8817.2004.04029.x.

[33] S. Egan, N.D. Fernandes, V. Kumar, M. Gardiner, T. Thomas, Bacterial pathogens, virulence mechanism and host defence in marine macroalgae, Environ. Microbiol. 16 (2014) 925–938. https://doi.org/10.1111/1462-2920.12288.

[34] GM Nylund, H. Pavia., Chemical versus mechanical inhibition of fouling in the red alga Dilsea carnosa. 299, , Mar. Ecol. Prog. Ser. 299 (2005) 111–121.

[35] K.N. Ingle, M. Polikovsky, A. Chemodanov, A. Golberg, Marine integrated pest management (MIPM)

approach for sustainable seagriculture, Algal Res. 29 (2018) 223–232. https://doi.org/10.1016/j.algal.2017.11.010.

[36] A. Baeta, R. Pinto, I. Valiela, P. Richard, N. Niquil, J.C. Marques, δ15N and δ13C in the Mondego estuary food web: Seasonal variation in producers and consumers, Mar. Environ. Res. 67 (2009) 109–116. https://doi.org/10.1016/j.marenvres.2008.11.005.

Solution combustion synthesis-derived materials in selective catalytic reduction of NO_x (NH_3-SCR). XRD analysis of Cu-Fe-Ce mixed oxides prepared by citric acid method

Agnieszka Szymaszek [1], Bogdan Samojeden [2], Monika Motak [3]

[1] AGH University of Science and Technology, e-mail: agnszym@agh.edu.pl
[1] AGH University of Science and Technology, e-mail: bogdan.samojeden@agh.edu.pl
[3]AGH University of Science and Technology, e-mail: motakm@agh.edu.pl

Abstract

Cu-Fe or Cu-Fe-Ce mixed oxides were synthesized by solution combustion synthesis (SCS) in "fuel rich" and "fuel lean" conditions. In order to investigate the influence of the chemical composition and the amount of fuel on the final structure of the samples, the detailed XRD analysis was performed. The different preparation procedures allowed to obtain the materials with diversified amounts of Fe_xO_y, CuO and CeO_2 (when applied) phases and different size of the crystals. It was noticed that the crystallinity was much higher for the samples prepared in "fuel lean" conditions. Additionally, for the materials with CeO_2 the crystallinity was noticeably lower. The influence of CeO_2 on the structure of the materials was more remarkable for the samples prepared in "fuel rich" conditions. Therefore, it is predicted that not the chemical composition of the sample and the fuel to oxidizer ratio is a key factor to obtain materials with desired structure.

Keywords: selective catalytic reduction, mixed metal oxides, citric acid method, solution combustion synthesis

1. Introduction

The constant development of many of the industrial processes and transport results in the increased combustion of fossil fuel. One of the most harmful compounds emitted by stationary and mobile sources are nitrogen oxides (NO_x). The main reason of the increasing emissions of NO_x is related to the application of mobile sources with improved fuel efficiency with the ratios of air-to-fuel is higher than stoichiometric [1]. In recent years, the emission of nitrogen oxides is rising successively resulting in the formation of acid rain, photochemical smog and ozone layer depletion. Moreover, NO_x contribute to ground-level O_3 and affect directly humans health [2–5].

According to the statistics, almost half of the NO_x emitted to the atmosphere are produced by mobile sources and the most effective technology applied for their abatement are catalytic converters [1,4,6]. Nitrogen oxides that are produced by stationary sources can be treated by in-furnance or post-combustion technologies. The techniques include for instance flue gas recirculation or steam/water injection and selective catalytic reduction (SCR) or non-selective catalytic reduction (NSCR), respectively [4,7]. In recent years, the most effective commercial technology used to decrease the amount of NO_x is SCR with ammonia as the reducing agent. The process is based on the reaction of nitrogen oxides with NH_3 on the surface of the catalyst. Most of the commercial systems used worldwide in SCR installations are honeycomb monolith that consist of V_2O_5-TiO_2 doped with promoters, for example MoO_3 or WO_3. The reaction proceeds usually at 200-400°C and the main products are molecular nitrogen and water vapor [5,8,9]. The simplified scheme of NH_3-SCR is presented in Fig. 1.1. and the possible pathways of the reaction depending on the initial conditions are described by equations 1.-3. [8].

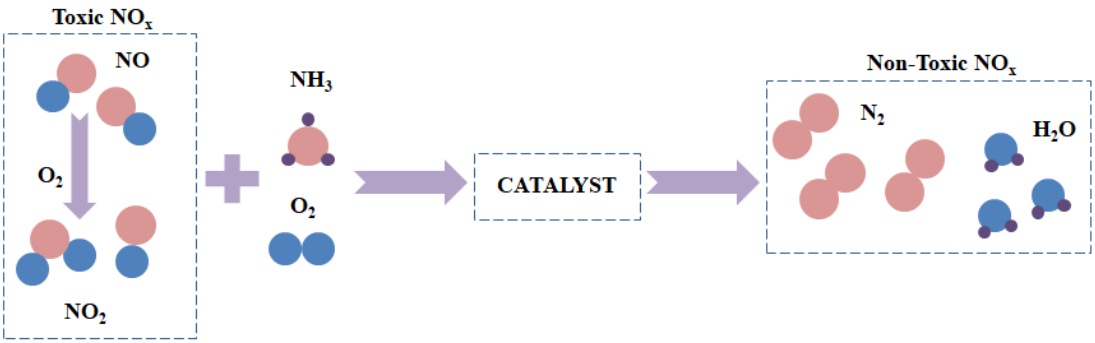

Fig. 1.1. Schematic pathway of selective catalytic reduction of NO_x by ammonia (based on [5,10]).

$$4\ NO + 4\ NH_3 + O_2 \rightarrow 4\ N_2 + 6\ H_2O \quad (1)$$

$$6\ NO_2 + 8\ NH_3 \rightarrow 7\ N_2 + 12\ H_2O \quad (2)$$

$$6\ NO + 4\ NH_3 \rightarrow 5\ N_2 + 6\ H_2O \quad (3)$$

Additionally, there are some undesired reactions of NH_3-SCR that lead to the formation of N_2O or to the non-selective oxidation of ammonia. These are described by equations 4. and 5., respectively.

$$2\ NH_3 + 2\ O_2 \rightarrow N_2O + 3\ H_2O \quad (4)$$

$$4\ NH_3 + 3\ O_2 \rightarrow 2\ N_2 + 6\ H_2O \quad (5)$$

Despite that NH_3-SCR is one of the most developed technologies of NO_x abatement, it has some drawbacks related to the properties of the commercial catalyst. First of all, it has a narrow temperature window (300-400°C). Therefore, it should be placed in so-called "high-dust" position, upstream of the dust removal equipment and the FGD unit, where the flue gas is hot enough to initiate the reaction. However, in this kind of system the catalyst is posed to the contaminations by fly ash, heavy or alkali metal compounds and other impurities present in the flue gas. Another problem of the commercial catalyst is that it promotes the reaction between NH_3 and SO_3. Sulphur dioxide can be oxidized to SO_3 and then react with ammonia giving ammonium salts. These compounds are extremely dangerous for the catalytic system, especially due to their poisoning influence and the risk of plugging and corroding of the equipment [4,9,11].

There are many materials described in the scientific literature that can be the substitutes for the commercial vanadium catalyst. The most promising are transition-metal modified zeolites [12–14], aluminosilicates [15–18], activated carbons [5, 19–21], modified hydrotalcites [9, 22] and metal-oxide supported systems [23–25]. These materials are attractive for industrial applications mainly due to their activity in the low-temperature range, low price and high resistance to contaminating compounds of the flue gas.

One of the recent approaches that were made to synthesize the effective catalyst is a solution combustion synthesis (SCS). The method is based on the self-sustained redox exothermic reactions between the oxidizer and fuel The most frequently used oxidizers are metal nitrates, mainly due to their good solubility in water and low temperature of decomposition, in comparison to other metal salts [26]. The most common fuels are urea, glycine, citric acid or glucose. The only condition is that these compounds are the source of carbon and hydrogen and form complexes with the metal ions. The preferable properties of the ideal fuel are good solubility in the solvent and low temperature of decomposition (less than 400°C). In most cases, oxidizer and fuel are dissolved in water [27, 28]. There are two modes of SCS: volume combustion, where the solution is slowly heated to the boiling point and to the ignition temperature or self-propagating combustion, where small volume of the solution is heated locally in order to initiate the exothermic reaction The simplified scheme of SCS according to the described modes is presented in Fig. 1. 2. (A).

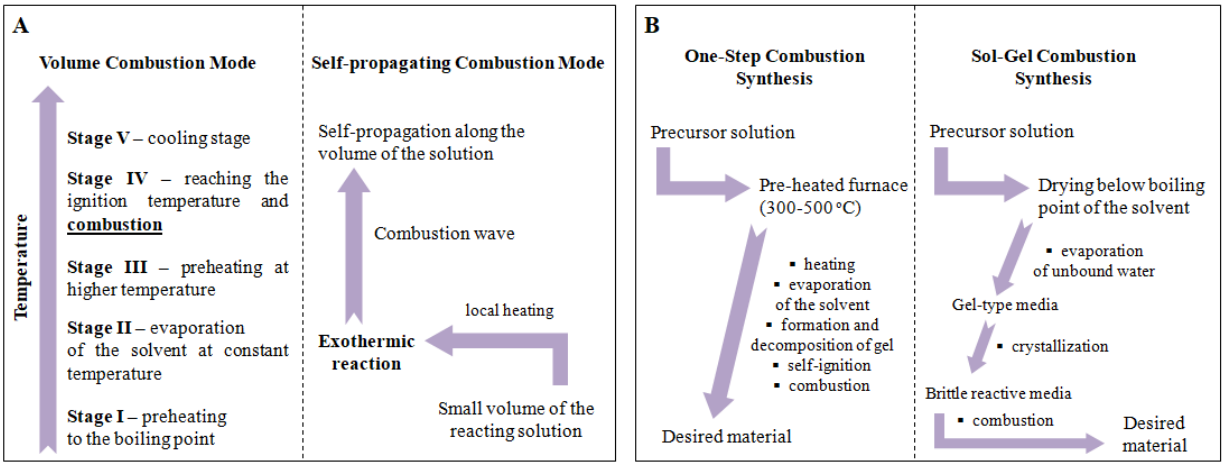

Fig. 1.2. The possible heating modes applied in solution combustion synthesis (A) and the schematic presentations of the most common pathways of solution combustion synthesis (based on: [26–31]).

What is more, heating of the initial solution can be performed according to two different routes. In the first one, all steps of the combustion reaction occur very rapidly [29,32]. In the second one, which is called sol-gel combustion, the initial solution is first dried below the boiling point of the solvent. As a consequence, the unbound water molecules are evaporated which results in the formation of gel-type media. Then the gel undergoes crystallization into a solid. Afterwards, the obtained medium is placed in the furnace at about 300-500°C and the self-ignition and combustion takes place [27, 30]. The possibilities of the initial solution heating are presented in Fig. 1. 2. (B).

According to the scientific literature, SCS-derived materials are good candidates for effective catalysts of many industrial processes, including CO oxidation [33], conversion of hydrocarbon to fuels and other chemicals [27, 33] or reforming of alcohol toward hydrogen [34]. It is mainly due to the fact that these formulations exhibit high specific surface area provided by the porosity generated under the influence of the combustion reaction. Additionally, their synthesis is relatively fast and easy in comparison to the other catalysts [26]. Moreover, the chemical composition can be adjusted in accordance to the nature of the reaction in which they will be used. The materials prepared by SCS were also considered as potential catalysts for selective catalytic reduction of NO_x [35–40].

Andreoli et al. [38] prepared MnO_x-CeO_2 via solution combustion synthesis and tested the obtained catalysts in low temperature NH_3-SCR. The authors investigated variable amounts of fuels (citric acid or glycine) with respect to the stoichiometry of the synthesis. Three different groups of materials with diversified Mn/Ce molar ratio were obtained. The results of XRD indicated that the samples prepared in so-called "lean conditions" that are characterized by low fuel to oxidizer ratio revealed more crystallized structure. According to the authors, it was typical for mixed metal oxides prepared by SCS. Additionally, S_{BET} analysis pointed at the fact that the specific surface area significantly increased with the decreasing amount of fuel used for the combustion reaction. What is more, the ratio of citric acid or glycine to the nitrates played an important role in the formation of the structure of mixed oxides. For the samples prepared in "fuel-rich" conditions the pore diameters were considerably wider in comparison to the "lean conditions" samples. The effect was explained by the higher amount of gases developed during the reaction. The influence of CeO_2 on the catalytic behavior of the Mn-based metal oxides was examined using H_2-TPR. The results of the analysis revealed that the addition of CeO_2 decreased the reduction temperature of MnO_x from 450°C to about 300°C. The results NH_3-SCR catalytic tests showed that the highest NO conversion occurred for the sample prepared with stoichiometric amount of fuel used for the combustion. It was suggested that the results were related to the highest specific surface area linked with the promotional influence of ceria. For the most active sample, 100% of NO conversion occurred at about 130°C. However, with the increasing temperature the selectivity to N_2 decreased significantly from 100% at 100°C to lower values. The result is related to the progressive promotion of ammonia oxidation at higher temperatures and consequent N_2O formation.

Another approach to the SCS synthesis of NH_3-SCR catalysts was presented by Zhijan et al. [41]. The authors investigated a series of TiO_2 supported $MnWO_x$ mixed oxides. The samples were synthesized with a different molar ratio of the metal precursors. Low temperature N_2 sorption results showed that the samples exhibited the specific surface area in the range of 168.5-253.5 $m^2 \cdot g^{-1}$ and it was observed that the pore volume and pore diameter determined by BJH method increased for the samples doped with tungsten. The dominant phase of anathase present in XRD patterns indicated that tungsten and manganese prepared by SCS were well-dispersed on the surface of TiO_2. $MnWO_x$-TiO_2 mixed oxides tested in NH_3-SCR reaction exhibited about 95% of NO conversion at 180-330ºC for the most active samples. It was observed that the catalytic performance of W-doped samples was enhanced, especially in the high-temperature SCR. What is more, the addition of W retarded the decrease of NO conversion above 250ºC to the higher temperature range. Hence, it was confirmed that the co-existence of Mn and W oxides prepared by SCS was beneficial for NH_3-SCR.

The next interesting attempt to prepare mixed metal oxides via SCS was made by Deorsola et al. The authors obtained unsupported MnO_x and examined the catalytic properties in the low temperature NH_3-SCR. The samples were prepared using glycine in fuel-lean (L) or fuel-rich (R) conditions and calcination at 400 or 600ºC. XRD analysis of the resulting materials showed that the samples obtained at 400ºC and at lean conditions exhibited lower crystallinity with respect to the other conditions of synthesis. Additionally, it was noticed that L samples were characterized by larger crystallites (40-50 nm) in comparison to R samples (10-20 nm). What is more, the specific surface area of the L samples increased with the increasing temperature of synthesis. The opposite effect was observed for R materials. NH_3-SCR catalytic tests showed that the materials prepared by SCS exhibited 75-100% of NO conversion and 100% of N_2 selectivity in the temperature range of 150-200ºC. Considering the whole temperature range, R samples were slightly more selective than L samples. Additionally, L catalysts exhibited broader range of 100% conversion (200-250ºC) in comparison to R catalysts for which 100% of NO conversion occurred only at 150ºC. The most active samples were the Mn oxide prepared in rich oxidant conditions at 400ºC. It was suggested that its good catalytic performance was facilitated by the presence of surface defect sites reflected in increased capability for NH_3 adsorption. Additionally, when the temperature of synthesis was lower, the oxidation ability of the catalyst was improved. Therefore, ammonia oxidation that is the side reaction of NH_3-SCR occurs at lower temperature.

Despite the high potential of Mn_xO_y prepared by solution combustion synthesis in NH_3-SCR, the Mn-containing catalysts exhibit very high oxidative potential [9]. Hence, the solution combustion synthesis of different transition metal oxides should be taken into consideration. A number of previous studies have confirmed catalytic activity of iron and copper in SCR [9, 39–42]. Another potentially advantageous component of SCR catalyst is CeO_2. It is mainly due to its non-toxicity, promoting impact on the structure stability and promoting influence of the redox properties of the catalyst [43, 44]. According to that, the paper describes the preparation and XRD characterization of Cu-Fe-Ce oxides. The materials were obtained using diversified molar ratio of the metal precursors. Additionally, the influence of fuel to oxidizer molar ratio on the final structure of the material was examined.

2. Experimental

2.1 Preparation of the materials

In order to prepare the Cu-Fe-Ce mixed oxides via citric acid method, the nitrate precursors of metals: copper nitrate trihydrate $Cu(NO_3)_2 \cdot 3H_2O$, iron nitrate nonahydrate $Fe(NO_3)_3 \cdot 9H_2O$, cerium nitrate trihydrate $Ce(NO_3)_3 \cdot 3H_2O$ (when used) and citric acid $C_6H_8O_7$ (where the $C_6H_8O_7$ to metal ion labeled as ω was 1:8, 1:6, 1:4, 1:2 and 1:1) were dissolved in 50 cm^3 of distilled water and mixed under vigorous stirring at room temperature for 1 hour. Subsequently, the solutions were dried at 120ºC for 12 hours. The obtained foam-like solids were calcined at 500ºC for 3 hours in air in a furnace. The preparation included diversified amounts of each metal. In order to investigate the influence of CeO_2 on the final structure of the catalyst, the reference CuFe sample was prepared. The list of the prepared materials and the designation of the samples are presented in Table. 2. 1.

Table. 2.1. List of the prepared materials

No.	Sample Code	Amount of Cu [mmol]	Amount of Fe [mmol]	Amount of Ce [mmol]	ω molar ratio
1	Cu6FeCe_8-1	10	60	10	1:8
2	CuFe_8-1	40	40	0	
3	Cu6FeCe_6-1	10	60	10	1:6
4	CuFe_6-1	40	40	0	
5	Cu6FeCe_4-1	10	60	10	1:4
6	CuFe_4-1	40	40	0	
7	Cu6FeCe_2-1	10	60	10	1:2
8	CuFe_2-1	40	40	0	
9	Cu6FeCe_1-1	10	60	10	1:1
10	CuFe_1-1	40	40	0	

2.2 Characterization of the materials

The structural properties of the prepared CuxFe(Ce) oxides were determined by the XRD analysis. The X-ray diffraction patterns were obtained using Empyrean (Panalytical) diffractometer. The instrument was equipped with copper-based anode (Cu-K_α LFF HR, λ = 0,154059 nm). The diffractograms were collected in the 2θ range of 2.0-80.0° (2θ step scans of 0.02° and a counting time of 1 s per step).
The size of the obtained crystallites was calculated using Scherrer's equation (eq. 6). :

$$T = \frac{K\lambda}{\beta cos\theta} \tag{6}$$

Where,

- T mean size of the ordered (crystalline) domains,
- K dimensionless shape factor, which value is close to unity,
- λ X-ray wavelength,
- β line broadening at half the maximum intensity (rad),
- θ Bragg angle.

3. Results and discussion

The obtained materials exhibited foamy structure and occupied the whole volume of the container. The obtained products were multicolor, and the individual phases were not separated. Therefore, no ion segregation occurred. Additionally, it was observed that the particles of the samples with the fuel to oxidizer ratio of 1:1 were softer in comparison to these with ω = 1:8 and it was far easier to ground them into mesh.

3.1 Crystalline Structure

The results of XRD analysis of the materials prepared by citric acid method are presented in Fig. 3.1. (A-E)

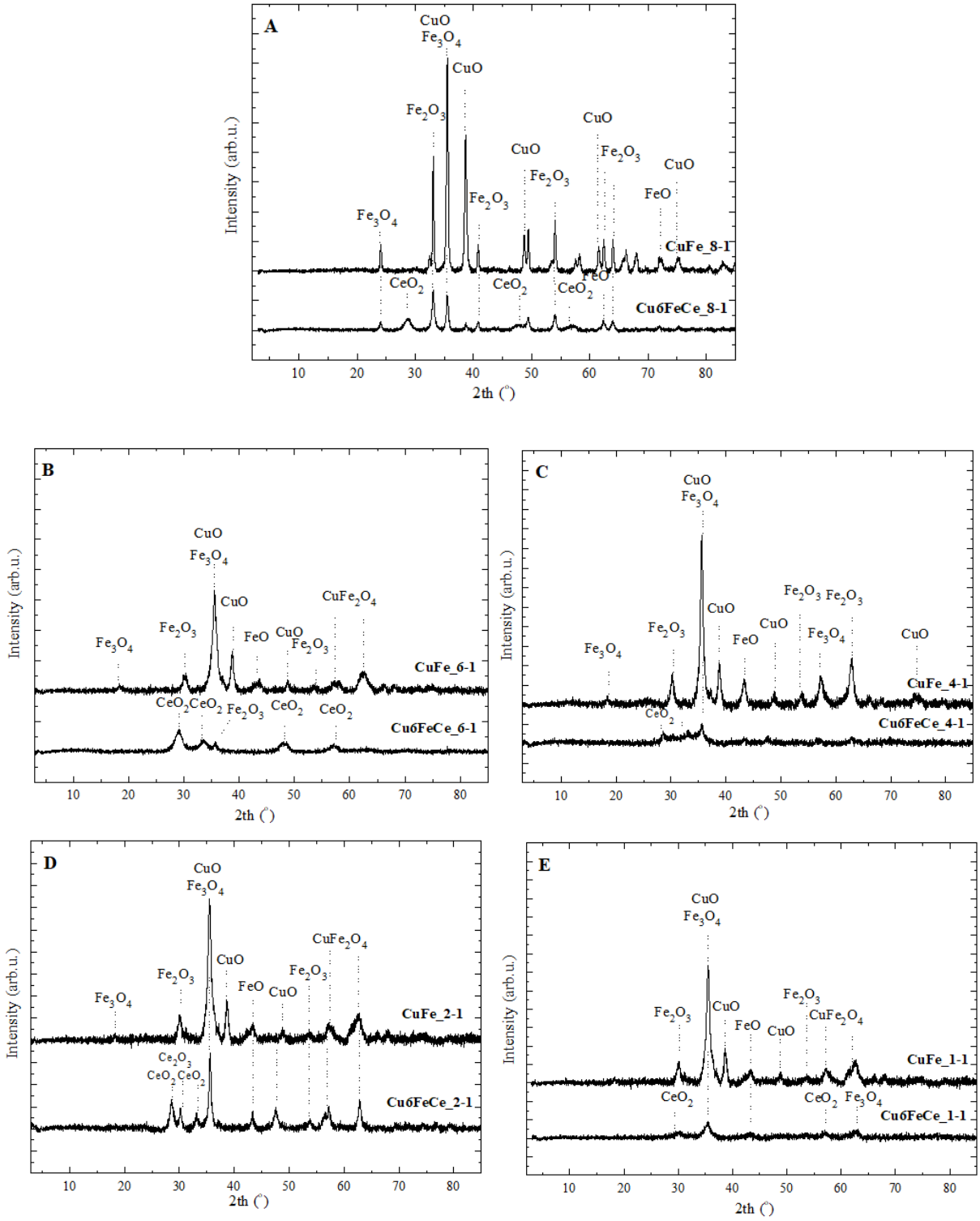

Fig. 3.1. XRD patterns obtained for the CuFe and Cu6FeCe mixed oxides prepared by citric acid method with the metal ions to fuel molar ratio of: 1:8 (A), 1:6 (B), 1:4 (C), 1:2 (B), 1:1 (A).

It can be observed that the dominant phase obtained for the CuFe samples, regardless of the applied ω molar ratio was Fe_2O_3. The presence of Fe_2O_3 was confirmed by the reflections at 2θ = 30.2°, 47.6°, 53.9° and 62.9°. Additionally, for the CuFe_1-1, CuFe_1-2 and CuFe_1-6 samples the mixed oxide $CuFe_2O_4$ was formed. It was confirmed by the presence of the reflection at 2θ = 57.2° and 62.4°. What is more, for the sample CuFe_1-8 the amount of CuO phase was the highest and it coexisted with Fe_2O_3. Therefore, it can be concluded that the "fuel lean" conditions facilitate the formation of copper oxide phase. Basing on the

obtained patterns, it was noticed that CeO_2 phase formation was strongly influenced by the ω ratio applied during the synthesis. Sharp and separated reflections of CeO_2 were obtained for the Cu6FeCe_8-1 and Cu6FeCe_2-1. Additionally, all of the samples containing CeO_2 fraction exhibited considerably lower amount of CuO. Hence, CeO_2 most probably inhibits the formation of copper oxide crystalline species species. CeO_2 crystallites were much bigger than CuO, thus the copper oxide phase possibly became undetectable for the XRD instrument. Therefore, the introduction of ceria affects the composition and the crystallinity of the resulting materials. However, it was observed for the most "fuel lean" conditions that the influence of ceria on the structure of the materials was reduced. The value of 2θ for the characteristic reflections of CuO, Fe_xO_y and CeO_2 in the patterns (A-E) are presented in Table. 3. 1. 1.

Table. 3.1.1. The values of 2θ angle detected for the obtained mixed metal oxides structures

Citric acid/metal ions ratio	**Sample Code**	***2θ* of the Compound [°]**					
		Fe_3O_4	**Fe_2O_3**	**FeO**	**CuO**	**$CuFe_2O_4$**	**CeO_2**
1:8	Cu6FeCe_8-1	23.9 35.5	33.2 40.9 54.0 64.0	62.4	49.5	-	28.7 47.9 56.5
	CuFe_8-1	23.9 35.3	32.9 41.1 54.0 64.2	72.4	35.3 38.5 48.8 61.5 75.4	-	-
1:6	Cu6FeCe_6-1	-	36.6	-	-	-	29.3 33.5 47.8 57.5
	CuFe_6-1	18.3 35.9	30.4 56.7	43.3	36.1 38.7	57.3 62.5	-
1:4	Cu6FeCe_4-1	35.6	-	-	-	-	28.6 32.5
	CuFe_4-1	18.3 35.6 57.2	30.4 53.7 63.0	43.3	35.6 38.7 48.5	-	-
1:2	Cu6FeCe_2-1	35.5	30.7 47.6 53.9 62.9	43.3	-	-	28.5 33.3 57.3
	CuFe_2-1	18.4 35.4	30.0 53.5	43.7	48.5 47.6	57.3 62.3	-
1:1	Cu6FeCe_1-1	35.5 62.8	-	43.2	35.7	-	29.4
	CuFe_1-1	35.5	30.2 53.7	43.2	35.7 38.6	-	-

The crystallinity of the obtained materials and the size of the crystals can be estimated by the analysis of the peaks present on the diffractograms. All of the CuFe samples, regardless of the ω molar ratio exhibited well separated, intense and sharp reflections. The effect was observed especially for the samples prepared in "fuel lean" conditions. Therefore, the co-existence of copper and iron oxides and low amount of fuel used for the preparation results in higher crystallinity of the final materials. The effect can be explained by different enthalpies of generation for different oxides. Lower temperatures that are reached in case of "fuel lean" conditions are suitable for the formation and crystallization of the oxides. On the other hand, in order to combust more fuel in "fuel rich" conditions, higher temperature is required and more amorphous fraction of the materials is obtained [38,40].

3.2 Size of the obtained crystallites

The size of the obtained crystallites was calculated by means of Scherrer's Equation (eq. 6.). The results are presented in Table 3.2.1. The ω molar ratio influenced significantly the size of the obtained crystallites. For the materials prepared in "fuel lean" conditions (1:8) the metal oxide species reached the biggest size, in the range of 47-58 nm. On the other hand, the samples prepared with the ω molar ratio of 1:1 exhibited the smallest crystallites, in the range of 20-25 nm. The results are in agreement with the scientific literature [40] for the estimated crystallinity obtained in "fuel rich" and "fuel lean" conditions. The average crystallites sizes of the meal oxides in each material are illustrated in Fig. 3.2.1.

Table. 3.2.1. The average size of the obtained crystals of mixed metal oxides

Citric acid/metal ions ratio	Sample Code	Average Crystal Size [nm]					
		Fe_3O_4	Fe_2O_3	FeO	CuO	$CuFe_2O_4$	CeO_2
1:8	Cu6FeCe_8-1	50.43	50.75	51.45	50.43	-	40.22
	CuFe_8-1	46.33	57.26	56.97	46.35	-	-
1:6	Cu6FeCe_6-1	-	31.45	-	-	-	33.54
	CuFe_6-1	31.58	31.52	32.56	24.96	37.74	-
1:4	Cu6FeCe_4-1	30.87	30.01	-	-	-	30.23
	CuFe_4-1	37.53	35.35	36.29	42.81	-	-
1:2	Cu6FeCe_2-1	33.01	37.76	29.65	21.39	23.18	21.58
	CuFe_2-1	32.02	34.87	27.32	23.12	24.56	-
1:1	Cu6FeCe_1-1	20.75	23.67	20.29	-	-	22.23
	CuFe_1-1	21.76	20.75	20.35	25.16	19.01	-

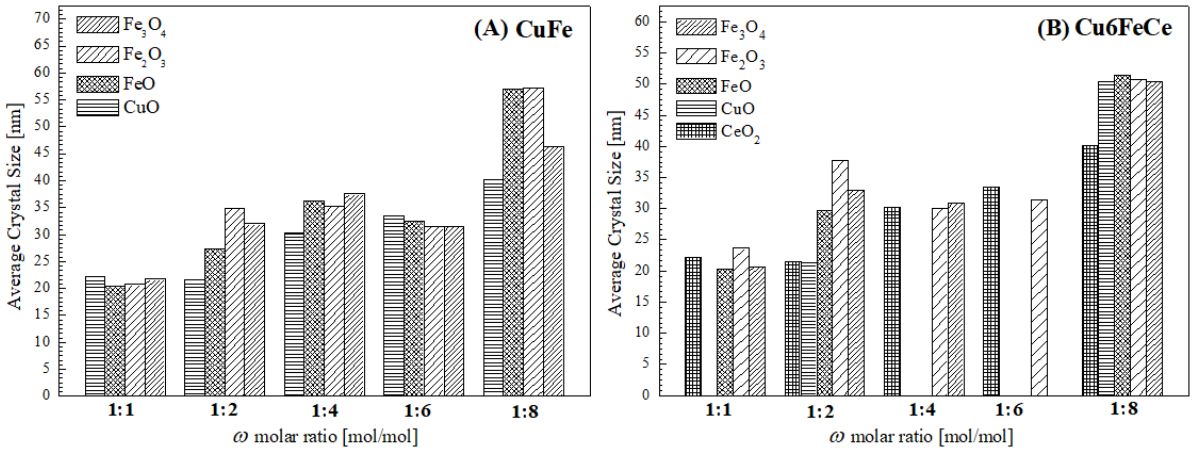

Fig. 3.2.1. Average size of the crystallites of the metal oxides obtained for the samples CuFe (A) and Cu6FeCe (B) in the function of ω molar ratio.

4. Conclusions

Solution combustion synthesis (SCS) is a very efficient, single- or two-steps synthesis of a wide range of metal oxides. In order to determine the influence of "fuel rich" and "fuel lean" conditions on the structure of the materials, five groups of Cu, Fe and Ce (when used) samples were prepared. It was observed that the materials prepared with the excess of fuel exhibited lower crystallinity and bigger particles than the other

analyzed group. The effect can be explained by a different amount of heat released at different temperatures. It results in the formation of diversified structure of the crystals. The introduction of ceria during the synthesis procedure led to the generation of more amorphous materials that contained mainly CeO_2 and Fe_xO_y fractions. This suggests that the presence of CeO_2 inhibits the formation of CuO fraction. Additionally, it is possible that low crystallinity of the selected samples arises from fast kinetics of some reactions during SCS. This effect might prevent the cation reorganization and, in consequence, makes crystallization difficult. However, one of the most important factors that should be considered in case of SCS is the variation of the synthesis parameters that can be applied. It enables to obtain materials with different crystallinity and morphology. The development of gases that occurs in a very short time, and high temperature reached during the synthesis, usually creates many defects on the surface of the materials, e.g. oxygen vacancies. Therefore, the adsorption of different gases is facilitated and as a result, the materials are suitable for many catalytic reactions, among them for NH_3-SCR. The active sites on the materials obtained via SCS promote their high catalytic activity in the sorption of NH_3 or NO, depending on the mechanism. Therefore, the materials can be successfully used as potential catalysts of selective catalytic reduction of nitrogen oxides.

Acknowledgment

The work was financed by AGH Research Subsidy 16.16.210.476

References

[1] Beale, A. M., Gao, F., Lezcano-Gonzalez, I., Peden, C. H. F., Szanyi, J. Recent advances in automotive catalysis for NOx emission control by small-pore microporous materials. Chem. Soc. Rev. 44, 7371-7405 (2015).

[2] Boningari, T., Smirniotis, P. G. ScienceDirect Impact of nitrogen oxides on the environment and human health : Mn-based materials for the NO x abatement. Curr. Opin. Chem. Eng. 13, 133-141 (2016).

[3] France, L. J., Yang, Q., Li, W., Chen, Z., Guang, J., Guo, D. Ceria modified FeMnOx—Enhanced performance and sulphur resistance for low-temperature SCR of NOx. Appl. Catal. B - Environ. 2017. 206, 203-215 (2017).

[4] Radojevic, M. Reduction of Nitrogen Oxides in Flue Gases. Elsevier Ltd. 685-689 (1998).

[5] Samojeden, B., Grzybek, T., Szymaszek, A., Ligęza, O. The application of modified cenospheres in $DeNO_x$ process. E3S Web of Conferences **108,** 02019 (2019).

[6] Guan, B., Zhan, R., Lin, H., Huang, Z. Review of state of the art technologies of selective catalytic reduction of NO_x from diesel engine exhaust. *Appl. Therm. Eng*. **66,** 395-414 (2014).

[7] Skalska, K., Miller, J. S., Ledakowicz, S. Trends in NO_x abatement: A review. *Sci Total Environ*. **408 (19),** 3976-3989 (2010).

[8] Forzatti, P., Nova, I., Tronconi, E. New "Enhanced NH_3-SCR" Reaction for NO_x Emission Control. *Ind. Eng. Chem. Res.* **49,** 10386-10391 (2010).

[9] Wierzbicki, D., Dębek, R, Szczurowski, J., Basąg, S., Włodarczyk, W., Motak, M., Baran, R. Copper, cobalt and manganese: Modified hydrotalcite materials as catalysts for the selective catalytic reduction of NO with ammonia. the influence of manganese concentration. *C. R. Chim*. **18,** 1074-1083 (2015).

[10] Brandenberger, S., Kröcher, O., Tissler, A., Althoff, R. The State of the Art in Selective Catalytic Reduction of NO_x by Ammonia Using Metal-Exchanged Zeolite Catalysts. *Catal. Rev*. **50,** 492-531 (2008).

[11] Ozkan, U. S., Cai, Y., Kumthekar, M. W. Selective Catalytic Reduction of Nitric Oxide with Ammonia over Supported and Unsupported Vanadia Catalysts. *CatalyticControl of Air Pollutants.* **9,** 115-124 (1992).

[12] Ryu, T., Ahn, N. H., Seo, S., Cho, J., Kim, H., Jo, D., Park, G. T., Kim, P. S., Kim, C. H., Bruce, E. L., Wright, P. A., Nam, I., Hong, S. B. Heterogeneous Catalysis Fully Copper-Exchanged High-Silica LTA Zeolites as Unrivaled Hydrothermally Stable NH_3 -SCR *Catal. Commun.* **56,** 1-6 (2017).

[13] Shakya, B. M., Harold, M. P., Balakotaiah, V. Simulations and optimization of combined Fe- and Cu-zeolite SCR monolith catalysts. *Chem. Eng. J*. **4323,** 1-11, (2014).

[14] Rutkowska, M., Pacia, I., Basąg, S., et al. Catalytic performance of commercial Cu-ZSM-5 zeolite modified by desilication in NH_3-SCR and NH_3-SCO processes. *Microporous Mesoporous Mater*. **246,** 193-206 (2017).

[15] Boxiong, S., Yan, Y. A. O., Hongqing, M. A., Ting, L. I. U. Ceria Modified MnO_x/TiO_2 -Pillared Clays Catalysts for the Selective Catalytic Reduction of NO with NH_3 at Low Temperature. *Chinese. J. Catal*. **32**,1803-1811 (2018).

[16] Chmielarz, L., Piwowarska, Z., Kuśtrowski, P., Gil, B., Adamski, A., Dudek, B., Michalik, M. Porous clay heterostructures (PCHs) intercalated with silica-titania pillars and modified with transition metals as catalysts for the DeNO $_x$ process. *Appl. Catal. B - Environ.* **91,** 449-459 (2009).

[17] Yuan, M., Deng, W., Dong, S., Li, Q., Zhao, B., Su, Y. Montmorillonite based porous clay heterostructures modified with Fe as catalysts for selective catalytic reduction of NO with propylene. *Chem. Eng. J*. **353,** 839-848 (2018).

[18] Motak, M. Montmorillonites modified with polymer and promoted with copper as $DeNO_x$ catalysts. *Catal. Today*. **137,** 247-252 (2008).

[19] Samojeden, B., Grzybek, T. The influence of the promotion of N-modified activated carbon with iron on NO removal by NH3-SCR. *Energy*. **116,** 1484-1491 (2016).

[20] Grzybek, T., Klinik, J., Samojeden, B. Badanie węgla aktywnego modyfikowanego związkami azotu i manganu w reakcji redukcji tlenku azotu amoniakiem. *Gospodarka Surowcami Mineralnymi.* **23,** 133-142 (2007).

[21] Klinik, J., Samojeden, B., Grzybek, T., Suprun, W., Papp, H., Gläser, R. Nitrogen promoted activated carbons as $DeNO_x$ catalysts. 2. The influence of water on the catalytic performance. *Catal. Today.* **176,** 303-308 (2011).

[22] Basąg, S., Kocoł, K., Piwowarska, Z., Rutkowska, M., Baran, R., Chmielarz, L. Activating effect of cerium in hydrotalcite derived Cu–Mg–Al catalysts for selective ammonia oxidation and the selective reduction of NO with ammonia. *React. Kinet. Mech. Catal*. **121,** 225-240 (2017).

[23] Li, J., Chang, H., Ma, L., Hao, J., Yang, R. T. Low-temperature selective catalytic reduction of NO_x with NH_3 over metal oxide and zeolite catalysts — A review. *Catal Today*. **175,** 147-156 (2011).

[24] Liu, C., Shi, J., Gao, C., Niu, C. Manganese oxide-based catalysts for low-temperature selective catalytic reduction of NO $_x$ with NH $_3$: A review. *Appl. Catal. A, - Gen*. **522,** 54-69 (2016).

[25] Liu, Z., Liu, Y., Li, Y., Su, H., Ma, L. WO_3 promoted Mn – Zr mixed oxide catalyst for the selective catalytic reduction of NO_x with NH_3. *Chem. Eng. J*. **283,** 1044-1050 (2016).

[26] Varma, A., Mukasyan, A. S., Rogachev, A. S., Manukyan, K. V. Solution Combustion Synthesis of Nanoscale Materials. *Chem. Rev.* **116,** 14493-14586 (2016).

[27] Patil, K. C., Aruna, S. T., Mimani, T. Combustion synthesis: an update. *Curr. Opin. Solid State Mater. Sci.* **6,** 507-512 (2003).

[28] Aruna, S. T., Mukasyan, A. S. Combustion synthesis and nanomaterials. *Curr. Opin. Solid State Mater. Sci*. **12,** 44-50 (2008).

[29] Erri, P., Nader J., Varma, A. Controlling Combustion Wave Propagation for Transition Metal/Alloy/Cermet Foam Synthesis. *Adv. Mater.* **20,** 1243-1245 (2008).

[30] Roy, S., Sharma, D. A., Roy, S. N., Maiti, H. S. Synthesis of $YBa_2Cu_3O_{7-x}$ powder by autoignition of citrate-nitrate gel. *J. Mater. Res.* **8,** 7-12 (1993).

[31] Bera, P., Hegde, M. S. Characterization and catalytic properties of combustion synthesized Au/CeO_2 catalyst. *Catal. Lett.* **79,** 75-81 (2002).

[32] Mukasyan, A. S., Costello, C., Sherlock, K. P., Lafarga, D., Varma, A. Perovskite membranes by aqueous combustion synthesis: synthesis and properties. *Sep. Purif. Technol.* **25,** 117-126 (2001).

[33] Bera, P., Patil, K. C., Jayaram, V., Subbanna, G. N., Hegde, M. S. Ionic Dispersion of Pt and Pd on CeO_2 by Combustion Method: Effect of Metal – Ceria Interaction on Catalytic Activities for NO Reduction and CO and Hydrocarbon Oxidation. *J. Catal.* **301,** 293-301 (2000).

[34] Kumar, A., Mukasyan, A. S., Wolf, E. E. Impregnated layer combustion synthesis method for preparation of multicomponent catalysts for the production of hydrogen from oxidative reforming of methanol. *Appl. Catal. A - Gen.* **372,** 175-183 (2010).

[35] Furfori, S., Russo, N., Fino, D., Saracco, G., Specchia, V. NO SCR reduction by hydrogen generated in line on perovskite-type catalysts for automotive diesel exhaust gas treatment. *Chem. Eng. Sci*. **65,** 120-127 (2010).

[36] Roy, S., Viswanath, B., Hegde, M. S., Madras, G. Low-Temperature Selective Catalytic Reduction of NO with NH_3 over $Ti_{0.9}M_{0.1}O_{2-\delta}$ (M = Cr, Mn, Fe, Co, Cu). *J. Phys, Chem. C.* **112,** 6002-6012 (2008).

[37] Chen, T., Lin, H., Cao, Q., Huang, Z. Solution combustion synthesis of $Ti_{0.75}Ce_{0.15}Cu_{0.05}W_{0.05}O_{2-\delta}$ for low temperature selective catalytic reduction of NO. *RSC Adv.* **4,** 63909-63916 (2014).

[38] Andreoli, S., Deorsola, F. A., Pirone, R. MnO_x-CeO_2 catalysts synthesized by solution combustion synthesis for the low-temperature NH_3 -SCR. *Catal. Today* **253,** 199-206 (2015).

[39] Andreoli, S., Deorsola, F.A., Galletti, C., Pirone, R. Nanostructured MnO_x catalysts for low-temperature NO_x SCR. *Chem. Eng. J.* **278,** 174-182 (2015).

[40] Deorsola, F. A., Andreoli, S., Armandi, M., Bonelli, B., Pirone, R. Unsupported nanostructured Mn oxides obtained by Solution Combustion Synthesis: Textural and surface properties, and catalytic performance in NO_x SCR at low temperature. *Appl. Catal. A - Gen.* **522,** 120-129 (2016).

[41] Zhijan, K., Cheng, W., Zhengnan, D., Yinfei, C., Zekai, Z. Enhanced activity of $Mn_xW_{0.05}Ti_{0.95-x}O_{2-\delta}$ for selective catalytic reduction of NO_x with ammonia by self-propagating high-temperature synthesis. *Catal. Commun.* **64,** 27-31 (2015).

[42] Chmielarz, L., Ku, P., Majda, D., Dziembaj, R. Catalytic activity of Co-Mg-Al, Cu-Mg-Al and Cu-Co-Mg-Al mixed oxides derived from hydrotalcites in SCR of NO with ammonia. *Appl. Catal. B - Environ.* **35,** 195-210 (2002). 2002;35:195-210.

[43] Ziemiański, P., Kałahurska, K., Samojeden, B. Selective catalytic reduction of NO with NH_3 on mixed alumina–iron (III) oxide pillared montmorillonite "Cheto" Arizona, modified with hexamminecobalt (III) chloride. *Adsorpt. Sci. Technol*. **35,** 825-833, (2017)

[44] Sun, M, Wang, S., Li, Y., Wang, Q., Xu, H., Chen, Y. Promotion of catalytic performance by adding Cu into Pt/ZSM-5 catalyst for selective catalytic oxidation of ammonia. *J. Taiwan. Ins.t Chem. Eng*. **78,** 401-408 (2017).

[45] Macina, D., Piwowarska, Z., Góra-Marek, K., Tarach, K., Rutkowska, M., Girman, V., Błachowski, A., Chmielarz, L. SBA-15 loaded with iron by various methods as catalyst for $DeNO_x$ process. *Mater Res Bull*. **78,** 72-82 (2016).

[46] Centeno, M. A., Hadjiivanov, K., Venkov, T., Klimev, H., Odriozola, J. A. Comparative study of Au /Al2O3 and Au/CeO2 -Al2O3 catalysts. J. Mo. Cat. A - Chem. 252, 142-149 (2006).

[47] Rodriguez, J.A., Liu, P., Hrbek, J., Evans, J. Activity of CeOx and TiOx Nanoparticles Grown on Au(111) in the Water-Gas Shift Reaction. Science 318, 1757-1759 (2007).

Properties of modified rigid polyurethane foam

Beata Zygmunt- Kowalska[1], Monika Kuźnia [2]

[1]AGH University of Science and Technology, Faculty of Metals Engineering and Industrial Computer Science, Department of Heat Engineering and Environment Protection, Mickiewicza 30 Av., 30-059 Krakow, Poland, e-mail: zygmunt@agh.edu.pl
[2]AGH University of Science and Technology, Faculty of Metals Engineering and Industrial Computer Science, Department of Heat Engineering and Environment Protection, Mickiewicza 30 Av., 30-059 Krakow, Poland, e-mail: kuznia@agh.edu.pl

Abstract

The article presents the mechanism of polyurethane (PU) foams production process with the addition of waste from coal-fired power plant. The PUR foams were made using a one-step method. The samples contained the addition of conventional and fluidized fly ash. Composite materials contained 5, 10, 15, 20 % of fly ash in PUR foams. In order to compare the properties of the composites with the reference (unmodified) foam, PUR without the addition of ash was produced. The following parameters were analyzed: the apparent density, calorific value, microphotographs from SEM and elemental analysis of carbon, hydrogen and nitrogen.

Keywords: rigid polyurethane foam, fly ash, properties of PUR

1. Introduction

The policy of reducing CO_2 emission to the atmosphere is associated with a decrease in the demand for thermal energy. The reduction of heat demand is achieved through thermal insulation. Rigid polyurethane foam (RPUF) is the most popular thermal insulation material. The mechanism of foams formation is based on mixing two substrates: isocyanate and polyol. This is one-step method of production [1]. Components for foams production are expensive, that is why scientists' interests are focused on new methods to reduce costs of production. Polyurethane foams are biologically and chemically inert, they are distinguished by a slight water absorption. The thermal insulation of PUR is distinguished by a low thermal conductivity, what is more, foam is resistant to petroleum solvents, diluted acids and bases. Their mechanical properties depend on apparent density, cell structure and content of various additions [2]. Very good thermal insulation properties caused that the RPUF is widely used in the industry, mainly in architecture. RPUF is flammable material. During combustion, the PUR foam generates substances harmful to health. RPUF decomposes above 200^{o}C. The desire to reduce the foam's flammability causes that various types of flame retardants are added. The current trend in the synthesis of PU materials is the modification by using recycled components [3]. Recycled materials can reduce production cost. What is more, polyurethane foams with recycled component can have better mechanical and thermal properties [4]. An example of PUR modifier can be fluidized bed combustion (FBC) fly ash (FB) or conventional pulverized coal combustion (PCC) fly ash (FC). Fly ash (FA) is captured from flue gas thanks for electrostatic or mechanical devices [5]. There are currently many methods of ash management. One of them is the application in building materials such as: building ceramics, cellular concrete and cements [6]. Fly ashes are also used in road construction and in mining as excavation fillers. Thermal energy is largely based on coal combustion. As a side effect, a large amount of coal by- products, including fly ash is produced. Therefore, new solutions for fly ash utilization are being developed. The innovative idea is used the fly ash as a filler in rigid polyurethane foams. The use of such the filler could contribute to improving the properties of the RPUF. Moreover, fly ash could fulfill the role of flame retardant.

2. Methodology of composite preparation

2.1 Composites

The following products were used to prepare rigid polyurethane foams:

- fly ash from conventional pulverized coal combustion (Fig.2.1.);
- fly ash from fluidized bed combustion (Fig.2.2.);

Fig. 2.1.1. Photo of PCC fly ash

Fig. 2.2.2 Photo of FBC fly ash

These fly ashes are obtained from one of the polish coal power plants. Process of ash removal is carried out using electrostatic precipitators. Fig. 2.3., Fig. 2.4. present photos of fly ash taken using a scanning electron microscope. It can be seen that diameters of FC ash particles are larger than FB ash. Conventional fly ash has a higher porosity. This may be due to the presence of unburned carbon particles in the ash. In addition, FB fly ash does not contain spherical particles (microspheres) that are present in FC fly ash [7].

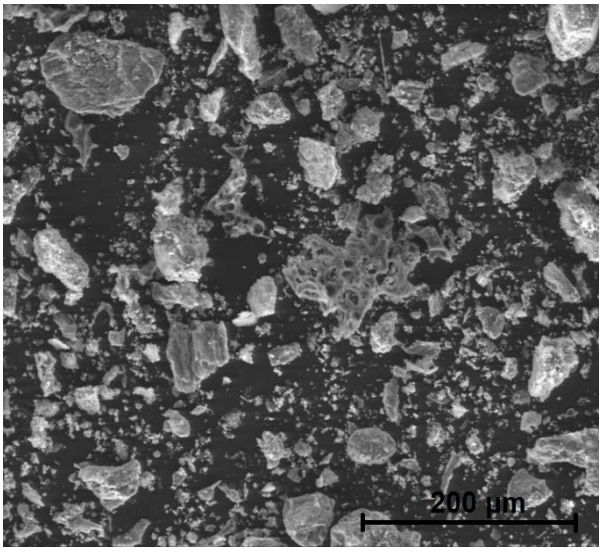

Fig. 2.3. Microphotograph of FBC fly ash

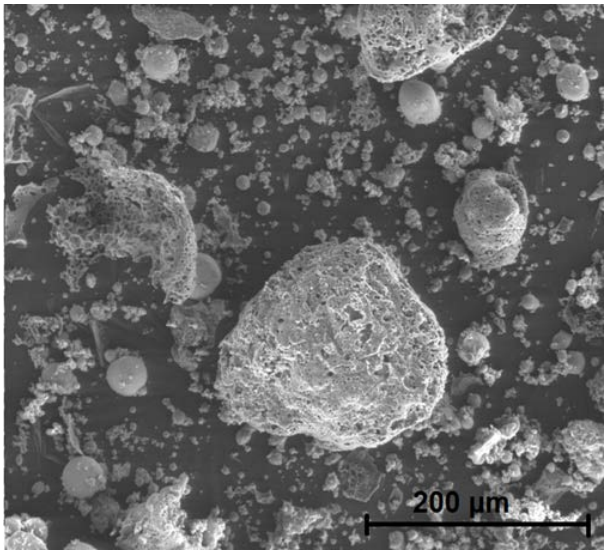

Fig. 2.4. Microphotograph of PCC fly ash

- EKOPRODUR BF5032

It is two-component system obtained from PCC Prodex (Poland). The system includes a polyol part (component A) and the second part isocyanate (component B), both products are shown in Fig.2.5.

Fig. 2.5. Photo of EKOPRODUR BF5032 system

2.2 Preparation of RPUF with fly ash

Samples of RPUF were prepared by hand mixing and casting method, using the EKOPRODUR BF5032 system. Component A-polyol was mixed with fly ash in cylindrical mold to obtain uniform mixture. Then the component B- isocyanate was added to mix of substances. Next all ingredients were mixed for about 20 seconds (according to the manufacturer's certificate the upper limit time was 42 s.). The mixture was transported to rectangular form. After two days, the sample was removed from the form. The RPUF was kept in room temperature for next 5 days. The above-mentioned activities were repeated eight times, for samples with addition of: 5,10,15, 20 % fly ash from conventional pulverized coal combustion (FC) and addition of 5,10,15, 20% fly ash from fluidized bed combustion (FB). Properly prepared foams were subjected to the analyzes described in chapter 3.

3. Analysis of the materials

3.1 Elemental analysis of C, H, N

Elemental analysis of C, H, N was carried out using a Leco CHN 628 device. An infrared absorption detector is used to determine the carbon and hydrogen content. The nitrogen content is determined using a thermally conductive detector [8]. Material samples from the range 25-45 mg were taken to study the elemental composition. Analysis was carried out three times for each type of foam. The table 3.1 presents the averaged results.

Table. 3.1. Elemental analysis of PUR materials

Type of RPUF	N [%]	C [%]	H[%]
PUR without FA	5.63	67.64	7.77
5 % FC	5.37	64.30	7.49
10%FC	5.05	60.80	7.10
15% FC	4.75	57.70	6.69
20% FC	4.41	54.50	6.24
5%FB	5.28	62.97	7.57
10%FB	5.14	60.77	7.21
15%FB	4.87	57.29	6.82
20%FB	4.65	53.95	6.47

Thanks to the C, H, N elemental analysis, the percentage of carbon, hydrogen and nitrogen in the polyurethane foams produces was examined. The largest content of all three elements can be found in pure rigid polyurethane foam. It can be noticed that with increase of ash addition, contents of carbon, nitrogen and hydrogen is decreasing. The biggest changes were observed in the case of carbon concentration in tested materials. Whereas the smallest decrease the element content in the samples refers to nitrogen.

3.2 Determination of gross calorific value

The gross calorific value was determined using a calorimetric method with LECO AC500 isoperibolic calorimeter. The gross calorific value is determined by combustion in oxygen of the sample placed in a pressure vessel immersed in water. The device is distinguished by its compact design and contains a closed water system. Thanks to above mentioned features, no additional temperature stabilizing devices are needed. On the basis of the obtained heat balance of the system, the heat generation is calculated [9, 10]. The results are summarized in the Table 3.2. and presented in Figure 3.1.

Table. 3.2. Gross calorific value of analyzed materials.

Type of RPUF	gross calorific value [J/g]
PUR without FA	27207.5
5 % FC	25215.4
10%FC	24434.8
15% FC	23315.6
20% FC	21857.8
5%FB	26033.9
10%FB	24665.8
15%FB	23514.0
20%FB	21708.7

The experiment allowed to obtain the results of gross calorific value modified foams. The highest value, 27207.5 $\frac{J}{g}$ was obtained for pure rigid polyurethane foam. The lowest value of heat of combustion was obtained for the sample with 20%FB. This value was 21708.7 $\frac{J}{g}$ and was slightly higher than the value for foam containing 20% FC.

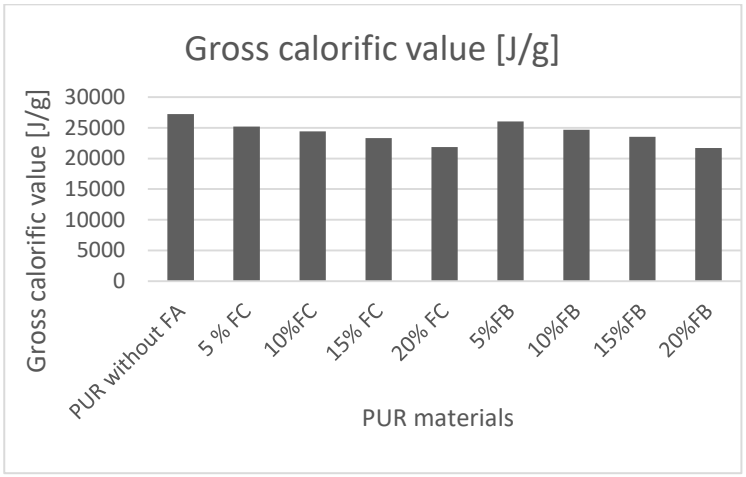

Fig. 3.1 Graph of gross calorific value

3.3 Apparent density

The apparent density of the modified foams was measured using the geometrical method. Apparent density measurements were carried out according to the PN-EN ISO 845:2010. Values of the calculated apparent density are presented in the Table 3.3. and in the Figure 3.2.

Based on the obtained results, a significant effect of fly ash addition on apparent density was observed. As the additive concentration increases, the density value increases. Higher foam densities were obtained in the case of RPUF with FB.

Tab. 3.3. Apparent density values of PUR foams.

Type of RPUF	apparent density $\left[\frac{kg}{m^3}\right]$
PUR without FA	35.5
5 % FC	36.0
10%FC	37.8
15% FC	41.4
20% FC	42.6
5%FB	37.4
10%FB	41.9
15%FB	43.5
20%FB	45.1

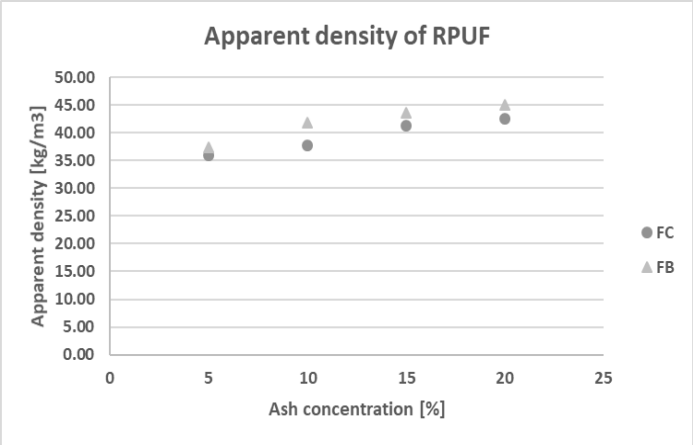

Fig. 3.2 Graph of apparent density

3.4 SEM images of rigid polyurethane foams

Scanning electron microscopy (SEM) is one of the most commonly used tools to characterize the cellular structure of rigid PU foams [11]. To examine the effect of ash addition on the foam structure, photos of samples were taken using SEM (Nova NanoSEM 200; FEI Company, USA). Foams were coated with gold and studied using an acceleration of 10 kV. Pictures were taken for 5% and 20 % fly ash addition (FB and FC).

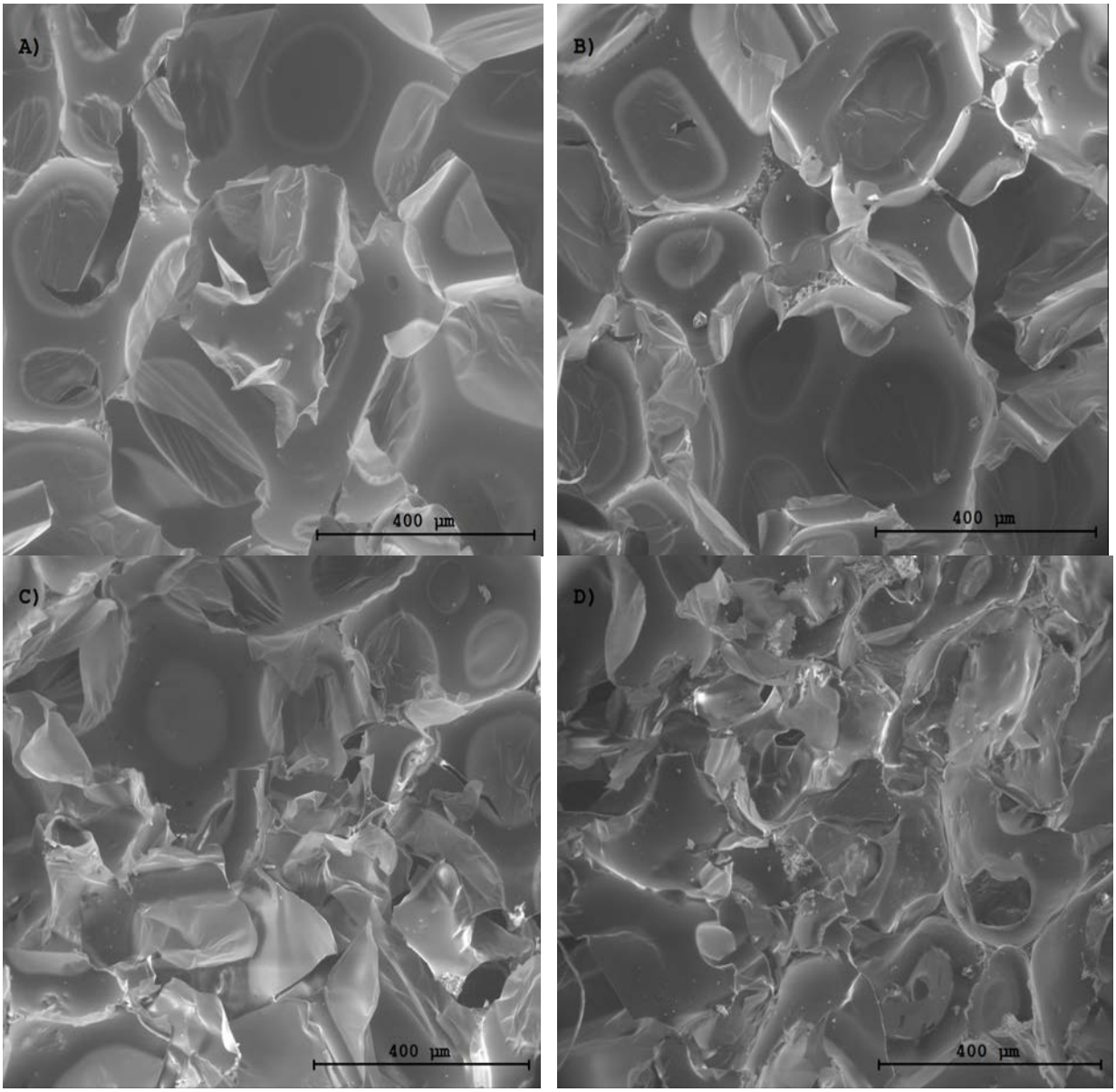

Fig. 3.3. Microphotographs of the modified rigid polyurethane foams with 5% FC (A), 5% FB (B), 20 % FC (C), 20% FB (D).

In the figure 3.2 the structure of modified polyurethane foams is depicted. It can be seen that ash addition impacts on the structure of rigid polyurethane foam. For foams with a content of 5% fly ash addition (for both types of additives) the structure has been preserved. In the case of a sample with 20% fly ash, the foam structure is completely disturbed and blurred. Each of the cells is different, no repeatability of cell shape has been observed. Material destruction is greater in the case of foam containing FB ash.

4. Conclusions

The article presents methods of foam production. Complex analysis was made to evaluate properties of PUR foam with fly ash additions. The use of FB and FC fly ash modifiers to polyurethane foam production significantly affects the change in the chemical composition of foam and its properties. This means that it can contributes to expanding the use of polyurethane foam. Moreover, fly ash is waste that if it is not used causes many problems connected with e.g. expensive storage. That is why it is crucial to seek for new possibilities of using waste such as fly ash from a coal power plant. The further development of RPUF with ashes as

insulation material would require additional tests. Due to influence of fly ash on the foam structure, the next steps could cover strength test, thermal analyses and conductivity.

Acknowledgment

The experimental work was done during the realization of master thesis *Combustibility tests of modified polyurethane* foams defended in 2019 under supervision of the PhD Monika Kuźnia at the AGH University of Science and Technology in Cracow.

References

[1] Prociak A., Rokicki G., Ryszkowska J., *Materiały poliuretanowe*, Wydawnictwo Naukowe PWN, 2016.

[2] Randall D., Lee S., *Polyurethanes Book*, J. Wiley, 2002.

[3] T. Calvo-Correas, L. Ugarte, P.J. Trzebiatowska, R. Sanzberro, J. Datta, M.A. Corcuera, A. Eceiza, *Thermoplastic polyurethanes with glycolysate intermediates from polyurethane waste recycling*, Polym. Degrad. Stab. 144 (2017).

[4] A. Reghunadhan, J. Datta, N. Kalarikkal, J.T. Haponiuk, S. Thomas, *Toughness augmentation by fibrillation and yielding in nanostructured blends with recycled polyurethane as a modifier*, Appl. Surf. Sci. 442 (2018).

[5] Strzałkowska E.: *Charakterystyka właściwości fizykochemicznych i mineralogicznych wybranych ubocznych produktów spalania*, Wyd. Politechniki Śląskiej, Gliwice 2011.

[6] Kruger R.A., *Superdrobny popiół lotny klasy F do betonu najwyższej jakości. Popioły z energetyki,* Wyd. Polska Unia UPS, Kraków 2006.

[7] Kuźnia M., Magiera A., Jerzak W., Ziąbka M., Lach R. *Study on chemical composition of fly ash from fluidized-bed and conventional coal combustion*, *Przemysł chemiczny* 96/8(2017), 2017.

[8] https://uk.leco-europe.com/, (10/11/2019).

[9] http://laboratoria.net/katalog-produktow/analizatory/rid,213.html, (10/11/2019).

[10] Porowski R., *Analiza metod określania ciepła spalania i wartości opałowej paliw,* Zeszyty naukowe SGSP 2016, nr59/3/2016, 2016.

[11] S. Pardo-Alonso, E. Solorzano, L. Brabant, P. Vanderniepen, M. Dierick, L. Van Hoorebeke, M.A. Rodríguez-Pérez *3D analysis of the progressive modification of the cellular architecture in polyurethane nanocomposites foams via X-ray microtomography* Eur. Polym. J., 49 (2013), 2013.

Novel strategies and future perspectives for phytoremediation of soils contaminated with heavy metals

Marta Jaskulak[1,2]

[1]*Institute of Environmental Engineering, Faculty of Infrastructure and Environment, Czestochowa University of Technology, Czestochowa, Poland; e-mail: martajaskulak@gmail.com*
[2]*University of Lille, Laboratory of civil engineering and environment (LGCgE), Environmental Axis, F-59650 Villeneuve d'Ascq, France*

Abstract

Contamination of soils with heavy metals is a major environmental concern and a great threat to all life on the earth. For human health, the risk is mostly associated with heavy metals entering food chain and the potential loss of agricultural land due to contamination. Currently, various physical, chemical and biological techniques are being implemented to remove heavy metals from soils. However, most of them are too expensive for a large-scale use. Thus, phytoremediation is a good strategy to harvest heavy metals from soils and have been proven as an effective and economical technique. In this article, we discussed the main sources of soil contamination with heavy metals and novel strategies that are being tested for remediation purposes. Moreover, since traditional phytoremediation approaches face some limitations regarding their large-scale use, we also focused on modern chemical, biological and genetic engineering tools that can modify the process to obtain better efficiency and shorter time of such process. In the end, we discuss different phytoremediation options to compare their applicability in different scenarios.

Keywords: phytoremediation, soil contamination, heavy metals

1. Introduction

Soil contamination with heavy metals is a continuously increasing problem worldwide that creates numerous threats to human health by its influence on crop production, and quality of groundwater and crops (tab 1.) [1]. Heavy metals are the most spread group of inorganic pollutants mostly due to anthropogenic activities such as manufacturing, use of synthetic fertilizers in agriculture and car emissions. Metal concentrations in soil range from even less than one to as high as 100000 mg kg-1 [2,3]. Accumulation of metals such as Lead (Pb), Chromium (Cr), Nickel (Ni) can seep through food chain and cause DNA damage due to their mutagenic abilities which can lead to carcinogenic changes in bodies of animals and humans. Since long-term persistence of heavy metals in the environment causes a threat to human health and crop production, technologies involved in remediation of contaminated areas gained an importance [4,5].

Phytoremediation is wildly accepted technology used in remediation of contaminants from soil by use of hyperaccumulating plants. Proper identification of suitable plant species for this process is one of the most important steps influencing efficiency of the process. Such plants are characterized by their remarkable biochemical mechanisms like an ability to accumulate and translocate metals in their cells [6].

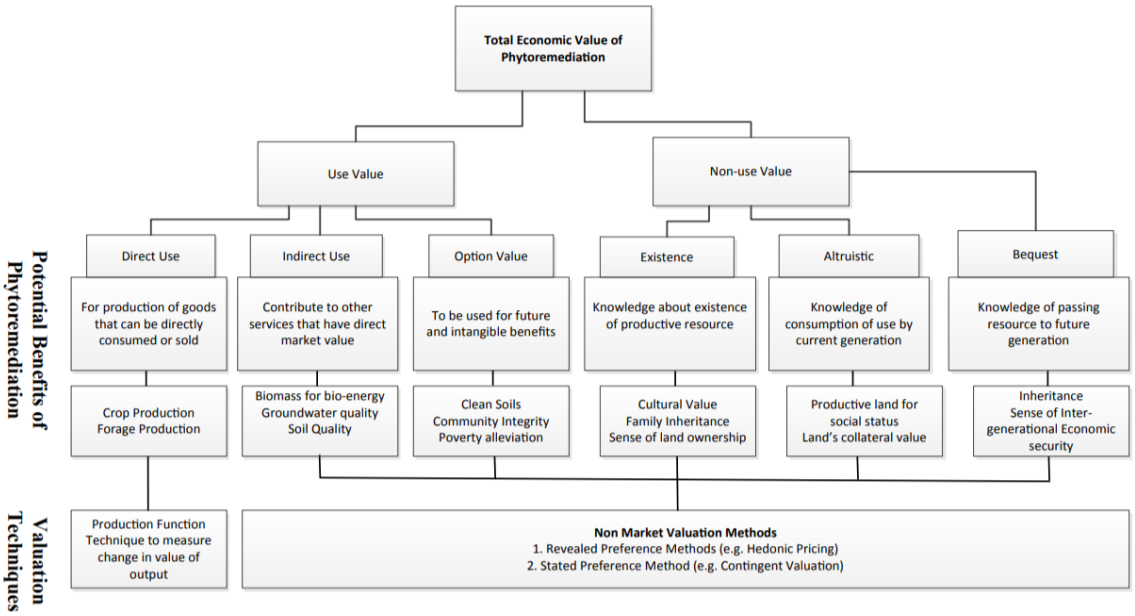

Fig. 1.1. Parameters involved in the economic value of phytoremediation [12]

As most other stress factors, heavy metals induce oxidative stress by disrupting metabolic chains. This leads to the imbalance in reactive oxygen species (ROS) generation and neutralization [6]. In normal conditions ROS such as superoxide radicals, singlet oxygen, hydrogen peroxide and hydroxyl radicals are removed by antioxidants (ascorbate, glutathione, α-Tocopherol, carotenoids) or enzymes such as superoxide dismutase (SOD), catalase (CAT) and peroxidases (POD, GPX, APX) [7]. Overflow of ROS, that cannot be properly neutralized by antioxidative system, cause damage in proteins and DNA. Toxic effects of that imbalance accumulate in cells and leads to plants death [5,8]. Activity of those enzymes can be used to determine stress levels and to determine environment toxicity long before any visible impact on growth appears. Such assay may be a useful tool in the environmental engineering, for example as an indicator in phytoremediation efficiency or in order to determinate severity of soil pollution. Artificial increase in the rate of ROS neutralization may lead to an increase in yield quality and enable some species to be cultivated outside their native climates [9].

2. Traditional phytoremediation

The term ‘phytoremediation’ refers to the use of plants to reduce the toxic effect of a contaminant in the environment. It has excellent potential for remediation of soils contaminated with heavy metals and was previously shown to be a more efficient and economically feasible than physical and chemical methods, including soil washing, solidification, incineration, or excavation. In addition, it has broad public acceptance and gains a lot of popularity in recent years since it can be applied to large areas. For the purpose of metal phytoremediation, the following approaches are the most used: phytostabilization (sometimes also called phytoimmobilization), phytoextraction, and phytovolatilization. Phytostabilisation uses plants to decrease the mobility and bioavailability of metals to prevent their leaching into the groundwater system or food chain by various mechanisms, including adsorption and complexation by roots. Even if phytostabilization is not a permanent solution since it only restricts the movement of contaminants, it is still a beneficial action, especially in large, post-industrial, contaminated areas. Phytovolatalization includes the conversion of metal into its volatile form and its release into the atmosphere through leaves. It is primarily useful for the contamination with mercury. Phytoextraction is currently the most crucial phytoremediation technique for the removal of metals not only from the soil but also water, sediments, and biosolids. It is even more suitable for commercial applications than other phytoremediation techniques. However, there are still a number of factors that can affect its efficiency, including species characteristics, metal availability to plants, and soil properties. Plants species selected for phytoremediation should possess some unique features including 1) rapid growth

rate, 2) high biomass production, 3) the ability to accumulate high concentration of metals, 4) the ability to translocate metals from roots to shoots, 5) be able to tolerate toxic effects of heavy metals, 6), be resistant to pathogens and pests, 7) be easy to cultivate and harvest.

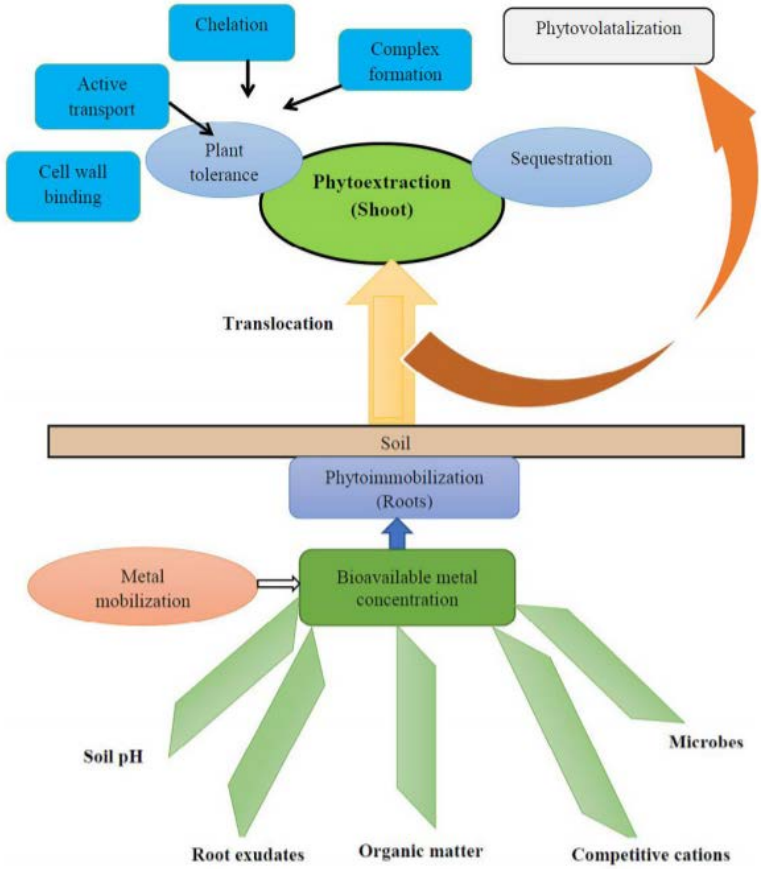

Fig. 2.1. Traditional phytoremediation

3. Novel approaches to phytoremediation

The use of plants to remediate contaminated soil could be a beneficial approach to deal with a growing issue of food safety due to metal contamination. However, traditional phytoremediation techniques still face several limitations such as 1) they require a long time, 2) most hyperaccumulating species produces a small amount of biomass, 3) metals need to be bioavailable for plants. Therefore, currently, researchers try to modify the traditional approaches to minimize their limitations and increase phytoremediation efficiency. Genetic engineering has played a vital role in the enhancement of plants toward the removal of both inorganic and organic contaminants. This technique is based on the over or under expression of specific genes involved in the uptake, translocation, sequestration, and tolerance of toxic compounds. The introduction of genes from microbes, plants, and animals can be achieved using either direct DNA methods of gene transfer of the transformation of Agrobacterium tumefaciens to develop transgenic plants. Generally, transgenic plants are designed to increase plants' tolerance against metal toxicity or to facilitate more translocation of metals from roots to shoots. Previous studies showed that transgenic plants with better endurance and metal sequestration and severely increase phytoremediation efficiency. However, a better understanding of specific mechanisms behind metal tolerance and metal detoxification is crucial to develop transgenic plants for phytoremediation.

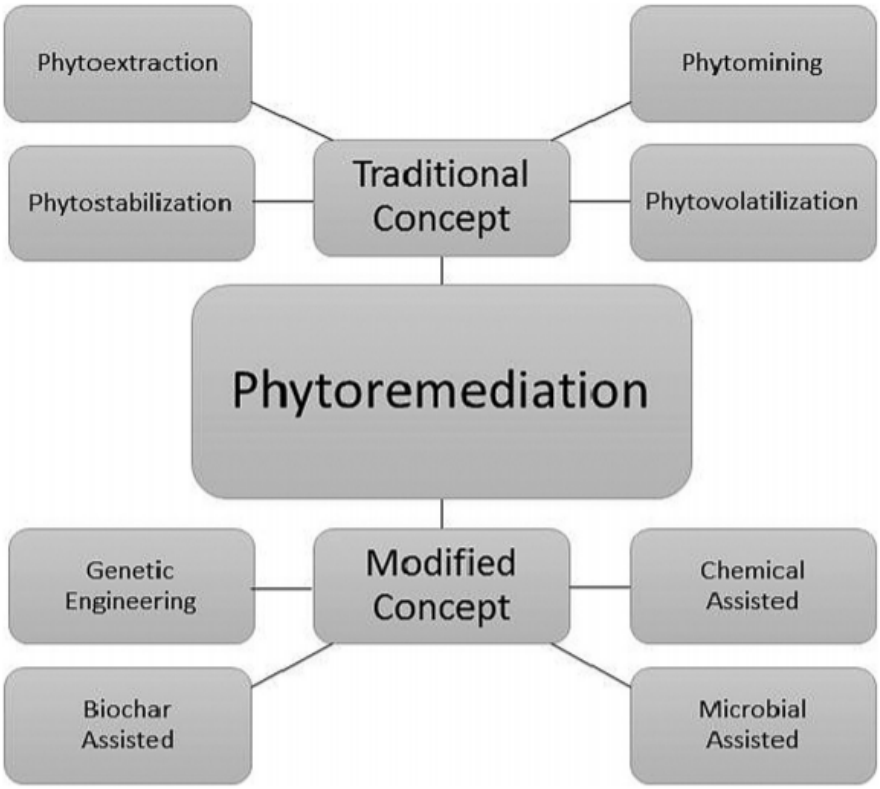

Figure 3.1. Types of traditional and novel phytoremediation approaches

3.1. Hyperaccumulation of heavy metals

Hyperaccumulation of heavy metals in plants occurs when concentration of a metals reaches to >0.1-1% of dry weight. Plant species known as hyperaccumulators. Can survive relatively contamination with metals and store metal ions in their cells and are characterized by their extraordinary abilities to absorb and accumulate metals [7]. Almost all species possess some abilities for metal tolerance based on 3 main processes: exclusion, chelation and sequestration. In current years nearly 400 of plant species have been reported as a hyperaccumulators for heavy metals [7,8].

Mechanisms of metals hyperaccumulation in plants is a complex phenomenon which involves many steps, starting with transport of metals from soil to root cells, translocation in xylem and finally sequestration and detoxification of metals in plans cells [9,10].

High efficiency in processes like sequestration and detoxification are a key property that allows hyperaccumulators to concentrate heavy metals in cells without phytotoxic effects. These elements are highly involved in homeostasis of essential metal micronutrients. Mechanisms of detoxification and sequestration in aerial organs consist mostly in complexation of heavy metals with ligands and transport to vacuoles and cell walls [11,12].

3.2. Influence of heavy metals on plants cells

When heavy metals enter cells cytoplasm, they are immediately bound with appropriate cellular compound which allows avoidance of toxic metal ions [13]. An example of metal chelators are organic acids such as citrate and nicotianamine (NA) which exhibits high stability for both binding and translocation of metals. In hyper-accumulating plants, concentration of NA is much higher than even in highly related species of non-accumulators [14]. Histidine has a major role in chelation of nickel and another amino acid – proline is probably involved in heavy metal chelation although the mechanisms of that role are still unknown [15].

Glutathione (GSH) is a low molecular weight chelator that can create complex formations with heavy metals which are necessary for induction of phytochelatin. Previous studies showed a direct link between overexpression of GSh and an increase in heavy metals tolerance in Arabidopsis thaliana which suggest lowering of oxidative stress caused by toxic concentrations of heavy metals by GSH [16].

Overexpression and overproduction of chelators like citrate, phytochelatins, metallothioneins, phytosiderophores or an overexpression of metal transporters leads to an increase in both tolerance and accumulation of metals in plants. Among all chelators, metallothioneins (MT) and phytochelatins (PCS) are widely studied in recent years [16,17]. When heavy metals enter plants cells a wide range of coping strategies occurs. One of them, is transporting metal ions out of the cell or to sequestrate it into vacuole in order to remove the contaminant form places with sensitive metabolic activi-ties. Vacuoles are suitable reservoir for excessive accumulation of heavy metals. Metal transporters play crucial role in protection of plant cells from phytotoxic effects induced by metals and in maintenance of the homeostasis. There are several classes of metal transporters in plants. Main ones include ATPases, Nramps, ZIP family, CDF's and finally ABC transporters. Overexpression of genes coding different types of transporters is often observed in hyperaccumulators [26,27].

Metallothioneins (Mts) are proteins containing sulfur with highly flexible structure. Flexibility allows for different coordination geometers to bind with different metals. MTs are divided into three main classes: first one – MT1 consist of polypeptides closely related to mammals and is characterized by the lack of aromatic amino acids and histidine's. Type 2 of metallothioneins was firstly discovered in yeasts and cyanobacterias. Saccharomyces cerevisiae Mt2, contributes to plant's tolerance of copper. Phytochelatins belong to the thing class of MT and were identified in a vast number of plant species including dicots, monocots, gymnosperms and algae. Heavy metals such as Pb, Cd, Hg, Zn can induce synthesis of metalotionein genes in plants and animals. Cadmium is the most powerful activator of MT genes in plants. Mt1 genes are expressed mostly in the roots and Mt2 in shoots of plants [18].

As mentioned before, overexpression of chelators can lead to an increase in tolerance and accumulation of heavy metals. One study showed that, accumulation of cadmium in tobacco can be increased when plants have the transgenes coding chelator – polyhistidine. Introducing metalotionein gene in tobacco also improved the tolerance of plant to Ni, Cd and Zn contamination. An increase in metal uptake, mostly for Fe, Cd, Mn and Zn was also observed in plants characterized with overproduction of ferritin through genetic modification. In transgenic *Brassica juncea* L., overexpression of ferratin, gamma-glitamylcsteine synthetase and glutathione synthetase caused higher accumulation of various metals – Cd, Cr and even Pb, in mixes or alone (tab. 2) [19,20].

Defense mechanisms based on antioxidant response to heavy metals keep formation of ROS at a low level. Still, contamination disrupts the balance between creation and detoxification of free radicals. Plant cells possess a wide range of antioxidant network based on non-enzymatic antioxidant's such as glutathione, ascorbate as well as enzymatic antioxidants like catalase (CAT), superoxide dismutase (SOD), peroxidase (POD) or glutathione reductase (GR). Accumulation of heavy metals can change the activity of those enzymes in a species-specific way. One example is cadmium accumulator – *Targets erecta* which exhibits a decrease in activity of SOD and CAT when exposed to cadmium but another Cd accumulator: *Avena strigose* showed an increase in activity of those enzymes when exposed to cadmium. Similar results occur in other plant species therefore patterns between enzyme activity are strictly specific for each species and should be taken into consideration when testing imbalance in oxidative stress induced by heavy metals [21].

4. Conclusions

Soil degradation becomes a rising threat to world agriculture. First global scale assessment in 1999 indicated that about 15% of global land area is affected by human induced degradation [1]. More recent studies revealed growth of that percentage to about 24% and about 19% of that area is used to produce food [2]. One of most notable soil contaminants around the world are heavy metals that not only decrease yield of crops but also can accumulate in biomass and pose a threat to humans and livestock [3–5]. Like many other abiotic

stress factors, heavy metals induce oxidative stress by interrupting cell metabolism. Improper flow of ions leads to excess of reactive oxygen species (ROS) [6]. With no stress factors present ROS (superoxide and hydroxyl radicals, singlet oxygen and hydrogen peroxide) are also produced, but in amounts low enough to be quickly neutralized by antioxidants (glutathione, ascorbate, αTocopherol, carotenoids) or enzymes - superoxide dismutase (SOD), catalase (CAT) and peroxidases (POD, GPX, APX) [7]. ROS that are not removed in time may cause oxidative damage to nucleic acids and proteins, ultimately leading to cell death [8, 9]. Assesment of activity of enzymes such as GPX or SOD may be viable way to determine stress levels and in consequence to assay environment toxicity. As phytotoxicity is traditionally evaluated in tests involving seed germination, result accuracy is limited due to many factors that are hard to control and foresee without extensive pretesting, such as seed genetic variability and natural tendency to sprouting [10,11].

Due to a rising problem of soil pollution with heavy metals in recent years special focus is putted on further development of quick but highly sensitive, plant stress detection methods that will allow to both: determinate the severity of contamination and possible options of phytoremediation as well as a indicator of efficiency of this phytoremediation processes. Further knowledge about plants ability to tolerate, ac-cumulate and detoxification metal irons is necessary for several purposes: (i) enhancing accumulation of metals that are microelements for nutritional purposes, (ii) for cleaning up contaminated soils, (iii) to mine rare metals which can be accumulated in plants, (iv) to predict health risk induced by metal accumulation in crops [28,29].

Areas with heavy metal-polluted soils are increasing significantly throughout the world, as a result of industrialization, mining operations, improper waste and water treatment [18,10,19]. It is widely known that heavy metals cause abiotic stress that results in plants improper development, lower yield and in high concentrations cause plant death. It was found that soon after exposure to heavy metals, metabolism of ROS gets altered and oxidative stress is induced [8,3].

Further knowledge on biochemical and physiological responses of plants to stress helps develop new strategies for purification of contaminated areas and overall improvement of the environment. In transgenic plants, capacity of metal uptake, transport and detoxification can be altered therefore, finding a suitable species with extraordinary antioxidant mechanisms is a key point in success of process. Overexpression of specific genes such as phytochelatin and metallothioneins is directly connected to heavy metal stress. Moreover, the role of miRNA and HSPs in plants stress tolerance induced by heavy metals is still unknown [30,31].

References

[1] Agostini E., Coniglio M.S., Milrad S.R., Tigier H.A., Giulietti A.M. Phytoremediation of 2,4-dichlorophenol by Brassica napus hairy root cultures. *Biotechnol Appl Biochem*, 2003, pp. 252-271.

[2] Arthur E.L., Rice P.J., Anderson T.A., Baladi S.M., Henderson K.L., Coats J.R. Phytoremediation—An overview. *Crit Rev Plant Sci*, 2005, 24, pp. 109–122.

[3] Boominathan R., Doran P.M.. Ni-induced oxidative stress in roots of the Ni hyperaccumulator, Alyssum bertolonii. *New Phytol*, 2002, 156, pp. 205–215.

[4] Harms H.H. In-vitro systems for studying phytotoxicity and metabolic fate of pesticides and xenobiotics in plants. *Pestic Sci*, 1992, 35, pp. 277–281.

[5] Lebeau T., Braud A., Jezequel K.. Performance of bioaugmentationassisted phytoextraction applied to metal contaminated soils. *Environ Pollut*, 2008, 153, pp. 497–522.

[6] Nedelkoska T.V., Doran P.M. Characteristics of heavy metal uptake by plant species with potential for phytoremediation and phytomining. *Minerals Eng*, 2000, 13, 549–561.

[7] Lodewyckx C., Taghavi S., Mergeay M., Vangronsveld J., Clijsters H., Van der Lelie D. The effect of recombinant heavy metal-resistant endophytic bacteria on heavy metal uptake by their host plant. *Int J Phytoremed*, 2001, 3, pp. 173–187.

[8] Van Nevel L., Mertens J., Oorts K., Verheyen K.. Phytoextraction of metals from soils: How far from practice? *Environ Pollut,* 2007, 150, pp. 34– 40.

[9] Coleman J.O., Blake-Kalff M.M., Davies T.G. Detoxification of xenobiotics by plants: Chemical modification and vacuolar compartmentation. *Trends Plant Sci,* 1997, 2, pp. 144–151.

[10] Schroder P., Scheer C.E., Diekmann F., Stampfl A. How plants cope with foreign compounds: Translocation of xenobiotic glutathione conjugates in roots of barley (Hordeum vulgare). *Environ Sci Pollut Res,* 2007, 14, pp. 114–122.

[11] Alexander M. Aging, bioavailability, and overestimation of risk from environmental pollutants. *Environ Sci Technol,* 2000, 34, pp. 4259–4265.

[12] Burken J.G., Schnoor J.L. Predictive relationships for uptake of organic contaminants by hybrid poplar trees. *Environ Sci Technol,* 1998, 32, pp. 3379– 3385.

[13] Groeger A.G., Fletcher J.S. The influence of increasing chlorine content on the accumulation and metabolism of polychlorinated biphenyls (PCBs) by Paul's Scarlet rose cells. *Plant Cell Rep,* 1998, 7, pp. 329–332.

[14] Nakazawa R., Kameda Y., Ito T., Ogita Y., Michihata R., Takenaga H. Selection and characterization of nickel-tolerant tobacco cells. *Biol Plant,* 2004, 48, pp. 497–502.

[15] Yoshihara T., Tsunokawa K., Miyano Y., Arashima Y., Hodoshima H., Shoji K., Shimada H., Goto F. Induction of callus from a metal hypertolerant fern, Athyrium yokoscense, and evaluation of its cadmium tolerance and accumulation capacity. *Plant Cell Rep,* 2005, 23, pp. 579–585.

[16] Chroma L., Mackova M., Kucerova P., In der Wiesche C., Burkhard J., Macek T. Enzymes in plant metabolism of PCBs and PAHs. *Acta Biotechnol,* 2002, 22, pp. 35–41.

[17] Khaitan S., Kalainesan S., Erickson L.E., Kulakow P., Martin S., Karthikeyan R., Hutchinson S.L., Davis L.C., Illangasekare T.H., Ngoma C. Remediation of sites contaminated by oil refinery operations. *Environ Prog,* 2006, 25, pp. 20–31.

[18] Boominathan R., Doran P.M. Cadmium tolerance and antioxidative defenses in hairy roots of the cadmium hyperaccumulator, Thlaspi caerulescens. *Biotechnol Bioeng,* 2003, 83, pp. 158–167.

[19] Eapen S., Suseelan K.N., Tivarekar S., Kotwal S.A., Mitra R. Potential for rhizofiltration of uranium using hairy root cultures of Brassica juncea and Chenopodium amaranticolor. *Environ Res,* 2003, 91, 127–133.

[20] Garnier L., Simon-Plas F., Thuleau P., Agnel J.P., Blein J.P., Ranjeva R., Montillet J.L. Cadmium affects tobacco cells by a series of three waves of reactive oxygen species that contribute to cytotoxicity. *Plant Cell Environ,* 2006, 29, pp. 1956–1969.

[21] Nedelkoska T.V., Doran P.M. Hyperaccumulation of cadmium by hairy roots of Thlaspi caerulescens. *Biotechnol Bioeng,* 2000, 67, pp. 607–615.

[22] Nedelkoska T.V., Doran P.M. Hyperaccumulation of nickel by hairy roots of Alyssum species: Comparison with whole regenerated plants. *Biotechnol Prog,* 2001, 17, pp, 752–759.

[23] Azevedo H., Pinto C.G.G., Santos C. Cadmium effects in sunflower: Membrane permeability and changes in catalase and peroxidase activity in leaves and calluses. *J Plant Nutr,* 2005, 28, pp. 2233–2241.

[24] Van Sint Jan V., Costa de Macedo C., Kinet J.M., Bouharmont J. Selection of Al-resistant plants from a sensitive rice cultivar, using somaclonal variation, in vitro and hydroponic cultures. *Euphytica,* 1997, 97, pp. 303–310.

[25] Schaider L.A., Parker D.R., Sedlak D.L. Uptake of EDTA-complexed Pb, Cd and Fe by solution- and sand-cultured Brassica juncea. *Plant Soil,* 2006, 286, pp. 377–391.

[26] Nedelkoska T.V., Doran P.M.. Hyperaccumulation of nickel by hairy roots of Alyssum species: Comparison with whole regenerated plants. *Biotechnol Prog*, 2001, 17, pp. 752–759.

[27] Olmos E., Hernandez J.A., Sevilla F., Hellin E. Induction of several antioxidant enzymes in the selection of a salt-tolerant cell line of Pisum sativum. *J. Plant Physiol*, 1994, 144, pp. 594–598.

[28] Kupper H., Lombi E., Zhao F.J., McGrath S.P. Cellular compartmentation of cadmium and zinc in relation to other elements in the hyperaccumulator Arabidopsis halleri. *Planta*, 2000, 212, pp. 75–84.

[29] Mackova M., Macek T., Kucerova P., Burkhard J., Pazlarova J., Demnerova K. Degradation of polychlorinated biphenyls by hairy root culture of Solanum nigrum. *Biotechnol Lett*, 1997, 19, pp.787–790.

[30] Davis D.G., Hodgson R.H., Dusbabek K.E., Hoffer B.L. The metabolism of the herbicide diphenamid (N-N-dimethyl-2,2-diphenyl-acetamide) in cell suspensions of soybean (Glycine max). *Physiol Plant*, 1978, 44, pp. 87–91.

[31] Eapen S., Suseelan K.N., Tivarekar S., Kotwal S.A., Mitra R. Potential for rhizofiltration of uranium using hairy root cultures of Brassica juncea and Chenopodium amaranticolor. Environ Res 91:127–133, 2003;

Underground pumped hydro energy storage in abandoned coal mines

Dawid Brzózka[1]

[1]*Silesian University of Technology, Faculty of Energy and Environmental Engineering, Konarskiego 18 St, 44-100 Gliwice, Poland; e-mail: dawid.brzozka96@gmail.com*

Abstract

The aim of this article was to investigate new application of the old technology. Pumped Hydro Energy Storage (PHES) systems are widely used all around the world. The basic principle is that the energy is stored in two reservoirs at different heights and the water is either pumped up consuming excess energy or let down through a turbine generating energy at peak demand. The concept that is new in this old idea is putting the lower reservoir together with machinery under the ground. One of the potential locations is abandoned coal mine. The principle of operation is very similar to conventional concept of UPHES. In an inactive coal mine the water is transported from the lower reservoir by the use of mine shaft equipped with turbines. There are several advantages of using coal mine infrastructure in UPHES: the voids are already excavated, there is a mineshaft that can access mine levels, mine's own underground pumping equipment (pumps, pipes, dams) but there are also limitations and challenges to be faced in order to build such a plant.

Keywords: pumped-hydro, pumped-storage, energy storage, coal mines, underground, hydroelectricity

1. Introduction

Power engineering in today's world and especially in Poland is at some kind of transitional state. Poland strongly relies on fossil fuels when it comes to production of electricity and heat generation – mainly hard coal, which is still available, and it is mined a lot. Unfortunately, because of this, it is necessary to fight with really dangerous smog lately. In order to deal with it, Polish energy policy is trying to involve more and more unconventional methods to obtain these two highly demanded products.

Fossil fuels, which are non-renewable sources of energy, are depleting very fast all over the world, because of the pace at which development progresses. Especially the less developed countries do not pay attention to global and ecological aspects of limited resources of fossil fuels, as they try to catch up to the most developed countries at all costs.

That is why more developed countries are trying to become independent of these non-renewable energy sources, at least to a certain degree. In order to obtain this independence, they rely on two main renewable energy sources – solar radiation and wind.

The potential of electricity production using wind is very high and widely used, although it comes with the disadvantages. Main one being the unpredictability of the wind and very high variation of the amount of produced electricity. As a result, other facilities producing electricity must adjust to it, as well as adjust to the load profile of the whole system. It may be that sometimes, conventional power plants work at such load that their efficiency drastically drops, causing losses.

Although the power from solar radiation is more predictable than the power from the wind and even in the cloudy days some electricity can be produced, this type of renewable energy source also strongly contributes to the load variation in Polish energy market.

This article will present some kind of solution to this problem. The concept is not new and is widely used known as pumped hydro energy storage, but the application of this process is quite interesting.

2. Pumped hydro energy storage

The increase in the renewable energy from wind and sun in the energy mix should always be accompanied with energy storage system. Crucial word here is **energy,** because to store electricity, not necessarily the electricity itself should be stored as it is difficult, but it can be stored in some other way i. e. potential energy. [1]

Here comes the pumped hydro energy storage, which is the only technology, which is so long-lived, mature and applicable to such a large scale. The first ideas date back to the beginning of 20th century.

The principle of operation is quite simple, yet so effective. The typical facility consists of:

- upper reservoir
- vertical tunnel called penstock
- headrace which conducts water between the upper reservoir and upper end of penstock
- pump-turbine on the same rotary shaft as motor-generator
- lower reservoir
- tailrace tunnel connecting the pump-turbine to lower reservoir

The system operates as a generator when the water plunges down the penstock, spins the turbine forward and generates electricity. The motor generator is supplied with electricity from the grid, when there is an excess of it to spin the turbine backwards and pump water from lower reservoir up the penstock, into the upper reservoir. Then the water stays there, waiting for an energy demand increase to kick in and the process starts over. [1]

Such systems are very reliable and can operate with efficiencies in the range of 70-85%. To confirm that this is one of the best solutions to store energy right now is the fact that as of 2017, the United States Department of Energy Global Energy Storage Database reports, that over 95% of all storage installations worldwide are pumped hydro technology, with installed capacity of over 184 GW.

The sample scheme of pumped-storage plant can be seen in Fig. 2.1.

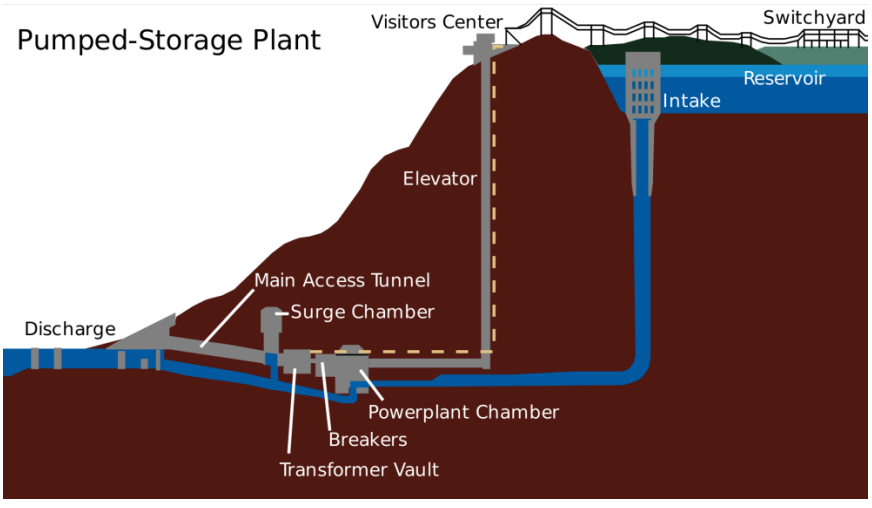

Fig. 2.1. TVA pumped storage facility at Raccoon Mountain Pumped-Storage Plant (USA)

3. Underground pumped hydro energy storage (UPHES)

The basic concept of pumped hydro energy storage relies on using natural landscapes and differences of height, such as mountain areas. That is why most of these type of energy reservoirs are located in the

mountains. However, it requires ideal topographic situation and also public acceptance related to the land use and environmental impact. [2]

That is not the only solution. Today more and more pumped hydro energy storages are being created in artificially made environments. Usually only the parts of PHES plants are located underneath the surface to i.e. preserve landscape.

However, it can be even designed in a way that both upper and lower reservoirs are not visible on the surface. On the other hand, the upper reservoir revealed is greatly preferred, which reduces the costs and increases the height difference.

3.1 Examples of existing UPHES solutions

It is difficult to point at already existing UPHES as most of them are still conceptual or at the level of feasibility studies.

The first realized project, not entirely hidden under the surface, but with one subsurface water cavern happened in Austria in 2006. [4]

It was not built like that from the beginning, but rather as an expansion of the existing plant Nassfeld which was created in 1980. The aim was to expand the lower reservoir motivated by economics. [4]

The expansion of the lower reservoir was not viable due to different legal, technical and landscape issues, so the solution was to put a subsurface system of pipes which is visualized in Fig. 3.1.

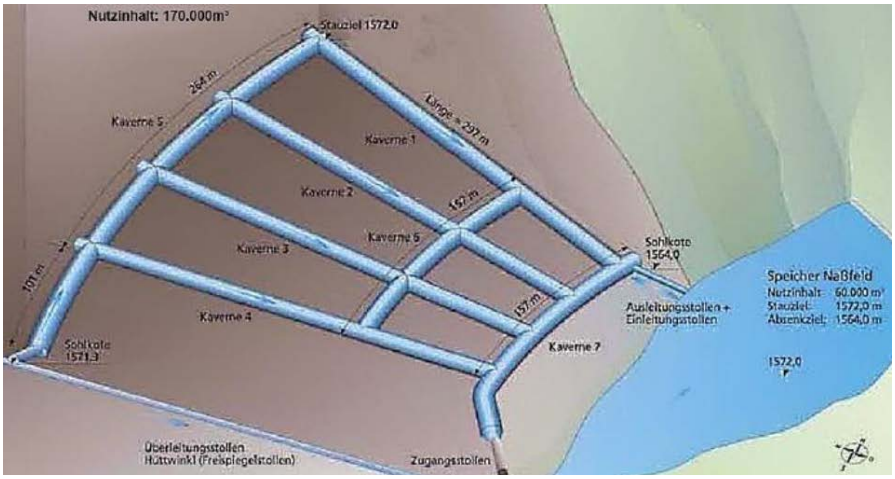

Fig. 3.1. Planned cavern structure for the extension of the intra-day PSHP plant Nassfeld, Austria [5]

The project was developed really fast - under 6 months, during which 160,000 m^3 of rocks were excavated, and tunnel of 1950m length was established. Capital cost ended up in ~8 million €. [4]

Some of the projects stopped at the planning phase and were abandoned for different reasons. One example could be Power Plant in Ritten, South Tyrol, Italy.

The plans were ambitious, and it assumed to be entirely subsurface power plant built by Austrian energy provider KELAG AG. Two caverns of 0.6 Mm^3 capacity were to be built, run by a 250 MW turbine, at a 900 m depth. [4]

Investment cost was much larger than the previous example of only expansion of existing power plant – 300 million €. The project was unfortunately abandoned due to protests of the population combined with bad PR claiming that the concession for construction would be unachievable. [4]

In many projects individual parts of PHES are being dug into the ground, however Underground Pumped Hydro Energy Storage has a potential of being located completely under the ground surface and next chapters will focus on what are the advantages of such concept, issues and possible solutions.

3.2 Viability of UPHES in coal mines

One way to approach Underground Pumped Hydro Energy Storage is to drill the hole to lower reservoir, but another option is to use already existing coal mines with its tunnels which average 500-1000 m.

Table. 3.1. Status of underground mines in Poland [2, 3]

Number of mines	State	Depth range (m)	Water outflow (Mm^3/year)
28	Active	300-800	209
26	Flooded	300-800	

Table 3.1 shows the current status of coal mining in Poland and the potential underground hydro pump storage facilities.

Coal mine considered for the UPHES must be obviously closed from its usual operation. It shouldn't be completely flooded, so abandoned coal mine which is still being dewatered can be taken into account.

The principle of operation is very similar to conventional concept of UPHES. In an inactive coal mine the water is transported from the lower reservoir by the use of mine shaft equipped with turbines. [2]

There are several advantages of using coal mine infrastructure in UPHES:

- the voids are already excavated,
- there is a mineshaft that can access mine levels,
- mine's own underground pumping equipment (pumps, pipes, dams)

What is more, the lower reservoir can be placed directly underneath the upper one, which reduces the distance that water has to travel compared to conventional PHES systems, while head stays the same. [2]

3.2.1 Potential issues and challenges

- Upper reservoir

It is possibly the least problematic aspect of the UPHES, as it can be located on the surface of the coal mine.

- Lower reservoir

It is crucial part of the whole concept and for sure should be placed underneath the ground at a great depth.

In order to achieve it the first thing that comes to mind is the usage of existing cavities. Today more and more coal mines are using advanced technique of mining which is called long-wall mining, which limits the presence of crews in the most difficult, dangerous places exposed to extreme conditions, i. e. very high temperatures.

It also means that the only drifts that remain were specifically created for the transportation of materials and equipment and caverns serve a role of hosting technical equipment. [4]

What is more extraction of additional large cavities would be very expensive and demanding.

The options that are left: making use of existing drift or dig new ones. For sure some of the old drifts could be used for this purpose as they are usually extensive and could store a large volume of water. However, it is no dispute that some new drift would have to be developed. [4]

In general, the best option for lower reservoir would be a rib-shaped storage system.

Table. 3.2. Drift extension cost [4]

Drift extension, m	Storable amount of water, t	Extension cost at 10 000 €/m, M€	Extension cost at 20 000 €/m, M€
2 000	96 000	20	40
5 000	240 000	50	100
10 000	480 000	100	200
15 000	720 000	150	300
20 000	960 000	200	400
30 000	1 440 000	300	600

Table 3.2 presents cost of drift extension with storable amount of water assuming that the diameter is about 7.8 m. Depending on what cost of extension is assumed, in the best-case scenario price for 1 m^3 of water stored oscillates around 200 €.

- Head

As stated in Table 3.1 majority of Polish coal mines are between 300-800 m deep. Up to 700 m Francis turbine type is preferred, which handles medium pressures. Above 700 m Pelton turbine is used instead, which can generate higher pressure. Larger heads would require an inter-stage in pumping which mine brines could be applied for. [4]

- Slope

The constraint in UPHES is that the downward slope must be maintained from the upper reservoir down to the lower reservoir where the whole water stays until it is pumped again to the surface.

When using an existing drift, it would have to be estimated if the slope is sufficient, while building a new system it would be easier, but it should also be taken into account. [4]

3.2.2 Available energy storage capacity

The amount of energy that could be stored in a plant hugely depends of the height difference and amount of stored medium. Typical storage capacities for PHES plants are presented in Fig. 3.2 for different heads and water mass. The assumption for calculation was g = 9.81 m/s^2 and turbine efficiency equal to 95%.

Range applicable for UPHES is between 500-750 m of head. Realistically not more than 1 Mm^3 could be stored under the ground as it would require more than 20 km of drift. Assumption that at the depth of 750 m, 1 million tons (~1 Mm^3) of water would be stored – results in 1941.6 MWh of potential energy.

This amounts to a little bit over a half of the biggest PHES plant in Poland – Żarnowiec – which has a capacity equal to 3600 MWh. This result however, being the best-case scenario, still looks impressive and for sure is realizable, the question is about the economic viability, which should be further investigated.

4. Conclusions

Pumped Hydro Energy Storage is the most mature technology of its kind. It has been there for a long time and one may think that nothing new could be surprising about this technology. However, from time to time some new applications of this old technology arise, using innovative new concepts, such as this Underground Pumped Hydro Energy Storage.

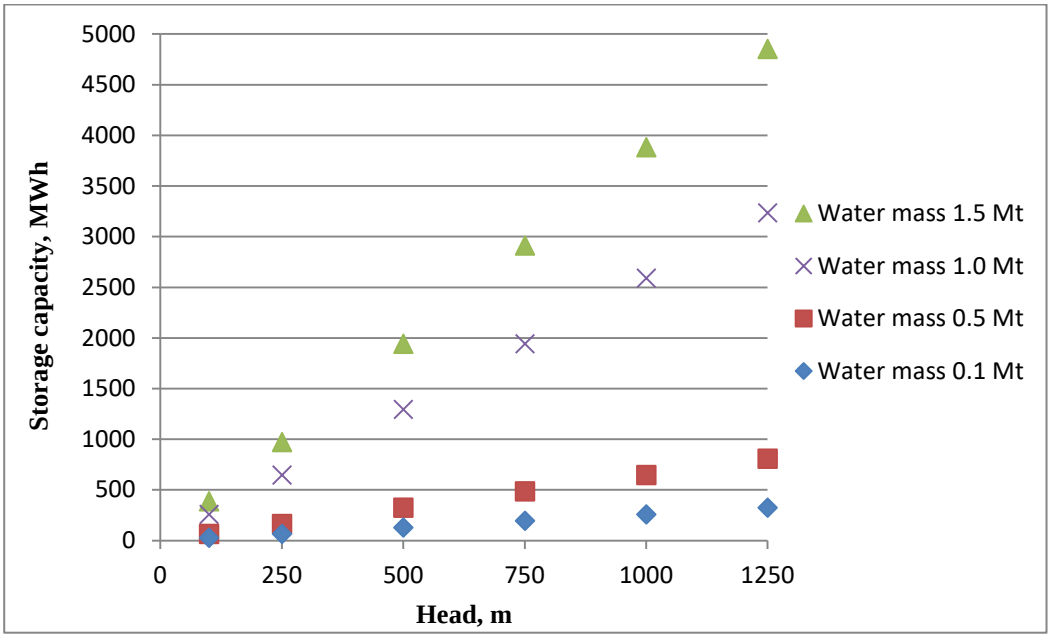

Fig. 3.2. Energy storage capacities of PHES plants [4]

As the world advances and new regulations are pushed by i. e. European Union about constantly increasing share of renewables in the energy mix. Taking into consideration that renewable energy sources are not fully predictable and can produce a lot of excess energy at the certain moment, introducing more energy storage systems is crucial.

Underground Pumped Hydro Energy Storage is a promising concept when considering abandoned coal mines and the fact that sooner or later coal mines could be closed, especially that today's world is trying to slowly move away from coal or at least European authorities are trying to make it happen.

For sure more advanced feasibility studies should be performed in order to assess, whether this concept is viable from the economic point of view, as technically it is possible to be constructed.

References

[1] W. F. Pickard. The History, Present State, and Future Prospects of Underground Pumped Hydro for Massive Energy Storage, in Proceedings of the IEEE, vol. 100, no. 2, pp. 473-483, Feb. 2012

[2] Javier Menéndez, Almudena Ordóñez, Rodrigo Álvarez, Jorge Loredo. Energy from closed mines: Underground energy storage and geothermal applications, Renewable and Sustainable Energy Reviews, Volume 108, Pages 498-512, July 2019

[3] Gombert P, Sracek O, Koukouzas N, Gzyl G, Tuñon S, Frączek R, et al. An overview of priority pollutants in selected coal mine discharges in Europe. Mine Water Environ 2018;38(1):16–23

[4] Madlener R., Specht J.M. (2013). An Exploratory Economic Analysis of Underground Pumped-Storage Hydro Power Plants in Abandoned Coal Mines, FCN Working Paper No. 2/2013, Institute for Future Energy Consumer Needs and Behavior, RWTH Aachen University

[5] Wall J. Pumpspeicherkraftwerke; Im Spannungsfeld zwischen der europäischen Wasserrahmenrichtlinie und der Liberalisierung der Strommarktes. Graz, Österreich; 2010.

Thermo-ecological assessment of import of natural gas to Poland

Tomasz Simla[1], Wojciech Stanek[2]

[1]Department of Thermal Engineering, Silesian University of Technology, e-mail: tomasz.simla@polsl.pl
[2]Department of Thermal Engineering, Silesian University of Technology, e-mail: wojciech.stanek@polsl.pl

Abstract

To correctly evaluate the impact of fossil fuels on the environment, not only the effect of combustion should be taken into account, but also the "upstream" effects, associated with processing and transporting the fuel to the final consumer. Since natural gas is transported over long distances, these effects are not negligible. Transporting natural gas in liquefied form is an alternative for traditional pipeline transport. Poland used to import natural gas mainly from Russia (via pipelines), but in year 2016 Poland joined the global LNG market through a regasification terminal built in Świnoujście. The paper describes the two methods of transporting natural gas and attempts to compare them by evaluating two thermo-ecological indices: cumulative consumption of primary energy and cumulative emission of greenhouse gases that burden the import of natural gas to Poland.

Keywords: cumulative energy consumption, greenhouse gas emission, liquefied natural gas, LNG, pipeline transport

1. Introduction

The fear of global warming caused by greenhouse effect has over recent decades become the reason for increasing public and legislative pressure against utilizing fossil fuels. This is evoked by the belief that anthropogenic emission of carbon dioxide (resulting from combustion of fossil fuels) has a crucial impact on global warming. International community has taken actions to reduce CO_2 emissions, hoping to prevent an adverse rise in the Earth's average surface temperature. The most notable treaty regarding this matter is the Kyoto Protocol adopted in 1997 [1], which obliged the signatory countries to control their emissions of greenhouse gases (GHG) and to meet the reduction targets (defined individually for each state). A successor of the Kyoto Protocol was signed in Paris in 2015. The Paris Agreement aims to reduce the increase of global average temperature to below 2°C by reaching global peaking of GHG emissions as soon as possible [2]. Another significant initiative is the European Union Emission Trading Scheme [3]. It determines the total amount of GHG that can be emitted in the system and distributes emission allowances between the companies which own industrial installations. Fines are imposed on companies that exceed emissions above their allowances. The allowances can however be a subject of trade. The limit is reduced in subsequent years in order to force the decrease of overall GHG emission. Another aim of the mentioned regulations is to slow down the depletion of natural resources, such as fossil fuels.

Among fossil fuels, coal is the one most often censured, while natural gas is universally perceived as more environmentally friendly [4,5]. This is justified by the results of combustion stoichiometry: obtaining 1 TJ of heat from natural gas is associated with emission of 56 Mg of CO_2; obtaining the same amount of energy from coal results in emission over 90 Mg CO_2 (the exact value depends on the type of coal) [6,7]. It is however a common misconception to compare fuels only by direct emission from combustion. Firstly, because often not heat but electricity is the final product of energy conversion. Therefore, the efficiency of power plant should be taken into consideration. And secondly, because the chain of processes before combustion (extraction, treatment and transport of fuel) requires an energy input which is associated with

additional emissions. An approach taking into account the abovementioned aspects is called life cycle assessment (LCA). LCA methods provide useful indicators (e.g. cumulative consumption of primary energy and cumulative GHG emissions per production of a unit of final product) that allow to properly compare different fuels and technologies.

Results of such studies may significantly differ from the usual fuel comparison based on stoichiometry, mainly because of methane leakages from coal mines and during transport of natural gas [7-9]. Methane is a much more potent greenhouse gas than carbon dioxide. The value of Global Warming Potential (GWP) for methane is estimated in the range of 21–30 (CO_2 being the reference substance has GWP = 1). When these upstream emissions are taken into consideration, the increase of equivalent CO_2 emission is much higher for natural gas than for coal [7]. This proves that in the case of fuel comparison with regards to their environmental impact, some elements of LCA should always be used.

The focus of this paper is the assessment of the methods of transport of natural gas using two thermo-ecological indicators: cumulative consumption of primary energy and cumulative equivalent emission of CO_2 per delivery of a unit of natural gas to the final recipient. The values of these indicators are estimated for the case of import of natural gas to Poland. Section 2 discusses the methods of transport of natural gas. Section 3 describes the role of natural gas in Polish economy. The methodology is explained in section 4 and the results of calculations are presented in section 5. Finally, section 6 contains the summary and conclusions.

2. Methods of transport of natural gas

Two most widespread, competing methods of transport of natural gas over long distances are: pipeline transport and LNG transport [10]. Pipelines are a traditional way of transporting natural gas, used for over a century. They are a stable and safe source of natural gas supply, suitable for large and conveniently located deposits of this natural resource. Gas trunk pipelines usually have 0.6–1.4 m in diameter and operate in the pressure range 4–12 MPa. Increasing the pressure reduces the specific volume of gas and allows to transport larger quantities of fuel. Due to hydraulic resistance of pipes (frictional flow), pressure drops over distance. Therefore, compressor stations need to be installed every 100–150 km to increase the gas pressure. The compressors are commonly driven by gas turbines fueled by natural gas extracted from the pipeline. Other purposes of compressor stations are to purify and cool the gas and to measure its flow. The rise of gas temperature is an unwanted side effect of compression. Higher temperature means higher specific volume, which induces higher pressure losses during flow. Hence the need of cooling, which is realized by air coolers powered by electric energy [11,12]. A downside of pipeline transport are leakages of natural gas occurring along the pipes and in compressor stations.

With discoveries of new deposits of natural gas, situated in remote locations, where construction of pipeline would be difficult and unprofitable, it became necessary to develop alternative methods of transporting large quantities of this fuel. Currently, the only alternative method that has become commercially widespread is the liquefaction of natural gas [13,14]. At temperature of −162°C and standard pressure, methane is a colorless, odorless, non-toxic and non-corrosive liquid with density about 650 times higher than in standard conditions. Therefore, liquefying methane increases its energy density from 32.8 MJ/m^3 to about 21 GJ/m^3, which makes transport in tanks (mainly by sea) reasonable. After delivering LNG to the receiver, it is reverted to gas state in a process called regasification.

A great advantage of transporting natural gas as LNG is the flexibility of this method. The supplier is not permanently bound to the receiver. Liquefied natural gas can be delivered to any regasification terminal around the world. This contributes to the increase of competitiveness on the global natural gas market. The receiver can freely choose between the offers on the market. A disadvantage of LNG is high investment cost of liquefaction and regasification terminals, but the distance between them does not have a significant impact on the unit cost of transport. It becomes lower than for pipeline transport at distances over 1000 km for offshore pipeline and 3000 km for onshore pipeline [15].

2.1 LNG delivery chain

The production and delivery chain of liquefied natural gas is presented in Figure 2.1. It consists of four stages: extraction, treatment and liquefaction, sea transport and regasification.

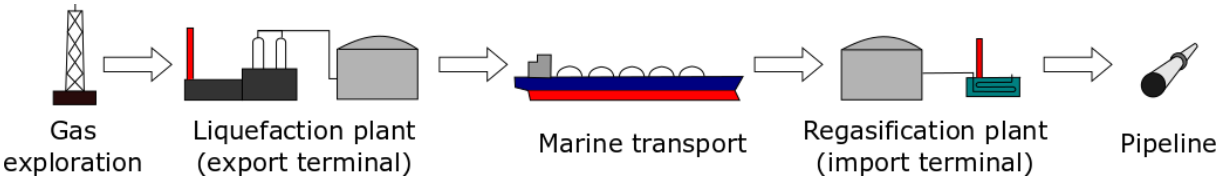

Fig. 2.1. LNG delivery chain

Natural gas needs to be treated before liquefaction. The aim of treatment is to meet the product specification by removing impurities and other unwanted components which are corrosive or would cause problems during liquefaction. Most notable of these substances are carbon dioxide, sulfur compounds (H_2S, thiols, OCS), moisture and mercury. Propane, butane and heavier hydrocarbons are usually also removed, because they can be sold separately with better profit. Nitrogen is unwanted as well, it is removed during the liquefaction process [5,13].

The liquefaction technology is based on the working principle of refrigeration cycles. Natural gas needs to be cooled down below its saturation temperature (−160°C at standard pressure). The most popular method, AP-C3MR (*Air Products propane precooled mixed refrigerant*) and its variations were responsible for 72% of the world's LNG production capacity in 2018 [16,17]. It is a vapor-compression refrigeration cycle which uses a carefully selected mixture of refrigerants as a working fluid, so that the temperature profiles of the working fluid and liquefied natural gas match closely. Liquefaction is the most energy-intensive process in the delivery chain. Driving the compressors requires a work input of about 1.2 MJ per kg of natural gas [18].

LNG is mainly transported by sea in special ships called LNG carriers. LNG is stored in insulated tanks at about −169°C and slight overpressure. Since it is not possible to insulate the tanks perfectly, heat from outside penetrates into the tanks, which causes LNG to boil off at rate of 0.1–0.15% per day. The boil-off gas (BOG) can be either used as a fuel to propel the ship or be reliquefied and returned to tanks, depending on the technical solutions implemented on the ship [13]. The cargo capacity of LNG carriers is in the range of 30,000–265,000 m^3. Modern ships called Q-Flex have capacity of approximately 216,000 m^3, and the largest ships called Q-Max – 265,000 m^3. At the end of 2018 the world's fleet of LNG carriers consisted of 525 ships with total capacity of over 75 million m^3 [13,16].

LNG carriers bring the fuel to receiving terminals, where it needs to be pressurized, warmed up and regasified. LNG unloaded from the ship is transported to insulated storage tanks. Their standard capacity is 160,000 m^3. The process of boiling-off occurs in these tanks as well, therefore regasification terminals should be equipped with small reliquefaction installations. LNG taken from the tanks is first compressed to pressure required in a gas sendout pipeline. It results from the fact that the work of compression is much lower for liquids than for gases. Compressed LNG flows into a heat exchanger, where it is vaporized and heated to ambient temperature. Depending on the source of heat utilized during regasification, methods can be divided into the following groups [13]:

- ORV (*Open Rack Vaporizers*), STV (*Shell and Tube Vaporizers*) – heat is taken from seawater. It is the most popular method of regasification, implemented in over 70% of existing LNG receiving terminals. Since the terminals are located close to the sea, seawater is a cheap and abundant source of heat. This method is simple, safe, easy to maintain and is characterized by low operation costs. However, the possibility of applying this method is determined by the climatic and environmental conditions at the site. If the temperature of seawater is too low (lower than 5°C), it cannot be used as a heat source to avoid freezing.

- AAV (*Ambient Air Vaporizers*) – heat is taken from atmospheric air. AAV is a more environmentally friendly method than ORV and it is not limited by the ambient temperature. However, because of low value of heat transfer coefficient, it requires much larger heat exchangers. This is the reason why this method is not suitable for terminals with large capacity.
- SCV *(Submerged Combustion Vaporizers*) – heat is obtained by combustion of a portion of regasified fuel. It is the second most popular method, used in about 20% of terminals. Due to high operation costs (fuel consumption is at the level of 1.5%) this method is used only if free heat sources are not available. The burners are situated on the bottom of a water tank and the heat exchanger is submerged in water. Flue gases migrate upwards in form of bubbles, which provides good heat transfer conditions. Moisture from the flue gases condenses, which increases the energetic effectiveness of the process, allowing it to reach 98%.
- IFV (*Intermediate Fluid Vaporizers*) – the intermediate fluid in heat transfer circulates in a closed loop, and heat may come from the environment or from another industrial process (waste heat). The intermediate fluid may additionally work in a power cycle, allowing for a partial recovery of cryogenic energy of LNG.

3. Natural gas in Polish economy

Polish energy mix is dominated by coal and lignite. Natural gas plays a relatively small role, but its consumption is predicted to grow in the future as a result of gradual withdrawal of coal technologies. In the year 2016 Polish economy consumed 11.33 Mtoe of primary energy of natural gas, which made up 16% of total consumption of primary energy [19]. Poland possesses own resources of natural gas, but they are insufficient to cover the whole demand. In the year 2017 the domestic production of natural gas amounted to 3.5 Mtoe, which made up almost 23% of the domestic consumption [19]. The remaining 77% of natural gas was imported. Until 2016, the whole import was being delivered via trunk pipelines. Thanks to a regasification terminal constructed in Świnoujście (north-western tip of Poland, on the coast of Baltic Sea), Poland recently joined the global LNG market. The first technical delivery of LNG occurred on 11th December 2015, and the first commercial delivery on 17th June 2016. The majority of deliveries will be realized under a long-term contract with Qatargas, a LNG company based in Qatar. The structure of origin of natural gas used in Poland in the years 2014 and 2018 is presented in Figure 3.1. Majority of imported gas still comes from Russia.

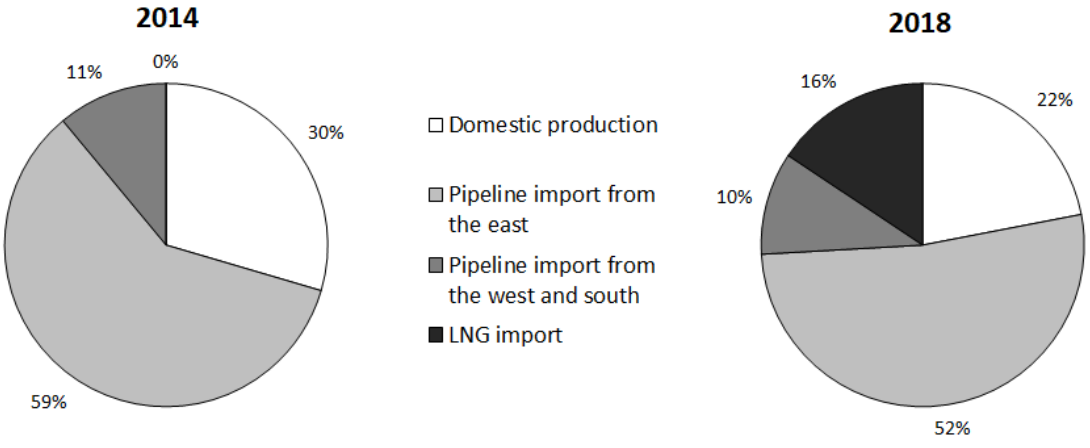

Fig. 3.1. Origin of natural gas used in Poland in 2014 and 2018 (based on [20])

The terminal in Świnoujście has a regasification capacity of 5 billion Nm^3 of natural gas per year. The largest components are two LNG tanks with capacity of 160,000 m^3 each. There is a space reservation for a third tank, which would increase the regasification capacity to 7.5 billion Nm^3 per year [21]. The port has the ability to berth LNG carriers with capacity in the range of 120,000–216,000 m^3. LNG is regasified using the SCV method. ORV technology was considered as a supplementary method, but it was rejected because of the

need to obtain an additional environmental permit and because it could only be used through several months in a year (due to rather cold climate) [21]. Regasified fuel is transported inland via a high pressure (8.4 MPa) pipeline.

4. Thermo-ecological indicators for the import of natural gas

To compare the two methods of import of natural gas to Poland, two indicators were estimated: the cumulative consumption of primary energy and the cumulative equivalent emission of CO_2 per delivery of a unit of natural gas to the final recipient. Note that the analysis presented here is not a full LCA approach, since it does not take into consideration the construction phase of the components of the transport system (which is generally negligible compared to the operation phase) nor the energy consumption during extraction of natural gas (which is assumed to be the same for both methods of transport).

The cumulative consumption of primary energy is defined as the sum of primary energy put into the process (including the primary energy of transported fuel itself) divided by the amount of energy of fuel delivered to the final recipient. It can be broken down into a sum of 1 and specific fuel consumptions for particular processes of the delivery chain:

$$w_{NG} = \frac{E_{in}^*}{E_{out}} = \frac{E_{out}+\Sigma\Delta E_{in\,i}^*}{E_{out}} = 1 + \frac{\Sigma\Delta E_{in\,i}^*}{E_{out}} = 1 + \Sigma\varepsilon_i \tag{1}$$

where:

- w_{NG} Coefficient of cumulative consumption of primary energy per delivery of a unit of chemical energy of natural gas (TJ/TJ),
- E_{in}^* Sum of primary energy put into the whole process, (TJ),
- E_{out} Chemical energy of fuel delivered to the final recipient, (TJ),
- $\Delta E_{in\,i}^*$ Additional primary energy put into *i*-th link of delivery process, (TJ),
- ε_i Specific consumption of primary energy in *i*-th link of delivery process (per unit of chemical energy of delivered natural gas), (TJ/TJ).

The cumulative emission of greenhouse gases is defined as the sum of carbon dioxide and other greenhouse gases (converted to equivalent of CO_2) emitted to the atmosphere during the delivery of a unit of energy of fuel to the final recipient:

$$e_{NG} = \sum e_i = \sum(\xi_i \cdot GWP_i \cdot \varepsilon_i) \tag{2}$$

where:

- e_{NG} Cumulative emission of greenhouse gases per delivery of a unit of chemical energy of natural gas, (Mg CO_2/TJ),
- e_i Specific emission of greenhouse gases in *i*-th link of delivery process (per unit of chemical energy of delivered natural gas), (Mg CO_2/TJ),
- ξ_i Unit emission of a greenhouse gas per a unit of chemical energy of fuel utilized in *i*-th link of delivery process, (Mg gas/TJ),
- GWP_i Global warming potential of a greenhouse gas emitted in *i*-th link of delivery process, (Mg gas/ Mg CO_2).

Carbon dioxide, as a reference substance, has *GWP* = 1. Global warming potential of methane is debatable. It is usually assumed at the level of 21, but recent studies imply that its value gradually increases over time, as its concentration in atmosphere gets higher [7]. In this paper it was assumed to be equal to 28 [22]. Direct emission of CO_2 from combustion of natural gas equals to 56 Mg per TJ.

4.1 Pipeline transport from Russia

Russian natural gas is transported to Poland via the Yamal-Europe pipeline. It runs from natural gas fields near Yamal Peninsula to Germany, through Minsk (Belarus) and central-northern Poland. Its length is 3075

km and pressure is maintained by 23 compressor stations [7]. The fuel consumption per compressor station, resulting from the analysis in [12], is 0.18% of natural gas flowing into the station. Using this value to calculate the total fuel consumption coefficient for compression ε_{comp} results in 4.23%. It is a probable value, since the total gas consumption in the Russian transmission system is estimated as 6% [11,23] and an optimization of energy consumption in a similar pipeline presented in [24] returned a result of 3.5%. However, a different study assumed that 0.33% of transported natural gas is consumed for each 100 km [25]. If this value is multiplied by the length of Yamal-Europe pipeline, ε_{comp} results in 11.3%, which is significantly higher.

The amount of methane leaking during transport and storage is difficult to quantify. The estimates are usually included in the range up to a few percent of throughput and can be as small as 0.7%–0.9% [25,26] or as high as 4% [27]. Other studies estimate the leakages (ε^*_{leak}) to be between 1.4% and 3.6% [28].

Note that the indicators such as energy consumption and leakages are usually presented in the literature as a percentage of gas inflow. For the purpose of this study, they need to be recalculated in reference to outflow, using the following equation:

$$\varepsilon_i = \frac{1}{1-\varepsilon_i^*} - 1 \tag{3}$$

where:

ε_i^* Specific consumption of primary energy in *i*-th link of delivery process (per unit of chemical energy of input natural gas), (TJ/TJ).

4.2 LNG transport from Qatar

As stated before, the work input in AP-C3MR liquefaction method is 1.2 MJ per kg of natural gas [18]. This value however needs to be recalculated to primary energy, considering the energy efficiency of compressor drivers. In most cases, gas turbines or combined cycles fueled with natural gas are used. Their efficiency may vary between 30% (for small gas turbines) and 60% (for combined gas-steam cycles) [13]. The coefficient of primary energy consumption for NG liquefaction ε_{liq} is therefore in the range 4.4÷8.9%, depending on the energy efficiency.

LNG carriers consume fuel for propulsion and driving the ship's auxiliary equipment. Q-Flex vessels (the ones that deliver LNG from Qatar to Poland) are equipped with an on-board reliquefaction installation to avoid losses of the cargo. This system contributes greatly to the overall fuel consumption of the ship. Analysis presented in [29] proves that the average fuel consumption with the BOG reliquefaction installation running is 6300 kg of marine diesel oil per hour, while the average fuel consumption with this installation turned off (in the case of return trip) is 4856 kg/hour. The voyage (via Suez Canal) takes 21 days. Taking the ship capacity as 216,000 m^3, the lower heating value (LHV) of marine diesel oil as 39.9 MJ/kg [30] and the LHV of LNG as 45 MJ/kg, the coefficient of primary energy consumption for LNG shipping ε_{ship} takes the value of 4.95%. This value includes both the delivery and return trips. The unit emission of CO_2 per a unit of chemical energy of marine diesel oil was assumed as 80 kg per GJ [31].

Regasification of LNG by the SCV method involves combustion of a small portion of regasified LNG, about 1.46% [32]. This value should be recalculated considering the induced additional upstream consumption (since some of the delivered fuel is used at the receiving terminal, more of it needs to be processed and delivered per unit of fuel at the end of the delivery process). This is done using the following equation:

$$\varepsilon_{regas} = \varepsilon_{regas\,0} \cdot \left(1 + \varepsilon_{ship} + \varepsilon_{liq}\right) \tag{4}$$

where:

$\varepsilon_{regas\,0}$ Specific consumption of primary energy for regasification in a local balance boundary, (TJ/TJ),

ε_{regas} Specific consumption of primary energy for regasification in a global balance boundary (TJ/TJ).

Such calculations result in a value ε_{regas} = 1.68%. The consumption of electric energy and resulting consumption of primary energy in a LNG regasification terminal is small compared to energy consumption (and its uncertainty) in other stages of the delivery chain, therefore it was neglected in this analysis.

5. Results of analysis

Figure 5.1 compares the two methods of transport of natural gas by the value of coefficient of cumulative consumption of primary energy. Figure 5.2 compares the specific emissions of greenhouse gases. Two variants are presented for both methods – optimistic and pessimistic. The optimistic variant assumes higher efficiency of compressor stations (for pipeline transport) or liquefaction installations (for LNG) and lower leakages during pipeline transport. The pessimistic variant assumes the opposite. Boundary values are presented in previous subchapters. Therefore, the actual consumption of primary energy and emission of GHG are likely to be in the range specified by the two variants.

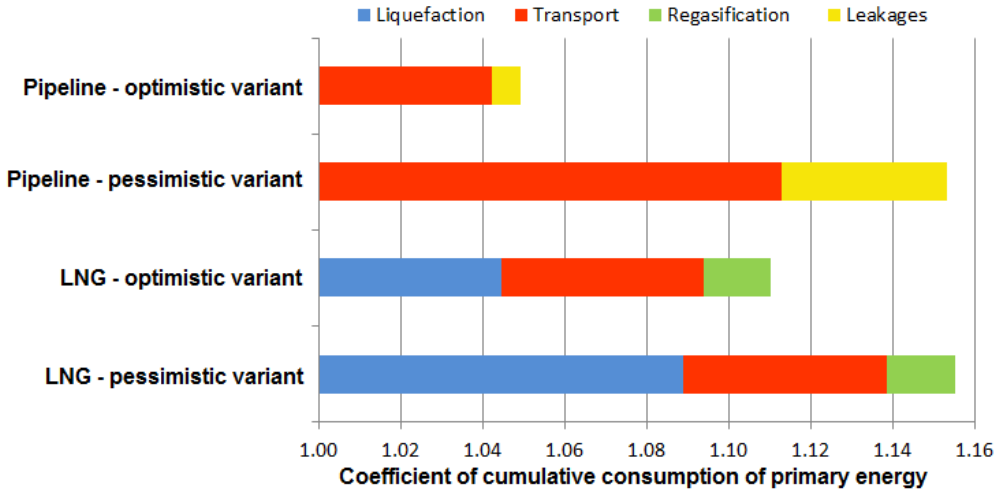

Fig. 5.1. Comparison of energy intensity of methods of transport of natural gas

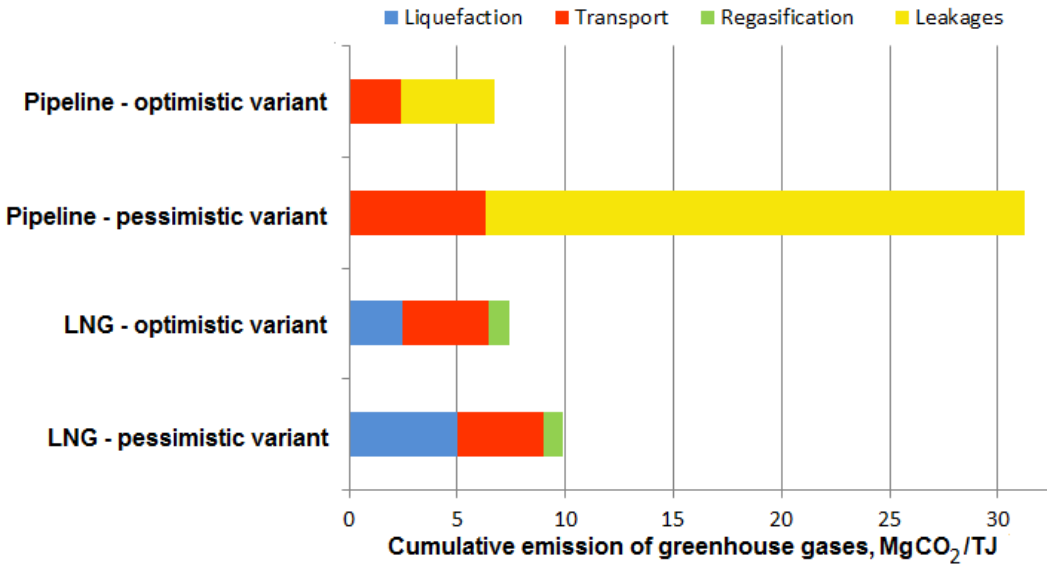

Fig. 5.2. Comparison of GHG emissions resulting from transport of natural gas

Value of w_{NG} fits in the range 1.05–1.15 for pipeline transport and 1.11–1.16 for LNG transport. A conclusion from these results is that transporting natural gas in liquefied form is most likely more energy intensive than transporting via pipelines. Therefore, it would be advisable to lower the cumulative energy consumption by recovering some of the cryogenic energy of LNG during the regasification process. Value of e_{NG} fits in the range 6.7–31.2 Mg CO_2/TJ for pipeline transport and 7.4–9.9 Mg CO_2/TJ for LNG transport. Due to high value of *GWP* for methane, leakages play a great role in the GHG balance and drive up the value of e_{NG}. Carbon footprint of pipeline transport in the optimistic scenario is at the same level as for LNG transport, but much higher if the pessimistic scenario (high leakages) is considered.

Note that the coefficients w_{NG} and e_{NG} are a function of distance between the source of natural gas and the recipient, so the results of analysis for other countries may be different from these presented in this paper.

6. Summary

In the present work, the process of delivering natural gas from deposit to recipient was discussed. Each link of the delivery chain requires an energy input. An attempt was made to evaluate the energy intensity and environmental impact of importing natural gas for the case of Poland by using elements of life cycle assessment. Two methods of transport were compared: trunk pipelines (gas from Russia) and LNG (gas from Qatar).

The data given in literature differs greatly and is burdened by uncertainties, therefore two variants were calculated: an optimistic one in which the energy intensity and losses are assumed at the lower limit, and pessimistic one, which assumes the opposite. Obtained results suggest that transporting natural gas as LNG requires a higher energy input than transporting it via pipelines. The coefficient of primary energy consumption is at the level of 1.05–1.15 for pipeline transport and 1.11–1.16 for LNG transport. There are however possibilities to improve the energy efficiency natural gas transport, especially for the case of LNG. Liquefaction is a very energy-consuming process. A portion of energy utilized in this process gets stored in LNG and can be recovered during regasification, though usually it is just released to the environment. Such energy recovery, for example in the form of production of electric energy, may significantly improve the outlook of LNG against pipeline transport.

On the other hand, the emissions of greenhouse gases are comparable for both methods, or even higher for pipeline transport. They take a value of 6.7–31.2 Mg CO_2 per TJ of chemical energy of delivered fuel for pipeline transport and 7.4–9.9 Mg CO_2/TJ for LNG transport. Large values for pipeline transport are due to methane leakages from pipelines, as methane has much higher global warming potential than carbon dioxide. When related to the stoichiometric emission of carbon dioxide from combustion of natural gas, it turns out that the actual emission is 12–55.7% higher for pipeline transport and 13.2–17.7% higher for LNG transport. These results confirm the incorrectness of evaluating the “eco-friendliness” of fuels just by the emission of CO_2 resulting from combustion stoichiometry.

References

[1] Kyoto Protocol to the United Nations Framework Convention on Climate Change. Available at: <http://unfccc.int/resource/docs/convkp/kpeng.html> [accessed 28.11.2019].

[2] Paris Agreement within the United Nations Framework Convention on Climate Change. Available at: <https://treaties.un.org/doc/Treaties/2016/02/20160215%2006-03%20PM/Ch_XXVII-7-d.pdf> [accessed 28.11.2019].

[3] European Commission. The EU Emissions Trading System. Available at: <https://ec.europa.eu/clima/policies/ets_en> [accessed 28.11.2019].

[4] Hausfather Z., Bounding the climate viability of natural gas as a bridge fuel to displace coal. Energy Policy 2015;86:286-294.

[5] Faramawy S., Zaki T., Sakr A.A.-E., Natural gas origin, composition, and processing: A review. Journal of Natural Gas Science and Engineering 2016;34:34-54.

[6] Marzec A., Carbon dioxide emission from fossil fuels; major component of greenhouse gases. Polish Journal of Applied Chemistry 2002; XLVI:143-149.

[7] Stanek W., Białecki R., Can natural gas warm the climate more than coal? Fuel 2014;136:341-348.

[8] Khan M. I., Comparative Well-to-Tank energy use and greenhouse gas assessment of natural gas as a transportation fuel in Pakistan. Energy for Sustainable Development 2018;43:38-59.

[9] Busch C., Gimon E., Natural gas versus coal: is natural gas better for the climate? The Electricity Journal 2014; 27:97-111.

[10] Wood D.A., Natural gas imports to Europe: The frontline of competition between LNG and pipeline supplies. Journal of Natural Gas Science and Engineering 2016;36:A1-A4.

[11] Albutov A., Reducing energy consumption through optimization of the operating conditions of the gas trunk pipeline [Master of Science thesis]. Stockholm, Sweden: KTH School of Industrial Engineering and Management; 2013.

[12] Chaczykowski M., Osiadacz A.J., Uilhoorn F.E., Exergy-based analysis of gas transmission system with application to Yamal-Europe pipeline. Applied Energy 2011;88:2219-2230.

[13] Mokhatab S., Mak J., Valappil J., Wood D., Handbook of Liquefied Natural Gas. Gulf Professional Publishing, Houston (2013).

[14] Mazyan W., Ahmadi A., Ahmed H., Hoorfar M., *Market and technology assessment of natural gas processing: A review.* Journal of Natural Gas Science and Engineering 2016;30:487-514.

[15] Foss M. M., Introduction to LNG - An overview on liquefied natural gas (LNG), its properties, organization of the LNG industry and safety considerations. Center for Energy Economics, Austin (2007).

[16] International Gas Union, 2019 World LNG report**.** Available at: <https://www.igu.org/sites/default/files/node-news_item-field_file/IGU%20Annual%20Report%202019_23%20loresfinal.pdf> [accessed 28.11.2019].

[17] Khan M.S., Karimi I.A., Wood D.A., Retrospective and future perspective of natural gas liquefaction and optimization technologies contributing to efficient LNG supply: A review. Journal of Natural Gas Science and Engineering 2017;45:165-188.

[18] Bin Omar M.N., Thermodynamic and economic evaluation on existing and prospective processes for liquefaction of natural gas in Malaysia [dissertation]. Berlin, Germany: Technischen Universität Berlin; 2015.

[19] Główny Urząd Statystyczny, Energia 2018**.** Available at: <https://stat.gov.pl/files/gfx/portalinformacyjny/pl/defaultaktualnosci/5485/1/6/1/energia_2018.pdf> [accessed 28.11.2019].

[20] Polskie Górnictwo Nafrowe i Gazownictwo S.A. Sprawozdanie Zarządu z działalności PGNiG S.A. i Grupy Kapitałowej PGNiG za rok 2018. Available at: <http://pgnig.pl/documents/10184/2580770/PGNiG_w_liczbach_2018_.pdf/6018f517-41da-4fc2-b15c-385118563764> [accessed 28.11.2019].

[21] Polskie LNG, Projekt terminalu LNG Świnoujście – Streszczenie nietechniczne. Szczecin (2010).

[22] Intergovernmental Panel on Climate Change, Climate Change 2014 – Synthesis Report. Available at: <https://www.ipcc.ch/site/assets/uploads/2018/05/SYR_AR5_FINAL_full_wcover.pdf> [accessed 28.11.2019].

[23] Gazprom, Gazprom in figures 2008–2012 – Factbook. Available at: <https://www.gazprom.com/f/posts/77/194006/gazprom-reference-figures-2008-2012-eng.pdf> [accessed 28.11.2019].

[24] Liu E., Li C., Yang Y., Optimal energy consumption analysis of natural gas pipeline. The Scientific World Journal 2014.

[25] Lechtenböhmer S., Dienst C., Future development of the upstream greenhouse gas emissions from natural gas industry, focusing on Russian gas fields and export pipelines. Journal of Integrative Environmental Sciences 2010; 7:39-48.

[26] Dedikov J.V., Akopova G.S., Gladkaja N.G., Piotrovskij A.S., Markellov V.A., Salichov S.S., Kaesler H., Ramm A., Müller von Blumencron A., Lelieveld J., Estimating methane releases from natural gas production and transmission in Russia. Atmospheric Environment 1999; 33:3291-3299.

[27] Reshetnikov A.I., Paramonova N.N., Shashkov A.A., An evaluation of historical methane emissions from the Soviet gas industry. Journal of Geophysical Research 2000; 105:3517-3529.

[28] Howarth R.W., Santoro R., Ingraffea A., Methane and the greenhouse-gas footprint of natural gas from shale formations. Climatic Change 2011;106:679-690.

[29] Adamkiewicz A., Cydejko J., The influence of energy consumption of gas vapour reliquefaction on the structure of the LNG carrier power plant. Naše More 2016;63:38-42

[30] American Bureau of Shipping, Notes on heavy fuel oil. Houston (1984).

[31] Intergovernmental Panel on Climate Change, Good practice guidance and uncertainty management in national greenhouse gas inventories. Montreal (2000).

[32] Simla T., Wykorzystanie egzergii kriogenicznej skroplonego gazu ziemnego do produkcji energii elektrycznej. Archiwum Instytutu Techniki Cieplnej 2016;1:113-151.

Modern district heating network for urban area with blocks of flats supported by a renewable energy source

Wiktoria Franiel [1]

[1]*Department of Energy and Environmental Engineering, Silesian University of Technology, e-mail: wiktoriafraniel@gmail.com*

Abstract

The work focuses on proposition of new modern heating network in the place of an old outdated one. The existing network in chosen urban in the Silesia region, Poland can be described as of the second generation of district heating. The chosen area is 13 blocks of flats with the heat supplied by a Cogeneration Plant built in the fifties of the last century and distributed over unnecessarily long distances. After analysis of the region, available space and other conditions, the next step was incorporation of an idea of a renewable energy source share increment in the heat production. Such actions can be treated as the introduction of some ideas from the concept of the Fourth Generation of District Heating that appeared in Denmark. It was treated as a role model and the proposed changes are result of its assumptions.

Keywords: Heating network, renewable energy source, district heating, solar energy, 4th Generation District Heating

1. Introduction

The paper concerns design of the heating network that ultimately aims to be of the 4th Generation of District Heating (4GDH). The current heating network supplying the buildings of interest is of the outdated technology. Heat is supplied by a Cogeneration Plant built in the fifties of the last century [1]. The length of the heating network is high therefore supplying water temperature is way above 100°C. The design of small distributed heating network will enable lowering the working medium temperature and usage of modern technical solutions. For that purpose, the analysis of the chosen area was performed - the factors influencing the network's final design and parameters. Later, the calculations of heat demand for one flat and whole considered neighborhood were made. Based on those and considering other factors, like e.g. available space, a renewable energy source was chosen to support the heating network by production of extra heat. This made the designed system more independent of fossil fuels. The following part considers how much heat can a renewable energy source supply and rough assessment of its profitability. As an addition, the calculation of design mass flow rate and then estimation of fluid's velocity, pressure losses and pipes dimensions were performed.

The discussion on other profits than those economical is also a very significant topic nowadays. Renewable energy sources' contribution to lowering the emission and savings of the fossil fuels is undeniable. Implementation of such network would be a huge step forward with modernization of existing networks towards 4th Generation District Heating, which is the direction the heating networks should be heading. The project is aimed at presentation of the problems of polish heating systems and showing the direction in which, they should be modernized on an example of small-scale application.

2. Generations of district heating

District heating can be simply defined as a network of pipes distributing produced heat within a centrally controlled system. One such network can include a few buildings or whole cities depending on the initial design. The basic idea of such system is to provide space and water heating to households. In Poland such

sources are mainly coal-fired Heating Plants or sometimes Combined Heat and Power Plants [2]. Currently, the tendency of District Heating development includes increasing the share of heat recovery from waste and heat production in Combined Heat and Power Plants (CHP). While those are being gradually realized, number of installed renewable energy systems to support efficient heating networks should also increase. To fully understand the characteristics of heating systems, there were distinguished four separate generations of district heating and cooling. [3] [4]

2.1. First generation

The first generation started in the 80s of 19th century in in the city of New York, when the idea of replacement of small apartment boilers with a common heating system appeared. Furthermore, steam was a heat carrier in the 1st generation networks. Those systems were not efficient enough, and the risk of malfunction or accident was very high. Example of such a solution is up to this day in the city of Paris. As for the polish heating systems, steam as a medium is used almost only in the industrial sector - this is due to very small distribution distances requirement. Another way of utilizing steam is for residential heat transportation but also over very small distances, meaning up to 3 kilometers in Poland and only when pressure is above 0.17MPa, those requirements are justified mainly by the heat losses. [5]

2.2. Second generation

The idea of water as a more efficient and safer heat carrier began the 2nd generation of district heating. The water was pressurized, and its temperature was over 100°C [5]. A huge drawback of this concept was the lack of any control system. Many such technologies were implemented in the former USSR, which included polish systems built mostly between the 30s and 70s of the last century. Based on the temperature of the working medium as the most important indicator, polish district heating systems can be mostly classified as the second-generation systems. Those networks are usually not well-distributed, and they transport heat over relatively long distances. For mentioned distances and significant heat demands, there is commonly used water with the maximal temperature of 150°C [5]. According to the tendencies in all processes of modernization of district heating, the temperature of heating water in Poland is currently being lowered typically to 130°C [5]. For distances smaller than 0.5km water of around or less than 115°C can be used [5]. The big concern is also the lack of flexibility of water systems when it comes to changing and adjusting loads, but on the other hand, it is much cheaper than a steam system and almost insensitive to corrosion. [5]

2.3. Third generation

“Scandinavian district heating technology” is the main term referred to when talking about the third generation. The very important feature of this technology is water temperature below 100°C. Many such solutions were developed in Scandinavia, among which there are modern pipes insulation or no concrete ducts for the pipes. For such solutions there are widely used plastic pipes, instead of those made of steel [4]. Since the 70s and 80s, the third-generation technology is the most popular solution in new installations in such regions as China or America. All the replacements on the areas of the former USSR systems were done with Scandinavian technology. This means that the main Polish improvements in district heating were done based on adapting the second generation’s systems into Scandinavian solutions [5]. The borders between generations are sometimes not too clear, but it can be said that in the 3rd generation the CHP concept was significantly enhanced, but it is supposed to be utilized since the second generation. Visible trends can be pointed out for the future: efficiency will be the crucial parameter, the temperature of the working medium will be decreasing, and more automated and flexible systems will be chosen.

2.4. The Fourth Generation of District Heating

The Fourth Generation District Heating (4GDH) concept first appeared in Denmark and “is defined as a coherent technological and institutional concept, which using smart thermal grids assists the appropriate development of sustainable energy systems. 4GDH systems provide the heat supply of low-energy buildings with low grid losses in a way in which the use of low-temperature heat sources is integrated with the

operation of smart energy systems. The concept involves the development of an institutional and organizational framework to facilitate suitable cost and motivation structures" [6]. This led to the formation of the set of five points that should be fulfilled by a heating system to be of the 4th generation:

"1. Ability to supply low-temperature district heating for space heating and domestic hot water (DHW) to existing buildings, energy-renovated existing buildings and new low-energy buildings.
2. Ability to distribute heat in networks with low grid losses.
3. Ability to recycle heat from low-temperature sources and integrate renewable heat sources such as solar and geothermal heat.
4. Ability to be an integrated part of smart energy systems (i.e., integrated smart electricity, gas, fluid, and thermal grids) including being an integrated part of 4th Generation District Cooling systems.
5. Ability to ensure proper planning, cost and motivation structures about the operation as well as to strategic investments related to the transformation into future sustainable energy systems. [4]"

Such systems should be flexible and sustainable. Big role in 4th Generation heating systems play renewable energy sources. This is a huge challenge for polish heating systems and implementation of newest solutions in systems should start as soon as possible, starting with a realistic scale projects to gradually invest in implementation of all aspects of 4GDH.

3. Region's description

Poland has a well-developed district heating system with one of the longest heating networks in Europe. According to [7] its length was 20745km in 2016 with visible development in length over past years. Taking a closer look, there can be noticed that the Silesia voivodship has the longest heating network in Poland - 3321km, while Mazowieckie voivodship with capital city of Warsaw in on the second place with 3026km in length [7]. Despite having very similar network lengths, those regions are different in one significant way. Mazowieckie voivodship is an owner of much more concentrated network, its center is in Warsaw, while all the other cities are much smaller (only 3 cities in total with more than 100000 inhabitants), therefore with shorter networks. In Silesia region there are 12 cities with more than 100000 inhabitants [8], resulting in much more evenly distributed heating networks.

One of such cities is Ruda Śląska, a city based on hard coal mining and its industry. The chosen district is of 13 blocks of flats located in the busy area with hardly any available green space. Each block has 40 flats with assumed 3 people per flat on average. This gives 520 flats with 1560 people total. The insulation is in poor condition and blocks are rather old. Surface area of a single flat is assumed to be 61m^2. The central heating is provided by Węglokoks Energia ZCP Sp. z o.o getting heat from CHP Plant "Mikołaj" in Ruda Śląska. The heating network can be classified as the second generation of district heating. Hot water is not provided by a network but is heated up in individual gas water heaters. The only available free space is one bigger area in the north direction from the neighbourhood. Those are post-mining areas. They can be described as small hills directed onto the South. There is no cooling network or renewable energy sources involved in heat production.

As can be seen on the map below, the blocks are numbered I-XIII. The available space is hatched and is limited by residential streets and old non-working railway (from north direction). The area of mentioned spot is about 8115m^2. The bold black lines represent the proposed new small, distributed heating network. As it can be noticed, it is not independent, but connected to the municipal heating network. This is due to unpredictability of the renewable energy sources and other factors. The habitants must be supplied at all times regardless of the meteorological conditions. In this area there are many other networks, such as electricity or gas, that cannot be omitted and during the design of the path of new heating network, the effort was made not to interfere with any existing networks. As this goal is practically unachievable, the heating network was designed to have as small impact on the neighborhood as possible.

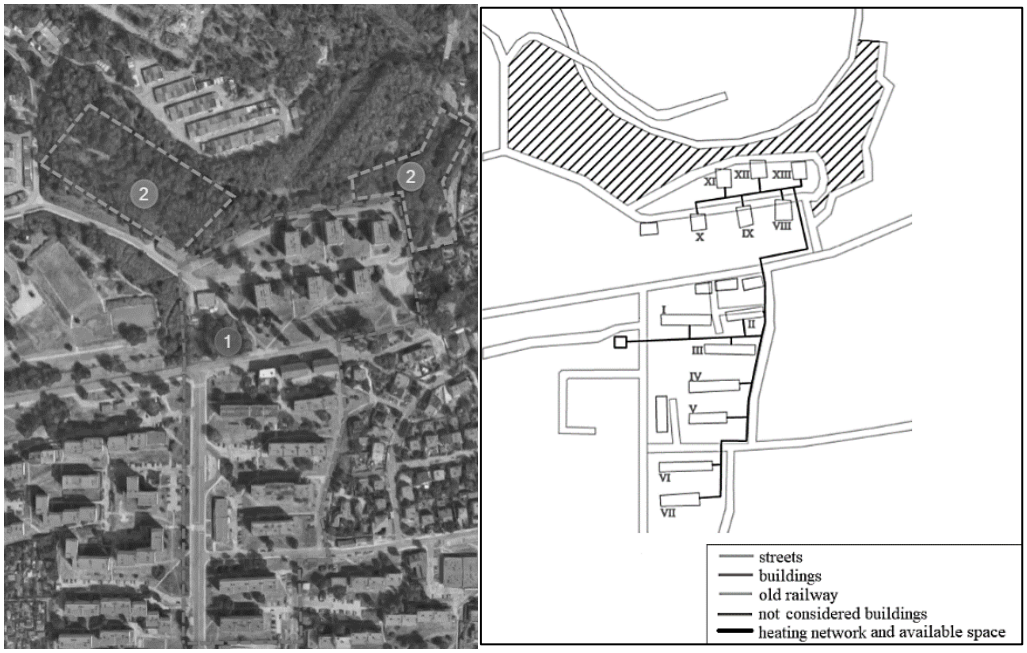

Figure 3.1. Map of the neighborhood (1 – Chosen urban area; 2 – Available space) [9];

Figure 3.2. Schematic representation of the area, blocks and heating network proposed [10].

4. Renewable energy sources and ecological aspects

Renewable energy sources are necessary to be implemented on much higher scale if the society wants to reduce the global carbon footprint, as well as solve more local problems, that are present in an excessive amount both in the whole Poland and also specifically in the Silesia voivodeship. Although most of the polish cities are connected to the heating networks, some of the buildings that are not, cause a lot of pollution, primarily to air. Also, many mines, industrial institutions and power plants of outdated technology exist and produce a lot of harmful substances. In Poland many of the environmental problems are significantly enhanced compared to European Union. The biggest source of smog and pollution are individual heat sources – the domestic coal-fired boilers of the previous generations. Also, the big trouble is people's awareness. Many households not only burn low quality fuel, but even throw old clothing, plastics and tires into their furnaces. District heating networks are also problematic themselves. Most of them are of the outdated technology from previous generations and in need to be adapted to the newer standards. Renewable energy sources are expected to play much bigger role in the newest solutions in district heating. It is a great opportunity for Poland to increase the share of renewables and meet EU requirements.

For the case where there is almost no open space, but we want to support the heating network with renewable energy source, the solar collectors seem to be the best choice. Flat plate type collectors are the most popular solar collectors, because of their efficiency, durability and relatively low cost. Such systems' payback time is shorter than evacuated tube collectors and they are preferably used in the climates where air temperature can go below zero. Their life span is up to even 30 years. [11] One can also try to receive a government's financial support or funding for production of energy from renewable energy source.

There are various reasons for rejection of other renewable sources. Firstly, any kind of biomass is unavailable in the area of interest and its transportation for long distance is highly unprofitable. Wind turbines require much more space and distance of 1km from urban area, which is impossible to realize in chosen neighborhood. Also, gas engine would be a bad choice, due to availability of other natural resources, such as hard coal, and the social aspect of most people in Silesia working in the mining industry.

5. Results

The choice of the solution for the selected area could not happen without knowing the needs of the neighborhood. This is why the calculations of the heat demand for: space heating, ventilation and domestic hot water were performed based on [12]. This enabled the creation of ordered graphs for heat demands, calculation of specific design and annual heat demands, design mass flow rates and hydraulic parameters choice.

5.1. Graphs of heat demand

The heat demand characteristics, where heat demands are firstly the function of time and then of the outside air temperature, is created to show the heat demands dependencies profiles in an ordered manner. They also clearly show the values for the peak demands.

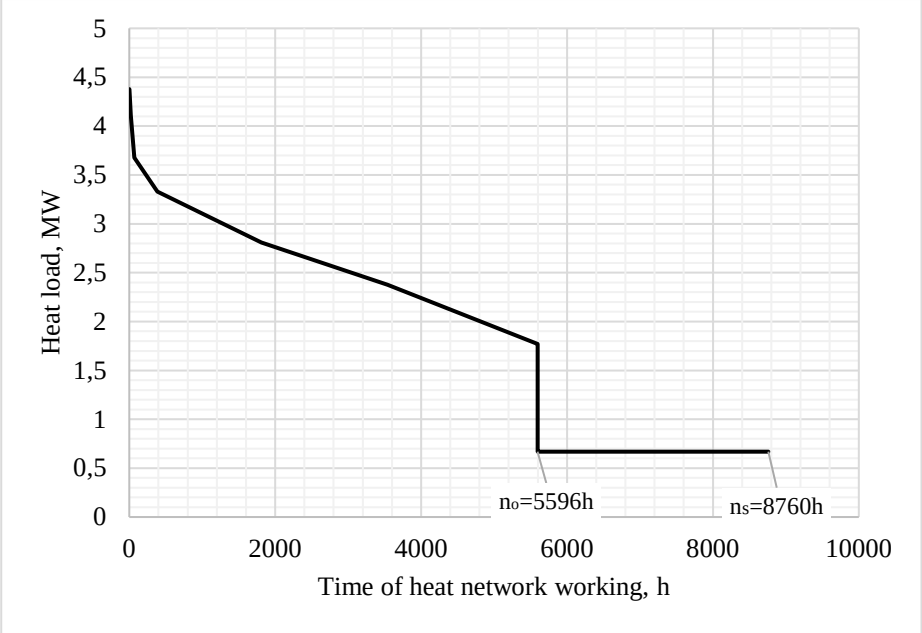

Figure 5.1. Ordered graph of heat demand

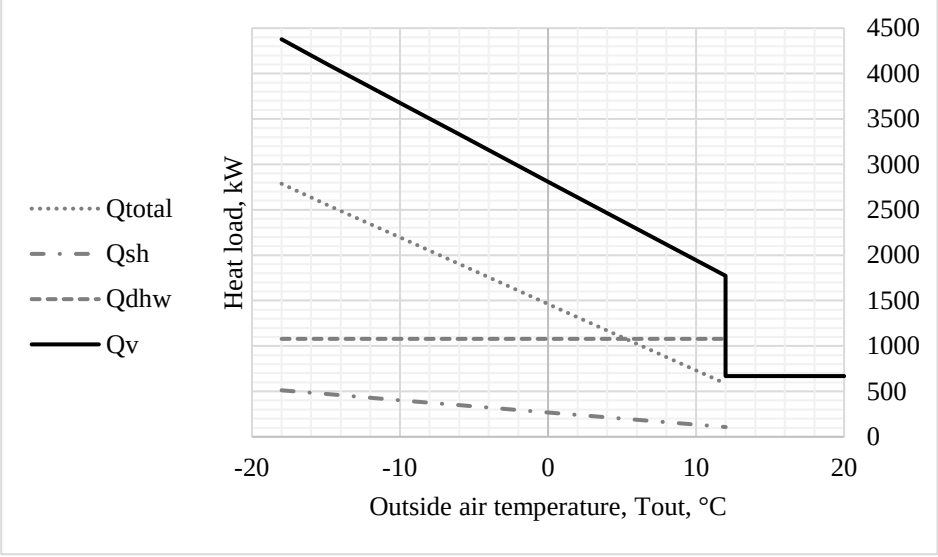

Figure 5.2. Annual graph of heat demand

5.2. Heat demand

The design heat demands results presented in the table below inform about the values for which the network must be designed. The average and annual values in the next table give a wider perspective about the habitants' needs.

Table 5.1. Design heat demand

Heat demand for:		Symbol	One flat		Whole neighborhood (520 flats)	
			Unit	Value	Unit	Value
Space heating		$\dot{Q}_{sh_{max}}$	kW	5.63	MW	2.92
Ventilation		$\dot{Q}_{v_{max}}$	kW	1.03	MW	0.54
Domestic hot water	heating season	$\dot{Q}_{dhw_{max}}$	kW	2.07	MW	1.08
	summer	$\dot{Q}_{dhw}^{summer}$	kW	1.29	MW	0.67
Sum for the heating season		$\dot{Q}_{tot_{max}}$	**kW**	**8.73**	**MW**	**4.54**

Table 5.2. Average and annual heat demands

Parameter	Symbol	Unit	Value
Average heat demand for space heating	$\dot{Q}_{sh}^{avg}$	kW	2.42
Annual heat demand for space heating for 1 flat	$\dot{Q}_{sh}^{annual}$	GJ	49.02
Annual heat demand for space heating for neighbourhood	$\dot{Q}_{sh,all}^{annual}$	GJ	25492.47
Annual heat demand for domestic hot water for neighbourhood	$\dot{Q}_{dhw}^{annual}$	GJ	8908.29

5.3. Mass flows and hydraulic parameters

To design a heating network, a hydraulic approximate calculation was performed. The information about mass flow rates in table 7 are needed to further estimate the basic hydraulic parameters, like pipes dimensions, pressure drop and velocity of water.

Table 5.3. Design mass flow rates of water

Parameter	Symbol	Unit	Value
Design mass flow rate of water for space heating	$\dot{G}_{w_{sh}}$	$\frac{kg}{s}$	11.64
Design mass flow rate of water for ventilation	$\dot{G}_{w_v}$	$\frac{kg}{s}$	2.14
Design mass flow rate of water for domestic hot water	$\dot{G}_{w_{dhw}}$	$\frac{kg}{s}$	7.35
Total design mass flow rate of water	$\dot{G}_w$	$\frac{kg}{s}$	21.13

Table 5.4. Hydraulic parameters values

Parameter	Symbol	Unit	Value
Unit pressure drop	R	kPa	0.098
Diameter of a pipe	d	mm	219
Thickness of a pipe	δ	mm	6
Velocity of water	v	$\frac{m}{s}$	1.3

5.4. Solar collectors analysis

The analysis of the solar irradiation, available space, technologies and other important aspects were later performed. This led to calculation of the total power gained from collectors and finally rough estimation of the average level of the heat demand that can be covered by the solar collectors alone (both in summer and during the heating season).

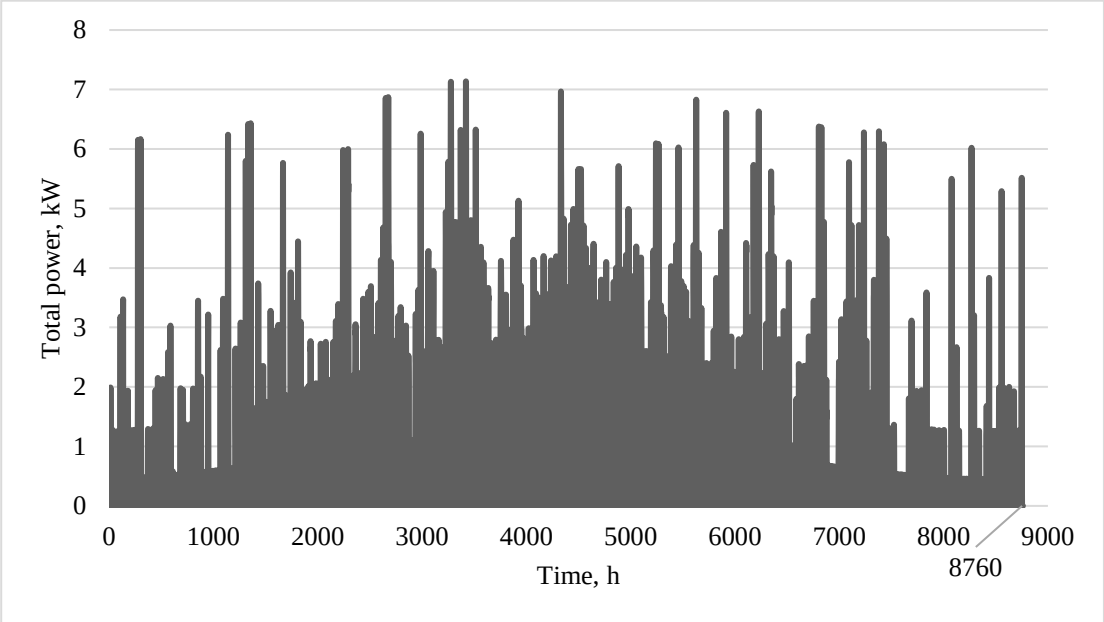

Figure 5.3. Total power from solar collectors

Table 5.5. Solar collectors' calculations results

Parameter		Symbol	Unit	Value
Area available		A	m^2	8114.82
Number of collectors		N_{sc}	-	3512
Average total power		$\dot{Q}_{sc}^{avg}$	MW	0.81
Maximal total power		$\dot{Q}_{sc}^{max}$	MW	7.14
Average level of heat demand covered	Heating season	η_{hs}	%	17.92
	summer	η_{summer}		121.70

6. Conclusions

The district heating networks existence is not enough to handle the environmental and social problems connected with heating systems in Poland. The role model for the nearest future of polish district heating should be e.g. Denmark with its well-developed district heating systems where many of them are already of the fourth generation. They are distributed, automated, supported by renewables and with significantly lowered working medium temperature, to name a few. This branch of Power Engineering has many great

opportunities to implement the newest available solutions. Thanks to those, the share of renewables can significantly rise in the overall energy sources structure.

In the city of Ruda Śląska there are hardly any renewable energy sources utilized to produce any form of energy. Certainly, there is no bigger heating network supported by renewables. The proposed small, distributed heating system enabled implementation of solar energy as the support for residential grid. The discussed area of 13 blocks received a new heating network and thanks to its short length and small number of receivers, the losses and temperature of working medium can be lowered in a significant way.

The design heat demand for the whole district is 4.54MW. This is not an enormous value, which justifies why such system was decided to be supported by the solar collectors' installation. The available free space was on the very favorably angled hill and the amount of sunshine received is optimal. Such solution gave almost 18% of heat demand covered on average during winter and over 120% during summer, when only domestic hot water is needed. Those are averaged values, which means that there were times with no solar irradiation noted and times with more than 7MW produced. In conclusion to this part, in winter in the polish climate, the support of the collectors with classical residential grid is necessary to ensure the habitants are always supplied with sufficient amount of heat. It is the other way around during summer season, when there can be noticed the excess of heat on average, which means that on sunny days, the heat could be sold to the national grid and the payback time of solar installation could gradually shorten. If this solution turns out to be not optimal, the heat storage should be taken into consideration. The energy storage is a very trendy topic and with good solutions chosen for the mentioned neighborhood, it could become even more independent on the grid and move significantly towards 4GDH.

The weather data used for the purpose of calculations are all averaged values and, for example, the solar irradiation is a very unstable energy source. This means, that in conclusion, except for the network itself, the system needs high level of automation and control. The traditional residential heating network must be prepared for load variations; therefore, it is highly recommended not only to modernize the networks themselves, but power plants too. The concept of Fourth Generation of District Heating assumes that already before implementation of renewables and development of smart grids, the classical heat and power sources are power plants and cogeneration plants of a high efficiency and modern solutions. The existing heating networks should be equipped with more efficient pipes prepared for heat transport over small distances and low water temperature. The biggest challenge for already existing polish networks is adjustment to transport different loads levels over small distances.

To sum up, the idea of a distributed heating network for small area with blocks of flats is a useful and beneficial concept. The implementation of such system would decrease the carbon footprint, emissions connected with poorly organized combustion and slow down the process of depletion of fossil fuels. Although it is a rather costly project, the growth of share of renewable is necessary to meet the EU requirements. This kind of an idea should be implemented in as many areas in Poland as possible.

References

[1] "Węglokoks Energia ZCP - Nasze Ciepłownie," [Online]. Available: http://weglokoksenergia.pl/zcp/pl/nasza-firma/nasze-cieplownie.

[2] "Heat generation by fuel," 2016. [Online]. Available: https://www.iea.org/statistics/?country=POLAND&year=2016&category=Key%20indicators&indicator=HeatGenByFuel&mode=chart&categoryBrowse=false&dataTable=ELECTRICITYANDHEAT&showDataTable=true.

[3] S. Werner, „International Review of District Heating and Cooling," *Elsevier, no. Energy*, nr 137, pp. 617-631, 2017.

[4] H. Lund, W. S. R. Wiltshire, S. Svendsen, J. E. Thorsen, F. Hvelplund and B. V. Mathiesen, „4th Generation District Heating (4GDH), Integrating smart thermal grids into future sustainable energy systems," *Elsevier, no. Energy,* nr 68, pp. 1-11, 2014.

[5] J. Szargut and A. Ziębik, Podstawy Energetyki Cieplnej, Warszawa : Wydawnictwo Naukowe PWN, 2000.

[6] "Definition of 4th Generation District Heating," [Online]. Available: http://www.4dh.eu/about-4dh/4gdh-definition.

[7] A. Buńczyk, "Energetyka Cieplna w liczbach – 2016," Urząd Regulacji Energetyki (URE), Warszawa, 2017.

[8] J. Stańczak, A. Znajewska and A. Daniłowska, Population in Poland. Size and structure by territorial division, Główny Urząd Statystyczny, Warszawa, 2014.

[9] [Online]. Available: https://www.google.pl/maps/

[10] [Online].
Available: http://rudaslaska.geoportal2.pl/map/www/mapa.php?CFGF=wms&mylayers=+granice+OSM

[11] Kolektory słoneczne płaskie [Online]. Available: http://www.kolektory.com/kolektory-plaskie.html.

[12] A. Szkarowski and L. Łatowski, Ciepłownictwo, Warszawa 2006: Wydawnictwo WNT, 2012.

Influence of climate change on soil organic carbon

Aneta Kowalska [1]

[1]*Faculty of Infrastructure and Environment, Czestochowa University of Technology, e-mail: aneta.kowalska@pcz.pl*

Abstract

Soil organic carbon (SOC) is one of the most important parameters which determines soil ecosystem quality and highly influences the plant biomass growth and development, and thus, the food availability. The sources of organic carbon in the soil are mainly residues of living organisms that are being decomposed by microorganisms, but also the carbon sequestration from the atmosphere. Soil carbon sequestration is mainly carried out in the process of photosynthesis where carbon dioxide consists a substrate and may contribute in a huge scale to the mitigation of climate change. Nowadays, progressive climate change consists one of the most important concern which affects all ecosystem compartments. The temperature is limiting agent for environmental processes, thus, increasing average temperature observed in the last years is increasing. The increasing mean temperature in the global scale may intense mineralization of SOC lowering the SOC stock and changing soil quality. Global warming alters soil microbial community and its functioning thus influencing mineralization of SOC by alternation in C use by microbes. Also changes in precipitation pattern and predicted flood in a global scale may alter the SOC content.

Keywords: soil organic carbon, soil carbon sequestration, climate change

1. Soil organic carbon

Soil consists the biggest reservoir of carbon in comparison to the atmosphere and waters and is crucial in global C carbon cycle [1,2]. It has been estimated that about 2500 Pg of C to 2 m depth is stored in the soil in organic form [3,4]. The definition of soil organic carbon (SOC) regards to the balance between carbon inputs and outputs. The SOC determines soil fertility, soil activity, soil productivity as well as food and waters security. Too low SOC content (<1%) in the soil is one of the major agents influencing the susceptibility to the negative impact of the environment including erosion, and thus, limiting the soil agricultural use [3]. Soil organic carbon is derived from the animal and plant residues as well as an effect of carbon sequestration from the atmosphere which is primarily conducted via photosynthesis [1]. Thus, the importance of soil organic carbon is focused not only in the aspect of the possible way to decrease the climate change but also in the aspect of soil quality or climate conditions [5]. Soil carbon sequestration may in a high scale contribute the mitigation of climate changes, since soil represents stable and safety storage sink for the carbon which is catch from the atmosphere lowering its concentration in the atmosphere. However, the scale of soil organic carbon sequestrationis strongly limited by several agents such as soil quality (figure 1). Nevertheless, during the soil respiration the labile forms of carbon are released back from the soil into to the atmosphere. [1].

The organic matter occurs in the soil in both, labile and non-labile fraction (figure 2). The lability of SOM is affected by chemical structure, and bioavailability (physical protection from microbes [28].

Soil organic carbon dynamics are driven by climate changes as well as changes in land cover and land use. Organic in the soil affects all soil properties including physical, chemical and biological properties consisting source of microbial nutrients. It has been observed that SOC stock are generally highest under cool humid conditions and decrease under warmer and drier climates both at the global scale and at the (sub)-regional scale [6,7]. Nevertheless, the influence of climate change relatively decreases with increasing soil depth. In deeper soil the factors controlling the stabilization of SOC have a higher importance [7].

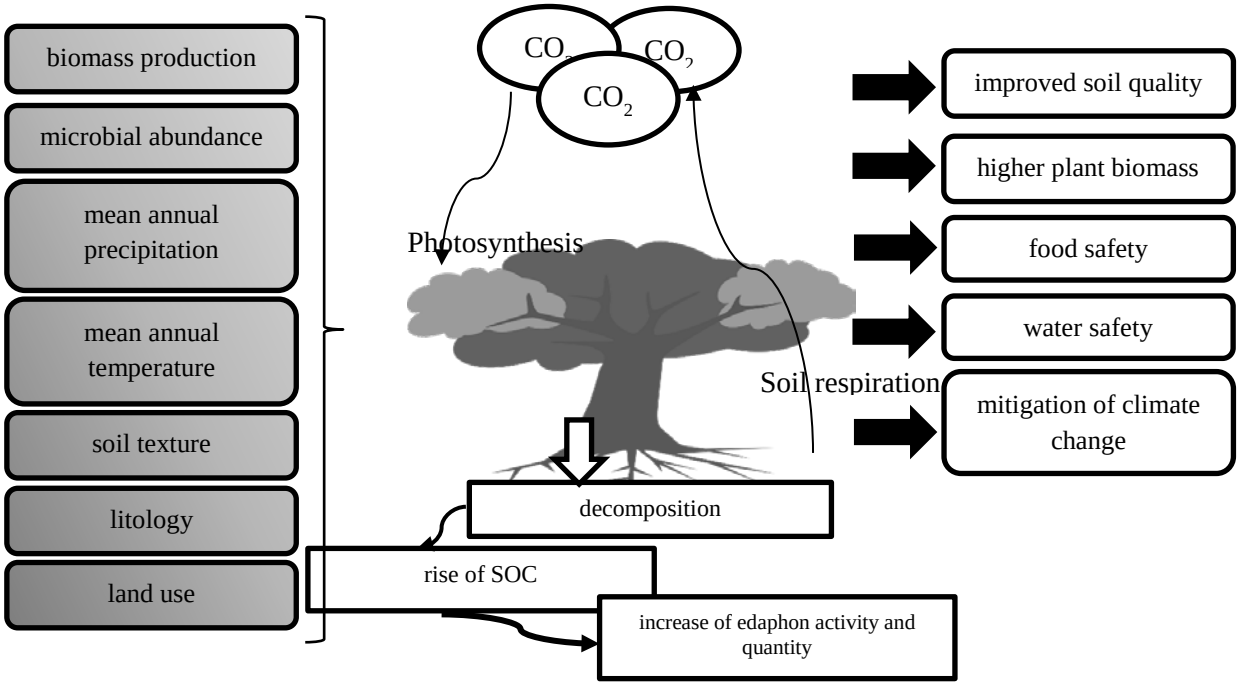

Fig. 1.1. Soil organic carbon sequestration, limiting agents and results.

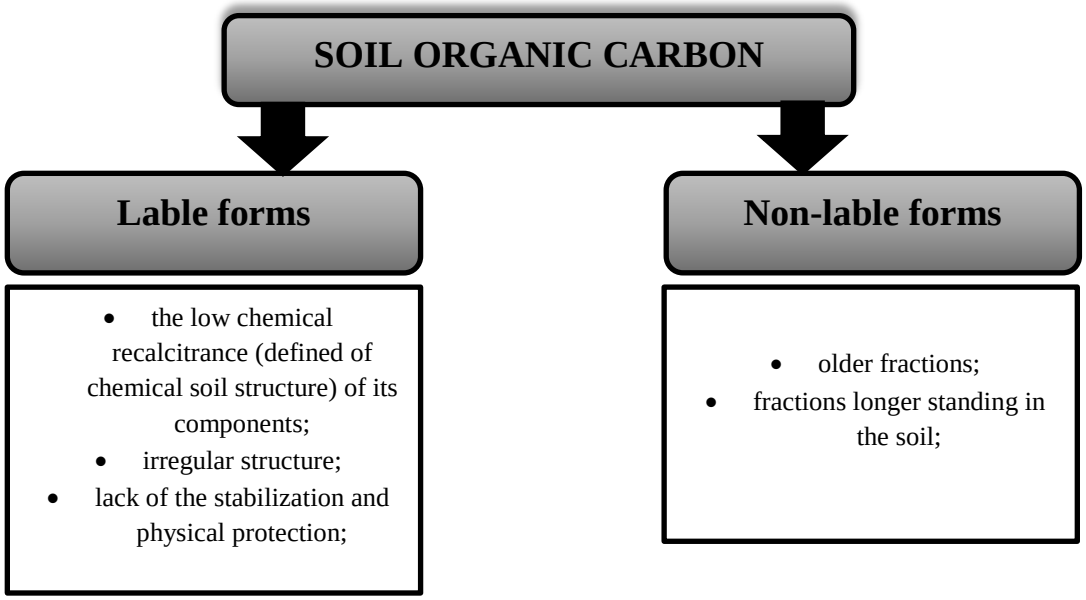

Fig. 1.2. Soil organic carbon clasification

However, at the local scale, the importance of climate changes is usually too small for the visible effect, thus, in contrast to others factor, the SOC storage is less relevant in context of climate change. The climate influence on the SOC sequestration and storage is more important in the global scale [7]. As a suitable indicator for SOC storage, the mean annual air temperature is proven. Less suitable indicator for estimating the global changes in SOC storage by climate changes is vapor pressure deficit [7].

2. The scale of climate changes

Anthropogenic activities, huge interference into the environment highly contributes to the observed climate changes worldwide. These changes have a strong impact on the amount and diversity of living organisms, and thus, affecting the ecosystems [8,9]. The long-term and progressive climate change contributes to the air and

ocean warming, sea level rising. The results of changing climate are different in many regions as an influence of, for instance, topographical features, and hence, differences in precipitation, water flow paths, water accumulation etc.

Increasing concentrations of greenhouse gases concentration in the atmosphere is considered as a crucial anthropogenic influence on the climate changes. The contamination of the atmosphere forced to the implementation of the actions for lowering the emission of the greenhouse gases (GHGs) as well as lowering the concentration of the CO_2 in the atmosphere since carbon dioxide is considered to have the highest contribution to the global warming. In this context, according to the 2020 Climate & Energy Package (Directive 2009/28/EC of the European Parliament and of the Council) and Strategy Europe 2020, European countries are obligated, among others, to cut greenhouse gas emission by -20% until 2020 to meet the RCP 2.6 goal. In 2016 the total emission of GHGs oscillated about 6.5 mln metric tonnes of CO_2 equivalent. Moreover, it has been estimated that carbon-climate response (CCR) is in the range 1.0-2.1°C/ Tt C emitted. According to the model provided by the Intergovernmental Panel on Climate Change (IPCC) by 2100 we may suppose the temperature rise up to 1.4-5.8°C [10]. Today, global mean surface temperatures about 1°C higher in comparison to the beginning of the 20th century, and rates of the rise of those mean temperatures is the highest in recent decades [11]. The increasing temperatures influence also on the sea levels. Melting glaciers, ice caps and ice sheets have a high influence on the rise of sea levels. At present, we observe approximately 17cm increase of the sea levels [12]. Climate change is also visible in the amount, intensity and frequency of the precipitation. The climate changes influence land degradation [13,14].

3. Soil organic carbon is changing climate

Global warming contributes to the increase of the temperature of soil. Such influence causes disrupting of the soil ecosystem and strongly influence on its quality, and thus usability for different applications [15,16]. Since, the area of the contaminated and/or degraded soils worldwide is large, the importance of the influence of climate change on SOC consists an emerging problem. The highest influence of climate change in a future projection will be visible in the labile forms of SOC. The growing temperature contributes to the intensification of SOC decomposition by terrestrial biosphere, and thus, emission of CO_2 into the atmosphere deeping the climate change [17]. In the further perspective such phenomenon may lead to the still growing problem with soil degradation and depletion by decreasing total SOC. Moreover, growing activity of soil microorganisms under increased temperature may lead to the changing their decomposition mechanisms and in consequence, to the decomposition of the more stable forms of the organic carbon stored in the soil. It has been observed that under rising soil temperature the degradation of simple sugar and alcohols in SOC is accelerated, what effects on the quick release of GHGs into the atmosphere in anaerobic fermentation [18,19]. The warming climate contributes to the changes in the soil microbial population, and thus, the projections on the SOC mineralization may be strongly affected by the lowering diversity of the soil microbiota [19, 20, 21]. Moreover, the growing mean temperature influences on the chemical processes of soil organic carbon adsorption and desorption onto mineral surfaces.

Changing precipitation pattern has an impact on the hydrologic balance affecting the water film thickness. Since diffusion of soluble organic carbon substrates and extracellular enzymes are present in this part of the soil, the content of the SOC may undergo strong changes [22]. On the other hand, due to the imbalance in precipitation pattern, longer drought periods especially in the summer may increase exposition of the soil organic-C to the aerobic decomposition.

While the several influences on carbon cycle are noticed in many laboratory studies referring to various environmental changes, the real influence of climate change on carbon cycle remains uncertain [23]. The prediction of the changes in SOC stock and its turnover brings many controversies [24]. The microbial activity and thus, decomposition of organic compounds is also dependent on the climate changes. Due to the sensitivity of enzymes to the temperature the carbon turns over may be seriously affected. It is predicted that organic matter depolymerization may be enhanced by the change microbial substrate preference [25].

However, the differences in SOM enzymatic decomposition may be a result of the desorption, and physical blockade in the enzyme-substrate system lowering the efficiency of the degradation [26, 27].

4. Changes in SOC under climatic changes and soil degradation by heavy metals

Metals occurs in the soil in various chemical forms: organic, minerals and/or ions [29]. Progressing anthropogenic activities such as mining leads to the higher contamination of the soils by heavy metals. The persistence of heavy metals in the soil causes long-term soil contamination. Due to the high interference of heavy metals into an enzymatic process the soil activity is limited [30].

The predicted intensive precipitations will affect the soil moisture content, and thus, heavy metal availability, and finally, for example reducing as (V) to the more toxic as (III) [31]. On the other hand, predicted lowering concentration of soil organic matter under global warming will affect the mobility of heavy metals, whereas organic matter immobilizes them decreasing their toxicity. Thus, as an effect of climate change, the availability of toxic metals increases changing soil quality and its usability. The combined influence of climate change on SOM content and pH value may contribute in an unpredictable significant increase of heavy metal mobility and toxicity [32, 33]. That means that their toxic potential will increase directly threating soil microorganisms and edaphon, as well, as plants.

Moreover, the remediation methods may be significantly disrupted under futuristic climatic changes. Lower pH value of soils (acid rains), higher leaching of heavy metals (more intensive precipitation) and increased heavy metals migration may significantly limit soil remediation. Since, the efficiency of remediation of soil contaminated by heavy metals strongly depends on the organic matter content and may be significantly correlated with the activity of plants growth promoting bacteria (PGPB) [33] the effectiveness of phytoremediation may be influenced (figure 3).

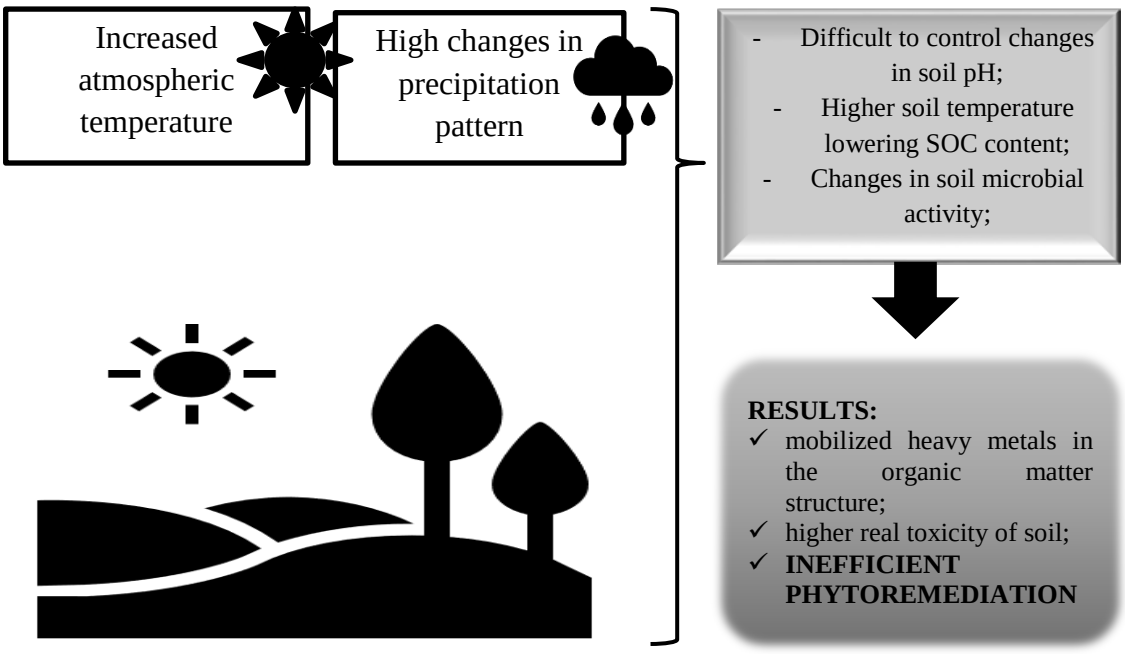

Fig. 4.1. Influence of climate change on remediation of the soil contaminated by heavy metals

5. Conclusion

The understanding of the interaction between soil organic carbon mineralization and global warming is crucial for predicting future atmospheric CO_2 concentrations. Climate change consists an extremely important

contributor to the variability of soil organic carbon stock as well as soil fertility. Since relatively labile soil organic carbon in a significant fraction is temperature-sensitive, the SOC stock may be limited under climatic changes. Global warming alters soil microbial community and its functioning influencing mineralization of SOC by alternation in C use by microbes.

Acknowledgment

The research has been funded by BS/MN-400-301/19.

The research leading to these results has received funding from the EnviSafeBioC project - contract No PPI/APM/2018/1/00029/U/001. The project is financed by the Polish National Agency for Academic Exchange (NAWA).

References

[1] Jia Z., Kuzyakov Y., Myrold D., Tiedje J. (2017). Soil Organic Carbon in a Changing World. Pedosphere, 27(5), 789–791. doi:10.1016/s1002-0160(17)60489-2 Author's name, *Name of the book*, Edition number, Publication house, page, year.

[2] Camino-Serrano, M., Guenet, B., Luyssaert, S., Ciais, P., Bastrikov, V., De Vos, B., Janssens, I. A. (2018). ORCHIDEE-SOM: Modeling soil organic carbon (SOC) and dissolved organic carbon (DOC) dynamics along vertical soil profiles in Europe. Geoscientific Model Development, 11(3), 937–957.

[3] Schiefer, J., Lair, G. J., Lüthgens, C., Wild, E. M., Steier, P., & Blum, W. E. H. (2018). The increase of soil organic carbon as proposed by the "4/1000 initiative" is strongly limited by the status of soil development - A case study along a substrate age gradient in Central Europe. Science of The Total Environment, 628-629, 840–847.

[4] Scharlemann, J.P., Tanner, E.V., Hiederer, R., Kapos, V., 2014. Global soil carbon: understanding and managing the largest terrestrial carbon pool. Carbon Manag. 5:81–91.

[5] Jobbagy, E.G. & Jackson R.B., 2000. The vertical distribution of soil organic carbon and its relation to climate and vegetation, Bellowground processes and global change 10(20), 423-436.

[6] Jobbagy, E.G., Jackson, R.B., 2000, The vertical distribution of soil organic carbon and its relation to climate and vegetation, Ecol. Appl., 10 (2), 423-436

[7] Wiesmeier, M., Urbanski, L., Hobley, E., Lang, B., Lützow, M. V., Marin-Spiotta, E., … Kögel-Knabner, I. (2019). Soil organic carbon storage as a key function of soils - A review of drivers and indicators at various scales. Geoderma, 333, 149–162. doi: 10.1016/j.geoderma.2018.07.026

[8] Sandel, B., Arge, L., Dalsgaard, B., Davies, R. G., Gaston, K. J., Sutherland, W. J., & Svenning, J.-C. (2011). The Influence of Late Quaternary Climate-Change Velocity on Species Endemism. Science, 334(6056), 660–664.

[9] Pearson, R.G., Dawson, T.P., 2003. Predicting the impacts of climate change on the distribution of species: are bioclimate envelope models useful? Global Ecology and Biogeography, 12 (5), 361-371.

[10] McMichael, A. J., Woodruff, R. E., & Hales, S. (2006). Climate change and human health: Present and future risks. *Lancet*, *367*(9513), 859–869.

[11] Ghimre, R., Norton, U., Bista, P., Obur, A., Norton J.B., Soil organic matter, greenhouse gases and net global warming potential of irrigated conventional, reduced-tillage and organic cropping systemsNutri Cycl Agroecosyst 2017, 107, 49-62

[12] Cheng, L., Abraham, J., Hausfather, Z., & Trenberth, K. E. (2019). How fast are the oceans warming? *Science*, *363*(6423), 128–129. https://doi.org/10.1126/science.aav7619

[13] McMichael, A. J., Woodruff, R. E., & Hales, S. (2006). Climate change and human health: Present and future risks. *Lancet*, *367*(9513), 859–869.

[14] Campbell-Lendrum D, Pruss-Ustun A, Corvalan C. How much disease could climate change cause? In: McMichael AJ, Campbell-Lendrum D, Corvalan C, Ebi KL, Githeko AK, Scheraga JS, eds. Climate change and health: risks and responses. Geneva: World Health Organization, 2003: 133–155.

[15] Grobelak, A., Placek, A., Grosser, A., Singh, B. R., Almås, Å. R., Napora, A., & Kacprzak, M. (2017). Effects of single sewage sludge application on soil phytoremediation. *Journal of Cleaner Production*, *155*, 189–197.

[16] Davidson, E. A., & Janssens, I. A. (2006). Temperature sensitivity of soil carbon decomposition and feedbacks to climate change. *Nature*, *440*(7081), 165–173.

[17] Pisani, O., Frey, S. D., Simpson, A. J., & Simpson, M. J. (2015). Soil warming and nitrogen deposition alter soil organic matter composition at the molecular-level. Biogeochemistry, 123(3), 391–409.

[18] Yang, Z., Wullschleger, S. D., Liang, L., Graham, D. E., & Gu, B. (2016). Effects of warming on the degradation and production of low-molecular-weight labile organic carbon in an Arctic tundra soil. Soil Biology and Biochemistry, 95, 202–211.

[19] Melillo, J. M., Steudler, P. A., Aber, J., Newkirk, K., Lux, H., Bowles, F. P., . . . Morrisseau, S. (2002). Soil Warming and Carbon-Cycle Feedbacks to the Climate System. Science, 298(5601), 2173-2176.

[20] Hartley, I. P., Hopkins, D. W., Garnett, M. H., Sommerkorn, M., & Wookey, P. A. (2009). No evidence for compensatory thermal adaptation of soil microbial respiration in the study of Bradford et al. (2008). *Ecology Letters*, *12*(7), 14–16.

[21] Streit, K., Hagedorn, F., Hiltbrunner, D., Portmann, M., Saurer, M., Buchmann, N., … Siegwolf, R. T. W. (2014). Soil warming alters microbial substrate use in alpine soils. Global Change Biology, 20(4), 1327–1338.

[22] Davidson, E.A., Janssens, I.A., Temperature sensitivity of soil carbon decomposition and feedbacks to climate change, Nature 2006, 440 (9), 165-173

[23] Carvalhais, N., Forkel, M., Khomik, M., Bellarby, J., Jung, M., Migliavacca, M., … Reichstein, M. (2014). Global covariation of carbon turnover times with climate in terrestrial ecosystems. Nature, 514(7521), 213–217.

[24] King, A. W., Post, W. M. & Wullschleger, S. D. The potential response of terrestrial carbon storage to changes in climate and atmospheric CO2. Clim. Change 35,199–227 (1997).

[25] Nottingham, A. T., Turner, B. L., Whitaker, J., Ostle, N., Bardgett, R. D., McNamara, N. P., … Meir, P. (2016). Temperature sensitivity of soil enzymes along an elevation gradient in the Peruvian Andes. *Biogeochemistry*, *127*(2–3), 217–230.

[26] Allison SD, Wallenstein MD, Bradford MA (2010) Soil-carbon response to warming dependent on microbial physiology. Nat Geosci 3:336–340

[27] German DP, Marcelo KRB, Stone MM, Allison SD (2012) The Michaelis-Menten kinetics of soil extracellular enzymes in response to temperature: a cross-latitudinal study. Glob Change Biol 18:1468–1479

[28] Xu, X., Shi, Z., Li, D., Rey, A., Ruan, H., Craine, J. M., … Luo, Y. (2016). Soil properties control decomposition of soil organic carbon: Results from data-assimilation analysis. *Geoderma*, *262*, 235–242.

[29] Jasińska, A. (2018). The Importance of Heavy Metal Speciation from the Standpoint of the Use of Sewage Sludge in Nature. Engineering and Protection of Environment, 21(3), 239–250. https://doi.org/10.17512/ios.2018.3.3

[30] Wuana R.A., Okieimen F.E., Heavy Metals in Contaminated Soils: A Review of Sources, Chemistry Risks and Best Available Strategies for Remediation, ISRN Ecology 2011, Article ID 402647

[31] Wani, A. L., Ara, A., & Usmani, J. A. (2015). Lead toxicity: A review. Interdisciplinary Toxicology, 8(2), 55–64. https://doi.org/10.1515/intox-2015-0009

[32] Ayangbenro, A. S., & Babalola, O. O. (2017). A new strategy for heavy metal polluted environments: A review of microbial biosorbents. International Journal of Environmental Research and Public Health, 14(1).

[33] Grobelak A, Napora A, Kacprzak M. Using plant growth-promoting rhizobacteria (PGPR) to improve plant growth. Ecol Eng. 2015;84:22–28. doi: 10.1016/j.ecoleng.2015.07.019

Water Loop Heat Pump Systems

Kubra Sultan Aba[1]

[1]*BSc-Cukurova University, Faculty of Architecture and Engineering, Mechanical Engineering Department, Adana/Turkey, e-mail: mecheng@cu.edu.tr*

Abstract

The improvement of energy efficiency and the use of eco-friendly working fluids are essential elements of prevailing European policies. Supermarkets are intense energy purchasers and nearly 40% of their yearly energy consumption is for refrigeration [1]. The oblique impact on the environment related to high electrical energy consumption, make shopping malls, not sustainable buildings.

Keywords: WLHP system, Heating, WSHP system

1. Introduction

Nowadays, with developing industries, the total energy consumption increases steadily to really high levels. An additional problem that we are facing is substantial energy waste along with increased energy demand. However, almost every sector strictly depends on energy usage and providing energy in an environmentally friendly way has become more difficult and expensive. Approximately 75% of European buildings do not meet current energy requirements [1]. Accordingly, improving the indoor air quality and energy efficiency of HVAC systems of occupied zones gives a huge opportunity for energy and cost savings.

An example of the above-described problem is providing energy for conditioning of large area and multi-zone buildings, such as malls, which started to be a substantial energy-consuming process. On top of a large scale of the building, individual zones may have different thermal condition requirements and energy needs. For such a problem, the Water Loop Heat Pump (WLHP) systems could be an appropriate system solution [1]. The starting point of this idea is to have opposite conditions for different zones in the same building.

This paper reviews the energy-saving potential of commercial buildings air conditioning and refrigeration systems using a Water Loop Heat Pump system (WLHP). In addition to this, to find the optimal values of the activation temperature for heat recovery, a supplemental heating system, and cooling towers are compared for traditional systems with Water Loop Pump (WLHP) system which has a heat exchanger (HX) and without HX. Two locations have been considered, representative of as many different European climatic zones.

2. System Description

A Water Loop Heat Pump (WLHP) system consists of a set of heat-pumps, that reject the excess heat from the zone which is cooled to a water loop. This heat is recovered by other heat pumps and transferred to spaces that need heating. Water Loop Heat Pump (WLHP) systems are a good option for space conditioning for commercial buildings, e.g. shopping malls. They allow us to save energy through heat recovery and temperature balancing when heating and cooling occur at the same time.

Those systems typically operate with a loop water temperature between 16 and 32 °C. When cooling loads are prevalent, loop water temperatures are maintained below 32 °C. To maintain this temperature, it rejects excess heat to a cooling tower. When heating is prevalent, loop water temperatures are maintained above 16 °C [2].

Energy exchange between the mixed cooling and heating modes of the Water Loop Heat Pump (WLHP) systems is a unique mode in air-conditioning, as well as space heating systems. The most effective operation occurs when the heating and cooling modes are balanced, which could happen when some zones require

heating or cooling during the whole year. For this reason, the Water Loop Heat Pump (WLHP) system is exclusively effective where zones have high internal loads. However, one operating mode is often dominated and water in the loop has to be heated or cooled.

Figure.2.1 is a typical model of a Water Loop Heat Pump (WLHP) system. Many buildings have large internal areas. Those areas often require cooling for all-year-round because of high internal heat gains. The chiller condenser that water heat is recovered, instead of rejected to the outside. This water used as a heat source for a water-source heat pump system. The water loop provides condenser water for the interior zone cooling units. Picking up the heat normally rejected to a cooling tower and transferring it as the heat source for the heat pumps. This largely increases the coefficient of performance (COP) and reduces the cost of operating the heat pumps over air-source heat pumps.

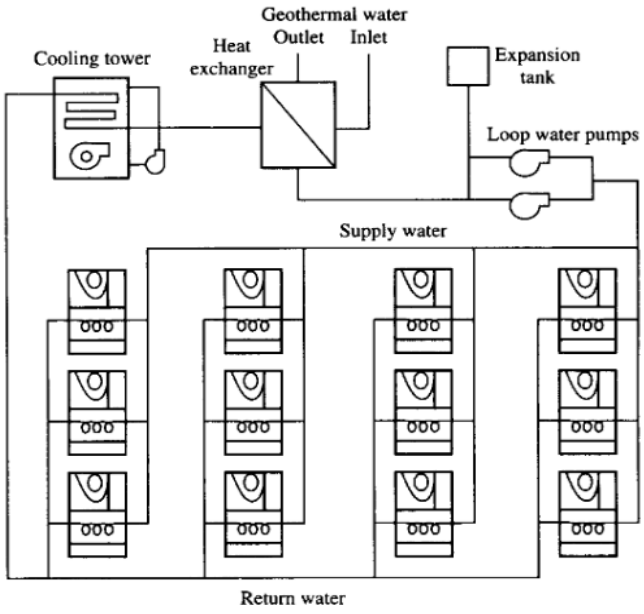

Fig. 2.1 Water loop heat pump system [2]

A WLHP system has been introduced years ago, and the idea is to take advantage of low condensing temperature and distributed heating-cooling generation with local control as well. The system consists of a water loop acting simultaneously as a sink or as a source for several reversible water-air heat pumps. Each heat pumps serving autonomously a limited space. The temperature of the water loop is a result of the balance between the units that are operating during cooling and heating mode.

The most effective operation occurs when these two modes are on balance. This balance can be reached during the mid-seasons or when multiple zones require heating-cooling all year around. Because of this reason, this system is effective mostly where zones have high internal loads. In addition to this, one operating mode is often frequent. Also, water in the loop has to be cooled or heated.

3. The Comparison Between WLHP Systems and Traditional Hydronic System Regarding Energy Demand

A first comparison was made between the traditional hydronic system and the WLHP system without and with heat recovery from the refrigeration plant. This comparison was made without any water reservoir in the water loop. Water loop temperature variable depending on outside conditions.

Table 3.1 presents a comparison results of these systems. The comparison is given for Mediterranean climate (Southern Europe) and Continental climates (Central Europe) separately.

Table.3.1 Annual global energy requirement for a traditional system and a WLHP system with and without Heat Exchanger (HX) or heat recovery [3]

	Continental			Mediterranean		
	Traditional System	Water Loop No HX	Water Loop HX	Traditional System	Water Loop No HX	Water Loop HX
	MWh	MWh	MWh	MWh	MWh	MWh
Refrigeration	537	537	520	604	604	595
HVAC	853	795	580	684	472	429
Total	**1390**	**1332**	**1100**	**1288**	**1076**	**1024**

Regarding the annual values, the difference is very small in the Continental climate. Nevertheless, it becomes enough in the Mediterranean climate. The result is related to the values of COP estimated for these two systems. In the previous reports by the researchers [4], the requirement for the global energy of these two systems was almost identical.

In both climates, the WLHP systems have better performance in terms of energy requirements. However, it is not 100% true for the Continental climate because of higher heating loads during the cold seasons, which provides better exploitation of the condensation heat rejected through the refrigeration systems. The energy need is increased up to 65% in October for the Continental climate and up to 36% in January for the Mediterranean climate.

In the Fig.3.1, comparison of monthly energy requirements (in MWh) shows between a traditional system, a WLHP system with and without HX for heat recovery in the Continental climate.

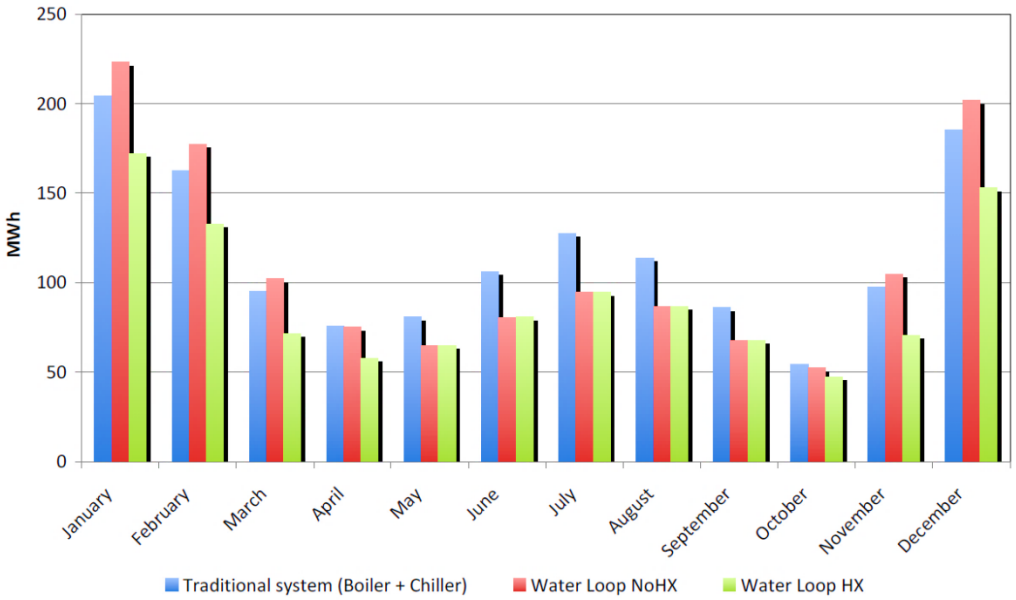

Fig.3.1 Monthly global energy requirements for a traditional system, a WLHP system with and without HX for heat recovery in the Continental climate. [3]

In the Fig.3.2, comparison of monthly energy requirements (in MWh) shows between a traditional system, a WLHP system with and without HX for heat recovery in the Mediterranean climate.

In both climates, the WLHP system with heat recovery has better performance in terms of energy requirement. Unfortunately, this is particularly true in the Continental climate. Due to higher heating loads in the cold season, which provide better exploitation of the condensation heat rejected by the refrigeration system.

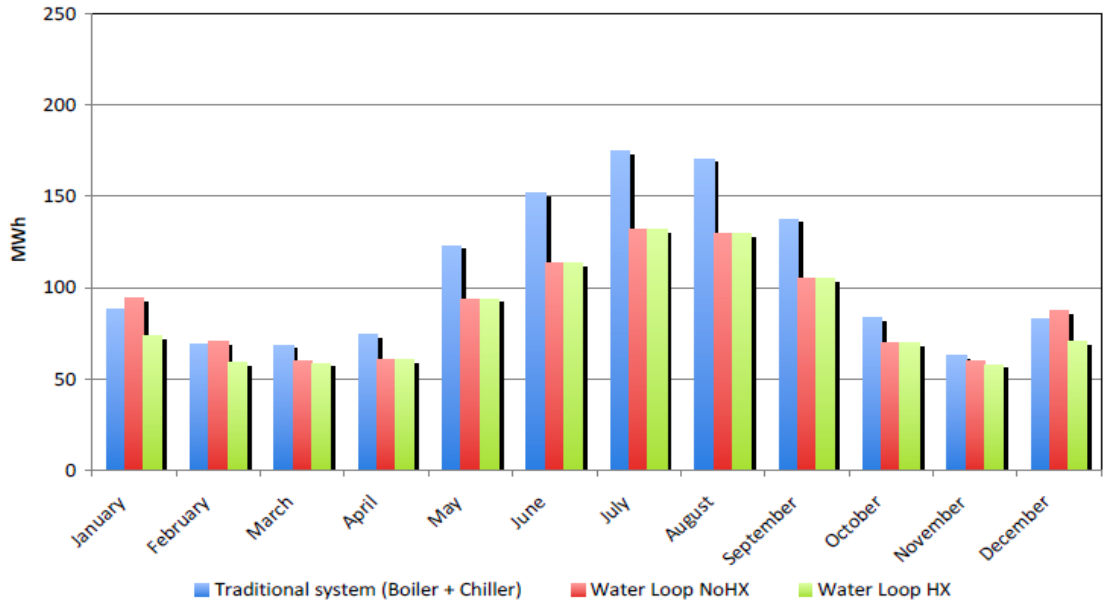

Fig.3.2 Monthly global energy requirements for a traditional system, a WLHP system with and without HX for heat recovery in the Mediterranean climate. [3]

4. Air Source Heat Pump

An air-source heat pump (ASHP) is a space-conditioning device that can provide both heating and cooling.

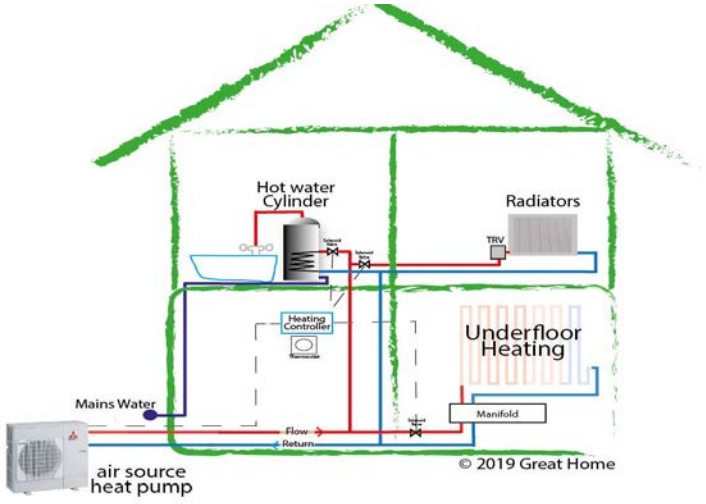

Fig.4.1. A typical Air Source Heat Pump (ASHP) System [7]

Although models exist that only provide one of them. In heating mode, the heat pump uses electricity to extract heat from the outside air, then transfers it to the inner zones. An ASHP uses a refrigeration cycle to “step up” the heat to a temperature proper for space heating. In cooling mode, the heat pump works like a refrigerator, shifting heat from the interior of a house and removing it outside.

4.1. How it works

An air-source heat pump transfers heat by the system of a refrigeration cycle. Heat is transferred by the refrigerant or the fluid that moves within the refrigeration cycle.

In heating mode, the refrigerant obtains heat from the outside air, during it travels through heat exchanger coils located in the outside unit. These coils are called the “evaporator” because the outside heat makes the refrigerant to evaporate into a gas. This gas then goes to a compressor, which uses electricity to increase the temperature of the refrigerant gas until it is enough for space heating. The gas then passes into a set of indoor heat exchanger coils where it abbreviates into a liquid, delivering heat. In an air-to-air ducted heat pump, a fan is used to move the heat into the zones. Finally, the liquid refrigerant moves into an expansion valve, which reduces its pressure, and starts the period again. [8]

5. Comparison Between ASHP System and WLHP System

Using the relative power method [8], two main tables (for winter Table.5.1 and for summer Table.5.2) are obtained to show the energy consumption of WLHP and ASHP systems.

Firstly, the degree of power change is greater at the load rate of 20–60% in winter than summer, because the use of the auxiliary heat source can improve the COP of a unit by heating circulating water. Secondly, the auxiliary heat source has a very negative effect on system efficiency when the load rate is raised to 80–100%. Noted that the key point occurs at a load rate of 80%. The operation of the WLHP system will lose its advantage over a traditional two-pipe HVAC system at a load rate of 80–100%, which also confirms its energy-saving range in winter.

Table.5.1 Energy consumption of heat pump systems in winter for ASHP and WLHP systems. [8]

Load rate/%	Unit power /kW		Energy consumption /kWh	
	ASHP	WLHP	ASHP	WLHP
100	11,76	7,63	3721	3228
80	7,71	4,82	14,184	11,03
60	5,39	4,08	16,911	12,263
40	3,41	2,77	5674	4271
20	1,59	1,41	1472	1198

Table.5.2 Energy consumption of heat pump systems in summer for ASHP and WLHP systems. [8]

Load rate/%	Unit power /kW		Energy consumption /kWh	
	ASHP	WLHP	ASHP	WLHP
100	32,31	16,56	2792	1520
80	24,03	9,31	10,665	4620
60	18,13	7,01	13,188	5910
40	13,01	4,69	4896	2196
20	9,11	2,33	1781	713

5.1. Advantages of a WLHP System

Almost any type of commercial buildings that has several temperature controls zones, some of which need to be heated while others need to be cooled, are prime candidates for a WLHP system. A Water Loop Heat Pump system is a good choice for office buildings, libraries, hotels, condominiums, and schools.

- It provides an opportunity for energy saving by recovering heat from internal areas as well as from waste heat. Also, there is another option to recover energy by storing the excess heat which is coming from day-time cooling for night-time cooling.
- When solar collector efficiency is high, this system allows for recovering solar energy at comparably low water temperatures.
- It provides a control system for the environment in distributed, occupied areas during the night or weekends. With this, there won't be any need to start a large central refrigeration machine.
- Units will have a longer service lifetime than air-cooled heat pumps.
- Units are not endangered by the outdoor weather, which allows installation in the waterfront and other destructive environments.
- Condenser fans are excreted, and the compression ratio is lower, that's why the noise level can be lower than air-cooled appliances.
- When a singular unit fails, the whole system is able to continue operation without the shut-down.
- Energy usage by the heat pumps can be measured for each occupant.

5.2. Limitations for WLHP System

As with any systems, there are some potential limitations with WLHP systems.

- Large places are required to place the boiler, pumps, heat rejector and heat exchanger.
- The initial cost may be higher than the systems that use various units.
- Basic WLHP equipment may have reduced airflow and this reduced airflow can cause the overheat on heat pumps and stall.
- The piping loop be must be maintained clear.

6. Conclusions

In this paper, general information about the Water Loop Heat Pump (WLHP) Systems have been studied. General description of the WLHP system with its advantages and limitations are shown. However, during the researches, some other systems such as Air Source Heat Pump (ASHP) System are referred to provide a comparison for the energy consumption of the systems.

According to the comparison between WLHP systems and traditional systems, WLHP systems with heat exchangers (HX) are more efficient for both warm and cold climates which are called as Mediterranean and Continental during the studies. However, this system is more efficient for cold climates because of more energy requirements for heating. Additional to this comparison, also the energy consumption of WLHP and ASHP systems are compared and it shows that ASHP systems are more suitable for small buildings.

Besides, the operation of WLHP system can achieve the higher efficiency for big buildings that have simultaneous heating and cooling and its energy-saving rates are 25.2% in summer and12.7% in winter, respectively, compared to an ASHP system.

References

[1] Arias, J., and Lundqvist, P, 2006. Heat recovery and floating condensing in supermarkets. Energy and Buildings 38 (2): 73-81

[2] Minea, V. Using heat pumps for energy recovery in supermarket refrigeration systems. IEA Heat Pump Centre Newsletter 2010, 28 (4), 24–30.

[3] M. Chaichian, H. Perez Rojas, A Tureanu. Basic Concepts in Physics: From the Cosmos to Quarks, Springer Press, Berlin, 2014.

[4] Arias, J., 2005. Energy usage in supermarkets - modelling and field measurements, Doctoral Thesis Royal Institute of Technology, Stockholm, Sweden.

[5] Buonomano, A., Calise, F., Palombo, A., Building dynamic simulation: Water loop heat pump systems analysis for European climates. Applied Energy. 2012; 91, 222-234.

[6] Carrier System Design Guide-Water Source Heat Pump

[7] Hubbard, R. 2009. Water-to-water heat pumps. ASHRAE Journal 51(1):28-35. IDEA. 2008. District cooling best practices guide. International District

[8] David A. Waddicor, Elena Fuentes, Marc Azar, et al., Partial load efficiency degradation of a water-to water heat pump under fixed set-point control, Appl. Therm. Eng. 106 (2016) 275–285.

Simulation of Kinetically Controlled Pressure Swing Adsorption Processes

Ewelina Brodawka[1], Mieczysław Bałys[1], Daniel Friedrich[2], Enzo Mangano[2]*

*[1] Faculty of Energy and Fuels, AGH University of Science and Technology, Al.Mickiewicza 30, 30-059 Krakow, Poland. * corresponding author, e-mail: brodawka@agh.edu.pl*
[2] School of Engineering, The University of Edinburgh, King's Buildings, Edinburgh, EH9 3FB, UK.

Abstract

Availability of a process simulator which can help in taking decisions on the operating parameters, operating configurations, selection of adsorbent and the number of beds is one of the important aspects in the design of adsorption processes, especially in the case of pressure swing adsorption (PSA) processes. This work makes an attempt at simulation using CySim simulator. Simulations of the kinetic separation of methane/nitrogen mixture are presented for a two-bed pressure swing adsorption (PSA) cycle using cycle simulator. The PSA process studied is the system of 50%-50% CH_4/N_2 –TAKEDA 3A carbon molecular sieve for enriching methane.
A methane product should be approximately 90% pure to be of industrial interest. Numerical simulations indicate that the purity of methane gas recovered can be greater than 90% for the proposed PSA cycle.

Keywords: pressure swing adsorption, kinetic separation, cycle simulator

1. Introduction

Pressure swing adsorption (PSA) processes have been applied for many gaseous separations and purification operations such as air separation [1,2] hydrogen purification [3,4], separation between linear and branched hydrocarbons [5], and recently, this technology has been applied in other areas like methane purification from natural and biogas [6, 7] or CO_2 removal [8,9]. In comparison with other processes as a membrane or cryogenic separation, PSA is suitable for middle-scale processes, which have a substantial interest in the gas processing industry [10-12].
Pressure swing adsorption (PSA) is a cyclic process for separation of gas mixtures. During high-pressure adsorption step, the gas feed mixture is introduced to a column packed with porous adsorbent where preferentially adsorbed components are retained producing a purified stream at the other end of the column. During desorption step, the adsorbed components are removed from the bed at low pressure producing a desorbed stream [13].
The optimum process variables and operating conditions to be used depend on the controlling mechanism for the process. Separation of gas mixtures by a PSA process can be accomplished on the basis of three different separation mechanisms: the differences of the selective adsorption amount of the adsorbed components (equilibrium separation), the differences in components gas diffusion rate in the adsorbent (kinetic separation) and the differences of molecular shape (steric separation) [14].
In the present study, the kinetic separation of a 50%-50% CH_4/N_2 gas mixture into the carbon molecular sieve (CMS) in a two-bed PSA unit have been simulated using *CySim simulator*. The effect of process cycle was investigated. The model for kinetic separation uses the linear driving force (LDF) model for diffusion rates, nonlinear mixed gas isotherms and is general for any number of adsorbing components. A modified Skarstrom-type PSA cycle was utilized to study the kinetically controlled separation. Moreover, the bed dynamics worked in cyclic steady-state regime. Approximately 10-15 cycles were required to reach CSS.

2. Simulation

The two-bed pressure swing adsorption (PSA) process has been designed and simulated by *CySim: Cycle simulator* developed at the University of Edinburgh. CySim is an efficient, software tool for the simulation of adsorption periodic processes designed to operate in cyclic steady state (CSS). The software's developers chose and linked the simulator with the SUNDIALS library to solve differential-algebraic equations (DAE) [4,8,14].

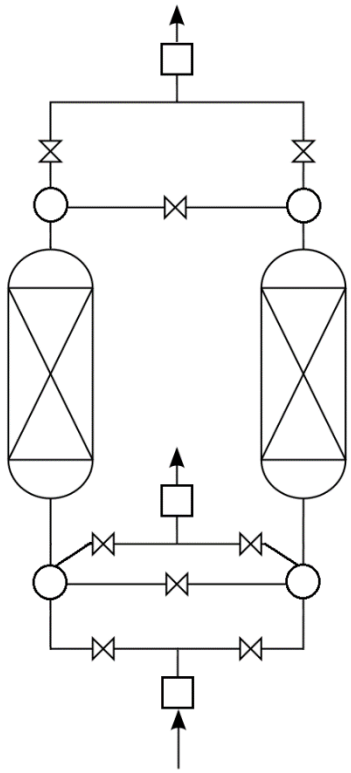

Fig. 2.1. Schematic diagram for the implementation of the two-bed PSA process within CySim.

2.1 Mathematical model

Mathematical models describing the PSA process were derived based on the assumptions that ideal gas law is valid, the effect of thermal excursions are negligible, the total pressure remains constant during high or low-pressure steps, the flow is governed by axially dispersed plug flow model, the equilibrium relations are given by the Langmuir isotherm, the mass transfer rates are represented by linear driving force (LDF).
Thus, the material balance for each component in the bed can be represented as follows [8]

$$\frac{\partial c_i}{\partial t} + \frac{(1-\varepsilon)}{\varepsilon} \cdot \frac{\partial Q_i}{\partial t} + \frac{\partial (c_i \cdot v)}{\partial z} + \frac{\partial J_i}{\partial z} = 0 \tag{1}$$

$$Q_i = \varepsilon_p c_i^m + (1-\varepsilon_p) q_i \tag{2}$$

$$\varepsilon_p \frac{\partial c_i^m}{\partial t} + \left(1-\varepsilon_p\right) \frac{\partial q_i}{\partial t} = k_i^p (c_i - c_i^m) \tag{3}$$

$$\frac{\partial q_i}{\partial t} = k_i^c (q_i^* - q_i) \tag{4}$$

Where,

c_i concentration of component *i* in the gas phase (mol/m^3),
c_i^m concentration of component *i* the macropore (mol/m^3),
Q_i concentration of component *i* the adsorbent pellet (mol/m^3),

q_i sorbate concentration of component *i* (mol/m^3),
q_i^* sorbate concentration of component *i* at equilibrium (mol/m^3),
ε void fraction of the bed,
ε_p void fraction of the pellet,
k_i^c LDF mass transfer coefficient of component in micropore (m/s),
k_i^p LDF mass transfer coefficient of component in macropore (m/s),
J_i diffusive flux of component *i* in the gas phase (mol/(m^2·s)),
v interstitial flow velocity (m/s).

2.2 Design and simulation strategies

In this study carbon molecular sieve TAKEDA 3A was used to separation CH_4/N_2 mixture for producing enriched methane by a PSA process. The physical parameters and adsorption constants are shown in Table 2.1. The geometrical data of a column, adsorbent and adsorption isotherm parameters have been adopted from [6, 16, 17, 18]. Carbon molecular sieves (CMS) are carbonaceous materials widely used in separation of gas mixtures, based on the differences in the rate of adsorption of the gases (kinetic separation). The CMS has a narrow pore size distribution and therefore discriminates molecules based on their size and shape [19].

Table. 2.1. Bed parameters and physical characteristic of CMS

Operating conditions		
feed pressure, bar	5	
evacuation pressure, bar	1	
temperature, K	293.15	
molar flow rate, mol/s	1	
Column dimensions		
diameter, cm	17.5	
length, cm	100	
Adsorbent		
particle size, cm	0.18	
pellet density, g/cm^3	0.90	
bulk density, g/cm^3	0.633	
Langmuir constants	CH_4	N_2
q_i^*, mmol/g	3.07	3.11
b_i, 1/atm	0.351	0.106
Diffusion time constant		
D/r^2, m^2/s	$4*10^{-5}$	$2*10^{-3}$

Due to the small difference in kinetic diameters of CH_4 (3.68Å) and N_2 (3.82Å), the relatively low diffusivities of both gases, the modest kinetic separation factor, and strong adsorptive characteristic of CH_4 on this CMS, separation of CH_4/N_2 on CMS is very difficult to obtain by kinetic adsorption-based separation process [18]. Consequently, the blowdown and purge steps in a simple Skarstrom PSA cycle (Fig.2.2. a.) was replaced with an evacuation step. The evacuation step was divided into a rapid depressurization step and a constant pressure desorption step. In addition, an equalization step was introduced to improve the recovery of the product [12]. Thus, the two-bed PSA cycle studied includes six steps, as shown in Fig.2.2. b. During step 1, bed 1 is rapid pressurized and bed 2 is rapid depressurized. In step 2, a high-pressure gas feed mixture containing 50% each of CH_4 and N_2 is introduced continuously to bed 1 in which preferential adsorption of nitrogen as faster diffusing component occurs. Methane as slower diffusing component is removed as purified product at the column outlet. The content of bed 2 is constantly evacuated in the reverse flow direction. In step 3, both columns are in pressure equalization. This completes one-half cycle. The other half cycle is accomplished similarly in steps 3, 4, 5 starting with bed 1 being depressurized and bed 2 pressurized.

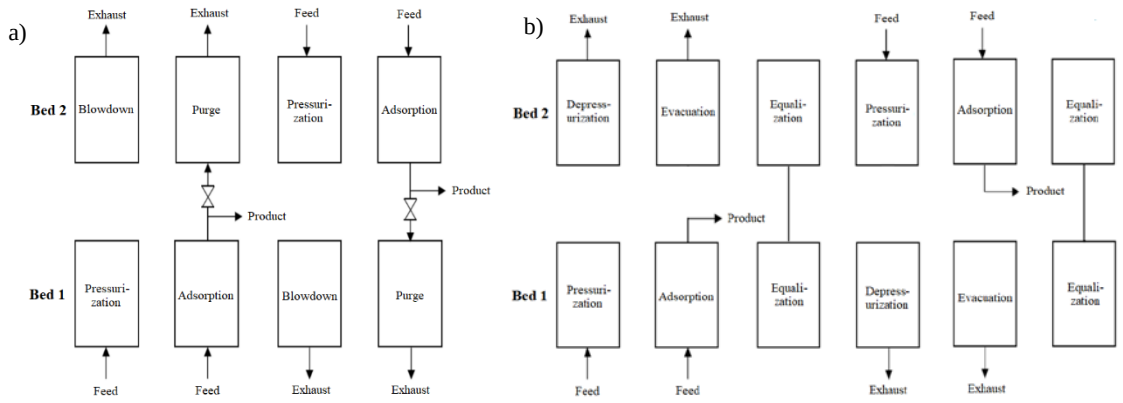

Fig. 2.2. Scheme of Skarstrom cycles: a) simple b) modified.

Furthermore, CySim gives opportunity choice an individual hierarchy model for the adsorption column that is described by mass, energy and momentum balances [8, 20]. According to assumptions in *2.1 Mathematical model*, and as discussed in detail by Rutherford and Do [21] the influence of macropore diffusion in the transport of molecules can be disregarded. Additionally, transport of nitrogen is rate-limited by the pore mouth barrier and is characterized by a linear driving force model (LDF) [22]. The following settings were chosen energy balance: isothermal operation, → momentum balance: no pressure drop, → mass balance: no external film resistance, no macropore, micropore LDF.

3. Results

The changes of CH_4 purity and recovery have been checked using the six-step, two-bed PSA cycle designed as shown in Fig. 2.2.b. The effect of adsorption was investigated. Gas stream flowrates and duration of the pressurization, depressurization and equalization steps were kept constant in all simulations. Simulation results are presented in Table 2.

Table. 3.1. Performance of six-step, two-bed PSA cycle

Adsorption time (s)	CH_4 purity (%)	CH_4 recovery (%)
150	96.3	56.5
250	91.6	65.6

Numerical simulation indicated that the purity of methane gas recovered can be greater than 90% for both adsorption times. It should be noted that the CH4 recovery decreases with adsorption time extension. As shown in Fig 3.1. the pressure profile of a column for all cycles corresponded to proposed six-step process.

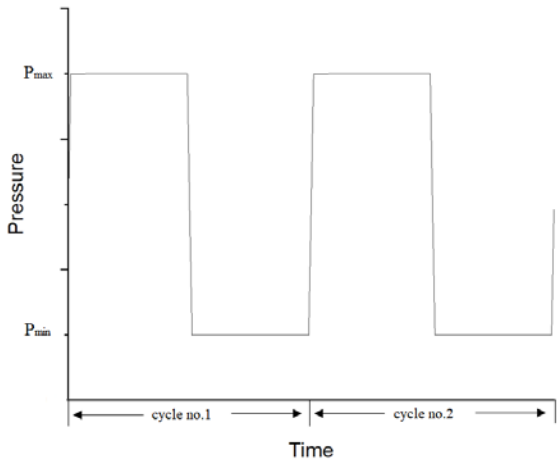

Fig. 3.1. Pressure profiles of a column.

4. Conclusions

The present study was undertaken as a step towards the development of the strategy for simulation pressure swing adsorption processes for methane/nitrogen mixtures. The simulations results indicated that the CySim simulator can be conveniently applied to investigate prospective adsorbents and different combinations of PSA process steps for a kinetic separation over a wide range of operating condition and their optimization (further investigations). In the example presented here, CH_4 of 90% purity is attainable using the two-bed PSA cycle for a 50/50 feed mixture.

Acknowledgement

The authors[1] are grateful to the AGH - University of Science and Technology (Project No 11. 11. 210. 374) and KIC Innoenergy PhD School for its financial support of this work.

References

[1] Ackley M.W., *Medical oxygen concentrators: a review of progress in air separation technology*, Adsorption, vol. 25, 2019, 1437–1474.

[2] Santos J.C., Portugal A.F., Magalhaes F.D., Mendes A., *Optimization of medical PSA units for oxygen production*, Industrial and Engineering Chemistry Research, vol. 45, no. 3, 2006, 1085–1096.

[3] Sircar S., Golden T. C., *Purification of hydrogen by pressure swing adsorption*, Separation Science and Technology, vol. 35, no. 5, 2000, 667–687.

[4] Luberti M., Friedrich D., Brandani S., *Design of a H_2 PSA for cogeneration of ultrapure hydrogen and power at an advanced integrated gasification combined cycle with pre-combustion capture*, Adsorption, vol. 20, 2014, 511–524.

[5] Silva J. A. C., *Separation of n/iso—paraffins by adsorption process* [Ph.D. dissertation], University of Porto, Porto, Portugal, 1998.

[6] Kim M.B., Bae Y.S., Choi D.K., Lee C.H., *Kinetic separation of landfill gas by a two-bed pressure swing adsorption process packed with carbon molecular sieve: nonisothermal operation*, Industrial and Engineering Chemistry Research, vol. 45, no. 14, 2006, 5050–5058.

[7] Bałys M., Szczurowski J., Czepirski L., *Adsorption technology for ventilation air methane enrichment*, [w]: Selected issues related to mining and clean coal technology, red: Borowski M. Swolkień J., Agencja Wydawniczo-Poligraficzna "ART.-TEKST", Kraków, 2016, 253–267.

[8] Farmahini A.H., Krishnamurthy S., Friedrich D., Brandani S., Sarkisov L., *From Crystal to Adsorption Column: Challenges in Multiscale Computational Screening of Materials for Adsorption Separation Processes*, Industrial and Engineering Chemistry Research, vol. 57, 2018, 15491−15511.

[9] Chaffee A.L., Knowles G.P., Liang Z., Zhang J., Xiao P., Webley P. A., *CO_2 capture by adsorption: materials and process development*, International Journal of Greenhouse Gas Control, vol. 1, no. 1, 2007, 11–18.

[10] Gomes, V. G., Hassan, M. M., *Coalseam methane recovery by vacuum swing adsorption*, Separation and Purification Technology, vol. 24, no. 1–2, 2001, 189–196.

[11] Fiandaca G., Fraga E. S., Brandani S., *A multi-objective genetic algorithm for the design of pressure swing adsorption*, Engineering Optimization, vol. 41, no. 9, 2009, 833–854.

[12] Grande C.A., *Advances in Pressure Swing Adsorption for Gas Separation*, ISRN Chemical Engineering, vol. 2012, Article ID 982934, 2012.

[13] Ruthven D.M., Farooq S., Knaebel K.S., *Pressure Swing Adsorption*, VCH Publishers, Inc., New York, 1994.

[14] Ruthven D.M., *Principles of adsorption and adsorption processes*, John Wiley and Sons, Inc., New York, 1984.

[15] Friedrich D., Ferrari M.C., Brandani S., *Efficient Simulation and Acceleration of Convergence for a Dual Piston Pressure Swing Adsorption System*, Industrial and Engineering Chemistry Research, vol. 52, 2013, 8897−8905.

[16] Rios R.V.R.A., Silvestre-Albero J., Sepulveda-Escribano A., Molina-Sabio M., Rodrıguez-Reinoso F., *Kinetic Restrictions in the Characterization of Narrow Microporosity in Carbon Materials*, Journey of Physical Chemistry C, vol. 111, no. 10, 2007, 3803−3805.

[17] Rutherford S.W., Do D.D., *Characterization of Carbon Molecular Sieve 3A*, Langmuir, vol.16, 2000, 7245−7254.

[18] Bae Y.S., Lee C. H., Sorption kinetics of eight gases on a carbon molecular sieve at elevated pressure, *Carbon*, vol. 43, 2005, 95–107.

[19] Bello G., Garcia R., Arriagada R., Sepulveda-Escribano A., Rodrıguez-Reinoso F., *Carbon molecular sieves from Eucalyptus globulus charcoal*, Microporous and Mesoporous Materials, vol. 56, 2002, 139–145.

[20] Friedrich D., Reid P., Brandani S., *CySim: Cycle simulator. User documentation for CySim v0.95*, University of Edinburgh, April 2013.

[21] Rutherford S.W., Do D.D., *Adsorption dynamics of carbon dioxide on a carbon molecular sieve 5A*, Carbon, vol. 38, 2000, 1339–1350.

[22] Rutherford S.W., Coons J.E., *Adsorption equilibrium and transport kinetics for a range of probe gases in Takeda 3A carbon molecular sieve*, Journal of Colloid and Interface Science, vol. 284, 2005, 432–439.

Opportunities to Implement Renewable Energy Sources in Mining Industry

Tugay Anıl Turan[1]

[1]*KIC Energy Transition, AGH University of Science and Technology, e-mail: tugayanilturan@gmail.com*

Abstract

The industry of mining is known with its massive use of energy and its negative impacts to the environment. The prime reason of this understanding is the scale of the operations and the nature of the industry. However, for so many years, professionals were unable see the clean and renewable energy's potential in the mining sites. It is known that both mining areas and the renewable energy installations occupy large amount of space. Furthermore, humanity may need the space occupied by these industries due to the significant increase rate of the world's population. In 30 years, forecasts show that the need for residential and agricultural land will also increase. Therefore, idea represented in this article is that the renewable energy installations being located in less productive or even disturbed lands. Because of the wrong practice of mining operations or some inevitable cavities, closed mines can be perfect homes for the renewable energy power plants if the basic requirements are met. In the scope of this article, open-pit mining method is examined, and possible renewable energy solutions are suggested. These renewable energy suggestions can be implemented simultaneous to the mining operations or as a mine closure project depending on the energy needs and the method of extraction. Moreover, the article provides examples on implementations of the renewable energy installations in mining sites.

Keywords: Renewable Energy, Mine Reclamation, Surface Mining, Photovoltaics, Wind Energy

1. Introduction

According to International Energy Agency (IEA), coal supplies a third of all energy used worldwide and makes up 38% of electricity generation, as well as playing a crucial role in industries such as iron and steel. This fact connects two of the biggest sectors, mining and energy sector. It is known that these two industries are also co-dependent which means mining sites cannot exist without energy use and energy sector cannot survive without raw materials (Copper, iron, coal) and would have massive issues related with energy security without mining.

Although, even in 2050 coal will be one of the main sources of energy, it is not desired due to its carbon intensive nature. Therefore, numerous solutions were investigated and developed in order to decrease carbon emission caused by fossil fuels. However, for so many years the sustainable and green energy potential in suitable mining sites were forsaken. Recent applications of renewable energy in mining sites show that these applications can be up to 70% less expensive than the diesel power.

In 2050, the population of the world will be approximately ten billion. This growth simply tells that humanity will need more energy, more food, wider space, greater number of employments. The only way to provide everything that mankind needs is to plan every meter square carefully. It is crystal clear that renewable energy installations and mining operations occupy significant space on the planet earth. However, if these two space occupying operations are combined, the available area for agriculture and residences may be provided. In the end, some of the post-mining areas might cause irreversible changes on the earth's crust, since certain amount of material is removed. Moreover, some of these sites might not turn to account except they are used for renewable energy. In other words, if the basic conditions are met, some mines can be perfect homes for green and carbon neutral energy installations after or during their mine life.

Under the light of the new developed technologies, mining companies must consider renewable energy usage (Solar, wind, biomass) in the whole life cycle of a mine. This life cycle includes the closing of mining operations which gives the opportunity to apply an energy transition at the end of the mine's life. The renewable energy solutions in mining sites which are implemented in the world and will be suggested in this article mainly focus on surface mining operations due to the nature of existence technology. Renewable energy use during mining operations and power generation after the mine closure can result various benefits like decreasing the operation cost, contribution to the economy, positive cash flow after mining operations, usage of disturbed land. These benefits can be diversified under three main categories which are economic, social and environmental.

2. Renewable Energy Solutions for Surface Mining Methods

In the scope of surface mining, open-pit mining, strip mining and Quarry mining method are suitable for renewable energy installations. Because, these types of operations usually have big potential for solar and wind power. Surface mining is a climate sensitive application. Therefore, most of the mines are located in the places where there is suitable working environment for machinery and employees.

Since, surface mining implementations occupy large areas, the possibility of installing wind turbines or photovoltaics is significantly increased. Mining sites are placed in the remote locations. This feature has advantages and disadvantages from the perspective of energy sector. On one hand, the main disadvantage is that the mines are far from the grids. Hence, while the mining operations continuing, the price of electricity is high due to the transportation cost. That's why most of the mining companies prefer diesel as the primer source of energy for their operations. On the other hand, the advantage is that those remote locations provide solar and wind energy opportunities which cannot be found in the residential areas. Being away from the city centers makes mined lands possible future renewable energy plants at the end of mine's lifetime.

Open-pit mining, is a surface mining technique that extracts minerals from an open pit on the ground. Open-pit mining is the most common method used throughout the world for mineral mining and does not require extractive methods or tunnels. This surface mining technique is used when mineral or ore deposits are found relatively close to the surface of the earth. Deposits mined by open-pit techniques are generally divided into horizontal layers called benches. The thickness (that is, the height) of the benches depends on the type of deposit, the mineral being mined, and the equipment being used; for large mines it is on the order of 12 to 15 meters.

The mining operation continues to dig deeper until it is not profitable to extract mineral by this method. Until it reaches this point, it can extract hundreds of meters vertically. Hence, the open pit mining operations leave a big scar or hole on earth's crust. A typical example of open pit mining and its impact to the land can be observed in Figure 2.1.

Fig. 2.1. A typical example of open-pit mining operation. (Picture by Tim Roberts)

Of course mining operations are responsible for the damage they cause to the environment and according to the regulations they cannot leave the mined area as it is. That is why the reclamation term is introduced to the mining industry. According to the definition reclamation is the process of returning an area, disturbed by mining, to its natural, economic and ecological state, or to a state suitable for equivalent or superior use or benefit. Since the ore mineral is extracted no open-pit mine can recover the cavities that they cause completely. However, the cavities comes with an advantage which is increased surface area of the land. While the Figure 2.2 is showing the surface area before mining operation, Figure 2.3 shows the increased surface area after mining operation. These increased land can be used both for plantation and photovoltaic power plant.

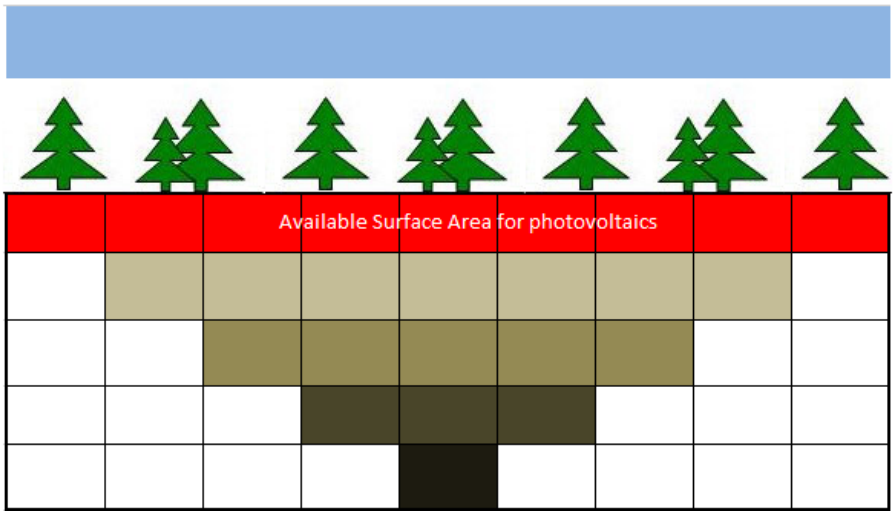

Fig. 2.2. Open-pit design before extraction and available surface area for photovoltaics.

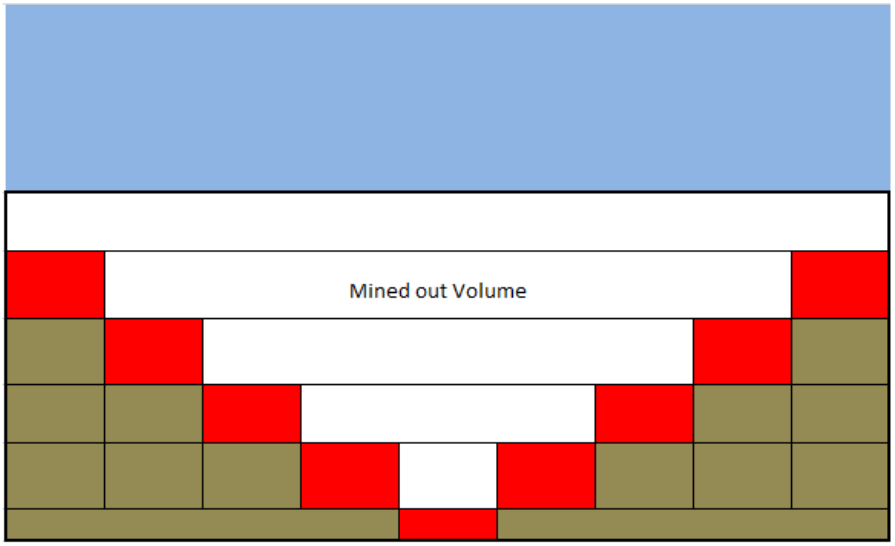

Fig. 2.3. Open pit after extraction and available surface area for photovoltaics.

In Figure 2.2 the available surface area for solar panels is 9 units. When the area is mined with a regular open pit mining method this area can be increased up to 14 units in 2D calculations. However, in 3D modelling the complex shape of the mine can increase the area even more.

The optimal solution as a mine closure project is to measure the yearly sun potential of the whole mining area. According to daylight and solar power intensity, photovoltaics should be placed in relatively high potential

areas. The relatively less sunny areas, which would not be efficient for power generation, can be used for vegetation and planting trees. As a result, a mixture of clean free power generation and the carbon capture by trees can be introduced to the post-mining area. The illustration of open-pit mine after the reclamation process with trees and photovoltaics is shown in Figure 2.4.

Fig. 2.4. Illustration of the open-pit mine after renewable energy installations are implemented as a mine closure project.

The very same kind of implementations can be performed in strip mines and quarries. If the conditions are suitable for wind energy where the solar power is not sufficient, wind turbines can be built since these mines are located at least 30km away from the residential area.

Renewable energy sources are already in use in the mining industry and it is expected that the number of installations will increase in the following years. Because, the technology is mature, and it provides cheaper electricity for the operating mines in long term. However, there are not examples of renewable energy power plants as a mine closure project. In the future, observing mine reclamation projects including renewable energy will be highly possible. Table2.1 shows the current practices of wind and solar energy applications all around the globe.

The power of these plants may seem insignificant when they are compared to a coal-fired or a natural gas-fired power plant. However, these power capacities can be highly significant for a single mining operation. Moreover, these applications do not contribute to the CO_2 emissions that is not wanted for environmental concerns.

Table 2.1. The list of renewable energy installations in mines

Name of the Mine	Location	Mining Method	Renewable Energy Type	Capacity
Galaxy Resources, Mt	Perth, Australia	Open-Pit Mining	Solar and Wind	1MW Solar, 1.2 MW

Cattlin				Wind
Sandfire DeGrussa Copper and Gold	DeGrussa, Australia	Open-Pit Mining	Solar	10.5MW (6MW Storage)
Rosebel Gold Mine	District Brokpond, Suriname	Open-Pit Mining	Solar	5MW
Gabriela Mistral Mine	Sierra Gorda, Chile	Open-Pit Mining	Solar Thermal	27.5MW
Amanecer	Copiapo,Atacama, Chile	Open-Pit Mining	Solar	100MW
Diavik Diamond Mine	Lac de Gras, Canada	Open-Pit Mining	Wind	9.2MW
Giencore Ragian Mine	Katinniq, Canada	Open-Pit Mining	Wind	12MW
Los Pelambres Mine	El Arrayán, Chile	Open-Pit Mining	Wind	115MW

3. Conclusions

Renewable energy and mining are concepts not so distinct from one another. Additionally, when these two sectors meet at the same location, there will be certain benefits. These benefits can be expressed in three main categories.

Firstly, starting from its development to the end of the mining, the operations in a mine require massive energy. Furthermore, this energy is produced by fossil fuels. While wind turbines and photovoltaics provide the opportunity to have cheaper and sustainable energy, they do not emit CO_2 or other greenhouse gases. Although, in most of the cases renewable energy will not be enough for the mining operations, these generations can be combined with fossil fuels as a hybrid solution.

Secondly, some of the environmental effects caused by mines cannot be reversed. However, with current solutions provided by renewable energy, these harmed areas may be used for a superior need. When the population growth is considered, the need for energy, agricultural land, and residential area will increase without question. The solution which is presented in the article is using post- mining areas for electricity generation with wind and solar power. The solution does not require the areas which can be used for agriculture or residents. On the contrary, it offers added value to the land which was damaged.

Thirdly, renewable energy installations provide continues economic value to the area even when mining operations are finalized. Mining industry in many sites is labor intensive and this manpower include experienced mechanical and electrical technicians and engineers. At the end of the mine life these people might be unemployed, and value added to the local people of the area will be decreased. Renewable energy power plants as a mine closure project can create many jobs for the locals. When sufficient training is provided the manpower in mines can be transformed to employment in renewable energy sector.

In conclusion, renewable energy sources can bring a big impact to the mining industry. The clean energy applications like wind or solar can be implemented both during operation and after the closure of the mine.

This new approach to mining may result in less consumption of fossil fuels and less CO_2 emission to the atmosphere. Using renewable energy in the mining sector will be economically, environmentally and socially beneficial.

References

[1] Geology. Retrieved November 25, 2019, from https://courses.lumenlearning.com/geology/chapter/reading-open-pit-mining/.

[2] 27.5 MW Provide Heat for Copper Mine in Chile. (2019, October 18). Retrieved November 27, 2019, from https://www.solarthermalworld.org/installation/275-mw-provide-heat-copper-mine-chile.

[3] At Mining Sites Renewable Energy Systems are up to 70 Percent Less Expensive than Diesel Power. (n.d.). Retrieved November 22, 2019, from http://www.mining.com/web/at-mining-sites-renewable-energy-systems-are-up-to-70-percent-less-expensive-than-diesel-power/.

[4] Coal: Our work. (n.d.). Retrieved November 28, 2019, from https://www.iea.org/topics/coal/.

[5] Database "Renewable Energy & Mining": wind & solar. (n.d.). Retrieved November 20, 2019, from https://www.th-energy.net/english/platform-renewable-energy-and-mining/database-solar-wind-power-plants/.

[6] Home. (n.d.). Retrieved November 26, 2019, from https://www.sandfire.com.au/site/operations/degrussa/solar-power-project.

[7] Open-Pit Mining Definition. (2019, December 10). Retrieved November 25, 2019, from https://www.angloamerican.com/futuresmart/our-industry/mining-explained/mining-terms-explained-a-to-z/open-pit-mining-definition.

[8] Safety in Open Pit Mining. (2018, February 25). Retrieved November 24, 2019, from https://www.911metallurgist.com/blog/open-pit-mining-safety.

[9] SunEdison, IFC and OPIC Close $212.5M Project Financing arrangement for a 100 MWp Solar Power Plant in Chile. (n.d.). Retrieved November 26, 2019, from https://www.opic.gov/press-releases/2013/sunedison-ifc-and-opic-close-2125m-project-financing-arrangement-100-mwp-solar-power-plant-chile.

[10] Thompson, A. (2011, April 6). A miner moves to renewables to power its site. Retrieved October 25, 2019, from https://www.abc.net.au/news/2011-04-05/a-miner-moves-to-renewables-to-power-its-site/2629936.

Climate positive district heating network for a small municipality using a local coal mine.

Karolina Serafin[1]

[1]*Faculty of Energy and Environmental Engineering, Silesian University of Technology, e-mail: karolina.serafin2@gmail.com*

Abstract

The article concerns implementation of a small-scale district heating network for a municipality located in Silesian Region in Poland. Currently in this municipality there is a very poor heating network and the heat demand is being covered in majority from individual hard coal fired boilers. In this work utilization of coal mine methane (CCM) from a local hard coal mine for residential heating purposes is considered. The methane from this mine is now only partially being captured and not whole acquired volume is being utilized. Introducing heating network in this area could bring environmental benefits in form of improvement of air quality and savings of the conventional fuels.

Keywords: district heating, heating network, heat demand, coal mine methane, CCM.

1. Introduction

The global energy demand continues to grow, and many countries face the challenge of supplying inhabitants with energy while also meeting the rising requirements imposed by the European Union. The struggle is even bigger for countries where the energy mix is based on fossil fuels, mainly coal. An example of such country is Poland, where, in terms of heat generation by heating plants, in year 2017 coal constituted almost 74% of fuels used, and in case of heat produced in cogeneration systems, where the diversification is slightly bigger, the share of coal was equal to 69% of all fuels.[1]

Situation is similar when concerning heat generation in individual households. The majority of houses in Poland utilizes fossil fuels for the heating purposes. In 2017 around 70% of households were provided with heat by coal-fired boilers, and even 50% of those boilers are aged 10 years and older. Only every fifth building is heated from sources that do not affect the air quality.[2] The abovementioned data indicate that single-family houses significantly contribute to the emissions of harmful substances to the atmosphere.

A solution may be shifting to small-scale district heating networks. District heating involves production of energy in a centralized source rather than in individual boilers. The heat is then distributed through piping network to multiple houses. Those systems can be based on renewable energy sources and cogeneration or even trigeneration. They provide higher efficiency and lower emissions, as well as give better control over the system, contributing to the improvement of the quality of life in the area.

With Poland being strongly dependent on hard coal and with limited possibilities to utilize renewable energy, it is a great challenge to find a cleaner alternative fuel for heating households. Hard coal still appears as the simplest and cheapest heat source, and it is widely available. There are many solutions to possibly minimize the influence of coal-fired boilers on the environment, but it does not solve the problem with the limited coal reserves being depleted in a close future.

There is however a great opportunity that comes with hard coal mining, namely Coal Mine Methane (CMM). It is a gas resulting from the mining operations, that for a very long time has been perceived mainly as a danger for miners and the priority was to lead it out of the mine by releasing it to the atmosphere. This contributed significantly to global warming, as methane is a gas with the estimated global warming potential

(GWP) to be 28 times higher than carbon dioxide.[3] But the potential of CMM for energy generation has finally been noticed and currently the trend is to capture it and use as a fuel.

The aim of this project is to design a district heating network for a residential area with single family detached houses to supply those recipients with heat from a cleaner, more environmentally friendly source. The project involves transition from individual heating sources installed in each building to one, bigger, central source, supplying all recipients. As the fuel for those recipients CMM from a nearby coal mine is considered. These efforts could contribute to decrease of emissions and savings of the conventional fuels.

1. Description of the analyzed region

The project is realized for a residential area in Ornontowice, a municipality located in the central part of Silesian region, about 20 kilometers south-west of the regional capital city, Katowice. The exact location is presented in the Fig. 2.1.[4] This is a relatively small municipality, with the area equal 15 km^2 and the number of inhabitants around 6 000 people.[5] Still, this is an important industrial region with the "Budryk Hard Coal Mine" located in the center.

Fig. 2.1. Localization of Ornontowice on the map

When it comes to the heat generation and distribution, on the premises of the municipality there is a heating network of length 5 550 meters, but it mainly supplies heat to the local coal mine, and only in a small part, less than 10%, is used for heating purposes in the housing sector. The rest of the buildings have individual heating sources. As for the family houses, they are mainly equipped with coal-fired boilers - in 65%. Then there are biomass boilers (11%) and gas boilers (10%). Electricity as a heating source is used only in around 4% of the households in Ornontowice.[6] The exact structure of the heating sources in the housing sector in Ornontowice is presented in the Fig. 2.2.

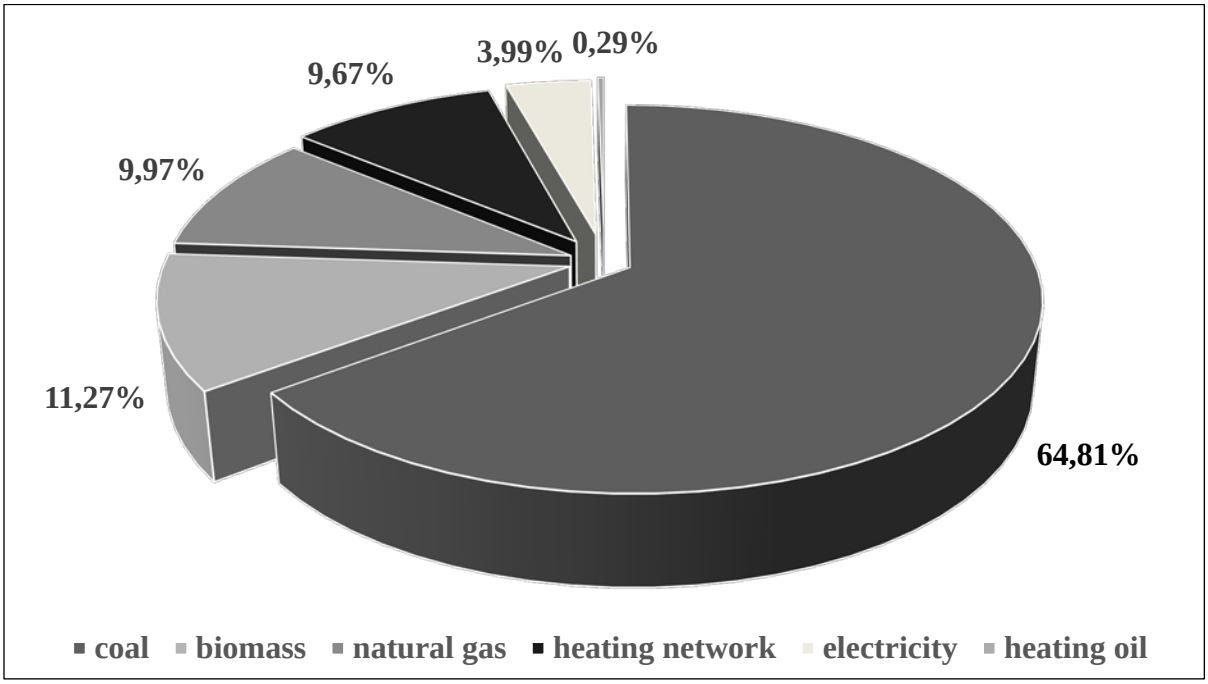

Fig. 2.2. The structure of the heating sources used in the housing sector in Ornontowice

For the simplification purposes for this project considered will be a small residential area located in the Ornontowice municipality, located close to the coal mine. The heating network will be designed for a housing district with 50 single-family detached houses, including also a kindergarten and a primary school. None of the buildings is connected to the existing heating network, each having its own individual heat source. The settlement of the buildings is quite compact, they are placed close one to another along the streets, yet having many available green areas around for placement of a small scale heat source.

A simplified map of the area for which the district heating network will be designed, with indicated borders of the parcels, outlines of the buildings and the streets, is presented in the Fig. 2.3.[7]

Fig. 2.3. The simplified map of the area under consideration

1. Heat demand estimation

1.1. Calculation procedure

In order to design a heating network, there was first conducted a simulation to estimate the expected heat demand to enable sizing of the system. For the sake of simplification of the calculations some assumptions and generalizations were made, namely the geometry of the buildings was simplified, the number of people inhabiting one house was taken to be 4 people on average, the heating season was assumed to last 212 days (October 1st – April 30th).

In all the calculations, meteorological data for a typical meteorological year, based on the 30-year long measurement (1971-2000), was used for the station in Katowice.[8] Additionally, according to the standards, which divide Poland into five climatic zones during the heating season, differing in the average annual outside temperature and the design outside temperature, the region analyzed in this project is placed in the 3rd climatic zone, with the design outside temperature of -20°C.[9]

The calculation procedure includes checking the energy demand for the purpose of space heating and hot water preparation, including also demand for covering the losses connected with ventilation. Calculations were conducted for the 50 single-family houses and separately for the kindergarten and the primary school, as the demand in public institutions differ from the residential sector. For this sake was used a computational procedure described by Aleksander Szkarowski and Leszek Łatowski.[10]

1.2. Calculation results

Results of the conducted heat demand calculations for the residential sector are presented in the Table 3.1., for the kindergarten in the Table 3.2. and for the primary school in the Table 3.3. In the Table 3.4. are collected values of the annual demand for the whole system.

Table 3.1. Calculation results for the residential sector

description	symbol	value	unit
total volume of the 50 houses	V	37 200	m^3
annual energy demand for space heating purposes	$\dot{Q}_h^a$	2 092	MW
		7 532	GJ
annual energy demand for the purpose of heating water	$\dot{Q}_{hw}^a$	281	MW
		1 010	GJ
annual energy demand for covering ventilation heat loss	$\dot{Q}_v^a$	446	MW
		1 606	GJ
overall annual energy demand for the houses	$\dot{\mathbf{Q}}^{\mathbf{a}}$	**2 819**	**MW**
		10 148	**GJ**

Table 3.2. Calculation results for the kindergarten

description	symbol	value	unit
total volume of the kindergarten	V	6 000	m^3
annual energy demand for space heating purposes	$\dot{Q}_h^a$	277	MW
		997	GJ
annual energy demand for the purpose of heating water	$\dot{Q}_{hw}^a$	24	MW
		86	GJ
annual energy demand for covering ventilation heat loss	$\dot{Q}_v^a$	37	MW
		133	GJ
overall annual energy demand for the kindergarten	$\dot{\mathbf{Q}}^{\mathbf{a}}$	**338**	**MW**
		1 217	**GJ**

Table 3.3. Calculation results for the primary school

description	symbol	value	unit
total volume of the school	V	23 490	m^3
annual energy demand for space heating purposes	$\dot{Q}_h^a$	859	MW
		3 092	GJ
annual energy demand for the purpose of heating water	$\dot{Q}_{hw}^a$	46	MW
		166	GJ
annual energy demand for covering ventilation heat loss	$\dot{Q}_v^a$	95	MW
		342	GJ
overall annual energy demand for the school	$\dot{\mathbf{Q}}^{\mathbf{a}}$	**1 000**	**MW**
		3 600	**GJ**

Table 3.4. Annual heat demand for the whole system

houses		kindergarten		school		total	
MW	GJ	MW	GJ	MW	GJ	MW	GJ
2 819	10 148	338	1 217	1 000	3 600	4 157	14 965

On the base of the calculation results were created two graphs - ordered annual heat demand graph depending on the outside temperature (Fig. 3.1.) and ordered annual heat demand graph depending on the frequency of occurring of given outside temperature (Fig. 3.2.).

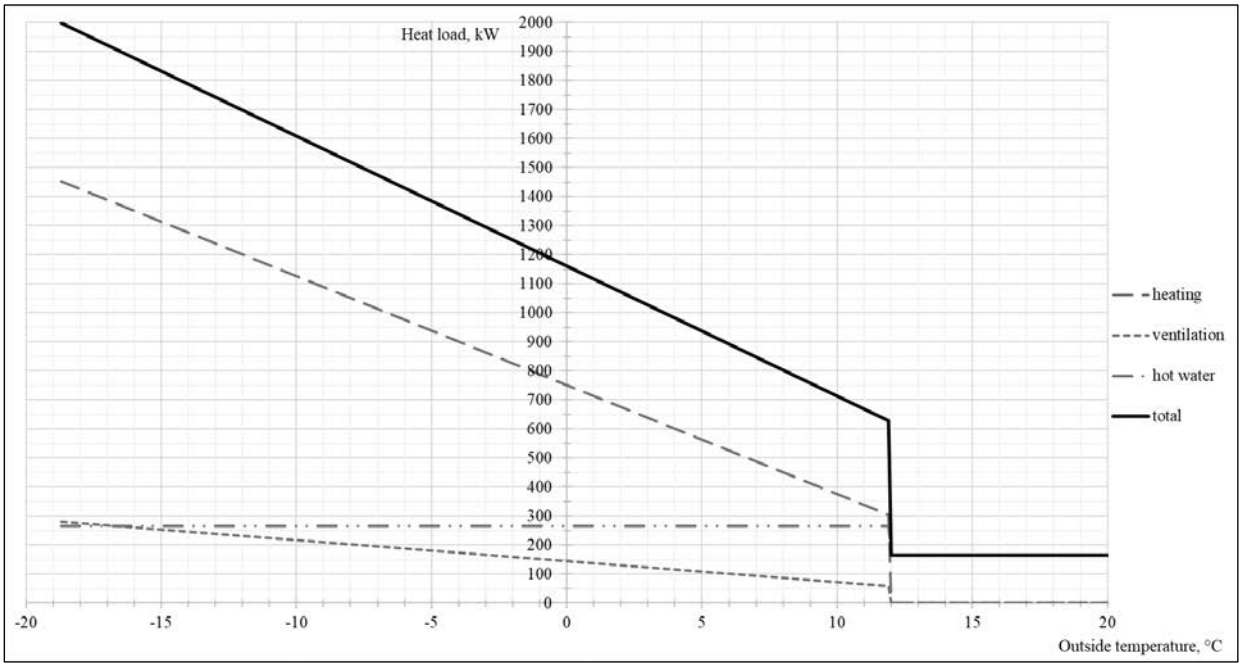

Fig. 3.1. Ordered annual heat demand depending on the outside temperature

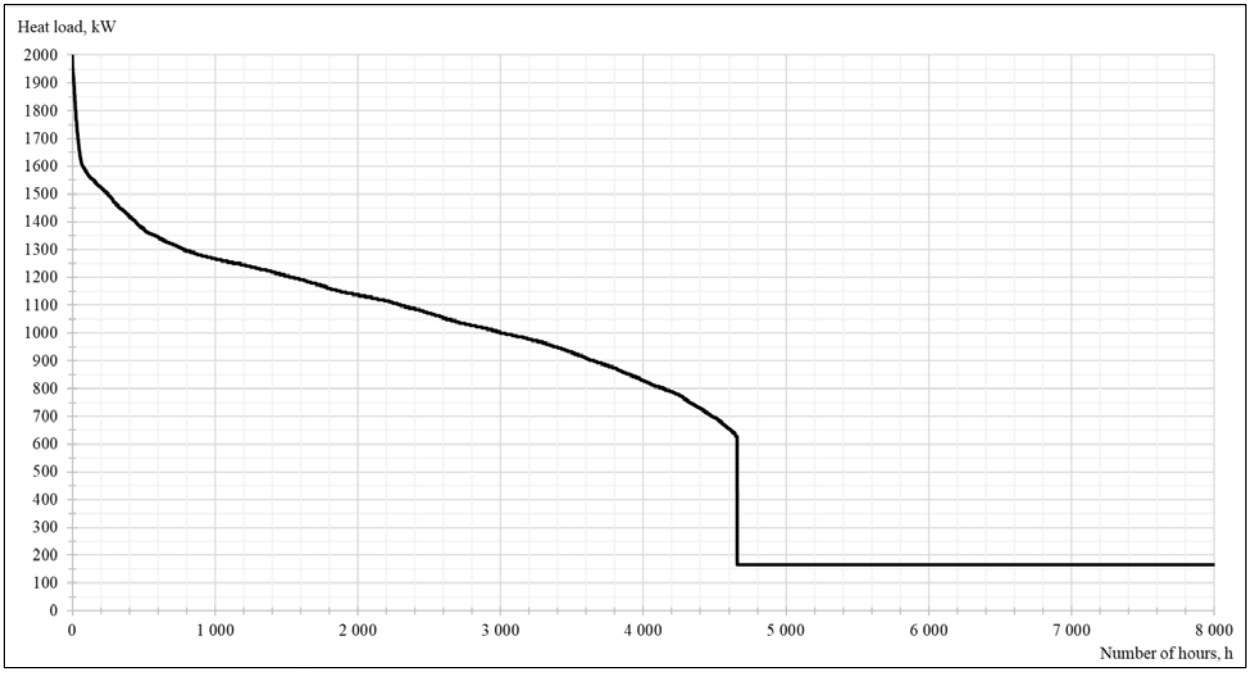

Fig. 3.2. Ordered annual heat demand depending on the frequency of occurring of given outside temperature

2. Coal Mine Methane utilization

2.1. CMM general information

Coal mining is a significant source of methane emissions. Methane is embedded in the coal layers and it can be emitted from active mines due to mining activities, but also from abandoned mines and, in smaller share, as a result of post-mining activities (including coal processing, storage and transportation). Methane resulting from coal mining is a great source of energy which is still largely untapped. In 2012, coal mines accounted for approximately 8% of global anthropogenic methane emissions.[11]

The coal mine gas has always been a known and important aspect of hard coal mining. Methane represents a safety hazard for the underground operation because it can form an explosive mixture in connection with air. The removal of this gas is therefore of great importance for the operation of the workers. For this reason, coal mine degasification grew out to help improve safety in mines. With the increase of awareness, the coal mine gas introduced to the atmosphere has become more important also in the context of climatic and environmental problems. Released methane significantly enhances the global warming effect, as it is a greenhouse gas with the effect 28 times higher than of carbon dioxide [3], therefore its capture and use brings serious environmental benefits.

Although currently in Poland the coal mining activities are consistently being reduced and many mines were closed in the last few years, the amount of methane emitted from the mining sector still constitutes a significant share. In 2016 gas released from the underground mines yielded 37% of the total methane emissions in Poland.[12] One of the main reasons is that the methanization of coal mines is progressively increasing. It is strongly connected to the coal mining operations moving deeper, where methanization is higher, hence more coal mine gas is being released. Comparing the data, in 2010 there was around 76 mln tones of coal extracted and the total methanization was 835 mln m^3 CH_4. In 2014 the amount of coal mined decreased to 72.5 mln tones but the methanization yielded 891 mln m^3 CH_4.[13]

Due to the technology development and spread of knowledge about coal mine gas potential, the amount of methane captured from coal mines and utilized increased. In 2010 in Poland was captured around 256 mln m^3 of CH_4 and about 161 mln m^3 (63%) was utilized. In 2014 the amount of methane captured increased to 321 mln m^3, and around 211 mln m^3 (66%) was utilized.[13] Those actions are however not enough to decrease the influence of coal mines on the environment. Despite all the efforts, the overall amount of methane emitted to the atmosphere increased. In 2010 around 674 mln m^3 of CH_4 was released due to mining activities in Poland, and this value increased to 680 mln m^3 of CH_4 introduced in 2014.[14]

2.2. CMM utilization from the local coal mine

Coal mine “Budryk” located in municipality Ornontowice is a highly methanous mine. During the exploration around 180 mln m^3 of CH_4 is released.[15] Until 2004 this gas was entirely introduced to the atmosphere. Then first capturing installations were introduced, but they captured only about 20 mln m^3 of CH_4. In 2016 a project was realized to increase the capture capacity and partly utilize the obtained gas. There was build a cogeneration system with two 4 MW generators and the amount of methane captured was increased to 90 mln m^3. The energy generated is used for covering the needs of the coal mine. In 2016, this system was covering around 30% of the mine’s demand.[16] The coal mine’s ultimate goal is to become energetically independent and cover the whole demand with use of CMM. New investments are being made to increase methane capture capacity and utilize most of it. Last year, the energy demand was covered in 46%. By 2030 it is planned to capture around 170 mln m^3 of CH_4.

The methane obtained from the coal mine is a great opportunity to be used as an alternative fuel source in the district heating area in the municipality. As stated before, the heat demand in Ornontowice is in 65% covered by coal fired boilers. Switching to gas fuel would bring many benefits. The emissions connected with using gas boiler are lower than for coal, which would contribute to the improvement of air quality in the area. The depletion of natural resources would be reduced, as CMM is a natural by-product of coal mining with a great

potential and introducing it to atmosphere is wasteful and harmful for the environment. The amount of methane that can be captured is substantial and would be enough to cover the needs of the coal mine and also at least a smaller region for the beginning, having potential to develop a strong heating network in the municipality.

3. Conclusions

Poland is gradually becoming more aware of the environment, however there is still a huge dependency on coal and outdated technologies. One of the reasons is that the implementation of renewable resources is limited due to the limited availability and high costs. Still, there are many chances of introducing environmentally beneficial changes to the system. One of the solutions may be taking advantage of the many coal mines in Poland and utilization of the coal mine methane. There are numerous benefits to capturing and using CMM, including conservation of a local and highly valuable source of energy, reduction of the greenhouse gas emissions, enhancement of the mine safety and providing of the revenue for the mine.

Implementation of the small-scale district heating system fueled with mine methane would be a very beneficial solution, having the potential for improvement in terms of ecology and comfort of users. Switching from individual coal-fired boilers to gas-fired source would reduce the emissions of harmful substances from the residential sector, resulting in improvement of air quality and comfort of life of the residents. Reduced would be also the carbon footprint. Additionally, the inhabitants connected to the network would not have to take care of heating of their houses, as heat would be provided from the external source. What's more, this fuel source, being a by-product of mining activities, would be a cheaper choice compared to hard coal.

In the future creation of a cooling network could also be considered. Although Poland is situated in a moderate climate zone and it would seem that the need for air conditioning is insignificant, a rising tendency can be observed lately. With changing atmospheric conditions and higher expectations concerning thermal comfort, the demand is also increasing. This demand could be covered by implementing cooling to the designed system, which would also help to balance the uneven need for fuel gas throughout the whole year. In this way, there would be a constant recipient of the methane and the inhabitants would gain access to cooling cheaper than home-scale air conditioners.

The problem with alarmingly bad air quality in Poland and emissions from households can be gradually tackled. Solutions and resources should be searched locally and should be fit for the local needs. There are many solutions available. Now it is a matter of scale and speed of transition.

References

[1] Buńczyk A., Bogusławski P., *Energetyka cieplna w liczbach - 2017*, Urząd Regulacji Energetyki, Warszawa, 2018.

[2] Zaborowski M., Walczak E., *Efektywność energetyczna w Polsce. Przegląd 2017*, Instytut Ekonomii Środowiska, Kraków, 2018.

[3] Myhre G., Shindell D., *Anthropogenic and Natural Radiative Forcing*, Cambridge University Press, Cambridge, United Kingdom and New York, USA, 2013.

[4] Google Maps, available on: https://www.google.com/maps/place/Ornontowice/@50.2293696,18.744318,11z/data=!4m5!3m4!1s0x471135113ea5829f:0x333d0a16148b7a9c!8m2!3d50.1811451!4d18.751126!5m1!1e2, available on 24.11.2019.

[5] Urząd Statystyczny w Katowicach, *Statystyczne Vademecum Samorządowca 2018 - Ornontowice*, available on: https://katowice.stat.gov.pl/vademecum/vademecum_slaskie/portrety_gmin/powiat_mikolowski/gmina_ornontowice.pdf, available on 24.11.2019.

[6] *Aktualizacja projektu założeń do planu zaopatrzenia w ciepło, energię elektryczną i paliwa gazowe dla Gminy Ornontowice na lata 2018-2033*, available on: https://www.bip.ornontowice.pl/res/serwisy/pliki/19747527?version=1.0, available on 24.11.2019.

[7] Geoportal 2, available on: http://mapa.mikolowski.pl/map/www/mapa.php?CFGF=wms&mylayers=+granice+dzialki+numery_dzialek+budynki+adresy+drogi+dr_kraj+dr_woj+dr_pow+dr_gm+dr_inne+&myqlayers=+dzialki+budynki+adresy+#, available on 24.11.2019.

[8] Ministerstwo Inwestycji i Rozwoju, *Typowe lata meteorologiczne i statystyczne dane klimatyczne - Katowice*, available on: https://www.gov.pl/web/fundusze-regiony/dane-do-obliczen-energetycznych-budynkow, available on 24.11.2019.

[9] Norma PN-EN 12831, *Nowa metoda obliczania projektowego obciążenia cieplnego*.

[10] Szkarowski A., Łatowski L., *Ciepłownictwo*, Wydawnictwo WNT, Warszawa, 2012.

[11] Global Methane Initiative, *The U.S. Government's Global Methane Initiative Accomplishments - Annual Report 2013*, available on: https://www.epa.gov/sites/production/files/2016-01/documents/usg_2013_accomplishments_0.pdf, available on 24.11.2019.

[12] *Klimat dla Polski. Polska dla klimatu. 1988-2018-2050*, Instytut Ochrony Środowiska - Państwowy Instytut Badawczy, Warszawa, 2018.

[13] Patyńska R., *Wskaźnik emisji metanu z kopalń węgla kamiennego w Polsce*, Zeszyty Naukowe Instytutu Gospodarki Surowcami Mineralnymi i Energią Polskiej Akademii Nauk, nr 94, s. 67-78, 2016.

[14] Wyższy Urząd Górniczy, *Ocena stanu bezpieczeństwa pracy, ratownictwa górniczego oraz bezpieczeństwa powszechnego w związku z działalnością górniczo-geologiczną w 2018 roku (porównanie od roku 2014)*, Katowice, 2019.

[15] Górnicza Izba Przemysłowo Handlowa, *Dla kopalni, dla gminy, dla ekologii* (BG 5-6/2017), available on: http://www.giph.com.pl/strony/dla-kopalni-dla-gminy-dla-ekologii-bg-5-62017, available on 24.11.2019.

[16] Biznes Alert, *Kopalnia Budryk w części zasilana energią z metanu*, available on: https://biznesalert.pl/kopalnia-budryk-metan-energia/, available on 24.11.2019.

Out-Of-Step Protection Modeling for Playback and Real-Time Testing

Mateo Toro Cárdenas[1]

[1]*Department of Electrical and Electronic Engineering, University of The Andes, Bogotá D.C., Colombia, e-mail: m.toro10@uniandes.edu.co*

Abstract

This paper describes the modeling and implementation process of a virtual out-of-step protection algorithm based on two commercial methods to develop playback and real time testing. The proposed methodology involves analyzing an existing COMTRADE file through specific digital signal processing (DSP) modules in order to detect an out-of-step operation condition in a simple power system using National Instruments software and hardware. The result brings a virtual tool able to analyze different generators in unique power systems presenting stable and unstable power swing events.

Keywords: Generators, Power system protection, out-of-step, LabVIEW

1. Introduction

Generators are one of the most important elements inside an electrical power system. They are not only responsible for providing the energy to attend the demand, also they are responsible to keep tension stability, frequency, and angle during a perturbation in the system [1]. Out-of-step operation is one of those possible perturbations. It is consequence of under voltages, low excitation on generators or high impedance between the generator and the system [2]. The above causes high currents and stress in the generator's windings and mechanical efforts in the stator of the machine which can even cause a break [3]. These are the reasons for the existence of the out-of-step protection function (ANSI 78) which recognizes if the behavior of the apparent impedance seen by the generator describes a characteristic path given a power swing in the power system which leads to a trip signal in the protection equipment. Simulation tools are ideal for exploring such fault scenarios and reaching the best settings [4].

In this paper a complete walkthrough the modeling and implementation process is presented. First, the configuration specifications necessary for the virtual tool are explained. In this part two commercial detecting characteristics are explained. This part applies equally for playback and real time testing. Then, playback DSP is presented as it differs from real time DSP, which is explained next. After that, the programing for the detection logic is presented. Again, this applies equally for both testing techniques. Results are presented using a single infinite bar system which will be explained at that moment. A final comparison between playback and real time testing is presented before conclusions.

2. Commercial Detecting Characteristics

For this virtual tool it is necessary to provide the following generator and system attributes. These are the transient reactance of the generator's direct axis (X'd), the reactance of the corresponding step-up transformer (XT) and the reactance of the system under maximum generation (Xmax). Also, it is possible to provide the critical angle between the generator and the system, δ (120° default) and a protection percentage of the transformer for internal oscillations, μ (between 70% and 90%).

The mho characteristic is proposed by IEEE Power System Relaying Committee in [5], while the quadrilateral characteristic is presented in [6]. Figure 2.1 shows the resultant geometry in a R-X graph and the corresponding formulas using the values described above in this section.

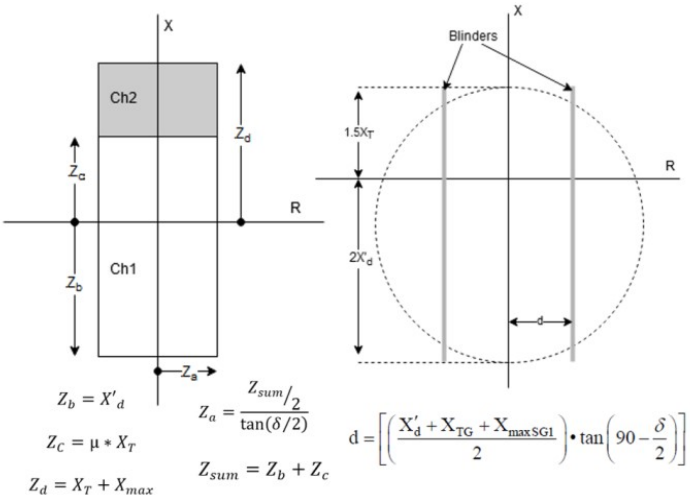

Fig. 2.1. Quadrilateral characteristic (left) and Mho characteristic (right) and associate formulas.

3. Digital Signal Processing (DSP)

This section starts explaining the process applied to the signals during the playback testing technique. LabVIEW is a software made by National Instruments which allows multiple programming possibilities using G language. This software is equipped with a complement called Electrical Power capable of analyzing COMTRADE files as voltage and current data vectors. A rational resampling process is applied to these vectors, then a low-passing 2nd order Butterworth filter is implemented [7]. The number of samples that exist per cycle is determined to adjust a mobile window on which a Fourier transform will be applied, obtaining a value of magnitude and phase for each voltage and current signal. With the above values, a phase impedance value seen by the generator is obtained. In other words, for each window that is analyzed, a complex value of voltage and current is obtained with which a complex phase impedance is calculated to move the window one sample then forward and repeat the process. The phase impedance vector is then transformed into a positive sequence impedance vector. This vector can be analyzed straightforward in the next section.

The DSP applied during the real time testing is quite different. A power injection device developed inside Universidad de Los Andes, Colombia, was used to transform COMTRADE oscillographies into analog signals which were received by a data acquisition hardware, CompacRio9082, developed by National Instruments. The 6 analog signals for 3 voltages and 3 currents in the form voltage were read cycle by cycle. Then the first cycle was connected to the second one and the analysis was performed. After that, the oldest part of the two-cycle cluster was deleted, and a new just-read cycle was joint to the remaining one. A new analysis is performed, and the operation repeats until the COMTRADE's end. The mobile window concept applied for the playback technique cannot be used during real time analysis due to computation capacities. The proposed alternative involves taking a user-determined number of photos of the two-cycle cluster previously mentioned. For each of these photos, which are one cycle long, a Fourier transform is applied to obtain a complex voltage and current values, then used to get a complex phase impedance value. Then, a positive sequence impedance is obtained. The maximum number of photos that can be taken in the two-cycle cluster is 46 due to computational capabilities. The more photos that are taken the closer the impedance path resultant to a point by point analysis. This concept is illustrated in figure 3.1 where a 6 and 46 photos' analysis (left and right respectively) in green is compared to a point by point analysis in blue.

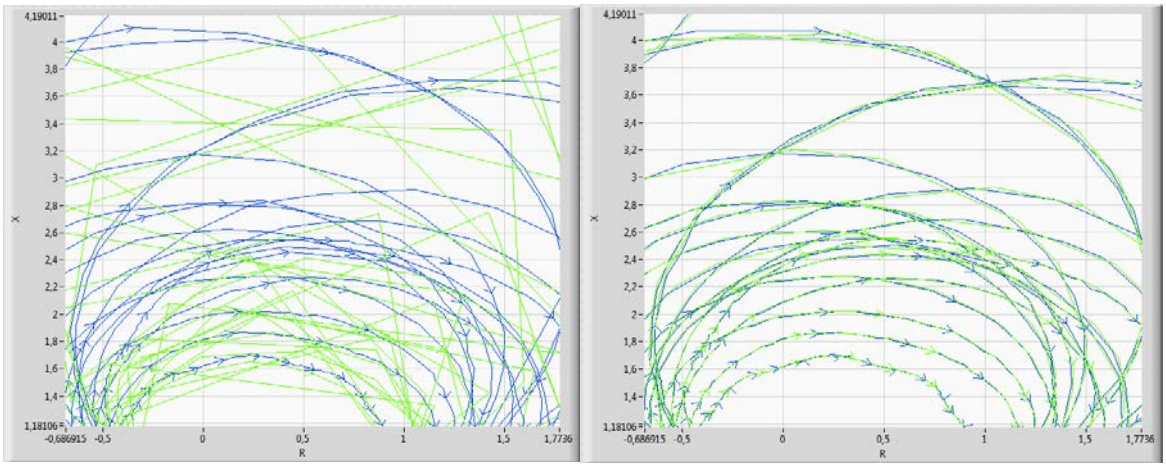

Fig. 3.1. Comparison in the impedance calculation point by point (blue) and taking 6 (left) and 46 (right) photos (green) in two cycles.

4. Out-Of-Step Detection Logic

The detection logic is based in the state machine presented in figure 4.1. The main idea is to count the times that the positive impedance path goes through the selected characteristic form right half plane to left half plane in a R-X graph.

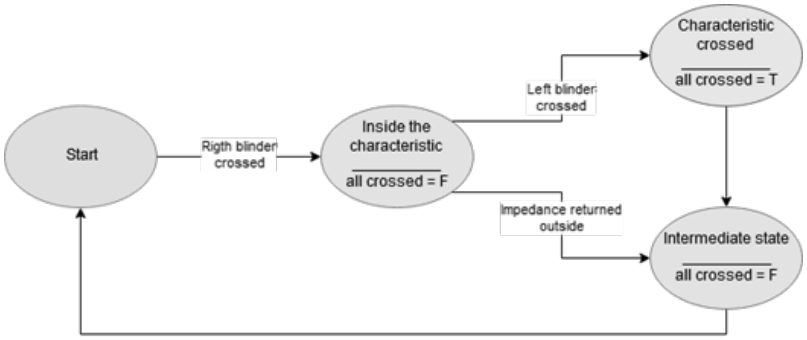

Fig. 4.1. Out-of-step detection state machine.

This state machine has three inputs and one output. The inputs are booleans that carry information about the movement of the apparent impedance within an R-X plot. These values are determined by analyzing two neighbor values of the impedance's behavior. If the first value is outside the characteristic and, the next value is inside the characteristic in the positive half plane, the right blinder (edge of the characteristic) has been crossed. If the first value is inside the characteristic in the negative half plane, and the next value is outside the characteristic, the left blinder (edge of the characteristic) has been crossed.

It is possible that the first value is inside the characteristic and the value is outside the characteristic but in the positive half plane which means that the impedance returned from where it came. The output of the state machine is a boolean that confirms if the apparent impedance crossed the characteristic from right to left.

There are four states in this state machine. A "start" state where the program waits for the impedance to cross the right blinder of the characteristic. Once that is done, the output "all crossed" is set to False in the "inside the characteristic" state and the program wait again for a left blinder crossed' flag or a signal that confirms the return of the impedance outside the characteristic through the right. If the left crossed blinder's flag arrives, the output is set to True in the "crossed characteristic" state.

On the other hand, if the second signal arrives the "intermediate state" is reached. From the "characteristic crossed" state, there is no condition for the transition which leads the algorithm to the "intermediate state"

immediately where the output is set to False. Again, there is no transition condition in the “intermediate state” so the “start” state is reached immediately closing the loop.

5. Results

For the system presented in figure 5.1 two events were analyzed. Line 1 was disconnected for 200 ms which resulted in a stable power swing. The unstable power swing was produced by disconnecting line 1 for 220 ms.

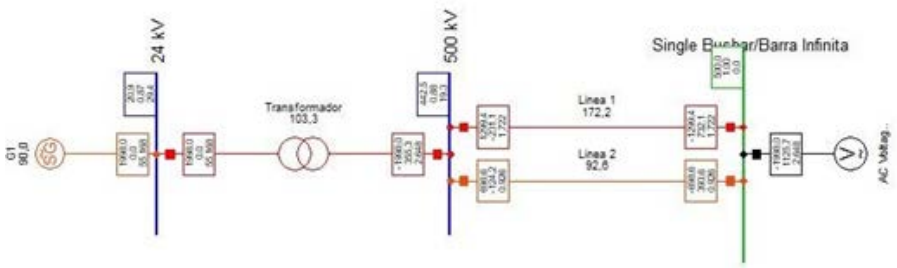

Fig.5.1. Case of study: Infinite bus.

The stable power swing being seen by the generator using quadrilateral characteristic is presented in figure 5.2. The left part represents the playback test while the right part represents the real time test.

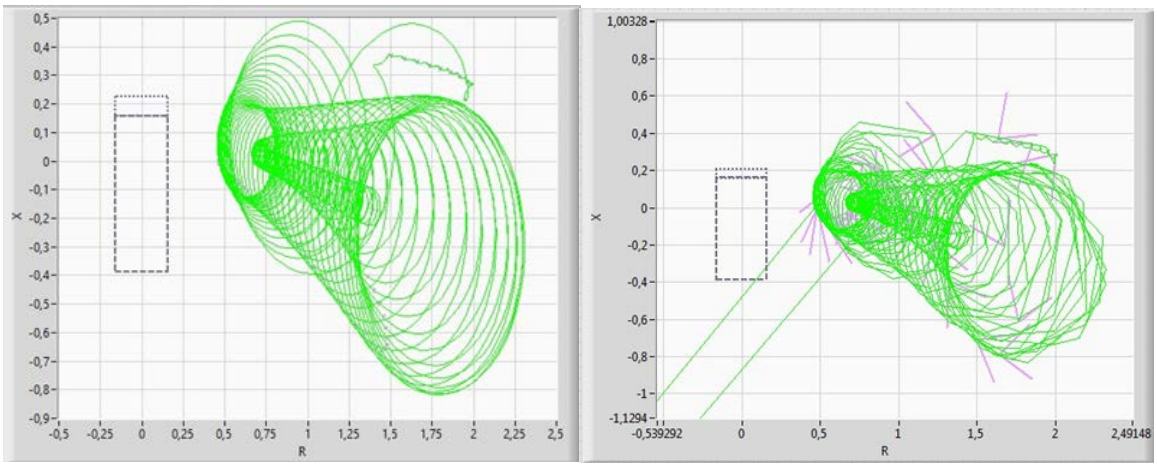

Fig. 3.2. Quadrilateral characteristic for stable condition using playback testing (left) and real time testing (right).

The paths illustrated by figure 5.2 are very similar using both testing techniques. Also, no out-of-step condition was detected.

Next, the unstable power swing condition is analyzed using the Mho characteristic comparing between playback test results and real time results. This can be seen in figure 5.3.

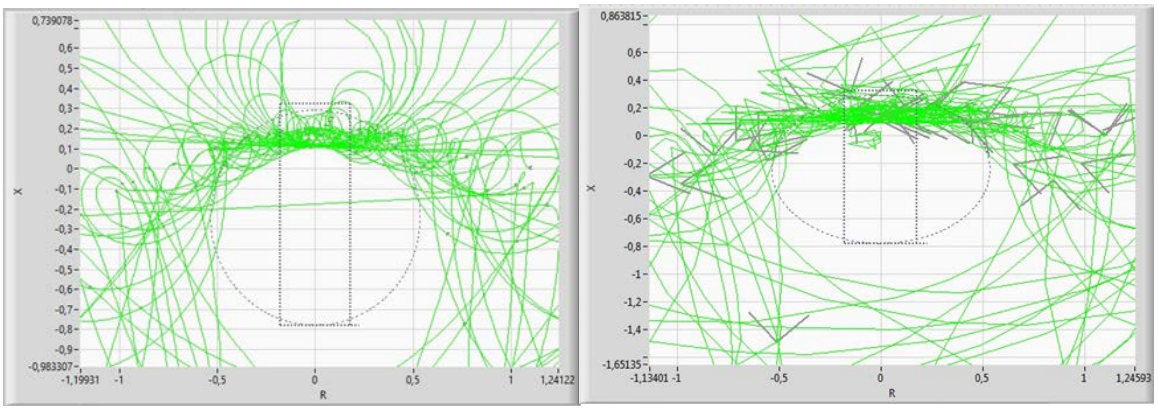

Fig.5.3. Mho characteristic for unstable condition using playback testing (left) and real time testing (right).

Again, the paths illustrated by figure 5.3 are very similar using both testing techniques. However, there is a small difference between the resultant counters, for playback testing 24 crosses were detected while 35 crosses were detected for real time testing.

6. Conclusions

This paper demonstrated the design and implementation process for an out-of-step virtual relay capable of performing playback and real time tests using National Instruments software and hardware. The development involved using commercial detection characteristics and analyzing standardized COMTRADE files which can be obtained from various simulation software and even from real on-camp relays. Also, a valid comparison was made between both testing techniques which required different programming approaches. In the future, this virtual tool can be used to analyze bigger power systems, and as part of more complex tests involving hardware-in-the-loop. Also, it can be used as template to implement other protection functions.

Acknowledgment

This paper is the result of a bachelor's degree thesis developed in the Department of Electrical and Electronic Engineering, University of The Andes, advised by associate professor Gustavo Ramos López Ph.D., David Felipe Celeita Ph.D. and Mario Tano Gutiérrez M.Sc.

References

[1] Granada Zapata, Juan David, *Determinación de los parámetros que afectan el ajuste y la coordinación de la protección de pérdida de sincronismo en generadores.* Master's Thesis, National University of Colombia – Medellín, 2016.

[2] *IEEE Guide for AC Generator Protection*, IEEE Std C37.102-2006 (Revision of IEEE Std C37.102-1995) 2006.

[3] Sistema Interconectado Nacional, Subcomité de Protecciones, *Guías para el buen ajuste y la coordinación de protecciones del SIN*. pp.193 – 200, 2016.

[4] D. Celeita, M. Gutierrez, M. Toro, and G. Ramos, *Out-of-step protection modeling for playback testing applied to industrial generators*, 2018 IEEE Industry Applications Society Annual Meeting, September 2018.

[5] IEEE Power System Relaying Committee, *IEEE Tutorial on The Protection of Synchronous Generators*, Second Edition, 2011.

[6] Siemens, *SIPROTEC Multifunctional Machine Protection 7UM62*, Manual. pp.165 – 174, 2010.

[7] K. Gadgil, *A numerical protection relay solution: High performance analog*, Tech. Rep. SLAA466, Texas Instruments, September 2010. Online: http://www.ti.com/lit/an/slaa466/slaa466.pdf

Review of energy storage technologies for cooperation with wind farm

Michał Rabiej[1]

[1]*Faculty of Energy and Environmental Engineering, Silesian University of Technology, e-mail: michal.rabiej11@gmail.com*

Abstract

This paper reviews the main energy storage technologies and their use in real objects. It also shows the maturity level of different storage technologies. Moreover, the article discusses energy storage technologies in the perspective of possible cooperation with a wind farm. Among the five technologies discussed, were selected these which could ensure efficient energy storage and discharge at expected time.

Keywords: energy storage, wind farm, energy transition

1. Introduction.

In the conditions of energy transition, the main challenge for scientists is to develop energy storage technologies. It is impossible to replace fossil fuels with renewable sources of energy without energy storage technology. Perhaps this is the most significant problem in today's energy sector. Renewable energy sources, although very promising and attractive, are not fully controllable sources, which means that the only possibility to use them on a larger scale is the possibility of energy storage. Especially in countries like Poland, where atmospheric conditions are unfavorable for renewable energy sources, such as wind farms. However, in recent years there has been a huge development and progress of energy storage systems such as lithium batteries, molten salt technology, flywheels energy storage, compressed air energy storage (CAES), thermal energy storage, flow batteries or pumped hydroelectric storage. Worldwide leading countries in this area are Japan, USA, Germany, Spain and Korea (Fig 1.1.). In 2014, USA was a leader with a total of 1500 MW non-pumped hydro energy storage capacity. Japan had 420 MW total, when whole Europe had only 550 MW [1]. In 2010 total capacity worldwide equaled 1.9 GW, while at the end of 2017 it was 6 GW. It was a rapid growth, which allows to believe that this trend will continue.

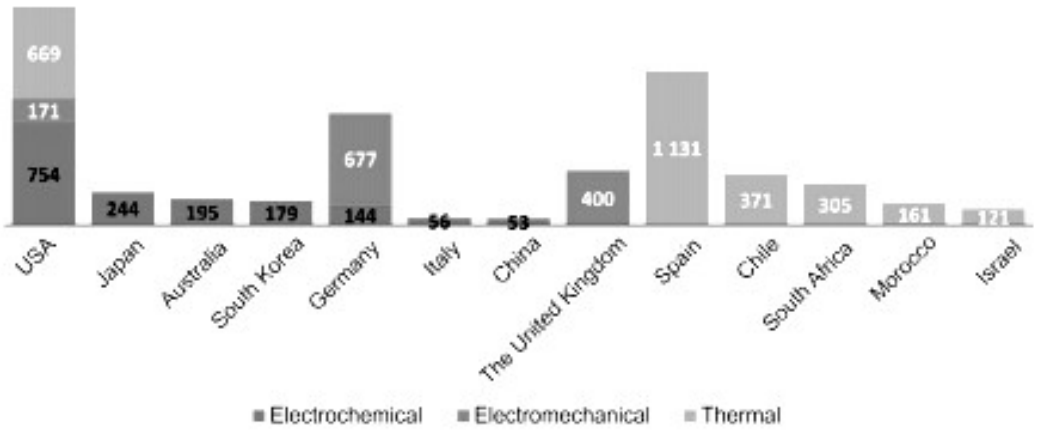

Fig. 1.1. The installed capacity of energy storage (excluding pumped hydro storage) at the end of 2017 [MW] [3].

Energy storage technologies can be divided in the consecutive systems:

- Thermal (Sensible heat storage (e.g. ceramic materials, rocks, molten salts), latent heat storage (e.g. phase change materials), cold storage),
- Mechanical (Pumped hydro power plants, flywheels, Liquid Air Energy Storage (LAES), Potential energy storage of large masses, Compressed Air Energy storage (CAES), AA-CAES (advanced adiabatic), LTA-CAES (low temperature adiabatic), CAES-AI (Air injected)),
- Chemical (batteries, flow batteries, fuel cells, synthetic fuels, hydrogen, reversible chemical reactions, methanol, synthetic natural gas),
- Electrical (capacitors, superconductive magnetic storage).

Table. 1.1. The worldwide installed capacity divided by method and technology of storage at the end of the year 2017 [MW] [2].

Method of energy storage	**Technology**	**Capacity [MW]**
Mechanical	Pumped-hydro storage (PHS)	169 557
Thermal	Molten salt	2 402
Chemical	Lithium batteries	1 412
Mechanical	Flywheels	931
Thermal	Other	406
Mechanical	Compressed-Air Energy Storage (CAES)	400
Chemical	Sodium-sulfur batteries (NaS)	189
	Lead-acid batteries	60
	Flow batteries	42
	Nickel batteries	30
Chemical	Hydrogen storage	17

Currently, the most developing technology is electromechanical storage, which has Compound Annual Growth Rate (CAGR) on the level of 30%. It also had 29% share in the total installed energy storage capacity at the end of 2017 [2]. Significant development could also be observed for thermal technology, especially molten salt technology. Thermal technology's average growth rate is 26% (CAGR 2010–2017), while its share of global installed energy storage capacity is approximately 47% [2]. The pumped-storage hydroelectricity (PSH) technology has evolved at a rate of 2% (CAGR) in the years 2010–2017, while chemical and electrical storage are treated to be at early stage of development [2].

The rapid development in energy storage sector related to huge investments in this area through recent years. For example, American Recovery and Reinvestment Act has provided approximately €185m to support projects of $772m total worth in the areas of battery storage for balancing frequency regulation, wind generation, compressed air storage technology and other. Additionally, the U.S. Department of Energy has provided additional research support, mostly focused on storage components and technologies, such as batteries, and thermal storage under the Advanced Research Projects – Energy Scheme [1].

2. Maturity of energy storage technologies.

Each energy storage technology is on the different level of development. Currently, only pumped hydro storage technology (PHS) has been fully commercialized. Pumped hydro storage is the main storage technology in the world. Nowadays about 30% of global storage capacity [6]. By 2020, capacity should rise to 47,8 GW. Notwithstanding the huge amount of installed capacity, there is still many plans of expansion and development of this technology. For example, the eStorage project calculated that in the EU-15, Norway and Switzerland there are 2291 GWh of areas ready for development with existing tanks for new hydro storage

power plants [6]. Despite some aspects which need to be improved flywheel technology is also mature. It is well introduced in the industry, mainly in the United States but also in France, United Kingdom, Spain, Germany and Portuguese islands. Technology which was introduced many years ago, then stopped a little bit and nowadays developed again is Compressed-Air Energy Storage (CAES). In 1978 the project of Diabatic Compressed Air Energy was started and since then CAES plant in Huntorf has been operating. Most of energy storage technologies already have practical applications in the industry but are still not widely used. Flywheel technology, which is characterized by fast response, a long cycle life, high charge and discharge rates and high energy density, has many applications as voltage and frequency regulation, pulsed power for the military, hybrid and electric cars, load levelling and even in spacecrafts. It seems that the future for flywheel technology will be bright because of ongoing work considering construction of a flywheel system for backup power and many other applications. Chemical energy storage is still in research and development stage but considerable funding from European Union introduced new possibilities and many projects – power-to-gas facilities and hydrogen storage. Chemical storage can be important factor of RES integration and probably will play important role in Europe. Regarding electrochemical storage methods the most mature technologies are Lead-Acid, Nickel-cadmium (Ni - Cd) and lithium-ion (Li-on). Li-on is the most popular and modern option nowadays. They have high energy density in comparison to Lead-Acid and Ni-Cd technologies. They also become cheaper every year and they are main development driver for electrochemical energy storage. There are also new technologies under development such as M-Air or Li-S batteries, which can compete with Li-ion in the future. Along with the development of solar farms there has been a significant development of molten salt technology. Currently, technology is used to store the heat collected by concentrated solar power. Heat can be converted into steam to power turbines and generate electricity. Technology is used in Spain. During summer 2013 the Gemasolar Thermosolar power plant has been producing electricity 24 hours per day for 36 day [7]. Figure 3.1 illustrates status of energy storage technologies in terms of their maturity.

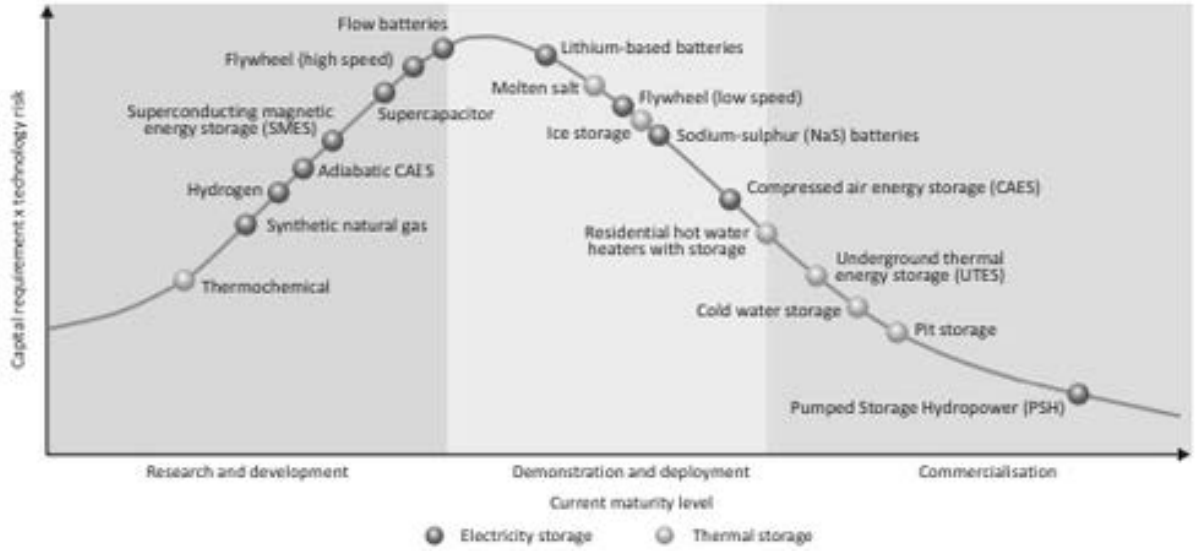

Fig. 2.1. Maturity of different energy storage technologies [5].

3. Considered wind farm problem.

One of the major disadvantages of wind farms is their unpredictability and instability when it comes to power generation due to weather conditions. The solution to this problem might be energy storage. Project aim was the selection of appropriate technologies for the needs arising from the operation and characteristics of a given wind farm. The maximum power generated by the farm was 12 MW. The problem was to enable charging of energy storage technology with maximum capacity during period of lower electricity prices and to discharge it during whole period of high prices.

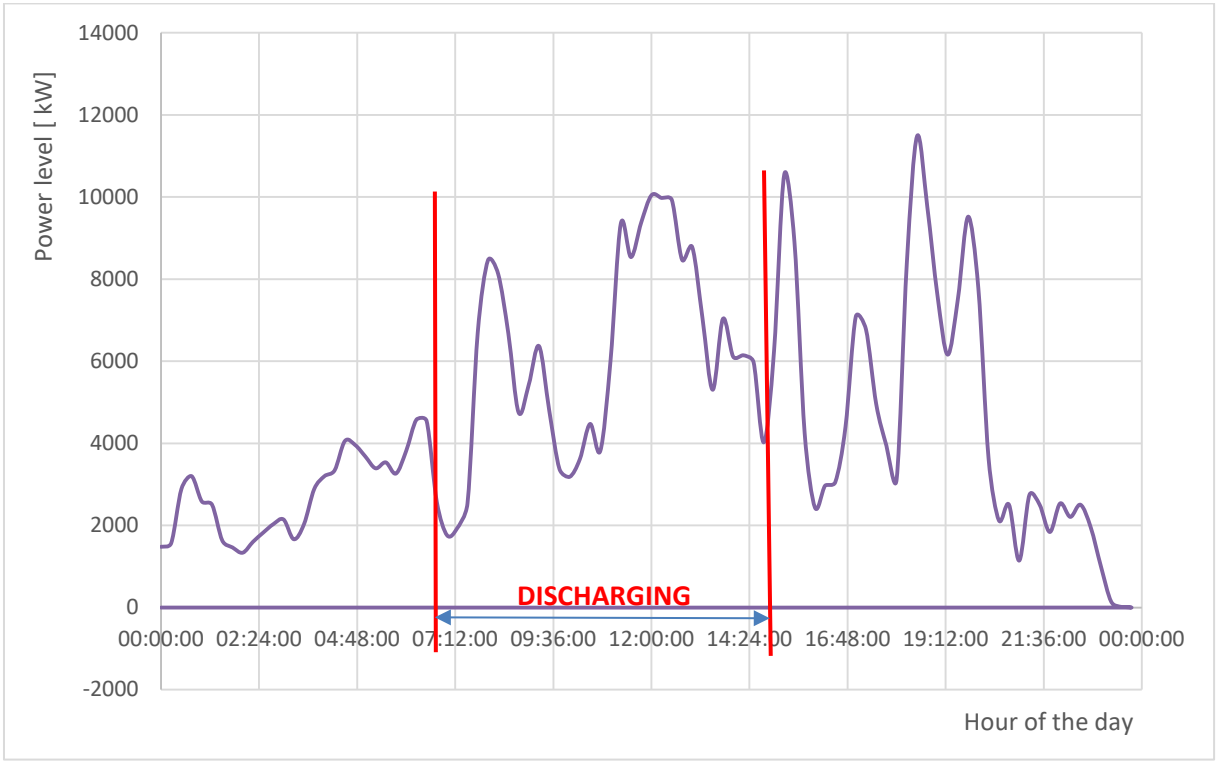

Fig. 3.1. Sample daily generation profile.

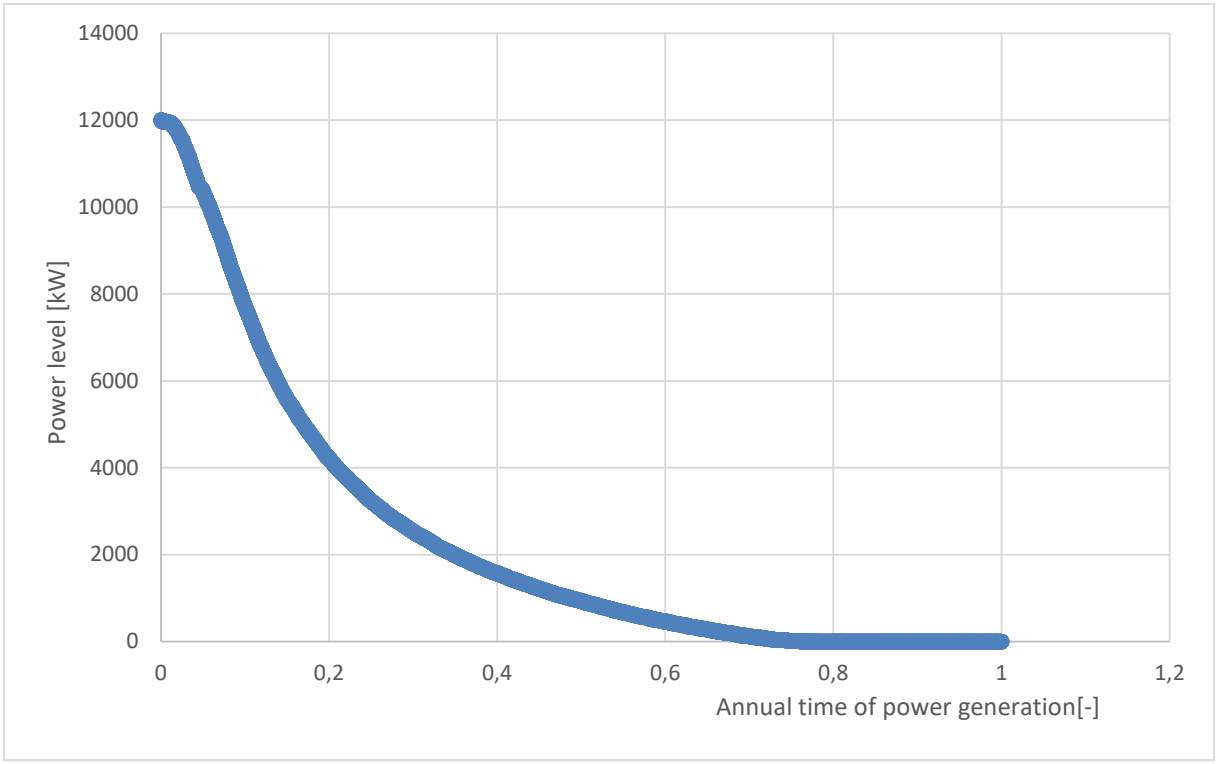

Fig. 3.2. Annual generation of electric power.

The figures 3.1. and 3.2. shows that there is a 7 hours period when energy storage installation has to discharged and for the rest of a day it may be in charge mode. The peak of power generation is 12 MW, but it is only for a short time of the year, so the installation has to be flexible in terms of energy discharged at any given time. It would also be very convenient to have a quick response of energy storage technology to the grid needs.

4. Discussion of considered energy storage technologies for the issue.

4.1. Pumped hydro storage (PHS).

The classic method based on the storage of potential energy. The principle of operation is to pump water from lower reservoir to higher one at low-demand period. The stored water is released through turbines during periods of high electrical demand to produce electrical power. The storage capacity depends on the height and volume of the water discharge. Considering losses in evaporation and conversion, the efficiency of PHS is between 70 and 85% [1].

Theoretically, as efficient, mature and with the ability to easily control the discharge time technology, using it enable to storage energy generated by a wind farm. However, this technology is generally used to store and produce much larger amounts of energy. In Poland, minimum is 95 MW Czorsztyn-Niedzica hydro power plant. So, the application of this technology for a given wind farm without cooperation with other source of energy would be completely unprofitable (cost of Pumped hydro storage plant ranges from $600/kW to upwards of $2000/kW) [9].

4.2. Compressed-Air Energy Storage (CAES).

Compressed-Air Energy Storage is based on ability of air accumulation by air compressors during off-peak periods and storing air under high pressure in appropriate underground storages (natural salt and hard rock caverns, natural gas formations and porous reservoirs). Similarly, to hydro-pumped storage agent is stored during low price period and during peak loads air is released from storages and its potential is used in turbines.

There are currently only two CAES plants in operation. There is one plant in McIntosh, Alabama (built in 1991, 110 MW) and the other one in Huntorf, Germany (built in 1978, 290 MW). For over 40 years, power plants serve safely and reliably. On the figure 4.2.1 there is a daily sample operation of installation in Huntorf.

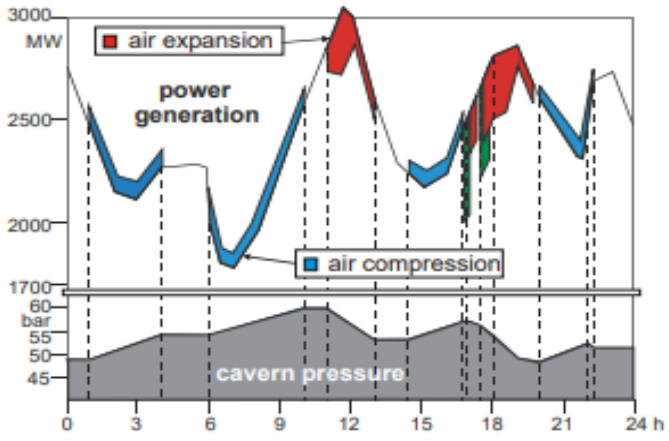

Fig. 4.2.1. Sample operation of CAES in Huntorf, Germany [10].

As a technology with very fast reaction time (plants can rise from a 0% to 100% charge level in in less than 10 min, from 50% to 100% in less than 15 s) [11], is ideally suited to act as a large sink for energy supply and demand, and for taking frequent starts and shutdowns. As it uses compressed air, plants do not suffer from any efficiency reduction due to lower air density. Also, technology does not have problem with excessive

heat, what make possible to use CAES for ancillary services such as frequency regulation, load tracking and voltage control.

This is the reason, why CAES is really good choice for the wind power energy storage. It is important for a given wind farm, that currently micro CAES plants are being under development, which would be ideal for our energy storage capacity demand. Also, it is possible to use an aboveground tank which simplify the implementation of solution.

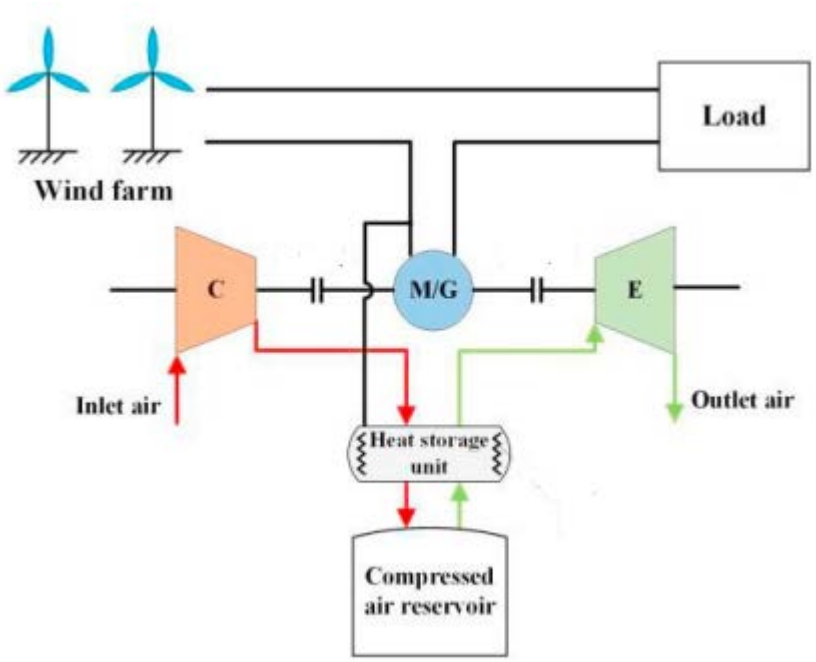

Fig. 4.2.2. Schematic CAES technology solution for wind farm technology [15].

4.3. Battery energy storage.

The market for Battery Energy Storage Systems (BESS) is developing rapidly and requests are coming from a wide range of industries. Principle of operation is common for all conventional technologies, electrodes are immersed in an electrolyte, which allows a chemical reaction to occur. Currently lithium-ion battery technology is the most popular one. They hold their charge much better than nickel metal hydride batteries (NiMH). NiMH batteries losses about 20% of its charge per month, when lithium-ion only 5%. Lithium-ion batteries do not have a memory effect, which means they do not need to be fully discharged before recharging, as with some other battery technologies. In addition, they are much more durable (charge/discharge cycles). Probably the most important feature is that they have much higher energy densities than lead-acid and nickel metal hybride batteries (Lithium ion energy density ≈ 150 $\frac{Wh}{kg}$, NiMH battery energy density ≈ 100 $\frac{Wh}{kg}$, lead-acid battery energy density ≈ 25 $\frac{Wh}{kg}$) [12]. Despite all pros, lithium-ion batteries still have a some disadvantages. Firstly, they are very sensitive to high temperatures. In such conditions, the batteries degrade much faster than normally. Secondly, completely discharged lithium-ion battery is broken. Exploding Samsung smartphones, electric cars fires and even airplane catching fire at the airport show that this technology is still not so stable.

Currently, the largest battery storage installations:

- Hornsdale Power Reserve in Australia (Power - 100 MW, Energy - 129 MWh, it provides a total of 129 megawatt-hours of storage capable of discharge at 100 megawatts into the power grid),

- Escondido Substation in U.S (Power – 120 MW, Energy - 30 MWh),
- Pomona Substation in U.S (Power – 80 MW, Energy - 20 MWh),
- Mira Loma Substation in U.S (Power – 80 MW, Energy - 20 MWh),
- Tesla Solar Plant in U.S (Power – 52 MW, Energy - 13 MWh),
- Stocking Pelham facility in United Kingdom (Power – 50 MW, Energy - 50 MWh),
- Jardelund in Germany (Power – 50 MW, Energy - 48 MWh),
- Minamisōma Substation in Japan (Power – 40 MW, Energy - 40 MWh) [4].

Nowadays, promising battery technology is flow battery. Such a battery is made of electrolyte tanks (catholyte and anolyte), cell stack which has inside two liquids (catholyte, anolyte) separated by Ion selective membrane and pumps to move a catholyte and anolyte from tanks to the cell stack. Flow battery can be compared to an electrochemical cell, with difference that the electrolyte is not stored in the cell around electrodes, but outside the cell and can be pumped into the cell in order to generate electric energy. The power capacity (kW) is determined by cell stack size, but the volume of electrolyte tanks determine the energy capacity (kWh). The efficiency of flow batteries is around 85%.

Therefore, there is a possibility to use batteries for energy storage at the level needed for a given wind farm. Costs of such an installation would definitely be competitive with CAES technology. The problem could be a rapidly falling capacity with a huge number of charge and discharge cycles. Another disadvantage is the risk of a major accident, even a fire, which unfortunately still happens when we talk about battery storage technologies. In the future, it seems that very interesting solution for wind farm cooperation can be flow batteries. With a very fast response (from charge to discharge in 0,001 s), high overload capacity and long estimated life (7- 15 years, 10000 charge/discharge cycles), it is very versatile and modern solution, which definitely could be used to work with wind farm. The disadvantage of this solution is higher price than conventional batteries and much more complicated construction.

4.4. Flywheel energy storage.

Flywheels are spinning mechanical machines that can store rotational energy which can be used almost instantaneously. Primary version contains a spinning mass in its centre that is driven by a motor. During necessity for energy, spinning force drives a device which is similar to turbine, which produce electrical energy. The charging process is carried out with usage of the motor to increase its rotational velocity. It is vital that the rotor spins in a nearly frictionless enclosure. Modern high-speed flywheel energy storage systems are made up of rotating cylinder (a rim attached to a shaft) supported by magnetically levitated bearings on a stator - the stationary part of an electric generator. The flywheel mechanism works in a vacuum to reduce drag in order to improve performance. The motor-generator connects the flywheel to the utility grid. There are many pros for current electric grid by usage of flywheels. Flywheels are able to capture energy from intermittent energy sources and deliver a continuous supply of power to the grid. Flywheels may also deliver frequency regulation and electricity quality improvements for the grid.

Currently, there are several examples of applications of this technology:

- Stadtwerke München in Germany which supplies electricity for more than 95% of Munich’s 750000 households, uses a flywheel storage system to stabilize the power grid and to compensate deviations from renewable sources of energy.
- Power plant in Ontario, Canada has flywheel energy storage for frequency regulation since 2014. It consists of 10 flywheels made of steel and the maximum power is 2 MW.
- On the island of Aruba (Caribbean Sea) there is a 5 MW flywheel storage power plant built. The flywheel installation ensures flexibility and resilience to the grid and enables gradual transition to renewable energy sources which is goal of Aruba island (The Aruba island is expected to have 100% energy from renewable energy sources).

Despite the many advantages of this technology, such as fast response, durability (approximately 20 years of lifetime), low maintenance requirements and being able to control irregular electrical output from other machine which would be very useful especially for working with wind turbines, the flywheels are only able to provide high power capacities in very short time (low speed flywheels) or low power capacities in a very long period (high speed flywheels), which prevents using this technology for cooperation with a wind farm.

4.5. Thermal energy storage (TES) - Carnot battery

Thermal storage is broadly regarded as the future of energy storage, it offers a “zero-emissions” technology with firm capacity and dispatchability characteristics. Relies on energy storage in a thermal reservoir which can be used later. Allowing the plant to be configured to optimize the electricity load profile to meet specific market needs. For example, a plant can be designed to maximize the output of electricity during a period of high demand or to continue producing electricity after sunset. Carnot Batteries are developing and promising low-cost and location-independent energy storage technology. The principle of operation is that in charging mode, energy is used to drive a heat pump cycle. Heat can be stored in pressurized water, thermal oil, PCM, ceramic materials or molten salt. In discharge mode, heat is converted into electricity in cycle with two heat exchangers, expander and pump. It can also work with storing cold, which becomes the heat sink during discharging mode [13] .

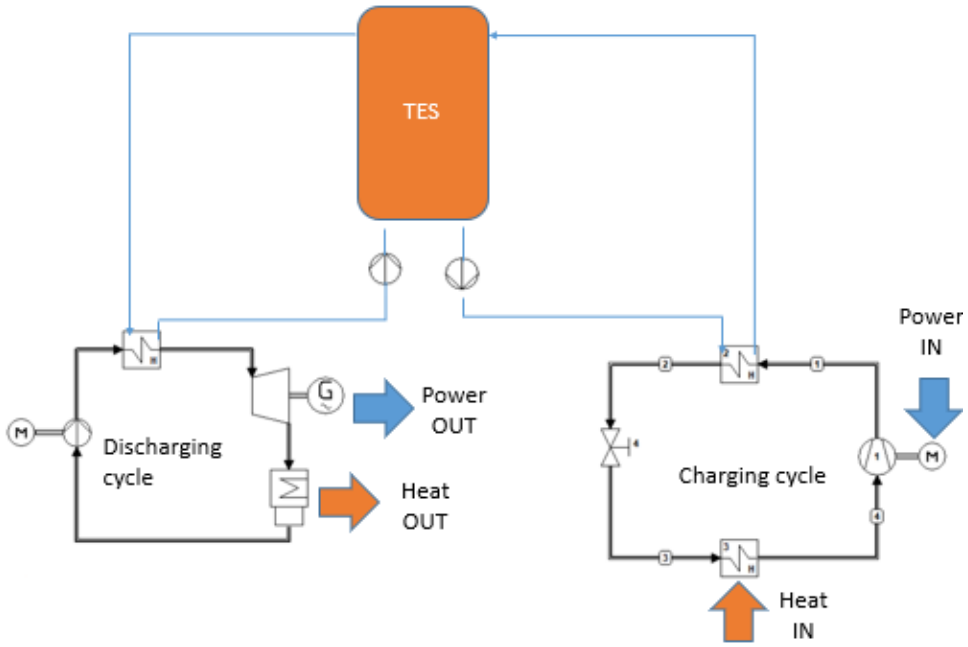

Fig. 4.5.1. Schematic Carnot battery installation [14].

Carnot battery installation would be also a possible cooperation solution for wind farm. High round trip storage efficiency, no restrictions on the location and the fact that technology of storing and consuming energy used in the solution is known and should not cause any problems are important factors supporting this technology. It also has very low unit cost of electricity storage similar to hydro power plant but with possibility of being deployed almost everywhere.

5. Conclusions and remarks.

Considering the selected energy storage technologies for analysis, the most appropriate for cooperation with a given wind farm would be compressed air technology or one of the battery technology. Certainly, flywheel technology is excluded for this cooperation due to the specification of the performance. Battery storage seems to be most conventional and easiest idea for given issue. Flexibility of flow batteries and long durability or simplicity of conventional batteries installation would be probably the most economically viable solution. However, with such power storage capacity requirements only lead acid batteries or li-ion batteries would

meet the needs of a given wind farm. CAES solution would be also convenient and possible solution. It would be more expensive than battery installation but more durable and effective in the long term of use. Very interesting would be usage of new, promising of Carnot Battery technology. It is not very widespread yet, but it will probably play an important role in the future and should work in cooperation with a wind farm very well.

References

[1] Catalina Spataru, Yen Chung Kok, Mark Barrett, *Physical energy storage employed worldwide*, Energy Institute, UCL, Central House, 14 Upper Woburn Place, London, WC1H 0NN, UK , Department of Civil, Environmental & Geomatic Engineering, UCL, Gower Street, London WC1E 6BT, UK, 2014.

[2] Krystian Krupa, Łukasz Nieradko, Adam Haraziński, *Prospects for energy storage in the world and in Poland in the 2030 horizon*, Polityka Energetyczna – Energy Policy Journal, 2018.

[3] *U.S. Department of Energy (DOE) 2018 results.*

[4] en.wikipedia.org, https://en.wikipedia.org/wiki/Battery_storage_power_station, 29.10.2019.

[5] Decourt, B. and R. Debarre (2013), "Electricity storage", Factbook, Schlumberger Business Consulting Energy Institute, Paris, France and Paksoy, H. (2013), "Thermal Energy Storage Today" presented at the IEA Energy Storage Technology Roadmap Stakeholder Engagement Workshop, Paris, France.

[6] Myriam Elisa Gil Bardajií (KIT; EERA JP Energy Storage); Dan Bauer (DLR); Thomas Bauer (DLR); Brittney Becker (EASE); Laurent Bedel (CEA); *"European energy storage technology development roadmap towards 2030"* Full list of contributing authors available on: https://www.eera-set.eu/wp-content/uploads/2017.01.16_Update-of-the-EASE-EERA-ES-Technology-Development-Roadmap_for-public-consultation.pdf.

[7] Wikipedia.org; https://en.wikipedia.org/wiki/Thermal_energy_storage; 10.11.2019.

[8] Energypost.eu; https://energypost.eu/can-vanadium-flow-batteries-beat-li-ion-for-utility-scale-storage/ ; 12.11.2019.

[9] Martin J. Leahy, David Connolly & Denis N. Buckley; „*Wind energy storage technologies*"; The Charles Parsons Initiative, University of Limerick, Ireland.

[10] Fritz Crotogino, Klaus-Uwe Mohmeyer and Dr. Roland Scharf Huntorf CAES: *"More than 20 Years of Successful Operation*"; KBB GmbH, Hannover, Germany, E.ON Kraftwerke Bremen, Germany.

[11] Gonzalez, A., Ó'Gallachóir, B., McKeogh, E. & Lynch, K., Study of electricity storage technologies and their potential to address wind energy Intermittency in Ireland. Sustainable Energy Ireland; 2004; http://www.sei.ie/Grants/Renewable_Energy_RD_D/Projects_funded_to_date/Wind/Study_of_Elec_Storage_Technologies_their_Potential_to_Address_Wind_Energy_Intermittency_in_Irl/.

[12] epectec.com; https://www.epectec.com/batteries/cell-comparison.html; 23.11.2019.

[13] event.dlr.de; https://event.dlr.de/en/hmi2018/carnot-batterien/; 26.11.2019.

[14] Jacek Kalina, PhD. DSc; Energy storage – grid scale - Carnot battery- lecture materials; Institute of Thermal Technology, Silesian University of Technology.

[15] Yi Zhanga,b, Yujie Xua, Xuezhi Zhoua, Huan Guoa, Xinjing Zhanga, Haisheng Chena; "Compressed air energy storage system with variable configuration for wind power generation" ; Institute of Engineering Thermophysics, Chinese Academy of Sciences, 100190 Beijing, China, University of Chinese Academy of Sciences, 100049 Beijing, China.

Environmental benefits of hovercraft

Fitim Halimi[1]

[1]*AEI, Silesian University of Technology, e-mail: fitimhalimi777@gmail.com*

Abstract

Knowing the damage that the human factor is causing to nature, to its flora, fauna and all the surrounding, our main goal is to figure out possibilities of how to decrease that bad impact to nature. Keeping that in mind we will focus on what is directly causing such damage and how to prevent it from happening. Any sort of transportation will somehow cause damage to the environment, but what would be a good replacement with less damaging factors, or even nil. Hovercrafts are one good example to mention if you want to have a multiple habitat vehicle which needs no extra modifications. It is always leading when it comes to comparison with boats or vessels, causing less damage to the environment and to the wildlife! Operating them is quite easy and they can also operate in areas where probably no other vehicle could, or at least at a much lower financial cost.

Keywords: Hovercraft, benefits, environment

1. Introduction

The main focus is on the benefits that the hovercraft can bring to the humanity and the environment, as the wildlife will have a peaceful habitat to live on even with the interaction of the hovercraft activity. The footprint that the hovercraft has is so small that a human's footprint actually can cause more damage to the ground, as the hovercrafts spread their pressure in all its area. Sea water is being polluted and that is the living environment of the biggest marine life and it is in the interests of everyone to keep it as clean as possible, but that is unlikely happening. Hovercrafts are the vehicles of the future as they cause much less pollution, also the electric models don't create pollution at all. They are fuel efficient, much safer in use as it can even cross over someone and still leave no casualties, they operate where other vehicles cannot even approach. It's time to stop polluting our world and switch to what is in the good of everyone. Is hovercraft the answer?

2. Hovercraft's benefits

The human activity has been causing damage to the marine ecosystems and now we need to act as fast as we can to save the nature we are living on, as this kind of damage still exists. The marine life is in danger as both it's flora and fauna are being polluted and damaged by boating collisions and that is causing habitats to wash away and decrease the population of the marine life. Hovercraft collisions also exist, but the impact is less harmful compared to vessels or boats. Wildlife is being damaged each year and the numbers are just increasing, causing also record-breaking damage to the marine life.

According to data from the state Fish and Wildlife Conservation Commission a total of **804 manatees** died in Florida waters last year, close to the record 830 set in 2013, **Boats killed 119** manatees in 2018, breaking the record of 106 set in 2016 and tied in 2017.

If we have a solution for this, why are we keeping up with the cruelty?

Most reports of collisions between whales and vessels involve large whales, but all species can be affected. Collisions with large vessels often go unnoticed and unreported. Animals can be injured or killed, and vessels can sustain damage. Serious and even fatal injuries to passengers have occurred involving hydrofoil ferries, whale watching vessels and recreational craft.

2.1 The wildlife benefits

Boats need to have their propellers under water to achieve their movement. That has been causing a lot of damage (killing species, damaging flora and fauna, noise pollution). The hovercraft's engines will provide with enough power for lift and thrust, so that way the hovercraft itself will just pass over the surface **without damaging flora or fauna**

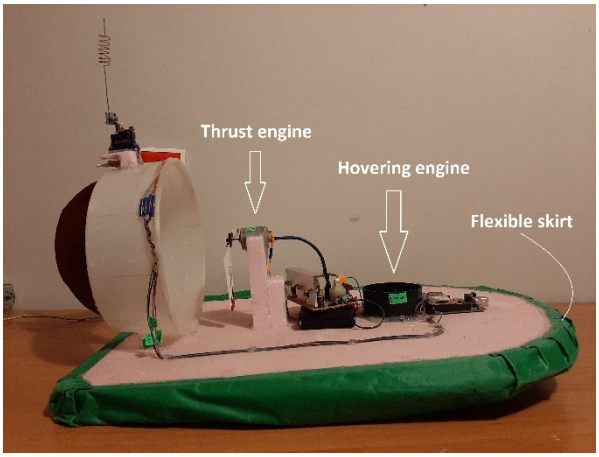

Fig. 2.1. Hovercraft functionality

A pressurized zone of air is created by lift fans to raise the craft above the surface, separating it from the environment below , that way the effect of the noise will be harmless ,so this is the solution of the noise problem.

Hovercraft can be used to best advantage in shallow water and drying areas, these areas often being remote and environmentally sensitive. Most of these areas are wetlands, swamps, and river delta. They are not only the feeding ground for a lot of different species of birds but as well very often used from marine live for hiding from predators. In these sensitive areas are nearly no transportation means available. Hovercrafts are able to operate in these areas in an environmentally friendly way.

2.2 Faced problems and their solutions

Wash is one of the most common problem mentioned. Hovercrafts are a good example when it comes to the wash as they do not create that much wash compared to vessels or same sized boats. All this is because hovercrafts do not need to pierce through water, they just glide on the surface, whether it is a surface of water, land, or snow. They always tend to not penetrate in the surface.

The wake created by the passage of a hovercraft is minimal, ensuring that river bank erosion caused by waves is zero. If we compare all the images of hovercrafts taken while they were on operation on water, the wash that they create is quite small and it is considerably less that the vessels and boats create. This is a good factor when it comes to the noise pollution or the waves that cause several damages to the marine life.

If you see the hovercrafts movement on water, the only disturbance you can tell is the air coming out of its soft skirt. All the boats or vessels have a big amount of their construction under the water level and they are always on a high friction contact which creates a lot of resistance and they have to keep pushing the water away on their path. Hovercrafts just keep gliding on the surface, and they are quite efficient when it comes to the fuel consumption, also the new four stroke engine technology is always more and more being used in hovercrafts which makes a huge difference also.

Noise, to be mentioned is the biggest problem that people think at first sight when we are talking about hovercrafts, as they tend to look gigantic and when you look at the propellers that's the first thing in mind. All advanced Hovercraft create no underwater noise, just atmospheric noise levels similar with other vehicles. The biggest amount of noise created by hovercrafts is the one that the propellers do.

They need to spin really fast to create the lift and the thrust that the hovercraft needs to realise its movement. Scientists during years have been working on this problem, and they came up with different ideas, involving special designed propellers which create considerably less noise.

To minimize this effect advanced hovercraft propulsion propellers have been designed with low tip speed to minimize atmospheric noise as well as most modern Hovercraft have a fully ducted thrust propeller which creates a more or less directional noise field. It is not possible to move air for the purpose of creating thrust without making some noise. What the scientists have achieved till now it's enough, as the rest of the noise which will be emitted is not a problem at all.

Hover ports:

- A hovercraft can land on any simple flat surface, it does not even need to be prepared. Let's say we want to make a **hoverport,** all that we will need is to have a big flat area that is enough for the hovercrafts to land and turn around.
- There is no need to excavate the area or disturb the local environment, so this will be at a very low cost and there will be no need for big machinery (that they also emit CO2) to be involved in the construction of the **hoverports**

Modern hovercraft benefits:

- One of the most important factors of the hovercraft is the '**hull'**, which is totaly sealed. This will prevent any kind of spillage in water. Including motor oil or any kind of fuels. Those can be eliminated after the hovercraft gets on a specific hoverport.
- All this eliminates the chance of polluting the marine by oil and fuel particles.
- The pollution of the atmosphere is also considerably less because of the fuel efficiency of the modern **four stroke** machinery (The fuel is consumed once every 4 strokes), and apart from that, the hovercraft **burns less fuel** as it glides on the surface (no need to pierce through water).
- No generation of slap noise, no propeller disturbance, also **damping sound engines**, which use water. Also, **refuelling** can be done on land to prevent any spillage of fuel on water during refuelling.
- Hovercrafts unlike motorboats, jet skis, have their own cooling system that does not use sea water, so they don't contaminate water while cooling. No emission of exhaust gases, or oil leakage into the water.

2.3 Hovercraft's accessibility

Global warming is a well-known problem for the whole world as it is causing sea levels to rise. There are places where this is already affecting the human community and there is a lot of need of vehicles to come and react for rescue .This is the aspect that makes hovercrafts lead as they have much more possibilities compared to other vehicles operating between communities (**Cars , boats, helicopters**)

- Hovercrafts can operate in areas where boats, vessels, cars, cannot and they can do it easily.
- All that by creating a cushion of air using lift fans which raise the hull up to **1.5m** above the surface.

That being said, it makes hovercrafts the best option for operating in these areas.

- **Cars** or any wheeled vehicle usually can't operate in mud, erosive areas, water.
- **Helicopters** are not an option that can be chosen often because of the high costs of maintaining them and also the power of wind they create in specific cases may cause damage. Apart from that helicopters do require a good landing area which cannot always be provided.

- **Boats** need a specific level of water to operate as their propellers can get in contact with ground and cause malfunctions.

2.4 The footprint

Most hovercraft therefore have a [kPa] of 0.7 – 3.3 [kPa]. In comparison the average person's footprint when walking is 20 – 25 [kPa]. One of the big factors that has to be mentioned is the footprint. It is harmful for the environment also because of that it allows access to specific areas with infrastructure damage and still be able to operate and not cause more harm to the environment. These benefits come from the way hovercraft functions.

- Damage to the shore environment, such as beaches, mudflats and vegetation is virtually zero because of the hovercraft's low pressure "footprint"
- Lightweight hovercrafts have a very light footprint, typically **15 grams** per centimeter when hovering on the surface.
- But also bigger sized hovercrafts such as: **SRN4 Mk3,** leave a light footprint which is less than a **human's footprint (average weight considered : 75 kg)**
- The Mk3 craft are around 56 m long and 23 m wide, and they can spread the pressure into all its area making it considerably less than a human's footprint!

Table. 2.4. Pressure comparison

Item	**Pressure [kPa]**
Hovercraft	2.2
Human foot	20 - 25
Car	205

3. Conclusions

Having all this told above, hovercrafts are crafts which can cause a huge good impact on the environment, they can replace boats, vessels, even different vehicles as they can operate in multiple habitats (land, snow, water).
Carrying cargo can also be one good reason as they can easily manage that and with a lower cost as they are fuel efficient. The wildlife has reacted good to the contact with the hovercrafts as they do not cause a lot of disturbance. Operating these crafts is quite easy and they can come in handy in a lot of cases where no vehicle can, or it can but in high financial costs. There are multiple good factors whenever we are mentioning hovercrafts, and there is no reason to not put them in use more day by day, as doing so we will be giving a good hand on the environment that we are all destroying more and more.

References

[1] *Hovercraft Definition and Meaning collinsdictionary.com*, date of access (18/11/2019).

[2] European Hovercraft Federation, europeanhovercraftfederation.org , date of access (25/11/2019).

[3] Hoveraid-Home, hoveraid.org , date of access (24/11/2019).

[4] 25-th research contest, mefproje.com, date of access (24/11/2019).

[5] World Hovercraft Federation, whf.hovercraft.org.uk, date of access (24/11/2019).

[6] BBC ON THIS DAY - 11 - 1959: Hovercraft marks new era in transport, news.bbc.co.uk, (22/11/2019*).*

[7] Hovercraft of hovermarine, bartiesworld.co.uk, date of access (22/11/2019*).*

[8] *RC Hovercraft, hovercrafthq.com*, date of access (22/11/2019*).*

[9] Hovercraft Cruising Club UK, hoverclub.org.uk, date of access (20/11/2019).

[10] Welcome to the Hovercruiser, hovercruiser.org.uk, date of access (20/11/2019).

Study of gasification kinetics of unconventional biomass and blends

A. Melle Sanchez[1], E. Moreno Piña[1], N. Szymus[1].

[1]Faculty of Energy and Fuels, AGH, Krakow, Poland. Author for correspondence: sanchez@student.agh.edu.pl

Abstract

Char gasification is the limiting step of the overall gasification process, so its kinetic study gives important information for gasification process operation. The present work studies the gasification kinetics of chars from diverse types of woody, agricultural and industrial biomass. Ten different samples of standalone and blended biomass chars have been gasified using steam as oxidizing agents. The evolution of the char transformation was followed by thermogravimetric analysis (TGA) at 800°C.

The results show a prominent influence of inorganic elements on gasification kinetics, which is in agreement with literature. The catalytic effect of K and Na and the inhibiting properties of Si and P have been highlighted through the successful correlation of mean reactivity to K+Na/Si+P ratio for several of the chars studied. Furthermore, the distinct conversion and reactivity evolution of the standalone feedstocks lead to a classification of the different samples in two families, which have been related to differences in catalytic behavior. The presence of chemical interaction between the two biomasses in the blends during gasification was observed.

Keywords: Biomass, gasification, kinetics, blending biomass, inorganic, catalytic, AAEM.

1. Introduction

Biomass gasification is a promising technology for the production of syngas from renewable sources. The current work aims to enlarge the biomass feedstock panel that is technically viable for gasification, and thus to bring more flexibility of the gasification plant towards the available biomass resources, as for now it is often performed with conventional stem wood only. The use of ashy biomass, such as forestry or agricultural residues (straw…) is often avoided because of their agglomeration propensity. This concerns in particular biomass with high alkaline (K, Na) and Si contents. These elements tend to form low temperature melting phases (carbonates, silicates, and molten salts), which lead to bed agglomeration, followed by defluidization of the bed, and possible shut down of the installation.

In this sense, the present work aims to study the gasification kinetics of the proposed atypical biomass feedstocks through thermogravimetric analysis (TGA), in order to further understand and predict their behavior under gasification conditions. In addition to this, a series of blends between wood and ashy biomass have been proposed as a solution to tackle the agglomeration problem, due to the chemical interaction between their individual inorganic compositions. These blends were therefore also investigated in the present work.

2. Gasification kinetics in TGA

2.1. Generalities and definitions

Char gasification is known to be the rate-determining step in the biomass gasification process [1]. The achievable conversion in the gasifier depends on the gasification rate of char, which is fundamentally linked to its kinetics. Therefore, understanding of mechanisms of char gasification is essential from a fundamental and technological point of view.

Gasification is a heterogeneous, endothermic chemical reaction between carbon contained in the solid and a reactive gas. The rate at which the chemical reactions can happen will increase as active sites are more rapidly accessible, as the atmosphere is more reactive and as the temperature is higher. Parameters such as composition and flow rate of the reactive atmosphere, morphological structure (porosity, tortuosity, and distribution of pore size) and geometry (size, shape) of the particle will play a more or less important role [2].

When studying intrinsic kinetics of gasification, it is important to clearly define the concepts of conversion, gasification rate and reactivity. These definitions are not consistent throughout literature. We will adopt the approach suggested by Dupont et al [3] which we consider to be quite extensive and generalized:

Conversion:

$$X = \frac{m_i - m(t)}{m_i - m_f} \qquad \text{equation 2.1}$$

Where *mi, m(t)* and *mf* are the masses of char before gasification, at the time t and at the end of gasification, respectively.

Gasification rate, dX/dt is then derived from the variation of conversion in time:

$$\frac{dX}{dt} = -\frac{1}{m_i - m_f}\frac{dm(t)}{dt} \quad \text{equation 2.2}$$

Gasification reactivity, or instant reactivity r, is defined as the normalized mass variation at each moment:

$$r(X) = -\frac{1}{m(t)}\frac{dm(t)}{dt} = \frac{1}{1-X(t)}\frac{dX(t)}{dt} \qquad \text{equation 2.3}$$

Finally, the average reactivity r_{integ} between two stages of conversion X_1 and X_2 was defined by:

$$r_{integ} = \frac{\int_{t_{X1}}^{t_{X2}} r(t)dt}{t_{X2} - t_{X1}} \quad \text{equation 2.4}$$

Gasification rate is commonly described according to the intrinsic reactivity of the occurring reactions, (which is accepted to be only a function of temperature and pressure of the reactive gas [4]) and the reactive surface (representative of the actual exchange surface between solid and gas). We can express it in the following general form:

$$\frac{dX}{dt} = k_{int}(T, P_i) * f(X) \quad \text{equation 2.5}$$

According to equation 2.5, the couple of variables (T, Pi) and X can be assumed to be independent in the mathematical sense of the term, allowing its study according to two different functions: one dependent only on operating conditions (T, Pi) and the other only on the conversion. This hypothesis has frequently been adopted and validated in literature by several authors [5]–[7] and although char structure can depend on temperature, under certain temperature and pressure ranges the evolution of the char structure can be considered to be independent of these magnitudes [2].

Authors studying coal and biomass gasification have arrived to a consensus on the expression for temperature and partial pressure dependence, which is commonly expressed according to a modified Arrhenius equation:

$$k_{int} = k_0 * exp\left(\frac{-Ea}{RT}\right) * P_i^n \quad \text{equation 2.6}$$

Where k_0 is the so-called pre exponential Arrhenius constant, R is the universal perfect gases constant, T temperature of the system, E_a the activation energy, P_i the partial pressure of the reactive gas and n an exponential factor related to pressure.

2.2. Influence of biomass composition on gasification kinetics

It is well known that the properties of biomass, such as morphological structure and content in inorganic elements, are very variable from one biomass to another. These properties determine the structural parameter, f(X) (see equation 2.5), which ultimately provides the expression for gasification rate. Butterman and Castaldi [8] underline the possible existence of a coupling of the degradation mechanisms and the presence of catalytic effects. Moreover, various studies comparing different types of biomass under similar gasification conditions conclude that biomass type, and therefore morphological structure, has very little influence on gasification reactivity compared to the effect of inorganic elements, particularly soluble minerals [9], [10]. Others, such as Bouraoui et al [11], observe that at low conversion levels, morphological structure and texture influence gasification rate along with inorganic contents, while at high conversion only the effect of these compounds is important.

However, the interpretation of the mechanisms and effects of these elements is not yet clear, becoming the main field of study related to biomass char gasification in the later years. Moreover, the fact that the biomass structure is constantly changing throughout gasification implies that the effect of the inorganic species varies with conversion [12] which increases its complexity and its scientific appeal. Researchers working in this field are trying to propose or modify existing models in order to describe gasification rate considering the effect of the inorganic compounds.

2.2.1 Effect of inorganic compounds on gasification kinetics

The inorganic elements present in biomass chars are, normally, alkali and alkaline earth metals [AAEM]. The form in which they are present in chars, which is distinct from forms presented in the raw biomass, is not yet precisely known (oxides or ions). Various types of tests have been conducted in the literature to highlight their influence on reactivity, knowing that their shapes and quantities are very variable.

It is important to note that in order to study the effect of these components, we can find two main approaches:

- The study of different biomasses which naturally present different concentrations of inorganic elements, depending on their origin. The problem of this method is that it is difficult to differentiate the effect of inorganic elements from morphological parameters.
- The study of the same biomass type by artificially impregnating or washing out the inorganic contents through chemical processes. The problem in this case is that morphological structure could be modified through acid washing [3], or the impregnation could fail to create the same bonds with the carbon matrix as the innate inorganic elements would, therefore affecting the experimental results due to unusually high volatilization [13].

In general, authors seem to agree on the catalytic effect of K, Na and Mg ([11], [14], [15] among others); while Si, P and Al seem to inhibit the effect of these catalyzers[1], [10], [16]. The mechanism driving this behavior is commonly explained by an oxidation-reduction cycle with oxygen transfer between the carbon sites (Cfas) and the AAEM species (M). The metallic species would create bonds with the carbon sites, Cfas (2M), attracting and reacting with the oxygen containing gasifying agents, therefore producing H_2, CO and leaving vacant the active sites [17], [18]:

$$Cfa(2M) + H2O \rightarrow M2O + H2 + Cfas \quad \text{reaction 2.1}$$

$$Cfa(2M) + CO2 \rightarrow M2O + CO + Cfas \quad \text{reaction 2.2}$$

The inhibiting effect of certain species such as Si, P and Al would be therefore explained by their ability to “encapsulate” the AAEM species[10], or to create permanent bonds with these, fixing them and repressing their interparticle mobility, therefore stopping them from further catalyzing the reaction [12].

The effect of calcium is particularly interesting. While most authors seem to agree that it would have a catalytic effect similarly to K and Na[19], others studies, such as the one developed by Gonzalez-Vazquez et al [20] on steam gasification of biomass, conclude that Ca would have an inhibiting effect on reactivity.

Moreover, it has also been observed that, while K would enhance gasification rate at high conversion, Ca would have the opposite effect, showing a peak of reactivity al low conversion for Ca-rich biomass chars [16], [21].

With the objective of describing the effect of inorganic species on gasification kinetics, various new models or modifications to the classic gasification models (volumetric, grain and random pore model) have been suggested. Dupont et al [3] based their work on the grain model, adding a new parameter which was varied in order to adjust the results of the model to their experimental findings. They then successfully correlated this parameter with the K/Si fraction of the biomass samples, thus taking into account with this ratio the phenomenon of encapsulation of potassium by silicon. The authors validated the model for a group of 21 different biomass chars.

Later on, various works have explored the differentiation between catalytic and noncatalytic gasification. In this regard, the works of Hognon et al [10] and Dupont et al [22] conclude that when there is an important concentration of inhibiting species, quantified by a low K/(Si+P) fraction (<1), the gasification is non-catalytic and its reactivity could be predicted through the volumetric model. However, for samples with high concentration of catalytic species (quantified by K/(Si+P) >1), the influence of the catalytic species would enhance the reactivity and provide a constant concentration of active sites. In this way, the evolution of the conversion with time would be linear and the surface function would be constant and equal to 1. Both works validate this model for the steam gasification of a large range and variety of biomass chars.

The work of Zhang et al [21] unifies the ideas previously presented. The authors work with the RPM, adding a new function to the gasification rate expression which describes the variation of the reactivity according to conversion and two dimensionless parameters successfully related to the content of calcium and potassium. The authors clearly distinguish between the biomasses which present reactivity peaks at low conversion levels, due to high concentrations of calcium and those which shows maximum rate at high conversion, due to high concentrations of potassium. The model proposed by the authors varies according to the main catalyst present in biomass, in order to represent reactivity peaks at high or low conversion, overcoming in this way the limitations presented by the classic RPM.

Finally, more recently Romero-Millan et al [14] have developed an interesting approach using model-free isoconversional methods and generalized master plots to determine the gasification kinetic parameters of the analyzed samples. In this way, no theoretical models were pre-supposed and as a result, a new model with a unique kinetic equation was proposed to predict gasification behavior based on the inorganic composition of biomass. The authors study a wide range of commonly used reaction mechanisms in solid state kinetic analysis to find the most suitable expression for the surface function and conclude that the variation in the reaction order identified in their experimental results could be related to the interactions between inorganic constituents and biomass, in particular potassium, silicon and phosphorous. The proposed model, which varies according to the K/(Si+P) fraction is presented below:

$$\frac{dX}{dt} = k_{int}(1-X)^m k_1 \qquad \text{equation 2.7}$$

Where:

- If K/(Si+P) ≥ 1:

$$\begin{Bmatrix} m = 0 \\ k_1 = 0.15\left(\frac{K}{Si+P}\right) + 0.7 \end{Bmatrix}$$

- If K/(Si+P) < 1:

$$m = -1.62\left(\frac{K}{Si+P}\right) + 1.64$$
$$k_1 = 1$$

k_{int} corresponds to the modified Arrhenius expression previously presented (equation 2.6)

2.3. Influence of biomass blending

Today, the industrial progress of biomass gasification in hindered mostly by the non-availability of a particular biomass round the year and the non-utilization of locally available biomass in a region. Hence co-gasification technology is a promising approach for deriving additional energy sources other than predominant feedstocks, optimizing the ratios of inorganic elements present and increasing the energy content of synthetic gas [23].

However, research on co-gasification of biomass is just recently gaining interest and the available studies in this field in quite limited. We will therefore extend our studies to cogasification of biomass and non-biomass feedstocks, which has already proven to have very positive results [5], in the hope of finding analogies which can be extended to the biomass blend gasification.

For example, Zou et al [5] study and compare the effect of mixing biomass feedstock with coal or with sawdust. The authors observe that when adding biomass to coal char, the ash of the biomass char is gradually transferred to the surface of the coal char, reacting with it and creating active sites. Since coal char is typically poor in inorganic content [24], a synergetic effect was observed for biomass-nonbiomass blends. However, when blending two different biomass chars, the authors observe no significant ash exchange and the two char samples seem to react independently.

However, the work of Wang et al [25] shows a positive effect of blending biomass with respect to the independent gasification of sole feedstocks, while the work of Zhang et al [26] on pyrolysis of biomass blends concludes that there is an overall positive effect due to a change in the blended char structure, and that this synergetic effect would also contribute positively to the blended char gasification reactivity.

With regards to the modelling of blended biomass char gasification, only Fernandes et al [27] have succeeded to propose a model, based on the RPM and modified to include certain synergy/inhibition expressions, and validate it with experimental results for biomass-coal char blends. However, the proposed approach is quite complex, and the parameters included must be defined through adjustment to the experimental results, which decreases its generalized applicability and interest.

It is important to note that Romero-Millan el al [14], using the model proposed in equation 2.7, were able to predict the conversion evolution of biomass blends, based solely on their inorganic content. Seeing that inorganic content of biomass blends is strictly related to the individual inorganic concentrations of the mother biomasses, this model presents a comprehensive and interesting approach to being able to derive biomass blend gasification behavior from that of the sole feedstock gasification.

3. Materials and methods

3.1. Biomass samples

The study was based on the analysis of various types of biomass:

- 4 different kinds of bark allow giving an insight on the variability of gasification within the same type of biomass.
- Wheat straw is an agricultural residue with high availability.
- Rapeseed cake and lignin residue from bioethanol refinery: 2 types of processed biomass.
- Finally, 3 different mixtures of bark and wheat straw were selected to account for the study of biomass blends. The composition of the blends are as follows: B15 (BarkFr 15%w - Straw 85%w); B50 (BarkFr 50%w - Straw 50%w); and B85 (BarkFr 85%w - Straw 15%w).

The samples studied were received after pyrolysis, which was carried out by third party, at high temperature (900°C) and under inert atmosphere (N_2). Therefore, the samples used for experimentation were the chars of the original biomasses. The chars received were analyzed via inductively coupled plasma (ICP) by a third party.

Table. 3.1. Description and composition determined through ICP for the biochars used in this study

Common name		*Wheat straw (WS)*	*Lignin*	*Bark ash*	*Bark PL*	*Bark 2017*	*Bark FR*	*Rape seed cake*	*B15*	*B50*	*B85*
Elemental analysis											
Ca	Total % Dry, ash	0,9	0,9	7,6	2,0	4,8	9,5	2,7	3,1	5,7	8,7
Al		<0,1	0,2	4,2	0,2	0,3	0,6	<0,1	0,2	0,4	0,6
K		3,8	0,2	1,7	0,3	2,6	0,8	4,6	3,6	2,2	1,3
Na		<0,1	1,4	0,9	<0,1	<0,1	0,1	<0,1	<0,1	<0,1	<0,1
Mg		0,2	0,1	1,4	<0,1	0,5	0,2	1,6	0,3	0,2	0,2
Fe		0,1	0,1	2,5	0,2	0,3	0,4	<0,1	0,3	0,3	0,4
P		0,2	0,2	0,1	<0,1	0,3	<0,1	4,1	0,2	0,2	0,1
Si		3,3	1,0	19,6	0,5	2,0	3,6	0,2	3,3	3,5	3,6

3.2. Isothermal TGA gasification experiments

Gasification of the chars was studied through thermogravimetric analysis (TGA) using a Setsys thermobalance (SETARAM, Caluire, France) coupled with a Wetsys steam generator. All samples were gasified at 800°C and atmospheric pressure in a mixture of steam and nitrogen. Steam concentration had to be limited under 20% partial pressure in order to ensure no water condensation in the conduct between the Wetsys and the TGA.

In order to properly study the intrinsic kinetics of a solid-gas reaction, the chemical regime must be guaranteed to be the phenomenon ruling the process. To achieve this, all limitations related to heat and mass transfer, such as external and internal diffusion, must be removed. Dahou et al [28] have studied the influence of char preparation on gasification kinetics using the same experimental setup and a crucible of almost identical dimensions. The authors found that a mass of around 5mg was not subject to mass transfer limitations for water vapor gasification. Therefore, this mass was used for our TGA experiments. Moreover, heat transfer limitations were avoided by maintaining the gasification temperature constant to assure the heating of the sample before injecting the reactive gas.

Reactor temperature was raised at a rate of 10°C per minute up to 800°C, under inert N_2 atmosphere which was injected at 50ml/min rate maintaining atmospheric pressure. Once gasification temperature is reached, it is kept constant for around 15 minutes, until no mass loss is observed. This pyrolysis phase is important to differentiate between the weight loss due to volatilization at high temperature and that due to interaction between the biomass and the reactive gases. Then, the flow is switched from nitrogen to the reactive gas, which is also injected at 50mL/min, and the reaction begins. The mass loss evolution is recorded until it reached minimal values. All experiments are carried out at least twice to verify the repeatability of the results.

4. Results and discussion

4.1. Standalone biomass char gasification results

Char gasification analysis was carried out for the 7 biomass char samples which were considered in this study. The temperature and sample mass were kept constant in order to be able to compare the results according uniquely to the biochar properties: morphological structure and/or inorganic content.

From the results we can distinguish two different trends: samples which react quickly and seem to have a linear variation with time up to conversion higher than 80%, and others in which the reaction rate decreases as the reaction evolves in time, characterized by a smooth curve-shape and longer times to attain total conversion.

Several authors ([7], [17] among others), have identified the curved shape of the char conversion in time with a non-catalytic gasification, which would be ruled by surface evolution, explaining the decrease in the conversion rate as less surface is available to the gasifying agent; therefore the reaction rate slows down logarithmically. This is the behavior which can be typically represented using the grain model. On the other hand, the linear evolution presented by the lignin sample, for example, is said to be related to a catalytic mechanism triggered by the presence of inorganic compounds. In this case the gasification evolution would not be limited by surface evolution but by the effect of these elements. The modeling of this kind of behavior has typically been achieved using the random pore model which is able to sustain more parameters and represent more complex gasification rate trends.

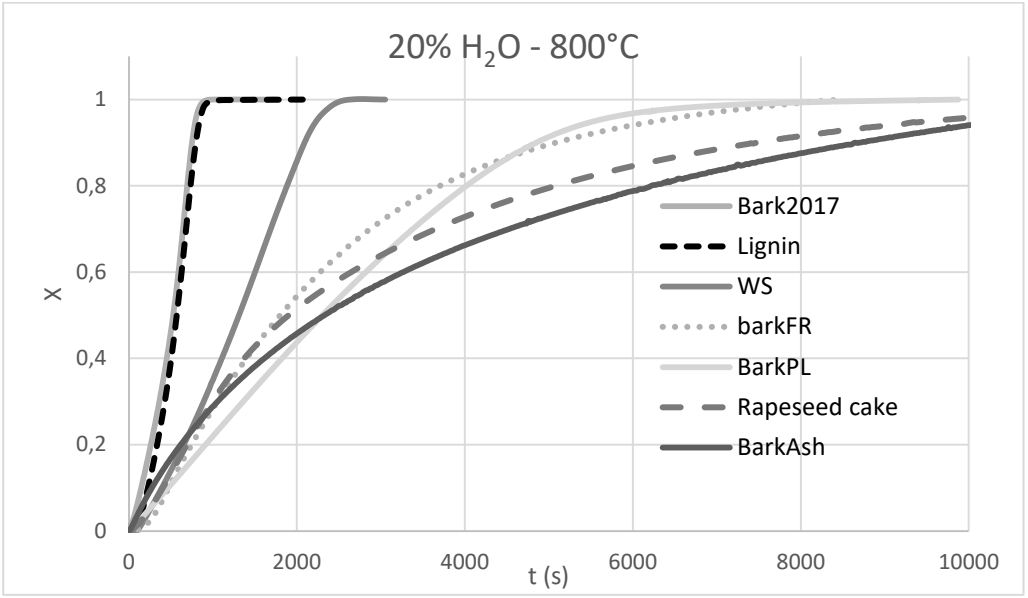

Figure 4.1 Temporal evolution of char conversion for the samples studied for gasification using 20% steam at 800°C.

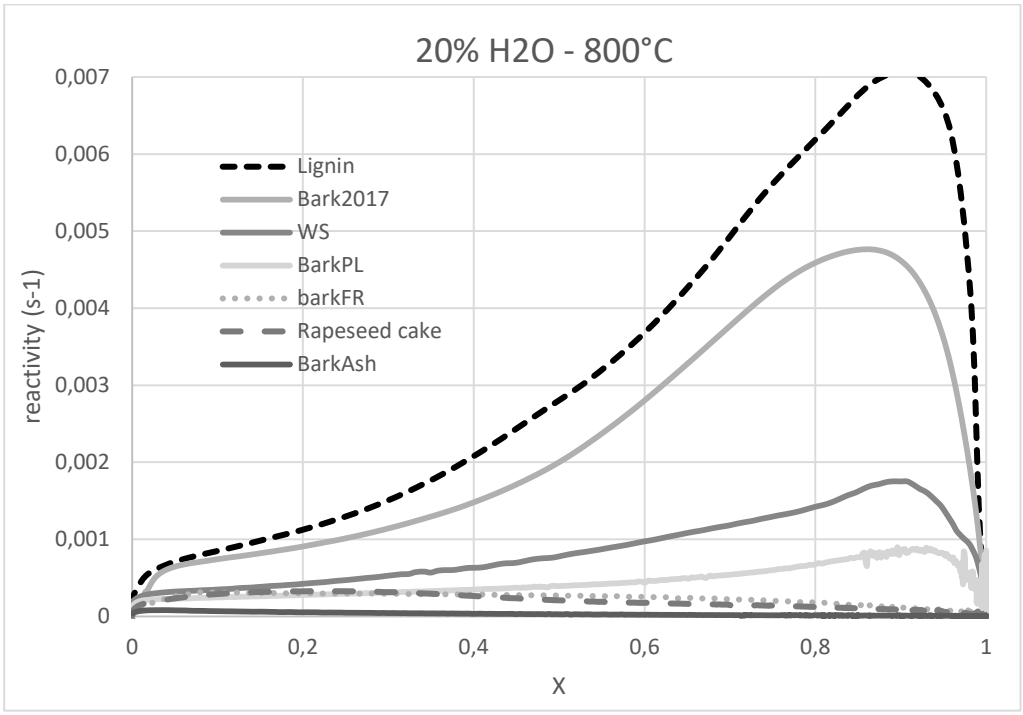

Figure 4.2 Reactivity as a function of conversion for the gasification experiments carried out using 20%H2O at 800°C.

Nonetheless, the observation of evolution of conversion with time is not always sufficient, as a non-linear evolution could seem linear in case of very rapid conversion. It is therefore interesting to also observe the reactivity profile, in order to confirm these differences. Once again, there seems to be two clear trends: for some for the samples, the reactivity increases with conversion, attaining a maximum in the range of $X \in [0,8-0,95]$, while others, such as BarkFR, present a maximum of reactivity at low conversion and then decrease with increasing conversion. Moreover, the samples which present a maximum at high conversion correspond to the ones which show linear dependence of conversion with time, while the samples characterized by rounded conversion curves match those for which reactivity decreases with increasing conversion.

These observations could be associated with the existence of catalytic mechanisms, due to which reactivity increases with conversion as the char particles evolve making the inorganic elements enclosed in them more accessible. This would increase their potential activity as the amount of volatile matter decreases and the ratio of carbon to inorganic elements increases. On the other hand, the reactivity trend of non-catalytic gasification normally presents itself in the form of decreasing reactivity as the amount of char surface is reduced, hence as conversion increases.

The observed results have led us to classify the samples in two categories according to the two distinct shapes of the conversion and reactivity curves, as suggested by various authors before. In this way a first "family" would be composed by the chars of WS, Bark2017 and Lignin, while a second family would be composed by the samples of BarkFR, rapeseedcake and BarkAsh. BarkPL is more complex to classify as its reactivity curve fits in with the trend shown by the first family while its conversion evolution seems to better match the second family. However, we considered that it should be placed in the first family as the reactivity peak observed at high conversion seems more compelling than the non-linear evolution of the conversion curve, which is more difficult to correctly assess.

4.1.1 Relationship between reactivity and inorganic content.

Following the example of various authors, we turn our interest to the verification of the catalytic effect of certain inorganic elements of the gasification kinetics. In this sense, the data collected from TGA experiments has been processed in order to calculate the mean reactivity in the range of $X \in [0\text{-}80\%]$, according to equation 2.4. This magnitude has then been correlated to the inorganic contents of the samples, through total content of these, or to ratios between contents in several inorganic elements in order to portray the inhibiting effect of elements such as silicon on the catalytic activity of AAEM.

It was found that, when the results were differentiated according to the families, they could be successfully correlated to inorganic ratio of the samples. In fact, this approach seems appropriate as in one case the evolution of reactivity is thought to be related to the inorganic content whilst in the second family the surface evolution effect may mask the effect of the inorganic elements, making it difficult to compare results of both families together. Nonetheless, it must be noted that even if the char gasification of family 2 samples may be ruled by the char surface evolution, the presence of inorganic elements can also have an effect on the overall reactivity.

Figure 4.3 reflects how there seems to be a linear increase in reactivity with the K+Na/Si+P ratio for the family 1 chars. This would confirm the findings of several authors [20], [14], [22] concerning the catalytic activity of K and Na which is partially suppressed by encapsulation of these by Si and P.

However, this relationship is quite different in the case of family 2. There seems to be no relationship between the inorganic ratio and mean reactivity. These observations can be attributed to the predominance of surface evolution of the gasification kinetics, which would blur the real catalytic effect, and to the fact that the rapeseed cake sample has a particularly high content of potassium and phosphorus, which makes it difficult to compare with the rest of the chars studied.

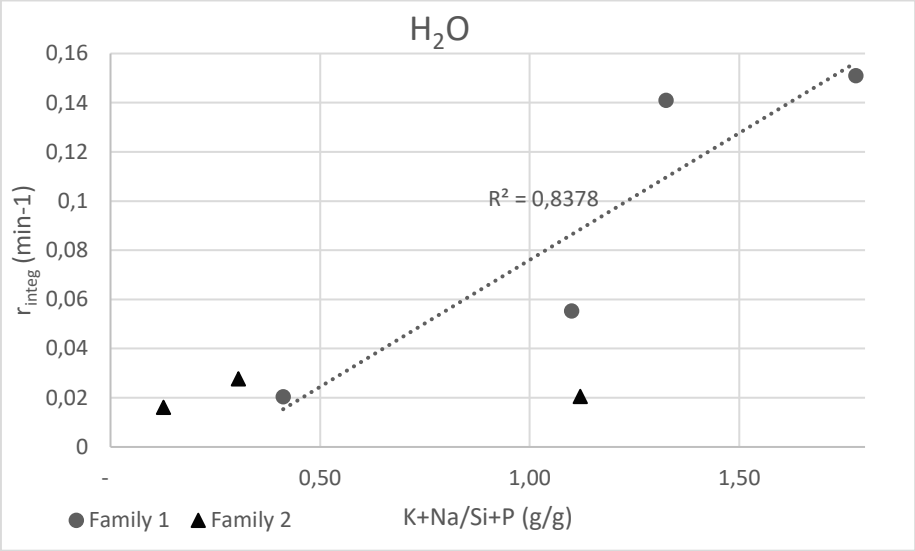

Figure 4.3 Relationship between the ratio K+Na/Si+P of the biochar samples and the mean reactivity for the 0-80% conversion range for the gasification experiments.

4.2. Biomass blends

Three different biomass blends of BarkFR and WS have been studied to observe the possible presence of interactions among the compounds during gasification. The char samples were prepared by a third party by mixing the dried biomasses at 85, 50 and 15% mass fraction before performing pyrolysis. Similarly, to the standalone samples, the blends where analyzed using 20% H_2O as gasifying agent through TGA.

The graphic results clearly showed conversion and reactivity evolutions of the blended samples to be between those of the mother biomass chars under the same gasification conditions. However, it was observed that the blend behavior was not exclusively conditioned by the fraction of each biomass in the blend, as it was observed that the three blends seemed to have low reactivity and behave much more similarly to the BarkFR sample than to the WS sample, independently of the content of WS in the blend.

In order to identify if there actually exists an interaction phenomenon between biomasses in the blends, an additive model was developed and compared to experimental results. The objective is to compare the experimental results of blended biomass chars to the results which would be expected from a perfectly non-interactive blend, in which the particles of each mother biomass react independently. This model was developed so that conversion and gasification rate of the blends can be expressed as a function of those of the mother chars only, which are known to us. Applying the definition of conversion presented in equation 2.1 for a blend and assuming that the mass of each fraction in the blend is an additive parameter derive the following definition:

$$X_M = \frac{\sum_i^N X_i * \alpha_i * \tau_{char,i}(1-\beta_i)}{\sum_i^N \alpha_i * \tau_{char,i}(1-\sum_i^N \alpha_i * \beta_i)} \quad \text{equation 4.1}$$

Where α(g/g) is the mass fraction of a biomass in the blend, β(g/g) represents ash fraction after TGA of char, τchar(g/g) represents the conversion fraction of dry biomass to char through pyrolysis and X represents conversion of each of the components of the blend (i) or blend itself (M).

Comparing the model to the experimental results we can infer that some samples greatly differ from the expected behaviour if there were no interaction between the different biomasses present in the blend. This is especially the case for the B15 sample, which we would be expected to react much faster taking into account it is mostly made up of rapidly reacting WS char. In the other cases, the experimental results seem to follow

the additive model more closely, although we cannot conclude that this means there is no interaction in these cases.

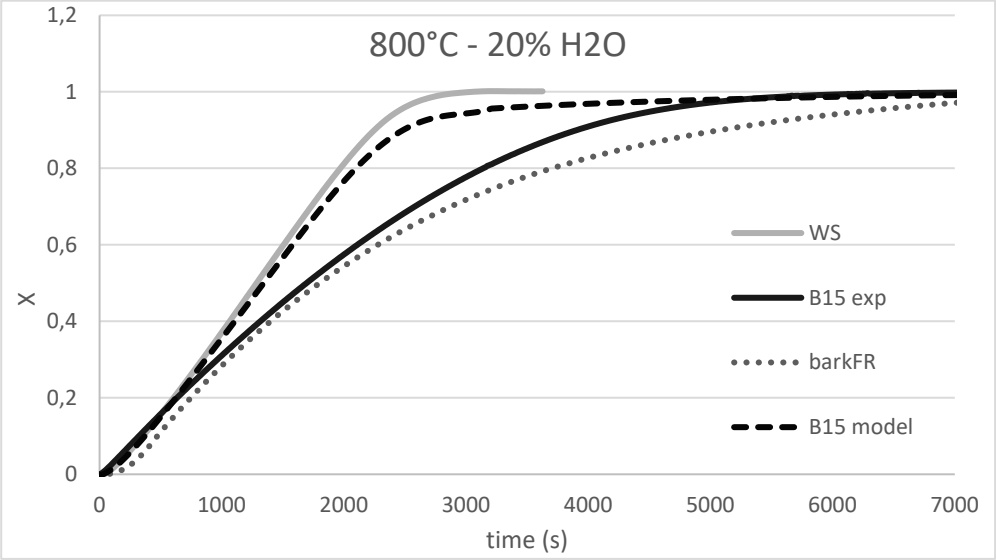

Figure 4.4 Char conversion versus time for the blended samples at 800°C in 20% H_2O.The results for the additive model are presented in dashed lines.

5. Conclusions

The char samples show 2 different behaviors according to the shape of their conversion and reactivity curves. Obtained results are in agreement with other authors which have found that there are certain biomasses for which the presence of catalytic inorganic elements rules gasification velocity, whilst others behave in a non-catalytic manner. Moreover, the sampling of similar biochars allowed to conclude that morphology of the sample has very limited effect on the gasification rate.

The study of the effect of inorganic compounds concentration on reactivity shows that the ratio (K+Na)/(Si+P) would be the most appropriate parameter to describe the catalytic effect of inorganic species on reactivity. However, a linear correlation between the mean reactivity and this parameter has only been identified for the family 1 char (identified as samples in which catalytic behaviors could be identified), but not for the family 2 chars. However, these observations are limited by the reduced number of samples which make up each family.

Blends of two different lignocellulosic biomass in varying proportions have been compared and analyzed using the developed “additive model” in order to study the existence of interaction mechanisms between then that would modify their behavior during gasification. The results have clearly shown there is an interaction between the different biomass char particles that lead to the conclusion that biomass blend samples can be characterized by homogenized properties. In this sense, they can be analyzed according to their overall inorganic content. This approach was suggested by authors such as [Romero-Millan 2019].

References

[1] Dupont C., Boissonnet G., Seiler J.-M., Gauthier P., Schweich D., Study about the kinetic processes of biomass steam gasification , *Fuel*, p. 32‑40, 2007.

[2] Tagutchou J. P., Gazeification Du Charbon De Plaquettes Forestieres Particule Isolee Et Lit Fixe Continu, Université de Perpignan, Via Domitia, 2008.

[3] Dupont C., Nocquet T., Da Costa J. A. Jr., Verne-Tournon C., Kinetic modelling of steam gasification of various woody biomass chars: Influence of inorganic elements , *Bioresource Technology*, p. 9743‑9748, 2011.

[4] Guizani C., Escudero Sanz F. J., Salvador S., The gasification reactivity of high-heating-rate chars in single and mixed atmospheres of H2O and CO2, *Fuel*, p. 812-823, 2013.

[5] Zou X., Ding L., Gong X., Study on cogasification of food waste char with biomass/coal char and thir interaction mechanisms, *Energy&Fuels*, p. 12644-12654, 2018

[6] Nilsson S., Gomez-Barea A., Fuentes Cano, D., Gasification reactivity of char from dried sewage sludge in a fluidized bed , *Fuel*, p. 346-353, 2012.

[7] Gomez-Barea A., Leckner B., Modeling of biomass gasification in fluidized bed, *Progress in Energy and Combustion Science*, p. 444-509.

[8] Butterman H. C., Castaldi M. J., CO2 as a carbon neutral fuel source via enhanced biomass gasification, *Environmental Science & Technology*, p. 9030-9037, 2009.

[9] Di Blasi C., Combustion and gasification rates of lignocellulosic chars, *Progress in Energy and Combustion Science*, p. 121-140, 2009.

[10] Hognon C., Dupont C., Grateau M., Delrue F., Comparison of steam gasification reactivity of algal and lignocellulosic biomass: influence of organic elements, *Bioresource Technology*, p. 347-353, 2014.

[11] Bouraoui Z., Jeguirim M., Guizani C., Limousy L., Dupont C., Gadiou R., Thermogravimetric study on the influence of structural, textural and chemical properties of biomass chars on CO2 gasification reactivity, *Energy*, p. 703-710, 2015.

[12] Kajita M., Kimura T., Norinaga K., Li C.-Z., Hayashi J., Catalytic and non-catalytic mechanisms in steam gasification of char from the pyrolysis of biomass, *Energy Fuels*, p. 108-116, 2010.

[13] Feng D., Zhao Y., Zhang Y., Xu H., Zhang L., Sun S., Catalytic mechanism of ion-exchanging alkali and alkaline earth metallic species on biochar reactivity during CO2/H2O gasification, *Fuel*, p. 523-532, 2018.

[14] Romero Millan L. M., Sierra Vargas F. E., Nzihou A., Steam gasification behaviour of tropical agrowaste: A new modeling approach based on the inorganic composition, *Fuel*, p. 45-53, 2019.

[15] Marquez-Montesinos F., Cordero T., Rodriguez-Mirasol J., Rodriguez J. J., CO2 and steam gasification of a grapefruit skin char, *Fuel*, p. 423-429, 2002.

[16] Wei J., Gong Y., Guo Q., Chen X., Ding L., Yu G., A mechanism investigation of synergy behaviour variations during blended char co-gasification of biomass and different rank coals, *Renewable Energy*, p. 597-605, 2019.

[17] Zhang Y., Ashizawa M., Kajitani S., Miura K., Proposal of a semi-empirical kinetic model to reconcile with gasification reactivity profiles of biomass chars, *Fuel*, p. 475-481, 2008.

[18] Chen S. G., Yang R. T., Unified mechanism of alkali and alkaline earth catalyzed gasification reactions of carbon by CO2 and H2O, *Energy&Fuels*, p. 421-427, 1997.

[19] Shadman F., Sams D. A., Punjak W. A., Significance of the reduction of alkali carbonates in catalytic carbon gasification, *Fuel*, p. 1658-1663, 1987

[20] Gonzalez-Vazquez M. P., Garcia R., Gil M. V., Pevida C., Rubiera F., Unconventional biomass fuels for steam gasification: Kinetic analysis and effect of ash composition on reactivity, *Energy*, p. 426-437, 2018.

[21] Zhang Y., Kajitani S., Hara S., Ashizawa M., Modeling of catalytic gasification kinetics of coal char and carbon, *Fuel*, p. 152-157, 2010.

[22] Dupont C., How inorganic elements of biomass influence char steam gasification kinetics , *Energy*, p. 430-435, 2016.

[23] Thiagarajan J., Srividya P. K., Balasubramanian P., Thermal Kinetics and syngas production on co-gasification of deoiled jatropha seed cake residues with wood chips, *International Journal of Renewable Energy Research*, p. 1105-1111, 2018.

[24] Wigmans T., Göebel J. C., Moulijn J. A., The influence of pretreatment conditions on the activity and stability of sodium and potassium catalysts in carbon-steam reactions, *Carbon*, p. 295-301, 1983.
[25] Wang G., Zhang J., Huang X., Liang X., Ning X., Li R., Co-gasification of petroleum coke-biomass blended char with steam at temperatures of 1173-1373K, *Applied Thermal Engineering*, p. 678-688, 2018.
[26] Zhang W., Yuan C., Xu J., Yang X., Beneficial synergetic effect on gas production during co-pyrolysis of sewage sludge and biomass in a vacuum reactor, *Bioresource Technology*, p. 255-258, 2015.
[27] Fernandes R., Hill J. M., Kopyscinski J., Determination of the synergism/antagonism parameters during co-gasification of potassium-rich biomass with non-biomass feedstock, *Energy&Fuels*, p. 1842-1849, 2017.
[28] Dahou T., The influence of char preparation and biomass type on char steam and gasification kinetics, *Energies*, p. 2126, 2018.

Experimental and numerical analysis of the hydrofluidisation freezing process

Edyta Piechnik[1], Michał Palacz[1], Wojciech Adamczyk[1], Michał Stebel[1], Jacek Smołka[1]

[1]Silesian University of Technology, Department of Thermal Engineering. Konarskiego 22, 44-100 Gliwice, Poland; e-mail: edyta.piechnik@onet.pl

Abstract

Hydrofluidisation freezing is relatively new food freezing method, which not only extends the shelf life of food but also provides high final quality of the frozen product. Nevertheless, the literature describing this method is not extensive and comprehensive experimental studies have not been conducted. The main purpose of this study was to determine the velocity profiles and the velocity fields around the stationary spherical sample as well as temperature distribution inside it. In order to capture fluid flow, the PIV method was used. Various parameters affecting the process were analysed, namely the orifice diameter (d), mass flow rate and the distance between the product and the orifice (H). The measurements were carried out for two orifice diameters of 3 mm and 5 mm. The distance between the orifice outlet and the sample varied from 50 mm to 70 mm. Consequently, the H to d ratio ranged from 10.0 to 23.3. The collected results indicate a significant influence of the H/d ratio on the local velocity magnitudes. In addition, an increase in the mass flow rate for H/d ratio above 14 did not affect significantly the fluid flow around the sample. The gathered results were used for the numerical model validation.

Keywords: Hydrofluidisation, food freezing, experimental investigation, fluid flow visualization

1. Introduction

Food freezing is one of the oldest and most commonly used methods for food preservation, which allows preservation of properties of processed products [1, 2]. An important factor in favor of freezing as a method of preserving food is its effect on harmful microorganisms. Moreover, the low process temperature achieved during the food freezing, affects the bacteria metabolism, which is disturbed or even stopped for the temperature ranged from -4°C to -10°C [3]. The selection of the freezing method depends on the type of groceries. Food freezing techniques significantly affects the structure of the processed products due to the formation of ice crystals [4]. Particularly noteworthy are products with high water content, such as fruits and vegetables in which it is over 90% [5]. The arrangement and shape of the crystals depend on the duration of the process. According to [4], quick freezing leads to the formation of a significant number of small ice crystals. As a consequence, the basic qualities of the fresh product are retained and the weight loss of the product after thawing is minimized. Slow freezing causes the creation of large dendritic crystals which affect morphological changes of the product, cells destruction as well as the denaturation of cell components [6, 7]. As the authors [4] presented, the choice of freezing method and process conditions determines the reduction of weight loss and has a significant impact on the food quality after thawing. Moreover, according to [7] to avoid significant ice crystal growth as well as structural damage, the temperature during the freezing process should be stable. On the other hand, due to temperature variations both in space and time, the measurement are challenging [8]. The effect of various freezing methods on the size and distribution of ice crystals inside the product has been discussed by Li et *al.* [9]. According to the aforementioned authors, the changes in food texture during freezing are highly dependent on the water distribution inside the product. Furthermore, the mechanism of cell damage during the freezing process was discussed. Li et *al.* [9] concluded that changes in the cell structure during freezing can affect the product quality, i.e. taste, color and texture, as well as the content of nutrients. Currently, the two most commonly used methods of food freezing can be distinguished, namely the air-blast freezing and the immersion freezing. Air-blast freezing is used for a wide range of products including fruits, vegetables, bakery goods, poultry, meats, and prepared meals [10]. There are two

types of air-blast freezers: batch and continuous both are based on convective heat transfer and use air as a freezing medium [11]. The main disadvantage of this method is the need for airflow at high speed and pressure. Consequently, a high fan power consumption is required [12]. In comparison to the immersion method, the lower heat transfer coefficients are obtained for that method. According to Dempsey and Bansal [3], the heat transfer coefficient for the air-blast method ranged from 25 $W \cdot m^{-2}K^{-1}$ to 300 $W \cdot m^{-2}K^{-1}$ for various types of air freezers. The immersion freezing method involves immersing the product in a liquid refrigerant, which is most often nitrogen or carbon dioxide [1] as well as aqueous solutions of NaCl, CaCl2, sucrose [13] or ethanol and glucose [14]. Because of higher heat transfer coefficient in liquids than in gases, the time required to conduct the process for the immersion freezing is shorter than in the air-blast freezing method. On the other hand, the main disadvantage of immersion is the possibility of absorption of refrigerant into the product [15]. Due to the disadvantages of currently used techniques, new methods of food freezing are constantly developed to improve the quality of the product and reduce energy consumption in the freezing process. James et. *al.* [2] and Li and Sun [16] reviewed and compared the methods being currently under investigation. The new methods of food freezing focus on increasing the rate of heat removal from food, as well as physical/chemical changes in a frozen product.

Hydrofluidisation freezing (HF), one of the most promising and innovative methods, is a combination of the air fluidization and the immersion freezing [2,12]. The origins of the method date back to the 1980s, when the first device was developed by Fikiin [17]. The freezing process proposed by Fiikin [17] is suitable for small-size product and it is based on submerging food products, e.g. small fruits or vegetables, inside a tank with an appropriate aqueous solution as a coolant. Within the hydrofluidisation freezing method, the coolant is pumped into the tank through orifices located at its bottom. That procedure leads to the creation of agitating jets and to intensify heat transfer coefficient between solution and food products. In consequence, freezing time is notably reduced, which results in a higher quality of the frozen product. The HF method is characterized by a very high heat transfer coefficients from 1000 $W \cdot m^{-2}K^{-1}$ to 3000 $W \cdot m^{-2}K^{-1}$ [12]. Further research has shown many advantages of HF systems, such as: reduced food weight loss, finer structure of ice crystals [12] and the use of natural coolants (e.g. sodium chloride aqueous solutions) [18]. Depending on the product, various fluidization media are used: brines, ice slurries and sugar-ethanol solution. The highest heat transfer coefficients were obtained for the ice slurry, namely of the order of 1000-2000 $W \cdot m^{-2}K^{-1}$, while the heat transfer coefficient for the classic immersion method is approximately 432 $W \cdot m^{-2}K^{-1}$ [19]. Moreover, the freezing time for small vegetables and fruits ranged from 1 min (for green peas) to 9 min (for strawberries) [19]. To describe the heat transfer in the HF system, Verboven et al. [14] conducted an experimental study in which the food was replaced with aluminum spherical samples. According to the results in this article, the heat transfer coefficient was in the range from 154 $W \cdot m^{-2}K^{-1}$ to 1548 $W \cdot m^{-2}K^{-1}$.

Recent studies on the HF method were performed using simultaneous laboratory-scale measurements and computational fluid dynamics (CFD). The CFD methods are based on the laws of fluid mechanics and heat transfer to accurately simulate the fluid flow and heat and mass transfer between products and the refrigerant. To determine the temperature change and the convective heat transfer coefficient on the surface of the sphere, the most basic model was formulated. The model covered simulation of the freezing system with one stationary spherical sample and a single orifice [20]. In the next stage of research, the formulated numerical model was extended by analysing the phenomenon inside the sample, which was the actual food product, namely potato [21]. These researches were focused on the analysis of the freezing of water inside the sample and the absorption of the refrigerant. Consequently, it was possible to determine the quality of the frozen product. Further analyses were focused on the numerical simulation for various numbers and positions of orifices and the distribution of the food samples inside the tank [22]. Next, the authors of [22] simulated the physical movement of products during hydrofluidisation, which corresponds to industrial scale process [23]. Nevertheless, the validation procedures were focused on a comparison of the global process parameters. Therefore, a more detailed experimental analysis is required to fully validate the heat and mass transfer phenomena during the HF process. The experimental effort should be focused on the local parameters of the

flow field as well as on the temperature distribution inside the HF tank. To capture the fluid, flow the particle image velocimetry (PIV) can be used.

2. Experimental rig and measurements

In order to investigate required parameters inside the hydrofluidisation chamber, a dedicated experimental rig was designed. The general design of that test rig was adapted from [18]. However, numerous modifications were introduced for more detailed experimental analysis. In particular, the construction of the hydrofluidisation chamber, as well as the sample mounting system, are more advanced comparing to the one described in the literature and mentioned above. The introduced changes are aimed at extending the measurements capability by using advanced flow visualization techniques (PIV) to determine the local flow field parameters. The general layout of the test rig with crucial elements marked is presented in Fig. 1. Two main elements of the experimental rig can be distinguished, namely the hydrofluidisation chamber and the refrigerant tank. The hydrofluidisation chamber is equipped with transparent elements at the front, the left and the right sides in order to enable the PIV measurements. Both elements were made of AISI 316L stainless steel and were thermally insulated. The refrigerant flow can be realized in two loops. The medium preparation loop is used to stabilise the coolant temperature throughout the system, while the freezing chamber loop supplies the refrigerant into the hydrofluidisation chamber.

2.1. Hydrofluidisation chamber

As it was previously mentioned the hydrofluidisation chamber is equipped with transparent elements to enable PIV measurements. As shown in Fig. 2.1. the transparent tank was installed inside the chamber. At the bottom of this tank, numerous stainless-steel plates having a different number of orifices with variable diameters can be installed. Therefore, a single jet as well as a multiple jet system can be analysed. Moreover, the experimental rig is adapted to investigate the freezing process of small vegetables and fruits e.g. strawberries or potatoes. In order to simplify the measurements of fluid flow, food products were replaced with copper spherical sample with a diameter of 20 mm. In the preliminary investigation of the heat transfer in processed product, the copper sample was replaced with the actual food product, namely radish. The sample is attached to the movable arm and its position can be precisely set using two step motors. The construction of the experimental rig allows for the simultaneous placement of one or more samples.

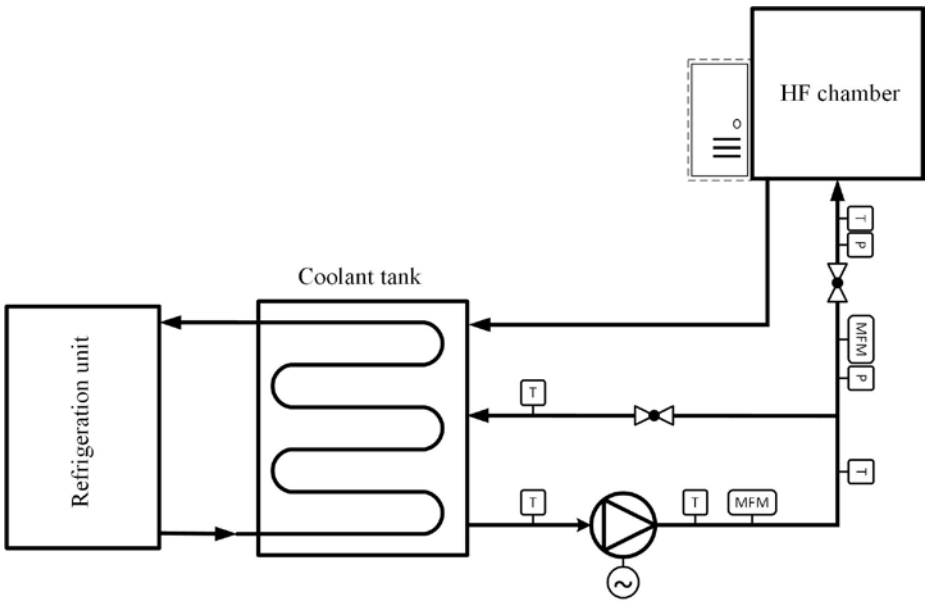

Fig. 2.1. The scheme of the experimental rig

2.2. Flow and thermal measurements

To ensure refrigerant circulation the experimental rig is equipped with a vertical multistage pump. The installed pump is rate 1.83 kW at 50 Hz. The maximum working pressure is 16 bar whereas the flow is in the range 2.4-7.8 $m^3\ h^{-1}$. The pump may operate within the temperature range between -30°C to 80°C. The whole pump was made of AISI 316L stainless steel. Mass flow rate is controlled by the TECO L510s inverter. The valve system is used to switch between the work in the medium preparation loop and the freezing chamber loop. The mass flow rate of the medium is measured by two Coriolis mass flow meters which are characterized by high accuracy of ±0.1% for the mass flow rates higher than 300 kg min^{-1} and max. ±2% of the reading for lower mass flow range. In order to analyse the temperature distribution, numerous T-type thermocouples were installed in the experimental rig. All sensors were installed in the piping system within the compression fittings. Three additional thermocouples can be placed inside the HF chamber, namely in the surrounding liquid, on the sample wall and in its core.

2.3. PIV system

As it was already mentioned, in order to analyse the refrigerant flow field around the spherical sample, the PIV method was used. This technique allows for the visualization of the fluid flow field in the laser light section within the region of the sample under examination. For this method, the equipment provided by Dantec (Dantec Dynamics Flow Sense 4M MK4 II) was used. The flow is recorded using a fast camera equipped with a 2048x2048 CCD sensor with a pixel size of $7.4 \cdot 10^{-6}$ m and with a Carl Zeiss APO-Sonnar T·135 mm f/2 lens. In order to illuminate the studied region, the Quantel Twin BSL 200 double pulsating laser was used. Two consecutive laser pulses illuminate a slice of a flow field with particles suspended in the flow. The scattered light from the particles is captured in two consecutive images on a digital camera. Registration of recordings can take place due to synchronization of both devices with Dantec Dynamics Synchronizer. Thanks to the Dantec Dynamics DynamicStudio 3.41 software, it is possible to process recorded recordings. To make these measurements possible, an appropriately selected particles of polyamide with an average particle size of 5 μm and the density of 1030 $kg \cdot m^{-3}$ are introduced into the medium. The measurement includes a 2D cross-section with a field of view equal to 63x63 mm. For each measurement, the camera position was selected to reach an area 20 mm below the spherical sample. Consequently, regardless of the H/d ratio, the arrangement of the frame was approximately the same for all considered cases. The laser was positioned on the left-hand side of the experimental rig and its beam illuminated only that side of the sample. Therefore, only the left-hand side of the recordings was analysed. It was assumed that the flow is symmetrical on both sides of the sphere. For each experimental run, 200 double frames were captured. Captured images are not ready for immediate processing. Pre-processing tools allow to perform a wide range of advanced features to optimise image quality, calibration and masking. In Fig. 2, the stages of processing are presented. Firstly, the high-pass filter was used to reduce the noise and enhance the contrast. In consequence, the seeding particles are better visible. Then the average flow field was calculated through an average correlation method. The images were divided into smaller areas for calculating the mean particle displacement between two corresponding sub-areas. Because the time interval between two laser pulses is known, the particle average velocity can be determined. Afterwards, the peak validation was used. This method compares the relative height of the highest peak in each sub-area to the second-highest peak. This tool is used to reject incorrect vectors, which relative height parameters exceeded the set value. In the next step, using range validation, it is possible to manually reject incorrect vectors based on the expected range of velocities. The vector length can be specified in the recipe. The last method used in the whole post-processing stage is moving average validation, which is based on comparing neighbouring vectors. If in a given neighborhood the vector deviates too much from the others, it can be replaced by the average of the surrounding vectors. Vector results can be represented using the 2D plot, as shown in Fig. 2.2. In order to obtain that plot, the scalar map function was used. In this method, individual velocities are represented by colours.

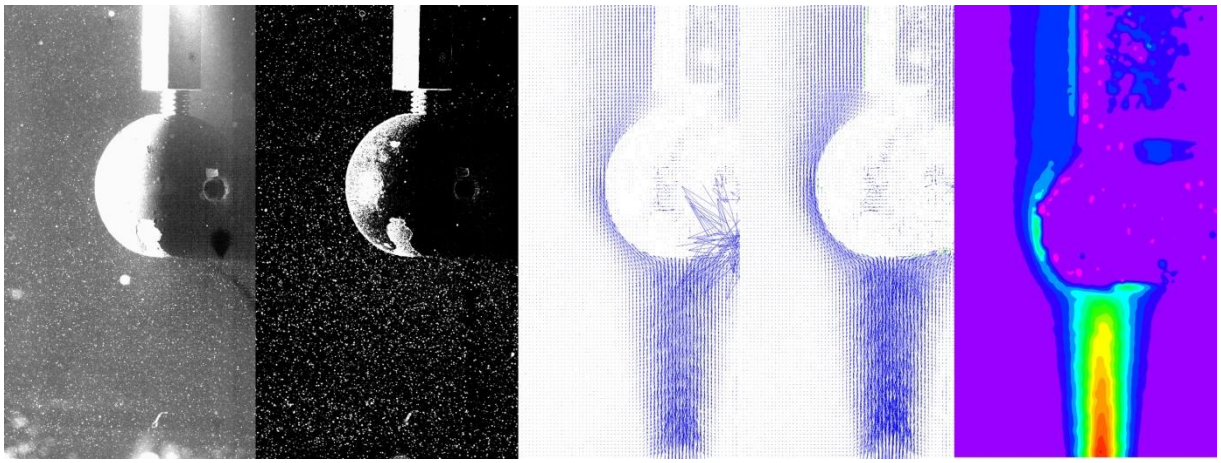

Fig. 2.2. PIV analysis stages [24]

3. Results

3.1. Fluid flow measurements

The results of fluid flow measurements presented in the current paper are selected cases from the most recent paper describing the experimental investigation of the hydrofluidisation method [24]. As it was previously mentioned, the experimental effort was focused on the analysis of the fluid velocity within the single jet and around the stationary spherical sample. The measurements included analysis of various ratios of the distance between the sample and the orifice (H) to the orifice diameter (d), as well as various mass flow rates. Two orifice diameters were investigated, namely 3 mm and 5 mm. The heat transfer was neglected for PIV measurements. Therefore, all of the PIV measurements were carried out for refrigerant at ambient temperature. The list of the analysed cases is presented in the Table. 3.1. The distance between the sample stagnation point and the orifice outlet varied from 50 mm to 70 mm for the orifice diameter of 5 mm and was equal to 50 mm for the orifice diameter of 3 mm. Consequently, the H/d ratio ranged from 10.0 to 16.7. The Reynolds number for investigated cases varied from 85 000 to 138 000.

Table. 3.1. Investigated cases

Case	d, mm	$\dot{m}$, kg·h^{-1}	Re	H/d, -
1	5	411.75	85000	10.0
2	5	407.57	85000	12.0
3	5	404.06	84000	14.0
4	5	657.48	138000	10.0
5	3	147.09	86000	16.7
6	3	185.84	110000	16.7

The velocity fields for H/d ratios of 10.0 and 16.7 and for Re numbers of 85 000, 86 000, 110 000 and 138 000 are presented in Fig. 3.1. The velocity reduction in the area directly under the sphere, i.e. the stagnation area, as well as the boundary layer of the solution, are clearly visible. As expected, an increase in the mass flow rate resulted in a higher fluid velocity. The velocity magnitude along the jet axis is significantly higher for the H/d ratio equal to 10.0, i.e. cases (a) and (b), and is approximately 6 m·s^{-1} and 10 m·s^{-1}, respectively. For the H/d ratio equal to 16.7 an increase in the mass flow rate did not influence the velocity significantly. The velocity values along the jet axis for this case range from 2 m/s to 4 m/s for cases (c) and (d), respectively. At the same time, clear differences in the flow within the boundary layer can be noticed. The fluid velocity in this area for cases (a), (c), (d) in Fig. 3 does not exceed 2 m/s, whereas in the case (b) it reaches the value of about 5 m/s. As a consequence of the mentioned observations, it can be concluded that for each case the increase of the H/d ratio

caused a drop in velocity magnitude along the jet axis and at the same time did not significantly affect the velocity near the sample wall for an H/d value of 16.7.

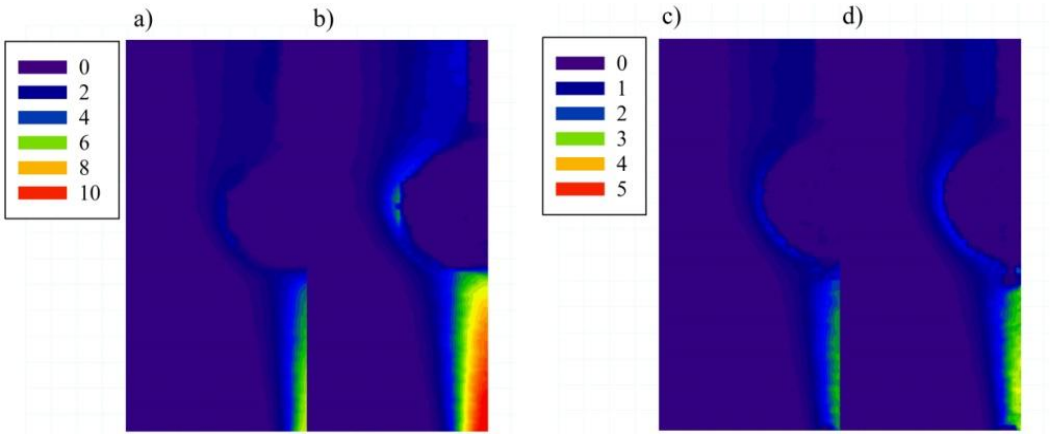

Fig. 3.1. Comparison of the velocity fields (m·s⁻¹) for various Re numbers: (a) Case 1 (b) Case 4 (c) Case 5 (d) Case 6 [24]

In Fig. 3.2. the velocity fields for various distances between the stagnation point of the sample and the orifice outlet are presented for the constant Re number of 85 000. The measurements were carried out for 5 mm orifice and the H value varied from 50 mm to 70 mm. Consequently, the H/d ratio ranged from 10 to 14. Each PIV recording was made to cover the area of 25 mm under the stagnation point. Therefore, regardless of the analysed case the location of the sphere in each frame is similar. According to the expectations, the jet velocity decreases with increasing H/d ratio. For thea H/d ratio of 10, the velocity in the jet axis is about 6 m·s⁻¹. For other H/d values, the velocity is lower, namely 5 m·s⁻¹ and 4 m·s⁻¹ for the cases with H/d=12.0 and H/d=14.0, respectively. Comparing the velocity fields near the sample wall, it can be noticed that the maximum difference in velocity magnitude is about 1 m·s⁻¹.

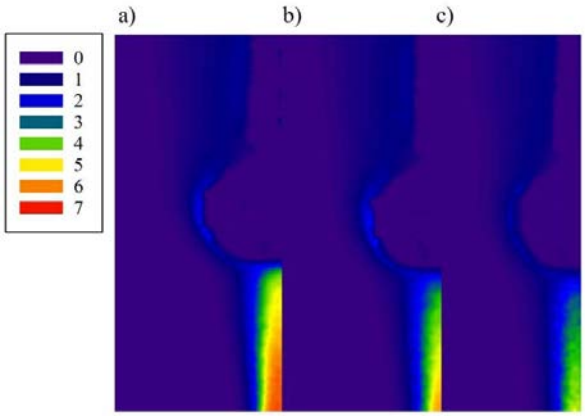

Fig. 3.2. Comparison of velocity field (m/s) for Re ≈ 85 000 (a) H/d = 10.0 (b) H/d = 12.0 (c) H/d = 14.0

In order to carry out a more detailed analysis of flow behaviour for various H/d ratios, the velocity profiles were prepared. The current paper presents the results of velocity profiles along the jet axis for selected cases. The comprehensive analysis of the velocity profiles in the discussed system is presented in detail in the study of Palacz et *al*. [24]. The aforementioned authors discussed the velocity distribution within the jet axis as well as within the horizontal line at the stagnation point level and at the sample centre level. In Fig. 3.3. the relation between the jet velocity and the H/d ratio is presented. These profiles were prepared for the Re number equal to 85 000 and two orifice diameters. In consequence, the ratio H/d ranged from 10.0 to 16.7. The cases H/d in the range from 10.0 to 14.0 refer to the 5 mm diameter orifice. According to the expectations, the velocity

magnitude within the jet rapidly decreases when the fluid reaches the stagnation point. The same trends can be observed on all characteristics. The decrease in velocity can be considered as steady and relatively slow. The difference in the maximum velocity of the jet for H/d equal to 10.0 and H/d equal to 14.0 is just about 2 m·s⁻¹.

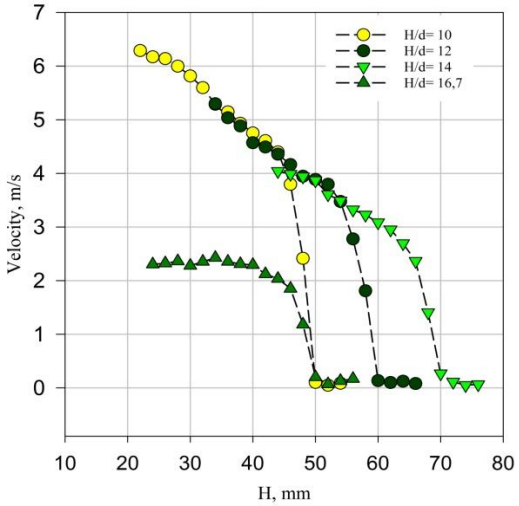

Fig. 3.3. Comparison of velocity profiles along the jet axis for Re ≈ 85 000

As it was previously mentioned, the results collected during the experimental investigation were used for the numerical model validation. The validation covers a comparison of the PIV measurements with the numerical calculations employing two turbulence models, namely k-ω SST and RSM (Reynolds stress model). PIV recordings were used to compare the velocity field within the jet region and around the sphere, while the mass flow measurements were used to control the operating conditions. The comparison of the obtained velocity fields is presented in Fig. 3.4. The measurements were carried out at ambient temperature. Therefore, the heat transfer during process was neglected. Velocity fields presented in Fig. 3.4. were compared for Case 3 from Table 1, namely the H/d ratio of 14.0. The field of observation for these velocity contours covers nearly 30 mm of the area below the stagnation point. As it can be seen in Fig. 8, for the k-ω SST model, the values of velocity within the jet core and the sample wall are close to the experimental results, while the RSM model is less accurate. Moreover, using the k-ω SST model, the phenomena of the stream detachment from the wall is much better simulated. For the RSM model the fluid flow near the sample wall is more dispersed.

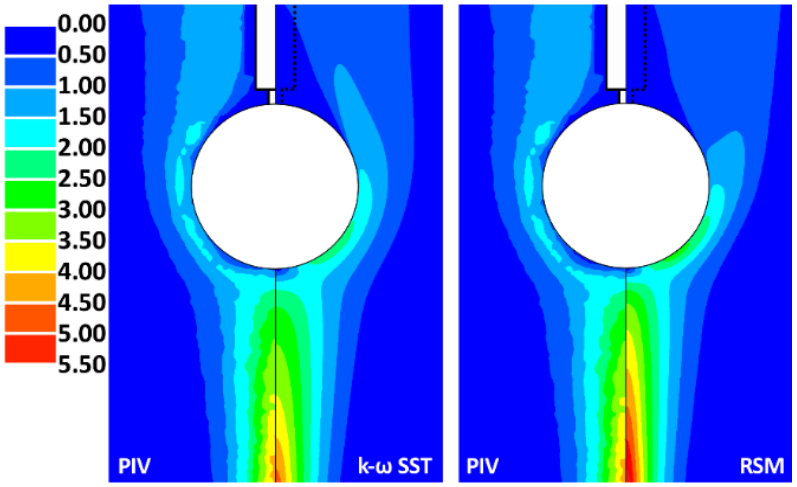

Fig. 3.4. Velocity magnitude field (m·s⁻¹) around the sphere obtained from PIV measurements and CFD model using two turbulence models for the H/d = 14.0, MFR=0,1132 kg·s⁻¹ [27]

3.2. Thermal measurements

The preliminary investigation of the heat transfer within the hydrofluidisation freezing process was conducted. In order to determine the temperature distribution two thermocouples were installed inside the analysed samples. The location of these thermocouples is presented in Fig. 3.6. The additional thermocouple was used to measure the temperature of the surrounding fluid. The cooling medium was an aqueous solution of ethanol (17% of the mass concentration). As it was already mentioned, the thermal measurements were carried out for the actual food sample. In the first stage of the thermal measurements, the analysed sample was strawberry. The measurements were carried out for H/d ratio of 10.0 and coolant temperature of -7.5 °C. Nevertheless, in Fig. 3.5. an example of temperature distribution during freezing process within previously mentioned locations is presented. The trends for the temperature profiles recorded during the experiments are consistent with the freezing process presented in the recent literature [25]. As it can be seen in Fig. 3.5., the sudden increase of the sample core temperature was noted during the process. In particular, the core temperature increased by 4K at 20th minute of the process. That phenomenon is directly associated with phase change and the release of latent heat. Moreover, the freezing time of the analysed sample was relatively long. According to the literature, the freezing time for strawberries is about 9 min [19]. This significant difference may be due to the non-spherical shape of the product and to the fact that the fluidisation effect was not achieved during experiments. In particular, the sample was attached to the sample mounting system. Hence, the sample position was fixed during the process. Consequently, the HTC values were significantly lower compared to those of the industrial HF freezing process. Due to problems with sample mass and shape repeatability, further research on strawberry samples was abandoned.

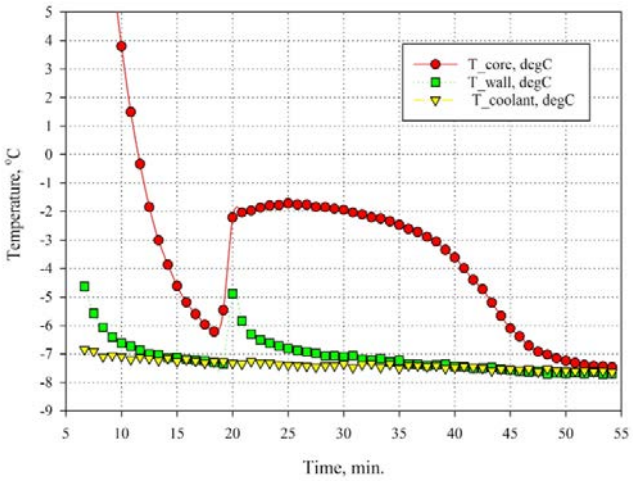

Fig. 3.5. Temperature distribution for strawberry sample

In the next stage of temperature investigation, the strawberry sample was replaced with a radish due to its spherical shape. The measurements were carried out for various H/d ratios. The full list of the analysed cases is presented in the Table. 3.2. The coolant temperature during the experiment was about -6°C while the Re number was about 85 000.

Table. 3.2. Investigated cases

Case	Type	H/d, -	d1, mm	d2, mm	Mass, g
1	radish	10.0	3.2	2.9	17.26
2	radish	12.0	2.9	3.4	17.93
3	radish	16.6	2.7	3.2	13.52
4	radish	20.0	3.2	3.1	17.04
5	radish	23.3	3.1	2.7	16.02

In Fig. 3.7. comparison of temperature distribution within the radish core for various H/d ratio is presented. It can be noticed that in the initial phase of the freezing process the temperature profiles were similar to all considered H/d. According to the presented results, it can be stated that the freezing process started after about 8 min. at the temperature of approximately -1°C for all cases. The core temperature of the radish, for the H/d of 20.0, reached the temperature of the surrounding liquid after about 30 min., while for the other cases, the time was about 38 min. In relation to the total duration of the freezing process, a difference of 8 min. can be considered as significant. However, it should be emphasized, that the investigated samples were slightly differed in mass and shape, which could also affect the freezing time.

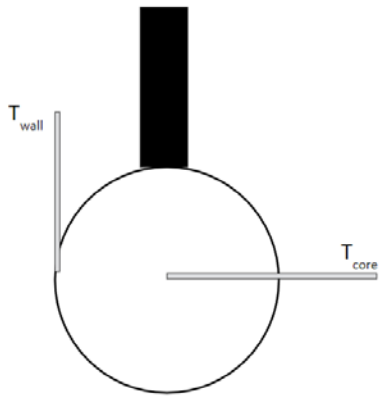

Fig. 3.6. T-type thermocouples location [26]

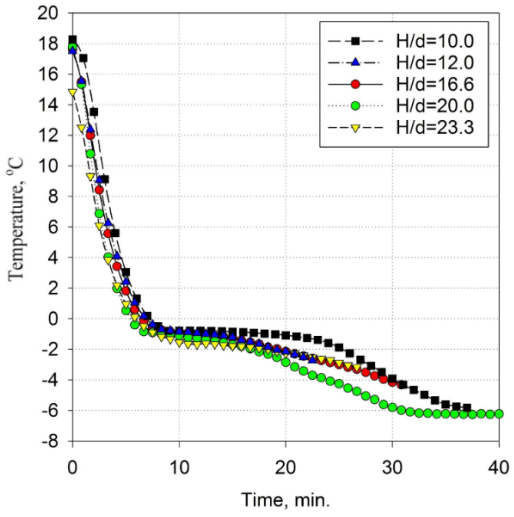

Fig. 3.7. The temperature profiles within the radish core [26]

4. Conclusions

To summarize, in order to analyze fluid flow inside the HF chamber, a dedicated experimental rig was designed and presented in this work. In addition, gathered results were used for the numerical model validation. Due to the use of transparent elements, namely transparent HF tank as well as transparent walls of the HF chamber, the test rig was adapted to perform PIV measurements. Moreover, it was equipped with high-quality measuring instruments. The main purpose of this thesis was to analyze the fluid flow around the stationary sample during the HF process. The presented measurements were carried out for a single spherical copper sample with a

diameter of 20 mm. Moreover, two orifice diameters of 3 mm and 5 mm were investigated. The influence of the orifice diameter, the refrigerant mass flow rate and the distance between the sample and the orifice outlet to its diameter on the jet velocity were investigated. The presented results indicate a significant influence of the investigated parameters on the course of the hydrofluidisation process. However, analysing the flow field around the sample, it can be stated that only for the H / d ratio in the range from 10.0 to 14.0 the increase in the number Re caused an increase in the velocity value around the sample walls. Moreover, it can be noticed that the distance between the sample and the orifice outlet for the Re≈ 85 000 has minor effect on the velocity fields near the sample surface. The maximum difference was about 0.4 $m \cdot s^{-1}$. As a consequence of the mentioned observations, it can be concluded that the H/d ratio has a greater impact on local velocity magnitudes than the distance change itself. Moreover, the results of the preliminary temperature measurements are discussed through this paper. Thermal measurement was carried out for two food samples, namely strawberry and radish. The freezing time for strawberry was about 50 min., which significantly exceeds the time reported in the literature. It was found that the reason could be the non-spherical shape of the sample. Therefore, in the next part of the experiment, radishes were used. To sum up the analysis of the impact of the H/d ratio on radish freezing time, it can be stated that the freezing process was the most effective for the H/d of 20.0. For the investigated cases the maximum difference in duration of the process was about 500 sec. In summary, the variation of H/d ratio for presented cases can be considered significant in terms of heat transfer. Nevertheless, in the next stages of the experimental investigation, the presented results should be repeated for food samples of similar shape and weight.

For the numerical model validation, two turbulence models were examined, namely k-ω SST and RSM. One arrangement of the single orifice and single sphere was analysed. The comparison of both turbulence models with gathered results from the PIV measurements shows that the numerical model predicts the refrigerating medium velocity with satisfactory accuracy. Nevertheless, according to results presented in Fig. 9, the k-ω SST approach performs better for the flow within HF system. The k-ω SST model predicts the fluid flow with higher accuracy within the region near the sample wall.

It is important to emphasize that the experimental investigation is a part of ongoing project. The further investigation of the HF freezing process will be enhanced by analysing the relation between the flow field and a various number of orifices as well as various number of samples installed inside the HF chamber.

Acknowledgments

Financial assistance was provided by grant no. DEC-2016/22/E/ST8/00517 funded by the National Science Centre, Poland and is here acknowledged.

References

[1] Singh R. P., Heldman D. R., Chapter 7 - food freezing, in: R. P. Singh, D. R. Heldman (Eds.), Introduction to Food Engineering (Fifth Edition), fifth edition Edition, Food science and technology, Academic Press, San Diego, 2014, pp. 521 – 563.

[2] James C., Purnell G., James S. J., A review of novel and innovative food freezing technologies, Food and Bioprocess Technology 8 (8) (2015) 1616–1634.

[3] Dempsey P., Bansal P., the art of air blast freezing: Design and efficiency considerations, Applied Thermal Engineering 41 (2012) 71 – 83, 13th Brazilian Congress of Thermal Sciences and Engineering.

[4] Goral D., Kluza F., Physical changes of vegetables during freezing by conventional and impingement methods, Acta Agrophysica (1).

[5] Schafer W., The science of freezing foods. usa: University of minnesota extension, Available from http://www.extension.umn.edu/food/food-safety/preserving/freezing/the-science-of-freezing-foods/

[6] Fellows P., Food processing technology.principles and practice.second edition (2000) 418–440.

[7] Kaale L. D., Eikevik T. M., Rustad T., Kolsaker K., Superchilling of food: A review, Journal of Food Engineering.

[8] Magnussen O.M., Hauglandb A., Torstveit Hemmingsen A. K., Advances in superchilling of food – process characteristics and product quality., Trends in Food Science and Technology 8 (19) (2008) 418–424.

[9] Li D., Zhu Z., Sun D.-W., Effects of freezing on cell structure of fresh cellular food materials: A review, Trends in Food Science & Technology 75 (2018) 46 – 55.

[10] Desrosier N. W., Singh R. P., Food preservation, Encyclopædia Britannica.

[11] Mascheroni R. H., Operations in food refrigeration, CRC Press, 2012.

[12] Fikiin K., Nolvelties of food freezing research in europe and beyond. institut national de la recherche agronomique. project no. qlk1-ct-2000-00040, 56p.

[13] Galetto C., Verdini R., Zorilla S., Rubiolo A., Freezing of strawberries by immersion in cacl2 solutions, Food Chemistry 123 (2010) 243–248.

[14] Verboven P., Scheerlinck N., Nicolaı B. M., Surface heat transfer coefficients to stationary spherical particles in an experimental unit for hydrofluidisation freezing of individual foods, International Journal of Refrigeration.

[15] Zorilla S., Rubiolo A., Mathematical modeling for immersion chilling and freezing of foods: part ii: model solution, Journal of food engineering 66 (3) (2005) 339–351.

[16] Li B., Sun D.-W., Novel methods for rapid freezing and thawing of foods – a review, Journal of Food Engineering 54 (3) (2002) 175 – 182.

[17] F. K, New method and fluidized water system for intensive chilling and freezing of fish food control 3 (3) (1992) 153–160.

[18] Peralta J., Rubiolo A., Zorilla S. Design and construction of a hydrofluidization system. study of the heat transfer on a stationary sphere, Journal of Food Engineering.

[19] Fikiin F. A., K.A., Individual quick freezing of foods by hydrofluidisation and pumpable ice slurries., Refrigeration Science and Technology 6 (1998) 319–326)

[20] Peralta J., Rubiolo A., Zorilla S.: Mathematical modeling of the heat transfer and flow field of liquid refrigerants in a hydrofluidization system with a stationary sphere. Journal of Food Engineering, 99, 2010, 303-313

[21] Peralta J., Rubiolo A., Zorilla S.: Mathematical modeling of the heat and mass transfer in a stationary potato sphere impinged by a single round liquid jet in a hydrofluidization system. Journal of Food Engineering, 109, 2012, 501-512

[22] Belis E., Zorilla S., Peralta J.: Effect of the number of orifices and operative variables on the heat and mass transfer in a hydrofluidization system with static spheres. Journal of Food Engineering, 153, 2015, 96-107

[23] Orona J., Zorilla S., Peralta J.: Computational fluid dynamics combined with discrete element method and discrete phase model for studying a food hydrofluidization system. Food and Bioproducts Processing, 102, 2017, 278-288

[24] Palacz M., Adamczyk W., Piechnik E., Stebel M., Smolka J., 2019. Experimental investigation of the fluid flow inside a hydrofluidisation freezing chamber. International Journal of Refrigeration 107, 52 – 62.

[25] Ericson M., Hung Y-C., Quality in frozen food, 1997, Springer

[26] Palacz M., Piechnik E., Adamczyk W., Stebel M., Smolka J.: Experimental analysis of the hydrofluidisation freezing system for small fruits and vegetables. The 25th Congress of Refrigeration, 2019, Montreal, Canada.

[27] Stebel M., Smołka J., Palacz M., Adamczyk W., Piechnik E.: Numerical modeling of the fluid flow and the heat transfer during food freezing with the hydrofluidisation method. ICCHMT 2019, Rome, Italy.

Ammonia as Storage Medium for Renewable Energies. Equilibrium modelling of ammonia combustion

Ewa Pazdur[1], dr hab. inż. Adam Klimanek[2]

[1]Faculty of Energy and Environmental Engineering, Silesian University of Technology e-mail: ewa.pazdur1@gmail.com,
[2]Faculty of Energy and Environmental Engineering, Silesian University of Technology e-mail: adam.klimanek@polsl.pl

Abstract

Increasing share of renewable energy sources in the power generation sector results in the need of having an intermediate storage system to support intermittent nature of energy produced from renewable sources. For industrial scale, energy storage can be realized by means of mechanical or chemical systems. Chemical energy storage is the branch intensely developed, as it possesses very big potential. One of the most frequently considered means of energy storage is via hydrogen production. This, however, brings a few difficulties connected with the properties of the hydrogen, its transportation and distribution. A solution to those problems, can be introduction of other, hydrogen containing energy carriers, as a part of hydrogen-based storage technology. One of the candidates is ammonia. Besides its high toxicity, ammonia handling is much easier than handling hydrogen. Ammonia can eventually be combusted, and energy stored in ammonia can be easily restored into electricity, by means of technologies very similar to those available today. Combustion of ammonia does not produce any CO_2, however considerably higher NOx generation is inevitable, which requires special attention. This study presents results of equilibrium computations of ammonia combustion for selected thermodynamic parameters (temperature and pressure), and air to fuel ratios. As expected, the maximum temperatures occur close to stoichiometric oxidizer to fuel ratios of n_{O2}/n_{NH3} = 0.75 and are increasing with increasing pressure. The predicted NO, NO_2 and N_2O are increasing to approximately the stoichiometric ratio and then remain virtually constant, where the NO is 3 orders of magnitude higher than NO_2. The predicted NO_x concentrations can be however considerably higher than in real systems due to the assumption of equilibrium.

Keywords: energy storage, ammonia for power, combustion of ammonia

1. Introduction

The current world is experiencing rapid energy transition process. In the topic of electricity generation, switching from the fossil into the renewable fuels is quite a challenging task, that, however, eventually will need to be implemented on a worldwide scale to prevent further great influence on the environment. The process of transition not only requires advanced technologies and better conversion of 'green energy' into electricity, but also the proper energy management systems. Part of the energy management is energy storage, that deals with the intermittent nature of some renewable energy sources and helps to mitigate the influence of over- and underproduction of electricity on the grid [1]. For the technical realization of a large-scale economy based on regenerative energy systems, an intermediate storage is required. Large-scale energy storage remains an issue, as most of the existing solutions are ineffective for a long-term storage or are not economically feasible. One of the promising technologies is energy storage via hydrogen production. This method, however, faces lots of problems connected with storage of the hydrogen, such as low volumetric energy density, high transportation costs or hydrogen's penetration through the solid walls, that cannot be easily nor directly solved. One of the possible ways to overcome this problem, is indirect use of hydrogen – using its derivatives as alternative energy carriers [2]. Very beneficial is use of carbon-neutral derivatives, as those don't cause emission of CO_2 while being burnt [2]. The carrier investigated in this paper is ammonia and its combustion. Ammonia is characterized by easier and more widespread production, lower storage cost, longer possible storage period, higher volumetric energy density, easier distribution and handling [3]. It is an energy carrier, which can be used just for transportation of

hydrogen, or be combusted directly [4]. Moreover, fully developed infrastructure for ammonia storage, transportation and distribution already exists, and the current power generation technologies can be applied for its utilization after introduction of minor changes. Thereby, it proposes solution to the hydrogen-based energy storage systems and can make possible to bring it into industrial scale. Several drawbacks of ammonia as a fuel exist, with the most important being its high toxicity [5]. If getting into contact with life organisms, it may cause permanent health damage [6].

2. General characteristics of ammonia

Ammonia (NH_3) is a chemical compound of hydrogen and nitrogen, the simplest stable one. It is colorless pungent gas [7] lighter than air. Ammonia is highly toxic, even small amounts are irritating for the living organisms. It is vastly used as fertilizer, refrigerant, in plastic, dyes, textiles, detergents and pesticides sectors [8]. Ammonia is characterized by low burning velocities in air (maximum of 0.09 m/s) approximately 4.5 times smaller than methane and 32.3 times smaller than hydrogen. Its high auto-ignition temperature (630 – 650 °C), indicate its low flammability. Combustion of ammonia is associated with high fuel NO_x generation and possible NH_3 emissions which can lead to health hazards. Ammonia-air flames are also characterized by lower radiation than hydrocarbon flames thus leading to lower heat transfer rates due to lack of CO_2 in the products [9]. The process of combustion characterizes with low combustion intensity, in comparison to other hydrocarbon fuels. The global reaction of ammonia combustion can be written as:

$$4NH_3 + 3O_2 \rightarrow 2N_2 + 6H_2O$$

In this idealized case of ammonia combustion, the only products are nitrogen and water, the real case, however, leads also to presence of many minor species, including the NO_x. Selected characteristic properties of ammonia are given in the Table. 2.1. The assessment of ammonia as a hazardous substance given in the Table. 2.2.

Table. 2.1. Properties of ammonia, [10]

Density, kg/m^3	0.86
Molar mass, g/mol	17.031
Flammability range, % of dry air	15.15-27.35
Energy density, MJ/kg	22.5
Volumetric Energy Density (liquid ammonia), MJ/L	11.5
Boiling point, °C	-33.35
Melting Point, °C	-77.7
Auto-Ignition Temperature, °C	630
Maximum burning velocity, m/s	0.09

Worldwide annual production of ammonia exceeds 170 Mt [11]. The production is dominated by China (around 32%). In Europe it is equal around 21 Mt, with Germany leading in the production [8]. The hydrogen used in ammonia synthesis is mostly produces by steam methane reforming or by gasification of coal, which is associated with CO_2 emissions. To produce the desired end-product ammonia, the hydrogen is then catalytically reacted with nitrogen (derived from process air) to form anhydrous liquid ammonia. This step is known as the ammonia synthesis loop (also referred to as the Haber-Bosch process) [12] [9]:

$$3H_2 + N_2 \rightarrow 2NH_3$$

Table. 2.2. Assessment of ammonia as hazardous substance, [13]

Hazard Rating (NFPA)	
Health	3
Flammability	1
Reactivity	0
Additional Information: Corrosive, may ignite and burn with explosive force, poisonous gases produced in fire, containers may explode in fire	
Hazard Rating Key: 0=minimal, 1=slight, 2=moderate, 3=serious, 4=severe	

3. Equilibrium modelling

The aim of this section is to model the combustion of ammonia assuming equilibrium of the products. In all the calculations the combustion process was assumed to be isobaric and adiabatic. Equilibrium modelling results provide important information about the process, however, due to the assumption of infinitely fast reactions (or infinite process time) the predicted products composition and thus the temperature may considerably differ from the real combustion systems. This is particularly important for predicting NO_x formation which, at typical combustion temperatures, is a relatively slow process, and thus the predicted NO_x concentrations with the assumption of equilibrium are considerably higher than those in reality. The calculations were performed using an open-source code Cantera, a suite of tools for problems involving chemical kinetics, thermodynamics, and transport processes. The data pre- and post-processing was realized by a code written in Python programming language. The set of species taking part in process were limited to those present in the GRI3.0 mechanism, from which also the thermodynamic data were taken. The computed parameters were the adiabatic flame temperatures and composition of products for various oxidizer-fuel ratios and for various pressures.

4. Results and discussion

4.1. Combustion in Oxygen

First computations were done for isobaric and adiabatic combustion of ammonia in oxygen for various molar oxygen to ammonia ratios. In Fig. 4.1. the adiabatic flame temperature is presented for pressures: 0.1 MPa (atmospheric pressure), 1 MPa, 5 MPa and 10 MPa. In Fig. 4.2., for the same range of pressures, molar fractions of products are presented. In Figure 3, NO_x emissions are presented, as, due to their order of magnitude, the values wouldn't be visible in Fig. 4.2.

The highest temperature occurs in the moment, when the ratio oxygen/ammonia is close to 0.75, which corresponds to stoichiometric parameters of ammonia combustion (0.75 moles of oxygen needed for 1 mole of ammonia combustion). Temperature in maximum point is equal to 2840 K for atmospheric pressure. For the highest pressure, maximum temperature is around 500 K higher. Possibility of obtaining high temperatures is important in designing the combustion stand, to choose proper materials. The maximum temperature appears in the moment when almost whole hydrogen coming from ammonia is oxidized to H_2O. The further drop is connected with appearance of excess oxygen, as it is seen on Fig. 4.2. The part of the enthalpy is used for heating it up, which causes drop of the temperature.

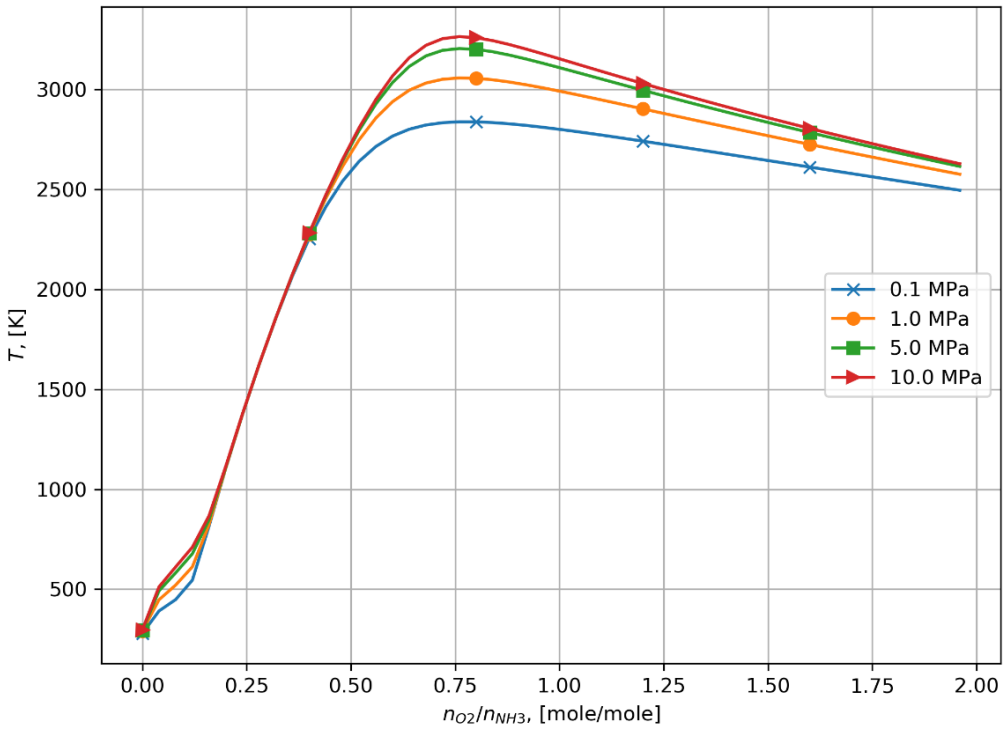

Fig. 4.1. Temperature profiles during ammonia combustion depending on the pressure, combustion in oxygen

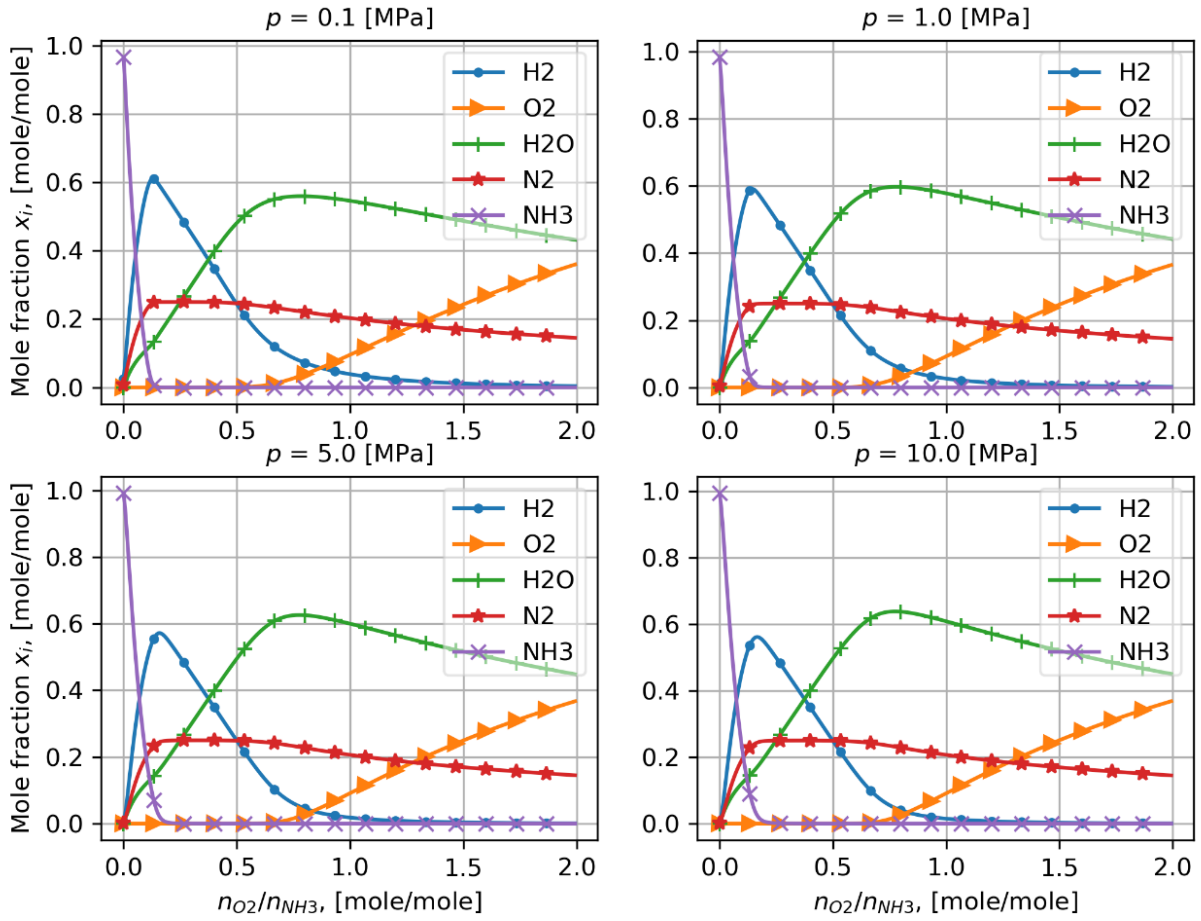

Fig. 4.2. Molar fractions of species during ammonia combustion in relation to pressure, combustion in oxygen

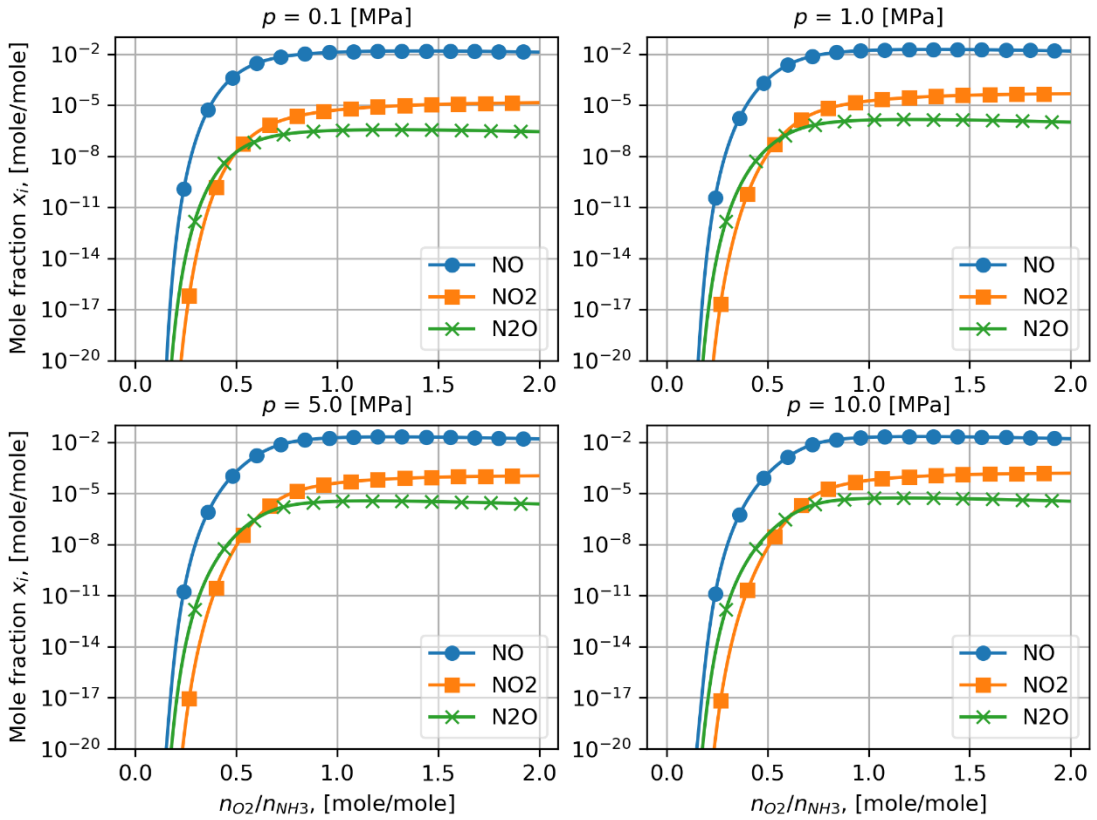

Fig. 4.3 NOx molar fractions in relation to pressure, combustion in oxygen

As shown in Fig. 4.2. the point where oxygen/ammonia ratio is equal to around 0.14 is where the biggest amount of hydrogen is released do to ammonia decomposition at high temperature at sub-stoichiometric conditions. Increasing water vapor fraction is a result of oxidation of hydrogen as the amount of oxygen increases. It stops increasing while excess amount of oxygen is provided. With increase of pressure, the amount of hydrogen released drops, but at the same time the amount of water vapor created increases. Fig. 1 shows, that with the rise in pressure, there is also an increase of temperature at equilibrium conditions. At the different pressures the particles behave differently. If the pressure **i**s higher it is more difficult to decompose the polyatomic species. But then, when they break**,** with bigger pressure they combine easily, and bigger amount of them will enter reactions, mostly with oxygen. As can be seen the higher the pressure the lower is the H_2 concentration at the same n_{O2}/n_{NH3} and more H_2O is formed, as can be seen in Fig. 4.2. This results in higher flame temperatures.

As a result of the oxidation reaction of ammonia mainly H_2O and N_2 is formed, however with the high temperature and excess amount of oxygen, the nitrogen undergoes oxidation, and is being transformed mostly into NO, and in smaller amounts to NO_2 and N_2O, as presented in Fig. 4.3. Maximum mole fraction of the formed NO is 0.0152 mol/mol. Generation of NO leads to formation of NO_2, as a result of proceeding chemical reactions. Restricting the emission of NO itself is also important, as, although it is not a pollutant itself, released to the atmosphere it would enter the reaction with oxygen present there and form NO_2. NO_2 is highly unwanted substance, which is considered to be on of major air pollutants. Maximum amount of NO_2 created is 0.0000147 mole. Majority of formed NO_x in typical combustion systems is thermal NO_x, created at the high temperatures in flame in oxidizing atmosphere. Since the fuel is ammonia, its decomposition will be associated with formation of intermediates, which will be then oxidized to nitrogen oxides. Therefore, the fuel mechanism will play an important role in NO_x formation. NO_2 concentration from combustion at 0.1 MPa is 11 times smaller than that at 10 MPa. Similarly, N2O concentrations are increasing. The NO_2 remains however 2-3 orders of magnitude smaller than NO and N_2O 2 orders of magnitude smaller than NO_2. Therefore, with the increase of pressure, the concentrations of the harmful substances increase as well, however the differences are not very large. This increment is a result of previously mentioned different behavior of particles at different pressures. It should be

also stressed that the assumption of equilibrium may lead to considerably higher NO_x concentrations than those in real systems.

4.2. Combustion in Air

Next computations were done for isobaric and adiabatic combustion of ammonia in air for various molar oxygen to ammonia ratios. Combustion in air is more probable to be performed in reality, as oxygen is expensive, and it might not be economically feasible to combust ammonia in pure oxygen. Fig. 4.4., 4.5., and 4.6. present cases analogical to Fig. 4.1, 4.2., 4.3., the differences between them are discussed below.

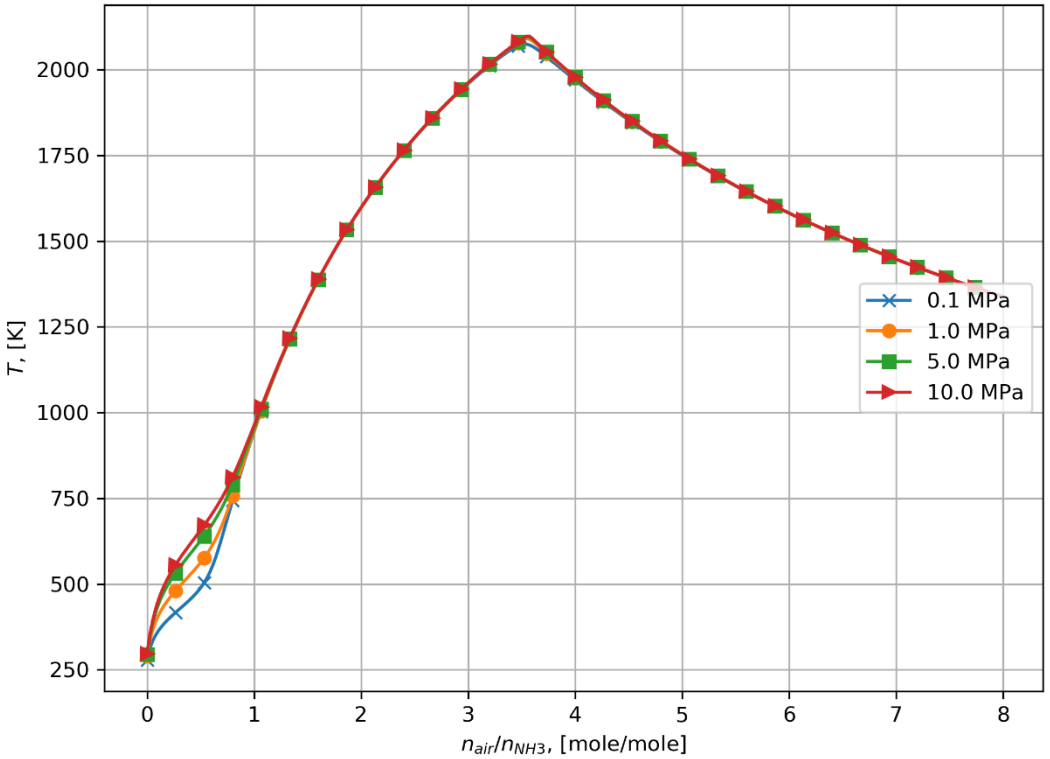

Fig. 4.4. Temperature profiles during ammonia combustion depending on the pressure, combustion in air

Temperature profile in case of combustion in air behaves similarly to the combustion in oxygen case. Temperatures obtained in combustion in air case are generally much lower (around 700 – 1000 K) and the differences between different pressures are not very noticeable. Lower temperatures are caused by the fact, that less oxygen is being provided and presence of oxygen is crucial for exothermic chemical reactions to occur. Those reactions are responsible for the heat release and rise in temperature. In each mole of air, there are only 0.21 moles of oxygen.

In Fig. 4.5. products of combustion in air are presented. What can be noticed is much higher amount of nitrogen released. Presence of nitrogen is a cause of NO_x creation, when it enters the reaction with oxygen. In case of combustion on oxygen, nitrogen comes only from ammonia, in case of combustion in air, additional 0.79 mole of nitrogen is provided per each mole of air. Molar fractions of hydrogen while combusting in air are generally much lower, around 30% less than in combustion in oxygen case, which is the cause of smaller temperatures. General behavior of species during combustion process is analogical to the combustion in oxygen.

In comparison with NO_x emissions presented in the Fig. 4.3., emissions of NO_x in Fig. 4.6. are lower. It could be expected, that since in second case, there is more nitrogen and thereby more NO_x could be formed. However, it needs to be noticed, that most of the NO_x created are created via thermal mechanisms, in presence of high temperatures. In case of combustion in air, temperatures are lower and thereby less NO_x are created as a result.

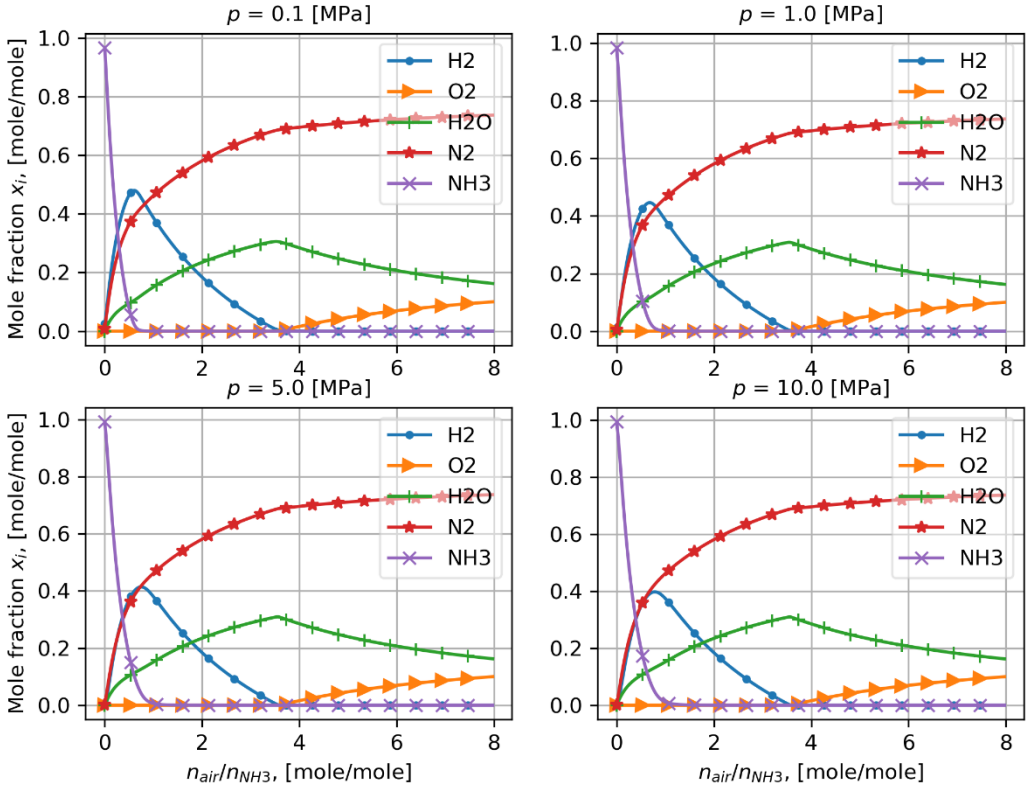

Fig. 4.5. Molar fractions of species during ammonia combustion in relation to pressure, combustion in air

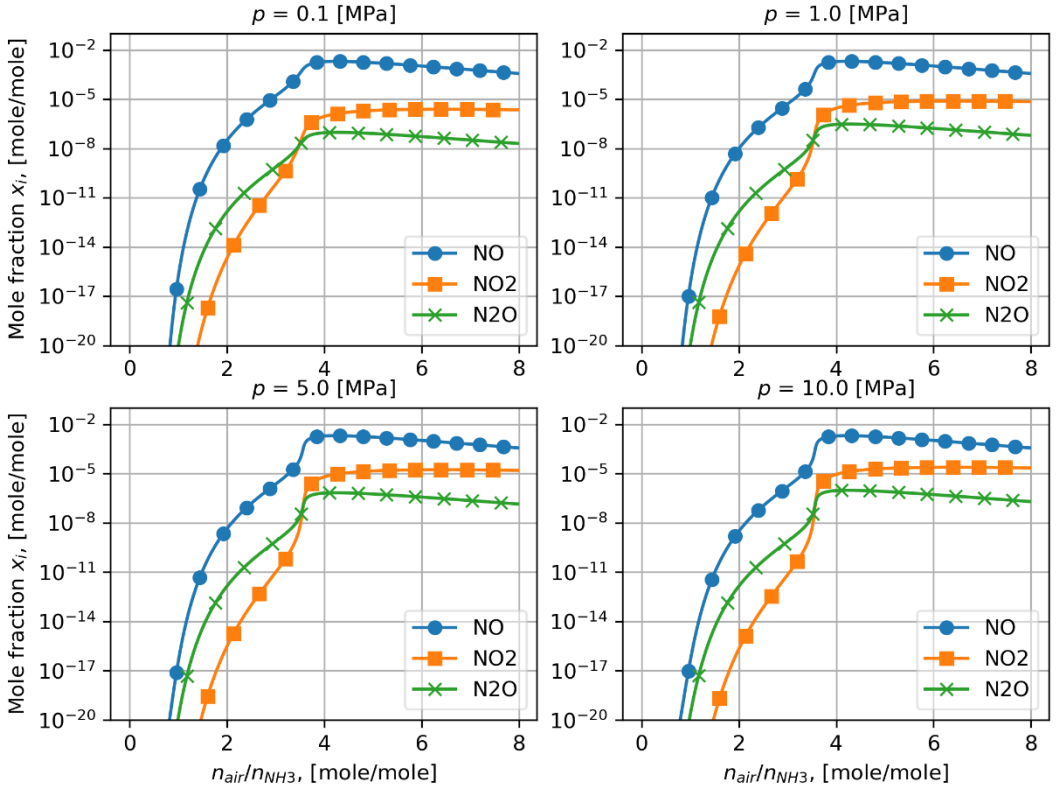

Fig. 4.6. NOx molar fractions in relation to pressure, combustion in air

5. Summary

Ammonia is more and more frequently considered as a future energy carrier. Its properties allow to handle and transport it in a more convenient way than hydrogen. Its main disadvantage is its high toxicity. It is believed that currently known combustion and power generation technologies can be used for ammonia utilization after minor modifications. The ammonia to power technologies will therefore contribute to decrease of carbon dioxide emissions, as its combustion does not produce any CO_2. The hydrogen from which it is produced should also be obtained from a carbon free source, like electrolysis or biomass gasification. The performed calculations allowed to predict the behavior of NH_3 at various oxidizer/fuel ratios and pressures with the assumption of equilibrium. As expected, the maximum temperatures were obtained for close to stoichiometric conditions and at the highest pressures. The predicted NO_x concentrations showed that the NO is the major pollutant formed and NO_2 concentration is 2-3 orders of magnitude smaller. Care should be however taken when interpreting the results due to the well-known over-prediction of NO_x concentrations when equilibrium is assumed. This research may contribute to developing ammonia combustion installations. It indicates on what aspects to focus while designing the combustion stand, and what is predicted outcome. It is shown that combustion in oxygen is not a proper method, and due to lower NO_x emissions, it is better to combust ammonia in air. The amount of obtained heat will be lower, but it will allow to avoid high costs of pure oxygen. A more detailed study, involving chemical kinetics, should be performed to analyze this behavior in more detail at the studied conditions. Ammonia is very versatile medium and there are many possible ways of its utilization. Further development and research are needed in this respect, to fully discover the advantages that can be obtained, and to bring the technology to a wider scale of use and proceed towards low-carbon economy.

References

[1] Posada JOG, Abdalla AH, Oseghale CI, Hall PJ. Multiple regression analysis in the development of NiFe cells as energy storage solutinos for intermittent power sources such as wind or solar. Int J Hydrogen Energy 2016;41:16330-7

[2] A.Valera-Medina, H Xiao, M. Owen-Jones, W.I.F David, P.J. Bowen, Ammonia for Power, Progress in Energy and Combustion Science 69 (2018) 63-102

[3] Kojima Y. A green ammonia economy. NH3-Association; 2013

[4] Xiao Ha, Howard MS, Valera-Medina A, Dooley S, Bowen P, Reduced Chemical Mechanisms for Ammonia/Methane CoFiring for Gas Turbine Applications, The 8th International Conference on Applied Energy – ICAE2016, Energy Procedia 105 (2017) 1483 – 1488

[5] Wang W., Herreros J.M., Tsolakis A., York, A.P.E., Ammonia as hydrogen carrier for transportation; investigation of the ammonia exhaust gas fuel reforming, International Journal of Hydrogen Energy, Vol. 38, Issue 23, 6 August 2013, Pages 9907-9917

[6] Health Protection Agency, (2007), Ammonia-General information, available at: http://tinyurl.com/p26qt66

[7] https://www.britannica.com/science/ammonia, (Accessed: 15/11/2019)

[8] Prof. Christian Egenhofer & Dr. Lorna Schrefler (Team Leaders), Vasileios Rizos, Federico Infelise, Dr. Giacomo Luchetta, Dr. Felice Simonelli, Wijnand Stoefs, Jacopo Timini, Lorenzo Colantoni, Final Report For A Study On Composition And Drivers Of Energy Prices And Costs In Energy Intensive Industries: The Case Of The Chemical Industry – Ammonia, Brussels, 13.01.2014

[9] H. Kobayashi, A. Hayakawa, K.D.K.A. Somarathne, E.C. Okafor, Science and technology of ammonia combustion, Proceedings of the Combustion Institute, 37, 2019, pp. 109–133, https://doi.org/10.1016/j.proci.2018.09.029

[10] https://pubchem.ncbi.nlm.nih.gov/compound/Ammonia#section=Boiling-Point, (Accessed: 15/11/2019)

[11] V. Pattabathula, J. Richardson, Introduction to Ammonia Production, CEP Magazine, An AIChE Publication, September 2016, pp. 69-75, www.aiche.org/cep

[12] https://en.wikipedia.org/wiki/Ammonia_production, (Accessed: 15/11/2019)

[13] https://nj.gov/health/eoh/rtkweb/documents/fs/0084.pdf, (Accessed: 15/11/2019)

CAES plant with above ground air vessel

Marek Utracki[1]

[1]*Affiliation: Institute of Thermal Technology, Silesian University of Technology, e-mail: marek.utracki@gmail.com:*

Abstract

One of problems with renewable energy sources is that some of them cannot guarantee continuous work or delivery of energy at given parameters. Example of such issue can be wind turbines. Those have priority in delivering electricity to the grid. It is hard to predict how long and how much electricity will be delivered to the grid from wind turbines, because wind is not steady. System DSR (Demand Side Response) is widely introduced in many countries as an insurance for stable work of electrical grid in peak hours. The operator of electrical grid is contracting companies for reducing their power consumption for certain amount of time. But those companies have to somehow maintain production and to do that they need electricity. One solution of accumulation of energy – besides pumped-hydro power pants – is Compressed Air Energy Storage (CAES). It allows to store energy in the form of compressed air. The air can be later released into turboexpander which connected to electric generator will produce electricity. Such installation can operate for few hours. Such system can deliver heat, cold and air at desired pressure. Depending which by-products are utilized the round-trip efficiency of such system changes. It ranges from 17% up to around 70% or even high for trigeneration.

Keywords: CAES, Mathematical modelling, Compressed Air Energy Storage, Trigeneration, Small scale system, Performance assessment

1. Introduction

One of the problems with renewable energy sources is that some of them cannot guarantee continuous work or delivery of energy at given parameters [9]. Example of such issue can be wind turbines. In Poland wind turbines have priority in delivery of electricity to electric grid. This regulation creates disturbances in work of conventional power plants. They have to decrease its load in order to create space for electricity from wind turbines. It is hard to accurately predict how long and how much electricity will be delivered to the grid from wind turbines, because wind is intermittent source of renewable energy.

System DSR (Demand Side Response) is widely introduced in many countries as an insurance for stable work of electrical grid in peak hours. The operator of electrical grid is contracting companies for reducing their power consumption for certain amount of time [10]. But those companies have to somehow maintain production and to do that they need electricity. The solution which is supposed to facilitate the integration of RES is energy storage.

One solution of accumulation of energy – besides pumped-hydro power pants – is Compressed Air Energy Storage (CAES). It allows to store energy in form of compressed air. The air can be later released into turboexpander which connected to electric generator will produce electricity. CAES system can be applied as regulator into electric grid [7] or as system which increases sustainability of work in facilities. Such installation can operate for few hours (discharge time for installation in McIntosh is set to around 26 hours) [5].

Such system can deliver heat, cold and air at desired pressure. Heat is extracted after each compression stage to increase efficiency of compression and reduce thermal strains inside vessel [8]. Air is then stored in natural caverns or above-ground vessel. After turboexpander cold is produced. It can be used for technological purposes or released into environment. Electricity is also produced during expansion.

This paper is a summary of the work on the mathematical model of the CAES system. This model simulates the charging and discharging of an air tank, as well as the production of electricity, heat and cool.

2. Aim of the project

Aim of the project is to design small scale CAES plant with above-ground vessel, investigate its performance as well as ways of integration with other systems. Depending on the needs the CAES can produce electricity, heat and cold. Maximum pressure of air in the tank is assumed to be 200 bar. Minimal pressure inside vessel is 10 bar. Vessel is charged to designed pressure and then air is discharged and expanded through turboexpander down to atmospheric pressure. Energy needed for compression and energy produced by turboexpander are calculated. Dynamic model will be programmed in Microsoft Excel.

3. Study of possibilities

This study of possibilities is mostly aimed at the CAES systems with above-ground vessels. Solution with above-ground vessel is location independent [2]. Higher pressure differences are possible which results in higher energy densities realizable [2]. But the investment costs and land consumption are high due to the size of the vessel [2]. Therefore, the critical issue of above ground air storage option is to make benefits of all products that can be potentially generated within the system. Creation of a relevant business model is typically based on the value stacking. In the case of distributed CAES system cogeneration or trigeneration solution is possible.

Applications are well presented by Briola [1]. “The CAES systems can be used in several different applications such as for space cooling by integration with a vapor compression cooling cycle, for the supercharge of diesel engine, for trigeneration, for storing of the mechanical energy produced by special devices (such as wind turbines) through direct connection with the compressor group, for power supply to isolated end-users by integration with diesel engine and in vehicle drivetrain. Moreover, Liquid Air Energy Storage and Underwater Compressed Air Energy Storage systems were proposed.”

Several configurations of CAES are possible. System A-CAES (Adiabatic-CAES) is a system in which no external energy is supplied while discharging. Configuration which utilizes some kind of external energy is Diabatic-CAES which is usually integrated witch Joule-Bryton cycle. Combination of those two above is also possible and is known as hybrid CAES [1].

3.1. Diabatic CAES

As for today there are only two existing CAES plants. One is in Huntorf, Germany and the second one in McIntosh, Alabama, USA. Both are based on Diabatic CAES solution. They have air storage in natural underground caverns. Compressor and gas turbine are on the same shaft and are coupled via gear box [3]. In Huntorf plant during discharging and expansion natural gas is used. Aforementioned plant has efficiency of about 42% without utilization of waste heat and about 55% with utilization [3].

3.2. Adiabatic CAES

Higher efficiency – up to 70% [5] – can be achieved while heat of compression is used for rising the temperature of air during expander operation. Such solution allows to rule out need of additional fuel combustion. Necessary technical solutions are currently developed independently in Germany and USA.

3.3. Air storage solutions

Aforementioned CAES plants are using natural salt caverns for air storage. There are also concepts for using drained gas caverns or porous sandstone layers [5]. Advantage of using salt caverns is that there are no losses in pressure during storage and no reaction between rocks and oxygen. Disadvantage of such solution is that those plants are location dependent, but on the other hand they consume only small part of land. The more mobile

solution is CAES with above-ground vessel. In such configuration land consumption is high due to size of vessel, but it can be built almost everywhere.

4. Methodology of calculation

Calculations are conducted for three main components which are shown in Fig 4.1:

a) Storage site which in this case is assumed to be a battery of vessels.
b) Charging cycle which consists of two compression stages (C_{LP},C_{HP}) with inter-cooler (HE_1) between them and post-cooler (HE_2) before storage vessel.
c) Discharging cycle which is turboexpander (T) coupled with electric generator (G).

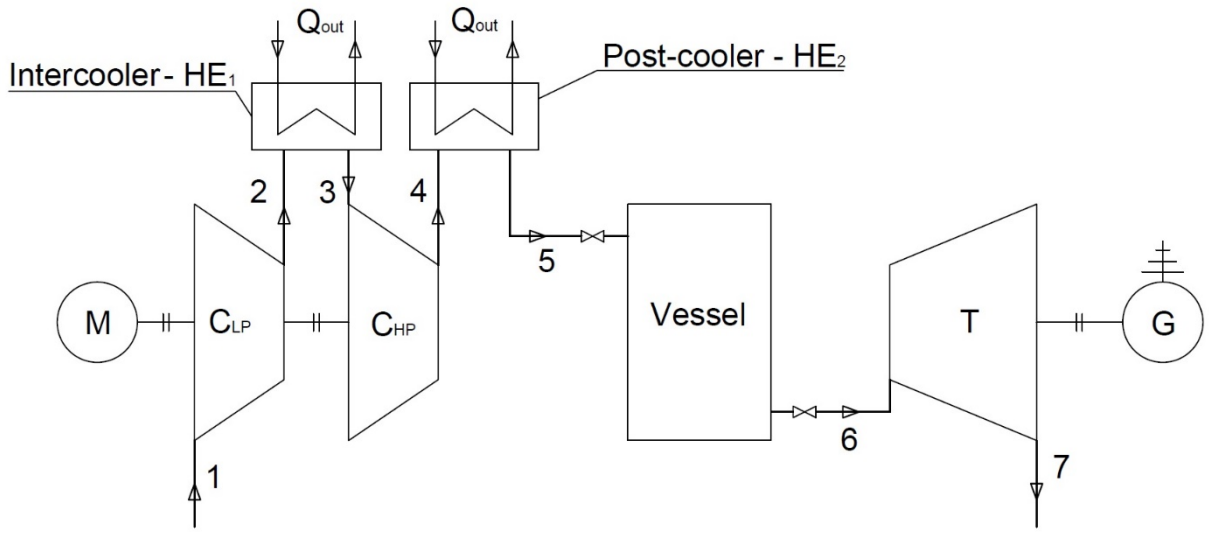

Fig. 4.1 – System scheme. C_{LP} – Low Pressure Compressor; C_{HP} – High Pressure Compressor; T – Turboexpander; M – motor, G - Electric Generator; HE – Heat Exchanger

Calculation step is assumed to be 15 minutes. Air is considered as ideal gas. Thermodynamic properties $\kappa(t_i), h(t_i)$ are evaluated using CoolProp 6.2.1 add in. It is assumed for whole cycle that there are no pressure losses. Heat losses through the walls are present only when air is in the vessel. Cycle is assumed to be operating for the first time, according to this knowledge author is aware of disturbances in workflow of system Pressure at the outlet of compressor is determined by pressure in vessel in given step. Mathematical models used for each component are described below. Model was programmed in Microsoft Excel.

4.1. Charging process

Charging model is dynamic model described by differential equations (1)(2). Solution of this system is numerical solution and is carried out step by step.

The calculations were based on mass (1), and energy (2) balances of the air vessel:

$$\frac{d\rho}{dt} = \frac{\dot{m}_{in}}{V} \tag{1}$$

$$\frac{dU}{dt} = \dot{m}_{in} h_{in} - \dot{Q}_l \tag{2}$$

where:
ρ - density,

t - time,
$\dot{m}_{in}$- input air mass flow,
V - cavern volume,
U - internal energy,
h_{in}-input air specific enthalpy,
$\dot{Q}_l$ - heat losses.
Differential equations of (1) and (2) are described below in (5)

Efficiency of compression η_{iCj} of *j*-th stage is assumed to be 85% for speeding up and simplification of the process of calculation.

$$\eta_{iCj} = \frac{h_{out,s} - h_{in}}{h_{out} - h_{in}} \tag{3}$$

Variables related to the *j-th* stage of compression and time (t_i), are defined as follows:

a) Mechanical power at the time step $N_{Cj}(t_i)$ of *j-th* stage of compression is calculated as follows:

$$N_{Cj}(t_i) = \dot{m}_{a,in}(t_i)[h_{Cj,out}(t_i) - h_{Cj,in}(t_i)] \tag{3}$$

b) Mass of air $m(t_i)$ inside vessel is evaluated as differential equation from (1):

$$m(t_i) = m(t_{i-1}) + \dot{m}_{a,in}(t_i - t_{i-1}) \tag{5}$$

c) Pressure at the outlet of compressor P_4 is determined by vessel and is calculated using equation (6):

$$P_v = P_4 = \frac{R\, T_v(t_i)}{V\, m(t_i)} \tag{6}$$

d) Value of temperature at the outlet of *j-th* compression stage is calculated as follows:

$$T_{2s,Cj}(t_i) = T_1 \frac{p_{Cj,out}(t_i)}{p_{Cj,in}(t_i)}^{\frac{\kappa(t_i)-1}{\kappa}} \tag{7}$$

$$T_{2,Cj}(t_i) = T_1 + \frac{T_{2s,Cj}(t_i)}{\eta_C} \tag{8}$$

e) Mass flow rate of air $\dot{m}_{a,in}$ for each step is calculated from ratio of real mass flow rate and nominal mass flow rate:

$$\dot{m}_{a,in} = \frac{y(t_i)}{y_N} \tag{9}$$

Dimensionless values of mass flow rate for compressor were taken from EBSILON software. Air is compressed from ambient conditions which in this case are:

Table 4.1 Ambient conditions

Parameter	Value	Unit
P_{amb}	101325	Pa
T_{amb}	293,15	K

For simplification it is assumed that the air is dry.

Specific points from dimensionless compressor chart (Fig. 4.2) were read manually and if necessary approximated based on following equation (10) for straight line. Such approximation is possible because lines between points can be regarded as straight lines:

$$\frac{y_s - y_1}{x_s - x_1} = \frac{y_2 - y_1}{x_2 - x_1} \tag{10}$$

Where subscript *s* indicates coordinate of point to be found, but one of values x_s or y_s must be already known.

CMV line on compressor chart indicates maximum available point of work for each flap position. Line was created by division of each flap line into ten parts where beginning is indicated as 0 and the end as 1. Point 0,9 on each flap position is the point where switching to next flap position must be done. This division was made manually by the author.

Energy balance in the intercooler and post-cooler (*j-th* heat exchanger) is described with equation (11). Intercooler cools down the air to temperature of 40°C

$$\left[\dot{m}_a(t_i)[h_{HE,in}(t_i) - h_{HE,out}(t_i)]\right] - \left[\dot{m}_w(t_i)[h_{HE,out,w}(t_i) - h_{HE,in,w}(t_i)]\right] = 0 \tag{11}$$

Where mass of water flowing through heat exchanger is calculated as follows:

$$\dot{m}_w(t_i) = \frac{\dot{m}_a(t_i)[h_{HE,in}(t_i) - h_{HE,out}(t_i)]}{c_w\, \Delta T_{w,out-in}} \tag{12}$$

Where $c_w = 4.19 \frac{kJ}{kgK}$ is specific heat of water.

Internal energy inside vessel is integrated in each step included mass of air flowing into the vessel and the heat losses. 13)

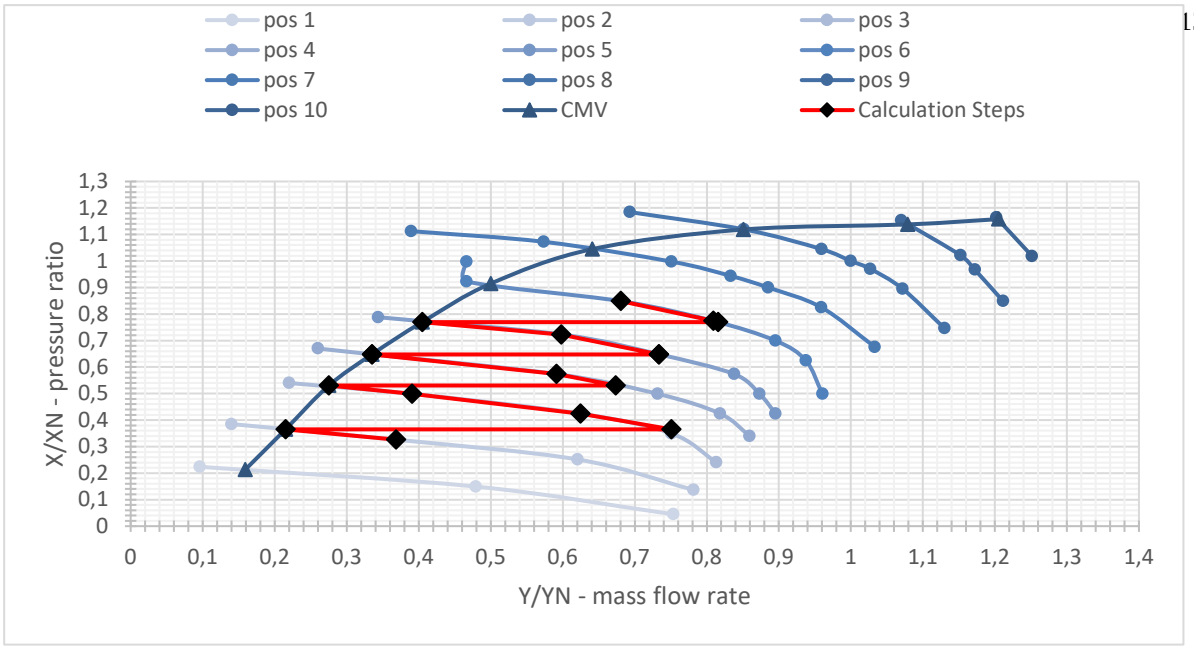

Fig 4.2 Dimensionless compressor map with CMV line indicating maximum possible operation points for each flap position. Red line indicates how author moved on this map and which points were choose for calculation.

Where heat losses Q_{out} are assumed as heat exchange between air and walls of the vessel only via convection and are calculated as follows:

$$Q_{out}(t_i) = kA_v[T_v(t_i) - T_{amb}] \tag{14}$$

Temperature inside vessel is calculated using Excel's "What if" tool. Knowing enthalpy inside vessel and mass of air in given time step, it is possible to calculate specific internal energy u. Specific internal energy is calculated second time for P_v and T_v using CoolProp. Having those values, specific internal energy from CoolProp is set to the value from the first u by changing temperature T_v value. The same algorithm is applied while discharging.

4.2. Air storage process

Evaluation of storing process is made simultaneously with charging or discharging. Conditions inside vessel determine work of compressor train and turboexpander. Moreover, in this paper discharging is assumed to be conducted immediately after charging to maximum pressure.

4.3. Discharging process

Discharging process is also described by differential mass (1) and energy (2) equations. Discharging model is calculated numerically step by step.

Emptying process is described by following energy balance and is written based on equation (2):

$$U_a(t_i) = U_a(t_{i-1}) - H_{a,v}(t_i)[t_i - t_{i-1}] - Q_{out}(t_{i-1})[t_i - t_{i-1}] \tag{15}$$

Mass of air inside vessel is evaluated using equation (16):

$$m(t_i) = m(t_{i-1}) - \dot{m}_{a,in}(t_i - t_{i-1}) \tag{16}$$

Designed value of mass flow rate for turboexpander was taken from AtlasCopco catalogue of turboexpanders [14] and was equal 100000 $\frac{m_n^3}{h}$. After recalculation for conditions inside vessel and kilograms it gives value of $\dot{m}_{a,out,D} = 39.791\frac{kg}{s}$. From this value will be calculated actual mass flow rate through turboexpander.

Mechanical power produced on turboexpander in time (t_i) can be evaluated with equation (17):

Since pressure inside vessel, temperature of air in vessel and pressure at the output of turboexpander are known

$$N_{Ti} = \dot{m}_{a,out}(t_i)[h_{Tj,in}(t_i) - h_{Tj,out}(t_i)] \tag{17}$$

the mass flow rate of air flowing into turboexpander must be determined. In order to do that Stodola's Ellipse Law is applied [11]

$$P_{T,in}(t_i)\sqrt{1 - \phi_{in}^2(t_i)Y(t_i)} \tag{18}$$

Where:

$$\phi_{in}(t_i) = \frac{\dot{m}_{a,out}(t_i)\sqrt{T}(t_i)}{P_{T,in}(t_i)} \tag{19}$$

$$Y(t_i) = \frac{{P_{T,in,D}}^2(t_i) - {P_{T,out,D}}^2}{{P_{T,in,D}}^2(t_i)\,{\phi_{in,D}}^2(t_i)} \tag{20}$$

By algebraic rearrangement equation for mass flow rate through turboexpander was obtained:

$$\dot{m}_{a,out}(t_i) = \frac{P_{T,in}(t_i)\sqrt{\frac{-\left[\frac{P_{T,out}}{P_{T,in}(t_i)}\right]^2 - 1}{Y(t_i)}}}{\sqrt{T}(t_i)} \tag{21}$$

where T – is the temperature of air flowing into turboexpander expressed in Rankine

Variables related to the turboexpander operation in time $(t_i)$are defined as follows:

a) Pressure at the inlet to turboexpander $P_{T,in}$ is determined by vessel and is calculated in similar way as equation (6) using appropriate values.
b) Mass flow rate $\dot{m}_{a,in}(t_i)$ is calculated using Ellipse Law (19) (20) (21).
c) Temperature after turboexpander is calculated using equation (7)(8).
d) Efficiency of turboexpander is read from characteristic Fig 3.2 dimensionless compressor map with CMV line indicating maximum possible operation points or each flap position. Line marked with diamonds indicates how author moves on this map and which points were chosen for calculation.

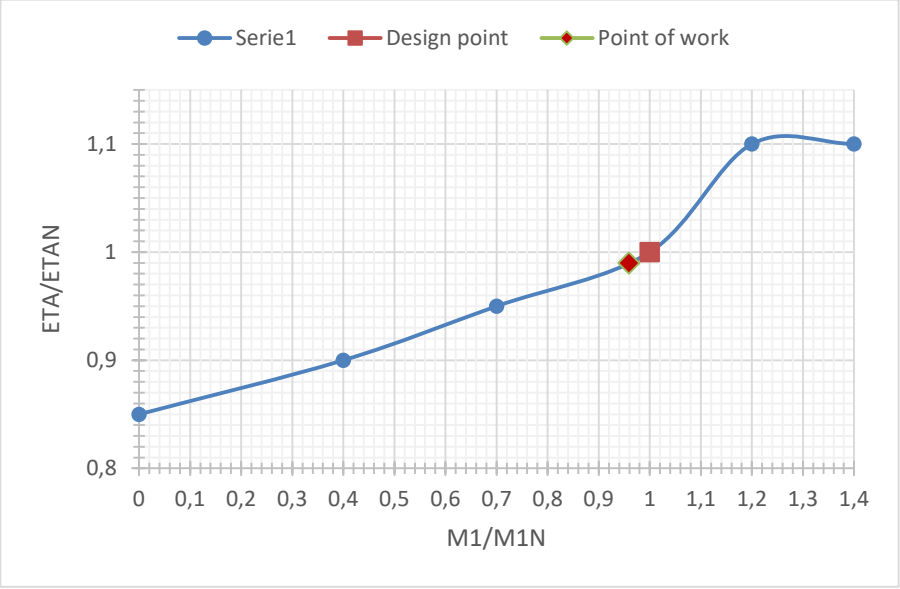

Fig 4.3 Dimensionless Turboexpander Performance Map from EBSILON software. Design point and point of actual work are shown.

5. Results

5.1. Energy balance of one cycle

The components of energy balance are listed below. Fig 5.1 shows how those components relate to CAES plant.

a) Energy of inflowing air, calculated using following equation :

$$E_{a,in} = \int_{t_1}^{t_2} \dot{m}_{a,in}(t) h_{a,in}\, dt \tag{17}$$

In this paper specific enthalpy of inflowing air is always the same since the ambient conditions remains unchanged through the whole process of calculation.

b) Electric energy needed for compression:

$$E_{el,Cj} = \int_{t_1}^{t_2} \dot{m}_{a,in}(t)\Delta h_{a,out-in}\, dt \tag{18}$$

Electric energy required to drive the compressor will be calculated twice since there are two stages of compression in the system.

c) Cold obtained at the outlet of turboexpander:

$$E_{cold,T} = \int_{t_1}^{t_2} \dot{m}_{a,in}(t)\Delta h_{a,in-out}\, dt \tag{19}$$

d) Heat removed in heat exchangers

$$E_{HE,j} = \int_{t_1}^{t_2} \dot{m}_{a,in}(t)\Delta h_{HE,in-out}\, dt \tag{20}$$

Heat exchangers will be also calculated twice since there are two of them in system.

e) Heat losses during charging and discharging :

$$E_{v,l} = \int_{t_1}^{t_2} Q_l(t)\, dt \tag{21}$$

f) Internal energy of turboexpander

$$E_{Ti} = \int_{t_1}^{t_2} \dot{m}_{a,in}(t)\Delta h_{a,in-out}\, dt\, \eta_{Ti} \tag{22}$$

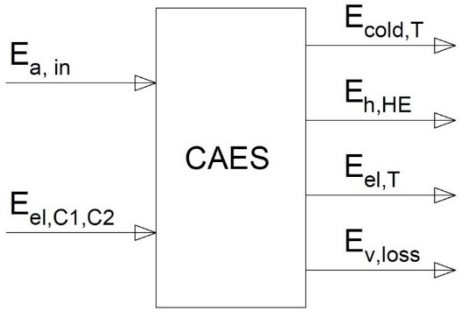

Fig 5.1 Energy Balance components

Results from calculation of energy balance for one cycle are shown in Table 5.4.

Table 5.4 Results of Energy balance for one cycle

Parameter	Vaule	Unit	Reference
Energy entering Control Volume			
$E_{a,in}$	11790565.817	kJ	(17)
$E_{el,C1}$	4611643.966	kJ	(18)
$E_{el,C2}$	4964484.947	kJ	(18)
$\sum E_{in}$	21366694.730	kJ	–
Leaving Control Volume			
$E_{cold,T}$	4022295.299	kJ	(19)

$E_{HE,1}$	6801706.240	kJ	(20)
$E_{HE,2}$	44390.991	kJ	(20)
$E_{v,l,charg}$	1991802.619	kJ	(21)
$E_{v,l,discharg}$	-20604.469	kJ	(21)
$E_{i,T}$	3395588,172	kJ	(22)
$\sum E_{out}$	16235178.852	kJ	–
$\sum E_{in} - \sum E_{out}$	5131515.878	kJ	–

From the results it can be seen that the difference in energy that needs to be put into the cycle and energy gained from the cycle as heat, cold and energy on turbine is around 5 GJ.

5.2. Behavior of temperature and pressure inside the vessel

Since the plant is assumed to be new build the vessel is being charged for the first time. Due to this knowledge the shape of temperature line and pressure line from Fig 5.2 can be explained. The vessel is trying to achieve energy balance with surrounding but is still charged which results in “sinusoidal” shape of abovementioned lines. The other cause for that maybe mass flow rate – which is showed in Fig 5.3 – at which air was compressed into the vessel.

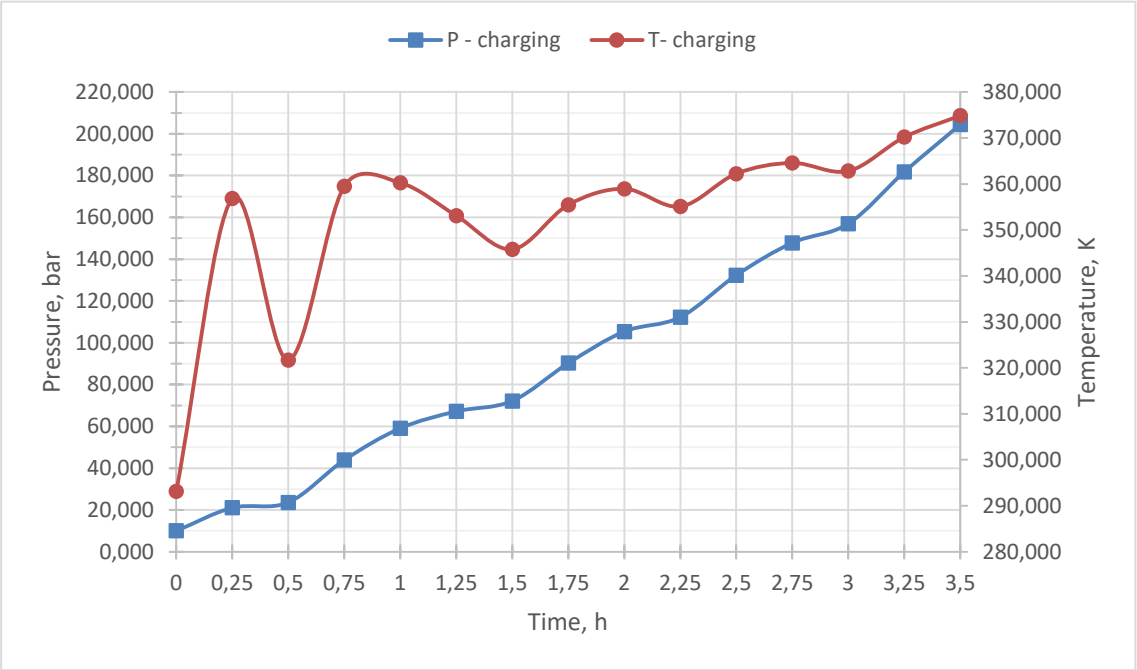

Fig 5.2 Temperature and Pressure inside vessel during charging process

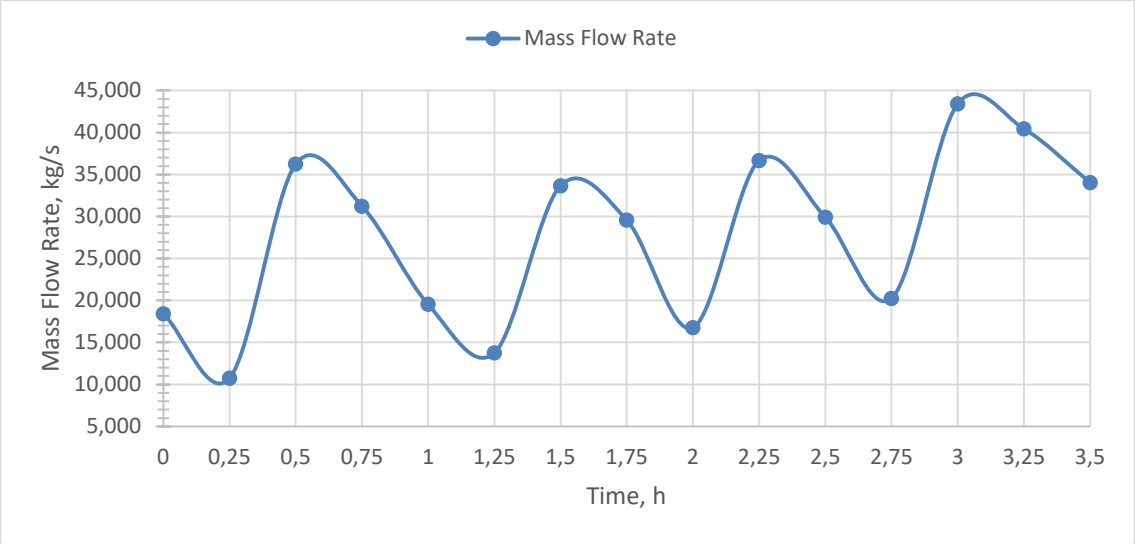

Fig 5.3 Mass Flow Rate of air in compressor train

The sinusoidal shape of mass flow rate through compressor is a result of changing flap positions to maintain required level of compression. The work points are shown in Fig 4.2 indicated by the red line.

As seen in the next Fig 5.4 the discharging process is conducted smoothly. This is due to constant mass flow rate through the turboexpander.

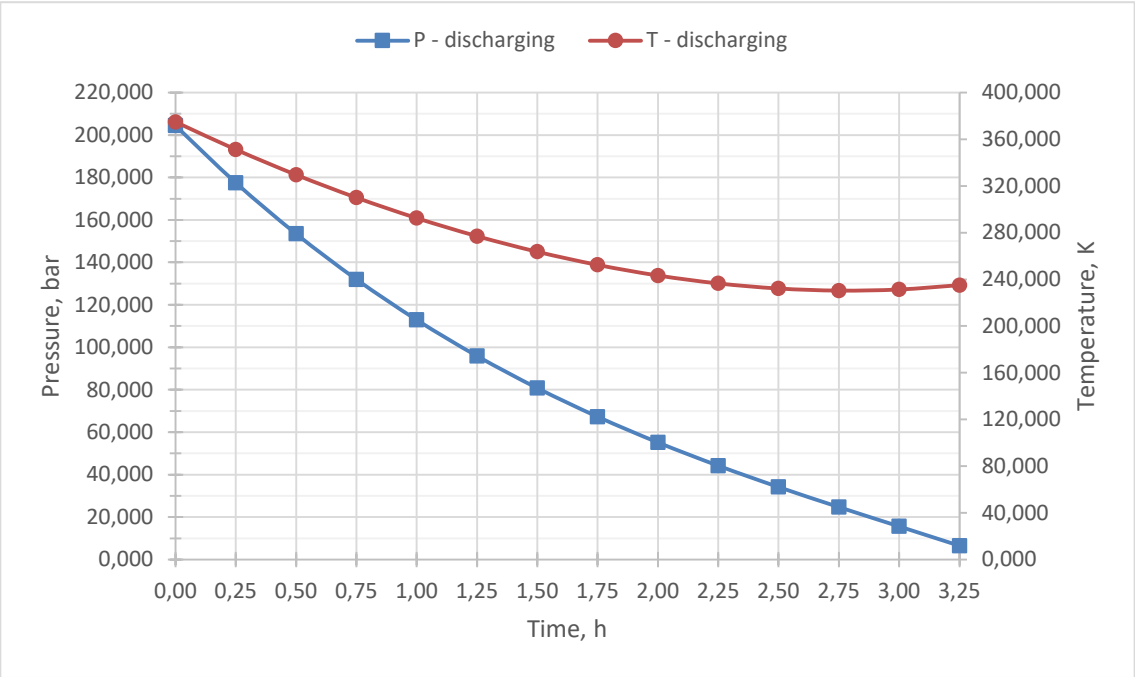

Fig 5.4 Discharging process. Pressure and Temperature inside vessel are shown

5.3. Results from whole period of work

Designed CAES plant is capable to charge fully in 3.5 hour. Discharge time is equal 3 hours and 15 minutes. The time strongly depends on size of vessel and performance of compressor and turboexpander. The most important results are shown in Table 5.5 and values are given in GJ for legibility.

Table 5.5 Results from whole operation

Parameter	Vaule	Unit
$\int_{t_1}^{t_2} N_{el,C}\, dt$	3180.147	GJ
$\int_{t_1}^{t_2} Q_{out,HE}\, dt$	1429.947	GJ
$\int_{t_1}^{t_2} Q_{cold,T}\, dt$	664.868	GJ
$\int_{t_1}^{t_2} N_{Ti}\, dt$	561.276	GJ

5.4. Efficiency of CAES plant

Efficiency of abovementioned plant can be calculated in four ways. First, simple efficiency η_P , which shows

$$\eta_P = \frac{\int_{t_1}^{t_2} N_{Ti}\, dt}{\int_{t_1}^{t_2} N_{el,C}\, dt} \tag{23}$$

ratio of power generated on turbine to the power that is necessary to drive the compressor train.

$$\eta_h = \frac{\int_{t_1}^{t_2} N_{Ti}\, dt + \int_{t_1}^{t_2} Q_{out,HE}\, dt}{\int_{t_1}^{t_2} N_{el,C}\, dt} \tag{24}$$

Since the heat from compression is removed, it can be utilized and the second efficiency η_h is obtained.

Utilizing cold along with electricity we obtain the third efficiency η_{cold}.

$$\eta_{cold} = \frac{\int_{t_1}^{t_2} N_{Ti}\, dt + \int_{t_1}^{t_2} Q_{cold,T}\, dt}{\int_{t_1}^{t_2} N_{el,C}\, dt} \tag{25}$$

When all three useful energies are utilized we obtain trigeneration η_{tri}.

$$\eta_{tri} = \frac{\int_{t_1}^{t_2} N_{Ti}\, dt + \int_{t_1}^{t_2} Q_{out,HE}\, dt + \int_{t_1}^{t_2} Q_{cold,T}\, dt}{\int_{t_1}^{t_2} N_{el,C}\, dt} \tag{26}$$

Table 5.6 Efficiencies of CAES plant

Parameter	Vaule	Unit	Reference
η_P	17.65	%	(23)
η_h	62.61	%	(24)
η_{cold}	38.56	%	(25)
η_{tri}	83.52	%	(26)

6. Conclusions

There are multiple ways to integrate CAES with other systems. It can deliver pressurized air at demanded level and in demanded amount. Use of more than one expansion stages and throttling valves gives opportunity to satisfy wide range of pressures. Amount and time of delivery of pressure, electricity or/and cold depends at most on size of vessel and mass flow rate through turboexpander.

In abovementioned cycle is no heating of air before turboexpander which gives very low temperatures at the exit of turboexpander. The average temperature at the outlet is the -151.25°C. This gives excellent opportunities of integration with cooling systems or use of the cold for technical purposes.

Heat from compression can be stored and then used for heating up the air before turboexpander if the cold is not needed - for example if air is used for technological purposes such as for tools which are driven by compressed air. Heat from compression -as well as cold from expansion - can be used for district heating or cooling. However, there is an issue with transportation of such medium due to probable heat losses during transport. Another way of utilizing waste heat are Thermal Energy Storages [11][13]

Electricity is used in motor to drive the compressor train. When CAES is integrated with wind turbines it gives opportunity of stable frequency and amount of delivered electricity.

References

[1] Briola S., Di Marco P., A novel mathematical model for the performance assessment of diabatic compressed air energy storage systems including the turbomachinery characteristic curves, Applied Energy, Elsevier, Volume 176, Pages 758 – 772, 2016

[2] Budt M., Wolf D., A review on compressed air energy storage: Basic principles, past milestones and recent developments, Applied Energy, Elsevier, Volume 170, Pages 250-268, 2016

[3] Compressed Air Energy Storage (CAES), [Online, 07.01.2019], Available in internet: http://energystorage.org/compressed-air-energy-storage-caes

[4] Cooke D., Modeling of off-design Multistage turbine pressures by Stodola's Ellipse, [Online, 08.01.2019], Available in internet: http://famos.scientech.us/Papers/1983/ 1983section11.pdf

[5] Dzierżanowski Ł., Elektrownie CAES, Energia Elektryczna, nr 2-3, 2011

[6] Li Y., Wang X., A trigeneration system based on compressed air and thermal energy storage, Applied Energy, Elsevier, Volume 99, Pages 316-323, 2012

[7] Lund H., Salgi G., The role of compressed air energy storage (CAES) in future sustainable energy systems, Energy Conversion and Management, Elsevier, Volume 50, Issue 5, Pages 1172-1179, 2009

[8] Luo X., Wang J., Overview Of Current Development On Compressed Air Energy Storage, Energy Procedia, Elsevier, Volume 62, Pages 603-611, 2014

[9] Owusu P. A., Asumadu-Sarkodie S., A review of renewable energy sources, sustainability issues and climate change mitigation, Cogent Engineering, Volume 3, Page 4, 2016

[10] Polska Agencja Prasowa, PSE: Udane letnie testy DSR, czyli redukcji zużycia energii na żądanie,[Online, 06.01.2019], Available in internet: http://biznesalert.pl/pse-testy-dsr/

[11] Prim E., Thermal energy storage (TES) using phase change materials (PCM) for cold applications, [Online, 09.01.2019], Available in internet: https://www.tdx.cat/bitstream /handle/10803/110542/Teop1de1.pdf?sequence=6&isAllowed=y

[12] Saadat M., Farzad A., Modeling and control of an open accumulator Compressed Air Energy Storage (CAES) system for wind turbines, Applied Energy, Elsevier, 2014

[13] Tola V., Meloni V., Performance assessment of Adiabatic Compressed Air Energy Storage (ACAES) power plants integrated with packed-bed thermocline storage systems, Energy Conversion and Management, Elsevier, Volume 151, Pages 343-356, 2017

[14] Turboexpander Brochure, AtlasCopco, 2017

Perovskite in solar cells application

Agata Horwacik[1]

[1]*Faculty of Energy and Environmental Engineering, Silesian University of Technology, e-mail: agata.horwacik@gmail.com*

Abstract

Recently the new technology has been developed namely the perovskite solar cells. It is considered as innovative substitute for the conventional silicone solar cells. Perovskite technology shows satisfactory results reaching the values of currently used solar cells. The material shows features such as high elasticity and low manufacturing cost which can be a revolution for the photovoltaic market. The concept is still being developed and upgraded as it requires many improvements before it meets the requirements to be fully released to the market and commercialized. The main issues which perovskite solar cells face is their instability and the presence of lead amounts in their structure. However, perovskite have already found use in many applications and show great potential to be applied in various branches.

Keywords: perovskite, solar cells, perovskite-based solar cells, photovoltaics

1. Introduction

Plans of energy transition in Poland take into account rising shares of renewable energy to 27% by 2030 [1]. So far data from 2018 shows that Poland hardly reached 12% [2]. Therefore, it is clear that the challenge is big. One way of achieving that goal is by introducing solutions for solar energy conversion into useful energy, as this technology is gaining more potential every year. Solar energy has the highest potential among available renewable energy sources. It can be transformed into electricity with the use of photovoltaic solar cells. The weather conditions in Poland are not the most favorable, however it is enough to develop this area and increase shares of renewables in total energy production. This aim could be achieved by introducing innovative solutions into the energy production not only in Poland, but all over the world to meet the requirements. In Poland the annual solar radiation on the horizontal plane takes values between 950 - 1250 kWh / m^2 while the average insolation is 1600 hours per year [3]. By now the efficiency of standard silicon-based photovoltaic panels is about 17% and keeps improving [4].

Recently perovskite solar cell technology is getting more and more attractive. The potential of photovoltaics in general is very promising and still being developed showing better results each year. The use of perovskite in power generation is another breakthrough that could bring the solar technology of energy production to the next level. Over last ten years the efficiency of perovskite solar cell reached almost 22,7% in 2018 , while in 2009 it was on the level of only 3% making it the fastest improving solar technology in history [5]. Right now the research shows efficiencies reaching even up to 25% [6], and theoretical efficiency of 30% according to Clean Energy Institute in Washington [7].

Generally, perovskite is naturally occurring mineral forming a crystal lattice or most commonly a hybrid of organic-inorganic lead or tin halide-based material. The mineral was first discovered in Ural Mountains in 1839. perovskites material is a class of semiconductors which can be processed on many ways, where one of them enabled patenting first perovskite solar cell in 2009. The pioneering device however would only work for couple of minutes as the electrolyte dissolved the perovskite structure almost instantly. Perovskite solar cells have become highly efficient in a very short time, which is a huge success of research and development, however a number of challenges still remain before they can become a competitive commercial technology. Although still imperfect the perovskite solar cells can revolutionize the market and solar technology in the future allowing to meet the energy transition requirements and goals towards clean, carbon-neutral environment.

2. What is a perovskite?

Perovskite solar cells is a type of thin-film cell made with the use of perovskite material as a semiconductor layer absorbing the light. The construction is very similar to the conventional silicon-based solar cells. However, the perovskite solar cells show extraordinary features thanks to the great capabilities of perovskite. A perovskite solar cells are considered a great alternative for most popular on the market silicone solar cells as they show great absorption features, relatively high-power conversion efficiency (PCE) and those are relatively cheap in manufacturing. Moreover, the material enables producing very thin cells that can be used for many applications, for example in the construction sector for covering, not only the rooftops, but also whole building walls.

Perovskites show a unique crystallographic structure that contributes to high performance and effective photons conversion. Perovskite material has the same crystal structure as calcium titanium oxide. The term perovskite generally states for the mineral $CaTiO_3$, but is used interchangeably for any structure that has the same generic form and the structure as the perovskite mineral. In general, perovskites have chemical formula ABX_3 , where A and B state for cation, where A comprises organic compounds and B states for elements such like lead (Pb) or tin (Sn). X anion bonds to both A and B, and states for halide ions like I, Br, and Cl. The perovskite crystallographic arrangement is as demonstrated below in [Fig. 2.1.].

The ideal perovskite structure designated by general formula ABX_3 contains a metal cation B surrounded by six anions X in such a way that they form a regular octahedron. A is a metal cation located between successive octahedrons and balancing the network charge. The structure can be arranged on multiple ways. One of the simplest representations of perovskite lattice structure is positively charged cation B in the center of the structure. The external corners are occupied by as well positively charged cations A and the faces of the cube occupied by negatively charged anion X visibly smaller than the cations A and B.

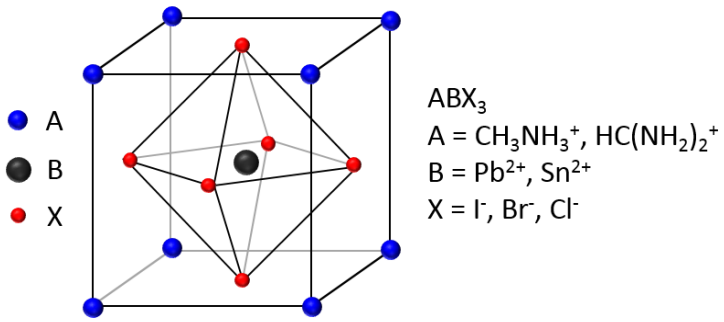

Fig. 2.1. Perovskite crystal structure, source: [11]

The elements that create a perovskite structure can be combined on many different ways. The selection and combination of material is crucial in determination of physical and chemical properties of the perovskite like bandgap, the lengths of spectrum absorbed, diffusion lengths etc [8]. It may influence e.g the bandgap which for perovskites usually is in the range of 1.55eV corresponding to an absorption of wavelenghts of about 800 nm for $MAPbI_3$ to bandgap of around. 2.3 eV in case of $MAPbBr_3$ which therefore has higher voltage potential [9].

Most of efficient perovskites is based on metal halides from Group IV like previously mentioned lead or tin. In case of metal halide perovskites the most popular and often encountered are caesium lead halide ($CsPbX_3$) and methylammonium lead halide ($CH_3NH_3PbX_3$). This type of lead-based perovskie solar cells are particularly effective due to their features such as strong light absorption, long charge-carrier diffusion lengths, a tunable band gap and the ease of manufacturing. Moreover, the material has a high defect tolerance and can be processed at low temperatures [10].

3. Perovskite solar cell principle of operation

The perovskite solar cells operation is based on the same principle as in case of traditional solar panels, namely they consist of a semiconductor that absorbs solar energy and initiates the flow of electrons. Negatively charged electrons surrounding the atoms in the crystal lattice absorb the photons that have energy beyond the band gap.

Then those are prompted to the conductive electronic states in crystal known as the conduction band. In turn the conductive pass of the charge causes a hole is left behind in the lower energy states of the crystal known as the valence band. Then the positive and negative charges are collected in the opposite electron nodes known as anode and cathode. The excited electrons are captured then by wiring and converted into usable electricity.

The typical perovskite solar cell is composed of 5 functional layers including respectively glass cover, anode in form of transparent conducting film, n-type compact layer, perovskite absorber, p-type hole transport material layer and cathode [15] . More specifically the perovskite solar cells are composed of layers such as in standard solar cells. As shown in [Fig. 3.1.], the basic construction of PCS consists of a layer of glass, Fluorine-doped Tin Oxide (FTO). FTO is a media for the electron's transportation on top of which a metal such as TiO_3 is placed which combined with FTO creates an anode in the perovskite solar cell. On top of that the perovskite material which is a semiconductor absorbing the light is being deposited to generate electrons and holes. As well known, the perovskite absorber can generate the charges by directly absorbing the insight light. Next the layer of spiro-OMeTAD is placed on the perovskite layer which enables the holes transportation and finally the gold wires which both makes the cathode in the solar cell. The perovskite layer absorbs light and creates electrons in the conduction band and holes in the valence band. On one side TiO_3 selectively transfers electrons from perovskite to the FTO anode, and on the other side spiro-OMeTAD selectively transfers holes through the carbon particles to the FTO cathode. Once the electrons are placed on the anode and holes are transported to the cathode the external load can be connected. The electrons themselves are free to travel through the circuit executing work, then the electrons return refilling the holes and that completes the circuit.

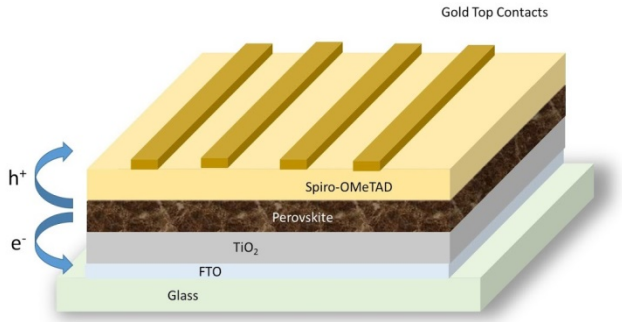

Fig. 3.1. Perovskite solar cell structure source: [7]

The wavelengths of visible light are in the range of 400 and 700 nm, where those lengths correspond to the bandwidth wavelength absorbed by silicon solar cells. In this case any radiation with a longer wavelength lacks the energy to produce electricity [16]. At the same time the optical absorption spectrum of the solar cells made from perovskite material can covered up to 800 nm [17]. Hence strong absorption of visible light is considered as the main strength of the perovskite material in the solar cell.

4. Perovskite promising potential

One of the biggest perovskite solar cells success is the rapid technology development. The concept improved a lot since the release of first perovskite solar cell and quickly achieved results close to ones shown by standard silicone or galium-based solar cells. The efficiency of perovskite cells is impressive for such a fresh concept and relatively low time of research; therefore, the idea seems to be very promising at this stage. Research shows that in the close future the results of perovskite-based cells might exceed the conventional solar technology.

Another great advantage of perovskite solar cell is that they are based on a material that can be produced in a laboratory environment which significantly decreases costs comparing to the silicon-based panels where the silicon is first extracted and has to be undergone processing before being applied. Moreover, the perovskite can be obtained thought process called "solution-processing" which is based on the same principle as printing

newspapers [13]. Thus, it can be seen that the process of perovskite solar cell production is much simpler and not only cheaper but also less time-consuming.

What is more, perovskite solar cells have unique features and properties that make them an attractive material used for the solar cells production. The solar cells made of perovskite, however very thin still maintain the reliable efficiency, thus the cost of material is highly reduced and the cells can be incorporated to any surface, those less demanding but also more challenging as a building facades or small electronic devices. Also due to their properties the material and overall cell mass is significantly reduced which additionally lowers constructional stresses and allows for wider range of applications.

From the point of view of energy production, the perovskites also show range of useful features such as great conductivity, magnetoresistance and ferroelectricity [14]. Perovskites can be also combined on many different ways of compounds resulting in various desired properties. Therefore, the technique of perovskite manufacturing makes them adjustable to the required conditions of operation and environment. All of above allows researches for optimization and selective design of the perovskite solar cells.

In addition, the advantage of perovskites is their very high absorption coefficient, even exceeding the absorption of gallium arsenide or silicon solar cells [19]. This allows manufacturing of extremely thin cells with a thickness of only a few hundred nanometers. Reduced thickness corresponds to significantly smaller distances charges generated in the cell need to cover which minimizes losses.

The possibility of choosing the composition of the perovskite from a wide range of organic and inorganic materials allows obtaining varied properties. An example is the modulation of the wavelength of absorbed light, which allows for the production of solar cells of various colors. Therefore the perovskite solar cells might be additionally considered not only as a device generating electricity, but also a decorative elements, e.g. in photovoltaics integrated with the building [19].

Application of the organic component in the perovskite structure allows the production of flexible thin-film cells, which significantly expands the range of possible applications. For comparison the silicon-based solar cells are very brittle and fragile therefore those require application of thick safety glass covers. Additionally, by adjusting the thickness of the active material in the perovskite cell, it is possible to produce modules with different levels of transparency.

Last but not least, the perovskite technique can be used for the production of tandem-type solar cells. More specifically the perovskite come together with silicon-based solar cells combining great properties of both types. This concept allows the cost reduction and boosting the cell efficiency as with the use of one cell [13].

5. Perovskites' limitations

One of the biggest problems of perovskite that limits its mass production is their long-term instability. The lack of stability in case of perovskite solar cells is often caused due to such factors as water, light or oxygen. More specifically the PCS still hard it finds to overcome the high temperatures and moisture degradation due to the material properties. The perovskite material undergoes decomposition in the humid ambience due to the hydrolysis of the compounds. The further degradation decreases significantly device efficiency as the compounds dissolve out of the perovskite resulting in porous structure that accelerates further oxygen and water absorption [18].

Several strategies have been proposed to resolve this problem such as replacement of the compounds or by surface passivation. Namely, it is necessary to substitute the faulty material with perovskite of better resistance to external factors or additionally providing proper insulation which influences significantly the efficiency the price of solar cells. Recently, utilizing passivation interface strategy is also one of the methods minimizing the moisture influence and improving the stability of cells. The passivation layer reduces the defects at the perovskite surface and facilitates electron extraction in the active layer. Also its hydrophobic properties influence enhanced solar cell stability as it protects the device from water damage and contributes to the moisture-resistance of perovskite solar cell [18]. Another solution to improve perovskite solar cell stability is combining

2D-layered perovskites instead of 3D, which rises their intrinsic stability but also causes poorer overall performance [8].

The second weakness of perovskite technology is the presence of lead in the active layer. Through leaching of the perovskite into the environment concerns still remain about exposure to toxic lead compounds. Although those are not numbers high enough to eliminate the perovskite technology completely, the research is being done in order to find lead-free perovskites. On the contrary some research has found the lead toxic impact to be negligible. Compounds such as $CH_3NH_3SnI_3$ are taken into consideration as a substitute that could prevent negative lead effects for human health and environmental safety. Although lead-free perovskite solar cells are a good alternative, their power conversion is significantly lower than lead-based devices. Therefore, at this point this is what holds back the perovskite solar cells commercial production on a higher scale [19].

The perovskite solar cells at this stage in terms of performance suffer current-voltage hysteresis. This issue is critical as it is related to the power conversion efficiency and stability of the device. The considered factors influencing the device characteristics might be connected with bulk or surface defects, ferroelectric properties of perovskite related to its slow polarization or the excess of ions being able to migrate as a result of interstitial defects [20].

What is more, despite of the general low production cost, the overall cost is also problematic in the perovskite solar cells manufacturing. Currently most common electrode material for perovskite solar cell production is gold which significantly contributes to the higher overall cost. On the contrary the cheaper solar cells have a short lifespan, thus they do not meet the requirements. The solutions for expanding the lifespan of perovskite solar cells and increase their durability most often has an impact on rising prices of manufacturing and also increased mass which is to be solved before introducing this device to the market.

6. Conclusions

In summary, the perovskite solar cell is definitely a great breakthrough in the solar energy sector. It is clear that perovskies will able not only to compete with silicon as a large-scale technology in the solar power plants, but they also have the potential to revolutionize and take over the thin-film cells market. In addition to their high-power conversion efficiency, the fabrication of thin film organic-inorganic solar cells would bring a significant commercial benefit. Those light, elastic, cheap and efficient cells can find application in many sectors and devices used on daily basis such as smartphones, tablets or notebooks. Great features will allow application of perovskite solar cells in the production of energy-generating clothing, buildings elevations made of solar batteries and electric cars supported by solar energy. All those challenges together with reaching the standards of carbon neutral policies can be achieved thanks to perovskite technology. Despite the limitations still holding back the perovskite solar cells to be commercialized, it is highly probable that in the near future the solar energy might be dominated by the perovskite technology. Future research of the perovskites is likely to focus on improving the stability and reducing defect of the technology. The strategies for improving the perovskite solar cells performance consider inter alia passivation, inclusion of 2D perovskites and better optimization of interface materials. Improving the stability and reduction in the environmental impact of lead are to be continued areas for research. Beyond solar there is still a broad range of application and potential use for perovskites such as fuels cells, light-emitting diods or electrochemical sensing.

References

[1] Paska, Józef, and Tomasz Surma. "„PAKIET ZIMOWY" KOMISJI EUROPEJSKIEJ A KIERUNKI I REALIZACJA POLITYKI ENERGETYCZNEJ DO 2030 ROKU." Rynek Energii 129 (2017): 21-28.

[2] Gram w zielone, https://www.gramwzielone.pl/trendy/34065/ministerstwo-energii-okreslilo-cel-oze-na-rok-2030-ambitny , 15.01.2019

[3] Sala, Krzysztof. "Energetyka słoneczna jako czynnik rozwoju regionów i gmin w Polsce." Przedsiębiorczość-Edukacja 14 (2018): 125-138.

[4] Zhang, Yaoju, et al. "Theoretical analysis of improved efficiency of silicon-wafer solar cells with textured nanotriangular grating structure." Optics Communications 410 (2018): 369-375.

[5] Cheng, Yuanhang, Franky So, and Sai-Wing Tsang. "Progress in air-processed perovskite solar cells: from crystallization to photovoltaic performance." Materials Horizons (2019).

[6] Zheng, Yifan, et al. "Perovskite solar cell towards lower toxicity: a theoretical study of physical lead reduction strategy." Science Bulletin (2019).

[7] Clean Energy Institute University of Washington, https://www.cei.washington.edu/education/science-of-solar/perovskite-solar-cell/ , 2019

[8] Ossila Perovskites and Perovskite Solar Cells: An Introduction, https://www.ossila.com/pages/perovskites-and-perovskite-solar-cells-an-introduction

[9] Marinova, Nevena, Silvia Valero, and Juan Luis Delgado. "Organic and perovskite solar cells: Working principles, materials and interfaces." Journal of colloid and interface science 488 (2017): 373-389.

[10] Varma, PC Reshmi. "Low-Dimensional Perovskites." Perovskite Photovoltaics. Academic Press, 2018. 197-229

[11] Research Center for Photovoltaics, https://unit.aist.go.jp/rcpv/cie/r_teams/eFTFT/index.html

[12] Energy Sage, Perovskite solar cells: the future of solar? https://news.energysage.com/perovskite-solar-cells/

[13] Liu, Heng-Rui, et al. "Origin of the superior conductivity of perovskite Ba (Sr) SnO3." Applied Physics Letters 102.11 (2013): 112109.

[14] Yue, Liyang, et al. "Light absorption in perovskite solar cell: Fundamentals and plasmonic enhancement of infrared band absorption." Solar Energy 124 (2016): 143-152.

[15] Sciencing, The Effect of Wavelength on Photovoltaic Cells, https://sciencing.com/effect-wavelength-photovoltaic-cells-6957.html, 01.12.2018

[16] Asian Scientist, Wider Wavelengths For Perovskite Solar Cells, /https://www.asianscientist.com/2015/11/in-the-lab/nims-perovskite-absorb-long-wavelength-sunlight/, 03.11.2015

[17] Li, Zhiqi, et al. "Surface Passivation of Perovskite Solar Cells Toward Improved Efficiency and Stability." Nano-Micro Letters 11.1 (2019): 50.

[18] Deltami, PEROWSKITY – PRZYSZŁOŚĆ FOTOWOLTAIKI, http://www.deltami.edu.pl/temat/fizyka/materialy/2014/12/27/Perowskity_przyszlosc_fotowoltaiki/, 01.2015

[19] Kang, Dong-Ho, and Nam-Gyu Park. "On the Current–Voltage Hysteresis in Perovskite Solar Cells: Dependence on Perovskite Composition and Methods to Remove Hysteresis." Advanced Materials (2019): 1805214.

Review on Compressed Air Energy Storage Technology

Novi Dwi Saksiwi[1], Arun Koomar Nagaraj[2]

[1]KIC Energy Transition, Silesian University of Technology, e-mail: novisak569@student.polsl.pl:
[2]KIC Energy Transition, Silesian University of Technology, e-mail: arunnag524@student.polsl.pl

Abstract

Energy Storage is one of crucial tool for enabling effective integration between renewable energy and unlocking the benefits of local generation, the resilient energy supply. The development of the technology continually proves the value to the grid operators around the world. This article will describe more about the principles of Compressed Air Energy Storage (CAES), type of the technology, advantages and disadvantages of the technology. There will be a brief description about ocean compressed air energy (OCAES) as a potential development and challenge in the future.

Keywords: CAES, Renewable Energy, Compression, OCAES

1. Introduction

Environment and ecosystem balance are severely damaged over the past year. Renewable energy power generation become one of many solutions and attract attentions for ecological economy. But the big problem in the power generation of renewable energy is the stability of the grid system according to energy source that has been used.[2] The power is intermittent and fluctuant.[3] The electrical energy storage (EES) has recognized as one of the most promising approaches in addressing the challenge of intermittent source of renewable energy. [2]

After more than 20 years of EES development, there are various energy storage technologies with different characteristic to suit different capacity and requirements. The most accepted EES that have been proved in large scale is pumped hydroelectricity storage (PHS) and compressed air energy storage (CAES). PHS is a mature technology but the development is constrained by special geology. Recently, CAES has been proven to be an alternative to PHS based on high reliability, feasibility and low environmental impact. [4,5] Figure 1 shows costs that is needed for CAES development is relatively similar with other energy storage technologies, but at the same time produce extensive cost of capital power.

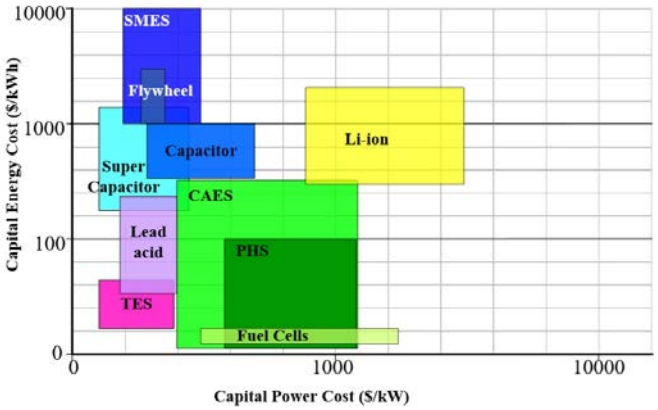

Fig.1.1. Comparation of energy storage technologies according to capital energy cost and capital power cost [1]

The present article gives an overview of basic principle and description of each CAES types. Advantages and disadvantages of using CAES will be discussed followed by challenge in the CAES development. Ocean compressed air energy storage will be explained briefly in the potential development of energy storage.

2. Basic Principles of Compressed Air Energy Storage

Compressed air energy storage (CAES) plants are largely equivalent to pumped hydro power plants in terms of their applications. In CAES plant, the work of system is not about pumping water from lower zone to the upper pond. But it is used the ambient air or other gas that will be compressed and stored in an underground container. When the electricity demand is rising, the pressurized air is reheated and expanded in an expansion turbine before going through a generator for power production. [4,5]

The special thing about compressed air storage is that the air heats up strongly when being compressed from atmospheric pressure to a storage pressure of approximately 70 bar. Standard multistage air compressors use inter- and after-coolers to reduce discharge temperatures to around 149 and 177°C and cavern injection air temperature reduced to around 43 - 49°C. The heat that has been compressed is either being extracted during the compression process or removed by an intermediate cooler. The loss of this heat energy then has been compensated for during the expansion turbine power generation phase by heating the high-pressure air in combustors. The heating process is using natural gas fuel, or in the other way using the heat from combustion gas turbine exhaust in a recuperator to heat the incoming air before the expansion cycle. Alternatively, the heat of compression can be thermally stored before entering the container and used for adiabatic expansion extracting heat from the thermal storage system. [2]

2.1 Compressors and Expanders

The design of compressors and expanders are chosen according to the application of storage. Capacity of the storage will determine the pressure of air and type of compressor that will be used. Multi-stage compressors with higher energy storage density can reach 30MPA of storage pressure. The CAES system pressure is about 8 MPa and combined with axial flow compressors and centrifugal compressors. [6]

3. Current Development of Compressed Air Energy Storage

3.1 Type

3.1.1 Diabatic

Diabatic Cycle dissipates the extra heat with intercoolers into atmosphere as waste. Upon removal from the storage, air must be reheated to expansion in the turbine to power a generator. It can be accomplished with a natural gas fired burner for utility grade storage. Additional heat from fuels and the lost heat due to expansion will degrades efficiency. [9]

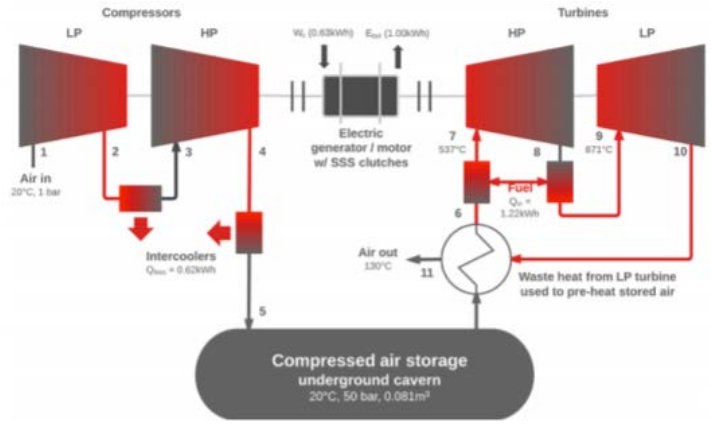

Fig. 3.1. Diabatic Cycle for CAES [7]

3.1.2 Adiabatic

In the adiabatic cycle the thermal energy recovered during the compression cycle is stored and used later to reheat the stored air during the generation cycle to reduce or even eliminate any fuel consumption. Adiabatic cycle uses sensible or latent heat storage and recovery materials. Adiabatic CAES plant is the plant where no fuel is used during the plant's generation cycle. The roundtrip efficiency for this type of plant has been estimated to be 65% [10]

Adiabatic cycle retains the heat produced by compression and returns it to the air when the air is expanded to generate power. With adiabatic compression, some of compression work goes into heating the gas. Efficiency will be reduced if this heat is lost to surroundings, and the same quantity of heat is not added to the gas upon expansion. [7]

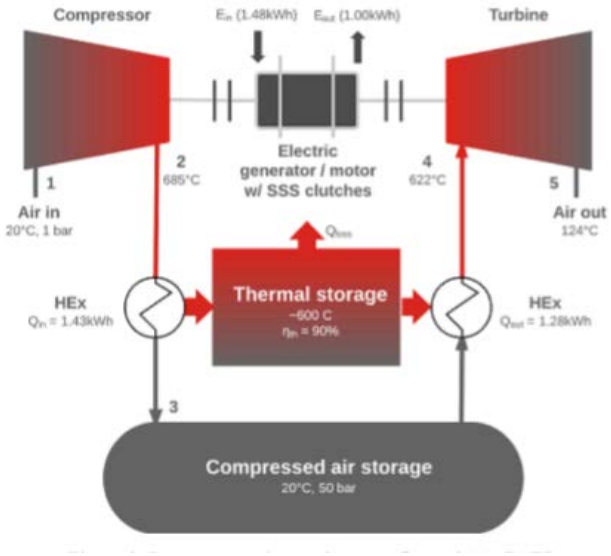

Fig. 3.2. Adiabatic Cycle for CAES [7]

3.1.3 Isothermal [7]

Isothermal cycle approaches attempt to maintain operating temperature by constant heat exchange to the environment. They are only applicable for low power levels without adding other heat exchangers. The theoretical efficiency of isothermal energy storage approaches 100% for small and slowly cycled devices and perfect heat transfer to the environment. In practical things, both of these cycles are hardly obtainable because heat losses sometimes are unavoidable.

The isothermal process maintains constant temperature. Compression process that generate heat must flow to the environment so the temperature will remain constant. In practice this is often not the case, because proper intercooling requires a compact internal heat exchanger that is optimized for high heat transfer and low pressure drop. Isothermal compression can be approximated only at low flow rates when there is no internal heat exchanger in the particularly small system. For higher inherent heat exchanger, small compressors are needed due to a higher ration of surface area to volume.

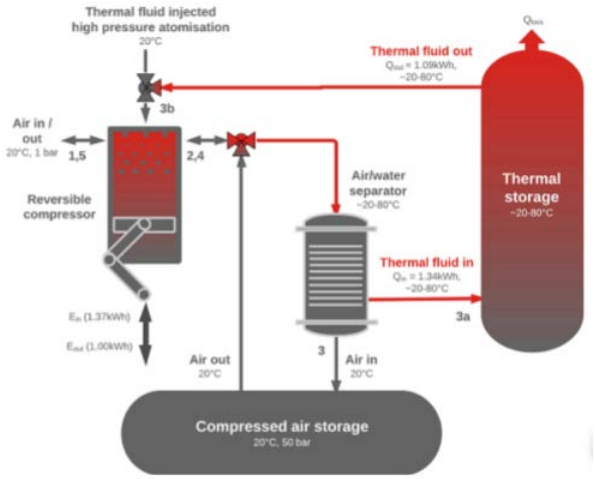

Fig. 3.3. Isothermal Cycle for CAES [7]

4. Advantages and Disadvantages of Using Compressed Air Energy Storage

4.1 Advantages

Compressed air energy storage designed for specific application which can provide benefit to owners, operators of power generation facilities. Economically said, that CAES plant can provide significant energy storage at relatively low costs. The plant has unlimited flexibility for providing precise amount of load management at the utility or regional levels. [8]

From electrical department, the utilization of CAES can provide VAR support. It can supply reactive power in the synchronous condenser mode. It can be operated 24 hours a day in the synchronous condenser mode, since it does not require any air from the storage reservoir. Other than that, CAES provide frequency regulation which can provide much better frequency control than a base load power plant.

From optimization point, CAES can store nighttime wind energy for delivery during the higher priced daytime. It will increase use of generation facilities during off-peak hours when it is on charging mode. CAES will absorb excess generating capacity with its compressor during times when the demand is decreasing. Furthermore, CAES plants have fast startup time. On the emergency mode, the startup times from cold conditions are about 5 minutes, while on normal startup times are about 10 to 12 minutes. [11]

4.2 Disadvantages

The development of CAES still ongoing on many parameters. Despite on many development plans on research and development on CAES, there are a few potential reasons that can be barriers. The underground geology is one of the main risk issues by utilities. Site selection is something limited since there still needs on the presence of mines, caverns, and certain geological formations. That is why the land or site selection for CAES is one of the main issues. [11]

From technological point, the requirement for additional heating in the expansion process is one of disadvantages that still trying to make progress on research to be solved. Other from that, in the case with energy conversion, certain losses are inevitable. There will be less energy makes it to the grid if it passes through the CAES system than in a similar system without storage. But, still there will be more improvement from research in the future to minimize the loss in the grid lines.

5. Future Development of Compressed Air Energy Storage

5.1 Potential

The 70% of world is surrounded by Ocean source, which has the potential to provide a significant amount of renewable energy. Ocean compressed air energy storage (OCAES) system is a promising system for ocean resources. In OCEAS, energy is stored in the form of highly compressed air in the underground storage tank. To store compressed air at high constant pressure, OCEAS uses hydrostatic pressure in Deep Ocean. Compared to land based, OCEAS has significant improvement on isothermal energy compressed air. Ocean compressed air energy storage system can be designed for a large-scale energy storage with the use of hydraulic/pneumatic components. [12]

In OCAES, energy will be stored as a compressed air in an underwater storage. OCAES takes the advantages of hydrostatic pressures in the deep ocean to store compressed air. It will be constant high pressure in the certain position deep in the ocean. When electricity demand is needed and for the energy recovery, compressed air will be passed through the expander to produce the electricity. [12]

Generally, OCAES use isothermal type of CAES. Isothermal OCAES has a potential to have high roundtrip efficiency. Other benefits from isothermal OCAES is this system can eliminate the need for fuel and high-temperature thermal energy storage. Ideal isothermal compression will not add thermal exergy which lead to avoid loss of exergy. Meanwhile in expansion process, exergy from compressed air is completely converted to electrical energy. Round trip efficiency for isothermal OCAES is between 50-70%. [13]

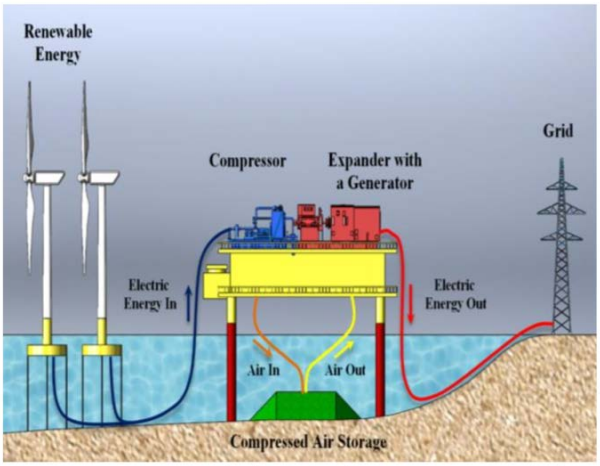

Fig. 5.1. Schematic of Ocean Compressed Air Energy Storage system [13]

5.2 Challenge

The prime challenge in installing a compressed air storage system is the infrastructure and space requirements which eventually results in higher cost and complexity. This concept has distinct benefits such as close location to energy sources and relatively large volume of storage. Nevertheless, feasible studies are still immature and certain problems must be overcome in order to develop a fully functional, large-scale operating concept. The major problems are related to the safety of operation i.e. isolation of workings designated for air storage from the remaining coal, provide leak tightness at high pressure, underground storage integrity and stability during injection/withdrawal cycles. Only after overcoming and solving these major issues this concept might be feasible. [11]

6. Conclusions

CAES systems can be used on very large scales. Unlike other systems considered large-scale, CAES is ready to be used with entire power plants. Apart from the hydro-pump, no other storage method has a capacity as high as CAES. Typical capacities for a CAES system are around 50 to 300 MW. The storage period is also the longest since its losses are very small. A CAES system can be used to store energy for more than a year.

Fast startup is also an advantage of CAES. A CAES plant can provide a startup time of about 9 minutes for an emergency start, and about 12 minutes under normal conditions. By comparison, conventional combustion turbine peaking plants typically require 20 to 30 minutes for a normal startup. If a natural geological formation is used (rather than CAS), CAES has the advantage that it doesn't involved huge, costly installations. Moreover, the emission of greenhouse gases is substantially lower than in normal gas plants.

The main drawback of CAES is probably its reliance on a geological structure. There is actually not a lot of underground caverns around, which substantially limits the usability of this storage method. However, for locations where it is suitable, it can provide a viable option for storing energy in large quantities and for long times. In summary, a CAES system: can be used in large scales, has a fast startup time, and is a low-cost installation when geological formations are used. The main drawback is its reliance on geological structures.

7. References

[1] Jacek Kalina, PhD. DSc; Energy storage – grid scale – Carnot battery- lecture material; Institute of Thermal Technology, Silesian University of Technology

[2] Budt M, Wolf D, Span R, Yan Jinyue. A review on compressed air energy storage: Basic principles, past milestones and recent developments. Elsevier: 250-268, 2016.

[3] Zakeri B, Syri. A comparative life cycle cost analysis. Renewable and Sustainable Energy Reviews 42:569-596, 2015.

[4] Luo X, Wang J, Dooner M, Clarke J, Krupke C. Overview of current development in compressed air technology. Energy Procedia 62: 603-611, 2014.

[5] Luo X, Wang J, Ma Z. Overview of energy storage technologies and their application prospects in Smart Grid. Smart grid 2:7-12, 2014.

[6] Wang J, Lu K, Ma L, Wang J, Dooner M, Miao S, Li J, Wang D. Overview of Compressed Air Energy Storage and Technology Development. Energies 10, 991, 2017.

[7] Rogers A, Henderson A, Wang X. Compressed Air Energy Storage: Thermodynamic and Economic Review

[8] Evans A, Strezov V, Evans T. Assessment of utility energy storage options for increased renewable energy penetration. Renewable and Sustainable Energy Reviews 16, 4141-4147, 2012.

[9] Zhang J, Zhou S, Li S, Song W, Feng Z. Performance analysis of diabatic compressed air energy storage (D-CAES) system

[10] He W, Wang J. Optimal selection of air expansion machine in Compressed Air Energy Storage: A review. Renewable and Energy Reviews 87:77-95, 2018.

[11] Lee Layton. Compressed Air Energy Storage. PDH Center Course. 2012.

[12] Patil V, Ro P. Energy and Exergy Analysis of Ocean Compressed Air Energy Storage Concepts. North Carolina State University, 2018.

[13] Patil V, Ro P. Design of Ocean Compressed Air Energy Storage System. North Carolina State University, 2019.

Passive Car Cabin Cooling System

Tarun Kumar Shanmugam[1]

[1]*KCG College of Technology, Department of Mechanical Engineering, India, email: hodmech@kcgcollege.com*

Abstract

Heat pipes are extensively used in the recent trend as highly efficient passive heat transfer devices. One such application is focused by this paper. Here, a study has been made to evaluate experimentally and numerically the performance of a two phased closed thermosyphon heat pipe, and its implementation in car cabin, so as to remove the accumulated thermal radiations and to restore the thermal comfort of the passengers, after being parked for a long time under sunny areas.

Keywords: Heat pipe, Car cabin cooling, Cooling systems

1. Introduction

A heat pipe is an evacuated cylindrical sealed tube containing a working fluid. It is divided into three sections which are evaporator section, adiabatic section and condenser section. Heat and mass transfer of the working fluid occurs inside the heat pipe primarily due to the transfer of latent heat, in and out of the heat pipe. There are many different kinds of heat pipes but for simplicity purpose, this paper considers the two-phase closed thermosyphon heat pipe incorporating a six layered screen mesh wick. Fig. 1.1 shows the schematic of the heat pipe.

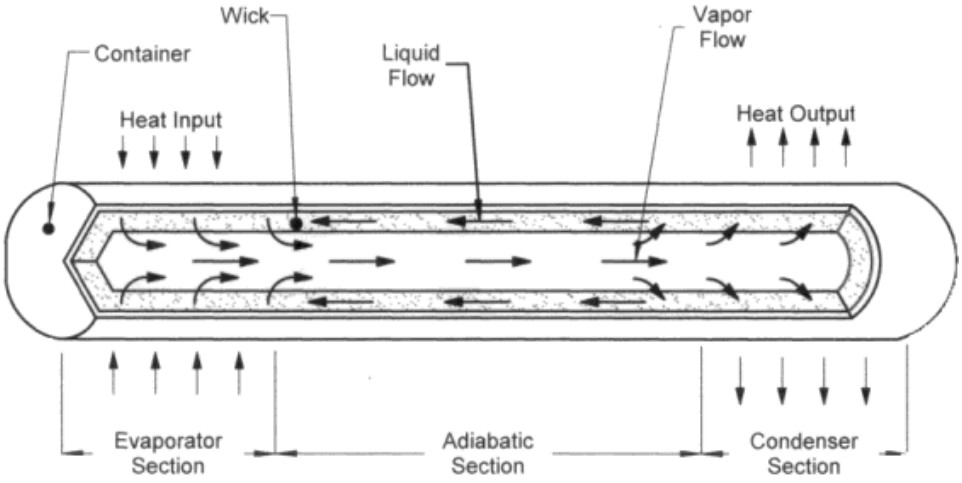

Fig. 1.1. Schematic diagram of the heat pipe

2. Heat Pipe Design

2.1. Design constraint

Table. 2.1. Design requirements of heat pipe

Design type	Dimensions
Heat pipe length (lhp)	10.16 cm
Evaporator length (le)	02.54 cm
Condenser length (lc)	02.54 cm
Adiabatic length (la)	05.08 cm
Outer diameter of heat pipe (do)	01.58 cm
Inner diameter of heat pipe (di)	01.39 cm
Wall thickness (tw)	00.17 cm
Vapor space radius (rv)	00.69 cm
Surface area of heat pipe (Ahp)	01.53 cm2
Area of vapor space (Avs)	00.38 cm2
Capacity (Q)	300.0 W
Operating temperature range (Tmin – Tmax)	300 – 343 K

2.2. Heat pipe geometry

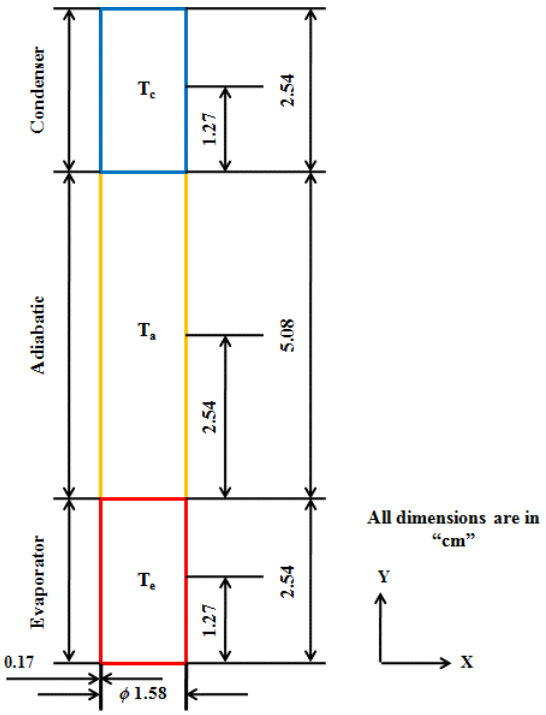

Fig. 2.1. Heat pipe geometry and dimensions

3. Material Selection

3.1. Heat pipe

- Material: ACR – L type soft copper pipe
- Outer diameter – 1.5875 cm
- Wall thickness – 1.7780 cm

Legierski et al [1] investigated the simulation of transient characteristics of heat pipes and they found that the effective thermal conductivity of the heat pipe is time dependant during its transient state of operation.

Annamalai and Ramalingam [2] performed experimental and CFD analysis of air cooled heat pipe and they found that an increase in evaporator heat flux causes the system to attain steady state at a higher temperature.

3.2. Wick

Kempers et al [3] attempted to characterize the evaporator and condenser thermal resistance of a screen mesh wicked heat pipes and found that conduction is the dominant mode of heat transfer across the wick in the condenser while conduction or boiling heat transfer can happen at evaporator depending on the vapor pressure and heat flux

Kempers et al [4] investigated the effect of number of mesh layers and fluid loading on the performance of screen meshes wicked heat pipes and they found that by increasing the number of mesh layers increases the maximum heat transfer quantity along with a slight increase in thermal resistance.

Putra et al [5] evaluated the thermal performance of screen mesh heat pipes with nanofluids and found that using nanoparticles form coatings over the screen mesh that aids in reducing the thermal resistance of the heat pipe.

- Material: Copper mesh 100
- Wire diameter – 0.1143 cm
- Opening – 140 microns
- Opening area – 30%

3.3. Working fluid choices

Per Wallin [6] provided certain guidelines on the determination of operating limits of heat pipe as a function of temperature, that helps in selection of appropriate working fluid.

- Distilled water
- Acetone
- Methanol

The selection of working fluid is based on the operating limits of the heat pipe which are evaluated in the next topic.

4. Operating limits and working fluid selection

In order to make sure that the heat pipe operates satisfactorily, the limitations of the heat pipe must be evaluated. There are five different limitations that are critical to the performance of the heat pipe. They are viscous limit, sonic limit, entrainment limit, capillary limit and boiling limit. Fig. 4.1. shows the different limitations to be considered as a function of temperature and axial heat flux

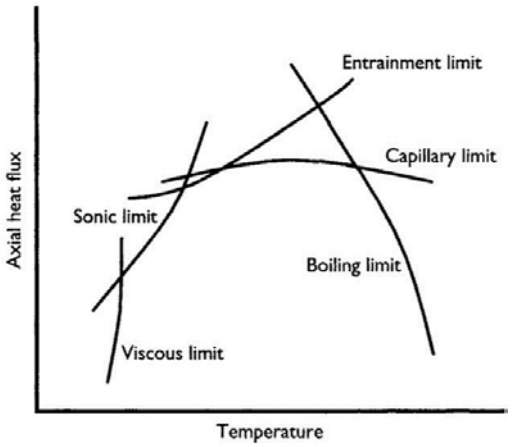

Fig. 4.1. Operating limits of the heat pipe

4.1. Viscous limit

The vapor pressure difference between the evaporator and condenser end is very small at low temperatures, then the viscous forces may be dominant. During start-up when the temperatures are low, the dominant viscous forces prevent the operation of the heat pipe until the working range is achieved. The criteria for the consideration of viscous limit [8] is given by (1)

$(\Delta Pv/Pv) < 0.1$ (1)

Viscous limit is of minimal importance for normal temperature applications according the Handbook of heat transfer.

4.2. Sonic limit

The sonic limit is to be considered at the minimum working temperature. Equation (2) is used to calculate sonic limit

$$\dot{q}_s = \rho_V L \sqrt{\frac{\gamma_V R T_V}{2(\gamma_V + 1)}}$$

Table. 4.1. Sonic limit heat flux

WORKING FLUID	SONIC LIMIT HEAT FLUX
Water	1.448 KW/cm2
Methanol	5.870 KW/cm2
Acetone	4.660 KW/cm2

The heat pipe has a circular cross section and is required to transport 300 W, so the actual heat flux is 0.048 KW/cm2. Comparison with the sonic limitations of various working fluids as shown in Table. 4.1. we can see that the limit is not going to be reached for the fluids.

4.3. Boiling limit

The degree of superheat ΔT required to cause boiling in the evaporator is given by (3). ΔT is evaluated at maximum temperature, as the lowest permissible degree of superheat will occur at maximum temperature

$$\Delta T = \left(\frac{3.06\sigma_l T_{sat}}{\rho_V L \delta}\right)$$

Table. 4.2. Sonic limit heat flux

WORKING FLUID	SONIC LIMIT HEAT FLUX
Water	9.000 K
Methanol	0.717 K
Acetone	0.690 K

The calculated values of degree of superheat for the three choices of working fluid are given in Table. 4.2. Preference must be given to those fluids that have the highest degree of superheat since the chances of boiling in the wick will be reduced. In our case water gets the first preference as the working fluid followed by methanol and acetone.

4.4. Entrainment limit

The entrainment limit is evaluated at maximum temperature of operation and is given by (4)

$$\dot{q}_{ent} = \pi r_v^2 L \sqrt{\frac{2\pi\rho_V\sigma_l}{z}}$$

Table. 4.3. Entrainment limit

WORKING FLUID	ENTRAINMENT LIMIT
Water	15786.20 W
Methanol	10917.34 W
Acetone	7401.33 W

The heat pipe has a circular cross section and is required to transport 300 W. Comparison with the entrainment limitations as given in Table. 4.3. we can see that the limit is not going to be reached for the fluids.

4.5. Capillary limit

The performance of the working fluids can be evaluated by the Merit Number. The formula for evaluating merit number is given by (5). The Merit number for different fluids are shown the figure below

$$\rho_l\left(\frac{\sigma_l L}{\mu_l}\right)$$

Capillary limit is only a comparative criterion that can be used to select the working fluid. Capillary limit plays a very significant role when the heat pipe is operated in orientations other than the vertical

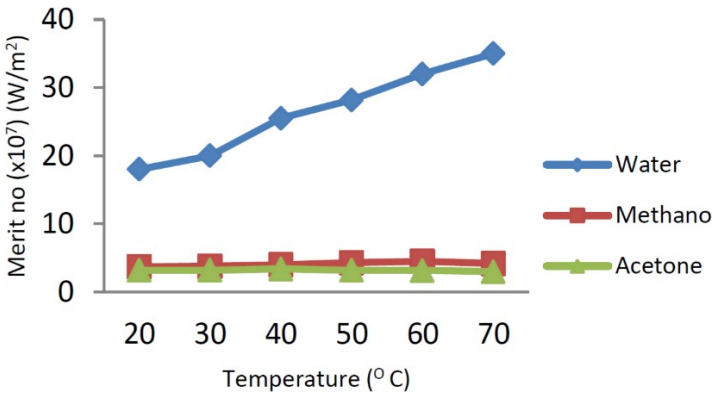

Fig 4. Merit number of selected working fluids

From the results of evaluation of the above limits, we can infer that water suits as the best working fluid.

5. Experimental analysis

Fig. 5.1. shows the experimental setup of the heat pipe. The adiabatic section and the protruding ends of condenser and evaporator section are insulated by means of glass wool. Fig. 5.2 shows the front view of the heat pipe setup.

Fig. 5.1. Experimental setup

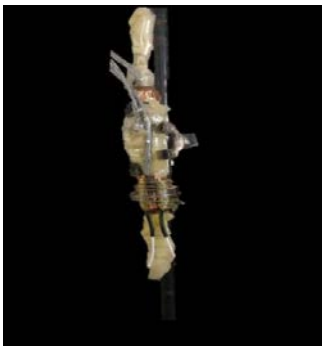

Fig. 5.2. Front view of the heat pipe setup

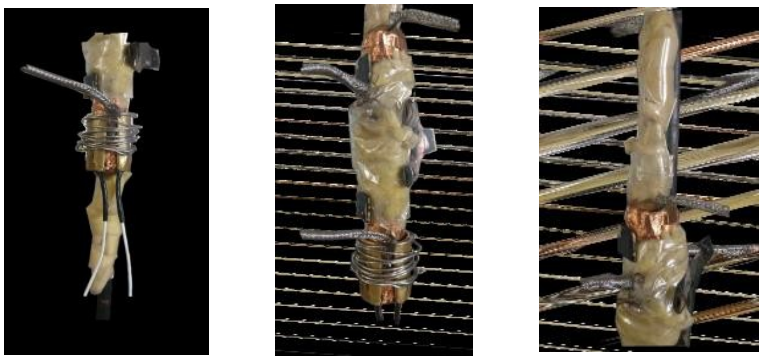

(a) (b) (c)

Fig. 5.3. Close up view of (a) evaporator, (b) adiabatic and (c) condenser

Three thermocouple wires are connected to the heat pipe, one for each region, and the other end to a multipoint scanner for temperature measurement. The voltage is controlled by means of a voltmeter to provide a supply power of 18W. Three sets of readings were taken and the average of them is tabulated in Table. 5.1.

Table. 5.1. Experimental results

Evaporator (°C)	Adiabatic (°C)	Condenser (°C)	Time (Sec)
65	45	42	3
62	49	44	6
59	50	54	12
56	51	46	24
53	51	47	45

51	50	46	54
49	49	46	75

6. Implementation

Hussain H. Al-Kayeim [7] et al investigated the accumulation of thermal radiations and its distribution inside a parked car cabin and they found that most of the hot air accumulates in the top part of the cabin and natural circulation takes place due to differential heating.

Peyghambarzadeh et al [8] investigated the thermal performance of different working fluids in the heat pipe and found that increasing the evaporator heat flux increases the evaporator heat transfer coefficient and increasing the inclination angle of heat pipe decreases its thermal resistance.

The heat pipe system is implemented in Maruti 800 car for practical testing and four locations are marked where the heat pipe is to be placed. They are

- Two on either side of the A pillar of the car
- Two on either side of the C pillar of the car

Fig. 6.1. Installed heat pipe system

Three thermocouple wires were connected in the car, one to measure the ambient temperature, one to measure the temperature of the car cabin and the other to measure the temperature of the heat pipe. Fig. 6.1. shows the installed heat pipe on the car. As it can be seen, the evaporator is located below the roof of the car while the condenser is located above the roof of the car.

Table. 6.1. Results after installing heat pipes

Before heat pipes		After heat pipes	
Peak inside temperature	59°C	Peak inside temperature	43°C
Ambient temperature	40°C	Ambient temperature	38°C
ΔT	19°C	ΔT	5°C

7. Conclusion

The results of the experimental and practical implementation of passive car cabin cooling system proves the temperature drop inside the car cabin. The temperature inside the car came down from 19°C to 5°C after installing the heat pipes, thus proving that the heat pipe is an efficient passive heat transfer device that effectively satisfies the application of car cabin cooling.

Acknowledge

Laboratory support offered by Department of Mechanical Engineering, KCG College of Technology.

Reference

[1] Leigierski J., Wiecek B., and Gilbert de Mey, "Measurements and simulations of transient characteristics of heat pipes," Microelectronics Reliability, Science Direct, vol. 46, 2006, pp. 109-115.

[2] Annamalai A.S, Ramalingam V., "Experimental Investigation and computational fluid dynamics of a air cooled condenser heat pipe," Thermal Science, vol. 15, 2011, pp.759-772.

[3] Kempers R., Robinson A.J, Ewing D., Ching C.Y., "Characterization of evaporator and condenser thermal resistances of a screen mesh wicked heat pipe," International Journal of Heat and Mass Transfer, Elsevier, vol. 51, 2008, pp. 6039-6046.

[4] Kempers R., Ewing D., Ching C.Y., "Effect of number of mesh layers and fluid loading on the perfromance of screen mesh wicked heat pipes," Applied Thermal Engineering, Science Direct, vol. 26, 2006, pp. 589-595.

[5] Putra N., Septiadi N., Ridho Irwansyah, "Thermal performance of screen mesh wick heat pipes with nanofluids," Experimental Thermal and Fluid Science, Elsevier, vol. 40, 2012, pp. 10-17.

[6] Per Wallin, "Heat pipe, selection of working fluid ," Energy Sciences, Lund University, Sweden, 2012.

[7] Hussain Al-kayiem H., Noble B., Sneddon I.N., "Study on the thermal accumulation and distribution inside a parked car cabin," American Journal of Applied Sciences, January 2010.

[8] Peyghambarzadeh S.M., Shahpouri S., Aslanzadeh N., Rahimnejad M., "Thermal performance of different working fluids in a dual diameter circular heat pipe," Ain Shams Engineering Journal, Elsevier, vol. 4, 2013, pp. 855-861.

Future of Fossil Fuels and Renewable Energy – A Review

Saman Hussein Aljaf [1],Vishal Gorecha1[2], Chrisanthemum Wadwadan[3]

[1]Department of Energy and Environmental Engineering, Silesian University of Technology, e-mail: samanhussein8@gmail.com;
[2]Department of Energy and Environmental Engineering, Silesian University of Technology, e-mail: visgor318@gmail.com;
[3]Department of Energy and Environmental Engineering, Silesian University of Technology, e-mail: ctwadwadan@gmail.com

Abstract

With the increasing pressure from the Paris Agreement, big companies are starting to invest on technologies towards the use of renewable energy sources such as photovoltaics, wind turbines, biomass, and others in order to ensure that the temperature increase will not exceed 2ºC in this century. One of the drivers for energy transition includes the fact that fossil-based fuels are expected to be depleted in 100 years considering the continuous increase in energy demand. With this in mind, suppliers of fossil fuels who are the key players in the energy transition are continuously researching, seeking, and experimenting new technologies in order to develop reliable and renewable sources of energy. Energy transition cannot be stopped or hindered. It is the future that needs to be embraced by everyone – industries, suppliers, policy makers, and consumers.

Keywords: energy transition, renewable energy, fossil fuel

1. Introduction

Climate change is a hot topic for the past few years already due to the observed occurrences in the environment. Some occurrences include shifting of weather patterns and rising sea levels. Over the past centuries, greenhouse gases (GHGs) kept on accumulating in the atmosphere, therefore trapping the sun's heat on earth. According to the United Nations, the average global temperature on earth is related to the concentration of GHGs in the atmosphere [1]. Moreover, it was observed that ever since the time of Industrial Revolution, the GHG concentration in the earth's atmosphere has been increasing progressively along with the global mean temperature. It was also mentioned that the most abundant GHG is carbon dioxide (CO_2) and it comprises around two-thirds of the GHG in the atmosphere. Carbon dioxide is produced mostly from burning of fossil fuels [1]. In addition to this, the increase in the consumption of fossil fuel-based resources and varying ways of life is one of the key drivers of global resource usage and the leading contributor of increasing GHG emissions [2].

Due to the concerns about GHG emissions and its effect on the increasing average global temperature, the Paris Agreement was created with the purpose of uniting all nations with the goal of combating climate change [3]. The main aim of the Paris Agreement is to limit below 2ºC the global temperature increase this century and to lessen it more to 1.5ºC. The agreement also aims to help and support other countries to deal with the effects of climate change [4].

It was identified that the energy supply sector is the leading contributor of GHG emissions [5]. Since economic growth is linked with the increase in the demand for power, coal and other fossil fuel-based products plays the major share in the global fuel mix. Global demand of energy consumption is expected to rise in the next decades, and fossil fuel will still remain as dominant source. Currently, with the growing desire of low hydrocarbon emission and clean energy, society faces a real challenge of how to obtain clean, reliable, and affordable energy - energy that directly impacts climate change. According to a study that was conducted by University of Oxford, since 1900, the energy consumption has increased at a rate of 2.8% per year and has continued to increase at a rate of 2.2% annually in the 21st century [6]. Therefore, the energy consumption demand is expected to exceed

100,000 Terawatt Hours in 2050 if the demand of energy increases by 1.7% per year. Moreover, increasing demand of energy in the future is beginning to concern the society and governments to seek for alternative energy which can minimize the carbon dioxide emissions into the environment. It is also important to mention that this prediction has been based on increasing global population, increasing incomes, and declining poverty. Fig. 1.1. shows that fossil fuels are still big contributors on the energy mix by 2050.

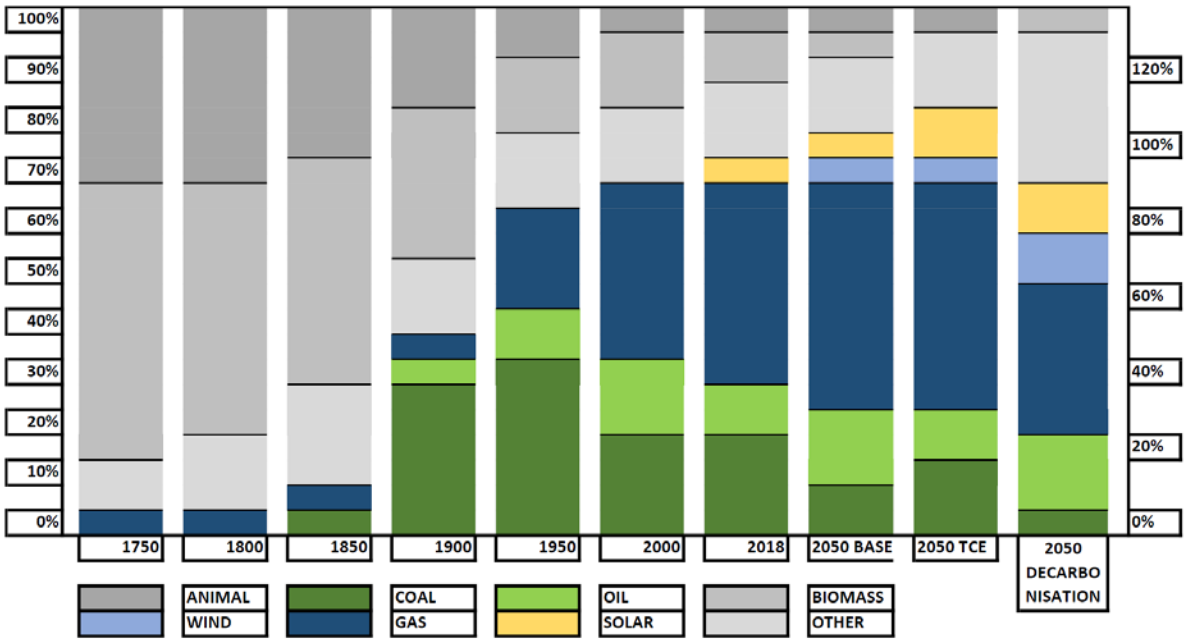

Fig. 1.1. Share of Energy Mix by 2050 [6]

There is a general concern that the current renewable technologies will not be able to meet the required demand of energy consumption in the future, due to low producing energy from renewable sources. To demonstrate, in 2017, the energy produced from solar and wind sources were 1850 Terawatt-, and the estimation of combined annual growth rates are around 270 Terawatt-hour. Consequently, to provide 50% of the total energy consumption to the world, it will take more than 175 years [6]. Fig. 1.2. and 1.3. shows share of fossil fuels and renewable sources for years 2017 and 2018, respectively.

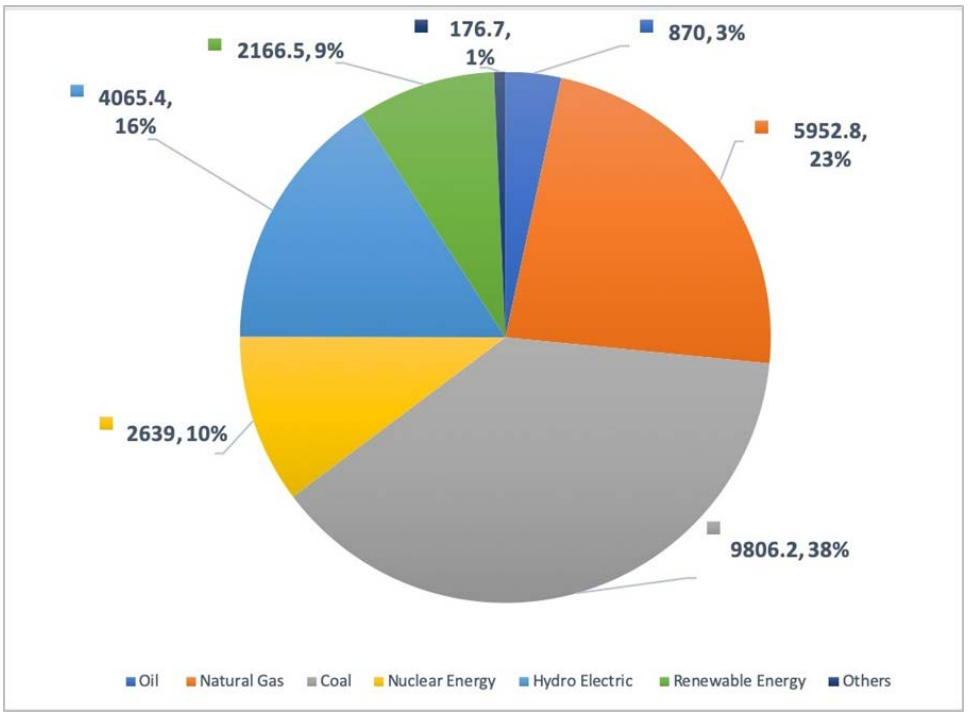

Fig. 1.2. Electricity Generation (TWH) by Fuel in year 2017 [7]

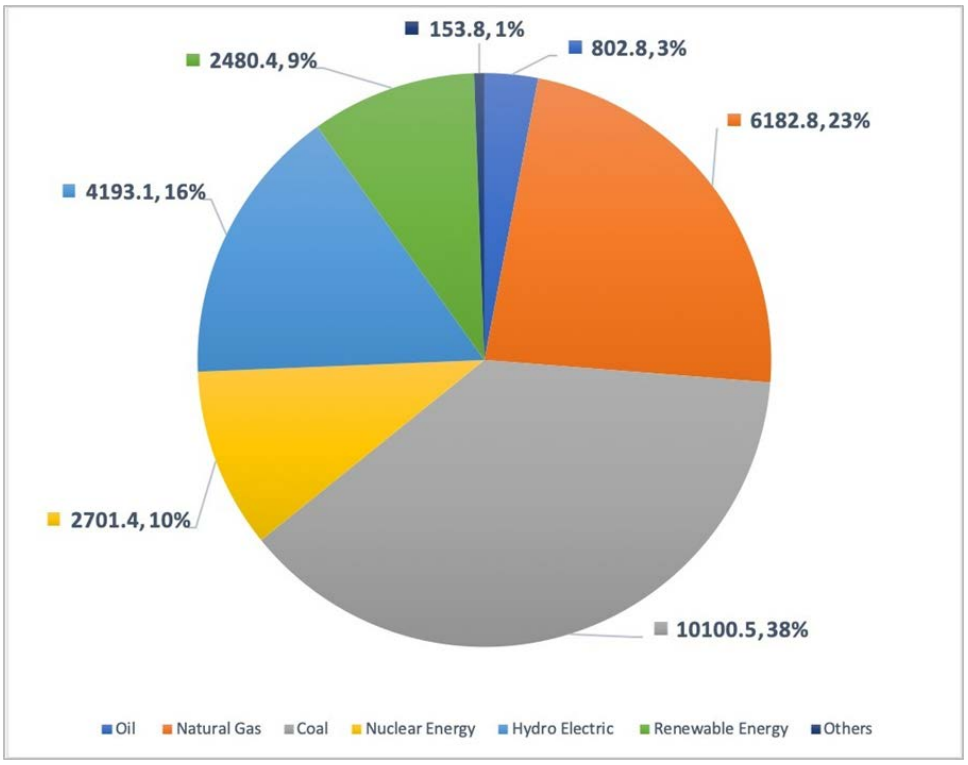

Fig. 1.3. Electricity Generation (TWH) by Fuel in year 2018 [7]

Besides the wind and solar sources, hydro power has been continually growing at its peak by an average of 180 Terawatt-hour annually, while the nuclear is increasing gradually 10% per year which is around 50 Terawatt-hour [6]. Even though the renewable energy constantly increases each year, fossil fuel is still very essential to fill the global energy needs. According to the study from University of Oxford, 120 million barrels per day, and 400 trillion cubic feet of natural gas will still be needed to meet the required energy of the world in 2050 [6]. Therefore, a huge amount of hydrocarbon emissions will be released into the environment as shown in Fig. 1.4.

[7]. It can also be observed from Figure 1 and Figure 2 that the process of energy transition is very slow due to many factors such as how the renewable technologies will evolve, which sort of energy will society choose, and most significantly, the implementation of government policies on the power plants. Therefore, it will take a very long period of time in order to provide enough energy to meet the global demand with zero emission.

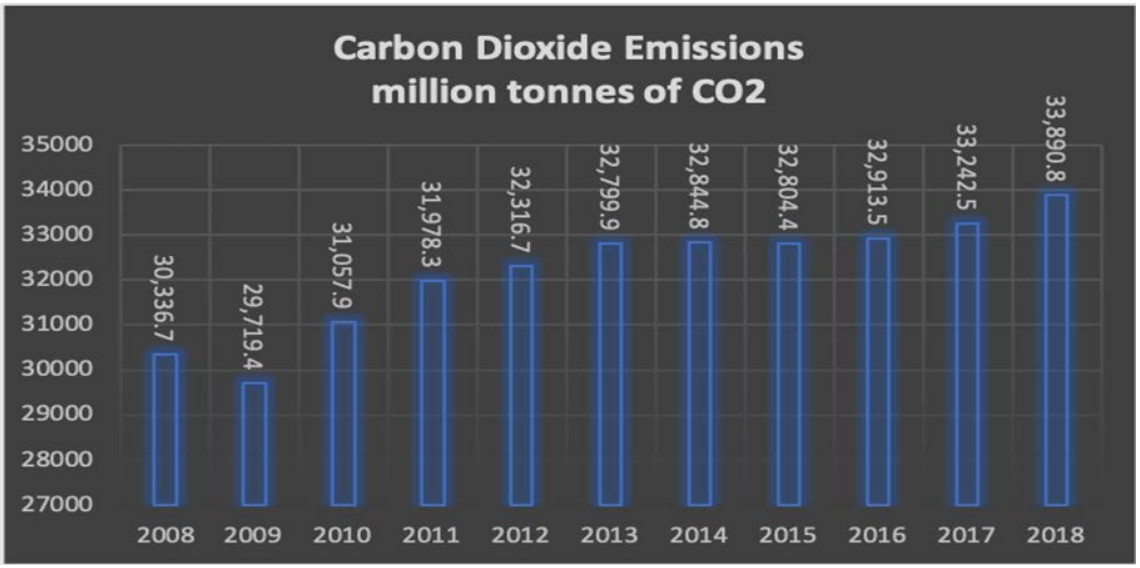

Fig. 1.4. Carbon Dioxide Emission [7]

2. Energy Transition Narratives

There are different setups which can be considered for the future of energy in terms of the speed of transition. It can be grouped into two primary narratives – gradual and rapid [8]. The Gradual Narrative infers that the energy world of tomorrow will look roughly the same as that of today – implying that the global energy system has an inertia incompatible with the Paris Agreement. On the other hand, the Rapid Narrative infers that the current and new clean energy technologies are rapidly supplying all the growth in energy demand and together with new policies will reshape markets, business models and patterns of consumption leading to a peak in fossil fuel demand in the course of the 2020s [8].

Whether the world will follow a path of a gradual or rapid transition will also make a significant difference to business across the energy spectrum. The rapid transition will bring new opportunities but the need to adapt to faster change will be greater. While the global energy system and the factors that impact it are more complex than any scenario or narrative can capture, this paper builds on different existing scenarios and summarizes the main ways in which they differ. It also highlights what to look for over the course of the next decade to see which narrative plays out.

2.1. Implications for the Fossil Fuel Sectors

Growing economies and populations will drive continued growth in demand for natural gas, oil and, to a lesser extent, coal and that the impact of the transition on these sectors will be muted with a gradual shift towards natural gas within the fossil fuel mix. And as technology improves, the fungibility between fossil fuels and renewables will further increase [8]. Table. 2.1. compares different factors that affects energy transition under gradual and rapid narratives.

Table. 2.1. Factors for Arguments [8]

FACTORS	GRADUAL NARRATIVE	RAPID NARRATIVE

What matters	**Storage** New energy technologies are relatively small and will take decades to overtake fossil fuels [9]	**Flow** New energy technologies will soon make up all the growth in energy supply [10].
Technology growth	**Linear** New energy technologies are expensive and face insoluble economic or technical impediments to growth, meaning that growth rates will only be linear [8].	**Exponential** Solar and wind are already cheaper than fossil fuels for the generation of electricity and that electric vehicles (EVs) are about to challenge internal combustion engines (ICEs) on price, that the barriers to growth are soluble for the foreseeable future, and that these disruptive new energy technologies will continue to enjoy exponential growth. They anticipate the rise of new technologies, such as green hydrogen [11], to lead to further waves of change.
Policy	**Static** It is necessary only to model policies that are certain to happen, that the forces of inertia are very powerful and that policy-makers will remain cautious and slow-moving.	**Dynamic** The forces for change are considerably greater than those for inertia, and that technology opens up the opportunity for policy-makers and regulators to design markets to better provide for all consumers' needs. As the necessity for action becomes clear, there will be an Inevitable Policy Response [12]. Modelling only the existing policy environment understates trends in policy-making.
Emerging market energy pathways	**Copy** The emerging markets (i.e. China and India) will broadly follow the path taken by developed markets and use more fossil fuels as they get richer and energy demand rises. Recent years' investments in infrastructure, such as coal-fired plants, are seen to lock in consumption for years to come and increase the costs of transition, thereby slowing down its pace [13].	**Leapfrog** The emerging markets will enjoy an energy leapfrog to new energy technologies and significantly less energy-intensive forms of economic development, while providing critical improvements in the quality of life.
Is the energy transition just about solar and wind?	Solar and wind are too small to drive an energy transition [14].	Technology disruption started with solar and wind, has since spread to renewable integration technologies, is now moving into transport, and will shift into other areas of energy. As in any transition, the low-hanging fruit of change is plucked first, leaving the more problematic areas for later.
How important are different fossil fuels?	Coal, oil and natural gas and every fossil fuel sector in every country are different, and highlight the areas that appear to have few renewable energy alternatives	The energy transition will drive peaks in one fossil fuel sector after another. First coal, then oil, then gas will be impacted, in one country after another, in a pattern whose shape and trajectory will become increasingly familiar.
What is the role of finance in the energy transition?	The capital invested in the fossil fuel sectors and the market need for fossil fuels are so considerable that investors in aggregate will not speed up the transition but will be a neutral force investing across the energy spectrum where they see the best opportunities for returns on capital.	The financial sector as a whole will act to increase the speed of change as it searches for new growth opportunities, becomes more environmentally sustainable and restricts the flows of capital to declining industries.
What about countries that resist the energy	Many fossil fuel exporters and the current US administration are resistant to an energy transition, and large emerging economies like China and India will continue to fuel demand	Four out of five people live in countries that import fossil fuels, meaning that they would stand to benefit from a transition to local renewable energy sources. In particular,

transition?	growth for all energy sources.	China and India are the largest and third largest fossil fuel importers and are strongly committed to a transition.
Recent developments	Rapidly rising energy demand, the roll-back of environmental protection in the US and the fact that renewable energy capacity growth in 2018 was similar to that in 2017.	Continued and unexpected fall in renewable costs, the continued S curves [15] of new energy technology growth, and the rising pressure from financial markets and society for policy-makers to take more assertive action. They note that disruption is already happening in a series of energy and related sectors, from coal to electricity, turbines to cars.

2.2. Questions and Argument

Table. 2.2. Questions and Argument

QUESTIONS	**ARGUMENT**
What should people count on?	The key issues to watch over the course of the next decade have been laid out to see which narrative will prevail. In technology, the focus is on the cost and growth rates of the key disruptive technologies – solar, wind, batteries, EVs and green hydrogen. In policy, the focus is on whether politicians implement more rigorous actions to make fossil fuel users pay for their greenhouse gas externalities. In the emerging markets, the question is whether China and India will be able to continue to implement new clean energy and energy efficiency technologies at scale and whether the path they are setting will be followed by South-East Asia and Africa.
Signals?	A series of signposts are presented. Pass these and the Rapid narrative is on track. Fail to pass them and the Gradual narrative is playing out. Three targets have been set for 2030: solar electricity at $20-30 per megawatt hour (MWh); advanced lithium-ion batteries at $50-100 per kilowatt hour (kWh); and carbon taxes implemented on around half of emissions at $20 per ton, with three peaks to take place in the 2020s in the event of Rapid transition: peak demand for new ICE cars; peak demand for fossil fuels in electricity; and peak demand for all fossil fuels.
Can technology solve everything?	Technology is helping to solve dynamic problems that will drive an energy transition, the forces of inertia are very powerful. So, strategists and planners will help to reach the goals in time.
Don't rage activists?	Activists are now focused on the increasing effects of climate change and are demanding policy makers to take an action with regards to this problem.
Should the voice of nonprofit organization's research towards environment and economy be ignored?	The voice of nonprofit organization's research towards environment and economy must be heard and most especially it must be supported by the government.

3. Conclusions

Both the gradual narrative and rapid narrative are both right, but it depends on the driving forces that will affect the decision making of key players in the world especially government and different unions of countries. One of the drivers for energy transition includes the fact that fossil-based fuels are expected to be depleted in 100 years considering the continuous increase in energy demand. With this in mind, suppliers of fossil fuels who are the key players in the energy transition are continuously researching, seeking, and experimenting new technologies in order to develop reliable and renewable sources of energy.

Another factor that affects the energy transition is the current economic state of different countries. Even if they wanted to transition to an environmentally friendly option or renewable sources of energy, their economic state will decide for it. Especially if the cheapest option are fossil fuel-based products such as coal and oil. Unless these countries receive support from the developed countries, the energy transition specifically in the third-world countries will be very slow.

With the increasing pressure from the Paris Agreement, big companies are starting to invest on technologies towards the use of renewable energy sources such as photovoltaics, wind turbines, biomass, and others in order to ensure that the temperature increase will not exceed 2^{o}C in this century. Energy transition cannot be stopped or hindered. It is the future that needs to be embraced by everyone – industries, suppliers, policy makers, and consumers. Policy makers play a very important role in energy transition. They must create policies that will dynamically stimulate study into new low, zero and negative-carbon technologies, as well as assisting in investigations with innovative business models that promotes decarbonization.

Acknowledgment

The researchers acknowledge the help of dr inż. Marcin Landrat of the Silesian University of Technology in reviewing and accepting this paper.

References

[1] https://www.un.org/en/sections/issues-depth/climate-change/, date of access (17/12/19).

[2] https://www.ipcc.ch/sr15/chapter/chapter-1/, date of access (17/12/19).

[3] https://unfccc.int/process-and-meetings/the-paris-agreement/the-paris-agreement, date of access (17/12/19).

[4] https://ec.europa.eu/clima/policies/international/negotiations/paris_en date of access (17/12/19).

[5] https://www.ipcc.ch/site/assets/uploads/2018/02/ipcc_wg3_ar5_chapter7.pdf date of access (17/12/19).

[6] The Oxford Institute for Energy Studies, https://www.oxfordenergy.org/wpcms/wp-content/uploads/2019/07/The-Energy-Transition-and-Oil-Companies-Hard-Choices-Energy-Insight-51.pdf, date of access (30/11/19).

[7] bp Homepage, https://www.bp.com/content/dam/bp/business-sites/en/global/corporate/pdfs/energy-economics/statistical-review/bp-stats-review-2019-full-report.pdf, date of access (30,11,19).

[8] World Economic Forum, http://www3.weforum.org/docs/WEF_the_speed_of_the_energy_transition.pdf, date of access (30,11,19).

[9] Smil, Vaclav, Energy Transitions: History, Requirements, Prospects, Praeger, 2010. date of access (30/11/19).

[10] ETC, Mission Possible. date of access (16/12/19).

[11] International Energy Agency (IEA), The Future of Hydrogen, 2019. date of access (17/12/19).

[12] Principles for Responsible Investment (PRI), "Inevitable Policy Response", https://www.unpri.org/newsand-press/take-action-on-climate-now-or-risk-disruptive-policies-in-future/3625.article. date of access (17/12/19).

[13] International Renewable Energy Agency (IRENA), Renewable Power Generation Costs in 2018. date of access (30/11/19).

[14] IEA, World Energy Outlook 2018. date of access (14/12/19).

[15] IDTechEx, "Electric Vehicles 2020-2030", https://www.idtechex.com/en/research-report/electricvehicles-2020-2030/670. date of access (17/12/19).

[16] Organization of the Petroleum Exporting Countries (OPEC), date of access (30/11/19).

Waste management: alternatives to landfilling

Piotr Mazur 1[1]

[1]*Silesian University of Technology, e-mail: piotrmazur96@gmail.com*

Abstract

Waste managements is a very serious issue at the moment. Due to growing problem of currently dominating method – landfilling – alternatives are sought-after. Out of many possibilities, several are considered most promising – combustion, gasification, pyrolysis, anaerobic digestions and landfill gas. Combustion is most common alternative for landfilling while other methods are only developing. They differ in the extent of feedstock, product of process, possible application and impact on environment. All of them have advantages and disadvantages but keeping in mind problems with landfilling they should all be considered. No best method can be selected – the preferred one should be chosen based on several criteria, for specific place and requirements.

Keywords: waste management, combustion, gasification, landfilling

1. Introduction

One of natural parts of human life is generation of waste. With the population constantly growing, the amount of produced waste is also increasing. For many years the most common method of waste disposal was storing them on landfills. It allowed the problem to be moved, both physically and in time. Permanent growth of amount of waste on landfills and increasing generation eventually became a problem. The most basic issue was related to people inhabiting more and more areas and simply lack of place for location of landfills.

Another important aspect was the escalation of interest in environmental issues. It became known that certain wastes are in fact very harmful to surroundings. Storing them on landfills does not only make the vicinity dangerous; often the pollution penetrates the soil contaminating it, sometimes can reach water and pollute it influencing reservoirs located far away [1].

Thus a search for a better solution began. A simple way seemed to be burning of waste; until it was realised that if not performed under proper condition, that also emits severe pollution to environment. Improvement of combustion installations and cleaning of exhaust gas helped to make it safer.

Development of new technologies, as well as growing interest in alternative fuels, due to depletion of fossil fuel sources, led to further insight into possible use (and at the same time removal) of wastes. Often the methods applied to fossil fuels were considered, after introducing certain modifications. Nowadays the most common technologies considered when it comes to thermal utilization of wastes, apart from afore mentioned combustion, are gasification, pyrolysis, anaerobic digestion and landfill gas.

In this paper all those methods shall be discussed and compared, keeping in mind the products of their application and environmental impact.

2. Combustion

Combustion is the simplest and most common mean of use of fossil fuels, transferred later to wastes. It is a process of oxidation of fuel with release of thermal energy. The wastes are destroyed by controlled burning in high temperature, with at least minimal stoichiometric amount of oxidizer required. Currently it is the most common method of waste disposal after storing on landfills.

Usually the temperature during the process is about 800 degrees Celsius or more; heat energy, gases and ash is released. The exact calorific value depends on waste composition, which varies, but it is estimated that about 65

to 80% of energy content can be recovered [2]. The heat is then for thermal applications (e.g. when it is needed for an industrial process) or to generate steam for electricity production.

Of course only organic wastes undergo oxidation; maintaining high temperature allows to also melt some part of inorganics. In certain systems, designed mainly for waste volume reducing, auxiliary fuel is used to obtain much higher temperature and melt all inorganic materials, allowing for up to 97% reduction of volume – all is turned into ashes.

Regarding the gases released, due to mixed content of wastes and often presence of undesired substances, flue gas control is necessary. Before realising to environment, the gases are cleaned, usually in few stages, to avoid the release of harmful substances and also to eliminate odour [3]. Since now incineration plants are often built in cities to lower the costs of transportation, that second reason is very important.

Another product of combustion is slag – if plant is operated properly, it will contain small amount of organic materials and of course heavy metals from wastes. It can be used for example in road construction to avoid the need of storing. Other residues generally require storing. Considering the nature of waste, they are all considered hazardous and need to be disposed of in a safe manner. Ashes undergo treatment to minimise their toxicity before disposing of them [2].

Amongst advantages there is less space required than when storing on landfills, possibility to apply even with hazardous wastes which cannot be stored, elimination of risk of contamination of soil and water, generation of heat and electricity. Main problem related to combustion of wastes is related to people attitude to the subject. Before the awareness on the topic increased it was quite common for people to burn the household wastes in house furnaces. That method is very dangerous since it is emitting dangerous substances to environment during combustion. Although modern waste incinerators are nothing like burning in house furnaces and process is completely safe, unaware people still are afraid of this solution. Social opinion may cause problems with building of waste incineration plants, and in fact have led to some of them being cancelled in the past. Other problem is very high investment cost, significant part of which is flue gas cleaning system, and the fact there are some ashes and residues left which need to be disposed of properly.

3. Gasification

Gasification is a conversion process of carbonaceous materials into gas. The product of gasification is gas usually called syngas – gas composing mainly of CO, H_2, CO_2 and H_2O. The process is run by partial oxidation of feedstock with oxygen, air or mixture of one of those substances with steam [4]. Although the process itself is known for many years, the application of biomass and waste as feed is much less investigated than that of coal. Many concepts prepared for fossil fuels can also be used with solid waste, obviously in certain conditions requiring some modifications.

The term ‘gasification’ is merely the name of the process itself, yet when ‘gasification plant’ is discussed it usually refers to the whole system, including conversion of produced syngas into energy carriers which may later be used. An important aspect of gasification is that it comes in many options. The first division that can be made is the application of obtained syngas. It can be either combusted or processed.

3.1. Combustion

Combustion of unprocessed syngas is often referred to as ‘two-step oxidation’ due to similarity with waste incineration process (‘one-step oxidation’) [5]; raw syngas is combusted and heat can be used for a cycle, in most cases Rankine cycle with steam as working medium. Steam is expanded in turbine producing electricity, of course there is also possibility extract useful heat – just as in conventional Rankine cycle. With two-step oxidation the main question occurring is whether it is reasonable to apply gasification instead of incineration. It has several significant advantages over combustion: syngas is a better fuel than waste, since it can be measured and controlled in an easier manner; combustion of syngas is more controllable than of waste due to its uniform

composition and homogenous reaction (oppose to waste being a heterogenous reaction); residues from combustion of syngas are easier to handle; certain pollutants are reduced in flue gas from syngas.

On the other hand, the disadvantages should not be disregarded. Syngas needs controlled storage due to its toxicity and explosiveness, so it is more difficult and costly than municipal solid waste (even though hazardous waste also has some limitations of storage); addition of 'second stage' of oxidation results in greater investment costs. The two greatest difficulties in the process are the quality of raw syngas and flue gases composition. With mixed municipal waste their exact composition is nearly impossible to establish. That creates additional difficulties when considering the system for gasification and results in variable syngas composition produced. Since in most cases air is used as oxidizer – it is much cheaper than application of pure oxygen – syngas contains non-combustible nitrogen. The exact composition depends on the waste, system and its parameters, but a sample composition can be presented [6]: 34% CO, 28% H_2, 29% CO_2, 7% CH_4 and others.

Discussing the flue gas, it is possible to obtain it cleaner than with combustion of waste, mainly lower amount of dioxins, furans and NO_x can be achieved. All of that depends however on the system and its properties, for example the temperature – higher (and system associated with it) allows for lower emission of NO_x and dioxins, lower for better removal of metals [5]. In most cases the flue gases still require cleaning. Usually the system for removing harmful substances from exhaust gas is very similar or even the same as when wastes are incinerated, so this aspect is not advantageous when comparing those systems.

An interesting aspect to consider is a social one. Waste incineration plants are often regarded by society as harmful to environment and emitting unpleasant smell, even though in modern systems it is not the case. Gasification is considered as more modern approach, which could result in less negative feedback from society.

3.2. Processing

The second main option with gasification is processing of syngas. The result is much wider range of possible applications. It can be cleaned-up for increased heating value and from undesired components (such as acid gases, particulates, impurities) and used in more efficient systems, for example gas turbines or internal combustion engines for electricity production and possibly also heat. Syngas can also be processed after clean-up and transformed into chemicals or liquid fuels. The main advantage of that solution is the independence from other sources – no need for import and more constant price than constantly variable market prices of resources.

Also further processing of syngas and its purification may result in production of hydrogen. Hydrogen is often referred to as 'fuel of the future' and has many possible applications, some of which are still being investigated. It could be used in fuel cells for clean production of electricity or even as transportation fuel. The greatest issue with hydrogen is its limited availability – this system allows for its production, making it very interesting [4].

The greatest advantages of further processing of syngas is of course the amount of possible applications; also, less pollutants are released to the environment if no combustion is taking place, or if combusted syngas is clean. The problem is that the cost of cleaning and processing of syngas is very high; if the obtained raw syngas is of low quality, the expense is even greater.

4. Pyrolysis

Pyrolysis is a thermochemical decomposition of carbonaceous material. The process is conducted at high temperature in absence of oxygen. The products of pyrolysis are generally gaseous, liquid or solid. It is regarded as more flexible than incineration, also the emission of certain pollutants is lower – thus making it a rather interesting solution. Several types of reactors may be used for pyrolysis – usually rotary kilns are applied, due to their high heat transfer and low energy consumption [7].

In studies, usually a certain type of wastes is analysed for pyrolysis – such as garden waste, food, paper, rubber plastics etc. However, in municipal solid waste a mixture of waste is present – even if segregation is introduced (and still it is not mandatory in many places), some wastes get mixed. Since the process yields certain

differences depending on type of waste, building a reactor for very heterogenous mixture, with variable moisture content, is rather problematic, but it also has some advantages.

Inorganic wastes do not undergo combustion process, they may cause slag or in high enough temperature can only be reduced to ash; in case of pyrolysis, addition of inorganic to organic waste (which is often the case for mixed municipal waste) results in improved quality of obtained product: gas has lower CO_2 fraction and more hydrocarbons, liquid better heating value. Nonetheless, if for example electric or electronic equipment is present in the mixture, emissions must be monitored thoroughly and controlled, since there is a risk of hydrogen chloride, sulphide and several other harmful substance release. [7]

As it was already mentioned, the products of pyrolysis are either gas, liquid or solid. Increasing of temperature of the process results in higher gas yield and lower contribution of two other phases. Generally speaking, the aim of pyrolysis is to recover energy from waste. More specific application, related also to the composition, depend on type of the product.

Pyrolytic gas is used in combustion process. It composes of CO_2, CO, hydrogen, methane and some light hydrocarbons [7]. The heat from combustion can be used in cycles for producing of electricity and possibly heat; the most common use, however, is as energy source for the process of pyrolysis. The problem is the presence of H_2S in pyrogas, possibly in relatively high concentration. As a result the emissions must be controlled, or the gas needs to be cleaned prior to use, especially if the exact composition of waste is not known.

Pyrolytic oil has a wider range of applications; the problem is its composition which is highly dependent on the feedstock and parameters of the process and also influences possible use of the oil. It can be used in some industries, e.g. detergent industries, for the process of manufacturing; similar to pyrogas, it is sometimes applied to run the process of pyrolysis; it can be combusted (or co-combusted) for generation of heat for steam production to obtain electricity [8].

Pyrolytic char is generally less desired than products in other phases. Although the heating value is similar to that of coal, heavy metals and hazardous elements are present, making combustion more problematic. It is still realised, but could cause problems in boilers and will certainly require exhaust gas monitoring and cleaning. Heat from combustion can also be used for steam generation.

The technology of waste pyrolysis is still being developed, yet it seems to have a very high potential. Its greatest advantage is the possibility to use almost any type of waste. A good example is pyrolysis of tyres. Pyrolysis allows the separation of carbon black from tyres and the released volatile matter has energy recovery potential related to natural rubber presence in tyre composition [9]. It is an opportunity for safe disposal of tyres and recovery of energy from it. Generally tyre utilisation after their use is very problematic and not many satisfying solutions have been found to solve that issue.

5. Anaerobic digestion

Anaerobic digestion is a process which breaks down organic matter in strict anaerobic conditions (lack of oxygen) to produce biogas and digestate. Biogas is the main and desired result and can be used as fuel; digestate still has some valuable properties and can also be utilised.

First step is selecting the feedstock source. Many can be used – e.g. agriculture wastes, food wastes (municipal, commercial), wastewater and certain sludges - but there are some strict limitations. It must not contain inorganic materials, wood wastes, soil, antibiotics or pesticides [10]. Pre-treatment is mandatory – to eliminate the waste which do not undergo anaerobic digestion – but is also highly recommended for increased efficiency and to minimise the possibility of damaging the system. Physical, chemical, biological or combined pre-treatment can be applied.

The process has several options. Apart from classification depending on size of the installation, digestion can be either single-stage or multi-stage. The first one is more economical and simpler in use, the second offers better

efficiency and greater production of biogas. The process requires monitoring to ensure its proper proceeding – amongst others pH, carbon to nitrogen ratio and methane content should be controlled [11].

The result of the digestion is biogas. Typical composition of biogas produced from waste is about 45% methane, 35% carbon dioxide and other gases – water vapour, oxygen, nitrogen, impurities [12]. Biogas is usually cleaned prior to use for improved heating value or simply to eliminate harmful substances which would be released to environment or could damage the systems. The main threat is hydrogen sulphide – that substance is very dangerous to installations due to corrosive properties. Then it can be used by replacing natural gas in production of steam and possibly heat, either in gas turbines, internal combustion engines, boilers or even fuel cells [13]. After upgrading it could be transformed into biomethane and used in transportation fuels or injected to natural gas system.

The digestate contains nitrogen, phosphorus and potassium, making it possible to use as fertilizer. However, in some countries it is forbidden to avoid excessive amount of those elements in soil, in which case its disposal is more problematic. Since it still has relatively high heating value (approximately 14MJ/kg) [14], possible applications as heat source are being researched.

The greatest advantage of anaerobic digestion is wide range of application and possibility of using waste with high moisture content. In afore mentioned solutions, since heat needs to be delivered, high moisture content requires more heat for drying, sometimes making the process unprofitable. The problems are mainly the need for processing of fuel and obtained biogas.

6. Landfill gas

Landfill gas basically comes from the process of anaerobic digestion, but the situation is different than in previous chapter. Here the wastes are not moved to another facility for the process of digestion. The gas is collected from wastes already stored at landfills; in lower layers anaerobic conditions occur, and presence of organic waste leads to natural process of landfill gas generation.

The gas is collected by a system of underground pipes and transported to a facility, in most cases near the landfill – for simple reason of lower transportation costs. Since it comes from unsorted waste, as it is in the case of anaerobic digestion, it requires more cleaning. Usually it is realised in two stages – the gas is cleaned upon entering the facility, then it is compressed – since collected from landfill has rather low pressure – then it is cooled down and cleaned again [15].

Sample composition of landfill gas is about 48% methane, 32% carbon dioxide, 18% nitrogen, other gases [16] – generally it is similar to biogas produced in process of anaerobic digestion, since it undergoes the same process. Also the possibilities of application are similar, so they shall not be discussed again.

Apart for the extraction of landfill gas to use as fuel and for economical reasons, mainly it is important for the environment. If it is not collected, the gas, of which nearly half is methane, is released to the surroundings. Global warming potential of CH_4 is much higher than that of CO_2 – 1kg of released methane is considered an equivalent of 25kg of carbon dioxide [17]. The installation cost for landfill gas recovery is high but due to the influence on environment the solution should be considered.

7. Summary

Five methods of energy recovery from wastes were considered. Each of them has some strengths and weaknesses. The main difference is in limitation of feedstock as well as in products obtained, along with possible application, and environmental impact, which assessment was the main purpose of this paper. For the sake of wider consideration, gasification is divided depending on whether raw syngas is combusted or processed further. The comparison of the solutions is given in Table. 7.1.

Table. 7.1. Comparison of methods

Method	Feedstock	Product	Application	Environmental impact
Combustion	All waste, inorganic may cause problems	Heat	Steam production (for electricity) and useful heat	CO_2, N_2O, NO_x, NH_3, dioxins, furans [18]
Gasification + combustion	Recommended only organic waste	Raw syngas	Externally fired cycles	Similar to combustion but lower amounts [5]
Gasification + processing	Recommended only organic waste	Clean syngas, hydrogen, chemicals or fuels	Internally fired cycles - in internal combustion engines, gas turbines, fuel cells; transportation	Minimal [5]
Pyrolysis	All waste	Pyrogas, pyrolysis oil, pyrolysis char	In internally or externally fired cycles, fuel for pyrolysis	Mainly PM, HF, HCl [19]
Anaerobic digestion	Biodegradable waste	Biogas or biomethane, digestate	Gas turbines, internal combustion engines, boilers, fuel cells, transportation, injection to natural gas system	CO_2 (non-ideal anaerobic conditions), NH_3, S in biogas, CH_4 losses [20]
Landfill gas	Landfill with biodegradable waste	Biogas or biomethane	As above	As above; preventing of methane release to environment

The products, described in Table 1, are in most cases fuel (except for combustion – the product is already heat). It may have different applications, but the concept is the same – energy from waste is recovered as fuel and can be put to use.

The environmental impact is quite similar in most methods. The focus is put on emissions during the process, less combustion of fuels (except gasification with combustion). Although different substances are released, regulations make it mandatory to apply filtration systems which must bring them below limits. In case of biogas as product, cleaning is usually conducted to eliminate undesired substances – mainly sulphur – to avoid emission of sulphur oxides during combustion later on. When it comes to landfill gas, it prevents from methane release to environment – and methane has a high global warming potential. All this methods prevent wastes from being stored on landfills, where they could contaminate soil or water – this is a great influence of all of them on environment.

A question may be raised as to which of those technologies is the best. Ideal solution for waste management would be minimising waste generation by people and secondary achieving as high recycling level as possible. However, those options are very time consuming and problematic to implement, also they still leave some wastes which cannot be processed. Methods described in this paper are ready for implementation and mainly only require funding for their introduction. Regarding which one should be selected – it depends on several factors, such as technological limitations – whether or not they can be separated to organic and inorganic; location – to avoid high transportation costs over long distances. A very important aspect is demand for product: wastes can be used to produce heat, electricity, hydrogen, natural gas – if a product can be put to use, that would allow for more rapid return of investment, and in some cases that could be the critical argument. Basically, financial aspect is possibly the most important factor in choosing one technology. Although it was not described thoroughly in this paper, often the decision comes down to choosing the most financially justified solution. Considering the environmental gain and elimination of problem of storing wastes, subsidies are usually provided, both from countries governments and in Europe from European Union. Still, the investment cost may make some of the solutions impossible to implement. Overall, there are many criteria and it is difficult to say which method is the best. It needs to be assessed based on specific cases, based on many aspects.

References

[1] Aziz H. A., Mohd. Zahari M. S., Bashir M. J. and Hung Y.-T., "Groundwater Contamination at Landfill Site," in *Handbook of Environment and Waste Management*, World Scientific, 2014, pp. 781-817.

[2] Patil A. A., Kulkarni A. A. Patil B. B., "Waste to energy by incineration," *Journal of Computing Technologies*, vol. 3, no. 6, pp. 2278-3814, 2014.

[3] Mikus M., Dziedzic K., Jurczyk M. P., "Flue gas cleaning in municipal waste-to-energy plants," *Infrstructure and ecology of rural areas*, vol. 4, pp. 1179-1193, 2016.

[5] Consonni S., Vigano F., "Waste gasification vs. conventional Waste-To-Energy: A comparative evaluation of two commercial technologies," *Waste Management*, vol. 32, pp. 653-666, 2012.

[6] Shehzad A., Bashir M. J., Sethupathi S., "System analysis for synthesis gas (syngas) production in Pakistan from municipal solid waste gasification using a circulating fluidized bed gasifier," *Renewable and Sustainable Energy Reviews*, no. 60, pp. 1302-1311, 20016.

[7] Czajczyńska D., Anguilano L., Ghazal H., Krzyżńska R., Reynolds A., Spencer N., Jouhara H., "Potential of pyrolysis processes in the waste management sector," *Thermal Science and Engineering Progress*, no. 3, pp. 171-197, 2017.

[8] [Online]. Available: https://www.btg-btl.com/en/applications. [Accessed May 2019].

[9] Martinez J. D., Puy N., Murillo R., Garcia T., Navarro M. V., Mastral A. M., "Waste tyre pyrolysis - A review," *Renewable and Sustainable Energy Reviews*, no. 23, pp. 179-213, 2013.

[10] Mata-Alvarez J., Mace S., Llabres P., "Anaerobic digestion of organic solid wastes. An overview of research achievements and perspectives," *Bioresource Technology*, no. 74, pp. 3-16, 2000.

[11] Global Methane Initative, "Overview of Anaerobic Digestion for Municipal Solid Waste," Global Methane Initiative, 2016.

[12] Kuźnia M., Jerzak W., Łyko P., Sikora J., "Analysis of the combustion products of biogas produced from ogranic municpal waste," *Journal of Power Technologies*, no. 95, pp. 158-165, 2015.

[13] Holm-Nielsen J., Al Seadi T., Oleskowicz-Popiel P., "The future of anaerobic digestion and biogas utilization," *Bioresource Technology*, no. 100, pp. 5478-5484, 2009.

[14] Neumann J., Meyer J., Ouadi M., Apfelbacher A., Binder S., Hornung A., "The conversion of anaerobic digestion waste into biofuels via a novel Thermo-Catalytic Reforming process," *Waste Management*, no. 47, pp. 141-148, 2016.

[15] Niskanen A., Varri H., Havukainen J., Uusitalo V., Horrtanainen M., "Enhancing landfill gas recovery," *Journal of Cleaner Production*, no. 55, pp. 67-71, 2013.

[16] Gewald D., Siokos K., Karellas S., Spliethoff H., "Waste heat recovery from a landfill gas-fired power plant," *Renewable and Sustainable Energy Revies*, no. 16, pp. 1779-1789, 2012.

[17] Marten A. L., Newbold S. C., "Estimating the social cost of non-CO2 GHG emissions: Methane and nitrous

oxide," *Energy Policy*, no. 51, pp. 957-972, 2012.

[18] Johnke B., "Emissions from waste incineration," *Waste Sector*, pp. 455-468.

[19] LAPČÍK V., and NIMRÁČEK T., "Emissions from Pyrolysis of Tyres and Municipal Waste," *Journal of the Polish Mineral Engineering Society*, pp. 177-182, 2015.

[20] Baldasano J. M., Soriano C., "Emission of greenhouse gases from anaerobic digestion processes. Comparison with other MSW treatments," *Water Science and Techonlogy*, no. 41, pp. 275-283, 2000.

Energy comparative analysis of solar power plants with a central and a linear absorber.

Łukasz Korcz[1]

[1]*Institute of Thermal Technology, Silesian University of Technology, e-mail: lucas.korcz@gmail.com*

Abstract

Energy comparative analysis of solar power plants with central and linear absorber was conducted to compare different technologies of solar electricity generation using Rankine Cycle to produce power. In this way, the most important parameter was to find their efficiencies for the same chosen location therefore same solar irradiation data and decide which one is better or if there are no significant differences. The central receiving system yielded an efficiency at the level of 28%, and the parabolic trough solar power plant at the level of 24%. Those values are for the averaged hour by hour solar data. The power output for both system was also different, the parabolic trough produced 7.05 MW of electricity and the central receiving system generated 7.99 MW. The additional calculations were done to see the improvement while using thermal storage tank. It was assumed that the nominal power of the power plant is 7.05 MW. The analyzed case showed that for both parabolic trough and central receiver system efficiency raised, but again the efficiency was higher in case of central receiving power plant 26% to 23% in the parabolic trough solar power plant.

Keywords: central receiving solar power plant, parabolic trough, direct normal irradiation, gross electrical power, nominal efficiency, annual efficiency, thermal storage

1. Introduction

Nowadays, the electricity production from solar irradiation is a direct process. To produce electricity from solar radiation, one has to use the so- called solar concentration technology. This kind of process is a very interesting option, especially when living in a world where the emission of CO_2 and other gaseous substance is rising tremendously fast, which affects health and the way of living. Additionally, regulations from the European Union cause that Poland has to adapt to European standards regarding gas emissions. Four different Concentrated Solar Power technologies can be distinguished, that are available on the market and can be used to absorber the sunlight and change it into heat: central receiver system, parabolic troughs, Fresnel reflectors and parabolic dishes. Two main leading technologies are the central receiver system and parabolic trough system that are used together with the Rankine Cycle to produce electricity.

Parabolic trough power plant shown in figure 1.1 contains of many parabolic troughs (1) field through which the heat carrier is heated up. The trough shaped mirrors are reflecting sun rays onto the thermally efficient tubes placed in the focal line which contains the heat carrier. The heat transfer fluid transports the heat to the steam generator (3). Created steam runs into the turbine (4) where is expanded generating the mechanical work, and thus producing the electricity in the generator (5). Then steam condenses in the condenser (6) from where is transferred via the pump (7) back again to the steam generator (3), and the whole process is repeated again.

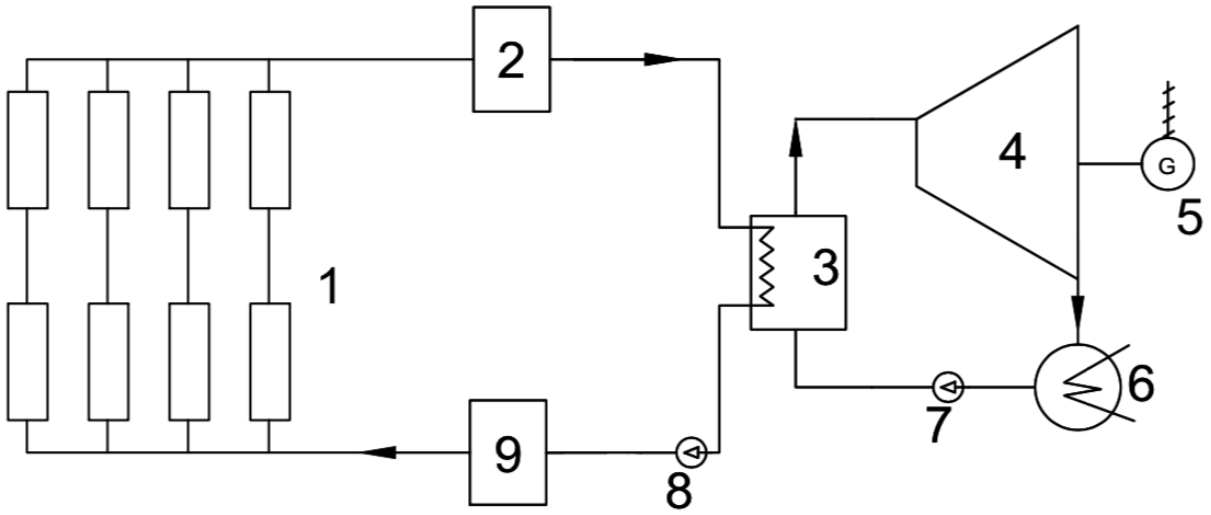

Figure 4.1 Scheme of parabolic trough power plant; 1- parabolic trough solar field, 2- heat transfer fluid hot tank, 3- steam generator, 4- turbine, 5- generator, 6- condenser, 7,8- pump, 9- heat transfer fluid cold tank

Figure 1.2 shows the central receiver power plant with the solar tower (1) as a main point which is equipped with absorber- containing the heat transfer fluid to deliver the absorbed heat to the Rankine Cycle. The solar tower is surrounded by heliostat field (10), each heliostat is tracking the sun to reflect the sun's rays into the receiver, located on a tower.

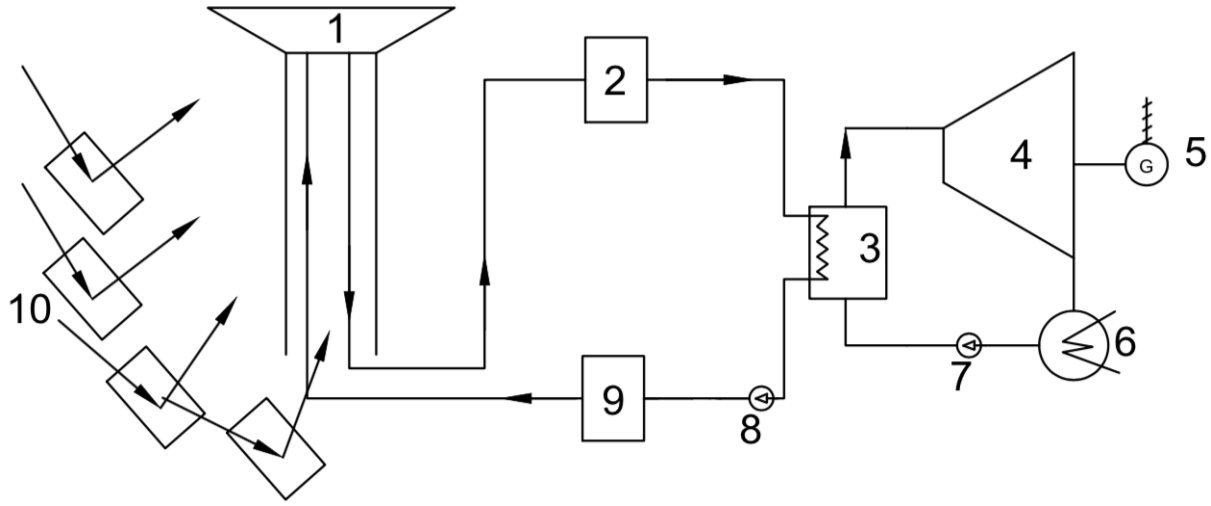

Figure 1.2 Scheme of central receiver power plant; 1- solar tower- absorber, 2- heat transfer fluid hot tank, 3- steam generator, 4- turbine, 5- generator, 6- condenser, 7,8- pump, 9- heat transfer fluid cold tank, 10- heliostat field

2. Aim and scope

Aim was to compare different technologies of solar electricity generation using Rankine Cycle to produce power, find their efficiencies for the same chosen location therefore same solar irradiation data and decide which one is better or if there are no significant differences. For the purpose of this project it was chosen that the solar data will be for Poland, more specifically for Katowice region- the precise data are presented later in the project.

The main value that controls everything in the whole process is the mass flow rate of the molten salt ($\dot{m}_{salt}$). Results of mass flow rate shown further are the maximum available values at certain sun's radiation. This value

is calculated taking into account the energy delivered from solar irradiation, assumed temperatures at the inlet (t_{in}) and outlet (t_{out}) of the collector/absorber and the specific heat capacity of salt (c_{p_salt}). The area of aperture (A) of both power plants is presumed to be the same, however the number of heliostat is different than the number of parabolic trough collectors in the same area- those numbers are calculated according to the manufacturer's data base. Based on those assumptions, the electric power output (N_{el}) of the steam turbine is calculated, as well as the nominal efficiencies (η_{eNomPT} ; η_{eNomCR}) and the annual efficiencies ($\eta_{e\_year\_PT}$; $\eta_{e\_year\_CR}$) of both systems. However, the main calculations are done for the annual average values, just to show what is the average electricity energy output (N_{el}) as well as the average efficiencies. First, the case with straight electricity production will be used and then the assumption of thermal storage case with the also assumed nominal power output.

3. Solar data for chosen location

The selected location is nearby small villages, where a gigantic piece of land is located which is intended for agricultural purposes and might be a suitable area for such project. The place (figure 3.1) is in the southern part of Poland, in the Upper Silesia province, close to the city of Pyskowice. The solar data for this location (figure 3.1) with coordinates 50.486° North and 18.593° East is generated using the interactive tool from European Commission website. The solar data is the hour by hour direct insolation.

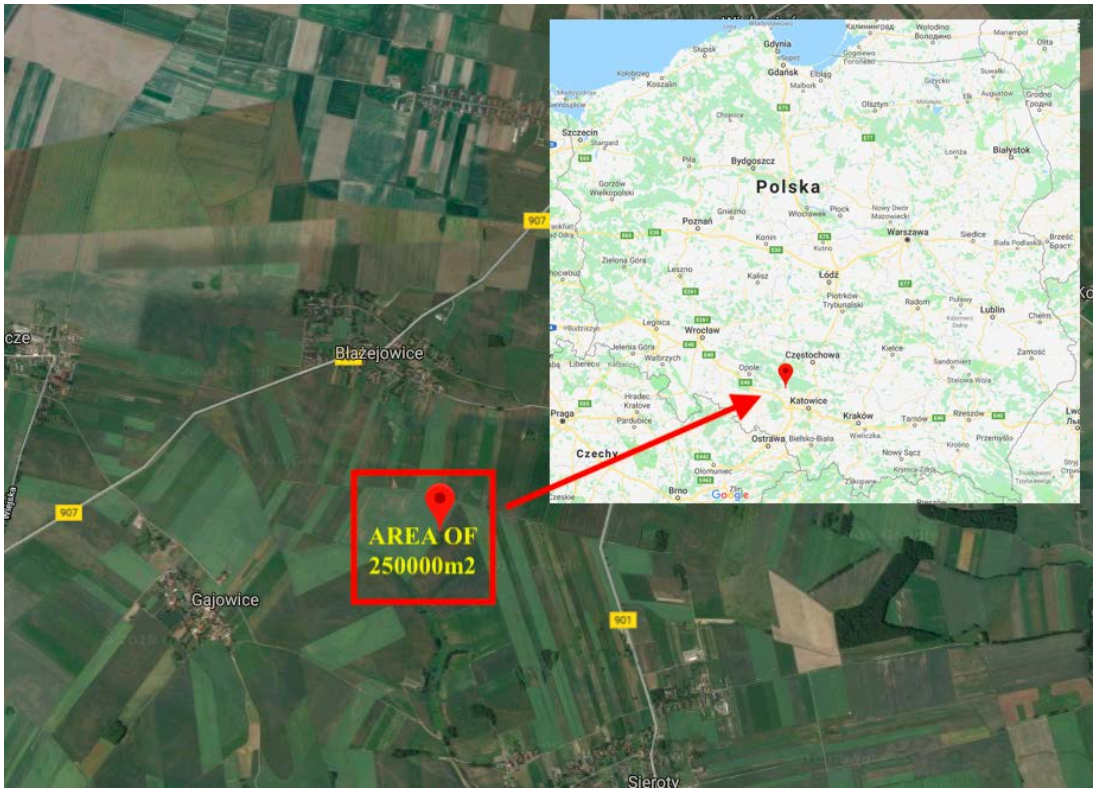

Figure 3.1 Precise location of Solar Power Plant in Poland [5]

Table 3.1 is showing the solar irradiation data gathered from the European Commission interactive tool for years from 2007 until 2016, for the slope of 30° and for the chosen location. All the values in this interactive tool are the hour by hour data. Then they are averaged for each month of the year and again recalculated to achieve the final result in two different units.

Table 3.1 Average solar irradiation for each month

MONTH	IRRADIANCE, $\frac{W}{m^2}$	INSOLATION, $\frac{kWh}{m^2*day}$
January	35.66	0.86

February	52.54	1.26
March	87.02	2.09
April	143.80	3.45
May	212.74	5.11
June	197.03	4.73
July	215.33	5.17
August	169.54	4.07
September	130.06	3.12
October	74.82	1.79
November	42.08	1.01
December	31.59	0.76
Yearly average	**116.016**	**2.78**

Table 3.2 was calculated to show how many hours in a month one have the access to sun rays thus the solar power might work. Even though the data was accurate, the number of sun hours does not take into account the intensity of radiation.

Table 3.2 Number of sun hour in a month

MONTH	SUN HOURS	HOURS IN MONTH	% OF SUN HOURS	AVERAGE SUN HOURS PER DAY
1	252	744	33.87%	8.13
2	267	672	39.73%	8.61
3	365	744	49.06%	11.77
4	415	720	57.64%	13.39
5	483	744	64.92%	15.58
6	480	720	66.67%	15.48
7	492	744	66.13%	15.87
8	448	744	60.22%	14.45
9	374	720	51.94%	12.06
10	317	744	42.61%	10.23
11	253	720	35.14%	8.16
12	248	744	33.33%	8.00
SUM	**4394**	**8760**	**50.16%**	

4. Energy comparative analysis

Nomenclature

c_{p_water} - water specific heat capacity, $\frac{kJ}{kg*K}$;

c_{p_salt} - molten salt specific heat capacity, $\frac{kJ}{kg*K}$;

h_1 - specific enthalpy in point 1, $\frac{kJ}{kg}$;

h_2 - specific enthalpy in point 2, $\frac{kJ}{kg}$;

h_{2s} - specific enthalpy in point 2s, $\frac{kJ}{kg}$;

h_3 - specific enthalpy in point 3, $\frac{kJ}{kg}$;

h_4 - specific enthalpy in point 4, $\frac{kJ}{kg}$;

m - month;

$\dot{m}_{steam}$ - steam mass flow rate, $\frac{kg}{s}$;

$\dot{m}_{salt}$ - molten salt mass flow rate, $\frac{kg}{s}$;

p_1 - pressure in point 1, MPa;

p_2 - pressure in point 2, MPa;

p_3 - pressure in point 3, MPa;

t_1 - temperature in point 1, °C;

t_{salt} - temperature of the molten salt, °C;

t_{in} - temperature at the inlet of the collector, °C;

t_{out} - temperature at the outlet of the collector, °C;

t_{year} - number of sun hours in year, h;

t_{m} - number of sun hours in a month, h;

t_{add} – additional number of hours, h;

A - field aperture area, m^2;

E_{el} - annual electricity production, kWh;

I_s - direct normal solar irradiation, $\frac{W}{m^2}$;

N_{el} - gross electrical power, MW;

N_{iT} – internal power of the turbine, MW;

$\dot{Q}_{av}$- available solar heat flow rate, MW;

$\dot{Q}_{sf}$ - solar gain energy transfer rate, MW;

$\dot{Q}_g$ – heat transfer rate delivered to the steam generator , MW

$\dot{Q}_d$ - thermal power delivered to the steam cycle, MW;

$\dot{Q}_{year}$- annual average solar heat transfer rate, MW;

$\Delta\dot{Q}_s$- surplus of solar available heat transfer rate, MW;

Q_{stored}- stored heat, TJ

η_a - absorber efficiency, %;

η_{opt_PTC} – optical efficiency of the parabolic trough , %;

η_{opt_CRS} – optical efficiency of the central receiver system , %;

η_{iT} - internal turbine efficiency, %;

η_{mT} - mechanical turbine efficiency, %;

η_{sG} - steam generator efficiency, %;

η_{G} - electricity generator efficiency, %;

η_{ST} – efficiency of storage tank, %;

η_{stored} – efficiency with stored energy, %;

η_{eNomPT} -nominal efficiency of the parabolic trough system,%;

η_{eNomCR} - nominal efficiency of the central receiver system,%;

$\eta_{e\_year\_PT}$ - annual efficiency of the parabolic trough system,%;

$\eta_{e\_year\_CR}$ - annual efficiency of the central receiver system,%

Two different solar power plants are studied in this subsection. Both are using the same heat transfer fluid-molten salt: solution of 60% sodium nitrate ($NaNO_2$) and 40% potassium nitrate (KNO_3). Temperature and pressure in each point of the cycle are taken from real cases and for typical thermodynamic cycles using steam turbine. Turbine internal and mechanical efficiency again are taken from real cases. All values that were used to calculate the efficiency of both cycles are shown in table 4.1. It is assumed that temperature, pressure and efficiencies of each component does not change to produce electricity. The main factor that produces the desired power is the mass flow rate, obviously that much as the solar radiation allows to.

Table 4.1 Values for calculation

QUANTITY	VALUE	UNIT
c_{p_water} - water specific heat capacity	4.19	$\frac{kJ}{kg*K}$
c_{p_salt} - molten salt specific heat capacity	1.51	$\frac{kJ}{kg*K}$
p_1 - pressure in point 1	17	MPa
p_2 - pressure in point 2	0.01	MPa
p_3- pressure in point 3 - saturation	0.01	MPa
t_{in} - temperature at the inlet of the collector	300	°C
t_{out} - temperature at the outlet of the collector	550	°C
t_{salt} - temperature of the salt	425	°C
t_1 - temperature in point 1	530	°C
A - area	2500000	m^2
$\dot{Q}_{av}$- available solar radiation	29	MW
η_{opt_PTC} - optical efficiency of the PTC	75	%
η_{opt_CRS} - optical efficiency of the CRS	85	%
η_{iT} - internal turbine efficiency	80	%
η_{mT} - mechanical turbine efficiency	97	%
η_{G} - electricity generator efficiency	96	%
η_{ST} – storage tank efficiency	90	%
η_{sG} - steam generator efficiency	95	%

4.1 Parabolic trough solar power plant analysis

Scheme in figure 4.1 is showing the parabolic trough power plant. Values of points shown in red color are all presented in the table 4.1 except the point 4, which is the value of enthalpy which is equal to enthalpy in point 3 and will be calculated later in the project.

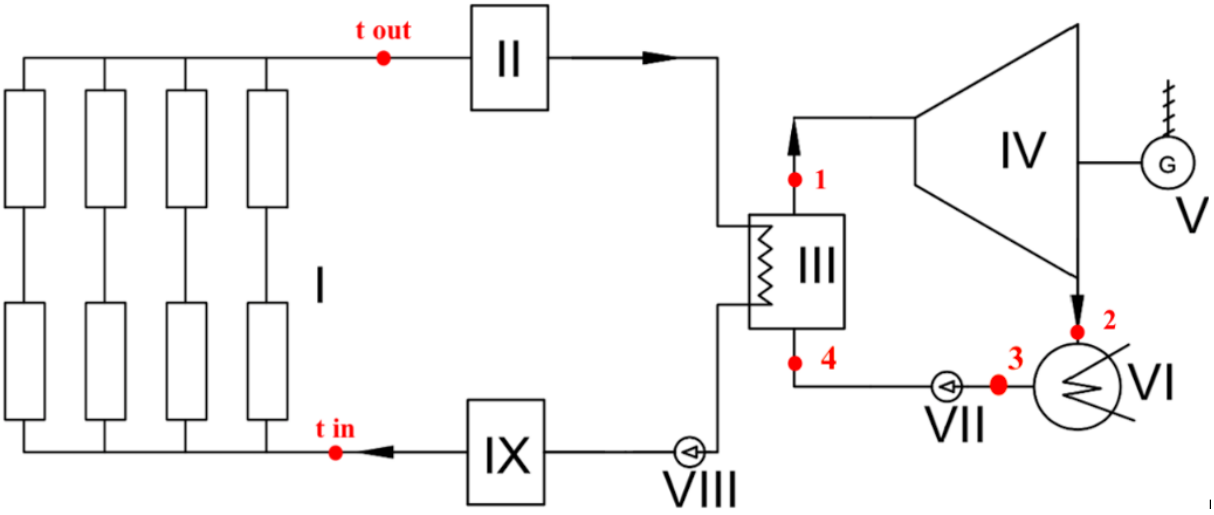

Figure 4.1 Scheme of parabolic trough power plant; I- parabolic trough solar field, II- heat transfer fluid hot tank, III- steam generator, IV- turbine, V- generator, VI- condenser, VII,VIII- pump, IX- heat transfer fluid cold tank

Firstly, the available power (4.1) for given solar field aperture area is calculated for each hour and then averaged to receive one value.

$$\dot{Q}_{av} = I_s * A \tag{4.1}$$
$$\dot{Q}_{av} = 116.016 * 250000 = 29003993.08\,W \approx 29\,MW$$

Secondly, knowing the field aperture area, hour by hour solar data and optical efficiency (which is the multiplication of mirror reflectivity, transmittivity of the glass, absorptivity of the absorber tube and interception factor) of the parabolic trough, the collected heat by the absorber tubes (4.2) is calculated.

$$\dot{Q}_{sf} = \dot{Q}_{av} * \eta_{opt} \tag{4.2}$$
$$\dot{Q}_{sf} = 29003993.08 * 0.75 = 21752994.81\,W = 21.75\,MW$$

Next point is to calculate the mass flow rate ($\dot{m}_{salt}$) (4.3). To get this value one have to have the specific heat of salt (c_{p_salt}), temperature at the inlet of the collector (t_{in}) and at the outlet of the collector (t_{out}) and collected heat by the tubes ($\dot{Q}_{sf}$).

$$\dot{m}_{salt} = \frac{\dot{Q}_{sf}}{c_{p\_salt} * (t_{out} - t_{in})} \tag{4.3}$$

$$\dot{m}_{salt} = \frac{21752994{,}81}{1516.1 * (550 - 300)} = 57.39\ \frac{kg}{s}$$

Additionally, the heat (4.4) which is delivered from the parabolic through field to the steam generator ($\dot{Q}_g$) is calculated. In this case, it is assumed that there are no losses to the environment in the transmission of heat thus the value will be similar to the (4.2) equation

$$\dot{Q}_g = \dot{m}_{salt} * c_{p_{salt}} * (t_{out} - t_{in}) \tag{4.4}$$
$$\dot{Q}_g = 57.39 * 1516.1 * (550 - 300) = 21.75\ MW$$

Then the heat delivered to the steam cycle ($\dot{Q}_d$)(4.5) knowing the efficiency of the steam generator (η_{sG}).

$$\dot{Q}_d = \dot{Q}_g * \eta_{sG} \tag{4.5}$$
$$\dot{Q}_d = 21752994.81 * 0.95 = 20665345\ W$$

Next, using the T-s diagram the enthalpies in point 1 and 2s are determined.

Enthalpy in point 1 – h_1 = 3372.88 $\frac{kJ}{kg}$
Enthalpy in point 2s – h_{2s} = 2020.00 $\frac{kJ}{kg}$
Using the formula for internal efficiency of the turbine (4.6), the enthalpy in point 2 is calculated (4.7).

$$\eta_{iT} = \frac{h_1 - h_2}{h_1 - h_{2s}} \tag{4.6}$$

$$h_2 = h_1 - \eta_{iT} * (h_1 - h_{2s}) \tag{4.7}$$
$$h_2 = 3372.88 - 0.8 * (3372.88 - 2020) = 2290.58\ \frac{kJ}{kg}$$

Calculation of the enthalpy in point 3 (h_3) knowing that in this point the pressure is the saturation pressure, so one can read this value from steam saturation tables.

Enthalpy in point 3- saturation (p=0.01 MPa) – h_3 =417.44 $\frac{kJ}{kg}$

Then knowing that in the pump is no increase of enthalpy since the compression work in pump two orders of magnitude lower than expansion work in turbine, one can say:

$$h_3 = h_4$$

Enthalpy in point 4 h_4 =417.44 $\frac{kJ}{kg}$

Afterward, the steam mass flow rate is calculated ($\dot{m}_{steam}$) (4.8) knowing the pressure (p_1) and temperature (t_1) of steam after the steam generator, so also knowing the specific enthalpy (h_1).

Other values that are known are the enthalpy in point 4 (h_4) and the heat delivered to the steam cycle ($\dot{Q}_d$).

$$\dot{m}_{steam} = \frac{\dot{Q}_d}{(h_1 - h_4)} \tag{4.8}$$

$$\dot{m}_{steam} = \frac{20665345}{(3372.88 - 417.44)} = 6.99\ \frac{kg}{s}$$

Later on in order to achieve the electrical power generated (N_{el}) the internal power of the turbine is calculated (N_{iT}) (4.9).

$$N_{iT} = \dot{m}_{steam} * (h_1 - h_2) \tag{4.9}$$
$$N_{iT} = 6.99 * (3372.88 - 2290.58) = 7567.79\ kW = 7.57\ MW$$

Finally, the electrical power of the turbine (N_{el}) (4.10) is calculated since the mechanical efficiency of the turbine (η_{mT}) and generator efficiency (η_G) is known.

$$N_{el} = N_{iT} * \eta_{mT} * \eta_G \tag{4.10}$$
$$N_{el} = 7567.79 * 0.97 * 0.96 = 7047.12\ kW = 7.05\ MW$$

The nominal efficiency of the parabolic trough system (η_{eNomPT}) is calculated (4.11).In general, it is the output divided by the input. In this case it is the electrical power generated (N_{el}) divided by the real available heat from sun ($\dot{Q}_{av}$).

$$\eta_{eNomPT} = \frac{N_{el}}{\dot{Q}_{av}} \tag{4.11}$$

$$\eta_{eNomPT} = \frac{7047127.96}{29003993.08} * 100\% = 24\ \%$$

The annual efficiency of the plant ($\eta_{e\_year\_PT}$)(4.12) depends on the annual production of electricity and on the atmospheric conditions that affect the amount of solar radiation falling on the mirror.

$$\eta_{e\_yearPT} = \frac{N_{el} * t_{year}}{\dot{Q}_{year}} \tag{4.12}$$

t_{year} (4.13) value is the value taken from table 3.2

$$t_{year} = \sum_{m=1}^{12} t_m = 4394\ h \tag{4.13}$$

$\dot{Q}_{year}$ value (4.14) was calculated taking into account the table 3.1, number of days in a year and the solar field aperture (*A*).

$$\dot{Q}_{year} = A * I_s * 365 \tag{4.14}$$
$$\dot{Q}_{year} = 250000 * 2.78 * 365 = 254054655\ kWh = 254.05\ GWh$$

Finally, the equation number (4.12) is used which is written above and calculation of the annual efficiency of the parabolic trough solar power plant is done.

$$\eta_{e\_yearPT} = \frac{7.05 * 4394}{254.05 * 10^3} * 100\% = 12\ \%$$

4.2 Central receiver solar power plant analysis

Scheme in figure 4.2 is showing the central receiver solar power plant. All values of points shown in red color are all presented in the table 4.1 except the point 4, which is the value of enthalpy which is equal to enthalpy in point 3 and is calculated later in the project.

First of all, the determination of the available power, the formula (4.1) was used. It is calculated for given solar field aperture area for each hour and then averaged to receive one value. The value is the same as in the case of parabolic trough power plant.

$$\dot{Q}_{av} = 116.016 * 250000 = 29003993.08\ W\ \approx 29\ MW$$

Secondly, knowing the value above and optical efficiency of central receiving system (η_{opt_CRS}) (which is the multiplication of mirror reflectivity, transmittivity of the glass, absorptivity of the absorber tube and interception factor) of the central receiver , the collected heat by the absorber tubes ($\dot{Q}_{sf}$) is calculated by using the equation-(4.2).

$$\dot{Q}_{sf} = 29003993.08 * 0.85 = 24653394.81\ W = 24.65\ MW$$

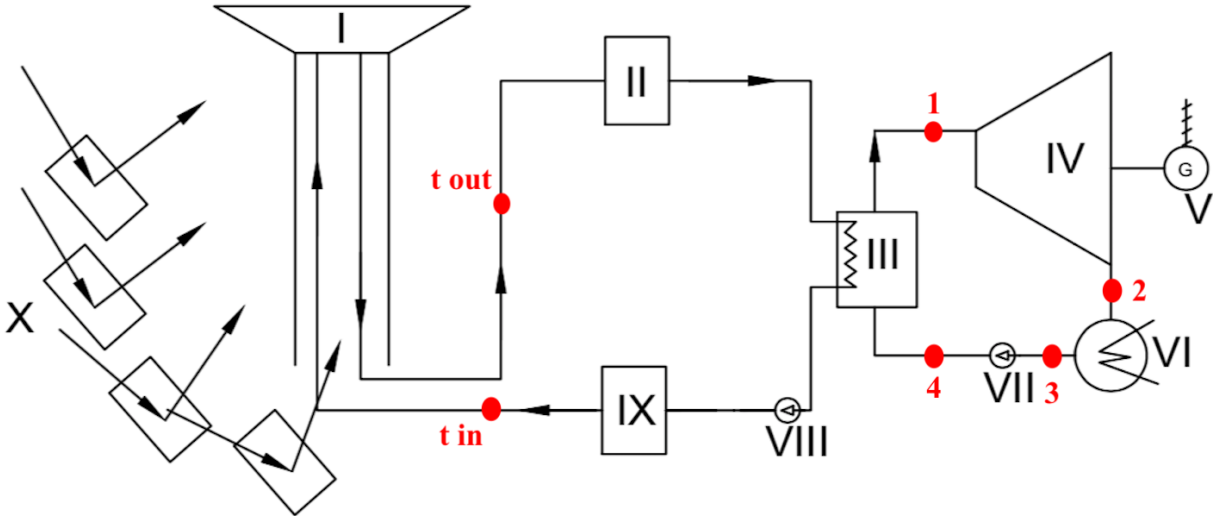

Figure 4.2 Central receiving solar power plant I- solar tower- absorber, II- heat transfer fluid hot tank, III- steam generator, IV- turbine, V- generator, VI- condenser, VII,VIII- pump, X- heat transfer fluid cold tank, X- heliostat field

Then the mass flow rate ($\dot{m}_{salt}$) is calculated using equation- (4.3). To get this value one have to have the specific heat of salt (c_{p_salt}), temperature at the inlet of the collector (t_{in}) and at the outlet of the collector (t_{out}) and collected heat by the absorber ($\dot{Q}_{sf}$).

$$\dot{m}_{salt} = \frac{24653394.81}{1516.1 * (550 - 300)} = 65.04\ \frac{kg}{s}$$

The heat from equation- (4.4) which is delivered from the central receiver field to the steam generator ($\dot{Q}_g$) is calculated. In my case, I have assumed that there are no losses to the environment in the transmission of heat thus the value will be similar to the ($\dot{Q}_{sf}$).

$$\dot{Q}_g = 65.04 * 1516.1 * (550 - 300) = 24.65\ MW$$

Then the heat delivered to the steam cycle ($\dot{Q}_d$) using equation- (4.5) knowing the efficiency of the steam generator (η_{sG}).

$$\dot{Q}_d = 24653394.81 * 0.95 = 23420724\ W = 23.42\ MW$$

Next, the enthalpies are determined, and are the same as in the case of parabolic trough solar power plant are taken from table 4.2. [10]

Enthalpy in point 1 – h_1 = 3372.88 $\frac{kJ}{kg}$

Enthalpy in point 2s – h_{2s} = 2020.00 $\frac{kJ}{kg}$

Enthalpy in point 2 from the equation (4.7)

$$h_2 = 2290.58\ \frac{kJ}{kg}$$

Calculation of the enthalpy in point 3 (h_3) knowing that in this point the pressure is the saturation pressure, value is taken from table 4.3. Plus the calculation of enthalpy in point 4 (h_4) which is the same as in point 3 (h_3)

Enthalpy in point 3 – h_3 = $417.44\,\frac{kJ}{kg}$

Enthalpy in point 4 – h_4= $417.44\,\frac{kJ}{kg}$

The steam mass flow rate is calculated ($\dot{m}_{steam}$) using formula- (4.8) knowing the pressure (p_1) and temperature (t_1)- (table 4.1) of steam after the steam generator, so also knowing the specific enthalpy (h_1). Other values that are known are the enthalpy in point 4 (h_4) and the heat delivered to the steam cycle ($\dot{Q}_d$).

$$\dot{m}_{steam} = \frac{23420724}{(3372.88 - 417.44)} = 7.92\ \frac{kg}{s}$$

Later on, in order to achieve the electrical power generated (N_{el}) the internal power of the turbine is calculated (N_{iT}) using the equation (4.9).

$$N_{iT} = 7.92 * (3372.88 - 2290.58) = 8576.83\ kW = 8.58\ MW$$

Lastly, the electrical power of the turbine (N_{el}) using the -(4.10) equation is calculated since the mechanical efficiency of the turbine (η_{mT}) and generator efficiency (η_G) is known.

$$N_{el} = 8576.83 * 0.97 * 0.96 = 7986.75\ kW = 7.99\ MW$$

The nominal efficiency of the central receiver system (η_{eNomCR}) is calculated just like the equation- (4.11) which is the . It is the electrical power generated (N_{el}) divided by the real available heat from sun ($\dot{Q}_{av}$).

$$\eta_{eNomPT} = \frac{7986745.02}{29003993.08} * 100\% = 28\ \%$$

The annual efficiency of the central receiving plant ($\eta_{e\_year\_CR}$) shows the formula (4.12) depends on the annual production of electricity and on the atmospheric conditions that affect the amount of solar radiation falling on the mirror. (t_{year}) is equal just like in the parabolic trough power plant so 4394 h. The annual available heat is the same like in (4.14)

$$\eta_{e\_yearPT} = \frac{7.98 * 4394}{254.05 * 10^3} * 100\% = 14\ \%$$

5. Conclusions

Even though Poland is not one of the main countries in the production of energy from renewable energy sources, has relatively not bad solar conditions. The sun is the basic source of free energy and does not make any harmful damages to the environment. That is why the production of energy from solar radiation becomes more and more popular. In the analysis carried out, comparing a solar power plant with a central absorber to the solar power plant with a linear absorber the efficiencies were found. The central receiving system yielded an efficiency at the level of 28%, and the parabolic trough solar power plant at the level of 24%. Those values are for the averaged hour by hour solar data. The power output for both system was also different, the parabolic trough produced 7.05 MW of electricity and the central receiving system generated 7.99 MW. Another very important parameter is the annual efficiency, probably the most reliable value in order to compare both technologies. The annual efficiency for central receiving system equals 14%, and for the parabolic trough system it is equal to 12 %. This efficiencies are significantly lower than previous ones, because it is affected by the weather conditions, the demand and production of electricity. It should be noted here that, this is due to the insufficient amount of solar heat in the fall and winter months. On the other hand, during the summer months, the Sun is able to provide much more energy than it is needed for the work.

References

[1] Lewandowski W. M., Proekologiczne źródła energii, Warszawa: WNT, 2007.

[2] Cieśliński J., Mikielewicz J., Niekonwencjonalne źródła energii, Gdańsk: Politechnika Gdańska, 1996.

[3] Szargut J., Ziębik A., Podstawy Energetyki Cieplnej, Warszawa: Wydawnictwo Naukowe PWN, 1998.

[4] Chmielniak T., Technologie Energetyczne, Gliwice: Wydawnictwo Politechniki Śląskiej, 2004.

[5] Google maps, https://www.google.com/maps/place/, date of access (11/11/2019)

[6] Steam tables, https://www.steamtablesonline.com, date of access (11/11/2019)

Sequestration of CO_2 in coal deposits case of Poland - modeling by thermodynamic model

Grzegorz S. Jodłowski[1], Marta Wójcik[2]

[1]AGH University of Science and Technology, Faculty of Energy and Fuels, Krakow, Poland, e-mail:jodlowsk@agh.edu.pl
[2]AGH University of Science and Technology, Faculty of Energy and Fuels, Krakow, Poland, e-mail:mwojcik@agh.edu.pl

Abstract

Based on the measurement data of sorption isotherms on coal samples, the sorption capacity was estimated using the Multiple Sorption Model. Then, based on *ex-situ* research, the sequestration capacity of coals in the field of Polish resources of this raw material was estimated with the use of literature data, taking into account only unexploited deposits. The theoretical sequestration capacity of all balance, but not mining deposits was estimated at 200 billion tons of CO_2, which will cover demand for many years of storage. At the same time, it was found that this theoretical value would be severely limited due to the actual conditions of the deposits and the technical possibilities of injecting this gas.

Keywords: greenhouse gases, sequestration, coal, sorption modeling

1. Introduction

As climate change is a major problem meet by the civilization, scientist and engineers search the method to mitigate the one of main cause of the greenhouse effect – emission of CO_2. Many works were done till now to fit this need, starting from increase of process effectiveness in main branches (power, steel or cement production or transportation), development of less CO2 emission technologies to CCS methods. The methodology of carbon dioxide capture and sequestration is mature in oil industry, till it is used from decades for separation of CO2 from natural gas and its injection to exhausted shale with simultaneous enhanced oil recovery (EOR)[1]–[5]. Technology is adopted to power industry and is continuously developed on the step of CO2 separation, compression and transport. Main way for the gas sequestration is geologic storage in: porous rock structure or geosynclines under insulating cap rock, underground saline water levels and in porous organic deposits, which are with weak exploration potential. Last geologic structure involves coal bed in closed coal mines, unused deep coal seems with no commercial meaning.

Coal is a porous substance with organic origin transformed in geochemical conditions and in the geologic time-scale. Coal matter is very complex mixture of different organic compounds resulting in partially rigid and partially elastic structure. Another property of this geologic form is presence of texture in many levels – nano, micro or macro porous system in so called coal bricks and butt-cleat composition in extra-macro scale. Butt-cleat formation of coal substance cause presence of transport channels for gases and liquids (especially water in shallow levels). Such a complicated structure of coal gives possibility to continuous and stable storage of gas in the sorption way. Many authors publish their works within this subject trying to understand the process and fitting the idea to possible technology[6]–[23]. Simultaneously it appear that injection of CO2 to coal bed induce the methane production which increases the economic efficiency of the technology [10], [18], [24], [25].

The aim of the work is research the CO2 sorption capacity by the use of numerical modeling of sorption process in hard coal samples (ex situ method). Consecutively, results of modeling are transformed to the field conditions. Multiple Sorption Model elaborated by the team is applied to the analysis of sorption capacity.

2. Copolymeric coal structure

Coal is a complicated organic copolymer substance formed as a result of geochemical changes. Its genesis also causes the occurrence of a mineral substance which sorption properties are negligible compared to those of a carbonaceous substance. From the point of view of sorption modeling, the components of carbon mass were divided into groups called components (Fig. 1):

- arene domains - quasi-crystalline deposits made of joined plates containing condensed benzene rings: their size, structure and molar content depend on the degree of transformation of the carbonaceous substance - these parameters remain in an increase relation to the degree of carbonization;
- crosslinked chains - aliphatic, alicyclic and heterocyclic compounds: their molar partition also increases in relation to the degree of carbonization;
- noncrosslinked chains - aliphatic, alicyclic and heterocyclic compounds with a molar partition decreasing along with the increase of carbonization of the carbonaceous substance;
- pores (especially submicropores or nanopores): holes in the carbonaceous material constituting sorption centers for sorbate particles;
- mineral admixtures: deposits derived from admixing a sedimentation basin by natural minerals.

The first two components constitute the macromolecular network of coal, constituting a limitedly rigid structure covering the entire volume of coal mass. The displacement of macromolecular phase objects is associated with overcoming large cohesion forces, and therefore requires a lot of energy. The third component is an elastic molecular phase whose objects can move inside the macromolecular network under certain conditions. The energy necessary to overcome the cohesion forces of the molecular phase is definitely smaller. The pores present in the carbonaceous substance are high-energy contacts for sorbate particles (especially submicropores - holes comparable with the size of the sorbate molecule, sometimes called nanopores in the point of view of their real size).

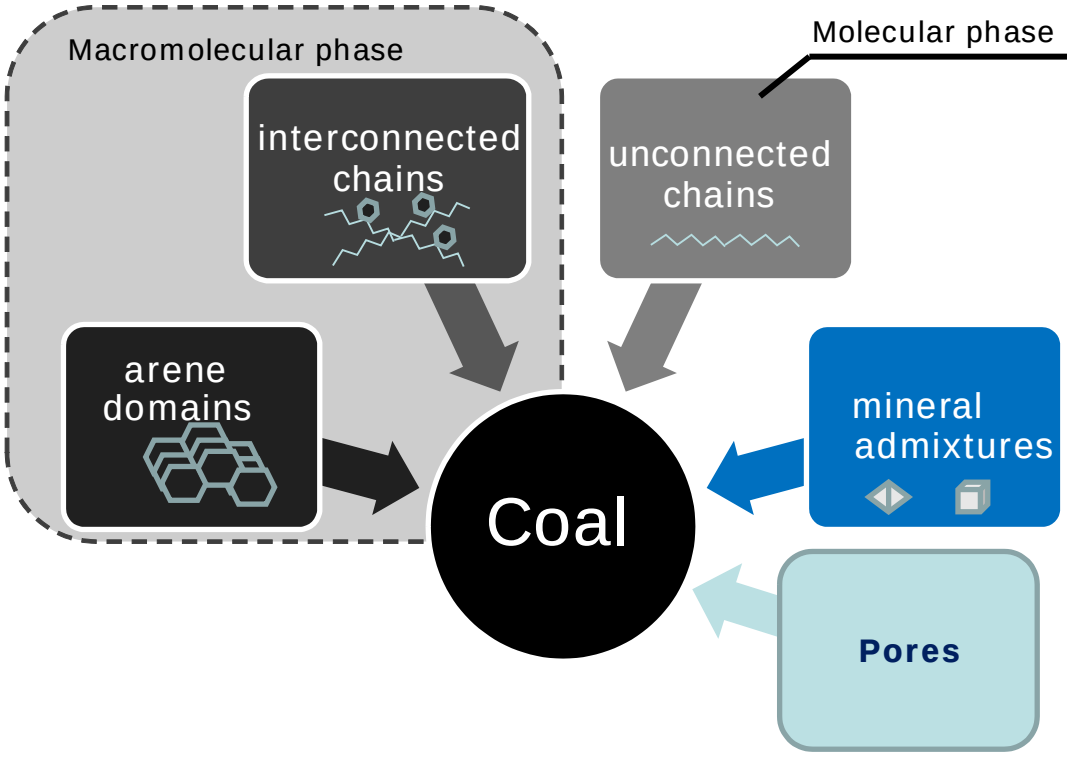

Fig. 2.1. Components of coal structure accordingly to Multiple Sorption Model

3. Multiple Sorption Model (MSM)

Described in chapter 2 copolimeric structure of coal results in the composition of model describing thermodynamic dependences taking part in the process of gas molecule location in the system. Presence of both: rigid macromolecular phase and elastic macromolecular phase cause co-existence of several phenomena like adsorption, expansion of pores, contraction of pores and absorption. Adsorption is a surface phenomenon involving adhesion forces while absorption is a bulk sub-process in which molecules need to introduce the energy necessary to producing of free volume not present earlier in coal matter and it happens in the cost of cohesion forces. Expansion and contraction of pores are contradictory processes mixing cohesion-adhesion forces to widen the submicropores filled with molecules of a gas or to shrink empty pores in their neighborhood. Such a properties of sorption system result in set of model formulas based on the Flory Polymer Solution Theory [26]. Model take into account sets of parameters like structural (partition of arene domains, crosslinked and noncrosslinked chains, partition of pores divided in group micropores and bigger pores), energetic (cohesion energy density of coal and penetrant, solubility parameter of coal [27], parameter of adsorption energy, parameter of absorption energy). The set of distributions is calculated under simulation experiment, i.e. pore volume (before location of gas), pore capacity (after location of gas), energy correction parameter (introducing non-ideal contact of penetrant molecules to coal components surface) and finally energy distribution. System is *a priori* divided to 11 subsystems (absorption, 9 for expansion and adsorption) giving poly-sorption isotherms and after summarizing it effects in isotherms of total sorption, adsorption (mono and polylayer), expansion and absorption as multisorption set of isotherms (Fig 3.1). [13], [28]–[30]

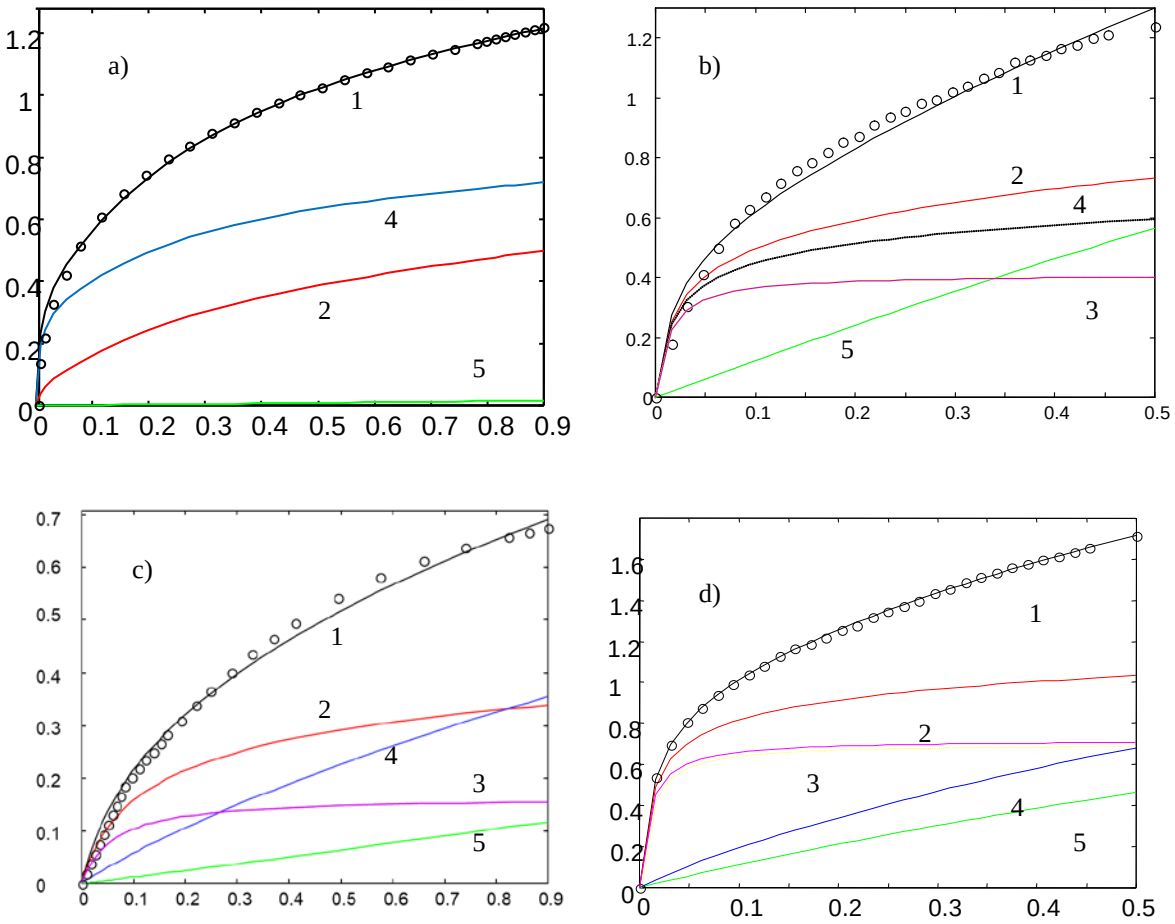

Fig. 3.1. Multi-isotherms of CO_2 sorption in different types of coal; a) lignite, b) sub-bituminous, c) bituminous, d) anthracite; circles - measured sorption isotherm, lines: 1 - total sorption, 2 - polylayer adsorption, 3 - monolayer adsorption, 4 - expansion, 5 - absorption; y-axis - a [mmol/g], x-axis - p/p_0.

It should be remembered that the process of gas sorption in coal is complex and the location of molecules in specific places is accompanied by their flow both in transport channels and in mass in the form of absorption, as a result of which gas molecules move throughout the entire coal deposit over the elastic part of the carbonaceous substance. These properties result in the need to consider all sorption sub-processes in the calculation of the sequestration capacity.

4. Samples of coal

Ten samples of coal from Polish collieries are taken into investigation. Characteristic of samples is presented in Table 4.1

Table. 4.1. Proximate analysis of coal samples

Sample →		**Be**	**Tu1**	**Tu2**	**Br**	**B82**	**A-K**	**Th**	**Vi**	**Wa**	**M85**
		Lignites			Sub-bitumin		Bituminous			Anthracites	
C^{daf}	%	65.9	70.2	75.9	79.6	80.88	86.4	86.4	87.6	89.1	92.41
V^{daf}	%	57.39	54.06	54.04	40.9	40.8	29.2	27.2	27.9	16.4	6.09
A^{a}	%	3.8	n.a.	12.3	15.5	2.48	6.15	7.89	7.78	8.92	3.7
W^{a}	%	21.1	8.3	8.3	1.65	3.76	1.55	1.13	1.25	0.9	0.81

C^{daf} - content of coal in dry and ash free sample, V^{daf}- volatile mater content in dry and ash free sample, A^{a} - ash content in analytical state of sample, W^{a} - humidity content in analytical state of sample

Selected coal samples covers the range of coal from lignite up to anthracite and are representative to Polish coal deposits. However sorption of CO_2 is possible in all types of coal but shallow deposits like lignites are less suitable for carbon dioxide sequestration because of weak layer of cap rock. This situation results in high-possible gas escape from the storage facility. Figure 4.1 schematically present the situation.

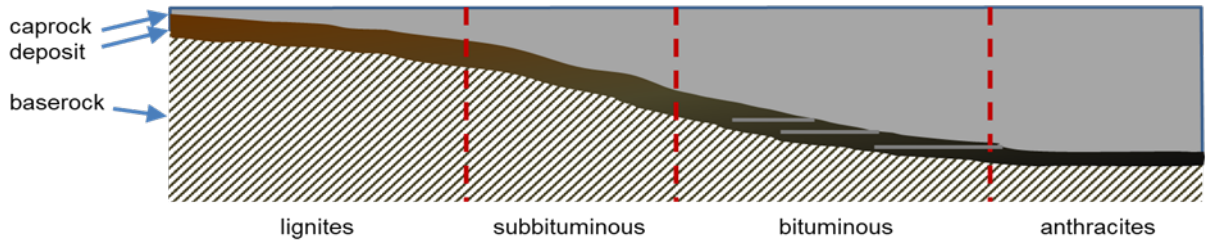

Fig. 4.1. Schematic presentation of coal deposit location in Poland

Together with so-called maturity of coal the depth of deposit increase. Lignite has a shallow bed with thin layer of over burden and possibility of gas leakage, sub-bituminous coal lays deeper and possibility of stable storage is bigger. The better situation is observed for bituminous coals which are located in large depth hundreds of meters but in some cases layers of coal are in direct contact with surface due to the tectonic activity in the past. So, the most suitable for CO_2 storage are deposits of sub-bituminous coals. Unfortunately, most of them are heavily exploited and only the levels under 800 m are possible for sequestration or deeper. This levels of coal are defined as non-technical or non-economical for exploration.

5. Sequestration capacity calculations

Firstly, the total sorption capacity of coal samples is calculated from the MSM model. One could understand that molecules of a gas permeate through coal deposit and find pores in distant part of deposit by the migration commonly by the butt-cleat structure and penetrative (absorption) way. Some investigations shows that butt-cleat structure squeeze and stop the flow of CO_2 after several days, as a result of coal matter swelling [11]. There are still place for the flow of gas molecules but in the penetration/absorption way which is significantly slower.

Molecules are located in coal in every stated earlier way (adsorption, expansion and absorption) in the coal mass. Sorption capacity evaluated by the application of MSM in the average pressure 3,4 MPa is used for calculation of sequestration capacity. Selection of such a pressure is an effect of achievable results for sorption isotherms measurements.

Information about available non-technological coal resources was taken from the publication [31]–[33].

Values given from MSM in moles per gram of coal are recalculated with using of data from [29] and [30] to obtain the total sequestration capacities for different types of coal. Results of calculations are presented in the Table 5.1 and on Figure 5.2.

Table 5.1. Resources of coal possible for sequestration and sequestration capacity

Coal Type	Accesible for sequestration*	Theoretic sorption	Total capacity
	Gg	mmol/g	Gg
Lignites	14 200	0,0963	60 168,2
31-33	3 416 555	0,754	113 347 628,7
34	664 322	0,93	27 184 056,2
35	1 095 284	1,18	56 867 145,3
36-38	164 461	0,875	6 331 748,5
41-42	145	0,815	5 199,7
Total →			203 795 946,6

This rough estimation shows the possibility of placing in off-balance deposits over 200 milions of tonnes of CO_2. Certainly, one should evaluate the real possibility of the gas injection. This number means the total theoretical capacity and probably would be decreased by the real technical possibility of gas injection and storage. Situation is presented in the chart (Fig 5.1) as the pyramid of potential-cost balance.

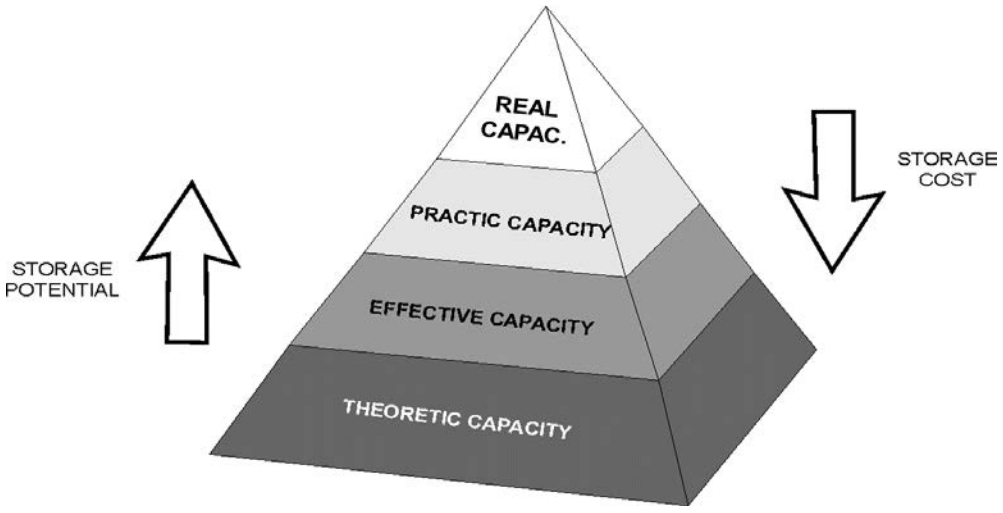

Fig 5.1 Effect of technology cost on the possibility of realization

The best storage potential is related to the smaller amount of gas introduced to the geologic structure. Increasing the amount of gas stored in the coal deposit is connected to the increasing cost of technology.

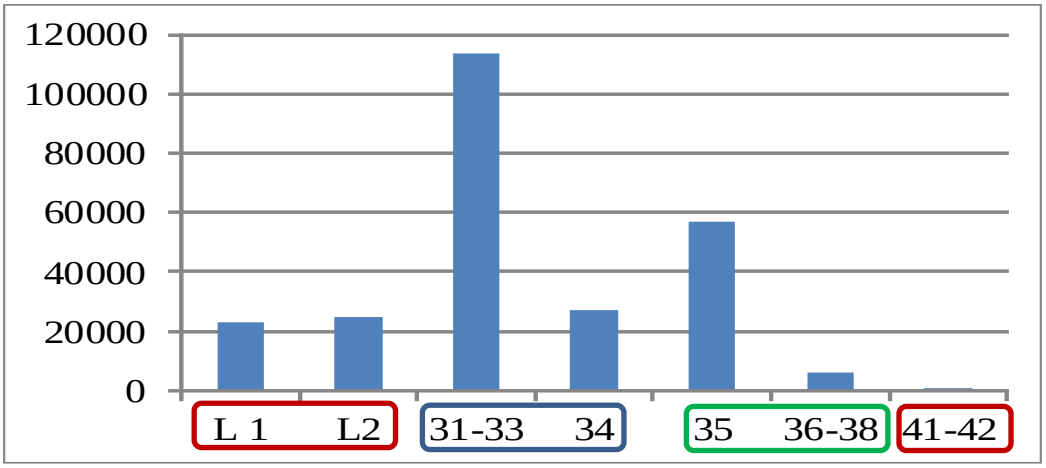

Fig. 5.2. Possible, theoretic amount of CO_2 storage in different types of coal in Polish resources

Lignites are generally less suitable for sequestration from the reason stated earlier (Fig 5.2). Sub-bituminous coal types 31 - 34 (accordingly to Polish national coal classification) are suitable conditional because of extensive exploration of this resources for power production purpose. Samples of bituminous coals types 35-38 comes from mines which are recently closed and could be involved to the sequestration methodology. Last class of coals - anthracites are meaningless because of very small amount off such coal types in Poland.

Another problem is the assumption of relatively low gas pressure which is injected to the coal bed. Most of acquired data on the accessible coal for sequestration proof that depth of sequestration exceeds 800 m. In bed conditions it means overcritical conditions in which carbon dioxide forms overcritical fluid with nearly constant density (Fig. 5.3). If one assume the density of gaseous CO_2 on the surface as 100% than it could be obtained that volume of the same gas at 800 m is 0.32 % and density is about 700 kg/m^3. This property of the gas in one hand gives possibility to increase sequestration capacity, in second hand this state of gas could cause appearance of reactions with coal matter with changing of its properties as well as properties of surrounding strata[34], [35]. These issues demand further investigations.

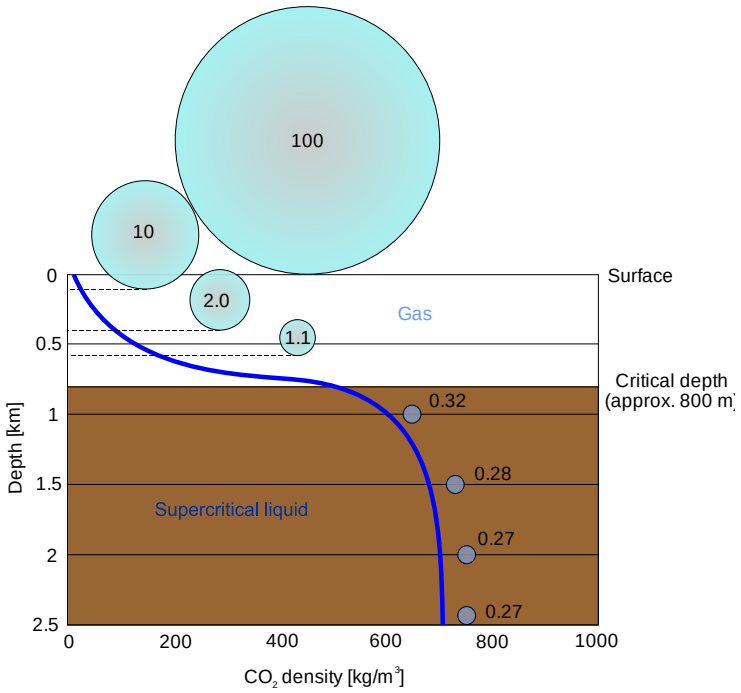

Fig. 5.3. Schematic presentation of changes of CO_2 volume with increasing pressure at different depth of cap rock.

6. Conclusions

Approach connecting ex-site modeling of sorption isotherms of CO_2 gives possibility to evaluate the theoretical sorption capacity in different way than ECBM-CO_2 methodology [10], [36], [37]. Preliminary works lets to state the possibility of long term storage of CO_2 in the coal deposits recognized in Poland (Fig. 6.1)

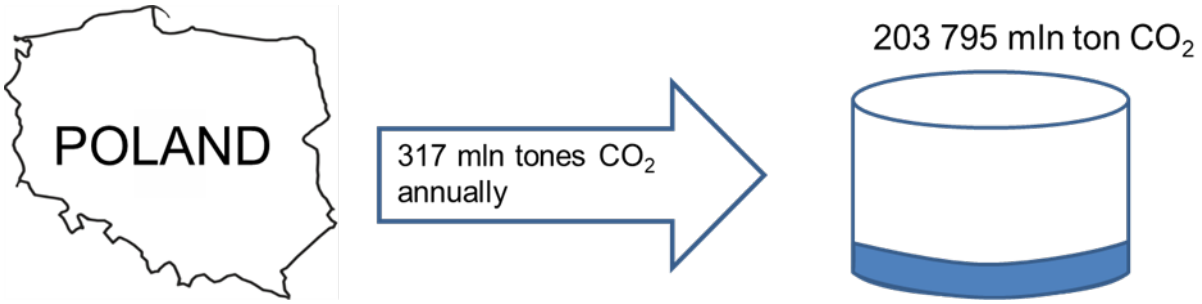

Fig. 6.1. The scheme of CO_2 sequestration process in Poland. Data on CO_2 emission are acquired from Eurostat.

There is possibility to accumulate about 600 years of CO_2 production from industrial burning of fuels (theoretically) in all types of coal and about 190 years of CO_2 production in bituminous coal (theoretically). Certainly, these numbers are overestimated in the technical point of view but it gives the picture of possible solution for problem of greenhouse effect by the CCS techniques. Every location should be evaluated separately for this purpose, not only in the point of view of theoretic capacity but especially in the direction of sealing of the gas. Problem of CO_2 sequestration in coal deposits should be further studied in the purpose of accurate forecast.

Acknowledgment

Investigations are made under financial support of AGH University of Science and Technology scientific subvention No. 16.16.210.476.

References

[1] Gozalpour F., Ren S. R., and Tohidi B., "CO2 EOR and storage in oil reservoirs," *Oil and Gas Science and Technology*. 2005, doi: 10.2516/ogst:2005036.

[2] Wall W., "OPTIMIZATION OF CO2 STORAGE IN CO2 ENHANCED OIL RECOVERY," 2010.

[3] Godec M., Kuuskraa V., Van Leeuwen T., Melzer L. S., and Wildgust N., "CO2 storage in depleted oil fields: The worldwide potential for carbon dioxide enhanced oil recovery," in *Energy Procedia*, 2011, doi: 10.1016/j.egypro.2011.02.102.

[4] Kokal S. and Al-Kaabi A., "Enhanced oil recovery: challenges and opportunities," *Glob. Energy Solut.*, 2010.

[5] Muggeridge A. *et al.*, "Recovery rates, enhanced oil recovery and technological limits," *Philosophical Transactions of the Royal Society A: Mathematical, Physical and Engineering Sciences*. 2014, doi: 10.1098/rsta.2012.0320.

[6] Tang Y., Yang R., and Bian X., "A review of CO2 sequestration projects and application in China," *Scientific World Journal*. 2014, doi: 10.1155/2014/381854.

[7] Liu C. J., Wang G. X., Sang S. X., and Rudolph V., "Changes in pore structure of anthracite coal associated with CO2 sequestration process," *Fuel*, 2010, doi: 10.1016/j.fuel.2010.03.032.

[8] Lal R., "Sequestration of atmospheric CO2 in global carbon pools," *Energy Environ. Sci.*, 2008, doi: 10.1039/b809492f.

[9] Mac Dowell N., Fennell P. S., Shah N., and Maitland G. C., "The role of CO2 capture and utilization in mitigating climate change," *Nature Climate Change*. 2017, doi: 10.1038/nclimate3231.

[10] White C. M. *et al.*, "Sequestration of carbon dioxide in coal with enhanced coalbed methane recovery - A review," *Energy and Fuels*. 2005, doi: 10.1021/ef040047w.

[11] Siriwardane H., Haljasmaa I., McLendon R., Irdi G., Soong Y., and Bromhal G., "Influence of carbon dioxide on coal permeability determined by pressure transient methods," *Int. J. Coal Geol.*, 2009, doi: 10.1016/j.coal.2008.08.006.

[12] Baran P., Jodlowski G. S., and Zarebska K., "Sorption of CO<inf>2</inf> in lignites from Polish coal mines: measurements and thermodynamic analysis," *Adsorption*, vol. 22, no. 4–6, 2016, doi: 10.1007/s10450-016-9789-6.

[13] Jodłowski G., Florencka N., Vogt E. B., Wójcik M., and Ziółkowska M., "Application of multiple sorption model to estimation of CO<inf>2</inf> sequestration capacity or CH<inf>4</inf> recovery in polish hard coals," in *E3S Web of Conferences*, 2017, vol. 14, doi: 10.1051/e3sconf/20171402028.

[14] Ceglarska-Stefańska G., and Zarebska K., "Sorption of carbon dioxide-methane mixtures," *Int. J. Coal Geol.*, 2005, doi: 10.1016/j.coal.2005.01.003.

[15] Baran P., Cygankiewicz J., and Zarębska K., "Carbon dioxide sorption on polish ortholignite coal in low and elevated pressure," *J. CO2 Util.*, 2013, doi: 10.1016/j.jcou.2013.09.003.

[16] Mack J. and Endemann B., "Making carbon dioxide sequestration feasible: Toward federal regulation of CO2 sequestration pipelines," *Energy Policy*, 2010, doi: 10.1016/j.enpol.2009.10.018.

[17] Folger P., "Carbon capture and sequestration: Research, developement, and demonstration at the U.S. Department of Energy," 2014.

[18] Prabu V. and Mallick N., "Coalbed methane with CO2 sequestration: An emerging clean coal technology in India," *Renewable and Sustainable Energy Reviews*. 2015, doi: 10.1016/j.rser.2015.05.010.

[19] Boot-Handford M. E. *et al.*, "Carbon capture and storage update," *Energy and Environmental Science*. 2014, doi: 10.1039/c3ee42350f.

[20] Vishal V., Ranjith P. G., and Singh T. N., "CO2 permeability of Indian bituminous coals: Implications for carbon sequestration," *Int. J. Coal Geol.*, 2013, doi: 10.1016/j.coal.2012.11.003.

[21] Miller B. G., *Clean Coal Engineering Technology*. 2011.

[22] Haljasmaa I. V., *et al.*, "North Dakota lignite and Pittsburgh bituminous coal: A comparative analysis in application to CO2 sequestration," *Int. J. Oil, Gas Coal Technol.*, 2011, doi: 10.1504/IJOGCT.2011.040839.

[23] Santarosa C. S., *et al.*, "CO2 sequestration potential of Charqueadas coal field in Brazil," *Int. J. Coal Geol.*, 2013, doi: 10.1016/j.coal.2013.01.005.

[24] Gentzis T., "Economic coalbed methane production in the Canadian Foothills: Solving the puzzle," *Int. J. Coal Geol.*, 2006, doi: 10.1016/j.coal.2005.04.017.

[25] Gentzis T., "Subsurface sequestration of carbon dioxide - an overview from an Alberta (Canada) perspective," in *International Journal of Coal Geology*, 2000, doi: 10.1016/S0166-5162(99)00064-6.

[26] Flory P. J., and Krigbaum W. R., "Thermodynamics of High Polymer Solutions," *Annu. Rev. Phys. Chem.*, 1951, doi: 10.1146/annurev.pc.02.100151.002123.

[27] Lindvig T., Michelsen M. L., and Kontogeorgis G. M., "A Flory-Huggins model based on the Hansen solubility parameters," *Fluid Phase Equilib.*, 2002, doi: 10.1016/S0378-3812(02)00184-X.

[28] J. Milewska-Duda, J. T. Duda, G. Jodłowski, and M. Kwiatkowski, "Model for multilayer adsorption of small molecules in microporous materials," *Langmuir*, vol. 16, no. 18, 2000, doi: 10.1021/la000027w.

[29] G. S. Jodlowski, P. Baran, M. Wójcik, A. Nodzenski, S. Porada, and J. Milewska-Duda, "Sorption of methane and carbon dioxide mixtures in Polish hard coals considered in terms of adsorption-absorption model," *Appl. Surf. Sci.*, vol. 253, no. 13 SPEC. ISS., pp. 5732–5735, 2007, doi: 10.1016/j.apsusc.2006.12.058.

[30] Jodłowski G. and Wójcik M., "Comparative analysis of sorption of small molecule hydrocarbons and polar substances in polish hard coals," *Adsorption*, vol. 19, no. 2–4, 2013, doi: 10.1007/s10450-013-9523-6.

[31] Olkuski T., "Analysis of Domestic Reserves of Steam Coal in the Light of its Use in Power Industry," *Gospod. Surowcami Miner. - Miner. Resour. Manag.*, 2013, doi: 10.2478/gospo-2013-0023.

[32] Paszcza H., "Ocena stanu zasobów węgla kamiennego w Polsce z uwzględnieniem parametrów jakościowych i warunków zalegania w aspekcie zapewnienia bezpieczeństwa energetycznego kraju," *Zesz. Nauk. Inst. Gospod. Surowcami Miner. i Energią PAN*, vol. 83, pp. 147–162, 2012.

[33] Naworyta W., "Analiza dostępności zasobów w polskich złożach węgla brunatnego ze względu na ochronę przyrody i zagospodarowanie powierzchni terenu.," *Zesz. Nauk. IGSMiE PAN*, vol. 95, pp. 23–34, 2016.

[34] Middleton R. S., *et al.*, "Shale gas and non-aqueous fracturing fluids: Opportunities and challenges for supercritical CO2," *Appl. Energy*, 2015, doi: 10.1016/j.apenergy.2015.03.023.

[35] Cole D. R., Chialvo A. A., Rother G., Vlcek L., and Cummings P. T., "Supercritical fluid behavior at nanoscale interfaces: Implications for CO2 sequestration in geologic formations," in *Philosophical Magazine*, 2010, doi: 10.1080/14786430903559458.

[36] Busch A., and Gensterblum Y., "CBM and CO2-ECBM related sorption processes in coal: A review," *International Journal of Coal Geology*. 2011, doi: 10.1016/j.coal.2011.04.011.

[37] Yu H., Zhou G., Fan W., and Ye J., "Predicted CO2 enhanced coalbed methane recovery and CO2 sequestration in China," *Int. J. Coal Geol.*, 2007, doi: 10.1016/j.coal.2006.10.002.

Review of the Carnot Battery Technology: Concepts and Applications

Ruiz Amantegui Jorge[1], Andreoletti Matteo [2], Banini Massimiliano [3]

[1]Faculty of Energy and Environmental Engineering, SUT University, e-mail: jorgeamantegi@gmail.com
[2]Faculty of Energy and Environmental Engineering, SUT University, e-mail: m.andreoletti004@studenti.unibs.it
[3]Faculty of Energy and Environmental Engineering, SUT University, e-mail: massimiliano.banini@yahoo.it

Abstract

The increasing use of renewable energy technologies for electricity generation, many of which have an unpredictably intermittent nature, will inevitably lead to a greater need for electricity storage. Although there are many existing and emerging storage technologies, most have limitations in terms of geographical constraints, high capital cost or low cycle life, and few are of sufficient scale (in terms of both power and storage capacity) for integration at the transmission and distribution levels.

This paper presents Carnot Batteries, that want to resolve these problems: using an electric heater, we can convert power to heat, store it and then (when we want to discharge) pass it through a conversion cycle, converting it to power again. Principles, performance parameters and implementations of this technology will be showed in this review.

This article will show the great potential we have inserting this system in small applications, but also in huge thermal plants, resolving geographical limitations, with low capital cost and long cycle life

Keywords: Carnot Battery, PTES, Pumped thermal Energy Storage

1. Introduction

Many countries worldwide turn to the exploitation and utilization of renewable energy because of severe environmental problems caused by the use of fossil fuels. It is predicted that renewable energy will account for 29% of total power generation in 2040[1]. However, because of intermittence, fluctuation and other uncertainties, renewable power generation faces with challenges of reliability and stability. [2]

Since the power grid cannot store electricity by itself, this has led to the development of Electrical Energy Storage (EES) technologies. Energy can be stored in various forms, such as mechanical, chemical, electrostatic, magnetic, biological, and thermal.Despite the large number of available storage technologies, only three of them can be considered as large-scale electricity storage technologies currently (>100 MWh): pumped hydro storage (PHS), compressed air energy storage (CAES) and flow batteries.

Currently, Pumped Hydro-Electricity Storage (PHS) and Compressed Air Energy Storage (CAES) are the main technologies employed at large scale, but they both suffer from geographical constraints, environmental issues and high capital cost. In this scenario, Carnot Batteries (also called PTES, Pumped thermal Energy Storage) are a promising storage option: they can combined them with all the renewable sources and retrofit existing thermal plant, they don't have geographical limitation, and they will have a lifespan longer than Lithium-Ion Batteries for a longer storing time. Potentially, there are some studies that show that roundtrip efficiency of Carnot Battery can be 80%, that is more or less the efficiency of Pumped Hydro, and it is for sure more than Compressed Air Energy Storage.

"Today we are at a point where we can also bring the benefits of the technology to the places where we don't have so much sunshine, and therefore to help them to get from the ColdAge to the StorAge"[1]

- Michael Geyer (Senior Advisor, DLR-German Aerospace Center)

2. Carnot Storage Principle – State of the Art

A Carnot Battery operation could be divided in two part: charging of the Thermal Energy Storage (with an electrical heater or a heat pump), and the discharging of the Thermal Energy Storage (delivering power to the cycle).

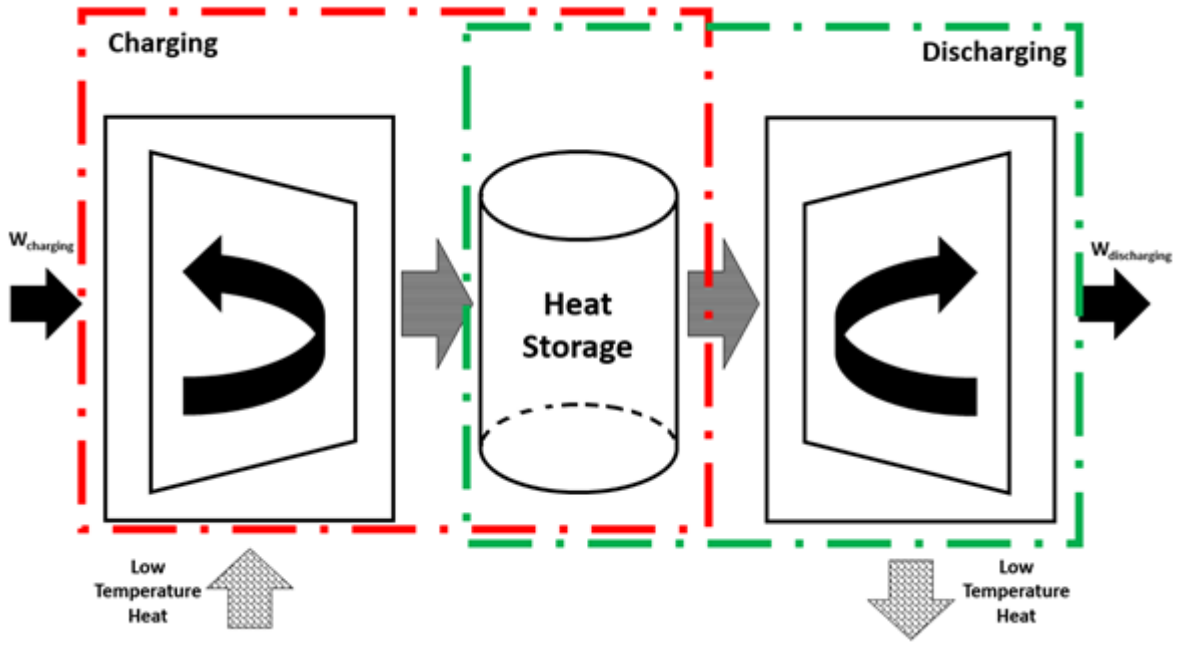

Fig. 2.1. Carnot Storage Principle

Carnot Battery uses thermal energy storage: there is a tank of same materials (there are different concepts about it), then we charge it with heat. The simplest approach is to place electric heater (a resistance) and heat up this storage medium to a certain temperature. To discharge this unit, we simply pump the heat currier (that is usually thermal oil) which takes heat from the tank, and deliver it to the evaporator of the discharging cycle. [4] [5] [6] [7]

If we install a thermal energy storage system in power plant, we can switch off the boiler, and we can produce steam using this cycle. We have evaporator then we have expander, where we produce power back to the grid, and also we release some heat to the atmosphere.

$$\eta_{\text{round}} = \frac{\text{electric energy delivered during discharging}}{\text{electric energy consumed during charging}} = \frac{W_{\text{discharge}}}{W_{\text{charge}}}$$

If we consider that in Organic Rankine Cycle (ORC) the highest efficiency we can obtain is 25%, and that the compressor has an efficiency of 95%, we can obtain the round trip efficiency (of the all system) that is 22-25%, not very high.

η_{round} is limited by the Carnot efficiency resulting from the maximum and minimum temperatures of the power cycle used in the discharge process. In technical implementations, a thermodynamic cycle with external heat supply will be applied.

There are three different approaches to increase the efficiency, rearranging the cycle.

1) We replace resistance heating with heat pump cycle. With heat pump cycle we deliver heat to the compressor (we compress energy fluid and not air), then we have condenser, we store in condensation the energy heating (in charging cycle), and we have evaporator. With a heat pump we not only use electrical energy for charging, but we are able to absorb some energy from environment (can be ambient heat). The losses are compensated with additional energy that we can absorb from environment (so for nothing). If we want to deliver power back, we have discharging cycle (that can be Rankine, Transcritical, or Brayton cycle). We have Heat Pump COP (Coefficient of Performance) greater than 1 (even 5 sometimes). So for the all system we have to multiply to something higher than one: if we had 22% *3 = 66%. The issue is that, at the moment, we need a high temperature heat pump cycle, that are not so common. Many companies are working with high temperature heat pump: we are able to store heat in high temperature, but actually on the market we can store it only to 165°C (it's not so very high). But even if we run the cycle with low temperature, the equation is always true, so we can have high efficiency also with low temperature. [10]
2) If we don't have the possibility to use some energy, we can close the cycle (using for example waste heat energy). Sometime is not possible use energy from environment, due to the working fluid used in charging cycle (for the property of the fluid, sometimes we need to have evaporation at high temperature, like 40-60 °C). For example, each industrial factory has waste heat, even low temperature (for conditioning, air system, chillers, compressors, …), so we can store this waste heat. If this energy from different sources of wasting heat is not use (for example it is dissipated and wasted in atmosphere), then we don't put it in the input energy (we could use the energy somehow). It's always case sensitive.
3) To close the cycle, we can use two thermal storage systems. During discharging, we don't have to discharge heat in the atmosphere, but we can discharge heat in the low temperature tank. Then, in charging, we take heat from low temperature tank and we pump it to a high temperature tank.

Increasing the roundtrip efficiency of storage systems does not only allow ensuring the security of supply with a lower total capacity of renewable energy generators but also helps to reduce the investment in the infrastructure required to transfer electricity between sources and storage systems, reducing the size of the thermal storage systems.

To charge and discharge the thermal storage we usually use three thermodynamic cycle solutions:

1) Linde-Rankine cycle: Linde cycle for charging (for heat pump) and Rankine cycle for discharging. It is the simplest one, so it will have the lowest temperature, and the lowest efficiency. If we look at temperatures, the system is quite difficult to apply in reality because the storage will take place at very low temperature (-25°C and -50°C), so it can be combined with some industrial refrigerator tank. If we have a demand from the factory for a very low temperature fluid, this cycle can be used[9]

2) Transcritical cycle. It means that condensation takes place over critical point, and then we cold down on saturation line (for discharging). But in charging, we have traditional evaporation cycle. So, Transcritical cycle will work partly under umbrella and partly over umbrella.

3) Brayton cycle. It can be located at any temperature, even 400-500°C). Brayton cycle is the cycle of gas turbine: we have compression, then we have the delivery of heat (in case of power cycle). Brayton can be reversible, so it can work as power cycle or as heat pump cycle, but it uses two heat exchanges (compressor and expander).

3. Performance parameters

There are three main performance parameters:

- Round trip efficiency:

$$\frac{net\ work\ output}{net\ work\ input}$$

- Energy Density:

$$\frac{net\ work\ output}{reservoir\ volume}$$

- Power Density:

$$\frac{average\ power\ output}{hot\ cylinder\ volume}$$

The important factors to evaluate an electrical energy storage technology are its round-trip efficiency and its capital costs per MW installed capacity and per MWh of storage. In this matter, PTES have relatively high energy density, which translates into a small plant footprint and low capital cost per MWh. [11]

Energy density of PTES is generally much higher than other energy storage systems due to the possibilities of thermal storage materials. With temperatures ranging between 500ºC to -150ºC, correspond to energy densities of 130kWh*m^{-3} to 60kWh*m^{-3} (using magnetite as a thermal storage material). [3]

Regarding round trip efficiency, this is most simply computed through the entropy budget. The system entropy must be the same before and after a storage cycle because it is a property of state, so any entropy generated during the cycle must be discarded as waste heat. This heat represents a loss from the stored energy that cannot be re-transmitted as grid power [10].

We can divide the main losses of the systems in three sectors:

1. Compression and expansion losses

Turbomachines have an achievable polytropic efficiency of 90% [12], compression efficiencies varies from 75 to 80% [11]. This low values for compressor may be associated with valve pressure drop and hence there is a possibility to increase this efficiency. In a PTES system the gas will stay longer in the device (in comparison with a turbo-compressor) meaning there will be considerable heat transfer to the environment. Main losses can be due to: pressure drop through the valves, cyclic heat transfer through the cylinder walls and mixing of fresh intake gas with the residual gas [11].

2. Pressure losses

Due to pressure losses in pipework, heat exchangers, reservoirs and valves the expander has a lower pressure ratio than the compressor. Pressure losses will have a greater impact in performance if it occurs in the low pressure part of the cycle[3] [11].

3. Thermal reservoir losses

Main sources of heat loss in the reservoir occur due to frictional pressure loss and heat transfer irreversibility. Thermal losses occur because heat exchange takes place across a finite gas-solid temperature difference [11].

4. Limitations and constrains

We can divide the limitation and constrains of Carnot Batteries in Materials and Design.

4.1. Materials

I) Steel Limitations

Closing the Brayton cycle enables the background working fluid pressure to be raise, greatly reducing the cost per engine watt. The turbine rotation speed and blade angles fix the working fluid velocity to first approximation, therefore, increasing the pressure simply increases the number of moles of working fluid passing a given point per second which increases total power.

Nonetheless, the use of high pressure severely limits the temperatures that can be employed. Raising the temperature of a steel eventually causes it to exhibit creep, a deformation that ends in full mechanical failure at

higher temperatures. This effect does not have an influence in short time but is a big design constrain on the scale of 40 years. This phenomena must be taken into considerations for high pressure systems which will work with temperatures above 700 K, although this limit can be raised to about 800 K by adding some impurities to the carbon steel[10].

II) Storage Media

Electricity is stored in the form of thermal potential (there is a temperature difference between environment and the reservoir). Thermal storage materials can be solid, liquid or phase change materials. Each of these have their own advantages. Solids, such as gravel or metal oxide are cheap, abundant and non-toxic. Liquids allow the system to be pressurized to reduce the cost and the thermal energy to be stored statically at a single temperature. Phase change materials tend to have a much higher energy density than the previous materials.

Temperature limitations due to usage of steel make solar salt a good choice for the high temperature storage medium. Solids and liquids have heat capacities of approximately $3R$ per mole, where R is the ideal gas constant, in the temperature range of interest. The great advantage of gravel or solar salt is their low cost, plus solar salt is liquid, so it enables heat transfer by counterflow, minimizing entropy creation. Solar salt also has low vapor pressure, high compatibility with steels, it is environmental friendly, does not disintegrate in response to thermal cycling stress the way a solid would and creates no explosion hazard[10].

The upper operating temperature of solar salt exposed to air is not presently known. Corrosion of stainless steel by these salts is mild and amounts to approximately ten micrometers per year at 550ºC[10].

The storage media should be chosen based on the temperature range we want. Water under pressure will be the cheapest option for the range of 120-150 ºC. For 200-300 ºC thermal oil can be used. We can store heat in ceramic materials (like in magnesite block, where we are able to store heat up to 600°C). But if we want to have different temperature profiles we have to use PCM (phase change materials): molten salt are used as PCM, there are different molten salt on the market, and with them we are able to reach 700-800°C.

III) Working Fluid in Heat Pump

The working fluids in this application is limited to gases that are extremely stable at high temperatures and far from liquefaction or solidification phase transitions at mildly cryogenic ones. Mechanical advantages of working near a critical point are not as important in this case as the danger of fluid raining or snowing out and damaging the turbine blades. For this application CO_2 is discarded because it suffers from liquefaction and freezing transitions in the range of 200-300 K. Taking into account these considerations and requirements for economic viability and environmental friendliness restrict the possibilities to Ar and N_2. Argon has a lowered compression ratio and, potentially, higher adiabatic efficiency due to it being a gas with no internal degrees of freedom. However, N_2 requires only minor modifications for being use in some jet engines [3] [10].

Other working fluids currently used in industrial compression heat pumps are shown in the following table:

Table. 4.1.1 Refrigerants used in industrial compression heat pumps

Refrigerant	**Maximum Sink Temperature [ºC]**	**Minimum Source Temperature [ºC]**
R245fa	140	15
R600a (Isobutane)	140	0
R717 (Ammonia)	110	-30
DR-2	160	35
SES36	160	35
R744 (CO_2)	130	About -10

IV) Working Fluid in ORC Cycle

- Dry working fluid. When we start expansion, we have always any points in dry region. During charging, to avoid enter in the wet region (we could destroy the compressor otherwise), we need to super-heat the fluid. So, dry fluids need super-heated steam at the entrance of the compressor, that means we need to use regenerate heat exchange to regenerate some heat from cooling, to super-heat this steam. In discharging, we have typical Organic Rankine Cycle, so we can start expansion from saturation line, then we expand, and then we have to cool (we also use regeneration), then we have condensation, pumping and re-heating.
- Isentropic fluids: part of their saturation umbrella is vertical, so entropy is almost constant (that's why we called isentropic). Charging and discharging are isentropic
- Wet fluids (example, carbon dioxide): the umbrella is open. If we start expansion from any points of saturation line, we always go to liquid. So, the issue is that we need to have super-heated fluid during discharging. If we have high isentropic efficiency, we can go down and enter the wet region.

If we want to operate with evaporation temperature around environment condition (15 °C) we have pressure around 1 MPa. Theoretically if we end up close to the saturation line, then the heat that we could be able to absorb from environment would be from 300 kJ/kg to 600 kJ/kg. So we are able to absorb around 300 kJ from each kg of working fluid.

Another issue is throttling: if it is too much (with an high pressure difference), we will not enter the condenser with the fluid close to the saturation line but we are going to evaporation with a sort of mixture. Then the ability to absorb heat will be limited by throttling. In this case we can look for isobutane. For isobutane is quite convenient, because in any point we are always able to absorb some it: it doesn't matter if we have the ending point after throttling, it's always left some space to absorb some energy for the external source of heat. This energy will compensate the losses. In case of toluene, it will be a limitation, because the ability to absorb heat will be limited. So, what we have to look at if we want to select the perfect working fluid? Not only pressure and temperature but also some balance energy issues.

4.2. Design

At fixed pressure ratio, the efficiency and energy density are both improved by either increasing T_1 or decreasing T_3 seen in Fig.1. If compression and expansion losses dominate, then the efficiency is governed mainly by the ratio T_2/T_3 since this determines the ratio between compression and expansion work. Increasing this ratio makes the cycle less susceptible to compression and expansion losses. On the downside, improvements regarding these parameters result in increased costs and technical difficulties since they imply higher top temperatures or pressures, or lower bottom temperatures. The benefits of higher work ratios might be diminished by increased thermal losses in the reservoir[11].

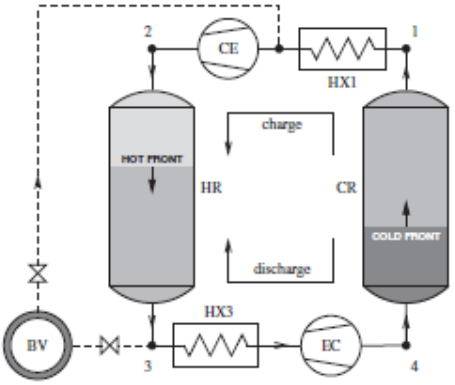

Fig. 4.2.1 Layout of PTES system. Key: BV buffer vessel; HR/CR hot/cold reservoir; CE/EC reversible compressor-expanders; HX1/HX3 heat exchanger[11]

Geometry parameters can also be varied, such as the hot and cold reservoir aspect ratios (L/D) and particle diameters. Small particles five large heat exchange but increase the frictional effects. Similarly, long reservoirs give lower thermal losses, but the reduction in cross-sectional area means higher fluid velocities and therefore higher pressure drop. In the cold reservoir, due to lower gas density, pressure losses are more significant and therefore the optimum aspect ratio is lower and optimum particle size larger than for the hot reservoir [11].

Overall, there are two main design options:

I) Two different machines (charging and discharging cycle). Integrated devices concept can be used, this means there is a compressor and an expander as two machines, but remaining elements are the same so they are heating exchangers (that can work reversibly). During charging, the compressor is switched off, the valves are closed (cycle runs in reverse) so the evaporator becomes a condenser and condenser becomes an evaporator.

II) Most advanced concept at the moment is a reversible machine. We can use scroll compressors in low temperature cycle (below 100 ºC): some of these scroll compressors can work reversibly. When we deliver mechanical power, the compressor will compress the fluid, but if we put some pressure (by delivering high pressure fluid from one side), it will work reversibly, so it will turn to a mechanical power up.

5. Concepts for technology implementation from small to large scale (from domestic applications to power plants)

We have now 10 year experience worldwide with molten salt tanks, and they have shown that they are operating in large commercial sizes up to 250 MWe for 6 hours, and that they can have a lifetime up to 35 years (where basically, for the electrochemical batteries is still a dream to come). We can implement them not only on thermal plants, but also on nuclear plants and combined them with all intermittent renewable's sources, to shoveling the peak of electricity demand. In the following table we will show the projects already on the market, and the researches going on:

Table. 5.1 Actual projects and researches

Name	**Capacity**	**Energy**	**Storage**
1. NADINE (National Demonstrator for Isentropic Energy Storage) [7] [13] [14] [15] [16]	research		
2. CHESTER Challenge [17] [18]	research		
3. University of Edinburgh experimental test [19]	research		
4. Small-scale prototype at Liege University, Belgium [20] [21]	research		
5. Southern Australia, Adelaide-based "1414 Degrees" Startup [22] [23] [24]		10 MWh	
6. SandTES Pilot Plant, Wien [35]	280 kWth		
7. Siemens Gamesa: 3 ETES (Electric Thermal Energy Storage) Solutions [25] [26]	1,4 MW		24 hours

8. Newcastle University small scale demonstrator [27] [28]	2-5 MW		8 hours
9. Start-up Malta Inc. [29] [30]	10 MW		6 hours
10. SaltX Pilot Plant, Berlin [31] [32] [33] [34]		10 MWh	
11. Torresol Gemasolar power tower, Spain [36]	19,9 MW		15 hours
12. Noor Ouarzazate 3, Morocco [37]	150 MWe		7,5 hours
13. Solana Plant, Arizona, USA [1] [38]	280 MW		6 hours
14. Noor Energy 1, Dubai [39]	950 MW		24 hours

6. Retrofitting of coal plants

"Retrofitting former coal plants with giant Carnot Batteries could be the key technology for storing large quantities of energy in a carbon-neutral energy system of the future".

- Institute of Engineering Thermodynamics at DLR (German Aerospace Center) [1]

German coal committee is a commission that is constituted by all basically social stakeholders, politicians, unions, industry, etc and they have made a publication and a recommendation that Germany would gradually step out from its coal power generation by 2038.

Actually, there are 46 gigawatts of coal plants in German, 7 gigawatts will be shut down by 2022, the total of 23 gigawatts (half of it) should be shut down by 2030, and the remaining would be shut down by 2038. If we want to shut down the fossil plants and minimize the carbon emissions, we need lots of storage to convert the variable electricity production into a dispatchable electricity production, that will supply the electricity when the demand is needed. So, at the DLR (German Aerospace Center), they are studying with a large German utility the possibility of converting existing coal plants into storage plants, giving coal plants a second green life by adding a storage system to them. We can bank on over 10 years of experience of concentrating solar power, expanding the solar power technologies to the cloudy countries by just adding a molten salt thermal storage.

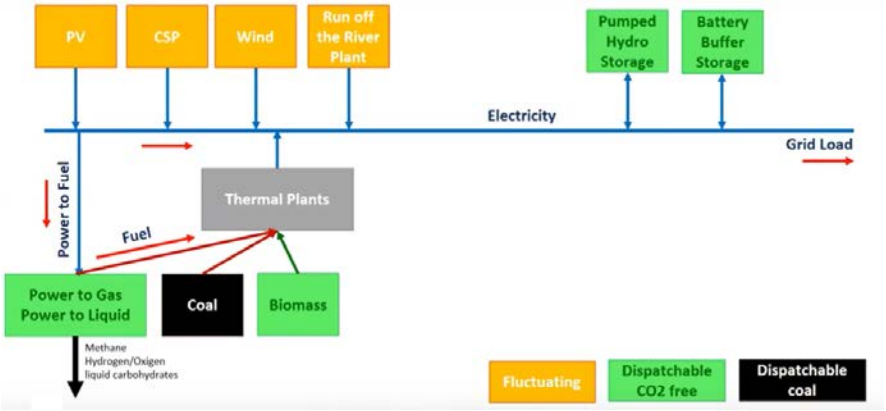

Fig. 6.1 (DLR - Michael Geyer presentation - 8 April 2019) Actual thermal plants grid[1]

The thermal plants are usually operating with coal, biomass, etc... and in future the idea is to eliminate the coal and add thermal storage (what we call the “Carnot battery”): it will be charged with electricity from the grid and then it will deliver its heat to the existing plants, being converted into the existing cycles.

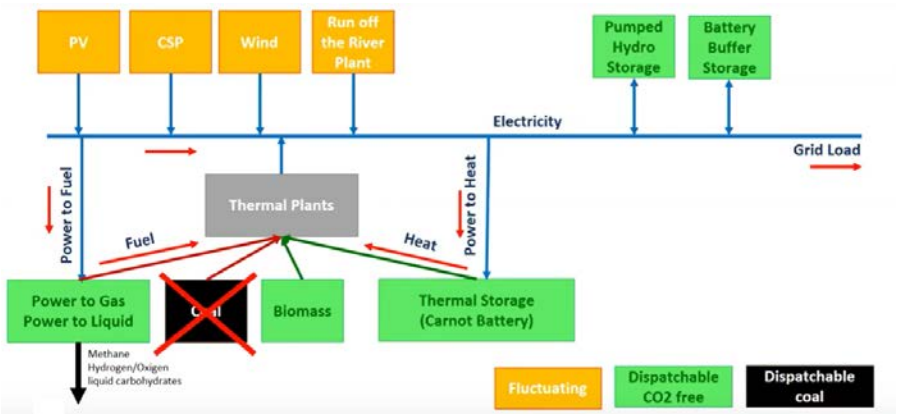

Fig. 6.2 (DLR - Michael Geyer presentation - 8 April 2019) Implementation of a Carnot Battery in the grid[1]

The advantage of these plants is that they are already there: they exist, they have a grid connection, they have permits, they have people who operate them, and so this means this is much easier to convert them. How a coal plant can be converted into a storage plant? Starting with an existing coal plant, with his thermodynamic cycle, we have the coal boiler that produces high-pressure steam that goes into the turbine, then the turbine moves the generator and the generator makes electricity: it successively goes back and closes the cycle.

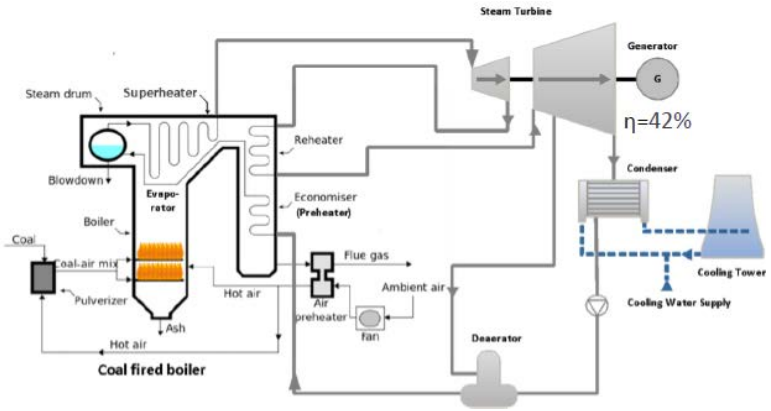

Fig. 6.3 Existing coal plant [1]

The conversion will not be difficult:

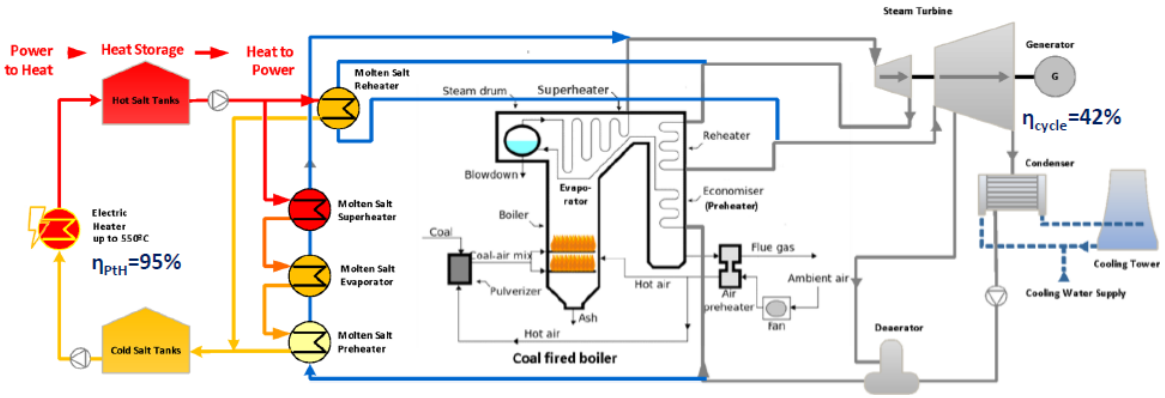

Fig. 6.4 Existing coal plant with the suggested electric heater/heat storage implementation [1]

We add the part on the right, that we know perfectly from the concentrating solar power plants. There is a hot tank with molten salt at the temperature of 565°C, and the cold tank at 270°C. We have then the molten salt steam generators: we come there with the feed water that we preheat, we evaporate it, superheat it, and then mix it (with the exact settings) with the existing steam from the coal boiler, that will run through the existing turbine to produce electricity.

The innovations is that on the right part we do not have mirrors (in the lack of sunshine), but we have electrical resistance heaters, which work with the excess production from renewable electricity or directly from the grid (when the electricity is cheap). In such a system, we have an efficiency of the right part of 95%, and we will have a cycle-efficiency of 42%. We could improve the system adding a heat pump (but this doesn't exist today). So, instead of using the electric heater, we use a heat pump, and by this we could have a coefficient of performance which around 120%, increasing the round-trip efficiency to 50%.

An additional improvement could be using the heat pump for discharging: we would not use anymore the steam cycle, putting a heat pump heat engine in it for the reconversion, reaching over 60% or close to 70% efficiency round-trip, during charging and discharging. It would become pretty close to what lithium-ion battery or other electrochemical batteries do, but in this system, we have the big advantage first of all that we can do this in many hundreds of megawatts for many hours, and with an expected lifetime of 35 years.

Actually, we don't have proof of technical concept for retrofit an existing coal plant with a molten salt storage, but what is completely proven is the molten salt system with its molten-salt heat exchangers.

In small-scale, the resistance heaters are proven to heat up to 565°C, so this is a conventional technology, but nowhere is build one for 100-200 MWe. So, basically, the systems would use a proven technology, learning day after day.

Further, coal plant in the world so far ran baseload of 6000 hours per year,, they did not need to start and stop daily, and it is more to get acquainted with this technology to integrate it in the plant then a technical proof of concept, because the molten salt storage steam cycle is running and proved for almost 10 years in utility-scale.

In detailed engineering and detailed simulations, this new system works quite well, but of course it hasn't been built yet. The heat exchanges are also challenging at least for the motor system. There are lots of technical challenges that can be overcome, but they remain big challenges, engineering-wise and economically.

Another great advantage is the persistence of the people working in the coal sector: often towns or cities are very dependent on this one source of employment and so on, and with this technology option we can at least save jobs in the coal plant. There are lots of jobs here commit in the power plants and converting these coal plants into two storage plants will conserve quite an amount of those jobs, because the plant will still be run as a thermal plant (basically with the same skills).

In conclusion, if the concept works, it could help safeguard coal generation jobs while giving, for example Germany, tens of gigawatts of storage capacity for renewable energy load-shifting on the German grid.

Furthermore, a single pilot could be enough to prove the commercial viability of the concept, since the technology, described as a Carnot battery, is based on commercially available industrial components and standard engineering practices.

Thermal storage tanks are relatively low-tech, low-risk engineering concepts, he said, requiring only a steel tank, concrete base and the salt itself. The principal engineering task is to fit the tank into a coal plant, he said. These plants were not designed to house molten salt storage containers, he admitted, and a Carnot battery built from scratch would likely not resemble a coal plant. The cost of converting the coal plants is not expected to be overly significant because a large amount of the existing infrastructure would be reused and permits plus grid connections are already in place.

For operation, meanwhile, the batteries would rely on renewable energy that is currently being curtailed. Carnot batteries would likely complement lithium-ion battery plants on the German grid, Geyer said, with the latter delivering primary and secondary frequency control services. The combination of lithium-ion and Carnot batteries could maintain grid stability and deliver load-shifting to keep grids running on high levels of renewable energy for hours or possibly days, he said. However, to cope with extended periods of low wind and poor sunlight, for instance during winter calms, some of the converted coal plants could be equipped with gas boilers.Nevertheless, the Carnot battery concept only makes sense as a way of taking advantage of coal plant equipment and excess renewable energy that would otherwise go to waste, Geyer conceded, because the round-trip efficiency of the storage process is only about 40 percent. [1] [40] [41] [42]

7. Conclusions

In this review, we showed the huge potentiality of Carnot Batteries, from small scale application to the implementation in power plants. It a reliable technology based on a simple principle, already used in CSP plant for over 10 years. We can use different cycles, and each material (solid, liquid, phase change) used to store the heat have his own advantage. We have losses like in all storage systems, and the efficiency actually is not competitive with the solution on the market, but it was showed that it will become more competitive combining it with an heat pump and using higher temperature (both not yet implement in operating system).

In conclusion, a lot of prototype and experimentations are carried actually, and they will have more and more importance during next years, above all implement Carnot Battery in existing thermal power plant, reconverting and improving the actual ones, to shoveling the load peak, and reducing the cost. The possibility to install Carnot Battery everywhere without geographical limitation will be a huge advantage in comparison with the other storage system, and next years this technology will become more and more famous, leading to improvements of it and with more existing system implemented in the world.

References

[1] Geyer M., *"Webinar: Carnot Batteries – facilitating the transition from fossil to renewable generation"* (8 April 2019), date of access (09/11/2019), https://www.youtube.com/watch?v=fWuc_PwVqBc

[2] Guan-Bang W., Xin-Rong Z., *"Thermodynamic analysis of a novel pumped thermal energy storage system utilizing ambient thermal energy and LNG cold energy"* (15 September 2017), date of access (09/11/2019), https://www.sciencedirect.com/science/article/pii/S0196890417305897

[3] Xue H., *"A comparative study of the Adiabatic Compressed Air Energy Storage (A-CAES) and Pumped Thermal Energy Storage (PTES) systems"* (10 July 2019), date of access (09/11/2019), https://ieeexplore.ieee.org/document/8867354

[4] Desrues T., Ruer J., Marty P., Fourmigué J.F., *"A thermal energy storage process for large scale electric applications"* (5 April 2010), date of access (09/11/2019), https://www.sciencedirect.com/science/article/pii/S1359431109002932

[5] White A., Parks G., Markides C.N., *"Thermodynamic analysis of pumped thermal electricity storage"*, (2 May 2013), date of access (09/11/2019), https://www.sciencedirect.com/science/article/pii/S1359431112002141

[6] *"Carnot's principle – Carnot's rule"* date of access (09/11/2019), https://www.nuclear-power.net/nuclear-engineering/thermodynamics/laws-of-thermodynamics/second-law-of-thermodynamics/carnots-principle-carnots-rule/

[7] Steinmann W.D., Jockenhöfer W., Bauer D., *"Thermodynamic Analysis of High-Temperature Carnot Battery Concepts"*, (9 October 2019), date of access (09/11/2019), https://onlinelibrary.wiley.com/doi/full/10.1002/ente.201900895

[8] *"Schematic of PTES"*, date of access (09/11/2019), https://onlinelibrary.wiley.com/action/downloadFigures?id=ente201900895-fig0001&doi=10.1002%2Fente.201900895

[9] Agency I. E., Conservation E., Storage E., and Tcp E., *"Carnot Batteries"* pp. 1–3.

[10] Laughlin R. B., *"Pumped thermal grid storage with heat exchange"* vol. 044103, no. July 2017.

[11] Mctigue J. D., White A. J., and Markides C. N., *"Parametric studies and optimisation of pumped thermal electricity storage"*, *Appl. Energy*, vol. 137, pp. 800–811, 2015.

[12] Hall D. K., Greitzer E. M., and Tan C. S., "GT2012-6 9709 Performance limits of axial compressor stages," pp. 1–11, 2018.

[13] NADINE: Power-Plant-Scale Energy Storage (9 October 2018), date of access (15/11/2019) https://www.kit.edu/kit/english/pi_2018_126_nadine-power-plant-scale-energy-storage.php

[14] NADINE: Power-plant-scale energy storage (17 October 2018), date of access (15/11/2019) https://www.eurekalert.org/pub_releases/2018-10/kift-npe101718.php

[15] New Concepts in Energy Storage Could Break Barriers (20 April 2018), date of access (15/11/2019) https://climatecrocks.com/2019/04/20/new-concepts-in-energy-storage-could-break-barriers/

[16] Energy storage on a gigawatt-hours scale (1 October 2018), date of access (15/11/2019) https://www.uni-stuttgart.de/en/university/news/press-release/Energy-storage-on-a-gigawatt-hours-scale/

[17] Peña X., - Tecnalia, *"The CHESTER challenge Compressed Heat Energy Storage for Energy from Renewable sources"*, date of access (15/11/2019) https://www.chester-project.eu/wp-content/uploads/2018/11/International-Workshop-on-Carnot-Batteries-CHESTER-challenge-20180810_nonConfidential.pdf

[18] *"Compressed Heat Energy Storage for Energy from Renewables sources"*, date of access (15/11/2019) https://www.chester-project.eu/

[19] *"Pumped-Heat Energy Storage: Experimental - Dan McKinley"*, (28 November 2018), date of access (15/11/2019), https://www.youtube.com/watch?v=RJbM5-xGOZ8

[20] Lemort V., *"Carnot batteries, an interesting solution to solve the problem of Renewable Energy storage"*, (14 may 2019), date of access (15/11/2019), https://www.linkedin.com/pulse/carnot-batteries-interesting-solution-solve-problem-renewable-lemort/

[21] *"Mapping of performance of pumped thermal energy storage (Carnot battery) using waste heat recovery"* (9 September 2019), date of access (15/11/2019), https://orbi.uliege.be/bitstream/2268/239271/1/orc_ptes_review.pdf

[22] *"Startup Says Molten Silicon Will Make Lithium-Ion Storage 'Uneconomic.' Here's the Full Story"*, (28 April 2019), date of access (15/11/2019), https://www.greentechmedia.com/articles/read/1414-degrees-says-it-will-make-lithium-ion-totally-uneconomic

[23] *"1414 Degrees kicks off molten silicon storage project in Australia"*, (28 December 2018), date of access (15/11/2019), https://www.energy-storage.news/news/1414-degrees-kicks-off-molten-silicon-storage-project-in-australia

[24] *"1414 DEGREES Highly efficient, clean and scalable thermal energy storage offering combined heat and power solutions"*, date of access (15/11/2019), https://1414degrees.com.au/

[25] *"Setting new standards in flexible energy storage"*, (28 November 2018), date of access (15/11/2019), https://www.youtube.com/watch?time_continue=151&v=PAs7UA1UYyM&feature=emb_logo

[26] *"Setting new standards in flexible energy storage"*, date of access (15/11/2019), https://www.siemensgamesa.com/products-and-services/hybrid-and-storage/thermal-energy-storage-with-etes

[27] *"Carnot Battery Energy Storage Rushlight Show 30 Jan 2019 A more cost-effective and flexible solution for grid-scale energy storage"* (30 January 2019), date of access (15/11/2019) https://www.rushlightevents.com/wp-content/uploads/2019/02/RUSHLIGHT-SHOW-2019-CLEANTECH-CONF-PANEL-1-NEWCASTLE-UNIV.pdf

[28] *"National Facility for Pumped Heat Energy Storage"* (2 June 2017), date of access (15/11/2019) https://www.youtube.com/watch?v=IMD_CptGayc

[29] *"Malta Solution"*, date of access (15/11/2019) https://www.maltainc.com/our-solution

[30] *"Malta Electro-Thermal Energy Storage Overview"* (29 may 2019), date of access (15/11/2019) https://www.youtube.com/watch?v=f5I2-RmZeYQ

[31] *"SaltX Pilot plant in Berlin - thermal energy storage"*, (15 May 2019), date of access (15/11/2019), https://www.youtube.com/watch?v=y3862TjPk8U

[32] *"SaltX Berlin pilot plant shows very promising results"*, (19 September 2019), date of access (15/11/2019), http://saltxtechnology.com/saltx-berlin-pilot-plant-shows-very-promising-results/

[33] *"ECO18 Berlin: Karl Bohman SaltX"*, (15 May 2018), date of access (15/11/2019), https://www.youtube.com/watch?v=XYLS44-zvGs

[34] *"Germany plans to convert coal plants into renewable energy storage sites"*, (15 may 2019), date of access (15/11/2019), https://energytransition.org/2019/05/coal-plants-into-renewable-energy-storage-sites/

[35] *"Highly efficient thermal energy storage system"*, (23 October 2019), date of access (15/11/2019), https://www.youtube.com/watch?v=LlhQCP0UFoo

[36] *"Gemasolar Concentrated Solar Power"*, date of access (15/11/2019) https://www.power-technology.com/projects/gemasolar-concentrated-solar-power/

[37] *"Central receiver plant Noor Ouarzazate III"*, date of access (15/11/2019), http://www.poweroilandgas.sener/project/central-receiver-plant-nooro-iii

[38] *"Solana Solar Power Generating Station, Arizona, US"*, date of access (15/11/2019) https://www.power-technology.com/projects/solana-solar-power-generating-arizona-us/

[39] *"Noor Energy 1 Power Plant, Dubai"*, date of access (15/11/2019) https://www.nsenergybusiness.com/projects/noor-energy-1-power-plant-dubai/

[40] *"Germany Looks to Put Thermal Storage Into Coal Plants"*, (18 march 2019), date of access (15/11/2019), https://www.greentechmedia.com/articles/read/germany-thermal-storage-into-coal-plants

[41] "Germany plans to convert coal plants into renewable energy storage sites", (15 may 2019), date of access (15/11/2019), https://energytransition.org/2019/05/coal-plants-into-renewable-energy-storage-sites/

[42] "New Concepts in Energy Storage Could Break Barriers", (20 April 2019), date of access (15/11/2019), https://climatecrocks.com/2019/04/20/new-concepts-in-energy-storage-could-break-barriers/

Small-scale Algae Electric Generator

Rishabh Golchha[1]

[1]*Department of Energy Technology, Royal Institute of Technology, KTH, Stockholm, Sweden: e-mail: rishabhgolchha95@gmail.com*

Abstract

Even after numerous efforts by many global organizations and national governments, the carbon dioxide emissions are daily on a rise. Renewables like solar, wind and hydropower are in primary focus to accelerate the efforts to reduce emission from the electricity sector. However, they constantly face problems of intermittency. The present article presents the idea of a small-scale algae-based electricity generator. A technical feasibility of the same is presented along with the economics. The breakeven electricity price for this is calculated to be $0.15 USD/kWh

Keywords: Algae, biomass, anaerobic digestion, renewable,

1. Introduction

The International Energy Agency (IEA) reports that the global emissions in the year 2018 were 33.4 Gt from fuel combustions [1]. If the world continues with the current policies this could increase to 42 Gt of CO_2 emissions from fuel combustion by 2040[2]. Figure 1 depicts the predicted emission from the energy sector if new policies are implemented by various nations and what are the transitions needed to achieve the sustainable development targets. There are three main steps identified by IEA: energy efficiency, change of fuels to more renewable options and carbon capture and storage (CCS).

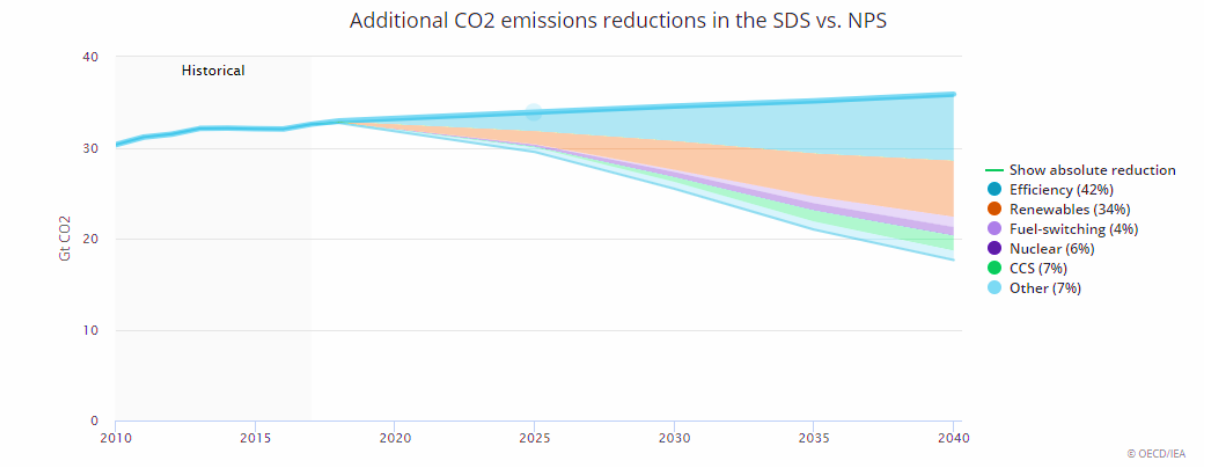

Fig. 1.1. CO_2 emissions in Sustainable Development Scenario (SDS) vs New Policy Scenario (NPS) [3]

To reduce emissions, the renewables that are playing a major role presently are solar, wind energy, biomass and hydropower. Solar and wind have immense potential but have the major problem of being intermittent and hence usually needs a supporting powerplant to supply electricity when the sun doesn't shine, and the wind doesn't blow. Battery storage is seen as the most promising solution to this and there has been a constant decline in battery prices. The levelized cost of electricity from battery storage has fallen to $187/MWh in 2018. Comparatively, the LCOE of just solar PV was $57/MWh [4]. So, the cost of battery storage is falling but in most places is still quite higher than the present electricity prices.

Another major challenge is deploying batteries on a global scale is the waste disposal strategy. Although recycling methods exist which can help reuse 60-80% of the materials, there is a lack of framework in many countries to implement these methods. If not done responsibly, there might be a huge problem of stockpiles of battery waste.

With these problems in perspective, the present article discusses the technical and economic feasibility of algae-based electricity generation using anaerobic digestion and subsequent biogas combustion. The algae are grown in Photo Bio Reactors to prevent the competition with food cultivation which has been a major drawback for the first-generation food-based biomass. A small-scale design is preferred over one centralised generation for easy installation especially in places which lack grid connections presently.

2. Technical design of the proposed generator

Figure 2.1 shows the schematic of the proposed algae-based electricity generator. The steps in the process of electricity generation are discussed in the subsequent subsections

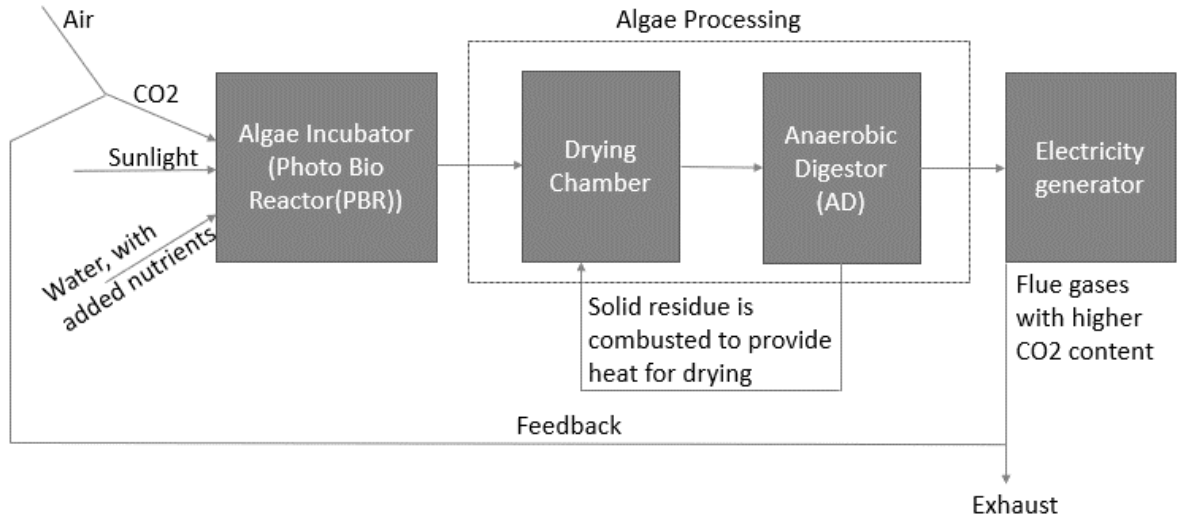

Fig. 2.1. Schematic of the proposed generator

2.1.Algae Incubator

The algae incubator is section is where the algae reproduces taking in sunlight, CO_2 from air and water along with nutrients. The exhaust air post electricity generation can be used to enrich the input air with CO_2 for better algae growth rates. For example, for Scenedesmus obliquus Zamalloa et al, used a concentration of CO_2 of 2% (v/v) [5].

The various design of the photobioreactor have been researched extensively in literature and the most common and successful design has been the tubular design [6] and the same is proposed to be employed in the present design.

2.2.Algae Processing

The algae processing section in where the anaerobic digestion (AD) of the algae take place. A complete or partial drying for thermal treatment might be employed to improve the efficiency of biogas generation as it is known that thermal pre-treatment can improve biogas generation from algae by about 20 to 40% [7].

The present design if for decentralised production of electricity and hence it might be a logistic issue to collect the solid waste from AD and use it for applications like fertilizers and hence it is rather burned to provide thermal energy for drying and thermal treatment.

2.3.Electricity Generation

The final step is to generate electricity from the produced electricity. Many commercial designs exist for the same and can be deployed as it is for this purpose.

2.4.Technical feasibility

Taking the case of a typical household in India, they consume 90 kWh of electricity per month [8]. However, with an increasing electrification and access to more technologies this is expected to increase. Hence, for the present analysis a household consumption of 125 kWh/month or 450MJ is taken.

Hakawati et al. [9] summarised the efficiency of heat, electricity and transport from biogas by evaluating 49 technologies. The efficiency of electricity generation varied from 8% to 54%, specifically for biogas power station from 35% to 40%. For the present analysis, an efficiency of 40% is taken for biogas to electricity generation. Taking the LHV of methane as 50 MJ/kg, this would give a need of 25 kg/month or 35 Nm3/month.

For S. obliquus, Zamalloa et al [5] evaluated that biogas production is approximately 0.5 m3/m3/day of incubator with 75% CH_4 content. This would provide 11.25 Nm3/m3/month of CH_4. Hence, an incubator size of approximately $3m^3$ is needed. Considering all the subsystems, the entire generator could be packed in a box of size 3m x 3m x 3m.

3. Economics of the proposed generator

Table 3.1 summarises the fixed cost od the proposed generator. Some of the costs available in literature were for larger subsystems and hence were scaled for the present design. Since installations are assumed to be done at home, no land cost is taken into the analysis.

Table. 3.1 Fixed cost for the proposed generator

Direct Fixed Costs heads	**Cost (USD) [9,10]**
Incubator (Photo Bio Reactor)	2,000
Anaerobic digestor	360
Electricity Generator	400
Total Direct Fixed Cost	***2,760***
Indirect Fixed Cost	**% of Total Direct Fixed Cost**
Installation	5%
Transportation	5%
Warehouse	4%
Total Indirect Fixed Cost (USD)	***390***
Total fixed cost	***3,150***

The recurring cost includes the cost for nutrients supply for algae growth and maintenance requirements. This is taken as 6 USD per month [10].

With a lifetime of 20 years for the generator and assuming it to have a zero-value post that, the breakeven electricity price is calculated to be $0.15 USD/kWh. The electricity price in India varies from 0.08 USD/kWh to 0.12 USD/kWh.

4. Conclusions

Some of the key challenges to the successful commercialisation and implementation of the proposed idea are:

- Since the proposed generator needs to run in a decentralised system, the PBR should work with almost no supervision.
- The system should ideally have an automatic fault detection to prevent any blackouts for the household.
- The levelized cost of electricity is still higher than the market's cost of electricity. The PBR comprises the bulk of the cost (0.07 USD/kWh). Technical improvements and local sourcing of components could reduce the cost to achieve competitive market prices
- Biogas is known to have problems with odour which would present a practical challenge in home installations
- Depending the microalgae, the growth rate varies with the intensity of sunlight. For example, for S. Obliqus, Zamalloa et al [5] used a intensity of 250 µmol/m^2/s. Usually a higher as well as a lower intensity reduces the growth rate. This could alter the rate of biogas production and hence electricity generation

Despite these challenges, the present technical and economic feasibility of the small-scale algae based electricity generation presented here is feasible and with some improvements soon be commercialised especially for regions with limited or no grid connectivity

References

[1] https://www.iea.org/statistics/co2emissions/ (accessed on 28/11/19)

[2] https://www.iea.org/weo2018/scenarios/ (accessed on 28/11/19)

[3] https://www.iea.org/topics/carbon-capture-and-storage/ (accessed on 28/11/19)

[4] https://www.pv-magazine.com/2019/03/26/lcoe-for-li-ion-batteries-down-35-to-187-mwh-since-2018-bnef/ (accessed on 28/11/19)

[5] Ilas A., Ralon P., Rodriguez A., Taylor, M.: Renewable power generation costs in 2017. International Renewable Energy Agency (IRENA): Abu Dhabi, UAE. 2018.

[6] Zamalloa C., Boon N., Verstraete W.: Anaerobic digestibility of Scenedesmus obliquus and Phaeodactylum tricornutum under mesophilic and thermophilic conditions, Applied Energy, 2012 Apr; 92:733-738.

[7] Cañedo J.C., Lizárraga G.L.: Considerations for photobioreactor design and operation for mass cultivation of microalgae, Algae-Organisms for Imminent Biotechnology, 2016 Jun; 29.

[8] González-Fernández C., Sialve B., Bernet N., Steyer J.P.: Thermal pretreatment to improve methane production of Scenedesmus biomass, Biomass and bioenergy, 2012 May; 40:105-111.

[9] Chunekar A., Sreenivas A.: Towards an understanding of residential electricity consumption in India, Building Research & Information, 2019 Jan; 47(1):75-90.

[10] Fasahati P, Saffron CM, Woo HC, Liu JJ. Potential of brown algae for sustainable electricity production through anaerobic digestion. Energy Conversion and Management. 2017 Mar 1;135:297-307.

[11] Zhu Y., Jones S.B., Anderson D.B.: Algae Farm Cost Model: Considerations for Photobioreactors, Pacific Northwest National Lab(PNNL), Richland, WA (United States); 2018 Oct 31.

Heavy metal ions removal by aerogels

Maciej Sobczyk[1], Tomasz Bajda[2]

[1]AGH University of Science and Technology, Department of Mineralogy, Petrography and Geochemistry, msobczyk@student.agh.edu.pl
[2]AGH University of Science and Technology, Department of Mineralogy, Petrography and Geochemistry, bajda@agh.edu.pl

Abstract

The aim of this research is to investigate the effectiveness of heavy metal ions removal (lead - Pb and cadmium - Cd) by alginate-based aerogel, derived from biodegradable precursor such as sodium alginate. The synthesis of desired material was composed of freezing in liquid nitrogen and followed by drying process - liophilisation. An investigation of synthetic, alginate-based aerogel properties was composed of Scanning Electron Microscopy (SEM-EDS), X-ray diffraction (XRD) , FTIR-analysis and thermo-gravimetric measurements (TG-DTA). The yield of the research suggests that alginate-based aerogel may be applicable as an effective and economically viable biosorbent of heavy metal ions. His biodegradability ensures highly effective process from waste point of view with simultaneous sorption of undesired pollutants.

Keywords: aerogels, sorption, biosorbents, polimer compounds

1. Introduction

An important issue of today's world is an environmental pollution caused by an anthropogenic pressure. The presence of numerous pollutants in water and soil ecosystems poses a huge danger for their consistency and integrity. Natural environment is polluted by carbon dioxide - CO_2, sulphur oxides - SO_x, nitrogen oxides - NO_x, heavy metal ions such as: Cu^{2+}, Zn^{2+}, Cd^{2+}, Pb^{2+}, Cr^{3+}, $Ni^{2+}$and Fe^{2+} , phenol and its derivatives, benzene and its derivatives further known as BTEX, pesticides, and volatile organic compounds - VOCs (Standeker et al., 2009). As mentioned one of the key issue of environmental remediation is to prevent or neutralize all of previously listed chemical agents via adsorption, membrane techniques, extraction or ion exchange.

In the literature an adsorption is considered as one of the most economically viable and simultaneously effective method of undesired chemical agents removal from water environments. An adsorption proces relies on proper adjustment of adsorptive material, therefore in this research paper a synthesis of polimer-based material - alginate-aerogel is conducted. His precursor is a biodegradable, polimer compound - sodium alginate, cross-linked by double-charged cation - Ca^{2+}. The parameters such as crystallinity, texture and surface functional groups were investigated followed by XRD measurements, SEM investigation, TG-DTA analysis and FTIR-analysis respectively.

Aerogels were initially investigated by Kistler (1931, 1932) when their interesting features were examined such as high porosity, well-developed active surface area, numerous macropores and mezopores followed by great thermal conductivity.

In general, an aerogel is a material, consist of three-dimensional, spatial structure, derived from organic, non-organic or organic-inorganic precursors in a process called gelation accompanied by proper drying technique (Maleki, 2016). Gelation proces - a creation of gel out of sol seems to be the key step in formation of 3D-structure of aerogel and its porosity. The overall scheme of gelation proces is presented in Fig. 1.1.

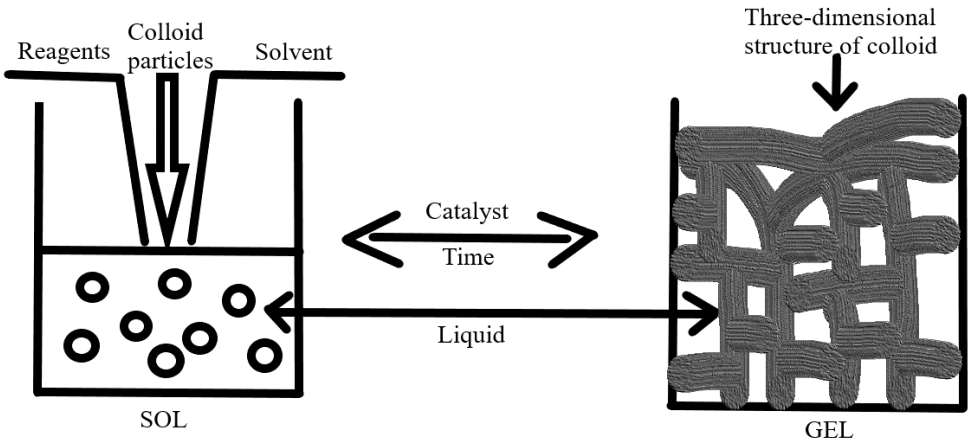

Fig. 5.1. Sol-gel process - general scheme

2. Application of aerogels in water treatment

According to the topic of presented research it is worth to mention that there are numerous of water pollutants. One could distinguish anthropogenic and natural pollutants as an effect of civilization development such as sewage, agriculture and heavy industry pollutants (Ali et.al., 2012; Barakat, 2011). Anthropogenic pollutants are highly toxic to the environment and could be divided into two main groups:

Inorganic pollutants:

- Metal ions, for example : Ni^{2+}, Cd^{2+}, Pb^{2+}, Cu^{2+}, Zn^{2+},
- Anions (acid residues) : AsO_4^{3-}, $HAsO_4^{2-}$, SO_4^{2-}, ClO_4^-, Cl^-, $H_2AsO_4^-$,
- Artificial fertilizers (nitrogen, phosphate) and their derivatives

Organic pollutants:

- Pesticides
- Phenol and its derivatives
- Dyes
- Pharmaceuticals

Pollutants entered to the environment via human activity are highly toxic and non-biodegradable therefore it seems to be crucial to neutralize them or capture form water-soil environments.

Aerogels, due to their high porosity, chemical groups on the surface and well-developed active surface area might be applicable as potential adsorbents of undesired pollutants from water. One of few effective ways of undesired heavy metal ions removal is their chelatisation with surface functional groups of an aerogel that contain nitrogen (N), phosphorus (P), oxygen (O) or sulphur (S). Those agents may serve as a donors of electrons that could create a coordinative covalent bonds with metal. Furthermore, one of the main advantage of a sol-gel process is a possibility of adjustment the surface chemistry of an aerogel with chelation groups via silicate aerogel usage. Modified by amines, silicate aerogels were proposed by Kłonkowski (Kłonkowski, 1999; Soliman, 1997) and co-authors (Kłonkowski et al., 1999) through bonding on their surface 3-aminepropyltrimethoxysilane (APTMS) and 3-amino-ethylene-2-aminopropylenetrimetoxysilane. This bonding reveals a possibility to create a coordinative covalent bond with Cu^{2+} cations and their chemisorption on an amine-modified aerogel.

Moreover a silicate aerogels with numerous of mono, di, tri and tetra amines poses an interesting sorption capacities toward heavy metal ions (Motahari, 2015; Motahari et al., 2009; Kumar Mena, 2005). They have studied an amine-modified resorcinol-formaldehyde aerogel aimed to remove Pb^{2+}, Hg^{2+} or Cd^{2+} cations from

water. They examined different sorption parameters such as pH, temperature, contact time, concentration and initial concentration. Authors of the research have found that sorption process is directly dependent on heavy metal ion solution's pH, with maximum sorption capacity equals to 157,73 mg/g of sorbent by pH = 6,6.

The results of sorption capacity might be adjusted to Freundlich and Langmuir models of sorption. Authors of aforementioned studies suggest that there is a chemical bond created between surface functional groups such as carbonyl group (C=O), carboxyl group (-COOH) and hydroxyl group (-OH) and heavy metal ion, namely Pb^{2+}, Hg^{2+} or Cd^{2+}. The highest sorption capacity was examined toward Cd^{2+} cations equal to 400,8 mg/g of sorbent, where the lowest sorption capacity was examined toward Pb^{2+} - 0,7 mg/g of sorbent.

3. Synthesis of aerogels

3.1. Sol-gel process

The synthesis of desired material - alginate-based aerogel was conducted in an ambient temperature and pressure with use of pipets, plastic bootles and liophyllisator. Sol-gel process as one of the key step in aerogel synthesis lasts for 10 minutes. It is worth to mention that this process is responsible for proper structure formation and desired chemistry of the surface of aerogel.

To a plastic bootle with a volume equal to 100 cm^3 filled with 50 cm^3 of 1% sodium-alginate solution, 10 cm^3 of calcium nitrate - $Ca(NO_3)_2$ was transfered with a molar concentration equal to 0,1 mol/dm^3. Throughout the proces stirring with use of glass spatula was performed. Afterwards the solution was freezing with the use of liquid nitrogen for 10 minutes and transfered to the liophyllisator with a power output equal to 10 mbar.

3.2. Drying process - liophilisation

Drying process lasts for 48 hours and took place in a liophilisator with a vacuum pump, presented below as Fig. 3.1.

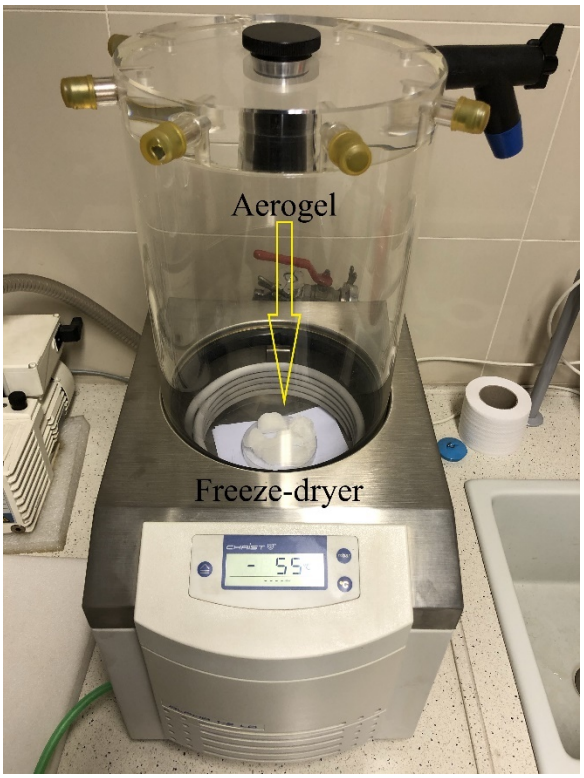

Fig. 3.1. An aereogel sample seen inside liophilisator

4. Laboratory work methodology

In order to investigate the crystallinity of an aerogels SmartLab RIGAKU X-ray diffractometer was used. The source of radiation was a copper lamp. An identification of mineral phases was performed utilizing XRayan software.

An observation of samples' surface and structure, scanning electron microscope Quanta 200 by FEI company was used. The microscope was equipped with EDS detector to microelementary analysis. During an analysis an accelerating voltage equal to 15 kV was used.

A FTIR analysis was performed utilizing Nicolet 6700 spectrometer from Thermo Scientific company. During an investigation a DRIFT scattered method was used.

Thermal analysis with thermo-gravimetric measurements coupled with quadrupled mass spectrometer (QMS) was performed via NETSCH STA 449 F3 thermal analyzer in a range of temperature from 30^{o}C up to 1000^{o}C. The heating rate was equal to 10^{o}C/min.

An analysis of two heavy metal ions, namely lead - Pb and cadmium - Cd was performed via atomic absorption spectroscopy (AAS) from SavantAA GBC company with acetylene burner.

Sorption process of two heavy metal ions was conducted via creating a series of solutions of lead and cadmium equal to 0.1 mmol/L, 1 mmol/L, 10 mmol/L and 100 mmol/L. Lead (II) nitrate – $Pb(NO_3)_2$ and cadmium nitrate tetrahydrate - $Cd(NO_3)_2 * 4H_2O$ were used for this purpose. Next step was consist of weightening of 25 mg of an alginate-based aerogel sample on an analytical weight. The samples were flooded with primary solutions of specific heavy metal ion and shaked on automatic shaker for 24 hours. After this process samples were transfered to a centrifuge and treated with a velocity of 14 000 rpm for 5 minutes. Afterwards an analysis of solutions' concentration was performed by AAS.

5. Laboratory work results

5.1. Phase analysis

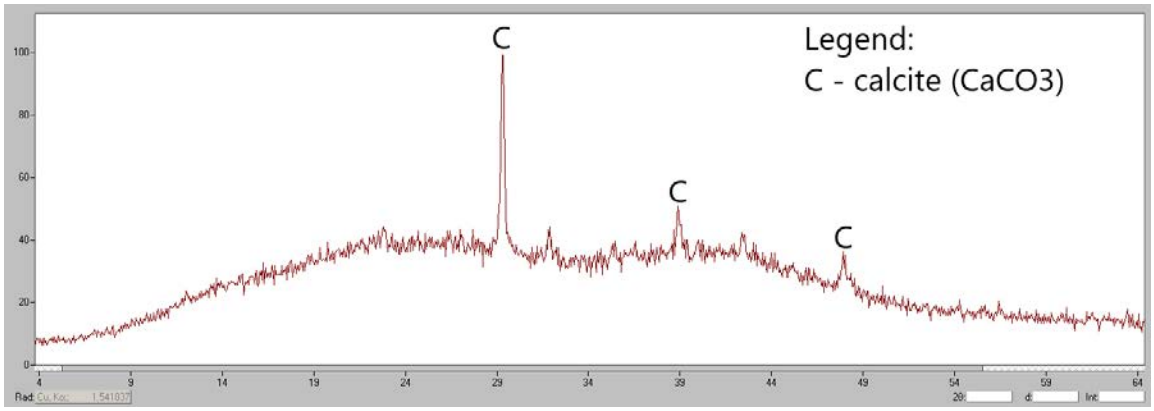

Fig. 5.1. Diffractogram of powdered sample of an alginate-based aerogel

As seen in the Fig. 5.1. above, an alginate-based aerogel is amorphous and only part of the sample possess crystalline structure, The only one phase detected by XRayan software was calcium carbonate – caclite ($CaCO_3$).

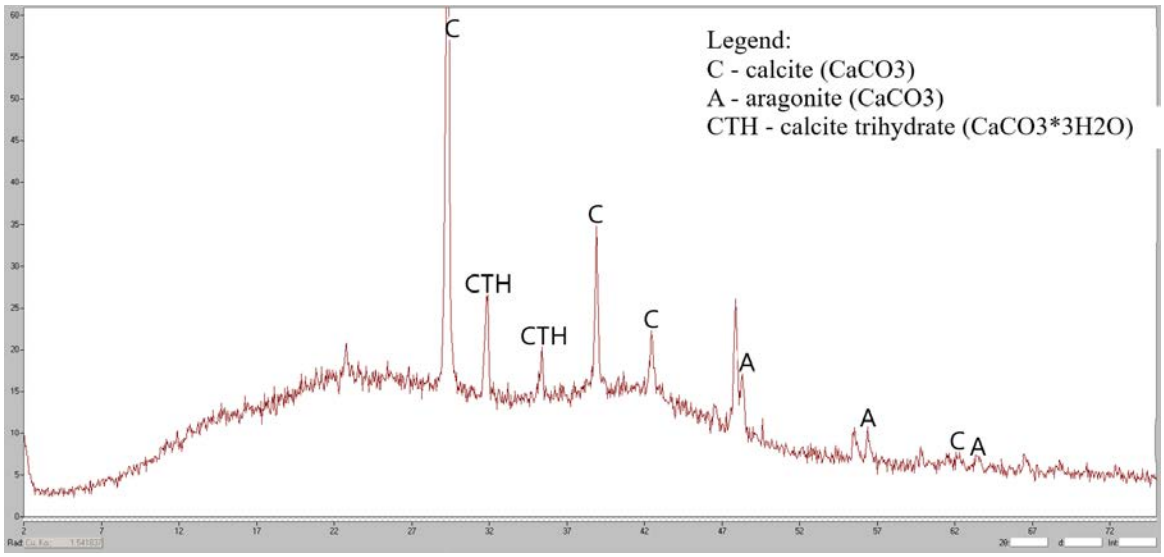

Fig. 5.2. Diffractogram of second, powdered sample of an alginate-based aerogel

Second investigated sample reveals a presence of three, mineral phases in an alginate aerogel powdered sample namely: calcite (α-$CaCO_3$), polymorphic form of calcite - aragonite (β-$CaCO_3$) and calcite trihydrate ($CaCO_3$*$3H_2O$).

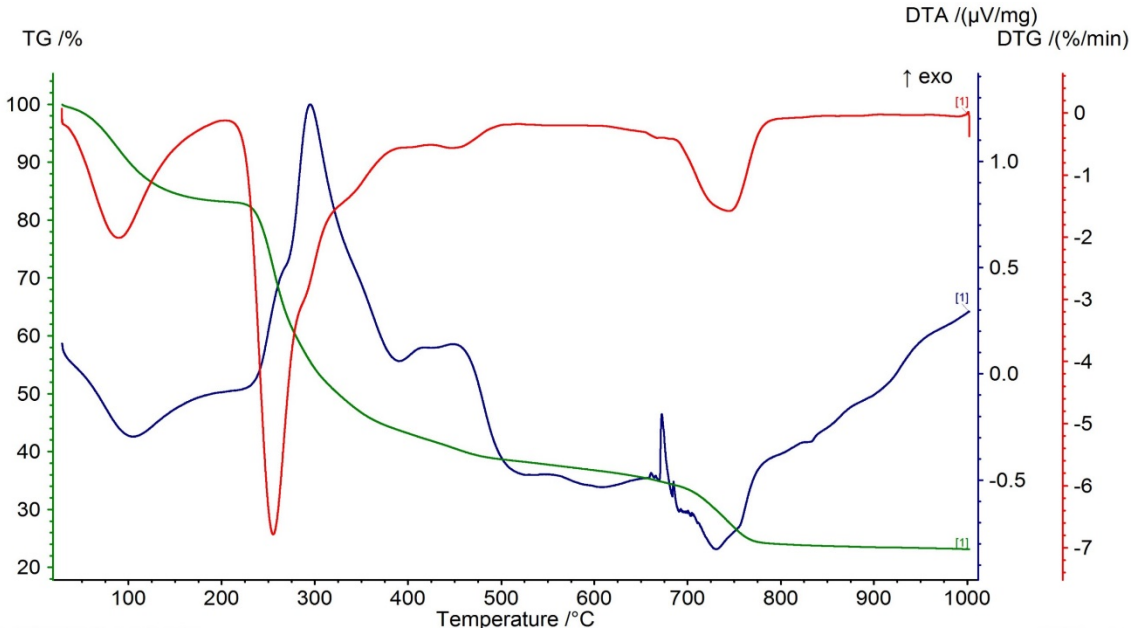

Fig. 5.3. Thermogravimetric curve of an alginate-based aerogel

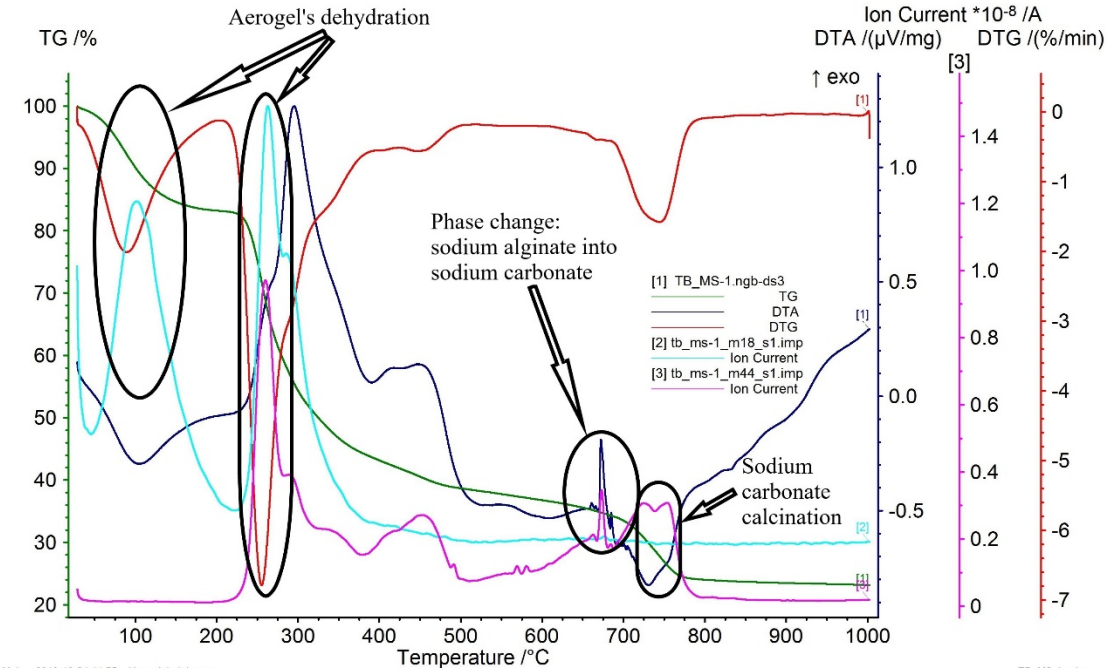

Fig. 5.4. Thermogravimetric curve with QMS analysis of an alginate aerogel (CO_2 - purple curve and H_2O - blue curve)

As seen on thermogravimetric curves, a two-step dehydration takes place at starting point equal to 45°C and ending point at 221°C. Mass loss in this range of the temperatures equals 16% (as seen on TG-curve - green line). Dehydration is considered as an endoenergetic effect. Second step of aerogel's dehydration starts at 227°C and ends at 376°C. Mass loss in this range of temperature equals 33%. Simultaneously from the sample carbon dioxide is released.

657°C is considered as starting point of phase change, namely sodium alginate changes into, simpler chemical compund - sodium carbonate. This exoenergetic effect ends at 700°C. Mass loss from 657°C to 700°C equals 1,85%.

In temperature equal to 705°C a thermal decay of sodium carbonate appears. Sodium carbonate changes into sodium oxide accroding to chemical equation (1). At the same time the release of CO_2 is present.

$$Na_2CO_3 \rightarrow Na_2O + CO_2\uparrow \quad (1)$$

sodium carbonatesodium oxide

5.2. FTIR analysis

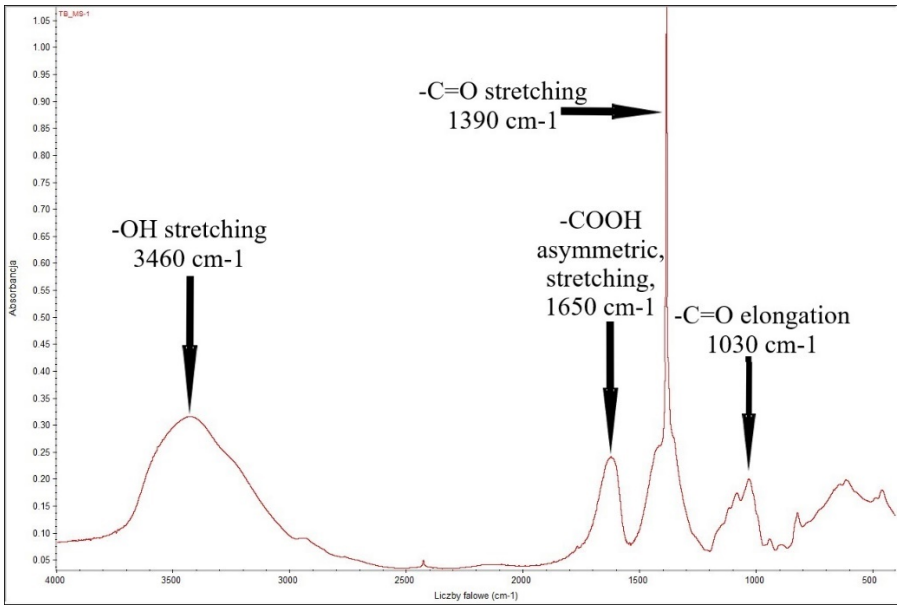

Fig. 5.5. FTIR spectra of an alginate aerogel

FTIR analysis reveals a presence of hydroxyl group (-OH) identified by 3460 cm^{-1} adsorption band. In addition a carboxyl group (-COOH) was present in a sampe identified by a band 1650 cm^{-1}.

Furthermore a carbonyl group (-C=O) was present with characteristic bands by a wavenumber equal to 1390 cm^{-1} and 1030 cm^{-1}.

5.3. Microstructure analysis

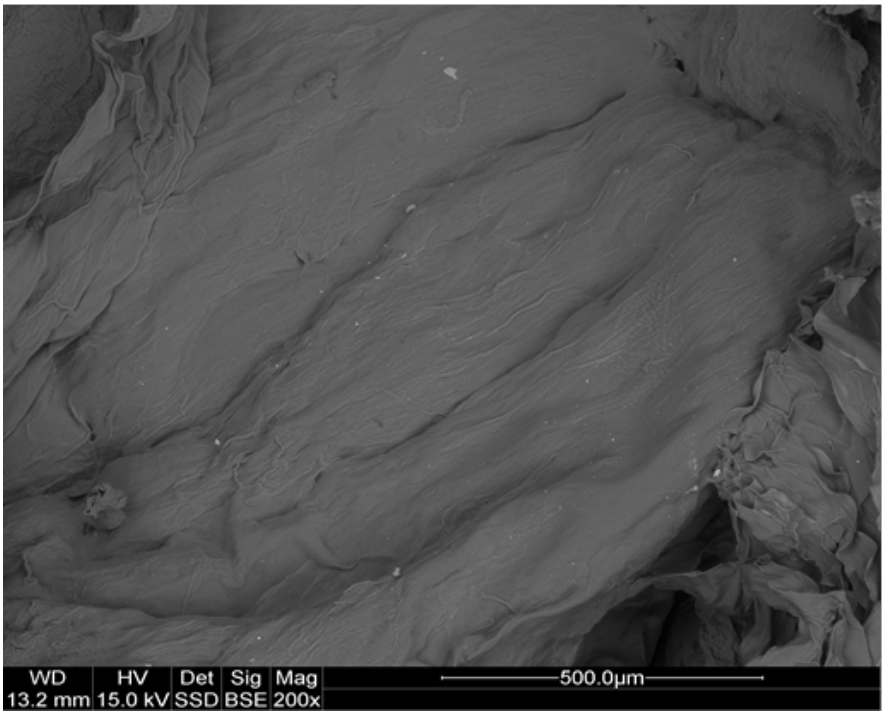

Fig. 5.6. Microstructure of a 1% alginate aerogel

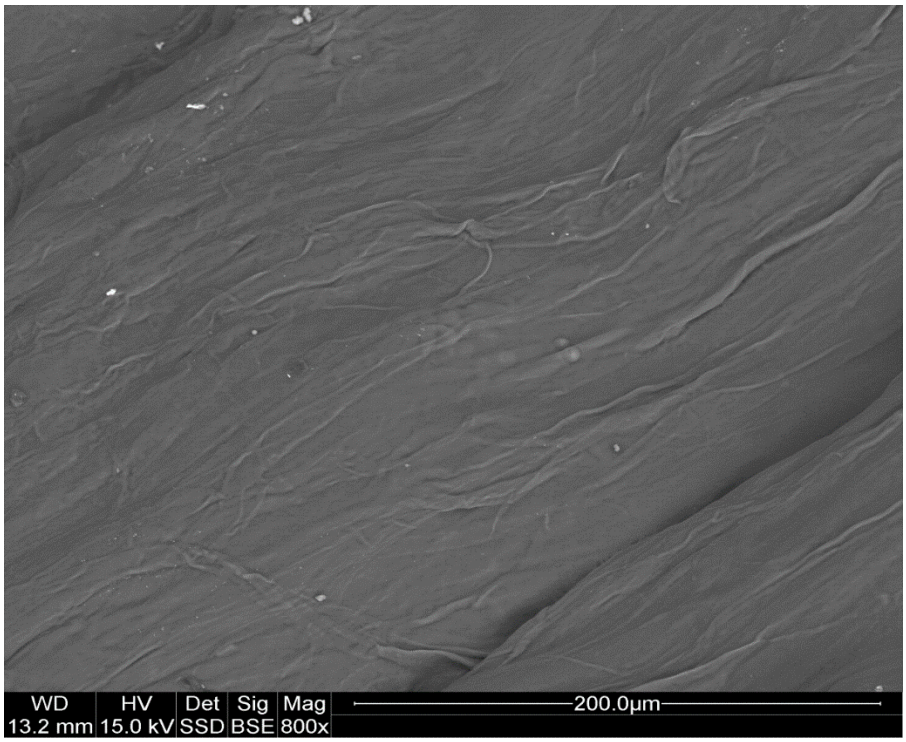

Fig. 5.7. Plain, homogenous microstructure of a 1% alginate aerogel

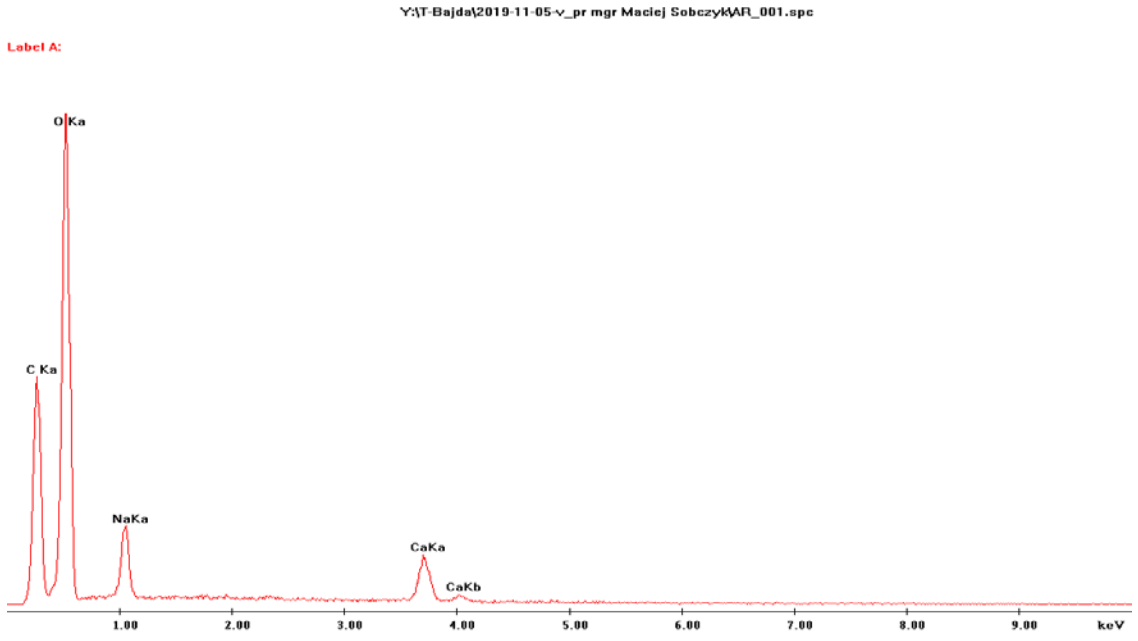

Fig. 5.8. EDS spectra of a 1% alginate aerogel

As seen (Fig. 5.6. and Fig. 5.7.) 1% alginate aerogel possess plain and homogenous structure without any protrusions and inhomogenity. An EDS spectra (Fig. 5.8.) reveals a presence of sodium (Na), carbon (C), calcium (Ca) and oxygen (O) in an invesytigated sample.

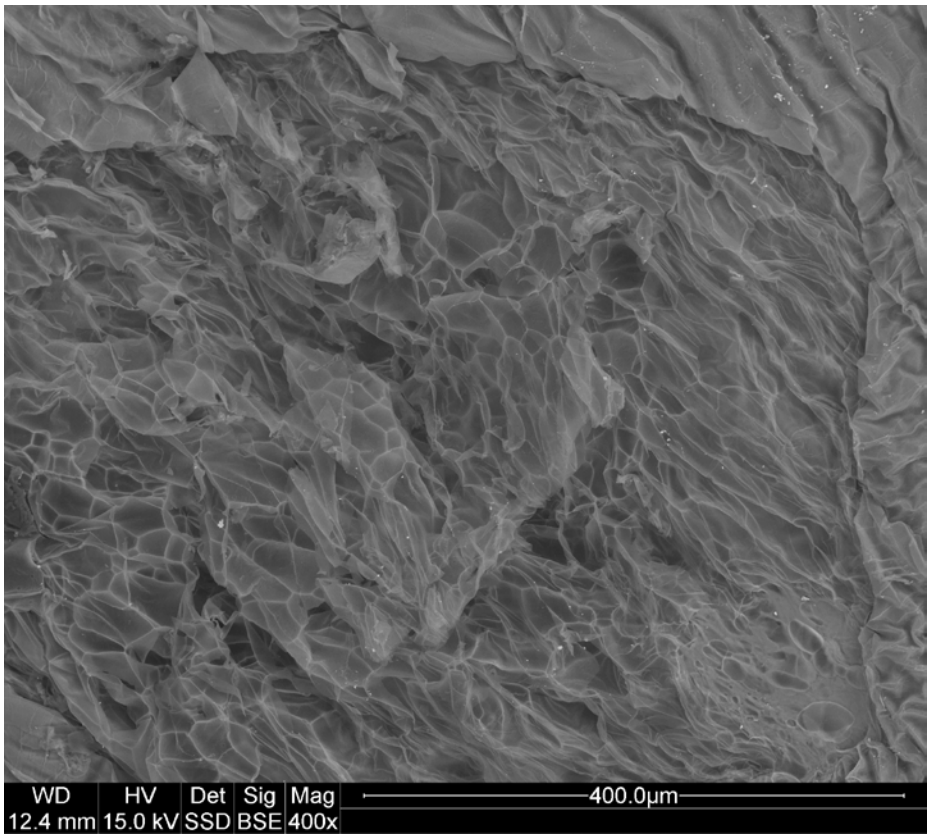

Fig. 5.9. Visble micropores - microphotography of 2% alginate aerogel

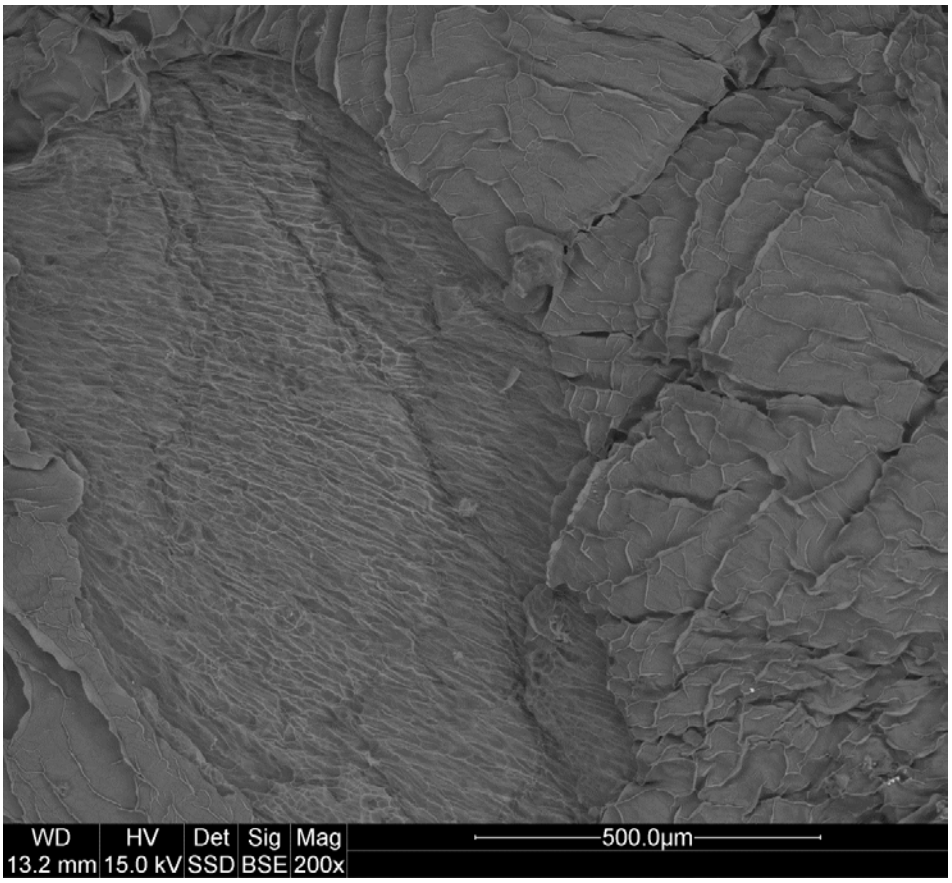

Fig. 5.10. Leaf-like structure with with given direction microporosity - 2% alginate aerogel

Fig. 5.9. and Fig. 5.10. reveal two new structures in a 2% alginate aerogel - leaf-like structure with numerous inhomogeneities on the surface, similar to a leaf of a tree and microporous structure with plenty of cavities visible as holes in a aerogel structure on the left-hand site of Fig. 5.11. Structure with leaves is presented in Fig. 5.11. on right-hand site.

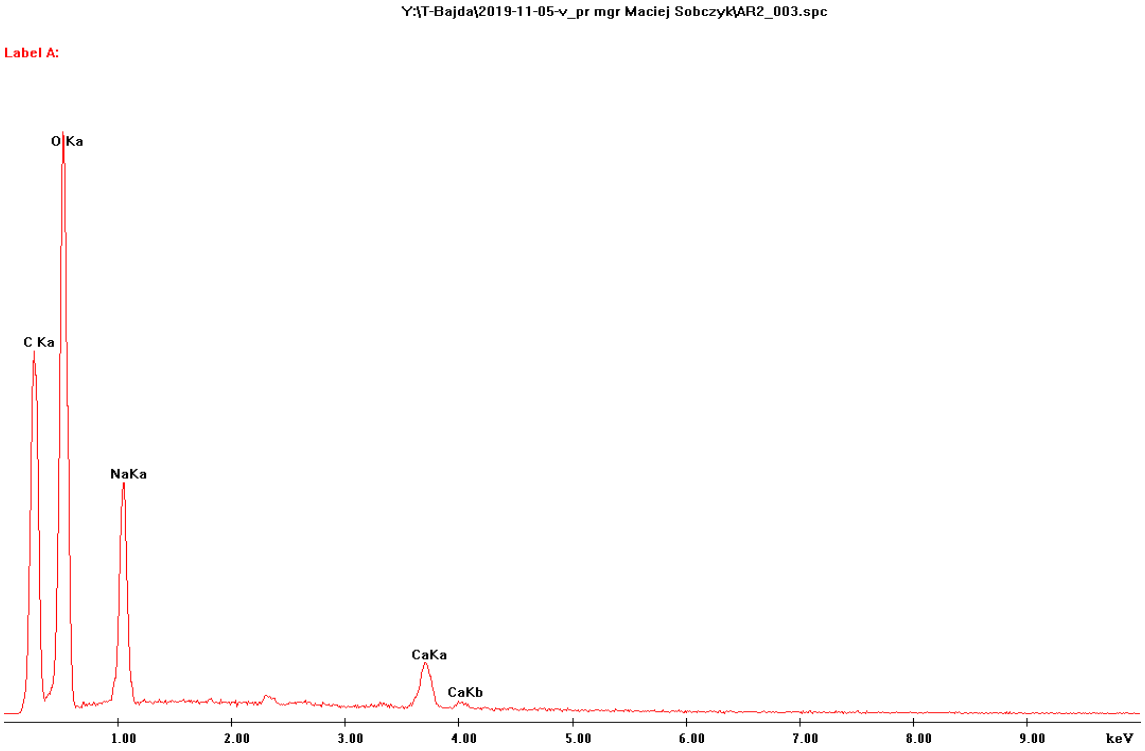

An EDS spectra of a 2% alginate-based aerogel reveals a presence of oxygen (O), carbon (C), sodium (Na) and calcium (Ca) similar to 1% alginate aerogel.

5.4. Sorption of lead

Sorption process of a lead was conducted at an ambient temperature and pressure. Absorbance scores for standard solutions of lead in a range from 0,25 mg/L Pb up to 20mg/L Pb is presented in Table. 5.1.

Table. 5.1. AAS indications in an analysis of standard solutions of lead

Standards [mg Pb/L]	AAS indications	Calculated concentration [mg Pb/L]
0,2500	0,025	0,284
0,2500	-	-
0,5000	0,059	0,684
0,5000	0,063	0,723
2,5000	0,171	2,089
2,5000	0,180	2,198
5,0000	0,400	5,447
5,0000	0,358	4,783
10,0000	0,695	10,767
10,0000	0,634	9,573
20,0000	1,134	20,736
20,0000	1,063	18,966

Based on standard solutions of lead a calibration curve was developed with polynominal fit. Pearson's match coefficient equals to 99,44%. Calibration curve is seen as Fig. 5.12.

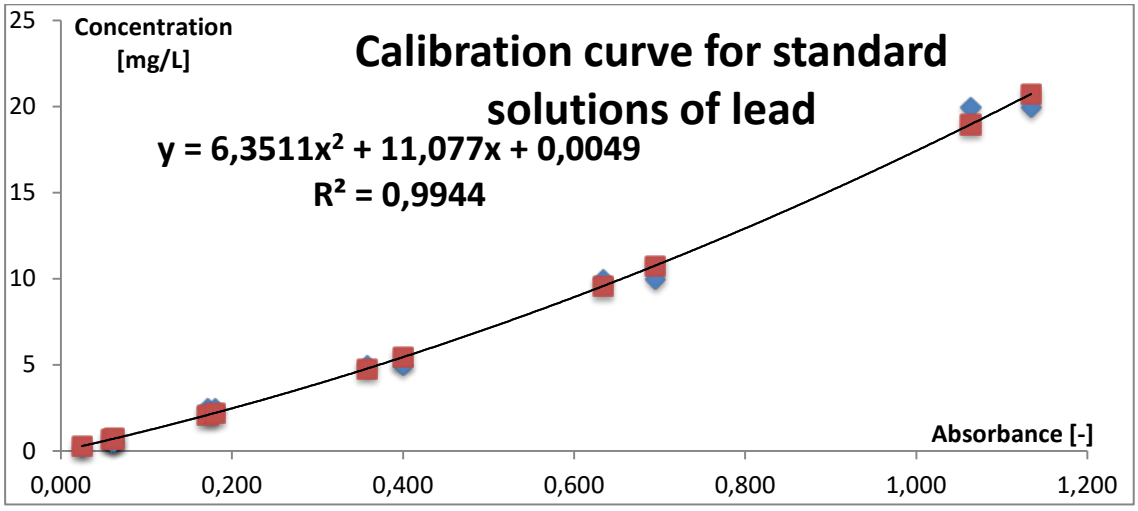

Fig. 5.12. Calibration curve for standard solutions of lead - Pb

After sorption process, scores were put into the table with proper values of dillution of the solutions and sufficient amount of weighted aerogels both 1% and 2%. The scores of an AAS analysis with sorption for 1%-aerogel and 2%-aergoel are presented in Table. 5.2.

Table. 5.2. Scores of sorption of a lead for 1%-aerogel and 2%-aerogel

Sample's symbole	AAS indication	Dillution	Mass	Solution's volume	SORPTION
[-]	[-]	[-]	[kg]	[L]	[mmol/kg]
RW-0,1	1,1439	1	-	-	-
RW-0,1	1,1332	1	-	-	-
RW-1	0,6920	10	-	-	-
RW-1	0,6845	10	-	-	-
RW-10	0,6792	200	-	-	-
RW-10	0,6263	200	-	-	-
RW-100	0,6436	2000	-	-	-
RW-100	0,6509	2000	-	-	-
AR1-1_1	0,138	10	0,0000258	0,00025	**0,045**
AR1-1_2	0,198	10	0,000026	0,00025	**0,041**
AR1-10_1	0,101	200	0,0000282	0,00025	**1,009**
AR1-10_2	0,082	200	0,0000261	0,00025	**0,855**
AR1-100_1	0,463	2000	0,0000258	0,00025	**3,257**
AR1-100_2	0,189	2000	0,0000259	0,00025	**7,578**
AR2_1_1	0,040	10	0,000026	0,00025	**0,051**
AR2_1_2	0,055	10	0,0000252	0,00025	**0,048**
AR2_10_1	0,096	200	0,0000266	0,00025	**0,958**
AR2_10_2	0,068	200	0,0000248	0,00025	**0,828**
AR2_100_1	0,467	2000	0,0000272	0,00025	**3,355**
AR2_100_2	0,494	2000	0,0000275	0,00025	**3,057**

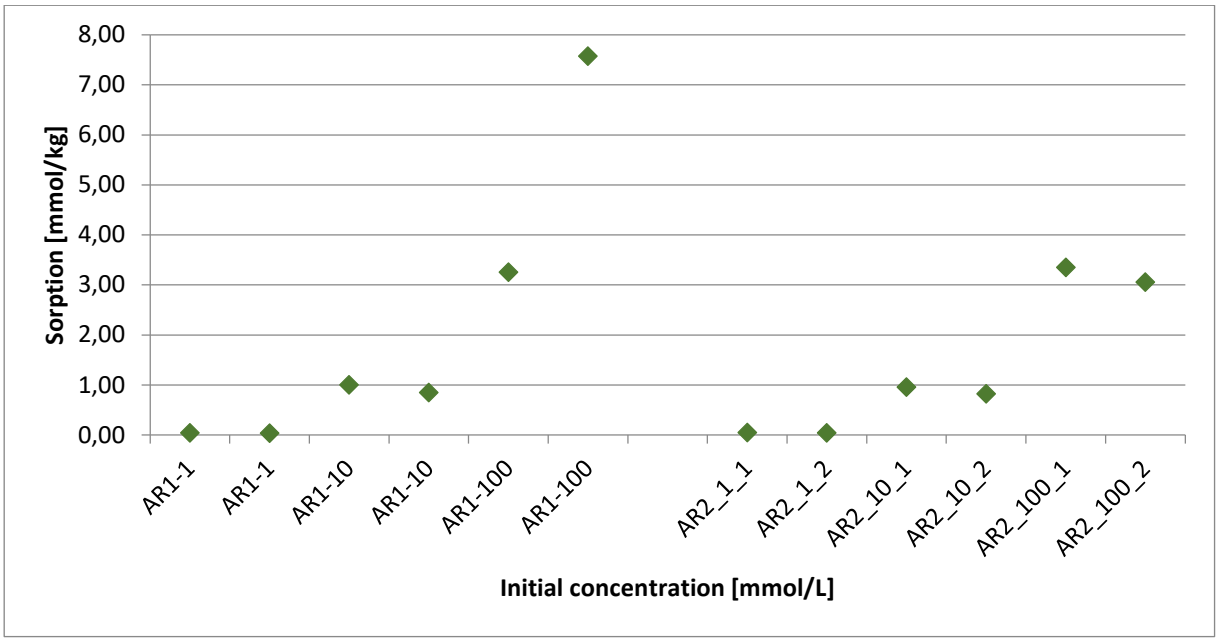

Fig. 5.13. A graph of sorption as a function of initial concentration for a lead Pb

Labels AR_1 and AR_2 in the Fig. 5.13. mean aerogel 1% and aerogel 2% respectively. Numbers 1, 10 and 100 are initial concentrations of lead in mmol/L. Numbers 1 and 2 are numbers of samples in duplicates. Based on scores presented in Table. 5.2. one could sugest that both aerogel 1% and aerogel 2% are characterized by highest sorption by initial concentration of lead equal to 100 mmol/L. The sorption for this concentration is equal 5,417 mmol/kg and 3,355 mmol/kg. According to the scores for 1 mmol/L and 10 mmol/L the differences are negligible and for both aerogels sorption is quite similar.

5.5. Sorption od cadmium

Table. 5.3.Scores of absorbance for standard solutions of cadmium - Cd

Standards [mg Cd/L]	AAS indication	Calculated concentration [mg Cd/L]
0,0500	0,027	0,067
0,0500	-	-
0,1000	0,043	0,099
0,1000	0,045	0,103
0,2500	0,103	0,236
0,2500	0,102	0,233
0,5000	0,202	0,501
0,5000	0,201	0,500
0,7500	0,276	0,735
0,7500	0,290	0,783
1,0000	0,360	1,035
1,0000	0,340	0,959
1,2500	0,434	1,329
1,2500	0,413	1,243
1,5000	0,477	1,514
1,5000	0,453	1,412

Based on AAS scores for standard solutions of cadmium, calibration curve was established, as was for lead. Polynominal fit yields Pearson's coeffcient equal to 99,48%.

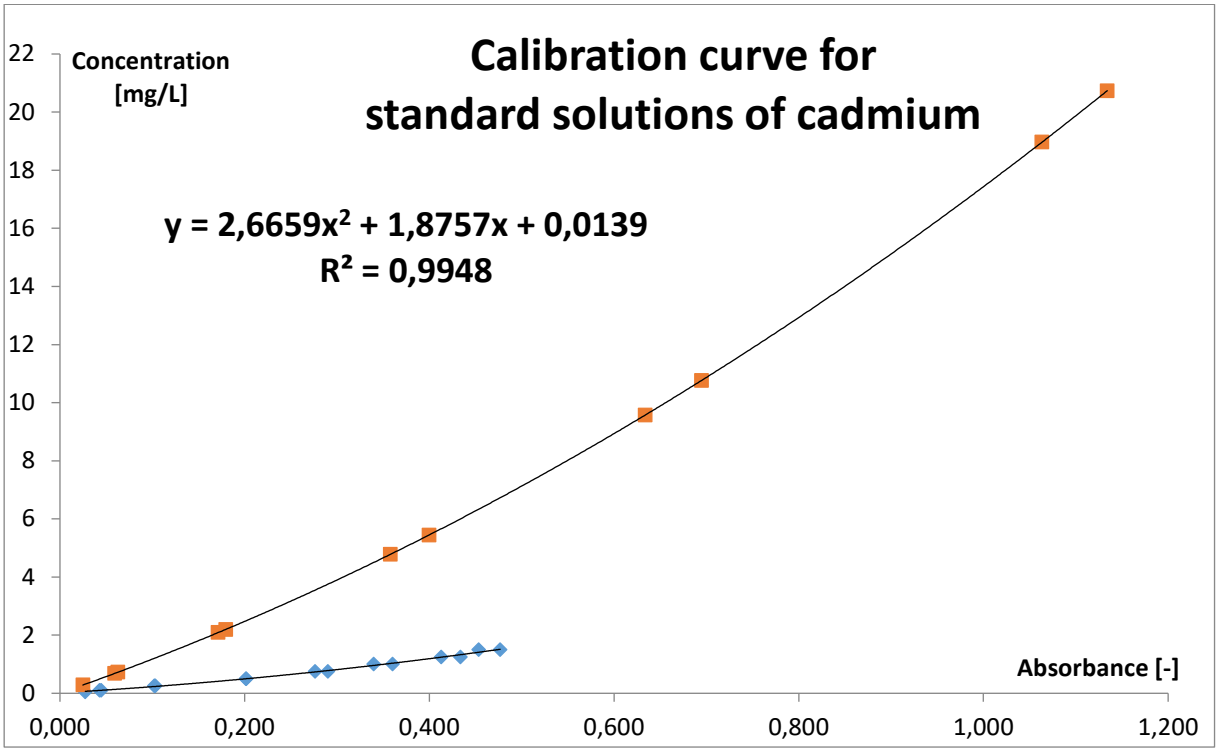

Fig. 5.14.Calibartion curve with Pearson's coefficient for standard solutions of cadmium - Cd

Having possessed calibration curve and formula for polynominal fit an equilibrum concentration of cadmium was calculated taking into consideration initial mass of an aerogel's sample and dillution of a standard solution. Scores regarding the sorption on aergels are presented in Table. 5.4.

Table. 5.4. Sorption scores of cadmium for two aerogels – 1% and 2%

Sample's symbole [-]	AAS indication [-]	Dillution [-]	Mass [kg]	Solution's volume [L]	SORPTION [mmol/kg]
RW-0,1	0,2855	10	-	-	-
RW-0,1	0,2846	10	-	-	-
RW-1	0,2866	100	-	-	-
RW-1	0,2973	100	-	-	-
RW-10	0,2519	1000	-	-	-
RW-10	0,2657	1000	-	-	-
RW-100	0,4235	10000	-	-	-
RW-100	0,4662	10000	-	-	-
AR1_0,1_1	0,1537	10	0,0000262	0,00025	**0,0038**
AR1_0,1_2	0,0438	10	0,0000232	0,00025	**0,0055**
AR1-1_1	0,021	100	0,0000245	0,00025	**0,0627**
AR1-1_2	0,038	100	0,0000242	0,00025	**0,0621**
AR1-10_1	0,229	1000	0,0000273	0,00025	**0,0720**
AR1-10_2	0,132	1000	0,0000252	0,00025	**0,3530**
AR1-100_1	0,317	10000	0,0000275	0,00025	**4,0373**
AR1-100_2	0,320	10000	0,000024	0,00025	**4,9647**

AR2_0,1_1	0,130	10	0,0000238	0,00025	**0,0039**
AR2_0,1_2	0,129	10	0,0000245	0,00025	**0,0041**
AR2_1_1	0,096	100	0,0000273	0,00025	**0,0539**
AR2_1_2	0,092	100	0,000026	0,00025	**0,0556**
AR2_10_1		1000	0,0000265	0,00025	**0,6073**
AR2_10_2		1000	0,0000262	0,00025	**0,6424**
AR_100_1	0,221	10000	0,0000263	0,00025	**6,8357**
AR2_100_2	0,225	10000	0,0000258	0,00025	**8,2725**

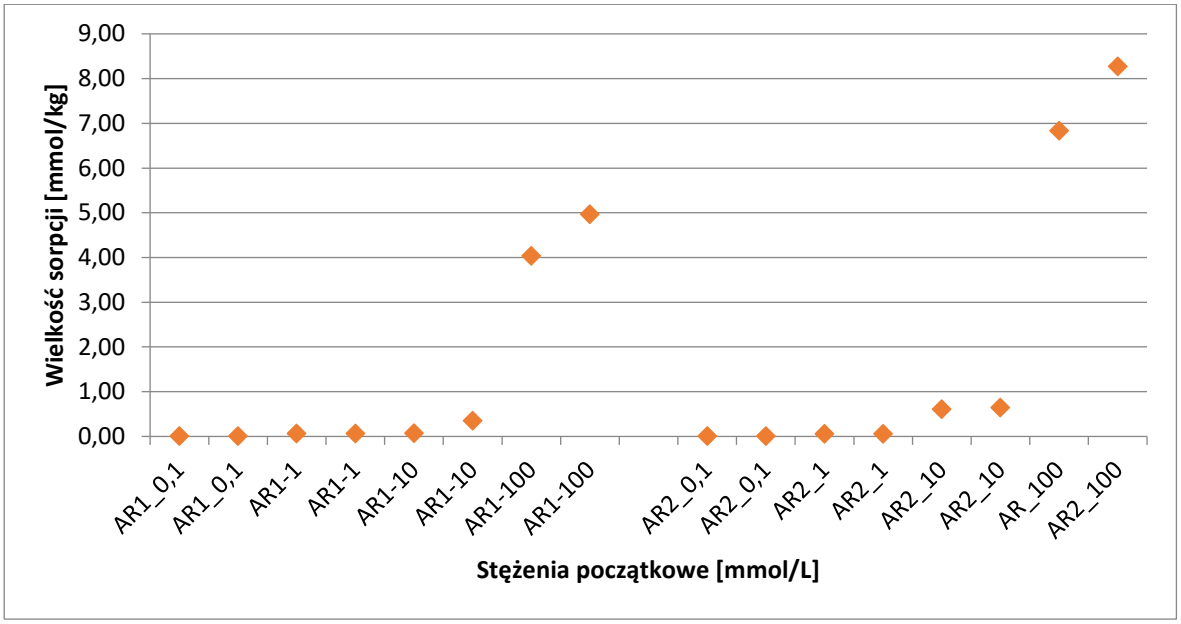

Fig. 5.15. A graph of sorption as a function of initial concentration forcadmium - Cd

Simlar to sorption of lead an AR_1 and AR_2 badges mean aerogel 1% and aerogel 2% respectively. Numbers 0.1, 1, 10, 100 mean concentration of standard solutions expressed as mmol/L. Sorption for initial concentration equal to 0.1 mmol/L and 1 mmol/L is similar for both 1% aerogel and 2% aerogel Fig. 5.15.

When it comes to standard concentration of cadmium equal to 10 mmol/L better sorption express 1% aerogel with sorpion equal to 0,72 mmol/kg, when for 2% aerogel this value is equal to 0,642 mol/kg.

The biggest difference between two aerogels in sorption is for standard solution equal to 100 mmol/L Cd. For this concentration sorption for 1% aerogel is equal to 4,5 mmol/kg when for 2% aerogel sorption is almost twice as much and equals 8,27 mmol/kg.

6. Conclusions

Alginate-based aerogel as a biodegradable material , being a biosorbent, yields great sorption properties as compare to materials such as zeolites, metal organic frameworks (MOFs) and activated carbons used in water cleaning. Sorption is equal to 7,58 mmol/kg for Pb^{2+} ions and 8,27mmol/kg for Cd^{2+} ions.

The most probable mechanism of sorption is an ion exchange, therefore both Cd^{2+} and Pb^{2+} were removed from water via this mechanism.

Another, probable mechanism of heavy metal ions removal on aerogel material might be adsorption on the surface of an aerogel, as an effect of poor hydrogen bonds and Van der Waal's interactions. Therefore it is an

effects of so called physisorption when only one mechanism that stands behind sorption is on the surface of a sorbent - aerogel.

Microstructure analysis reveals three main structures of an aerogels. For 1% aerogel a typical microstructure was leaf-like structure visible in Fig. 5.11. On the other hand for 2% aerogel the typical structure were porous one visible on Fig. 5.10 and three-dimensional structure similar to α-helix of a DNA in an eucaryotic organisms.

A FTIR analysis reveals inhomogeneity of the chemistry of the surface of aerogel with presence of functional groups such as hydroxyl group (-OH), carboxyl group (-COO) and carbonyl group (-C=O). Thanks to these chemical groups it is possible to create a permanent chemical bonds between a sorbent and sorbates both organic and inorganic.

On the other side of the coin, a phase analysis (XRD) reveals a presence of three mineral phases in powdered aerogel sample namely calcite (α-$CaCO_3$), aragonite (β-$CaCO_3$) and calcite hydrate - $CaCO_3$*$3H_2O$.

A thermal analysis gave a proof that alginate-based aerogel is stable in the temperature up to 650ºC. As an effect of this it is possible to utilize aerogel material in a high-temperature DeNO_x process (harmful nitrogen oxides - NO_x removal) and in selective catalytic reduction (SCR) where temperature window for typical vanadium catalyst on γ-Al_2O_3 support is between 350ºC up to 500ºC.

It is worth to highlight that we do not know how both cadmium and lead are linked by aergoel material. Therefore it would be beneficial to utilise XPS analytical method. Thanks to this method we could measure a distribution of elements on the surface and identify their chemical state and concentration. This analysis would straightforward give an answer regarding bond character between sorbent and sorbate and element's oxidation state.

To sum up all of previously mentioned passages, investigated in this research an alginate-based aerogel, being a biodegradable material, might be use in industrial applications especially in environmental protection and in material engineering. Based on conducted sorption experiments of inorganic pollutants (heavy metal ions) form water systems, one could conclude that this method is highly effective utilizing aerogels as sorbents.

What is more, removal of heavy metal ions via adsorption process and ion exchange on biodegradable biosorbents is waste-free method, which complies with circular economy trend.

References

[1] Araki S., (2013), Preparation and CO_2 adsorption properties of aminopropyl-functionalized mesoporous silica microspheres, Colloid Interface Science, vol. 339, s. 144-154.

[2] Barakat M.A, (2011), New trends in removing heavy metals from industrial wastewater, Arabian Journal of Chemistry, vol. 4, p. 361–377.

[3] Bartczak P., (2017) Ocena zdolności sorpcyjnych materiałów pochodzenia naturalnego w usuwaniu wybranych zanieczyszczeń nieorganicznych i organicznych z układów wodnych, Praca doktorska, Politechnika Poznańska, p. 9-10.

[4] Pierre A.C., Pajonk G.M., (2002), Chemistry of aerogels and their applications Lyon, vol. 102, p. 4243-4265.

[5] Choi S., Drese J.H., Jones C.W., (2009), Adsorbent materials for carbon dioxide (CO_2) capture from large anthropogenic point sources, Sustainable Chemistry, vol. 2, p. 796-854.

[6] Cui S., Cheng W., Shen X., Fan M., Russel A., Wu Z., Yi X., (2011). Mesoporous amine-modified SiO_2 aerogel: a potential CO2 sorbent, Energy and Environmental Sciences, vol. 6, p. 2070-2074.

[7] Dingicai W., Zhuoqi S., Ruowen F., (2006), Structure and adsorption properties of activated carbon aerogels, Applied Polymer Science, vol. 99, p. 2263-2267.

[8] Drese J.H., Choi S., Didas A., Bollini P., Gray M.L., Gray C., Jones W., (2005), Effect of support structure on CO_2 adsorption properties of pore-expanded hyperbranched aminosilicas, Microporus and Mesoporous Materials, vol. 151, p. 231-240.

[9] Ridha F.N., Macchi A., Anthony E.J., (2015), Enchanced CO_2 capture by biomass templated Ca(OH)2-baseed pellet's, Chemical Engineering Journal, vol. 274, p. 69-75.

[10] Fairen-Jimenez D., Carrasco-Marin F., Moreno-Castilla C., (2007), Adsorption of benzene, toluene and xylenes on monolithic carbon aerogels from dry air flows, Langmuir, vol. 23, p. 10095-10101.

[11] Fan X., Zhang. G., Shu Z., Shi J., Shi Z., (2014), Chitosan derived nitrogen-doped microporous carbons for high performance CO_2 capture, Carbon, vol. 61, p. 423-430.

[12] Gebald C., Wurzbacher J.A., Tingaut P., Zimmermann T., Steinfeld A., (2009), Amine-based nanofibrillated callulose as adsorbent for CO_2 capture from air, Environmental Science Technology, vol. 45, p. 9101-9108.

[13] Gil M.V., Alvarez-Guiterrez N., Martinez F.R.M., Pevida A.M.C., (2015), Carbon adsorbents for CO_2 capture from hydrogen and biogas streams: breakthrough adsorption study, Chemical Engineering Journal, vol. 269, p. 148-156.

[14] Gupta V.K., Carrott P.J.M., Ribeiro Carrott M.M.L., (2009) Low-cost adsorbents: growing approach to wastewater treatment - a review, Critical Reviews in Environmental Science and Technology, vol. 39, p. 783–842.

[15] Maleki H., Duraes L., Portugal A., (2014), An overview on silica aerogels synthesis and different mechanical reinforcing strategies, Journal of Non-Crystalline Solids, vol. 385, p. 55-74.

[16] Ismail, A.A., Ibrahim I.A., Ahmed M.S., Mohamed R.M., El-Shall H., (2004). Sol-gel synthesis of titania-silica photocatalyst for cyanide degradation, Journal of Photochemistry, Photobiology and Chemistry, vol. 163, p. 445-451.

[17] Kistler S. (1931). Coherent expanded aerogels and jellies, Nature, vol. 127, p. 741.

[18] Kistler S. (1932). Coherent expanded aerogels, Journal of Physical Chemistry, vol. 36, p. 52-64.

[19] Kong Y., Shen X., Cui S., Fan M., (2015), Development of monolithic adsorbent via polymeric sol-gel process for low-concentration CO_2 capture, Applied Energy, vol. 147, p. 308-317.

[20] Kumar Meena A., Mishra G.K., Rai P.K., Rajagopal C., Nagar P.N., (2005), Removal of heavy metal ions from aqueous solutions using carbon aerogels as an adsorbent, Journal of Hazardous Materials, vol. 122, p. 161-170.

[21] Kłonkowski A.M,. Grobelna B., Widernik T., Jankowska-Frydel A., Mozgawa W., (1999), The coordination state of copper (II) complexes anchored and grafted onto surface of organically modified silicates, Langmuir, vol. 114, p. 5814-5819.

[22] Linneen N., Pfeffer R., Lin Y.S., (2013), CO_2 capture using particulate silica aerogel immobilized with tetraethylenepentamine, Microporous and Mesoporous Materials, vol. 176, p. 123-131.

[23] Maldonado-Hodar F.J., Carlos M.C., Carrasco-Marin F., Perez-Cadenas A.F., (2007), Reversible toluene adsorption on monolithic carbon aerogels, Journal of Hazardous Materials, vol. 148, p. 548-552.

[24] Maleki, H. (2016), Recent advances in aerogels for environmental remediation applications - a review, Chemical Engineering Journal, vol.300, p. 6.

[25] Husing N., Schubert U., (1998). Aerogels - airy materials: chemistry, structure and properties, Chemistry International, vol. 37, p. 22-45.

[26] Leal O., (1995), Reversible adsorption of carbon dioxide on amine surface-bonded silica gel, Inorganic Chimica Acta, vol. 240, p. 183-189.

[27] Rachbereger F., Ilari G., Niederberger M., (2014), Assembly of antimony doped tin oxide nanocrystals into conducting macroscopic aerogel monoliths, Chemical Communications, vol.86, p. 13138-13141.

[28] Zeng S., Gao H., Zhang X., Dong H., Zhang X., Zhang S., (2014), Efficient and reversible capture of SO_2 by pyridinium-based ionic liquids, Chemical Engineering Journal, vol. 251, p. 248-256.

[29] Standeker S., Novak Z., Knez Z., (2009), Removal of BTEX vapours from waste gas streams using silica aerogels of different hydrophobicity, Journal of Hazardous Materials, vol. 165, p. 1114-1118.

[30] Zhang X., Bao D., Huang Y., Dong H., Zhang X., Zhang S., (2014), Gas-liquid mass-transfer properties in CO2 adsorption system with ionic liquids, AIChE Journal, vol. 60, p. 2929-2939.

[31] Xu X., Song J., Andersen J.M., Miller B.G., Scaroni A.W., (2016), Novel polyethylenimine-modified mesoporous molecular sieve of MCM-41 type as high-capacity adsorbent for CO_2 capture, Energy & Fuels, vol.16, p. 1463-1469.

A Technical Review on Potential of Oxy Combustion Process in CCGT Cycle

Deogratias Uwizeyimana[1], Tarikul Hassan[1], Bayron David Alvarez Rodriguez[1]

[1] MSc Student, AGH University of Science and Technology/Faculty of Energy and Fuels, al. Adama Mickiewicza, 30-059 Kraków, Poland:

Abstract

Oxy combustion process is one of the most promising technologies being implemented in the efforts to mitigate the anthropogenic impact on greenhouses gas by the fossil-fueled power plants. The ever-increasing unrest in the global climate evolution as a result of greenhouse gas emissions have challenged the power generation and industrial sectors to find technical solutions for strongly reducing these emissions to the atmosphere. These technologies are gathered under the appellation of carbon capture and storage (CCS), where three main CO2 capture pathways are possible: the post-combustion, the pre-combustion, and the oxy-fuel combustion routes. Oxy-fuel combustion capture is not limited to coal and can be applied to natural gas with an adapted technology for gas turbines. The maturity of this technology is much less advanced than for oxy-coal combustion, and available literature is mainly limited to fundamental combustion studies and thermodynamic process analysis. In this paper, we are reviewing the concepts and intricacies of the oxy combustion processes of natural gas and its applicability in combined cycle gas turbines (CCGT).

Keywords: oxy-combustion, CCGT, CCS

1. Introduction

Oxy-fuel combustion is the process of combusting hydrocarbon fuel in a nearly pure oxygen environment, as opposed to air. The main purpose for using oxy-fuel combustion is to generate flue gas with very high concentrations of CO2 and water vapor, making it possible to separate or capture the CO2 from the flue gas with high efficiency [1]. The benefits of oxy-fuel combustion include reduced NOx emissions, high CO2 purity, and lower gas volumes due to increased density [1]. The oxygen, used for this type of combustion, is obtained by air separation. The most widely used method for separating oxygen from air is cryogenic oxygen generation. The flue gas from this kind of combustion mainly consists of CO2 and H2O [2].

CCGT is a form of highly efficient energy generation technology that combines a gas-fired turbine with a steam turbine. The design uses a gas turbine to create electricity and then captures the resulting waste heat to create steam, which in turn drives a steam turbine significantly increasing the system's power output without any increase in fuel. Incorporating oxy-fuel combustion in CCGT serves at least two purposes, one being the increase in power generation efficiency and at the same time this technology is more ecologically friendly comparing to other conventional fuel combustion systems.

2. Oxy-Combustion Process Analysis

As in any other combustion process, temperature is one key parameter that affects the oxy-fuel combustion. During the oxy-fuel combustion, temperature is controlled by diluting the oxygen with a portion of recycled flue gas [1]. This also makes up the volume of the missing N2 to ensure there is enough gas to carry the heat through the boiler [2]. The substitution of N2 with CO2 in the oxidizer will lead to a reduction of the flame speed [2]. This causes poor combustion performance and a modified distribution of temperature and species in the combustion chamber [3]. A numerical investigation on the chemical effects of CO2 has been performed. A comparison between numerical and experimental data showed, that the decrease in burning velocity for the oxy-fuel combustion cannot entirely be described by only considering the material properties of CO2 [4].

Anderson et al. have performed experiments on a 100-kW test unit, which facilitates O2/CO2 combustion with real flue gases recycle. The tests comprise a reference test with air and two O2/CO2 test cases with different recycled feed gas mixture concentrations of O2 (OF 21 at 21% O2, 79% CO2 and OF 27 at 27% O2, 73 vol % CO2). The results showed that the fuel burnout is delayed for the OF 21 case compared to air-fired conditions as a consequence of reduced temperature levels. Instead, the OF 27 case results in more similar combustion behavior, as compared to the reference conditions in terms of in-flame temperature and gas concentration levels, but with significantly increased flame radiation intensity [5].

Another trial has been conducted in a 300-kWh pilot-scale facility, composed of a burner, a combustion chamber, a flue gas cooler and a flue gas recycle fan. Flue gas composition, O2 concentration in the feeding gas and the flame temperature were monitored. The results obtained showed that the flame temperature with 21% O2 concentration in the feed gas is lower for oxy-combustion than combustion in air. However, the recycling ratio can be adjusted to control the flame temperature and an O2 concentration of 24% in the feed gas is necessary to maintain a temperature profile similar to that observed for combustion in air. It has been observed also that oxy-combustion with flue gas recycling improves the heat transfer. Finally, the results showed also that the NOx emissions are highly reduced because of the absence of N2 in the feed gas [6].

Fig. 2.1. shows the centerline flame temperature profiles measured for combustion in air. It can be observed that the average temperature is smaller when the excess O2 increases because of the inert gasses' dilution effect (mainly due to N2). Indeed, for a higher air flow rate, the combustion energy is released in a larger inert gas volume and, thus, the temperature measured decreases. Fig. 2.2., 2.3., and 2.4. show the centerline flame temperature profiles measured during oxy-combustion trials. It can be observed again that the average temperature is smaller when the excess O2 increase because of the inert gasses' dilution effect (mainly due to CO2 and H2O in this case). For a given O2 concentration in the flue gas (4%), the pure oxygen flow rate is fixed and the O2 concentration in the oxidizer is controlled by adjusting the RFG flow rate. For a higher RFG flow rate, the volume of inert gases (mainly CO2 and H2O) is larger and, thus, the temperature measured decreases. To compare oxy-fuel combustion with conventional combustion, the baseline case chosen corresponds to combustion in air with an O2 concentration in the flue gas of 4%. From these results, it can be observed that the temperature profile in the combustor with 21% O2 concentration in the oxidizer is lower for oxy-combustion than combustion in air [6].

Oxy-fuel combustion generates a flue gas with high proportions of CO2 and H2O, which have high heat capacities compared to N2. This results in smaller average temperature in the combustion chamber. To attain a similar flame temperature to that observed for conventional combustion, the O2 concentration in the oxidizer must be higher than 21%. An O2 concentration of 24% in the feed gas is found to produce the closest conditions compared to air firing [6].

From this experiment, four temperature profile have been developed.

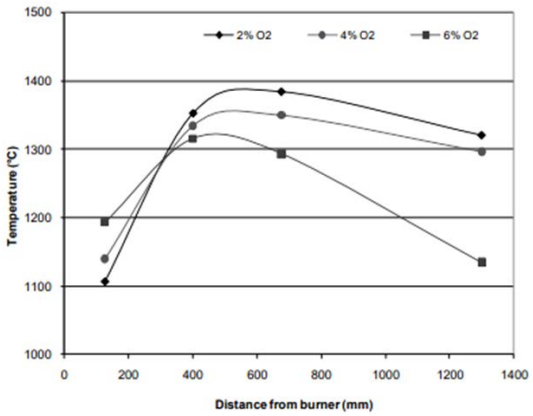

Fig. 2.1. - Temperature profiles for combustion in air (21% O_2 in air)

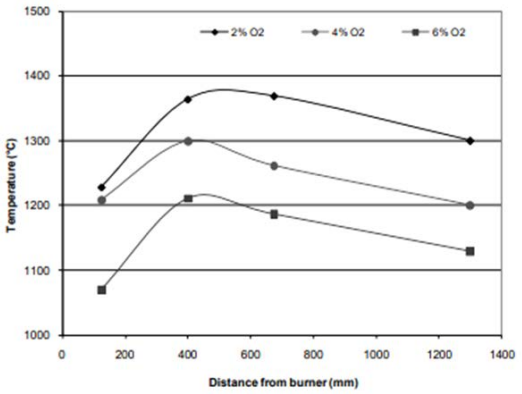

Fig. 2.2. - Temperature profiles for oxy combustion (19% O_2 in oxidizer)

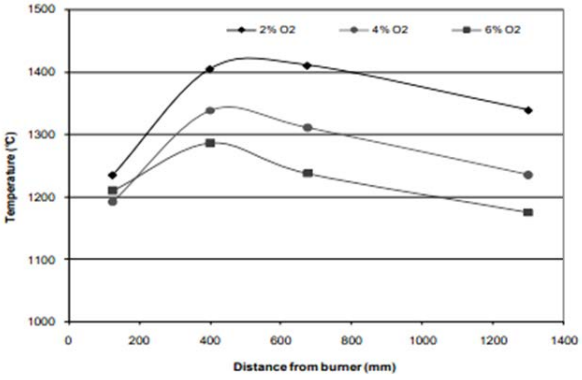

Fig. 2.3. - Temperature profiles for oxy combustion (21% O_2 in oxidizer)

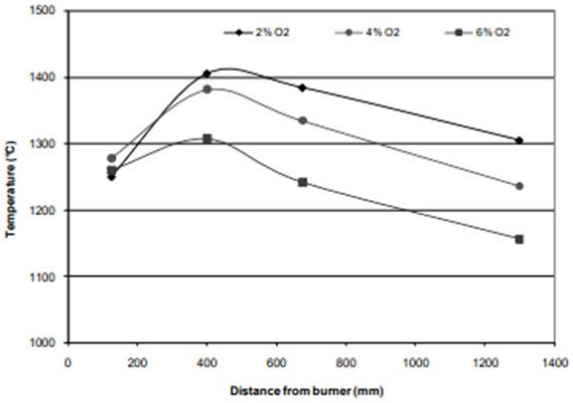

Fig. 2.4. - Temperature profiles for oxy combustion (24% O_2 in oxidizer)

The same experiment analysed NOx emission also. The following figure represents NOx concentration (ppm) for air/enriched air and O2/RFG combustion.

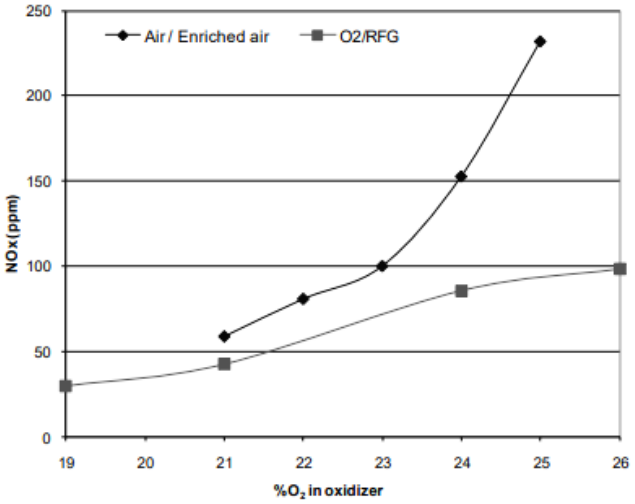

Fig. 2.5. NOx concentration (ppm) for air/enriched air and O2/RFG combustion

Fig. 2.5. shows the NOx concentrations measured in the flue gas in the range of 21−25% of O2 in the feed gas for combustion in air and enriched air and in the range of 19−26% of O2 for oxy-fuel combustion. An O2 concentration of 4% in the flue gas is used in each trial. In both cases, the NOx concentration increases when the O2 concentration in the oxidizer is higher. For larger O2 concentration, the average temperature measured is higher, which increases NOx production. It can also be observed that NOx concentrations are smaller for oxy-fuel combustion compared to combustion in air. This is mainly due to the absence of N2 in the feed gas and to lower temperatures in the case of oxy-combustion (for the same O2 concentration in oxidizer). However, the NOx concentration is higher for oxy-combustion with 24% of O2 in oxidizer compared to air firing (21% O2). In fact, an air leakage maintains a relatively high N2 concentration in the flue gas (approximately 10% on a wet basis). Thus, a higher NOx reduction can be expected. Moreover, oxy-fuel combustion highly reduces the volume of flue gas after recycling. The expression of NOx emissions in terms of concentration is not suitable because this flue gas volume has to be taken into account. Thus, it can be said that oxy-fuel combustion reduces NOx production rate.

The high proportions of CO2 and H2O in the furnace gases result in higher gas emissivity, so that similar radiative heat transfer for a boiler retrofitted to oxy-fuel will be attained when the O2 proportion of the gases passing through the burner is less than the 30% required for the same AFT.

The volume of gases flowing through the furnace is reduced somewhat, and the volume of flue gas (after recycling) is reduced by about 80%. The density of the flue gas is increased, as the molecular weight of CO2 is 44, compared to 28 for N2 [7].

A comparison between numerical and experimental data showed that the decrease in burning velocity for the oxy-fuel combustion cannot entirely be described by only considering the material properties of CO2. CO2 affects the combustion reactions especially by the reaction CO + OH• → CO2 + H•. The competition of CO2 for H• radical through the above reverse reaction with the single most important chain branching reaction H + O2 → O• + OH• significantly reduces the concentrations of important radicals, that is, O•, H•, and OH•, leading to significant reduction of fuel burning rate. This hypothesis is supported by a comparison of the burning velocity of methane flames and hydrogen flames in a CO2/O2 gas mixture. The influence of CO2 on the burning velocity of hydrogen flames is less significant because the concentration of hydrogen radicals is much higher. Finally, it was summarized, that the chemical effect of CO2 significantly reduces the burning velocity of methane, whereby the relative importance of this chemical effect increases with increasing CO2 concentration in the oxidizing mixture [6].

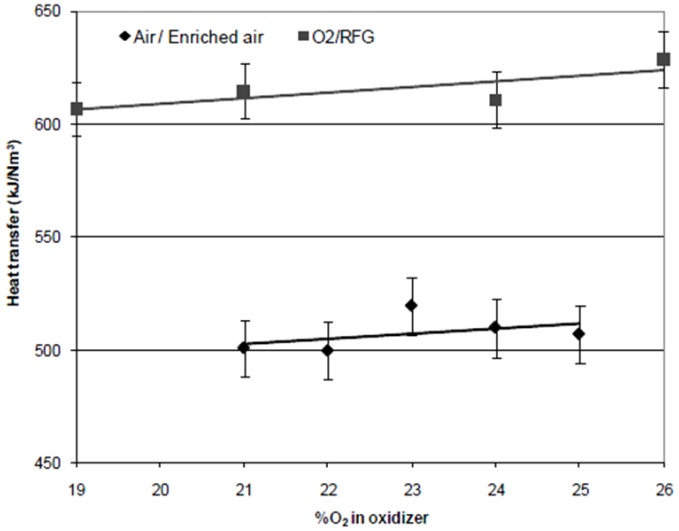

Fig. 2.6. Heat transfer for air/enriched air and O2/RFG combustion [6]

2.1 Economics and Efficiency of Oxyfuel Combustion

1. The oxy-fuel combustion contributes also to a higher boiler thermal efficiency with lower sensible heat in flue gas and offers the potential to lower oxy-fuel plant investment by reducing the scale of flue gas cleaning equipment [8].
2. As oxy-fuel combustion combined with sequestration must provide power to several significant unit operations, such as flue gas compression, that are not required in a conventional plant without sequestration, oxy-fuel combustion/sequestration is less efficient per unit of energy produced [9].
3. Oxy-fuel combustion will impose a 7–10% efficiency penalty on the power generation process. The major contributors to this efficiency penalty are oxygen production and CO2 compression [2].
4. Typical electrical power requirements range from 160 kWh to 270 kWh per ton of O2 with a commonly cited approximate value of 200 kWh per ton, depending on the desired purity [2].
5. Despite their complexity, commercial cryogenic units achieve low Second Law efficiencies in the range 15–24% [10].
6. The mass and volume of the flue gas are reduced by approximately 75%. Because the flue gas volume is reduced, less heat is lost in the flue gas. The size of the flue gas treatment equipment can be reduced by 75% [11].
7. The flue gas is primarily CO2, suitable for sequestration. The concentration of pollutants in the flue gas is higher, making separation easier [11].
8. Because nitrogen from air is absent, nitrogen oxide production is greatly reduced [11].

3. Combined Cycle Gas Turbine

Combined Cycle Gas Turbines (CCGT) are a form of highly efficient energy generation technology that combines a gas-fired turbine with a steam turbine. The design uses a gas turbine to create electricity and then captures the resulting waste heat to create steam, which in turn drives a steam turbine significantly increasing the system's power output without any increase in fuel. The technology is typically powered using natural gas, but it can also be fueled using coal, biomass and even solar power as part of solar combined cycle plants [12].

There are many natural gasses fired oxy-combustion turbine cycles, including ones that are being developed commercially and ones that have been proposed by academics. These include the following [13]: 1. Semi-Closed Oxy-Combustion Combined Cycle (SCOC-CC), 2. NET Power cycle, 3. Graz cycle, 4. CES cycle.

These cycles mainly differ for two criteria, the main component of the fluid used as moderator of the combustion temperature, being also the working fluid of the power cycle (water or CO2) and the technology used to produce oxygen: cryogenic distillation rather than membrane separation. Among the plants using a cryogenic air separation unit, the SCOC-CC and NET Power cycles use recycled CO2 as temperature moderator [13]. Among these cycles, Semi-Closed Oxy-Combustion Combined Cycle (SCOC-CC) is the most mature one and, also in practice commercially.

3.1 Semi-Closed Oxy-Combustion Combined Cycle (SCOC-CC)

The following figure shows a schematic of the SCOC-CC cycle. The SCOC-CC consists of five main parts: the topping cycle, the bottoming cycle, the air separation unit, the CO2 compression and the flue gas condenser [14].

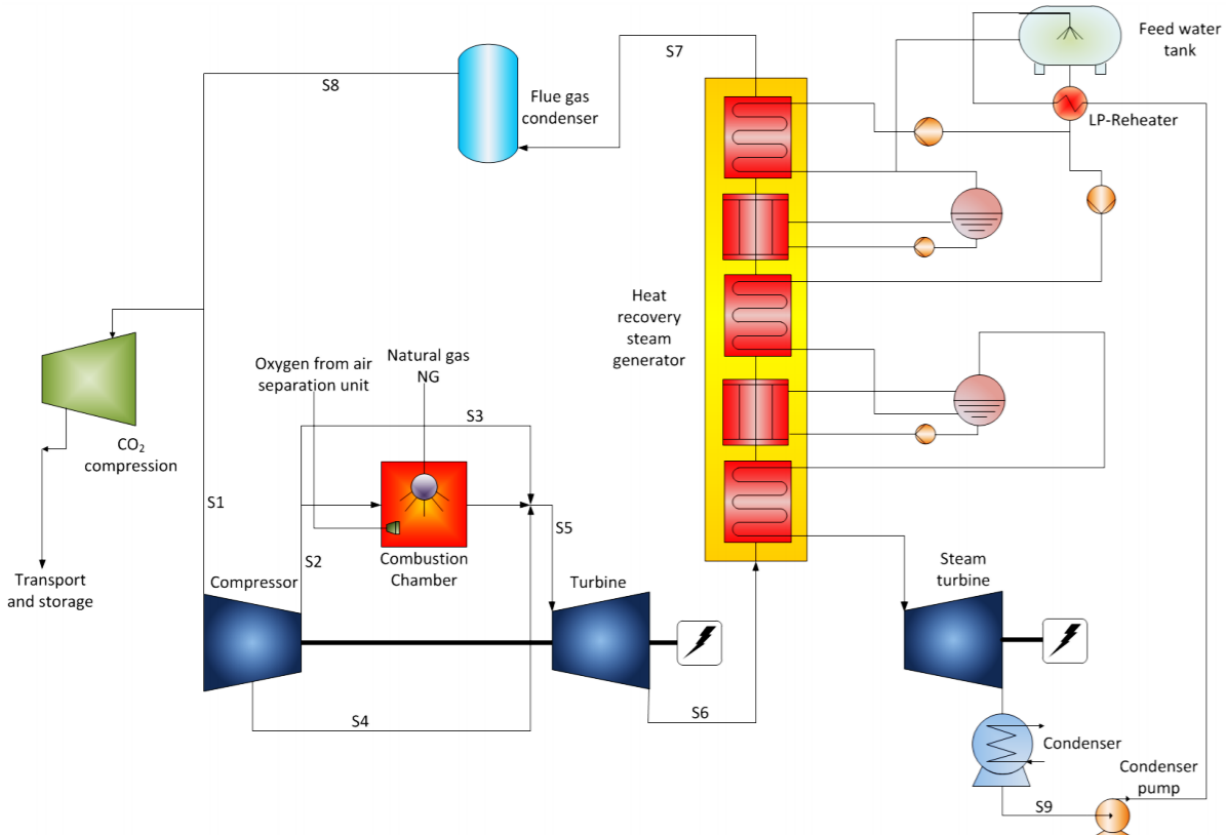

Fig. 3.1. Principle flow scheme for SCOC-CC [13]

3.2 Semi-Closed Oxy-Combustion Combined Cycle (SCOC-CC)

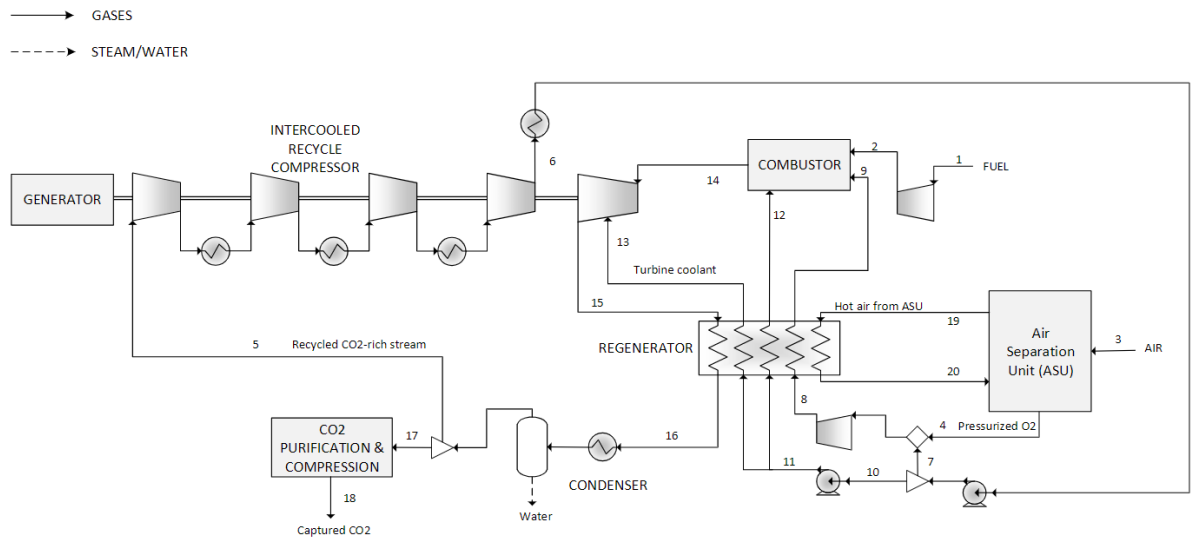

Fig. 3.2. NET Power Cycle [13]

The NET Power cycle utilizes carbon dioxide as the working fluid in a high-pressure, low-pressure-ratio Brayton cycle, operating with a single turbine that has an inlet pressure around 300 bar and pressure ratio around 9, set so that the turbine outlet pressure matches the requirements of the downstream CO2 purification unit. The high-pressure combustor burns natural gas in an oxidant stream resulting from the mixture of high-purity oxygen stream with the recycle gas stream and provides the feed to a direct-fired CO2 turbine. A regenerative heat exchanger transfers heat from the high temperature turbine exhaust to the high pressure recycle required to control the combustion temperature and cool the turbine blades. Heat from the hot air from the ASU main air compressor is recovered in the regenerative exchanger to enhance the cycle efficiency [13].

3.3 Modified S-GRAZ cycle

Different variants of the Graz cycle have been proposed and among the alternatives evaluated in the study, the Modified S-Graz Cycle presents the most attractive results. The cycle consists of a high-temperature cycle, including the gas turbine and associated compressors and combustion chamber, the HRSG, a high pressure steam turbine (back-pressure type) and a low temperature cycle, substantially including a low pressure turbine and condenser. The fuel along with the nearly stoichiometric mass flow of oxygen is fed to the combustion chamber, which is operated at a pressure around 45 bar. The working fluid, mainly composed of steam, is expanded to a pressure slightly above the atmospheric pressure and sent to a single pressure level HRSG, generating high pressure steam to be expanded in the back pressure steam turbine down to the pressure level required for steam injection in the gas turbine expander for blade metal temperature control. Part of the cooled gas from the HRSG are compressed and recycled back to the combustion chamber for combustion temperature control, while the remaining portion is sent to the low temperature cycle [13].

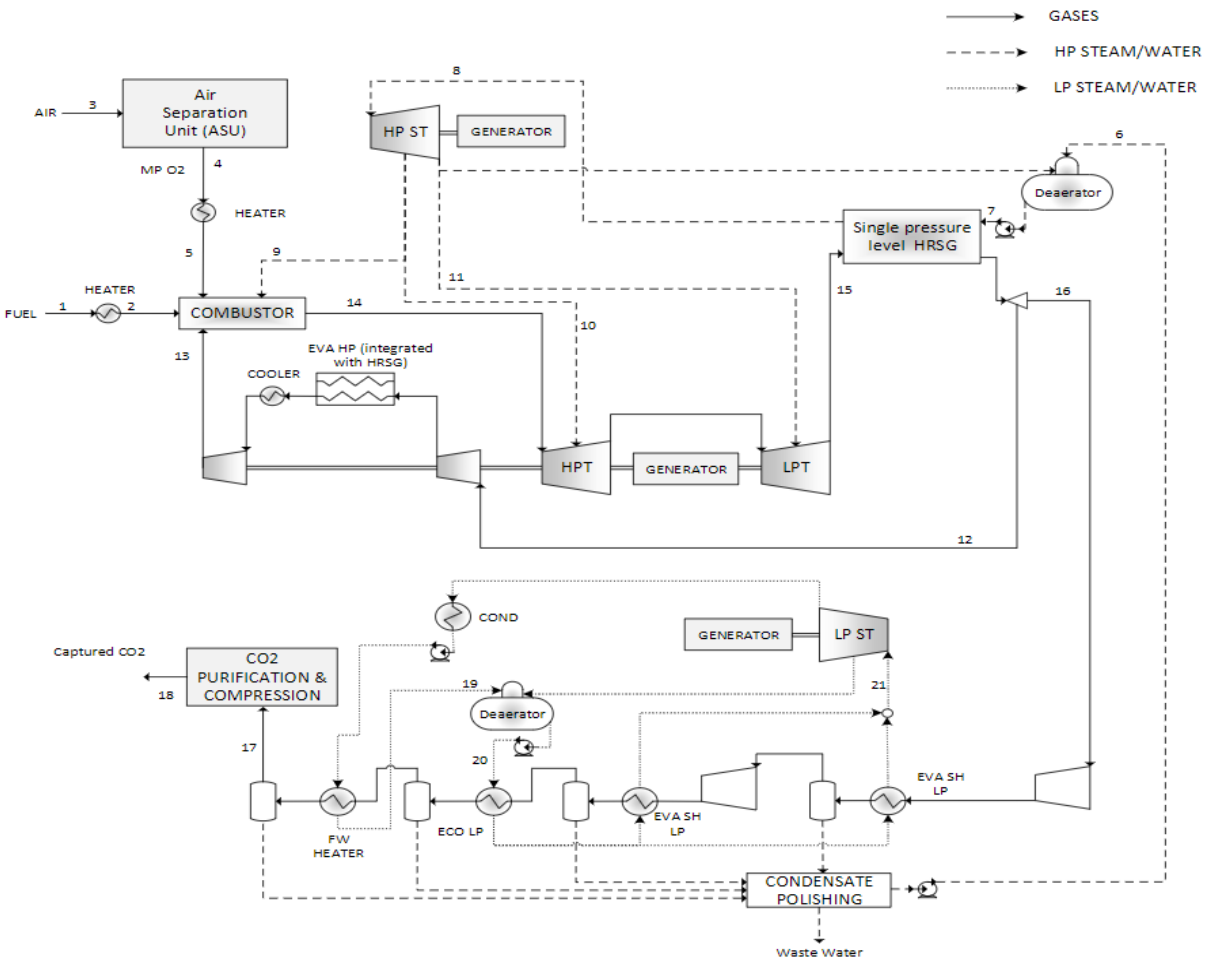

Fig. 3.3. Modified S-Graz Cycle [13]

3.4 CSE Cycle

This cycle, proposed by Clean Energy Systems (CES) uses water, both in vapor and liquid phases, as combustion temperature moderator. Though different versions have been proposed, the most promising cycle consists of a high pressure oxy-fuel combustor where part of the fuel and oxidant are combusted utilizing steam in supercritical conditions as temperature moderator, while hot gas produced in the gas generator is expanded in a steam cooled HP turbine. The HP turbine exhaust gas is double-reheated by supplementary oxy-fuel combustion and further expanded in a MP and a LP section of the gas turbine, down to vacuum conditions. The cooling stream for these gas turbine sections is part of the flue gas from the upstream turbine sections. This configuration

shows the best efficiency among the different schemes proposed by Clean Energy Systems, differing also for the different technology effort and time required to develop some of the key cycle components. CES considers this cycle as their long-term high-efficient solution for oxy-combustion natural gas cycle application [13].

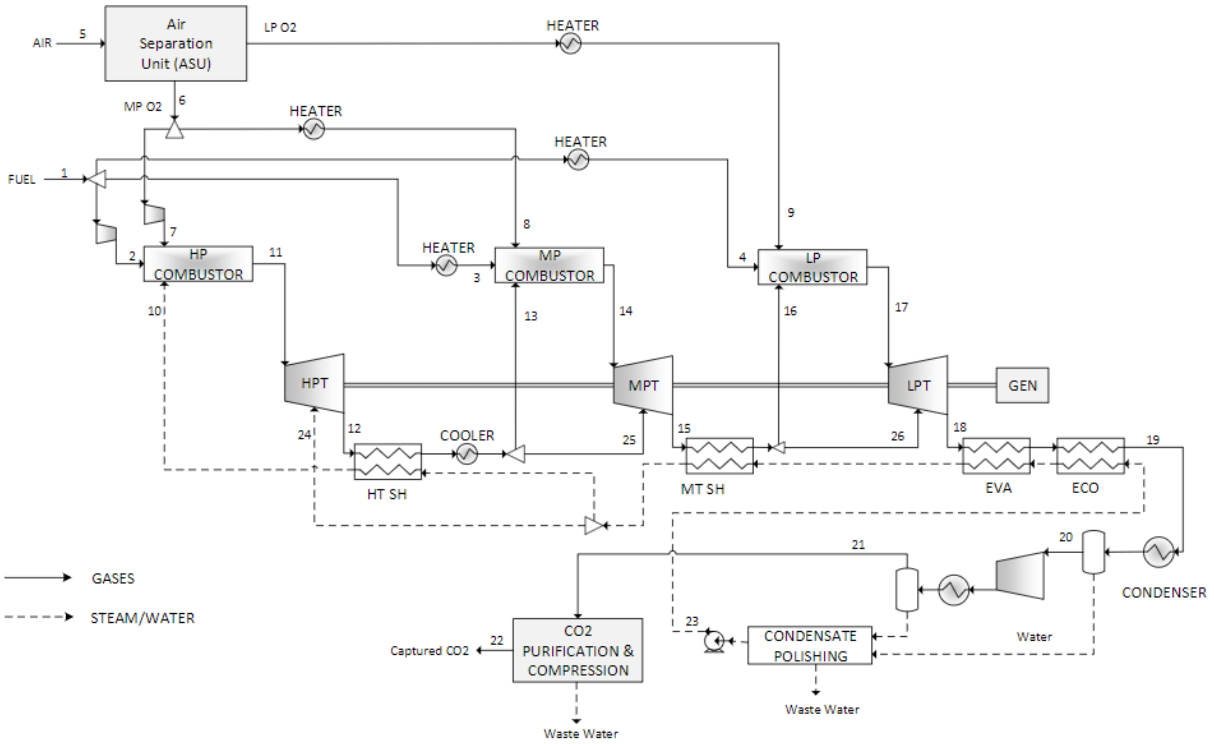

Fig. 3.4. CSE Cycle [13]

3.5. Efficiency of Different Cycles

In one study a contrast in efficiency and performance was made for the plants, all with the same natural gas feed rate of 1,536 MWh (LHV basis) [13]. The performance summary for different cycles is presented in the table below.

Table. 3.1. Performance Summary [13]

	Net power output, MWe	CO_2 captured, kg/MWh	CO_2 emissions, kg/MWh	Efficiency (LHV basis), %	Efficiency penalty for capture (LHV), %points
Reference NGCC	904	-	348	58.8	-
SCOC-CC	757	377	39	49.3	9.5
NET Power cycle	846	336	37	55.1	3.7
Modified S-Graz cycle	756	375	41	49.2	9.6
Supercritical CES	751	379	41	18.9	9.9

From Table. 3.1., we can say that the highest efficiency of 55% is for the NET Power cycle, the other three oxy-combustion processes have lower efficiencies of around 49%. The developers of the NET Power cycle have estimated an efficiency of 59% for their cycle using proprietary improvements and CES has estimated an efficiency of 53% for its cycle. The supercritical version of the CES cycle is a relatively recent innovation. Adopting a lower coolant temperature would be likely more advantageous and is currently being pursued by CES as part of their on-going cycle optimization work [13].

From the same study [2], the two most promising oxy-combustion turbine cycles were compared with the best performing NGCC with post combustion capture, using the new generation of proprietary MEA-based solvent in the capture unit. Main technical and economic results are summarized in Table. 3.2.

Table. 3.2. Comparison of oxy-combustion and post combustion capture plants [13]

	Efficiency, % (LHV)	Total plant cost, €/kW	LCOE, €/MWh	CO_2 avoidance cost
Reference NGCC	58.8	655	62.5	-
SCOC-CC	49.3	1470	92.8	98
NET Power cycle	55.1	1320	83.6	68
NGCC with post-combustion capture	52.0	1200	84.7	71

The Total Plant Cost of the oxy-combustion plants are higher than that of the NGCC with post-combustion capture, however, the higher efficiency of the NET Power cycle allows lowering the relevant LCOE and consequently the CO2 avoidance cost below those of the post combustion capture based plant [13].

4. Conclusion

Several technologies have been developed for carbon capture and storage (CCS). The purpose of this CCS is to reduce the CO2 emission during fossil fuel combustion and thus, mitigate the global warming effect. Among the developed technologies, post combustion carbon capture technology is in commercial use. But this system is expensive. Combining oxy-fuel natural gas in CCGT can be an economically viable solution for CO2 capture. Although oxy-combustion has its own energy penalty, usage of the waste heat for running steam turbine largely makes up for it.

In addition, flues gas from oxy-fuel combustion is better in heat transfer compared to flue gas generated from air combustion. Also, oxy-combustion generates negligible amount of NOx and the amount of flue gas is very small, thus, reducing the size and cost of flue gas handling facility. The efficiency of this kind of power generation systems ranges between 50% to 55%, which is reasonably good since this system captures most of the generated CO2 with almost zero NOx emission. Further development in the technology can increase the efficiency significantly.

References

[1] Shaddix C., Molina A., in Oxy-Fuel Combustion for Power Generation and Carbon Dioxide (CO2) Capture, 2011

[2] Habib M.A., Nemitallah M., and Ben-Mansour R. Recent Development in Oxy-Combustion Technology and Its Applications to Gas Turbine Combustors and ITM Reactors. Energy & Fuels 2013 27 (1), 2-19.

[3] Zhu, D.; Egolfopoulos, F.; Law, C. Symp. (Int.) Combust. 1998, 21 (Issue 1) 1419– 1426

[4] Liu, F.; Guo, H.; Smallwood, G. J. Combust. Flame 2003, 133 (4) 495– 497

[5] "Flame and radiation characteristics of gas-fired O2/CO2 combustion", Andersson, Klas; Johnsson, Filip, Fuel (2007), 86 (5-6), 656-668CODEN: FUELAC; ISSN:0016-2361. (Elsevier Ltd.)

[6] Bensakhria, Ammar, Leturia, Mikel. Natural gas oxy-combustion with flue gas recycling for CO 2 capture. 2010/01/01. 10.3303/CET1021107

[7] Combustion processes for carbon capture,Wall, Terry F.,Proceedings of the Combustion Institute (2007), 31 (Pt. 1), 31-47CODEN: PCIRC2; ISSN:1540-7489. (Elsevier)

[8] Marin, O., Châtel-Pélage, F., Perrin, N., Chen, S., Lu, Y. and Rostam-Abadi, M., 2003, Economic analysis of oxygen-fired coal boilers, The 28th international technical conference on coal utilization and fuel systems, Clearwater, FL

[9] Khare, S.; Wall, T.; Gupta, R.; Elliott, L.; Buhre, B.Coal Technology: Yesterday–Today–Tomorrow, The 30th International Technical Conference on Coal Utilization and Fuel Systems, 2005.

[10] Simpson, Adam P.; Simon, A. J. "Second law comparison of oxy-fuel combustion and post-combustion carbon dioxide separation". Energy Conversion and Management (2007), 48 (11), 3034-3045CODEN: ECMADL; ISSN:0196-8904. (Elsevier Ltd.).

[11] WIKIPEDIA | https://en.wikipedia.org/wiki/Oxy-fuel_combustion_process.(last visited on September 1, 2019)

[12] BusinessGreen|https://www.businessgreen.com/bg/glossary/1807455/combined-cycle-gas-turbine-ccgt.

[13] Ferrari N., Mancuso L., Davidson J., Chiesa P., Martelli E., Romano M.C. Oxy turbine for Power Plant with CO2 Capture. 13th International Conference on Greenhouse Gas Control Technologies, GHGT-13, 14-18. November 2016, Lausanne, Switzerland.

[14] Sammak M., Jonshagen K., Thern M. and Genrup M., Conceptual Design of a Mid-Sized Semi-Closed Oxy-Fuel Combustion Combined Cycle. DOI: 10.1115/GT2011-46299.

Neural Networks Applied to Garbage Sorting

Scientific statement

Jeon Ha Eun[1]

[1]*Silesian University of Technology, e-mail: h2dah_sum @hotmail.com*

Abstract

Artificial neural networks are very important tools to develop a wide range of technologies, nowadays. Although there are a lot of different kinds of neural networks, this document focuses on the fundamental artificial neural network, perceptron. The aim of this document is to propose a mechatronic system as a solution of garbage sorting, which is known as an important task before recycling, as well as, a big problem that the world is facing due to excessive consumption of products. The system is aimed to separate organic from inorganic trash by a reduced number of epochs, a manipulator robot, and odor sensor to detect easily the trash. Additionally, the advantages and disadvantages of the implementation of the system are presented for the reader to discriminate the viability of this implementation.

1. Introduction

Artificial neural networks (ANN) are sets of algorithms, modeled after the human brain, that are designed to recognize patterns. These patterns are numerical, contained in vectors, into which all real-world data (imagines, sound, text) must be translated. Neural networks help to group unlabeled data according to similarities among the example inputs, and they classify data when they have a labeled dataset to train on. Nowadays, ANN are used in our daily lives, such as speech, character and facial recognition. Mostly, ANN consists on separating a set of elements from another, therefore, it is possible to say that we can apply ANN for garbage sorting between organic and inorganic. There are many types of ANN but for this specific task it is proposed to used perceptron for it is the simplest and easiest method.

2. Perceptron

Perceptron is the simplest form of a neural network for the classification of a special type of patterns. Basically, this neural network consists on a neuron with synaptic weights and adjustable offsets. The algorithm implemented to adjust those parameters for a learning process was first developed by Rosenblatt in 1958. Rosenblatt demonstrated that if the patterns for training the perceptron were obtained from two linearly separable classes, then the algorithm converges and takes as the decision surface a hyperplane between these two classes. This algorithm is called the convergence theorem of the perceptron. Single-layer perceptron has only one neuron. The perceptron is limited to classification of patterns with only two classes. It is fundamental to emphasize that perceptron's learning rule is not guaranteed to converge if data is not linearly separable. The following figure gives a schematic representation of the perceptron.

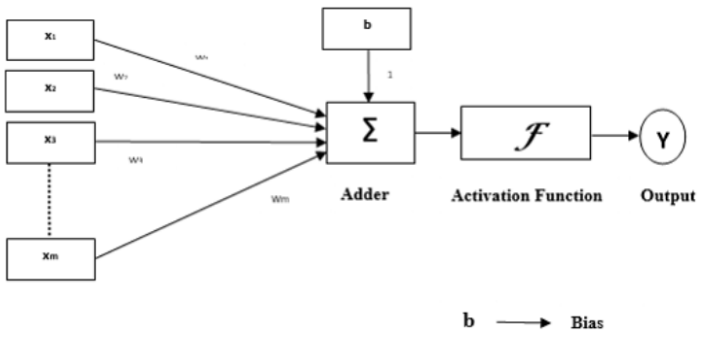

Fig. 2.1 - Schematic representation of perceptron

Learning rules for perceptron:

$$W^{new} = W^{old} + eP'$$
$$b^{new} = b^{old} + e$$

Where

$$e = t - a$$

This method is proposed because the error is a constant zero, it does make the separation between two groups without needing a learning rate and without having a lot of epochs.

3. System Proposal

For the garbage sorting task, a mechatronic system is suggested for it includes a mechanical, electronic, and programming subsystems that are strongly correlated. The strong dependence arises from the part that if one of the subsystems is dysfunctional the whole system is likely to fail.

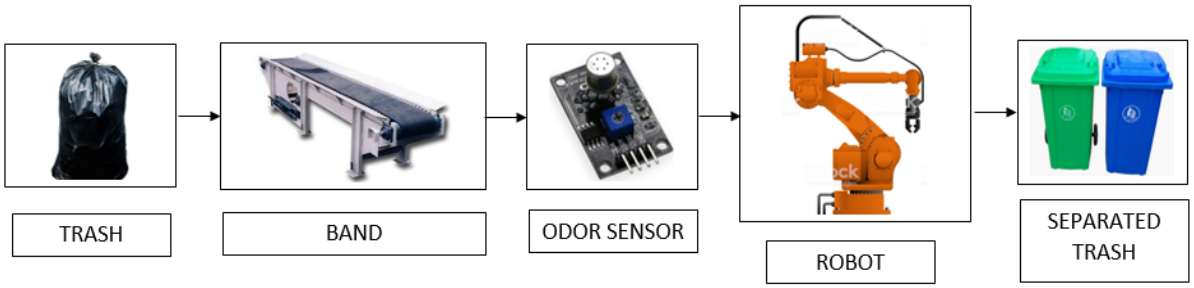

Fig. 3.1 Scheme of the proposed system and process.

Based on figure 3.1, the process consists on putting the trash into the band in a way that the trash is distributed along the band having one layer of trash (avoiding lumps). This task is manually done. The band will transport the trash to the robot to be separated. In between the band and the robot, it is installed an odor sensor which is already calibrated with the odor thresholds that the inorganic trash may have. Once that the sensor sends the signal, the robot will pick up the organic trash and store it in a bin. The robot has already implemented the algorithm of the neural network perceptron to be capable of the separation, also is needed to be implemented a control position to it. At the end of the band, the bins will be located to continue with the post-process (the following process after the separation may vary).

As it can be seen, the system is structured by a mechanical, electronic and programming subsystems. The mechanical is acquiesced by the robot and the band, the electronic subsystem has the sensor and its signaling, and the programming subsystem is immersed in the code for the manipulator and the sensor.

3.1. Advantages and disadvantages of the system

The implementation of the previous system has its advantages and disadvantages which are stated in the following table.

Table. 3.1 Advantages and disadvantages of the proposal

Advantages	Disadvantages
The system makes more efficient the process of separation of garbage.	The implementation of the whole system is very expensive.
The system is semi-automatic, therefore there is less human intervention with trash.	The machinery needed has high consumption of current and voltage.
Less human interaction with trash means less diseases and accidents.	

The biggest disadvantage of the proposed system is the cost of implementation and the consumption of current and voltage. The first inversion maybe hard to pay but after sometime the money can be retrieved and the profit will be higher. This system can be implemented in big industries or in schools for academic purposes, such as, implementation of different neural networks, or different approaches of control, programming, testing sensors. In the industry, the company may have big profits because when doing the recycling process, the company is forced to decrease the consumption of raw materials.

On the other hand, the advantages are focused on the employees or students. Regarding the price, the system is very to control and supervise. This process can be complemented as much as needed for it is a very dynamic system: more sensors, robots, can be implemented to make a lot of groups of trash (glass, paper, and metal). The proposed system has the simplest form with ability of being enlarged.

4. Conclusion

A lot of applications with ANN are used in our daily lives by making more efficient and accurate any task we need to be done. The garbage sorting is one of the main problems we are facing due to the over consumption and the production of large amounts of waste. This task is usually done by people, exposing their health and wellness. The proposed system does not need a lot of human interaction for it is semiautomatic. The implemented neural network, perceptron, is the most basic ANN that the error tends to zero with a small number of epochs, therefore, the process is going to be efficient by implementing the most basic and user-friendly ANN.

Acknowledgment

I want to thank Ph. D. Blanca Tovar for inspiring me to proposed this topic and my home institution, National Polytechnic Institute for giving me the opportunity of studying abroad. Also, I would like to thank Silesian University of Technology of receiving me in this institution and giving me the chance of presenting this article in the Environmental Protection and Energy Conference 2019.

References

[1] Supervised learning, retrieved May 9, 2019 in:
https://www.tutorialspoint.com/artificial_neural_network/artificial_neural_network_supervised_learning.htm

[2] T, A., (2017), The mostly complete chart of Neural Networks, explained, retrieved from:
https://towardsdatascience.com/the-mostly-complete-chart-of-neural-networks-explained-3fb6f2367464

[3] El perceptrón, retrieved from:
http://bibing.us.es/proyectos/abreproy/11084/fichero/Memoria+por+cap%C3%ADtulos+%252FCap%C3%ADtulo+4.pdf+

[4] A Beginner's Guide to Neural Networks and Deep Learning, retrieved from https://skymind.ai/wiki/neural-network

Is crowdfunding the missing puzzle piece to achieve rapid decarbonization?

Scientific statement

William Wiseman[1]

[1]*Department of Energy Engineering, Universitat Polítecnica de Catalunya, mr.wwwiseman@gmail.com, Seeds - Collective Greenvesting, seeds-investing@gmail.com*

Abstract

Adapting to climate change is commonly associated with sacrifice and reduction. People imagine a dramatic change from the status quo which often causes a psychological recoil. Rhetorically, people are quick to agree with ways to reduce their carbon footprint although in practice their actions are not reflective of their words. Governments are equally guilty of the same inaction due to deeper socio-political and economic roots which have a vested interest in maintaining the current course. In a menacing turn for the worst, global energy-related emissions have actually risen for the first time since 2013, reaching a record high of 33.1 Gt CO2 per year [1]. The sluggish actions of governments to mitigate climate change has resulted in a growing outcry from concerned citizens globally; most notably the Fridays for Future movement, founded by Greta Thunburg. The recent galvanization of millions of activists has some energy economists weighing the potential of a novel financing method which could change the public perception of climate change mitigation from sacrificial to beneficial. This revolutionary new financing channel is renewable energy crowdfunding.

Keywords: crowdfunding, renewable energy finance, democratic investing

1. Introduction

Crowdfunding has traditionally been used for donation campaigns, early-adopter sales, and recently some equity investing on platforms such as GoFundMe, Kickstarter and AngelList. Crowdfunding works by aggregating small investments from many investors to result in a large financing round for a company or project. These platforms have rapidly scaled a significant user base, with Kickstarter as the market leader. Since its founding in 2009, Kickstarter has raised over 4.6 billion USD for over 460,000 projects from roughly 17 million users [2]. In comparison, Seeds, the Collective Greenvesting financial technology platform uses an innovative repurposing of this funding mechanism to enable environmentally concerned citizens to invest and benefit from the renewable energy transition. Seeds' unique cash flow model uses a "round-up" feature in which the user's transactions are rounded up to the nearest Euro and the difference is automatically invested in the user's renewable energy project of choice. ex. You buy a coffee for 1.50€, Seeds identifies this purchase and makes a separate transaction of 0.50€ which is invested into your selected project for a total of 2€ spent. These micro-investments will lower the barrier of entry so that every financial level of environmental investor can benefit from the energy transition. Users will receive a return on investment from the loan repayments from the collectively funded project. Seeds strives to connect spending with responsible saving and investing with the added social value of helping to mitigate the climate crisis. The rapid growth in global environmental activism signals that people are demanding change; Seeds plans to unleash this collective energy while distributing the profits to the masses.

2. Review of Current Renewable Energy Finance

Financing the energy transition has always been a challenge. For a long time renewable energy sources required government subsidies to be economically viable, although now economies of scale and perpetual learning have made some commercial solar and on-shore wind farms reach a levelized cost of energy price parity with conventional fossil fuels. [3] While this pivotal tipping point will signal future investment potential, this has not been the case for the past or the present. To date, the energy transition has been regrettably underfunded.

According to the International Renewable Energy Agency "In the power sector, the global energy transformation would require investment of nearly USD 22.5 trillion in new renewable installed capacity through 2050. This would imply at least a doubling of annual investments compared to the current levels, from almost USD 310 billion to over USD 660 billion." [4] In 2018, humanity was below 50% of the investment required to avert the worst consequences of climate change. This staggering statistic clearly shows that financial investment needs to either be redirected to the energy transition, or new financing channels need to be opened. This is where crowdfunding can play a pivotal role in changing the course of the energy transition.

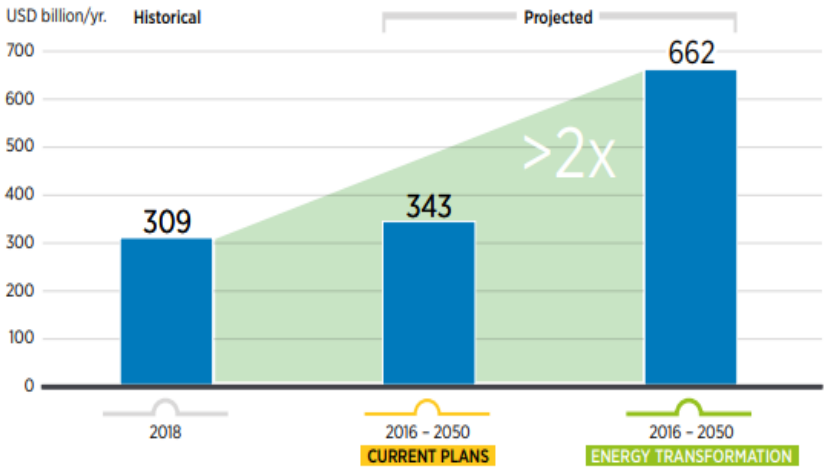

Fig. 2.1. Current vs. Required Investment in Renewable Energy [4]

3. Benefits of Renewable Energy Crowdfunding

To date, renewable energy crowdfunding has only accounted for a small fraction of total crowdfunding globally which is primarily centered in the Europe and the United States. Crowdfunding is primary geographically centered in developed countries with North American and Europe accounting for over 90% of the 2012 total. [5] Despite the concentrated nature of renewable energy crowdfunding, the potential is enormous. According to Bloomberg New Energy Finance, "Just 1% of current US retail investment in savings accounts, money markets and US treasuries would provide US$90 billion for clean energy crowdfunding, with 0.5% of the bond market adding a further US$190 billion." [6] This cumulative USD$280 billion of additional renewable energy investment would eliminate 79% of the financing deficit needed to meet the most ambitious global carbon reduction goals and limit the global temperature increase to 1.5°C while avoiding the most catastrophic environmental consequences.

Besides the obvious benefit of averting climate change, renewable energy crowdfunding has the secondary benefit of distributing the profits of the energy transition to regular people as opposed to institutional investors and international banks. As an alternative to traditional funding mechanisms which are focused primarily on the financial bottom line; renewable energy crowdfunding brings the additional social benefit of community involvement and improvement. As an example, a solar installation on a local school could help reduce the electricity bills of the school, provide jobs to local electricians, distribute the loan profits to the community and help diffuse the NIMBY ("not in my backyard") phenomenon. Additionally, projects that receive widespread community support are more likely to receive preferential treatment with respect to permitting and legal complications which can threaten to derail any project.

A more subtle benefit of renewable energy crowdfunding may actually be the most interesting facet of the financing model; democratic investing. Once a project's financial viability is verified by the responsible crowdfunding platform, it is up to the investors to choose which projects get funded thereby promoting the projects with the largest social impact. This fascinating evolution of project finance will couple profits with the ethical implications of the project and "If this perspective proves accurate and mass production of the 20th

century gives way to greater personalization in the 21st, then it is hard to see the world of finance avoiding a comparable transformation of its own. New mechanisms like crowdfunding that are disintermediated, personalized and ethical will be well poised to challenge the centralized and opaque structures of old." (5) With the growth of renewable energy crowdfunding, the energy and financial industry are poised to make simultaneous evolutions.

Fig. 3.1. Solar Panels Used to Offset School Energy Costs [12]

4. Limitations of Crowdfunding

While the renewable energy crowdfunding financing mechanism appears to be an extremely promising option to accelerate the energy transition it is not without limitations of its own. At the moment the limit for a crowdfunding campaign in the European Union is capped at 8 million Euros [7] and in the USA it is capped at 1 million USD. [8] These limits eliminate the ability to fund projects such as utility scale solar and offshore wind which tend to have the fastest payback rate. Additionally, "In the EU there is no EU-wide legislation specifically targeted at crowdfunding, although the European Commission has outlined its intention to monitor progress and report back on the need for further action." [9] The fractured nature of the European Union financial regulatory system complicates the flow of international capital. Finally, the inability to liquidate investments poses a challenge. Investments in renewable energy infrastructure tend to be medium to long-term investments of 5-10 years. This can be a significant deterrent to investors who may need to liquidate their assets in the short to medium-term. To eliminate this obstacle, some renewable energy crowdfunding sites have worked to develop a secondary market, essentially a stock market, which would allow their users to buy and sell their shares within the community. Operating a secondary market comes with significant additional financial oversight and development costs so, to date, no company has perfected this concept.

5. Conclusions

Just as no technology can single-handedly prevent climate change, it cannot be assumed that renewable energy crowdfunding will be the saving grace for humanity, although it could be a significant step in the right direction. Mitigating humanity's impact on the environment will require a diverse aggregation of technologies, business models and social movements. Each of these will represent a uniquely shaped puzzle piece that helps construct the plan to save the world; crowdfunding may just be a piece that nobody expected. Preventing a climate disaster will require a dynamic evolution of human society. Crowdfunding offers an opportunity to positively reform the financial system during a time of global adaptation. If people work together and "If people take back control of their own money and invest it transparently and tangibly in the real economy, ethics can be reintroduced into financial decision-making." [11] With Seeds, this is a chance to grow together and give power to the people.

Acknowledgment

This paper was written in cooperation with Seeds Investing, the Collective Greenvesting platform and within the framework of the Energy Resources course at Universitat Politecnica de Catalunya with direction from Professor

Lluís Batet. Seeds was a finalist in the EPAE entrepreneurial contest and is startup founded in conjunction with ESADE Business School and the InnoEnergy Masters in Renewable Energy.

References

[1] International Energy Agency. "Global Energy & CO2 Status Report," 2019. https://www.iea.org/geco/emissions/.

[2] Szmigiera, M. "Kickstarter - Statistics & Facts." Statista, October 29, 2019. https://www.statista.com/topics/2102/kickstarter/.

[3] PVEurope. "Solar and Wind Reaches Parity with Power Prices in Parts of Europe." PVEurope, October 29, 2019. https://www.pveurope.eu/News/Markets-Money/Solar-and-wind-reaches-parity-with-power-prices-in-parts-of-Europe.

[4] IRENA. "Investment Needs." International Renewable Energy Agency, June 2016. https://www.irena.org/financeinvestment/Investment-Needs

[5] Donovan, Charles W. *Renewable Energy Finance: Powering the Future*, 2017. pg.332. Print.

[6] BNEF. "All Renewable Energy - Research Note. Extraordinary Popular Solution: Funding from Crowds?" Bloomberg New Energy Finance, 2012. https://www.bnef.com/InsightDownload/7188/pdf/.

[7] Donovan, Charles W. *Renewable Energy Finance: Powering the Future*, 2017. pg.334. Print

[8] Kolinska, Dorota. "New EU Rules to Boost Crowdfunding Platforms and Protect Investors." Press Release. European Parliment, November 5, 2018. https://www.europarl.europa.eu/news/en/press-room/20181105IPR18253/new-eu-rules-to-boost-crowdfunding-platforms-and-protect-investors.

[9] Gabison, Garry A, and Institute for Prospective Technological Studies. *Understanding Crowdfunding and Its Regulations: How Can Crowdfunding Help ICT Innovation?*. Luxembourg: Publications Office, 2015. http://dx.publications.europa.eu/10.2791/562757.

[10] European Commission, The Council. "Unleashing the Potential of Crowdfunding in the European Union." Communication From The Commission To The European Parliament. Brussels: The European Economic and Social Committee And The Committee Of The Regions, 2014.

[11] Donovan, Charles W. *Renewable Energy Finance: Powering the Future*, 2017. pg.331. Print

[12] Chow, Lorainne. 5,500 K-12 Schools Have Already Gone Solar, School buses at Analy High School in Sebastopol, California. The Solar Foundation, https://www.ecowatch.com/amp/solar-schools-us-2513536603

The following publication consists of articles presented during the Environmental Protection and Energy Conference at Silesian University of Technology in Gliwice, 6th December 2019

This release is a result of the "learning by doing" approach of MSc Energy Transition students.

KTiUZO

eit InnoEnergy Knowledge Innovation Community

Silesian University of Technology